

Preface

In these several decades, the rapid development of magnetic resonance spectroscopy has been a capital event in chemical physics. Among many brilliant advances in its fundamental techniques and applications, the advent of the observation methodology of spin polarization, to my mind, is epoch-making. Efforts to climb over a wall of time-resolution that has been thought to be a limit of the ordinary resonance experiment in equilibrium should be highly appreciated and actually have become a motive power to find out various new research objects like the chemically induced dynamic electron and nuclear polarization (CIDEP, CIDNP) and related phenomena. This area of study however is still a young science which may be properly said to have just seen its dawn.

Judging from the present situation in this field, I took it into my mind to organize an international symposium which covers not only spin polarization but general magnetic field effects on photochemical reactions. Meanwhile, we recently named this field spin chemistry. What is meant by this word seems to be rather wider, since there are many branches of structural chemistry and magnetism which treat electron and nuclear spins in molecular ground states. If one wishes to discriminate, one may call it dynamic spin chemistry.

The Oji Conference on Spin Chemistry was thus held from 15th through 18th of July, 1991 at Tomakomai, Hokkaido under the auspices of the Japan Society for the Promotion of Science and the Fujihara Foundation of Science. Almost all distinguished research scholars in this field were invited from the inside and outside of Japan, and vivacious discussions were developed. The meeting ended in success and produced numerous invaluable results useful for the future of spin chemistry.

This book is a collection of the manuscripts contributed from the invited participants together with the authors presented in poster sessions. It should be noted however this is not a mere proceedings but contains articles in no small numbers that have been nicely completed. I am grateful to all contributors for submitting camera-ready manuscripts before the time set.

I hope that this book will play a dominant part in introducing up-to-date status of spin chemistry and at the same time in increasing the number of the specialist in this field.

Yasumasa John I'Haya, Tokyo

August 1, 1991

SPIN CHEMISTRY

Spin Polarization and Magnetic Field Effects
in Photochemical Reactions

Edited by

Y. J. I'Haya

Department of Applied Physics and Chemistry
University of Electro-Communications
Tokyo, Japan

Temperature Dependence of the Magnetic Field Effect of the CIDNP in the Photocleavage of Cycloalkanone. by N. Suzuki, K. Maeda, Q.-X. Meng, K. Suzuki, M. Terazima and T. Azumi	150
CIDNP and CIDEP Studies on Intramolecular Hydrogen Abstraction Reaction of Polymethylene Linked System. by K. Maeda, N. Suzuki, Q.-X. Meng, K. Suzuki, M. Terazima and T. Azumi	154
Effect of Coulomb Force on Diffusion as Studied by CIDNP Intensities of Photo-Induced Electron Transfer Reactions of trans-Stilbene. by T. Aizawa, T. Sakata, K. Maeda and T. Azumi	160
Photo-Induced Electron Transfer Reaction Between Hexamethyldisilane and Quinones as Studied by a CIDNP Technique. by M. Wakasa, M. Igarashi, Y. Sakaguchi and H. Hayashi	164
Magnetic Field Effects on the Decay Kinetics of Triplet Radical Pairs in Homogeneous and Organized Systems. by P. P. Levin and V. A. Kuzmin	174
Mechanisms of Spin-Orbit Coupling Dependent Magnetic Field Effects in Chemical Kinetics. by U. E. Steiner, D. Baumann, W. Haas, H.-J. Wolff and D. Bürssner	209
Magnetic Field Effects in Luminol Chemiluminescence. by M. M. Triebel, A. K. Morozov, M. M. Totrov and E. L. Frankevich	214
Temperature Dependence of Lifetime of Chain-Linked Biradicals in the Absence and Presence of a Magnetic Field. by Y. Tanimoto	238
Intermediates for Photoisomerization of Aromatic Olefins in the Presence of Electron Acceptors as Studied by Magnetic Field Effects. by K. Naitoh, T. Oguchi, R. Nakagaki, T. Arai, H. Sakuragi, K. Tokumaru and S. Nagakura	244
An Application of Spin Trapping to the Study of Magnetic Field Dependent Chemical Reactions. by M. Okazaki, K. Toriyama, Y. Tai and T. Shiga	258
External Magnetic Field Effects on Bichromophoric Photochemistry. by R. Nakagaki	264
Laser Flash Photolysis Studies of the Magnetic Field Effects on the Bifunctional Chain Molecules Containing Benzophenone and N,N-Diethyl-aniline. by Y. Tanimoto, Y. Fujiwara, A. Saegusa and M. Hayashi	271

Contents

Theoretical Aspects of Chemically Induced Magnetic Polarization. by F. J. Adrian	1
The Electron Spin Polarized (CIDEP) Spectrum of the Propan-2-oyl Radical. by K. A. McLaughlan, N. J. K. Simpson and P. D. Smith	26
CIDEP in the Photolysis of Benzoic Acid Derivatives. by A. S. Jeevarajan and R. W. Fessenden	47
Electron Spin Polarization by a Radical-Triplet Pair Mechanism. by C. Blättler and H. Paul	64
Diffusional Aspects of Spin Selective Reactions; Fundamental Quantities and Relations. by J. B. Pedersen	71
Formation of Novel Radicals from the $\pi\pi^*$ Triplet States of Aromatic Ketones. by H. Hayashi, M. Igarashi, Y. Sakaguchi and Y. J. I'Haya	90
CIDEP of Benzil. by M. Mukai, Y. Yamauchi and N. Hirota	99
Electron Spin Polarization Generated in Singlet-Doublet and Triplet-Doublet Systems. by K. Obi and A. Kawai	105
CIDEP Studies on the Photoinduced Electron Transfer Reactions from Metalloporphyrins to Quinone. by S. Yamauchi, T. Ueda, M. Satoh, K. Akiyama, S. Tero-Kubota, Y. Ikegami and M. Iwaizumi	112
CIDEP Measurement in Low Magnetic Field. by M. Terazima, S. Hayakashi and T. Azumi	117
Formation Mechanism of Spin Polarized Solvated Electron in Photoionization. by H. Murai and K. Kuwata	123
Investigation of Novel Radical Pair Interaction: Ionic System and Micellar System. by H. Murai, H. Honma, M. Ishiwata and K. Kuwata	131
Stimulated Nuclear Polarization and Related Phenomena. by R. Z. Sagdeev, E. G. Bagryanskaya, I. V. Koptyng, Yu. P. Tsentalovich and A. V. Yurkovskaya	138
Determination of the Enhancement Factor of CIDEP in the Photochemical α -Cleavage of Ketones. by T. Sakata, M. Terazima and T. Azumi	145

Magnetic Field Effects on Photoinduced Electron-Transfer and the
Succeeding Processes in Phenothiazine-Viologen Linked Compounds
Incorporated into Cyclodextrin.

by T. Matsuo, H. Nakamura and H. Yonemura

278

Paramagnetic Ion Quenching of the Magnetic Field Effect in the
Photochemical Reaction of Naphthoquinone in Micelles.

by Y. Sakaguchi and H. Hayashi

290

Magnetic Field Effects in Photoinduced Electron-Transfer in Porphyrin-
Viologen Systems.

by T. Matsuo, H. Nakamura and H. Yonemura

303

Applications of Electron Spin Echo Spectroscopy to Location Control
of Alkylphenothiazine Derivatives in Photoinduced Charge Separation
Across Vesicles, Micelles and Reverse Micelle Interfaces.

by L. Kevan

313

New Aspects of Photo-Induced Chemical Reactions Studied by FT-EPR.

by K.-P. Dinse, G. Kroll and M. Plüschauf

344

Electron Spin Echo Study of CIDEP in Photolysis of di-t-Butyl Ketone
at Low Temperatures.

by P. P. Borbat, A. D. Milov and Yu. N. Molin

353

Application of Pulsed EPR Spectroscopy to the Study of Radical Reactions.

by T. Ichikawa and H. Yoshida

368

Effect of Electron Spin Diffusion on Electron Spin Echo Decay.

by V. V. Kurshev and T. Ichikawa

375

An ODESR Study of the Phosphorescent States of trans-2,2'-Bipyridine,
Metal-Free cis-2,2'-Bipyridine and $[Z_n(\text{bpy})]^{2+}$.

by M. Yagi

387

Formation of Aminoxyl Radicals from 5,5-Dimethyl-1-pyrroline-N-oxide
by Ferric Ion.

by K. Makino, A. Hagi, H. Ide, A. Murakami and M. Nishi

396

Applications of ESE Spectroscopy in the Study of Electron Spin Polar-
ization in Bacterial Photosynthesis.

by M. K. Bosch, P. Gast and A. J. Hoff

402

The Role of Spin Chemistry in the Primary Events of Photosynthesis.

by G. Kothe, S. Weber, J. R. Norris, S. S. Snyder, J. Tang,
M. C. Thurnauer, A. L. Morris, R. R. Rustandi and Z. Wang

420

Electron Spin Polarization in Photosynthetic Bacteria. Anisotropic
Chemical Reactivity.

by P. J. Hore, D. A. Hunter, D. J. Riley and J. J. Semlyen

435

Theoretical Aspects of Chemically Induced Magnetic Polarization

Frank J. Adrian

Applied Physics Laboratory, The Johns Hopkins University^{a,b}
Laurel, Maryland 20723, USA

and
Department of Chemistry, Queen's University
Kingston K7L 3N6, Canada

Abstract

The role of theory in guiding and simplifying interpretation of electron spin resonance experiments on photochemical and other reactions involving free radical intermediates is surveyed. Emphasis is on models which provide a physical picture as well as quantitative estimates for such phenomena as the radical pair mechanism of chemically induced electron spin polarization (CIDEP), the closely related process of spin exchange during radical-radical encounters, and spin lattice relaxation. Some specific topics discussed are an improved quantitative model of ST_0 CIDEP combining an initial stage of polarization development followed partial loss of this polarization to spin exchange, the relation between the spin exchange and recombination rate constants, and simplification of spin-lattice relaxation in the common case of spin-rotation relaxation. The modification of the polarization processes in two-dimensional and closed three-dimensional systems is also discussed.

1. Introduction

Recent experimental advances in high energy, pulsed, excimer lasers operating at photochemically important wavelengths, and in time-resolved detection of transient paramagnetic species by pulsed and direct-detection electron spin resonance (ESR) spectrometers [1], offer exciting new possibilities for investigating the reaction dynamics of increasingly complex chemical reactions involving free radical intermediates. A particularly important example of this, and one where considerable progress has already been made, is reactions in dimensionally-restricted environments such as micelles [2-4]. Of special interest are those reactions involving electron-spin-dependent processes with consequent magnetic-field-dependent effects, of which chemically induced electron spin polarization (CIDEP) of the radical intermediates is arguably the most striking and informative [5,6].

One obstacle to progress in this field is that a large number of processes occur more or less simultaneously in these complex reaction systems and, consequently, the theoretical

(a) Permanent address.

(b) Work supported by the Department of the Navy, Space and Naval Warfare Systems Command under Contract No. N0039-89-C-001.

models used to interpret the experimental data often contain more parameters than can be determined from the data itself. Therefore, realization of the full capabilities of the recent experimental advances will require accompanying advances in the theoretical models, particularly those that minimize the number of parameters required to describe these reaction systems, and that can provide quantitative estimates of experimentally inaccessible quantities. This article will discuss some of the more important theoretical problems arising in these reaction systems, with emphasis on CIDEP mechanisms, and will suggest some approaches to them.

2. An Overview of a Photoinduced Reaction

Fig. 1 gives an overview of the stages in a photochemically induced reaction involving production of an initial geminate radical pair. Similar processes occur in thermal dissociations, and following the encounter of separately-produced radicals (random pair), except that triplet state involvement is unlikely in these cases.

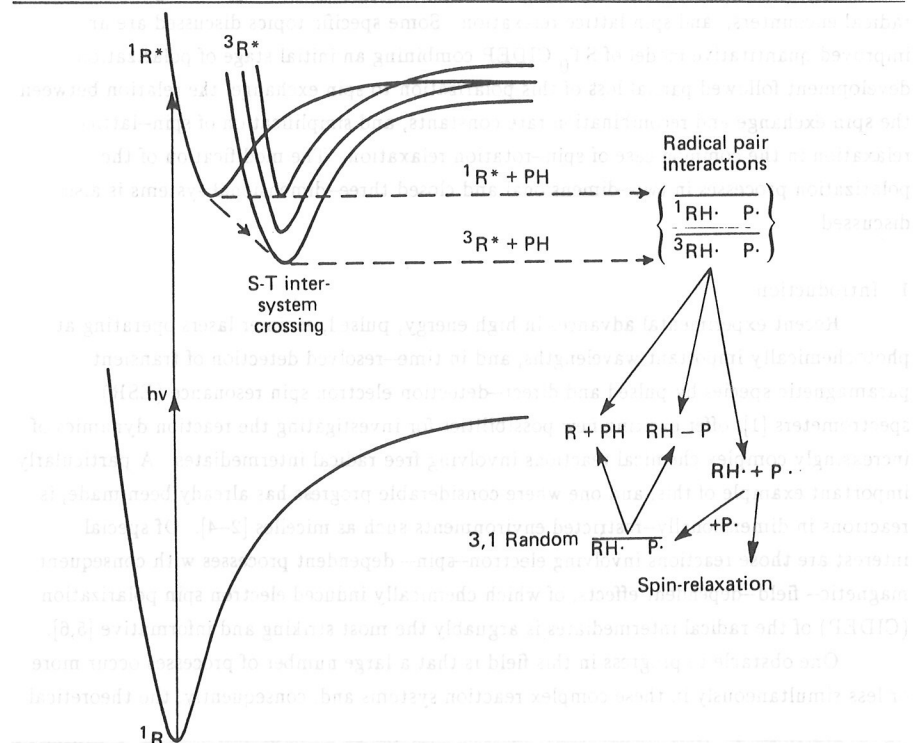


Fig. 1. Overview of a typical photochemical reaction involving free radicals.

The first stage of the process is formation of the geminate pair from the photoexcited species, during which electron spin polarization developed in the triplet precursor by the spin-selective singlet-triplet intersystem crossing may be transferred to the radicals (Triplet Mechanism) [6]. This stage typically lasts 10^{-11} to 10^{-9} s.

The second stage in which the radicals separate diffusively lasts approximately 10^{-9} to 10^{-7} s. During this period the radicals may acquire electron spin polarization through a combination of singlet-triplet mixing by the magnetic (hyperfine and electron Zeeman) interactions within the individual radicals and singlet-triplet splitting by the inter-radical exchange interaction (Radical Pair Mechanism or RPM).

Finally, about 10^{-7} s after the formation of the radical pair, the radicals are fully separated independent species in the sense that their diffusive reencounter is unlikely. These radicals individually undergo a number of processes, including: (1) encounters with other radicals leading to recombination, spin exchange, and/or the initiation of a new radical pair sequence, (2) reactions resulting in a new radical species, or, in the case of ion-neutral charge exchange, simply limiting the spin-state lifetimes of the radical species, (3) a variety of spin-lattice relaxation processes, and (4) electron spin transitions induced by the ESR observation process.

This rather large number of processes which can affect the concentrations and the spin polarizations of the radicals is reflected in the complexity of the kinetic equations for the magnetization of the various radical spin states and the corresponding ESR transitions. This is illustrated by the following equations for the concentrations of the four total electron-nuclear spin states of a pair of identical radicals with a single, spin $1/2$, magnetic nucleus. The corresponding energy levels are depicted in Fig. 2, and α and β denote, respectively, "up" and "down" electron spins, and $+$ and $-$ denote the corresponding nuclear spin states. These equations, whose derivation is described in detail elsewhere [7], are for a system in which the radicals are produced individually with reaction, polarization, and spin exchange occurring in random radical-radical encounters, however, similar equations apply to geminate radical systems.

$$\begin{aligned} \frac{d\alpha_+}{dt} = & \frac{1}{4}QI - \frac{1}{2}k_e p_s(\alpha_+ \beta_+ + \alpha_+ \beta_-) - \frac{1}{2}k_{ex}(\alpha_+ \beta_- - \alpha_- \beta_+) + \frac{1}{4}k_e p_s P(ST_0)(\alpha_+ \beta_+ + \alpha_- \beta_+) \\ & + \frac{1}{2}k_e P(ST_-)[\beta_+^2 - (1-p_s)\alpha_+ \beta_-] - [(W_e + W_2)(1 + \frac{1}{2}\delta) + W_n]\alpha_+ \\ & + W_e(1 - \frac{1}{2}\delta)\beta_+ + W_2(1 - \frac{1}{2}\delta)\beta_- + W_n\alpha_-, \end{aligned} \quad (1a)$$

$$\begin{aligned} \frac{d\alpha_-}{dt} = & \frac{1}{4}QI - \frac{1}{2}k_e p_s(\alpha_- \beta_+ + \alpha_- \beta_-) - \frac{1}{2}k_{ex}(\alpha_- \beta_+ - \alpha_+ \beta_-) - \frac{1}{4}k_e p_s P(ST_0)(\alpha_- \beta_+ + \alpha_+ \beta_-) \\ & + \frac{1}{2}k_e P(ST_-)[\beta_+^2 + 2\beta_+ \beta_- - (1-p_s)(\alpha_- \beta_+ + 2\alpha_- \beta_-)] - [(W_e + W_0)(1 + \frac{1}{2}\delta) + W_n]\alpha_- \\ & + W_e(1 - \frac{1}{2}\delta)\beta_+ + W_0(1 - \frac{1}{2}\delta)\beta_- + W_n\alpha_+, \end{aligned} \quad (1b)$$

$$\begin{aligned} d\beta_-/dt = & \frac{1}{4}QI - \frac{1}{2}k_e p_s(\alpha_+ \beta_- + \alpha_- \beta_+) - \frac{1}{2}k_{ex}(\alpha_+ \beta_- - \alpha_- \beta_+) + \frac{1}{4}k_e p_s P(ST_0)(\alpha_+ \beta_+ + \alpha_- \beta_-) \\ & + \frac{1}{2}k_e P(ST_-)[\beta_+^2 - (1-p_s)\alpha_+ \beta_-] - [(W_e + W_2)(1 - \frac{1}{2}\delta) + W_n]\beta_- \\ & + W_e(1 + \frac{1}{2}\delta)\alpha_- + W_2(1 + \frac{1}{2}\delta)\alpha_+ + W_n\beta_+, \end{aligned} \quad (1c)$$

$$\begin{aligned} d\beta_+/dt = & \frac{1}{4}QI - \frac{1}{2}k_e p_s(\alpha_+ \beta_+ + \alpha_- \beta_-) - \frac{1}{2}k_{ex}(\alpha_- \beta_+ - \alpha_+ \beta_-) - \frac{1}{4}k_e p_s P(ST_0)(\alpha_- \beta_+ + \alpha_+ \beta_-) \\ & + \frac{1}{2}k_e P(ST_-)[3\beta_+^2 + 2\beta_+ \beta_- - (1-p_s)(\alpha_- \beta_+ + 2\alpha_+ \beta_- + 2\alpha_- \beta_+)] \\ & - [(W_e + W_0)(1 - \frac{1}{2}\delta) + W_n]\beta_+ + W_e(1 + \frac{1}{2}\delta)\alpha_+ + W_0(1 + \frac{1}{2}\delta)\alpha_- + W_n\beta_-. \end{aligned} \quad (1d)$$

Here QI is the radical production rate, k_e is the reactive encounter rate, where p_s is the probability a singlet pair will react in such an encounter, and k_{ex} is an effective spin exchange encounter rate. The relation between k_e and k_{ex} is the subject of some controversy and will be discussed in more detail later. $P(ST_0)$ and $P(ST_-)$ give the radical pair polarizations resulting from $S-T_0$ and $S-T_-$ mixing, respectively, following formation of a triplet state pair by a reactive encounter. W_e , W_2 , W_0 , and W_n are the indicated spin-lattice relaxation transitions between the different electron-nuclear spin levels and $\delta = g\mu_B H/kT$ where $g\mu_B H$ is the electron spin transition energy.

As noted previously, the large number of terms in these equations reflects a correspondingly large body of information contained in and potentially available from the ESR spectra, but the same complexity of these equations usually will mandate the aid of theory in estimating some of the terms and justifying the neglect of others.

3. Qualitative Picture of the Radical Pair Mechanism

The radical pair polarization processes occur in the range of separations shown on the singlet-triplet energy diagram in Fig. 2. Here the dotted lines indicate the fully polarized spin states that would result from an initial triplet pair with a single (+) nuclear spin on radical 1 if the separation were slow enough (adiabatic separation) that level crossings are avoided. Of course the separation rate is nowhere close to being adiabatic as this would require separation times of the order of the reciprocal of the magnetic interactions within the radicals or roughly 10^{-8} sec. Nonetheless, the adiabatic separation concept is useful because it does predict the sense if not the magnitude of the radical pair polarizations. For example, the T_0 state of the pair with a single "up" nucleus on radical 1 (T_0^+) will adiabatically separate exclusively to the $(\alpha_+)_1(\beta)_2$ state of the separated pair, assuming the electron-nuclear hyperfine interaction is positive, yielding an emissively polarized low field transition of radical 1, as expected for $S-T_0$ mixing. The T_- state, on the other hand, adiabatically crosses to the S_- state, which, neglecting its possible adiabatic evolution, evolves into an equal mixture of $(\alpha_-)_1(\beta)_2$ and $(\beta_-)_1(\alpha)_2$ states. The effects of this $S-T_-$ mixing process are somewhat complicated, as will be discussed later, but the T_-S transition generally results in an excess of α spins in the separated radicals and a net emissive ESR spectrum.

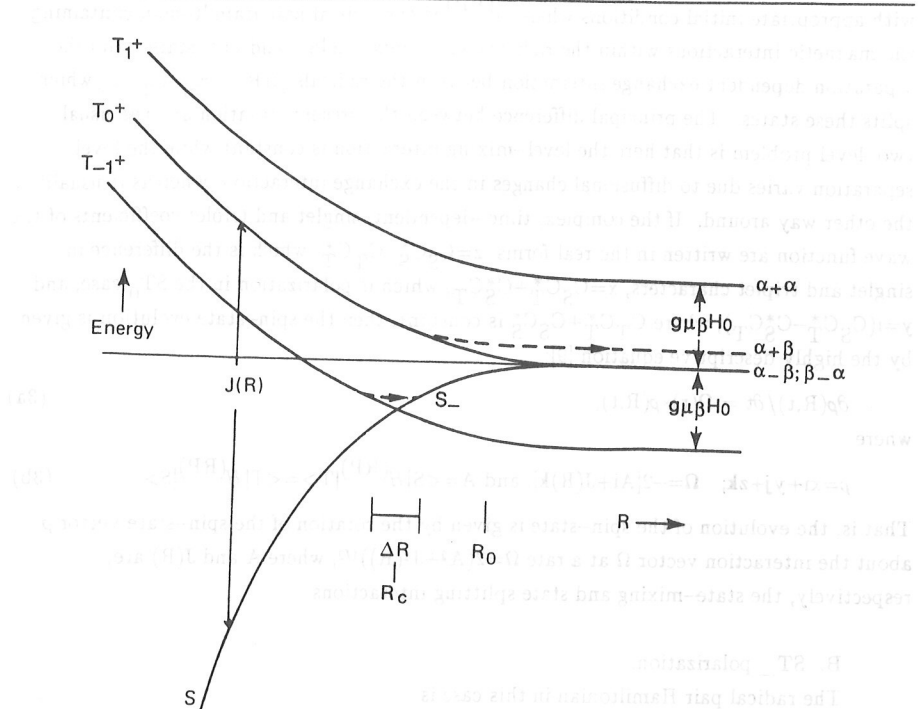


Fig. 2. Singlet and triplet energy levels of a separating radical pair in an external magnetic field. — rapid (diabatic) separation, - - - slow (adiabatic) separation. Final states at the right of the diagram result from adiabatic evolution of the initial states at the left of the diagram.

A. A vector model of CIDEP

A model for visualizing these polarization processes, and also spin exchange, which is closely related to the $S-T_0$ polarization process, on the usual, rather-far-from-adiabatic, time scales can be obtained from an adaption of the Feynman, Vernon and Hellwarth [8] generalization of the Bloch equation for a two-level quantum system. Here the two levels are the singlet and either the T_0 or T_- triplet, and their evolution is determined by the time-dependent Schrodinger equation

$$H^{(RP)}\psi = i\hbar \partial\psi/\partial t ; \quad \psi(t) = C_S(t)|S\rangle + C_T(t)|T\rangle, \quad (2)$$

with appropriate initial conditions where $H^{(RP)}$ is the radical pair Hamiltonian containing the magnetic interactions within the radicals which mix the $|S\rangle$ and $|T\rangle$ states, and the separation dependent exchange interaction between the radicals $[J(R) = (E_S - E_T)/2]$ which splits these states. The principal difference between the present situation and the usual two-level problem is that here the level-mixing interaction is constant while the level separation varies due to diffusional changes in the exchange interaction, whereas it usually is the other way around. If the complex, time-dependent, singlet and triplet coefficients of the wave function are written in the real forms: $z = C_S C_S^* - C_T C_T^*$, which is the difference in singlet and triplet characters, $x = C_S C_T^* + C_S^* C_T$, which is polarization in the $S-T_0$ case, and $y = i(C_S C_T^* - C_S^* C_T)$, where $C_T C_T^* + C_S C_S^*$ is constant, then the spin-state evolution is given by the highly descriptive equation [9]:

$$\frac{\partial \rho(R,t)}{\partial t} = \Omega(r) \times \rho(R,t), \quad (3a)$$

where

$$\rho = xi + yj + zk; \quad \Omega = -2[Ai + J(R)k]; \text{ and } A = \langle S | H^{(RP)} | T \rangle = \langle T | H^{(RP)} | S \rangle. \quad (3b)$$

That is, the evolution of the spin-state is given by the rotation of the spin-state vector ρ about the interaction vector Ω at a rate $\Omega = 2(A^2 + J^2(R))^{1/2}$, where A and $J(R)$ are, respectively, the state-mixing and state splitting interactions.

B. $S-T_-$ polarization.

The radical pair Hamiltonian in this case is

$$H^{(RP)} = -J(R)(2S_1 \cdot S_2 + \frac{1}{2}) + g\mu_B H \cdot (S_1 + S_2) + \sum_i A_{1i} S_1 \cdot I_{1i} + \sum_j A_{2j} S_2 \cdot I_{2j}, \quad (4)$$

that is, the sum of the inter-radical exchange interaction, the electron Zeeman interactions and the electron-nuclear hyperfine interactions on the two radicals. Usually only one of the hyperfine constants will be large enough to produce the required $S-T_-$ mixing, which simplifies the problem considerably. Even then the mixing can occur only in the level-crossing region where $J(R)$ and the electron Zeeman energy $g\mu_B H$ nearly cancel each other. In other regions either $J(R) > A$ or $g\mu_B H > A$ determines Ω and the state vector ρ rotates around the z axis with virtually no change in S vs T_- character. That $S-T_-$ mixing can only occur in the brief crossing interval is a stringent condition that requires an unusually large hyperfine interaction and/or slow diffusion for effective $S-T_-$ mixing. These conditions are embodied in the following equation for the $S-T_-$ polarization, which was obtained by adding a diffusion term, representing the variation of $J(R)$ in the diffusing radical pair, to Eq. (3) for the $S-T_-$ mixing case, and converting this Stochastic-Liouville equation to a single integral equation, whose analytic solution gave the result [10]:

$$P(ST_-) = (\pi A^2 / 4\mu_B g H_0) (R_c / \lambda D) \quad (5)$$

Here, $(R_c / \lambda D)$ estimates the time spent in the level crossing region at R_c , where D is the diffusion constant, and λ determines the range of the exchange interaction, $J(R) = J_0 \exp(-\lambda R)$. Although these conditions severely limit $S-T_-$ polarization, and it is less common than $S-T_0$ polarization, it is nonetheless more common than might be expected, especially in viscous solution at low temperature, because, unlike the $S-T_0$ polarization, it is an absolute polarization which cannot be destroyed by radical recombination or processes such as spin exchange which limit the lifetime of a spin state.

It should be noted, however, that even though the $S-T_-$ mechanism yields an overall absolute polarization, it does favor certain hyperfine states of that radical whose large hyperfine interaction led to the polarization. All hyperfine levels of the counter radical have the same polarization, however, provided that its hyperfine interactions played no role in the $S-T_-$ mixing. As a simple example of this point, which is sometimes overlooked, consider a radical pair with a single "up" magnetic nucleus in the T_+ state, as shown in Fig. 2. Conversion of this state to the $S-$ state in the $S-T_-$ process (the accompanying $+ \rightarrow -$ nuclear transition is required to conserve angular momentum) and the subsequent evolution of the singlet yields an equal mixture of α_- and β_- states of the radical with the magnetic nucleus. For this radical, therefore, $S-T_-$ mixing yields an unpolarized high-field high-field ESR transition ($\alpha_- \leftrightarrow \beta_-$) while its low field transition ($\alpha_+ \leftrightarrow \beta_+$) is emissively polarized because of the depletion of the β_+ state. A more complex example is Eq. (1) for the population of the spin states of a radical pair where the $S-T_-$ process clearly populates different states differently. Unfortunately, the resulting polarization pattern is very similar to the emissive/absorptive pattern produced by $S-T_0$ polarization and careful analysis involving examination of a number of hyperfine lines, temperature dependence, etc. is usually required when both types of radical pair polarization are present [7].

C. $S-T_0$ polarization.

The radical pair Hamiltonian in this case is

$$H^{(RP)} = -J(R)(2S_1 \cdot S_2 + \frac{1}{2}) + \mu_B H \cdot (g_1 S_1 + g_2 S_2) + \sum_i A_{1i} S_{1z} I_{1iz} + \sum_j A_{2j} S_{2z} I_{2jz}, \quad (6)$$

from which it can be seen that the difference in the magnetic interactions on the two radicals determines the $S-T_0$ mixing, the mixing rate being

$$A = \langle S | H^{(RP)} | T \rangle = \langle T | H^{(RP)} | S \rangle = \frac{1}{2}\mu_B H(g_1 - g_2) + \frac{1}{2} \sum_i A_{1i} M_{1i} - \frac{1}{2} \sum_j A_{2j} M_{2j} \quad (7)$$

The $S-T_0$ polarization process begins with the pair separating to a point where $J(R) << A$ because, as shown in Fig. 3a, the initial pure triplet (or singlet) state cannot evolve until this happens. After separation to a point where $J(R) \leq A$ $S-T_0$ mixing in the form of rotation about the x axis at a rate A begins, as shown in Fig. 3b. This, however, does not directly lead to CIDEP as this gives ρ a y component but not a spin polarization x component.

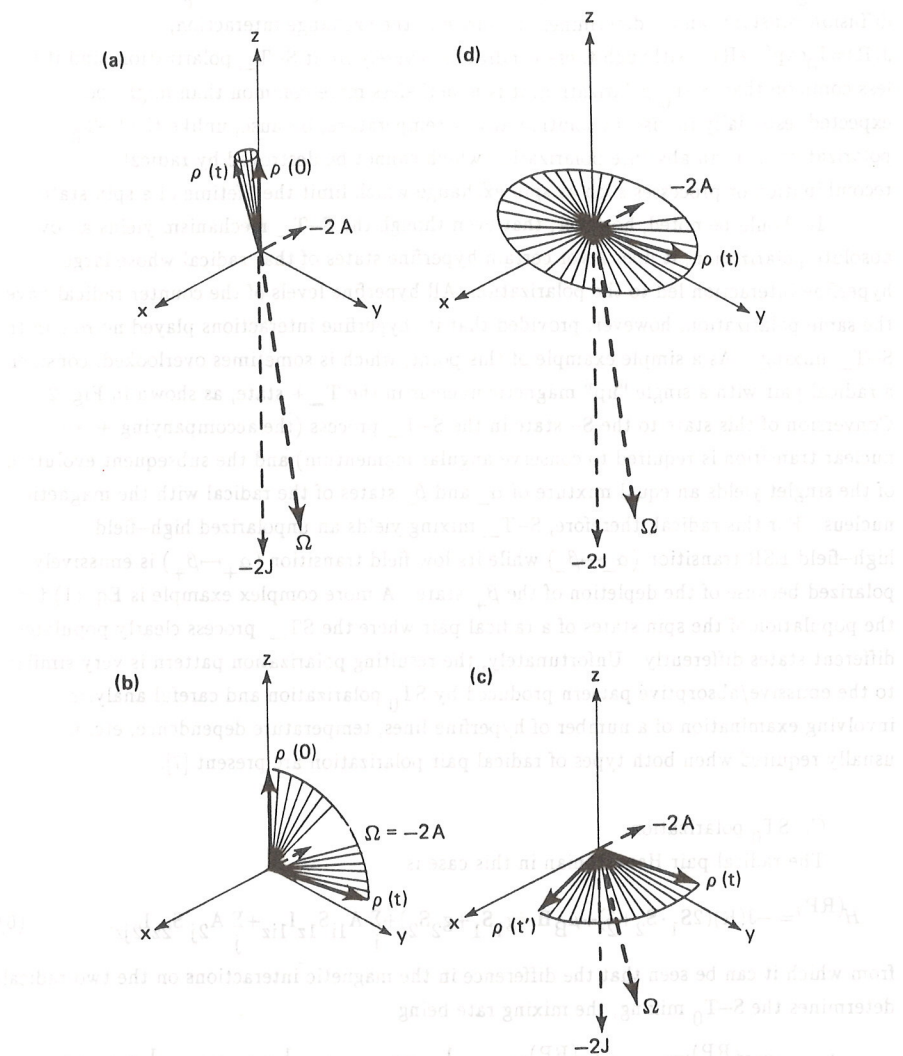


Fig. 3. Vector model of the S-T₀ CIDEP process. (a) S-T₀ mixing quenched when $J > A$. (b) S-T₀ mixing when $J < A$. (c) CIDEP results from limited reexposure to J after S-T₀ mixing. (d) Polarization destroyed by spin exchange if pair remains too long in region of large J .

Consequently, as shown in Fig. 3c, a subsequent limited reencounter [$J(R) > A$] is required to give ρ a spin-polarization component along x . Then, however, the pair must separate permanently before the reexposure to the exchange interaction is too prolonged or too strong. If this last occurs, the rapid rotation about the z axis averages the x and y components of ρ to zero, as shown in Fig. 4d. This is the phenomenon of spin exchange in which two encountering radicals have a 50–50 chance of exchanging spins. This process destroys any ST₀ polarization present in the pair because this polarization, unlike the ST₀ polarization, is only a relative polarization in which the electron spin states of the radicals are correlated with their nuclear spin states and their electronic g factors. As will be discussed in more detail later, ST₀ polarization and spin exchange are closely related, and it is often convenient to regard the ST₀ polarization process as weighting the spin randomization of the spin exchange process somewhat in favor of one of the two electron spin distributions according to the nuclear spin states and g factors of the radicals.

A useful semiquantitative aspect of this model is that it shows the time required for the polarization to develop is of the order of the S-T₀ mixing time ($\approx 1/A$) because the initial separation, and subsequent reexposure to the exchange interaction can be expected to be much shorter processes. Application of this result in support of more quantitative models, which usually only calculate the steady state limit of the polarization, will be discussed later.

4. Quantitative Models of Radical Pair CIDEP

A. The Stochastic Liouville equation.

Quantitative treatments of the rather complicated S-T₀ polarization process are based on the Stochastic-Liouville equation in which the time dependence of $J(R)$ due to the diffusive motion of the radicals is treated by adding a diffusive term to the equation for the evolution of the radical pair spin states [11,12]. With Eq. (3) for the spin state evolution, this equation is [9]:

$$\partial\rho(R,t)/\partial t = D\partial^2\rho(R,t)/\partial R^2 + \Omega\times\rho(R,t), \quad (8)$$

where it is to be noted that $\rho(R,t)$ is actually $R\rho$ (this definition simplifies the diffusion term) so that its volume integral is $4\pi\int\rho R dR$ not $4\pi\int\rho R^2 dR$. All solutions start by taking the Laplace transform of ρ , denoted as $(L\rho)$, to eliminate the time derivative, and solve for the steady state limit using the theorem: $\rho(r,t\rightarrow\infty) = \{sL[\rho(r,s)]\}_{s\rightarrow 0}$. The resulting coupled differential equations were solved numerically by Pedersen and Freed for a wide range of parameters [11,12]. Analytic solutions have been obtained by Monchick and Adrian [9,10], who used Green's function techniques to condense the three coupled differential equations into a single integral equation. Very recently, more comprehensive, albeit somewhat more complicated, analytic solutions for both the CIDEP and CIDNP cases have been obtained by Sushin who has used Green's function techniques to obtain separate solutions of the

Stochastic-Liouville equations in the regions of strong and weak exchange, and then joined these solutions [13].

The integral equation for the polarization can provide useful insights into the polarization process as well as numerical estimates, and a number of its applications will be discussed here. Semiquantitative methods for extending its range of applicability beyond that of relatively slow S-T mixing and fast diffusion will also be discussed. This integral equation, obtained from Eq. (8) following the procedures of Monchick and Adrian but written in a slightly different, more general form, is:

$$\begin{aligned}\varphi(r) = 4\pi j^{1/2}(r)x(r) &= -\frac{j^{1/2}(r)}{r_0} \int_1^\infty dp j(p) G_{\sqrt{s}}(r,p) Im[G_{\alpha\pm}(p,r_0)] \quad (9) \\ &- j^{1/2}(r) \int_1^\infty dp j(p) G_{\sqrt{s}}(r,p) \int_1^\infty dq j^{1/2}(q) Re[G_{\alpha\pm}(p,q)]\varphi(q)\end{aligned}$$

where the ST₀ polarization is

$$P(ST_0) = \lim_{r \rightarrow \infty} \varphi(r)/j^{1/2}(r). \quad (10)$$

Here, r_0 is the initial separation of the radicals, Re and Im denote the real and imaginary parts of the indicated quantities, and G_c denotes the Green's function of the operator $d^2/dr^2 - c^2$ with appropriate boundary conditions, in which c^2 is either the Laplace transform variable s , which is zero in the steady state limit, or is:

$$\alpha\pm = (\pm ia)^{1/2}; \quad (a\pm)^2 = \pm ia, \quad (11)$$

where a is the dimensionless form of the S-T₀ mixing rate A , to be defined momentarily. Previously these Green's functions were given for a reflective boundary at the distance of closest approach ($R=\sigma$) and an unrestricted outer boundary. Here we give them for the same inner boundary and an outer reflective boundary at $r=r_0$ in order to later investigate polarization in a confined system. The Green's functions in this case are [14]:

$$G_c(x,y) = \frac{[e^{cr_-} - \Gamma(c)e^{-cr_-}][e^{cr_+} - \Gamma(cr_0)e^{-cr_+}]}{2c[\Gamma(cr_0) - \Gamma(c)]}, \quad (12)$$

where $r_-(x,y)$ and $r_+(x,y)$ are, respectively, the lesser and greater of x and y . For $r_0 \rightarrow \infty$ one obtains the previously given Green's function for free diffusion in three dimensions with only a reflective inner boundary [9]. The expansion of this function for small c , which is always justified for $G_{\sqrt{s}}$, and which gives the polarization as an expansion in $a^{1/2}$ when used for $G_{\alpha\pm}$ is [9]:

$$G_c(x,y) = -r_-(x,y) + cxy. \quad (13)$$

Finally, it should be noted that all variables and parameters in these equations are

dimensionless, and related to the corresponding dimensioned quantities by the equations

$$r=R/\sigma; \quad j(r) = [2J(R)\sigma^2/D]; \quad a=[2A\sigma^2/D] \quad (14)$$

where σ is the distance of closest approach or reactive encounter separation of the radicals.

B. S-T₀ polarization in the unrestricted 3-D case

For the case of unrestricted 3-D diffusion except for a reflective boundary at $R=\sigma$ or $r=1$, Eq. (9) can be written in the following form:

$$\varphi(r) = P_0 g(r) - \int_1^\infty K(r,q)\varphi(q)dq, \quad (15a)$$

where

$$g(r) = [j^{1/2}(r)/\Lambda] \int_1^\infty j(p) p r_<(r,p) dp; \quad \Lambda = \int_1^\infty j(p) p^2 dp; \quad P_0 = (a/2)^{1/2} \Lambda, \quad (15b)$$

and

$$K(r,q) = j^{1/2}(r) j^{1/2}(q) \int_1^\infty j(p) r_<(r,p) r_<(p,q) dp. \quad (15c)$$

Although equivalent to the equation treated by Monchick and Adrian [9], this form reveals interesting relationships between its terms, which are the basis of a variational solution [15], to be discussed later.

With $j(r) = j_0 \exp(-\lambda \sigma r)$, this equation has been solved for the lowest-order term in the expansion in $a^{1/2}$. The method used was an expansion of $\varphi(r)$ in eigenfunctions of the symmetric kernel of the integral equation, $K(r,q)$ in Eq. (15c). Fortunately in this case it was possible to evaluate the required integrals of these eigenfunctions and sum the resulting infinite series for the polarization. The resulting equation for the polarization is [9]:

$$P(ST_0) = (\pi/2)(J_0/|J_0|)(A/D\lambda^2)^{1/2} \quad (16)$$

where the dimensionless quantity $(A/D\lambda^2)$ is the roughly the amount of S-T₀ mixing in the time it takes for diffusion to produce a significant change in $J(R)$. This equation is useful for the insight it provides into the process and for quantitative calculation of the polarization for small $(A/D\lambda^2)^{1/2}$. Extension to higher powers of $(A/D)^{1/2}$ are possible, but the approach of Sushin seems more versatile for this task [13]. We shall momentarily describe a simple heuristic approach combining the ST₀ polarization calculation and a calculation of the spin-exchange cross section, which yields a much more generally applicable ST₀ polarization formula as well as providing considerable additional insight into the polarization mechanism.

The necessity of calculating the polarization in the steady state limit $[sL(r,s)]_{s=0}$, in order to avoid the problem of inverting the Laplace transform, loses information about the

rate at which the polarization develops, and this information can be important in systems where there are fast competing processes or as ESR observation techniques reach shorter time scales. As shown earlier, however, this problem is largely resolved by the qualitative vector model which shows the polarization development time is of the order of $1/A$.

Another method for estimating the polarization development time, which we discuss later, is to incorporate a decay term into the Stochastic-Liouville equation.

C. Spin exchange

Unlike the absolute, magnetic energy, polarizations produced by the Triplet Mechanism and the ST₀ part of the RPM, ST₀ polarization does not change the relative number of "up" and "down" electron spins but is a relative, or magnetic entropy, polarization in which there is a correlation between the location of the "up" and "down" spins and the nuclear spin states and electronic g factors of the two radicals. Spin exchange, in which two encountering radicals with opposite electron spins trade these spins, removes ST₀ polarization but not an absolute polarization.

The spin exchange cross section can be calculated from an equation similar to Eq. (9) by starting with a fully polarized pair [$\rho(R_0, 0) = R_0 i$] at a separation R_0 such that $J(R_0)$ is very small, rather than an initial unpolarized pair in a singlet or triplet state in the strong exchange region [16]. The spin exchange cross section is related to the difference between the initial polarization and the final polarization of the separated pair as obtained by solution of the integral equation for the polarization using methods similar to those used in the ST₀ polarization case [9]. The result is [16]:

$$\Delta P_{ex} = 1 - P_\infty = \frac{\sigma}{R_0} \left[\frac{2\lambda\sigma+1}{2\sigma\lambda} \right]^3 + \frac{1}{\lambda\sigma} \left[\frac{4}{5} + 4n \frac{128J\sigma}{25\pi^2 D\lambda^2} \right], \quad (17)$$

where J_σ is the exchange interaction at the reactive-encounter separation σ . Since the rate constant for bimolecular encounters between radicals at a separation R_0 is $k_e = 4\pi R_0 D$, the spin-exchange encounter rate, which is usually significantly different from the actual spin exchange rate, is:

$$k_{ex}^{(enc)} = k_e \left[\frac{2\lambda\sigma+1}{2\sigma\lambda} \right]^3 + \frac{1}{\lambda\sigma} \left[\frac{4}{5} + 4n \frac{128J\sigma}{25\pi^2 D\lambda^2} \right], \quad (18)$$

Since $[(2\lambda\sigma+1)/2\lambda\sigma]^3$ is usually close to unity this result shows that the spin exchange process has a short-range component corresponding to encounters at the reactive separation σ , where radical recombination may also occur, and a long-range component due to grazing encounters which has no reactive counterpart. The implications of this result for the treatment of spin exchange in the kinetic equations, such as Eq. (1), for the formation and decay of spin polarization will be discussed momentarily, the important point being that the short-range part of the spin exchange term competes with radical recombination but the

long-range part does not. Next, however, we present an interesting, albeit somewhat heuristic, application of this result to extend Eq. (16) for the S-T₀ polarization to include higher terms in (A/D) .

D. Secondary spin exchange as a correction to S-T₀ polarization

The second term on the rhs of the Stochastic-Liouville equation for the ST₀ polarization, cf. Eqs. (9) and (15), represents the destruction of the developing polarization by spin exchange, and an exact solution of this equation will properly represent this effect. Nonetheless, it is both interesting and potentially useful, that a substantial improvement to Eq. (16) is obtained by the following relatively simple model in which a substantial portion of the loss of the polarization to spin exchange is assumed to occur after the formation of an initial polarization given by the approximate Eq. (16).

The basis of this correction is the previously discussed idea that the time required for the development of the polarization is determined largely by the S-T₀ mixing rate A , because the initial steps of pair separation to the point where $J(R) \leq A$, and the weak reencounter with $J(R) > A$ are relatively rapid processes. Thus, during the time (of the order $1/A$) required for the development of this polarization the radicals may not have been able to separate to a point where partial loss of the just-developed polarization to spin exchange can be neglected. To calculate the average separation $\langle R \rangle$ reached in time $1/A$, or actually $\langle 1/R \rangle$ because this is the factor in ΔP_{ex} , we need an expression for the distribution of separations at time t of a radical pair that was initially at a small separation R_0 , when the ST₀ polarization process began. We use the distribution:

$$P(R, t) = [1/4\pi R R_0 (4\pi D t)^{1/2}] \{ \exp[-(R-R_0)^2/4Dt] - \exp[-(R+R_0-2\sigma)^2/4Dt] \} \quad (19)$$

which is calculated with an absorbing barrier at the encounter separation $R=\sigma$, so that pairs encountering during t are removed from the distribution [17,18]. This distribution is believed more appropriate than the distribution resulting from diffusion with reflection at σ because pairs which undergo a strong encounter at σ during the polarization process are unlikely to be polarized. The average of $1/R$ over this distribution can be obtained in terms of standard integrals if one writes $R-R_0=(R-\sigma)-(R_0-\sigma)$ and $R+R_0-2\sigma=(R-\sigma)+(R_0-\sigma)$, notes that the time $t \approx 1/A$ will be long enough that $\exp[(R_0-\sigma)^2/4Dt] \approx 1$ and that the terms $\exp[\pm R(R_0-\sigma)/4Dt]$ can be expanded in powers of their arguments and only the first non-cancelling terms retained. The result, if one replaces the factor $(R_0-\sigma)/R_0$ by unity, because this factor represents the fraction of pairs that have escaped absorption at σ , and it is known that a polarized pair has escaped, is

$$\langle 1/R \rangle = (1/\pi D t)^{1/2} = (A/\pi D)^{1/2} \quad (20)$$

Then, from Eq. (17), the polarization surviving spin exchange is given by the expression:

$P(ST_0)_f = P(ST_0)_i(1 - \Delta P_{ex})$ where the initial polarization $P(ST_0)_i$ is given by Eq. (16). This equation accounts well for the spin exchange correction if A/D and ΔP_{ex} are not too large, but is flawed for large ΔP_{ex} (particularly $\Delta P_{ex} > 1$) because spin exchange can never do more than reduce the polarization to zero. A way out of this difficulty, in keeping with the present heuristic approach, is to replace $(1 - \Delta P_{ex})$ with $1/(1 + \Delta P_{ex})$ which reproduces $(1 - \Delta P_{ex})$ for small ΔP_{ex} and never becomes less than zero. The resulting expression for the polarization is

$$P_f(ST_0) = \frac{\pi}{2\lambda} (J_0/|J_0|) \left[\frac{A}{D} \right]^{1/2} \left\{ 1 + \left[\frac{A}{\pi D} \right]^{1/2} \left[\sigma \left[\frac{2\lambda\sigma+1}{2\sigma\lambda} \right]^3 + \frac{1}{\lambda} \left[\frac{4}{5} + \ln \frac{128J\sigma}{25\pi^2 D\lambda^2} \right] \right] \right\}. \quad (21)$$

In Table I below we compare $S-T_0$ polarizations calculated by the lowest-order Eq. (16) and the spin-exchange corrected formula above with the numerical results [11]. Clearly, Eq. (21), which is similar in form to Sushin's expression for $P(ST_0)$ [13], is a considerable improvement, particularly for the conditions of large hyperfine mixing, slow diffusion, and a long-ranged exchange interaction for which Eq. (16) fails completely. This suggests that the model leading to Eq. (21) does depict reasonably well the processes occurring after the polarization is initially formed. Also this approach may be useful for obtaining corrections to the lowest order approximation to the polarization in more complicated situations such restricted environments.

Table I. Comparison of polarizations calculated with the lowest order formula [P_i from Eq. (16)], the spin exchange corrected formula [P_f from Eq. (21)] and the results of numerical calculations (P_{num}).

$A 10^8 s^{-1}$	$D cm^2/s$	$\lambda = 5.756 \text{ \AA}^{-1}$			$\lambda = 1.439 \text{ \AA}^{-1}$		
		P_i	P_f	P_{num}	P_i	P_f	P_{num}
0.5	10^{-4}	1.93	1.90	1.68	7.72	7.53	6.79
2.0	10^{-4}	3.86	3.74	3.73	15.4	14.7	14.5
8.0	10^{-4}	7.72	7.25	7.02	30.9	28.0	26.3
32.0	10^{-4}	15.4	13.7	12.7	61.7	51.4	44.5
0.5	10^{-6}	19.3	16.1	14.9	77.2	55.9	48.5
2.0	10^{-6}	38.6	27.8	23.2	154.4	87.7	68.2
8.0	10^{-6}	77.2	43.4	32.8	302.7	122.5	88.5
32.0	10^{-6}	134.4	60.3	42.0	617.4	152.8	104.0

E. Variational solutions – CIDEP in two dimensions.

The range of conditions for which Eq. (9) can be solved can be extended by various methods such as the just discussed grafting of a spin-exchange process onto the initial polarization process, taking higher order terms in the expansion of the Green functions present in the integral equation, and by variational techniques [15]. The variational technique is based on the following interesting relationships that often exist between the terms of the integral equation when only the lowest-order terms in the expansion of its Green's functions are used. These conditions, exemplified by Eq. (15) are:

$$P(ST_0) = \lim_{r \rightarrow \infty} [\phi(r)\varphi(r)]; \quad \lim_{r \rightarrow \infty} \phi(r)g(r) = 1; \quad \lim_{r \rightarrow \infty} \phi(r)K(r,p) = \Lambda g(p) \quad (22)$$

where $\phi(r) = 1/j^{1/2}(r)$. These conditions are the same as discussed previously, except that the form of $j(r)$ is more general [15]. There they were shown to lead to a variational expression for $\varphi(r)$ in which the quantity minimized (or maximized) by choice of the variational parameter(s) in a trial approximation to $\varphi(r)$ is related to, and thus determines, the polarization. For Eq. (15) the variational function is

$$F = 1 - \Lambda \langle \varphi | g \rangle \langle g | \varphi \rangle / (\langle \varphi | \varphi \rangle + \langle \varphi | K | \varphi \rangle); \quad P(ST_0) = F \Lambda (a/2)^{1/2}, \quad (23)$$

where $\langle \varphi | g \rangle = \int \varphi g dr$. Furthermore, for a symmetric kernel $[K(r,q) = K(q,r)]$, such as present in Eq. (15), this method gives an upper limit to the polarization [15]. This equation was solved for diffusion in three dimensions with $j(r) = j_0 \exp(-\lambda r)$, using the trial function: $\varphi(r) = \exp(-\lambda \sigma r/2)$ for $r \geq r_c$ and 0 for $r < r_c$ where r_c was the variational parameter. The result was: $R_c = \sigma r_c = \lambda^{-1} \ln[(10/3)^{1/2} J_0/D\lambda^2]$ and $P(ST_0) = (10/3)^{1/2} (J_0/|J_0|)(A/D\lambda^2)^{1/2}$, which is only slightly greater than Eq. (16).

The form of Eqs. (15 and 23) show, moreover, that the method can be applied to any $J(R)$ that never changes sign, although the calculations may be more involved than in case of an exponentially decaying exchange interaction. Another interesting possibility, as yet unexplored, is whether the method could be applied to a more complicated diffusion model such as diffusion in a restricted environment where the diffusion rate changes with radical separation.

As an example of the variational approach we summarize briefly here its application to Monchick's model of CIDEP in two dimensions [19]. In order to avoid the problems posed by the inevitable reencounter of a radical pair diffusing in two dimensions he used an absorbing barrier to remove reencountering pairs and calculated the polarization as a fraction of the remaining pairs. The resulting integral equation had the form of Eq. (15) with

$$g(r) = \frac{j_0^{1/2} e^{-\lambda \sigma r/2}}{\Lambda} \sqrt{r} \int_1^{\infty} p \ln(p) \ln[r_{<}(r,p)] e^{-\lambda \sigma p} dp; \quad \Lambda = \int_1^{\infty} p \ln^2(p) e^{-\lambda \sigma p} dp; \quad P_0 = \frac{j_0 \ln(r_0)}{2 \ln a};$$

$$K(r,q) = j_0^2 \sqrt{r} e^{-\lambda \sigma r/2} \sqrt{q} e^{-\lambda \sigma q/2} \int_1^{\infty} \ln[r_{<}(r,p)] \ln[r_{<}(p,q)] p e^{-\lambda \sigma p} dp \quad (24)$$

where r_0 is the starting separation. The kernel of this integral equation is considerably more complicated than that of the three dimensional case and severe approximations had to be made to estimate its eigenfunctions and evaluate the resulting expression for the polarization [19].

The above equation also satisfies the conditions for the variational treatment, cf. Eq. (22) with $\phi(r) = \sqrt{r} \exp(-\lambda \sigma r/2)$, and here we summarize the variational result, to be reported in more detail elsewhere. The variational function in this case is:

$$\chi(r) = \sqrt{r} e^{-\lambda \sigma r/2} \quad r \geq r_c; \quad \chi(r) = 0 \quad r < r_c \quad (25)$$

where r_c is the variational parameter. This function is similar to that used in the 3-D case, and is based on the idea that the polarization is zero at small distances where $j(r)$ dominates and rises rapidly to its limiting value outside this region. The required integrals in Eq. (23) can be evaluated as expansions in $1/\lambda$, although the process is tedious and too lengthy to be included here. The results are:

$$R_c = \sigma r_c \approx \lambda^{-1} \ln(2J_0/D\lambda^2); \quad P(ST_0) \approx \frac{\ln(R_0/\sigma)}{\ln^2(2A\sigma^2/D) \ln(2J_0/D\lambda^2)} \quad (26)$$

where it is to be noted that the various distances, S-T mixing rates, etc have been written in their dimensioned form given by Eq. (14) rather than the dimensionless forms used in the integral equation. Interestingly, R_c is essentially the same as in the three dimensional case. The polarization obtained by Monchick [19] is similar except for the important difference that $1/\ln(2J_0/D\lambda^2)$ in Eq. (26) is replaced by $1/\lambda^2$. Thus, his model predicts the polarization is favored by a long-ranged $J(R)$ (i.e., λ small) whereas the above expression predicts the opposite, but with a much weaker λ dependence. Further examination of the two expressions is being carried out, however, the logarithmic dependence on the exchange interaction contained in Eq. (26) is typical of two dimensional problems. That the polarization increases with $\ln(R_0)$ is unphysical for very large R_0 , but given that the increase is only logarithmic probably does not present any problems for realistic values of the initial radical separation.

As of yet there are no experimental observations of CIDEP in two dimensions (practically, a system in which one dimension is considerably less than the others), however, this may be feasible given recent work in micellar systems. Although the above expression

indicates the polarization is zero in the limit of large exchange interaction, the logarithmic dependence should permit non-zero polarizations for typical exchange interactions. For example, with $A=10^8 \text{ s}^{-1}$, $D=10^{-6} \text{ cm}^2/\text{s}$, $J_0=10^{17} \text{ s}^{-1}$ [which gives $J_\sigma=J_0 \exp(-\lambda \sigma)=3 \times 10^{13} \text{ s}^{-1}$], $\lambda=2 \text{ A}^{-1}$, $R_0=8 \text{ \AA}$, and a collision separation $\sigma=4 \text{ \AA}$, Eq. (25) predicts a modest polarization of 0.025. Thus there is reason to hope that CIDEP may be observable in two dimensions, however, a more careful examination of two dimensional systems and particularly a probably more realistic system in which the radical pairs are being continuously created and continuously decaying, is needed. This investigation is currently being carried out.

F. CIDEP in a restricted 3-D environment.

The effect of both inner and outer limits on a pair diffusing in three dimensions may be useful as a model of a micelle, although it must be recognized that micelles are likely to be considerably more complex with diffusion limited by internal structure as well as boundaries. This case is investigated using Eq. (9) in which the Green's functions are given by Eq. (12) with a finite outer boundary at r_o . Treatment of this system is facilitated by having the radicals be both continuously produced at a rate k_f at a separation r_0 and continuously decaying at a rate k_r because the polarization due to an initial nondecaying radical population will go to zero in the steady state limit as all the radical pairs eventually undergo spin exchange in the confined space. This model also gives another estimate of the rate at which the polarization develops. Eq. (8) revised to include continuous production of radicals at rate k_f at an initial separation r_0 in an initial singlet state, and radical loss at rate k_r is:

$$\partial \rho(R,t) / \partial t = D \partial^2 \rho(R,t) / \partial R^2 + \Omega \times \rho(R,t) + k_f \frac{\delta(r-r_0)}{4\pi r_0} \begin{pmatrix} 0 \\ 0 \\ 1 \end{pmatrix} - k_r \rho. \quad (27)$$

Applying the procedures of Monchick and Adrian [9] to this equation gives an integral equation for the polarization similar to that obtained for diffusion without an outer boundary, provided that the outer boundary r_o is large enough that $j(r_o) \approx 0$. However, because of the continuous production and decay of radicals this equation yields the total polarization for all radicals, not the desired polarization per radical. This, however, is readily corrected for by dividing the resulting formula for the polarization by the radical concentration. The integral equation in this case is:

$$\varphi(r) = - \frac{k_f j^{1/2}(r)}{k_r r_0} \int_1^{\infty} dp j(p) G \sqrt{k_r} (r,p) Im[G \sqrt{k_r + ia}(p,r_0)]$$

$$- j^{1/2}(r) \int_1^{\infty} dp j(p) G \sqrt{k_r} (r,p) \int_1^{\infty} dq j^{1/2}(q) Re[G \sqrt{k_r + ia}(p,q)] \varphi(q), \quad (28)$$

where the fact that $k_r > s$ has been used, and it is to be noted that the loss process is represented by the addition of k_r to the Green's function parameters s and $\pm ia$. Let us consider the case in which the $S-T_0$ mixing rate is considerably larger than the recombination rate ($a > k_r$) and also large enough that $ar_0 > 1$, but that $k_r r_0$ is small. This corresponds to the situation where the $S-T_0$ mixing and initial phase of the polarization process is complete before the radicals can diffuse to the outer boundary but the radicals are unlikely to have reacted in that time. Thus, $G_{\sqrt{k_r+ia}} \approx G_{ia}$ because $a > k_r$ is given by Eq. (13) while expansion of Eq. (12) for $G_{\sqrt{k_r}}$ gives:

$$G_{\sqrt{k_r}}(x,y) = -3xy/[k_r(r_0^3-1)]. \quad (29)$$

Then Eq. (28) becomes

$$\begin{aligned} \varphi(r) = & \frac{3k_f(a/2)^{1/2}j^{1/2}(r)r}{k_r^2(r_0^3-1)} \int_1^r dp j(p)p^2 \\ & - \frac{3j^{1/2}(r)r}{k_r(r_0^3-1)} \int_1^r dp j(p)p \int_1^r dq j^{1/2}(q)r_{<(p,q)}\varphi(q). \end{aligned} \quad (30)$$

Inspection of this equation shows that because $G_{\sqrt{k_r}}(r,p)$ is a simple product of its arguments, rather than of the form $r_{<}(r,p)$ found for unrestricted 3-D diffusion, $\varphi(r) = Nrj^{1/2}(r)$. Substitution of $Nrj^{1/2}(r)$ for $\varphi(r)$ in the above equation, evaluation of the integrals with $j(r) = j_0 \exp[-\lambda\sigma r]$ up to only the leading term in $1/\lambda$, and recalling that the polarization is $\varphi(r)/f(r)$ gives

$$P_{\text{tot}}(ST_0) = \frac{3k_f(a/2)^{1/2}j_\sigma}{k_r^2(r_0^3-1)\lambda\sigma} r \left[1 + \frac{3j_\sigma^2}{k_r(r_0^3-1)(\lambda\sigma)^2} \right], \quad (31)$$

where, as discussed previously, this is the total polarization due to all radicals in the system, rather than the polarization per radical. The later polarization is readily obtained by dividing by the radical concentration, which is $(k_f r/k_r)$. If we note that the second term in the denominator of this expression will almost certainly be large compared to unity, we get, after converting to the demensioned form of the parameters using Eq. (14) and dividing by the radical concentration, the following simplified expression for the polarization per radical:

$$P(ST_0) = (A/D\lambda^2)^{1/2}/(2J_\sigma/D\lambda^2) \quad (32)$$

As in the case of CIDEP in two dimensions, and contrary to the results for CIDEP in an open 3-D system, the polarization decreases as the range of the exchange interaction increases, with the dependence being considerably stronger here than in two dimensions.

Eq. (32) indicates that ST_0 polarizations will be small unless the outer boundary is

large enough that both the polarization and observation processes are completed before the radicals can diffuse to the outer boundary, in which case the system is essentially an open 3-D system. If this time is roughly $t=10^{-7}$ s and $D=10^{-6}$ cm²/s, Eq. (19) shows the outer boundary would have to be roughly $R_0=(4Dt)^{1/2}=60$ Å. For a not untypical confined system with $A=5\times 10^8$ s⁻¹, $D=10^{-6}$ cm²/s, $J_\sigma=10^{13}$ s⁻¹, and $\lambda=2$ A⁻¹, one gets $P(ST_0)=2\times 10^{-4}$, which is considerably smaller than the thermal equilibrium population difference $g\mu_B H/kT \approx 0.0013$ for $H = 3000$ G and $T=300$ K. The fact that CIDEP is observed in micelles[1-3] whose dimensions are such that Eq. (32) should apply is an indication that the motion of the radicals in such systems is not free diffusion except for the boundary restrictions but is a more complex motion mandated by the internal structure of the micelle. It further should be noted that all the CIDEP equations are based on relative diffusion in which one radical is effectively fixed at the origin while the other diffuses at the sum of the two diffusion rates.. This is exact in an open system but is a considerable oversimplification in a closed system. Given that both radicals will tend to diffuse to the outer boundary because of the increase in volume with increasing r , the system might be better approximated as a 2-D system with the radicals diffusing about the outer boundary. Finally, the very interesting observation of another type of polarization associated with a small constant non-zero exchange interaction between the radicals in micellar systems[1-3] is another indication that the radical motions in such systems are more complicated than free diffusion. [20,21]

5. Kinetic Parameters and Relaxation Effects

Lastly, we consider some of the kinetic and relaxation processes occurring in a CIDEP-producing radical reaction. Often it is desired to determine the rates of one or more of these processes, especially the reaction rates, from the data, but often this will require that the rates of processes not being so determined be determined from other experimental data or from theory. One problem is that these different processes overlap to a considerable extent. An notable example is the spin exchange process which has much in common with both radical recombination, and the transverse or T_2 relaxation process.

A. Spin exchange.

Observation of spin exchange in free radical systems can provide information about the diffusive motions and the inter-radical exchange interactions. Observations of spin exchange in reactive free radicals systems has been limited up to now because of the difficulty of producing high enough radical concentrations for this bimolecular process to compete with the unimolecular spin-lattice relaxation, however, the new laser photolysis sources should overcome this restriction in many cases. There remains, however, the problem of separating spin exchange effects from the competing processes of reaction and spin-lattice relaxation.

There has been some confusion over the exact form of the spin exchange rate in equations such as Eq. (1) for the population of the different spin states of a radical undergoing reaction and polarization processes. This confusion seems to stem partly from the fact that its definition varies according to the specific quantity being measured and partly because it is not always recognized that recombination in a strong encounter precludes spin exchange.

The important quantity in an ESR experiment is the population difference between spin levels (magnetization). The effects of recombination, spin exchange, and relaxation on this quantity can be seen from a simplified version of Eq. (1) for the upper and lower electron spin states of a particular hyperfine level, in which the CIDEPE processes and all relaxation processes except those between the same hyperfine level (the W_e process) are neglected. These equations are:

$$\begin{aligned} d\alpha_\lambda/dt &= \frac{1}{4}QI - \frac{1}{2}k_e p_s \alpha_\lambda \Sigma_{\mu\mu} \beta_\mu - \frac{1}{2}k_{ex} [\alpha_\lambda \Sigma_{\mu\mu} \beta_\mu - \beta_\lambda \Sigma_{\mu\mu} \alpha_\mu] - W_e [(1 + \frac{1}{2}\delta) \alpha_\lambda - (1 - \frac{1}{2}\delta) \beta_\lambda], \\ d\beta_\lambda/dt &= \frac{1}{4}QI - \frac{1}{2}k_e p_s \beta_\lambda \Sigma_{\mu\mu} \beta_\mu - \frac{1}{2}k_{ex} [\beta_\lambda \Sigma_{\mu\mu} \alpha_\mu - \alpha_\lambda \Sigma_{\mu\mu} \beta_\mu] + W_e [(1 + \frac{1}{2}\delta) \alpha_\lambda - (1 - \frac{1}{2}\delta) \beta_\lambda]. \end{aligned} \quad (33)$$

It is helpful to recall that the factor 1/2 in the k_e term is because an $\alpha\beta$ pair has only 50% reactive singlet character, while the factor 1/2 in front of the k_{ex} term is because a spin randomizing exchange encounter has only a 50% chance of actually interchanging the $\alpha\beta$ spins. From these equations we can obtain the rate equation for the population difference ($\beta_\lambda - \alpha_\lambda$). In writing this equation, however, we simplify by noting that, if small population differences between the spin levels are neglected, $\Sigma_{\mu\mu} \alpha_\mu = \Sigma_{\mu\mu} \beta_\mu = R/2$ where R is the total radical concentration, and that $\alpha_\lambda + \beta_\lambda = f_\lambda R$ where f_λ is the weight of the λ 'th hyperfine level. Thus,

$$d(\beta_\lambda - \alpha_\lambda)/dt = -\frac{1}{2}Rk_e(\beta_\lambda - \alpha_\lambda) - \frac{1}{2}R(2k_{ex})(\beta_\lambda - \alpha_\lambda) - 2W_e(\beta_\lambda - \alpha_\lambda) + f_\lambda RW_e\delta. \quad (34)$$

From this equation we note that if k_e and k_{ex} are taken to be equal to the rate of encounters at the hard-core or reactive separation then the spin exchange rate is twice the reaction rate because reaction removes a given spin state with no accrual to another whereas spin exchange removes a spin from one level and transfers it to the other with a double effect on the population difference ($\beta_\lambda - \alpha_\lambda$).

The actual situation can be more complicated for two reasons. First, as shown in Eq. (18), k_{ex} has a short-range part corresponding to strong encounters, which can also lead to reaction, and a long-range part due to grazing encounters. At first glance the short range part can be set equal to k_e , as was done in Eq. (18), however, it must be realized that spin exchange can occur only if the radicals fail to react and that the probability of reaction at this separation is $p_s/2$. The long range part of the spin exchange process does not compete with relaxation, however. Therefore, the effective spin exchange encounter rate is, from

these considerations and Eq. (18) for the encounter rate,

$$k_{ex} = 2k_e \left(\left(1 - \frac{1}{2}p_s \right) \left[\frac{2\lambda\sigma+1}{2\sigma\lambda} \right]^3 + \frac{1}{\lambda\sigma} \left[\frac{4}{5} + \ln \frac{128J\sigma}{25\pi^2 D \lambda^2} \right] \right). \quad (35)$$

If the probability of reaction from the singlet state in strong encounters is unity then the short range part of the spin exchange rate is the same as the reaction rate, not twice it.

B. Spin lattice relaxation.

Spin-lattice relaxation processes are both an interesting and inevitable aspect of CIDEPE. As shown by Eq. (1) their effects can be quite complicated, with different hyperfine levels affected differently. In addition to the longitudinal or T_1 processes which, as shown in Eq. (1), involve transitions between spin levels, there are also the transverse or T_2 processes, which include both the T_1 processes and all other effects such as spin exchange, charge exchange reactions, etc., which limit the lifetime of a given spin state.

Given the potential complexity of these relaxation processes, it usually will be helpful to simplify them as much as possible. A useful simplification is to assume pure electron spin-lattice relaxation without accompanying nuclear spin transitions [only W_e is nonzero in Eq. (1)], and $T_1 = T_2$, although remembering that other processes may contribute to T_2 . This assumption is usually valid if the dominant spin relaxation mechanism is spin-rotation, as found experimentally for many small free radicals [22].

Whether spin-rotation relaxation is dominant in a particular system may be ascertained from the equations for spin-rotation relaxation [23], and using the Curl relation [24],

$$\gamma_{ii} = -\hbar(g_{ii} - g_e)/I_i, \quad (36)$$

to estimate the spin-rotation interaction constant (γ_{ii}) of the i 'th molecular axis from the usually better known g factor shift along this axis ($(g_{ii} - g_e)$ where g_e is the free spin g factor), and I_i is the moment of inertia which drops out of the final equation. A simplified version of the relaxation expressions given by Nyberg [23], for the case where γ_{ii} is much larger along one axis than the others (if there are large spin-rotation interactions along more than one axis a reasonable approximation is to add the individual spin-relaxation rates), is

$$\frac{1}{T_1} = \gamma^2 \left[\frac{\hbar k T}{3\hbar^2} \frac{2\tau_N}{1 + (g\mu_B H)^2 \tau_N^2} \right]; \quad \frac{1}{T_2} = \gamma^2 \frac{\hbar k T}{3\hbar^2} \left[1 + \frac{\tau_N}{1 + (g\mu_B H)^2 \tau_N^2} \right], \quad (37)$$

where τ_N is the rotational angular momentum correlation time, which is related to the rotational correlation time τ_2 by the equation;

$$\tau_N = I/6kT\tau_2. \quad (38)$$

For the values of I and τ_2 typical of small reactive free radicals ($I < 10^{-37}$ g cm²/s, and

$10^{-11} > \tau_2 > 10^{-13}$ s) one has $\tau_N(g\mu_B H) \ll 1$ and $T_1 = T_2$. Substituting Eq. (36) for γ and Eq. (38) for τ_N in Eq. (37) gives for the spin-rotation relaxation rate due to rotation about the i^{th} molecular axis:

$$T_{1i}^{-1} = T_{2i}^{-1} = (g_{ii} - g_e)^2 / 9\tau_{2i}. \quad (39)$$

Since the electronic g factors of radicals are usually at least partially known, or can be measured, the spin-rotation relaxation rates can be estimated if the rotational correlation times can be estimated from the dimensions of the radical and the viscosity of the solution. As the following examples show, however, it is important to estimate τ_2 using a rotational diffusion model with a slipping boundary condition [25] rather than the more common sticking boundary condition. This model also gives τ_2 a physically realistic dependence on rotation axis.

We illustrate the method with two examples: the CH_2O^- radical and the duroquinone anion (DQ^-). The molecular radii of these radicals were estimated from space-filling molecular models except that the radius in the direction perpendicular to the molecular plane of these π radical was taken to be half the thickness of an aromatic molecule or 1.7 Å [26]. The in-plane radii of CH_2O^- in the direction of the CO bond and perpendicular to it were each approximately 2 Å. The in-plane radii of the DQ^- radical were 4 Å in the direction of the CO bonds and 4.5 Å perpendicular to the CO bonds. To estimate the rotational diffusion times we somewhat arbitrarily extended the model of Hu and Zwanzig [25] for an axially symmetric spheroid to the case of a unsymmetric spheroid, obtaining

$$\tau_{2a} = (4\pi R_a R_b R_c \eta / 3kT) S_{bc} \quad (40)$$

where η is the viscosity of the medium, R_a , R_b , and R_c are the molecular radii along the three principal molecular axes, and S_{bc} is a slip/stick ratio determined by the ratio $R_{<} (R_b R_c) / R_{>} (R_b, R_c)$, that is the ratio of the lesser to the greater of the radii perpendicular to the direction of rotation. This quantity is given by Hu and Zwanzig for prolate and oblate axially symmetric spheroids. Here, we use the oblate and prolate spheroid value of S when the rotation is about the axis with the smallest and largest radius, respectively, and a weighted average of the oblate and prolate values when the rotation is about the intermediate axis. The rationale for this expression is that $4\pi R_a R_b R_c / 3$, the volume of the unsymmetrical spheroid, replaces the spherical volume $4\pi a^3 / 3$ in the expression for τ_2 without slip ($4\pi R_a R_b R_c \eta / 3kT$), and that the ratio of the axes perpendicular to the direction of the rotation is analogous to the minor/major axis ratio which determines the degree of sticking in the Hu-Zwanzig model of an axially symmetric rotor.

The g factor shifts of CH_2O^- are estimated from its isotropic g value of 2.0037 [27] and the assumption of equal g shifts along the in-plane axes and zero g shift in the direction perpendicular to the molecular plane, as is typical of π radicals. This gave $g - g_e = 0.0021$ for

both in-plane axes, so, in this case rotations about both in-plane axes contribute to the relaxation. The g shifts of DQ^- were taken from the benzoquinone values [27], which are $g_1 - g_e = 0.0042$, which is taken to be along the CO bonds, $g_2 - g_e = 0.0030$ which is taken to be the other in-plane axis, and zero perpendicular to the molecular plane. Again rotations about both in-plane axes contribute to the relaxation.

For CH_2O^- , with $\eta = 1.3$ cp [22], $T_1 \approx 0.2 \mu\text{s}$ in the slipping model of rotational diffusion and $10 \mu\text{s}$ in the sticking model, while the experimental value is $0.1 \mu\text{s}$ [22]. For the DQ^- radical, again with $\eta = 1.3$ cp, $T_1 \approx 5 \mu\text{s}$ in the slipping model and $14 \mu\text{s}$ in the sticking model, as compared with the experimental value of $6.6 \mu\text{s}$ [28]. T_2 is reported to be $0.67 \mu\text{s}$ in this system which the authors attributed to the lifetime limiting charge-exchange reaction $\text{DQ}^- + \text{DQ} \rightarrow \text{DQ} + \text{DQ}^-$ [28]. The close agreement between the calculated and experimental values is fortuitous and relatively unimportant. The important points are that in many cases spin-lattice relaxation is due to the relatively simple spin-rotation process, and that calculations of this sort usually can decide whether this is so in a given case. It is also readily shown that for the rotational correlation times found here ($\approx 10^{-13} \text{ s}$ for CH_2O^- and $\approx 10^{-11} \text{ s}$ for DQ^-) that rotational modulation of an anisotropic g factor hyperfine interaction does not contribute significantly to their spin relaxation. A final important point is that rotational diffusion is far better described by the slipping rather than the fixed boundary condition model of rotational diffusion, which result is consistent with other magnetic resonance evidence [7, 25].

6. Summary

The various phenomena covered in this article are believed to be among the most important factors in determining CIDEP in rapid reactions involving free radical intermediates, and, conversely, in extracting mechanistic information from CIDEP observations. As discussed here, it is believed that the relation between the radical recombination rate and the spin exchange rate given in Eq. (35) is a useful simplification, as is the assumption that spin-rotation usually is the dominant spin lattice relaxation mechanism. Advances to date in the theory of the radical pair mechanism of CIDEP provide both a good mechanistic picture of the process and adequate quantitative estimates for systems in which the radicals are freely diffusing. In confined media, such as micelles and solids, there are indications that the free diffusion model needs modification in at least some cases to deal with these interesting, and practically important, systems.

7. Acknowledgement

The author is grateful to Professor Jeffrey K. S. Wan and his colleagues in the Chemistry Department of Queen's University for their help and hospitality during visits when portions of this work was carried out. Helpful discussions with Dr. Louis Monchick are also gratefully acknowledged.

References

- [1] L. R. Dalton, A. Bain, and C. L. Young in *Annual Reviews of Physical Chemistry*, Eds. H. L. Strauss, G. T. Babcock, and C. B. Moore, Vol. 41 (Annual Reviews, Inc., Palo Alto, 1990), p. 389.
- [2] H. Murai, Y. Sakaguchi, H. Hayashi, and Y. J. I'Haya, *J. Phys. Chem.*, 90 (1986) 113, and references contained therein.
- [3] G. L. Closs, M. D. E. Forbes, and J. R. Norris, *J. Phys. Chem.*, 91 (1987) 3592.
- [4] C. D. Buckley, D. A. Hunter, P. J. Hore, and K. A. McLaughlan, *Chem. Phys. Letters*, 135 (1987) 307.
- [5] L. T. Muus, P. W. Atkins, K. A. McLaughlan and J. B. Pedersen, eds., *Chemically Induced Magnetic Polarization* (Reidel, Dordrecht, 1977).
- [6] F. J. Adrian, *Rev. Chem. Intermediates*, 7 (1986) 173, and references contained therein.
- [7] T. J. Burkey, J. Lusztyk, K. U. Ingold, J. K. S. Wan, and F. J. Adrian, *J. Phys. Chem.*, 89 (1985) 4286.
- [8] R. P. Feynman, F. L. Vernon, and R. W. Hellwarth, *J. Appl. Phys.*, 28 (1957) 49.
- [9] L. Monchick and F. J. Adrian, *J. Chem. Phys.*, 68 (1978) 4376.
- [10] F. J. Adrian and L. Monchick, *J. Chem. Phys.*, 71 (1979) 2600; *ibid*, 72 (1980) 5786.
- [11] J. B. Pedersen and J. H. Freed, *J. Chem. Phys.*, 58 (1973) 2746.
- [12] J. H. Freed and J. B. Pedersen, in *Advances in Magnetic Resonance*, ed. J. Waugh, Academic, New York, 1975), Vol. 8.
- [13] A. I. Sushin, *Chem. Phys.*, 144 (1960) 201.
- [14] J. T. Cushing, *Applied Analytical Mathematics for Physical Scientists*, (Wiley, New York, 1975) pp. 470–486 gives a good discussion of Green's functions and their derivation.
- [15] F. J. Adrian, *Chem. Phys. Letters*, 80 (1981) 106.
- [16] F. J. Adrian, *J. Chem. Phys.*, 88 (1988) 3216.
- [17] H. S. Carslaw and J. C. Jaeger, *The Conduction of Heat in Solids*, (Oxford U. P., London, 1959), p. 382.
- [18] F. J. Adrian, in L. T. Muus, P. W. Atkins, K. A. McLaughlan and J. B. Pedersen, eds., *Chemically Induced Magnetic Polarization* (Reidel, Dordrecht, 1977), Chap. V.
- [19] L. Monchick, *J. Chem. Phys.*, 72 (1980) 6258.
- [20] K. Tominaga, S. Yamauchi, and N. Hirota, *J. Chem. Phys.*, 92 (1990) 5175.
- [21] A. I. Sushin, *Chem. Phys. Letters*, 177 (1991) 338.
- [22] D. M. Bartells, R. G. Lawler and A. D. Trifunac, *J. Chem. Phys.*, 83 (1985) 2686.
- [23] G. Nyberg, *Mol. Phys.*, 12 (1967) 69.
- [24] R. F. Curl, *Mol. Phys.*, 9 (1965) 585.
- [25] C.-M. Hu and R. Zwanzig, *J. Chem. Phys.*, 60 (1974) 4354.
- [26] L. Pauling, *The Nature of The Chemical Bond*, 3rd ed., (Cornell, Ithaca, 1960), p. 260.
- [27] H. Fischer and K.-H. Hellwege, eds., *Magnetic Properties of Free Radicals*, Landolt-Bornstein, Numerical Data and Functional Relationships in Science and Technology, New Ser., Group II, Vol. 1, (Springer-Verlag, N. Y., 1965).
- [28] S. Basu, K. A. McLaughlan, and A. J. D. Ritchie, *Chem. Phys. Letters*, 105 (1984) 447.

The electron spin polarized (CIDEP) spectrum of the propan-2-oyl radical.

K.A.McLauchlan, N.J.K.Simpson and P.D.Smith.

Physical Chemistry Laboratory, South Parks Rd., Oxford OX1 3QZ (U.K.)

Abstract

It is demonstrated that the origin of the absorptive contribution observed in the spin polarized esr spectrum of the propan-2-oyl radical when it is created by flash-photolysis of propan-2-one (acetone) in a hydrogen-donating solvent is not the triplet mechanism of CIDEP, as previously assumed. It is shown to arise not in the photochemistry or photophysics of the parent molecule, but rather to be a property of the radical pair itself. Arguments are presented to demonstrate that its origins may lie in an unidentified novel polarization process, rather than the possible redistribution of level populations via very fast relaxation processes.

1. Introduction.

For some years it has been realised that the esr spectra of spin-polarized free radicals are consistent with two quite separate contributions to the line intensities (1,2). One is of a single phase, either emission or absorption, with the relative intensities as in unpolarized spectra. The origin of this contribution has always been believed to be the triplet mechanism (TM), in which radical polarization results from reaction of a fore-going triplet molecule, itself polarized by spin-selective intersystem crossing from a precursor singlet state. The second, more general, contribution, the radical pair mechanism (RPM), results from the production of free radicals in pairs and has the characteristic form that the low and high-field halves of the spectra are in opposite phase. For radicals formed from a triplet precursor and with a negative value of the electron exchange interaction, the lower half is in emission and the upper in absorption, an E/A pattern, whilst singlet-origin radicals exhibit an A/E one; in pairs of identical radicals the central RPM polarized line (if there is one) is of zero intensity.

There is strong qualitative and quantitative evidence that the TM does occur (3-6) although there are sound theoretical reasons for expecting it not to be inevitable in radicals produced from triplet precursors (7,8), in particular because certain kinetic criteria have to be met (see below). No evidence has yet been produced that hyperfine-undistorted emission spectra have any other possible polarization origin. Nevertheless, in all cases where a single-phase absorption contribution with undistorted line intensities has been reported, it has almost inevitably been assumed to have its origin in the TM also. Indeed the phase of the signal has been used to deduce the sign of the zero-field coupling constants in several aliphatic ketones on this basis (9,10). Despite an early suggestion from Adrian (11) that creation of radicals using plane-polarized photolysis light could provide a

diagnostic test for the occurrence of the TM, this test has been shown not to be useful in practice (12), although earlier claims were made that it was (13-15). In its absence, there exists no qualitative test for the action of the TM, and quantitative measurement of the polarization magnitude remains difficult, with few reliable results reported (5,6). In this paper we consequently have to take the approach of showing that the observations reported here are inconsistent with the qualitative predictions of TM theory to establish that, in some cases, the one-phase contribution may have a different origin.

The spectrum of the propan-2-oyl radical produced by the flash-photolysis of propan-2-one in propan-2-ol solution, in which an identical pair of free radicals is produced, has been a subject of CIDEP interest for some time (12,15-25). In the earliest observations, the appearance of a central line went unremarked, but it was soon realised that it was anomalous (23), and that it apparently indicated a source of spin polarization other than the RPM. It was shown that the central line had a non-Boltzmann intensity, and it appeared obvious that its origin lay in polarization due to the TM. Indeed, careful tests showed that the entire spectrum could be reproduced by adding a wholly undistorted absorptive contribution to the RPM one calculated for a pair of identical radicals. However, even in this early paper it was remarked that hydrogen abstraction by triplet propan-2-one from the alcohol proceeded at a known rate which appeared to be too slow, as compared with spin-lattice relaxation in the triplet, to carry the polarization to the radicals. In the absence of any other explanation, however, it has become accepted that the single-phase contribution does have a TM origin. It is our first task here to disprove this.

Very recently, an elegant time-resolved Fourier transform study has been made of the fully-deuterated propan-2-one/propan-2-ol system which has allowed, *inter alia*, a full investigation of the time-dependence of the intensities of the hyperfine components (26). This has shown, by methods quite independent of those used here, that the origin of the absorptive contribution to the polarized signal is not the TM; the authors assigned it rather to the result of the reaction of spin-equilibrated triplet, as originally suggested by Paul (17). This will be commented upon below.

2. Experimental.

All experiments were performed using the time-integration spectroscopy (TIS) method developed in this laboratory (27-29), often in the off-line mode in which an entire matrix of intensity-time-field information is stored on a minicomputer and manipulated away from the spectrometer. In this way the complete time dependence of esr signals from about 30 nsec. after radical formation until their disappearance by reaction is obtained in about 1.5 hour experimental runs. The radicals were produced by 308nm. flashes from a Lambda Physik 103M laser operating on a Xe/HCl/He/Ne fill, with a feedback unit ("intelligent laser control") to maintain an average constancy of output whilst the data set was gathered. This is particularly important in the comparatively lengthy off-line TIS

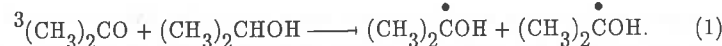
experiment, in which the information is obtained by performing a series of flashes as the magnetic field is stepped monotonically to display the spectrum. The samples were of the purest commercially-available forms, and were re-distilled as necessary; they were de-oxygenated by passage of nitrogen before flowing through the microwave cavity in which they were irradiated.

Several of the spectra shown have been acquired in a novel, stepped, surface mode. In this, the positions of the lines are first determined using our conventional mode 2 method, but then the computer running the experiment is programmed to display the spectrum for typically 5 gauss about each line position before jumping to the next line. In this way most of the laser flashes produce real signal, rather than simply monitoring the baseline between the lines, leading to improved signal-to-noise ratio over the period of the experiment. A second advantage comes from being able to display each line on an extended field scale, so that all of the second-order effects on each are evident in an overall spectrum which yet allows the overall intensity information to be shown. In this way all the information needed to characterise the radical and its polarization pattern is preserved in its most detailed, yet economic in time, form. For clarity, we have not shown the full surface, but rather have performed off-line TIS on the data set to display the spectral appearance at various times after the laser flash. In all the spectra shown, the intensities have been normalised, so that the only indication of the signal falling in time is from the deterioration of the signal-to-noise ratio.

3. Results and Initial Discussion.

3.1. Propan-2-one photochemistry.

The spectrum obtained on irradiation of propan-2-one in propan-2-ol solution is shown in fig.1. It is of the propan-2-oyl radical produced by the reaction



The emissive low-field lines and the enhanced absorptive high-field ones demonstrate that the radicals originate from a triplet precursor, as shown. The difference in the absolute intensities of the lines in the two halves, and the appearance of the central line are consistent with an absorptive contribution to the spectrum which shows no hyperfine distortion, that is the transition intensities due to this contribution are symmetric about the centre. It is the origin of this contribution to which we address ourselves.

The basic tenets of the TM mechanism are that spin-polarized radicals result from reaction of a spin-polarized molecular triplet state, and electron spin orientation is conserved on reaction. It follows that the sense of the polarization, emissive or absorptive, is the same in the radicals as in the triplet. The esr spectrum of one triplet state of propan-2-ol itself has been observed in low temperature experiments in the solid state, and it is emissive (30), and it follows that, if the single-phase contribution observed in the

radical, solution, spectrum is due to the TM, radical production cannot involve this same

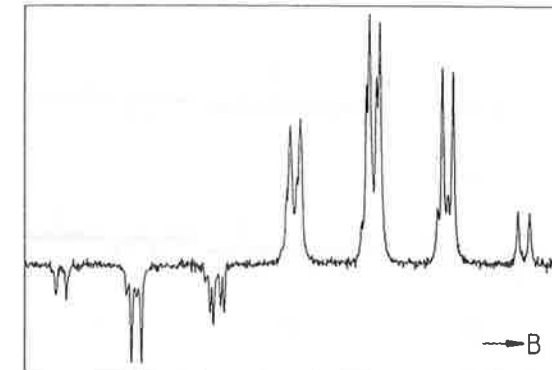


Fig.1. The field-stepped spectrum of propan-2-oyl radicals created as members of a symmetric radical pair by the flash photolysis of a 1:4 solution of propan-2-one in propan-2-ol, with observations between 2.0 and 3.0 μs after the photolysis flash. The spectrum shows the E/A intensity pattern expected for a RPM polarization process for radicals formed from a triplet precursor, together with an absorptive contribution which causes the absolute intensities of the low and high-field regions to be unequal, and yields a central line of non-zero intensity. Each line in this spectrum has been swept for 5 gauss about its centre, and consequently displays both the small hydroxyl splitting and the second-order effects, which would be difficult to discern in a conventional spectrum. The true separation of the lines can be appreciated by inspection of fig.2, where this presentation is not used.

triplet state. It has been postulated (25) that internal conversion leads to population of another triplet state (in which the sign of the zero-field coupling is opposite to that of the first) which is absorptively polarized, and it is the reaction of this state that gives rise to the radicals observed. This state has not been recognised, and no independent evidence seems to exist for it.

This may be put to direct experimental test by reacting excited state propan-2-one with a more efficient hydrogen donor than propan-2-ol to try to demonstrate radical formation in emission. In fig.2 are shown some results obtained by adding various amounts of tri-tert butyl phenol (TTBP) to the solution. This is an experiment that must be interpreted with caution, for TTBP is itself photo-active at the laser wavelength, reacting through an emissively-polarized triplet state. The nature of this reaction is not well known, but the spectrum observed in any solution containing TTBP is invariably that of the phenoxy radical; whilst propan-2-one is in large excess, we may assume that the dominant reaction is hydrogen abstraction from the phenol. In the spectra shown, all

obtained over the same time interval and at the same microwave field strength, the

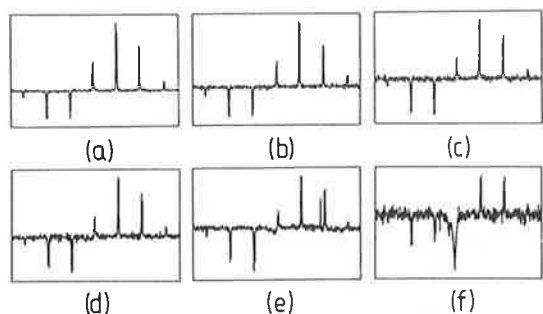
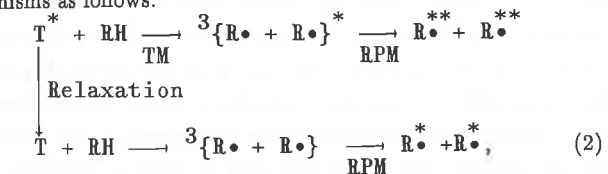


Fig.2. The effect of adding the efficient triplet scavenger TTBP to the system shown in fig.1, with an observation time of 1–2 μ s post flash, and with the following amounts added to 75ml of the solution: (a) 0, (b) 2gm. (c) 4gm. (d) 6gm (e) 8gm and (f) sufficient to saturate the solution. From the first, the emissive signal increases with added TTBP, but the behaviour is complicated by the photoactivity of TTBP itself (see text); the spectrum of the phenoxy radical is visible in traces (e) and (f). The field sweep was 140 gauss.

spectrum of the phenoxy radical is not evident until quite large amounts of TTBP have been added. Nevertheless, the relative magnitude of the emissive part of the spectrum increases continuously with TTBP concentration. The phenoxy radical itself has a g-value greater than that of the propan-2-olyl one, and a RPM calculation involving phenoxy and propanolyl radicals indicates that, from this source alone, the phenoxy radical should appear wholly in emission. This implies that the counter-radical should exhibit more absorption, than in the absence of TTBP, not more emission. It appears, therefore, that there is an emissive contribution to the spectra of both radicals, and this is presumably due to the TM. At low TTBP concentrations most of the light is absorbed by the propan-2-one, and the most probable origin of the TM contribution is from the reaction of triplet acetone, now in the phase expected from the direct low-temperature observation of the triplet itself. As the TTBP concentration is increased, the spectrum of the phenoxy becomes visible, in emission, yet the propan-2-olyl radical still exhibits net absorption; this is so even when, in the saturated solution, the central line of its spectrum can no longer be observed clearly. In consequence, although this reaction system is more complex than is ideal to demonstrate our point, it strongly suggests that triplet acetone does react to yield emissively-polarized radicals, and that the absorptive contribution to the spectrum is from another source.

This is confirmed in two further experiments based on a consideration of reaction

rates. We can summarise the total production of polarization in the radicals by both TM and RPM mechanisms as follows:



where the asterisk denotes spin polarization. In the radicals a single asterisk represents polarization via one mechanism only, and a double one denotes that both the TM and the RPM contribute (here we neglect a possible contribution to polarization in the radicals from reaction of equilibrated triplet; this is discussed below). It should be noted that whilst the quantum yield for radical formation is independent of which fraction of the overall reaction proceeds along the two routes to radical production, one involving polarized triplet and the other relaxed triplet, this is not the case where the contribution from the TM is concerned. In each radical pair formed the RPM polarization depends solely upon the nature of the radicals, here two propan-2-olyl ones, and is constant, and the magnitude of any TM contribution can be gauged by monitoring the size of the central peak relative to those of the RPM-dominated other peaks. According to eqn.(2), this should increase as the rate of the reaction is increased to compete with the relaxation process in the triplet. In fig.3 are shown the spectra observed when the propan-2-ol is diluted with an added inert



Fig.3. Tests which show that the relative magnitude of the central line in the spectrum is independent of the rate of triplet reaction, in contradiction to the expectation for TM polarization. The central five lines in the spectrum are shown (over a field sweep of 85 gauss) at times between 1–2 μ s post flash from solutions containing 50% (upper) and 75% (lower) of an inert hydrocarbon diluent, dodecane. The relative intensities of the central and other peaks are the same in each, and identical to those observed in the absence of any diluent.

solvent, dodecane, first by 50% and then by 75%. The TM contribution to the spectrum would be expected to change essentially linearly with the concentration of propan-2-ol, but inspection shows that the relative intensities of the peaks in the spectrum remain the same within experimental error, and are the same as in the undiluted system.

A further apparently obvious test of whether a triplet state of propan-2-one is the source of spin polarization in reactions involving its irradiation is to create the radicals via reaction of the precursor excited singlet state with an efficient scavenger. This experiment has been done using triethylamine in a simple mixture with propan-2-one alone (25), and has been repeated to give the spectrum shown in fig.4. It can be seen that the A/E pattern due to RPM polarization confirms reaction through the singlet state, but the extra absorptive contribution is still apparent. Even the ratio of the lines is similar in the two cases (although the initial radical pair is now of dissimilar radicals). It has been pointed out that this is not a definitive experiment, since reaction may occur through both singlet and triplet routes: the observation is compatible with the majority proceeding through the singlet pathway, but with possibly TM polarization from a small amount of triplet reaction contributing the extra absorptive intensity (25). Interestingly, if the experiment is performed in the correct concentration of added triethylamine, an apparently pure A/E



Fig.4. The central five lines in the spectrum produced on irradiating a 1.4M solution of propan-2-one in triethylamine, observed between 0.4–1.6 μ s post flash. The spectrum shows the A/E polarization pattern characteristic of radical production via the reaction of a singlet state, but the absorptive contribution to the signal remains, with even its relative magnitude unchanged from that shown in the preceding figures, within experimental error.

polarized spectrum is observed, with no central line. Since we know that the absorptive component is present in the neat solution, it appears that it is cancelled out here by a component in the opposite phase. This is not unexpected, for triethylamine reacts with both singlet and triplet states, and if not all the singlet is scavenged at a particular concentration, triplet propan-2-one is produced which then reacts quickly with triethylamine to yield a TM polarized contribution to the signal. As with TTBP, this appears to demonstrate that the true TM polarization in this system is emissive, not absorptive.

Several independent pieces of evidence suggest, therefore, that the single phase absorptive contribution to the spectrum of the propanolyl radical does not originate in the TM, and we seek other causes of it. An established phenomenon for producing single-phase polarized spectra with undistorted hyperfine intensities is that of secondary radical formation (31,32), under the condition that no significant coupling is correlated between the parent and daughter species (33,34). If the radical we observe is in fact a secondary one, this would depend upon producing a primary radical with excess absorptive polarization; in the absence of TM polarization this would have to be from a member of an asymmetric pair with RPM polarization. Irradiation of propan-2-one is known to produce methyl radicals in the gas phase by the reaction



with subsequent decarbonylation. The occurrence of a similar reaction in solution has been deduced from Chemically Induced Dynamic Nuclear polarization (CIDNP) studies, although it appears to be a minor route (34). Methyl radicals have been reported in one low temperature CIDEP study of propan-2-one photolysis in solution (25), but we have failed to detect them in our room temperature studies. Nevertheless, gas is evolved during photolysis (particularly of neat propan-2-one, with prevents tuning of our spectrometer), and it appears that methyl radicals are probably formed. Evidence that bond scission of this type can produce alkyl radicals in sufficient concentration to affect our observations is found in the irradiation of pentan-3-one (diethyl ketone), as shown in fig.5.

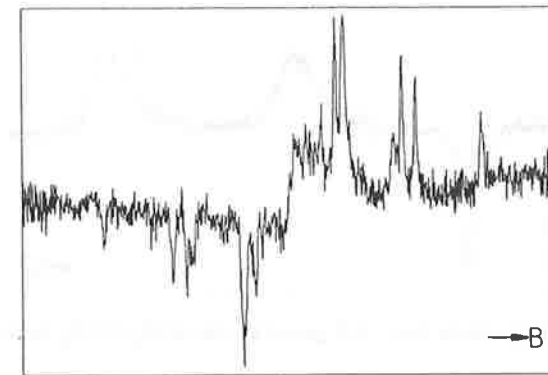
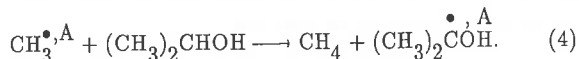


Fig.5. Photolysis of pentan-3-one in a variety of solvents yields the ketyl radical formed by hydrogen abstraction, together with the ethyl radical formed by direct bond scission. This spectrum was obtained, with observation between 0–1 μ s post flash, of a solution in a silicone, the radical derived from which exhibits a broad spectrum which allows the spectra of the ketone-derived radicals to be observed with less-confusing line overlap than occurs in other hydrogen-donating solvents. The field sweep was 180 gauss.

In this spectrum, the polarized spectrum of the ethyl radical can be observed along with that of the ketyl radical. It appears that the methyl radical from propan-2-one reacts too quickly to be observed in room temperature experiments. In other diketones containing aliphatic hydrocarbon groups, bond scission dominates over hydrogen abstraction (9,10) as a reaction route in photochemical studies. It is possible therefore that a source of polarized propan-2-oyl radicals is their formation as secondary species in the reaction of propan-2-ol with $\text{CH}_3\bullet$ radicals, the member of the initial pair with $\text{CH}_3\text{CO}\bullet$ which might be predominantly absorptively polarized when the radicals are formed by reaction of a triplet precursor:



This would produce absorptively polarized propan-2-oyl radicals, with undistorted hyperfine intensities, since reaction occurs with conservation of overall spin orientation, with no couplings correlated between the two radicals. Nevertheless, we believe that this is not the major source of the contribution in our case (since the absorptive contribution appears in the absence of propan-2-one itself, see below), although we are unable to remove this possibility completely.

Other radicals have been reported in solution in this system. Reaction (1) proceeds

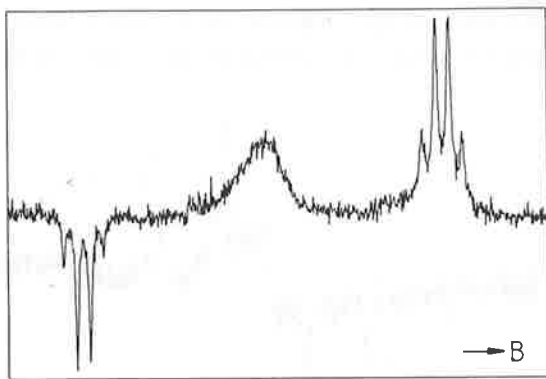
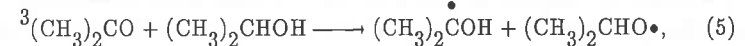


Fig. 6. The stepped spectrum (over 3×8 gauss) of the $\bullet\text{CH}_2\text{COCH}_3$ radical ($A_{\text{CH}_2} = 19.8$, $A_{\text{CH}_3} = 0.62$ gauss), produced by chlorine atom abstraction by the triplet, on irradiation of a 1:5 solution of 1-chloro propan-2-one in ethane-1,2-diol. This characteristic spectrum has not been detected in experiments with propan-2-one itself. An interesting feature of the spectrum, which we shall comment upon in the future, is that the central line fails to show the structure due to methyl coupling so evident in the others.

with a rate constant of $9.7 \times 10^5 \text{ M}^{-1}\text{s}^{-1}$ (36), and there is a rather slower one, with a rate constant of $5 \times 10^4 \text{ M}^{-1}\text{s}^{-1}$ which produces the $\bullet\text{CH}_2\text{COCH}_3$ radical by direct hydrogen abstraction from propan-2-one itself (37). We have not detected it in our experiments using propan-2-one, although it does appear in the photolysis of the monochloro compound (fig. 6.); its reaction and relaxation rates would be expected to allow its observation if it was present to a significant extent in the un-substituted system. In all of our experiments the concentration of the hydrogen donor has been maintained at a level at which this route should be suppressed. An interesting feature of the spectrum obtained from the monochloro system is that at early times it exhibits excess emission, with the central line in emission. This demonstrates unequivocally that the parent molecule reacts through its emissively polarized triplet state to produce the radical, as we have endeavoured to show for propan-2-one itself.

A second possibility is that the triplet molecule extracts the hydroxyl hydrogen from the propan-2-ol,



and a fast reaction, rate constant $2 \times 10^6 \text{ M}^{-1}\text{s}^{-1}$ (39), of the oxygen-centred species with the alcohol then generates another molecule of the ketyl radical. It is likely however that the expected fast relaxation rate of the electron on the oxygen atom would make this an inefficient route to polarization in the initial radical pair. Whether, if polarization was caused, any excess polarization in the oxygen-centred species would be absorptive depends upon the relative g-values of the radicals, and it may well be that emissive polarization would be the more likely.

The relative sizes of the absorptive and RPM contributions to the observed spectrum are unchanged on irradiation of aqueous solutions of propan-2-one in the pH range 5 to 8. Possible reaction routes involving radical ions appear to be insignificant. Furthermore, the behaviour is unaffected by isotopic substitution. It has been reported that photolysis of fully deuterated propan-2-one in fully deuterated propan-2-ol produces identical results (26,40), as do experiments we have performed with further isotopic variations of the molecules.

Only two products of the irradiation of propan-2-one in propan-2-ol have been identified in conventional photochemical studies (38), the combination and disproportionation products of two ketyl radicals; this again suggests that any other routes involving other radicals are negligibly important. We believe that we have eliminated any possible sources of polarization through complex chemistry. Nevertheless, this discussion has highlighted the importance of understanding the chemistry of the system in considerable detail before any firm conclusions on polarization mechanisms can be made.

The question might now be asked as to whether the absorptive contribution originates from spin-polarized or from relaxed radicals. An early study demonstrated

through the microwave power dependence of the spectrum that the line is indeed polarized (23); this is possible since the time decays of polarized lines differ from those of ones from equilibrated radicals, in a way that depends upon the microwave field strength (12), and the value of the polarization ratio obtained by curve-fitting was about $6-8P_{eq}$ (where P_{eq} is the polarization at thermal equilibrium). Later studies, performed at low temperature, still confirmed the presence of the absorptive contribution, despite complicating features from ST₋₁ RPM polarization processes (24,25); each also detected the esr signal from the spin-correlated radical pair itself. The absorptive polarization was said to be about eight times the Boltzmann one (P_{eq}), with the ST₀ RPM one four times this (24). In our room temperature experiments the two contributions to the polarization appear to have about equal polarization ratios. It seems apparent therefore that the absorptive, single-phase, contribution does originate in spin polarized radicals, despite the TM not being the source of the polarization.

Two other mechanisms are known via which a single-phase contribution could arise, through the spin-rotation interaction (41,42), and via triplet-doublet pair polarization (43). Both are attractive in being hyperfine-independent, but the former has been shown on theoretical grounds to be likely to be insignificant due to the rotational correlation times of the radicals (42). Furthermore we have observed that the absorptive contributions to the spin polarized esr spectra of hydroxymethyl and propan-2-oyl radicals, produced by hydrogen abstraction from the parent alcohols by excited state propan-2-one under similar experimental conditions, are the same relative to the RPM contributions in the systems within experimental error. Spin-rotation is known to be a major source of relaxation in the former (44), and would be expected to be less important in the latter (unless spin-internal rotation interactions are coincidentally of comparable importance), with similar implications for polarization production. The latter mechanism appears untenable too. In the first place, the polarization magnitude is expected to increase with increasing viscosity relative to the normal RPM contribution, but the converse is observed (24,25). Secondly, this mechanism can produce only emissive polarization (43). Finally, the only two sources of triplet in our experiments are propan-2-one itself, and dissolved molecular oxygen. We find the appearance of the spectrum is the same if the propan-2-oyl radical is produced by an alternative route in the absence of triplet propan-2-one (see below), and it is also unchanged by oxygen saturation of the solution.

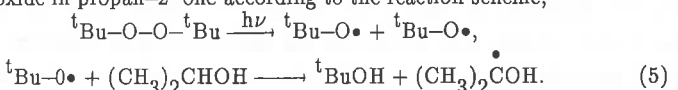
We now turn to the evidence from Fourier transform observations in which Levstein and van Willigen (26) have demonstrated a quite different behaviour in the deuterated propan-2-oyl system from those in which the TM is known to occur. In particular, the relative intensities of the various hyperfine lines show no appreciable variation during the first few hundred nanoseconds of the observation, as would be expected if the relative contributions of the TM and the RPM varied as the polarization developed, and the lines

exhibited no difference in the kinetics of signal growth. The results were analysed on the assumption that the absorptive contribution arose in the formation of radicals by reaction of spin-equilibrated triplet propan-2-one, which can produce a polarization of $1.3P_{eq}$ in the doublets; this is in agreement with a previous conclusion of Paul's (17). More precisely, it was realised that there was a hyperfine-independent absorptive polarization whose magnitude needed to be known to extract the kinetic constants in the solution, and the above value was taken. We have three difficulties in accepting reaction of equilibrated triplet as the sole source of the absorptive signal in the radicals. In the first place, so low a polarization ratio seems incompatible with our results, which consistently give values in the 6-8 range, admittedly with large errors. Secondly, the spin-lattice relaxation time of the deuterated radical, obtained using this assumption, is unusually large ($9\mu s$) for a small radical in a low-viscosity room-temperature solution, and larger than that found for the protonated species from spin-echo measurements ($3.5\mu s$ (45)). A suggestion that this is due to the reduced hyperfine couplings in the former implies that the relaxation in this radical should be hyperfine-dependent; no evidence exists for this and it is unlikely that these two radicals would have widely-different relaxation times. Fitting of the experimental curves using the known value of T_1 for the protonated species, rather than an assumed value for the polarization ratio, would imply a higher value of the polarization ratio, more consistent with our results, but would lose the apparent understanding of the polarization origin. Thirdly, we shall show below that the absorptive signal is present even when the propan-2-oyl radicals are formed from routes which do not involve reaction of triplet propan-2-one. The Fourier results are not in doubt and they do constitute the most direct evidence that the TM is not the source of the absorptive contribution to the spectrum, besides confirming that the signal does arise in spin-polarized, rather than relaxed, radicals.

3.2. Propan-2-oyl radicals and radical pairs.

In the first section we have largely eliminated the possibility that the origin of the absorptive component in the spectrum of the propan-2-oyl radical lies in the photochemistry or photophysics of the propan-2-one molecule. We now consider the possibility that it reflects an inherent property of the propan-2-oyl radical itself, or of a radical pair containing one or two of them. This is simply tested experimentally by making the radical from an alternative source.

In fig. 7 is shown the spectrum of propan-2-oyl created by photolysis of a solution of di-tert butyl peroxide in propan-2-one according to the reaction scheme,



We have CIDEP evidence that the peroxide dissociates through the excited singlet state (46). No report has ever been made of a direct observation of the butoxyl radical itself, and there is little evidence for it generating significant RPM polarization in the primary radical pair (34). Any possible polarization would be expected to be minimal for two reasons. Firstly, coupling to the γ protons will be small, and secondly spin de-phasing is expected to be fast for an oxygen-centred radical. Finally, pure ST₀ RPM polarization in a pair of identical radicals produces no net effect which might be transmitted to a secondary radical. It appears, therefore that the reaction shown in eqn.(5) cannot produce a net polarization in the secondary radical. Nevertheless, the spectrum in fig.7 is identical to those in which the radical is produced from the triplet reaction, and the possible intermediacy of CH₃[•] and CH₃CO[•] radicals, for example, in polarization development, discussed above, is irrelevant. It is apparent that in this system the observed effect arises in the encounters of identical propan-2-oyl radical pairs (here F-pairs) and that the absorptive contribution, besides the RPM one, originates either in these or in the isolated radical itself. It shows that whether or not the assignment, discussed above, of some of the absorptive signal to radicals formed by reaction of relaxed triplet is correct, another process contributes to it. This implies either the operation of an unidentified polarization mechanism or of population redistribution following a known one by spin relaxation.

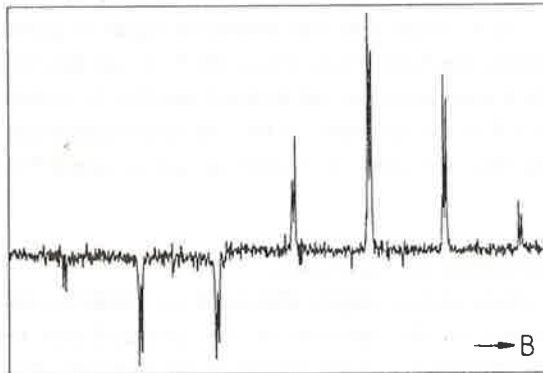


Fig.7. A spectrum of the propan-2-oyl radical produced by irradiating a 1:1 mixture of tert-butyl peroxide and propan-2-ol, with observation from 1.5–2.5 μ s post flash and a field sweep of 140 gauss. This spectrum, from a radical formed by hydrogen abstraction, and with no propan-2-one present, exhibits a similar absorptive contribution to that shown, for example, in fig.1. The polarization results from an identical pair of propan-2-oyl radicals. This shows that the absorptive signal originates from the radicals or radical pairs themselves, since no TM polarization can occur in this system.

4.Discussion.

Much of what follows now is speculative, and we are able only to describe, and criticize, possible explanations rather than reaching a firm conclusion. We shall assume, for the moment, that the generation of polarization and spin relaxation occur on different timescales, and consider the effect of relaxation on initially spin-polarized systems.

Since hyperfine-dependent polarization is apparent in the spectra, and it is also known that the absorptive contribution itself comes from polarized radicals, any relaxation mechanism must needs be hyperfine-independent and relatively inefficient so as to leave still polarized radicals at the observation times. In this way it diminishes the electron spin disequilibrium in the system without affecting the relative populations of the levels set up in the polarization processes. The electron-nuclear cross relaxation invoked recently to rationalise the phase inversions of some CIDEP spectra with time after radical creation cannot do this, and its effects anyway typically appear on the tens to hundreds of microseconds timescale of nuclear relaxation processes in solution (47–49). A suitable, and at first sight attractive candidate, is spin-internal rotation relaxation, which causes relaxational transitions without nuclear spin inversions, and indeed connects all electron levels of the same overall nuclear spin with identical rate constants. Any relaxation of an initial polarization set up in a RPM process would therefore vary the relative populations of the levels at rates which depended simply on the degeneracies of the states, and would give rise to an undistorted, absorptive, contribution to the spectrum, provided that the process happened faster than the overall electron spin relaxation in the system. That is, the relative state populations would reflect hyperfine-independent relaxation besides the initial RPM effects, and the spectrum would be an RPM one distorted by an absorptive contribution, as observed; electron relaxation could not however be complete since the latter is observed to be polarized.

This origin of the absorptive component is attractive in other ways. Firstly, in the spectrum from a symmetric pair of radicals with pure ST₀ RPM polarization, any exactly central line has zero intensity since it corresponds to connection of two equally populated levels. Relaxation between these levels immediately overpopulates the lower and gives rise to a characteristic central line in absorption. It was seen above that reaction of both singlet and triplet propan-2-one with propan-2-ol yielded spectra which showed this feature, and this is exactly what is expected: spin relaxation in an infinite room temperature bath produces the same end result whatever the starting condition. This conclusion holds for any hyperfine-independent relaxation process.

Spin-internal rotation relaxation cannot occur if there is no possibility of such rotation. An obvious test would seem to be to inspect the CIDEP spectra of cyclic aliphatic ketyl radicals created in symmetric radical pairs by irradiation of the parent ketone in solution in the corresponding secondary alcohol. We have published the spectra of

cyclohexyl and cycloheptanoyl, and of 4-tert-butyl cyclohexyl, radicals (50). At room temperature these encompass the whole range of rates of ring flipping from none, in the latter radical, to free flipping in the second and intermediate flipping in the first. None exhibit the absorptive component to the spectrum evident in the ketyl radicals from straight-chain ketones, and this appears consistent with spin-rotation relaxation in the latter. Nevertheless, this cannot be the source of the absorptive component to the spectrum of these species. The problem is that spin-internal rotation relaxation is a property of the isolated radical and it proceeds monotonically in time in an exponential manner. Our spectra exhibit a substantial absorptive signal from the earliest times that we observe them (roughly 30–500 nsec. post the photolysis flash) and thereafter the signals decay on the microsecond timescale. A single relaxation mechanism cannot change its rate in a discontinuous manner in normal isotropic solution.

This latter conclusion is important, for any relaxation mechanism capable of producing a substantial absorptive signal when the radicals are first observed, whilst relaxation is slow thereafter, must operate during the period of the generation of the polarization itself (or within nanoseconds of it) and be turned off subsequently. It is attractive therefore to speculate on hyperfine-independent mechanisms which involve the radical pair itself, that is on intermolecular electron-electron relaxation. There are two possible sources of this, the modulation of either the electron exchange interaction or the electron-electron dipolar interaction as the radicals diffuse apart. In experiments conducted at low temperature, a splitting of resonance lines due to the former has been reported in propan-2-olyl radicals (24,25), and a non-zero value of the interaction at room temperature has been deduced from the analysis of the magnitude of nuclear spin (CIDNP) observed in the products of their reaction (51). This has been confirmed in the recent Fourier Transform esr observations (26). This is significant, for the usual concept of polarization development in the RPM process is that the exchange interaction, although essential to the production of polarization in radical encounters, is expected to be zero for most of the pair lifetime. As Shushin (52) has pointed out, a non-zero observed value is consistent with the existence of a weak potential which holds the radicals together for a period in solution. In the case of propan-2-ol solutions its origins are probably hydrogen bonding. There is consequently direct experimental evidence that the polarized members of the radical pair remain comparatively close together for some period, and fluctuations in either of the two possible electron-electron interactions might cause very rapid spin relaxation, they being potentially both comparatively strong interactions; comparable relaxation processes in molecular triplet states are known, for example, to occur on the nanosecond timescale in solution. The longer-range nature of the dipolar interaction makes it perhaps the stronger candidate of the two. Both interactions are well known sources of spin relaxation in concentrated solutions of stable free radicals, and we might look upon the region of space including the radical pair simply as a particularly concentrated volume.

We now return to the assumption that polarization and relaxation occur on different timescales, using our concept that after the first has occurred there exists a very fast relaxation process which is switched off when the members of the pair separate. Once the radicals are separated, the slower relaxation associated with isolated radicals occurs. If this is a correct picture, relaxation can only proceed when some polarization has been generated, and we might expect that the absorptive component would become progressively more significant as time elapsed, reaching an asymptotic value as the pair separated. We have consequently investigated the appearance of the spectrum using the greatest time-resolution of our apparatus consistent with an adequate signal-to-noise ratio. That

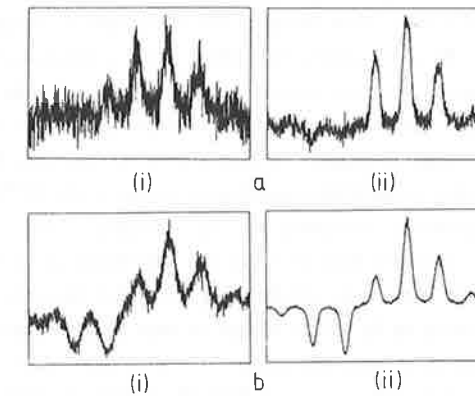


Fig.8. Stepped spectra obtained from photolysis of solutions of (a) tert-butyl peroxide in propan-2-ol, and (b) propan-2-one in propan-2-ol at (i) 0.0–0.2 μ s and (ii) 0.2–0.4 μ s post flash. In (a), the signal shows a more predominant absorptive contribution at the earliest time than it does later, in contradiction to the expectations of the simple relaxation theory outlined in the text; this is not the case in (b). The poor signal-to-noise ratio, and the line broadening as compared with later-time spectra, result from the production of radicals within the magnetic field of the spectrometer itself, and the comparatively slow tipping of the magnetisation vector into the measurement plane. It is an artifact of the continuous wave method but it does not affect the phase or the relative intensities of the signals (1,2).

from the peroxide/propan-2-ol mixture is shown in fig.8(a). At early times after radical creation in a continuous wave experiment, the lines are broadened, but it is immediately apparent that at this early time (0.0–0.2 μ s) the spectrum is entirely in absorption, with some E/A distortion. It is our experience that we are unable to detect relaxed radicals on this timescale, needing the extra signal-to-noise ratio available as a result of polarization; we believe, therefore, that this absorptive contribution does arise from a polarized species. The relative contributions of the single-phase and two-phase contributions are the reverse of what is seen at later times. This is contrary to what was expected, and the later time

spectrum implies that much of the RPM polarization observed arises at quite late times in the radical pairs' existence. That is, on this model, some of the polarization initially produced is largely removed by relaxation when the radicals are very close together, but further polarization occurs at inter-radical distances where the relaxation internal to the pair is insignificant. Since a non-zero exchange interaction is essential to the creation of RPM polarization, this explanation requires rather stringent conditions, and differentiation between the relaxation and later polarization regions, and may be un-tenable. However, it may be that this problem is artificial and arises through the simple model taken, for clearly both polarization and relaxation have both to occur within a few nanoseconds of radical pair creation if our idea is correct. Now, however, the short-time experiments seem to offer a different interpretation, for it is possible that there exists a second pairwise mechanism for creating spin polarization which occurs on a much faster timescale than the normal RPM one and, presumably, can occur when the exchange interaction is larger than the hyperfine couplings. The original suggestion that relaxation via two different processes acting on different timescales redistributes populations set up in the RPM process does not seem tenable. The spectrum obtained at a similarly early time from the propan-2-one/propan-2-ol system does not show the same variation of the magnitudes of the two contributions with time, but exhibits (fig.8(b)), for example, a similar excess absorption as is demonstrated in fig.1. The reason for this difference appears to lie in the RPM polarization arising in F-pair encounters in the former case, but in both the absorptively-polarized contribution is apparent from the earliest observation times.

There is however another more powerful reason for rejecting such a relaxation mechanism inside the radical pair, which can be appreciated by considering the central line of the spectrum. We have argued above that rapid relaxation between two equally populated states can yield an absorption signal and that this may be still polarized when it is observed since relaxation is incomplete at the time the pair separates. If this is the case the observed signal should relax towards the Boltzmann equilibrium one by increasing in size as time elapses. This is the converse of what is observed, the behaviour corresponding to the normal polarization condition in which the lower electronic state is overpopulated, rather than underpopulated. The weight of evidence is consequently against a relaxation origin of the polarized absorptive component.

We have provided a full discussion of the possible effects of relaxation in re-distributing state populations because, only by rejecting it have we been led to the possibility that the origin of the absorptive signal might be an unidentified polarization mechanism. In this paper we have eliminated the TM, spin-rotation, doublet-triplet polarization and secondary radical formation as its source. Our experiments indicate that it appears to arise in radical pairs, to be independent of the normal RPM process, and be capable of producing absorptive polarization independently of the spin multiplicity of the radical precursor. Since the absorptive signal is observed in systems of identical radicals, it

cannot arise in an electron-electron Overhauser process. It also appears that it does not operate in all radical pairs under all conditions, for many examples are known of systems which exhibit pure ST_0 RPM behaviour, including even propan-2-oyl radicals created in comparatively viscous ethane-1,2-diol solutions. This is significant, for one possible origin of a fully-absorptive polarization in this system would be the ST_{+1} form of radical pair mechanism (23), which would increase in magnitude with increasing viscosity. Furthermore the absorptive signal would have a hyperfine-dependent polarization, and the ST_0 polarization would be that corresponding to a positive value of the exchange interaction, both also in contradiction with the observations.

We have no satisfactory explanation of all the facts that we have assembled here, and can produce no convincing suggestions as to the nature of the missing polarization mechanism, if it indeed exists.

5. Conclusion.

The conclusions from this work are of some significance to polarization studies and their interpretation to yield molecular data. Since the absorptive contribution to the spectrum of the propan-2-oyl radical, produced by photolysis of propan-2-one, does not arise in the triplet mechanism of CIDEP, major doubts must exist that the use of the phase of this signal to deduce the signs of zero-field coupling constants in other aliphatic ketones (9,10) is soundly based. It also implies that experiments performed on aliphatic ketones to test Adrian's suggestion of using polarized light to diagnose TM activity have been performed on radicals where no TM polarization was present, and are therefore invalid to the test of the method; conclusions from observations on other radicals are unaffected. As was always apparent from the theory (7,8), TM polarization is not inevitable when radicals are produced from triplet precursors. Nevertheless, there remain cases in which the TM does occur, for example in the photolysis of solutions of nitrogen heterocyclics (4,53) and in radical anions (5,6). However the apparent simple test for the TM, that both radicals should have polarizations of the same phase and magnitude (37), cannot be used when the signal is absorptive.

The absence of a useful definitive test for the TM, and the difficulty in making absolute polarization magnitude measurements, has undoubtedly led to the misinterpretation of some published CIDEP spectra. Since only two polarization origins were recognised, and these appeared to rationalise all the observations in the semi-empirical way that the spectra could be reproduced by adding a single-phase undistorted signal to a RPM one, it was assumed that TM polarization was always its source. An article we wrote in 1978 (54) was prophetic in saying "that the TM and RPM theories are accepted as rationalising all the known phenomena of CIDEP owes more to Occam's razor than to hard fact". Since that time secondary polarization, polarization

through cross-relaxation and doublet-triplet polarization, all referred to above, have been demonstrated experimentally to occur, and the puzzle of the polarization in our apparently simple system remains. Its origin appears to lie in radical pairs, and it does not depend on how the radicals are created, but rather on the nature and environment of the radicals involved.

The work reported here emphasises that the photochemistry of even so simple a molecule as propan-2-one is potentially rather complex, and can involve many different radicals. The understanding of polarization behaviour requires this chemistry to be understood, and CIDEP observations are more sensitive to this chemistry than are studies on steady state concentrations of radicals or of conventional kinetic or product analysis studies. It is hoped that this paper will stimulate further theoretical and experimental work.

Acknowledgments.

Prof. van Willigen was very kind in providing a preprint of his elegant work. We are grateful to the S.E.R.C for maintenance awards to N.J.K.S and to P.D.S.

References.

1. McLauchlan.K.A. in "Advanced EPR. Applications in Biology and Biochemistry" ed. Hoff.A.J., Elsevier, Amsterdam. 1989, 345.
2. McLauchlan.K.A. in "Modern Pulsed and Continuous Wave Electron Spin Resonance" ed. Kevan.L. and Bowman.M.K., Wiley Interscience, New York. 1990, 285.
3. McLauchlan.K.A., Sealy.R.C. and Wittmann.J.M., 1977, J.Chem.Soc.Faraday Trans.II., **73**, 926.
4. Basu.S, McLauchlan.K.A. and Sealy.G.R., 1982, Chem.Phys.Letts., **88**, 84.
5. Prisner.T., Dobbert.O., Dinse.K.P. and van Willigen.H., 1989, J.Amer.Chem.Soc., **110**, 1622.
6. Plüschau.M., Zahl.A., Dinse.K.P. and van Willigen.H., 1989, J.Chem.Phys., **90**, 3153.
7. Atkins.P.W. and Evans.G.T., 1974, Molec.Phys., **27**, 1637.
8. Pedersen.J.B. and Freed.J.H., 1975, J.Chem.Phys., **67**, 1706.
9. Grant.A.I. and McLauchlan.K.A., 1983, Chem.Phys.Letts., **108**, 120.
10. Yamauchi.S. and Hirota.N., 1984, J.Phys.Chem., **88**, 4631.
11. Adrian.F.J., 1974, J.Chem.Phys., **61**, 4875.
12. McLauchlan.K.A. and Stevens.D.G., 1987, Molec.Phys., **60**, 1159.
13. Dobbs. A.J. and McLauchlan.K.A., 1975, Chem.Phys.Letts., **39**, 257.
14. Adeleke.B.B., Choo.K.Y. and Wan.J.K.S., 1975, J.Chem.Phys., **62**, 3822.
15. Yamauchi.S., Tominaga.K., and Hirota.N., 1986, J.Phys.Chem., **90**, 2367.
16. Paul.H., 1976, Chem.Phys., **15**, 115.
17. Paul.H., 1979, Chem.Phys., **40**, 265.
18. Atkins.P.W., Dobbs.A.J. and McLauchlan.K.A., 1975, J.Chem.Soc.Faraday Trans.II., **71**, 1269.
19. Aycsough.P.B., Lambert.G. and Elliot. A.J., 1976, J.Chem.Soc.Faraday Trans.I, **72**, 1770.
20. Choo.K.Y. and Wan.J.K.S., 1975, J.Amer.Chem.Soc., **97**, 7127.
21. Carmichael.I. and Paul.H., 1979, Chem.Phys.Letts., **67**, 519.
22. Wong.S.K., Chiu.T-M. and Bolton. J.R., 1981, J.Phys.Chem., **85**, 12.
23. Basu.S., Grant.A.I. and McLauchlan.K.A., 1983, Chem.Phys.Letts., **94**, 517.
24. Buckley.C.D., Hore.P.J., Hunter.D.A. and McLauchlan.K.A., 1987, Chem.Phys.Letts., **135**, 307.
25. Tominaga.K., Yamauchi.S. and Hirota.N., 1988, J.Chem.Phys., **86**, 553.
26. Levstein.P.R. and van Willigen.H, 1991, J.Phys.Chem., *in the press*.
27. Basu.S., McLauchlan.K.A. and Sealy.G.R., 1983, J.Phys.E., **16**, 767.
28. Basu.S., McLauchlan.K.A. and Sealy.G.R., 1984, Molec.Phys., **52**, 531.
29. McLauchlan.K.A. and Stevens. D.G., 1986, Molec.Phys., **57**, 223.
30. Yamauchi.S., Tominaga.K. and Hirota.N, 1985, Abstracts of the 5th Nodzu Memorial Lectures, 24.
31. McLauchlan.K.A. in "Chemically Induced Magnetic Polarization" ed. Muus.L.T., Atkins.P.W., McLauchlan.K.A. and Pedersen. J.B., Reidel.D., Dordrecht, 1977, 151.
32. Pedersen.J.B., 1979, FEBS Letts., **97**, 305.
33. McLauchlan.K.A. and Simpson.N.J.K., 1989, Chem.Phys.Letts., **154**, 550.
34. McLauchlan.K.A. and Simpson.N.J.K., 1990, J.Chem.Soc.Perkin Trans.II, 1371.
35. Münger.K. and Fischer.H., 1984, Int.J.Chem.Kinet., **16**, 1213.
36. Henne.A. and Fischer.H., 1977, J.Amer.Chem.Soc., **99**, 300.
37. Leuschner.R. and Fischer.H., 1985, Chem.Phys.Letts., **121**, 554.
38. Paul.H., Small.R.D. and Sciano.J.C., 1978, J.Amer.Chem.Soc., **100**, 4520.
39. Blank.B., Henne.A., Laroff.G.P. and Fischer.H., 1975, Pure and Appl.Chem., **41**, 475.
40. Tominaga.K., Yamauchi.S. and Hirota.N., 1988, Chem.Phys.Letts., **149**, 32.
41. Atkins.P.W. and McLauchlan.K.A. in "Chemically Induced Magnetic Polarization" ed. Lepley.A.R. and Closs.G.L., John Wiley and Sons, New York, 1973, 41.
42. Adrian.F.J. 1971, Chem.Phys.Letts., **10**, 70.
43. Blättler.C., Jent.F. and Paul.H., 1990, Chem.Phys.Letts., **166**, 375.
44. Kivelson.D in "Electron Spin Relaxation in Liquids" ed. Muus.L.T. and Atkins.P.W., Plenum Press, New York, 1972.
45. Bartells.D.M., Lawler.R.G. and Trifunac.A.D., 1985, J.Chem.Phys., **83**, 2686.
46. McLauchlan.K.A. and Simpson.N.J.K. *to be published*.
47. Valyaev.V.I., Molin.Yu.N., Sagdeev.R.Z., Hore.P.J., McLauchlan.K.A. and Simpson.N.J.K., 1988, Molec.Phys., **6**, 891.

48. Jent.F. and Paul.H., 1989, Chem.Phys.Letts., 158, 632.
49. Murkovskaya.A., Tsentalovich.Yu.P. and Sagdeev.R.Z., 1990, Chem.Phys.Letts., 171, 406.
50. McLauchlan.K.A. and Stevens.D.G., 1987, J.Chem.Phys., 87, 4399.
51. Itoh.S-Y., Terazima.M. and Azumi.T., 1990, Chem.Phys.Letts., 170, 565.
52. Shushin.A.I., 1990, Chem.Phys.Letts., 170, 78.
53. Buckley.C.D. and McLauchlan.K.A., 1985, Molec.Phys., 54, 1.
54. Hore.P.J., Joslin C.G. and McLauchlan.K.A., 1978, Chem.Soc.Spec.Period.Rept., Electron Spin Resonance, 5, 1.

CIDEP in the Photolysis of Benzoic Acid Derivatives

A. S. Jeevarajan and R. W. Fessenden

Radiation Laboratory and Department of Chemistry and Biochemistry
University of Notre Dame, Notre Dame, IN 46556, USA

Abstract

ESR spectra of basic aqueous solutions of a wide variety of benzoic acid derivatives taken during steady-state photolysis show that two types of radicals are formed in the presence of a hydrogen donor: anion radicals and cyclohexadienyl radicals. A typical system is 1,4-benzenedicarboxylic acid (terephthalic acid) and 2-propanol. The anion radical is well known; the cyclohexadienyl radical is that formed by net hydrogen atom addition at the position opposite one carboxyl group. Addition of acetone as sensitizer increases the yield substantially. The spectrum of this radical is notable in that the low-field half of the spectrum is in emission as a result of CIDEP. A number of time-resolved ESR and optical absorption experiments were done to identify the reaction mechanism and to try to understand the origin of the CIDEP. A triplet state of the acid has been identified as the reactive species. The largest yield of cyclohexadienyl radicals is produced with an alcohol as the hydrogen donor. This reaction is promoted by high base concentrations. CIDEP for this radical is by the normal F-pair mechanism and is large because of the long relaxation time. An initial ESR emission is observed for the anion radical in neutral solution, but this changes to an absorption in basic solution. The origin of this polarization is not yet clear.

1. Introduction

Steady-state photolysis ESR experiments using continuous illumination were carried out on solutions of 1,4-benzenedicarboxylic acid (terephthalic acid) containing 2-propanol as a hydrogen donor. Two radicals were identified in the spectrum: the anion radical (the single electron reduction product, a tri-anion at high pH) and a cyclohexadienyl radical (CHD) formed by net addition of hydrogen to a carbon bearing a carboxyl group.

The spectrum of the latter radical is notable in that the low-field half of the spectrum is in emission as a result of CIDEP. Part of the reason for the large polarization is the long relaxation time for the radical ~10 μ s as measured in experiments making use of the out-of-phase signal at the field modulation frequency [1]. However, the radicals involved all bear multiple negative charges so it is surprising that the reaction rate is fast enough to produce such a polarization. The purpose of the work reported here is to better understand the mechanism of reaction and the origins of the polarization.

Formation of cyclohexadienyl radicals has been observed by Sakaguchi et al. from xanthone [2,3] and by Hayashi et al. for acetophenone and 2-acetonaphthone [4] and is favored by hydrogen bonding solvents. The present work is also reminiscent of work on the photolysis of maleimide [5] and maleic anhydride [6] in which addition of hydrogen or a solvent radical produced a cyclic alkyl radical which showed emission from the low-field lines.

2. Experimental Section

The continuous photolysis experiments were carried out with the light source and ESR spectrometer described by Davis and Fessenden [7]. The laser experiments used a direct-detection ESR which is an update of the unit described by Fessenden et al. [8]. A Lumonics HyperEX-400 laser using XeCl was used for excitation at 308 nm. Laser pulse energies were in the range 20 mJ to 150 mJ. The AFC circuits of the ESR were pulsed at 100 Hz and the laser at 25 Hz. One radiolysis experiment was done with the same ESR and irradiation with 2.8 MeV electrons. A flat ESR cell of 0.4 mm spacing was used in a flow system with solution flow rates of about 10 cm³/min. Nanosecond optical absorption experiments used apparatus like that described by Nagarajan and Fessenden [9] with excitation either at 308 nm or 265 nm (from the fourth harmonic of a Nd-YAG laser).

The terephthalic acid or sodium terephthalate was obtained from Aldrich Chemical Co. as was sodium borohydride. The Methanol, ethanol, 2-propanol and acetone were from Fisher Scientific Company. Tetrahydrofuran without inhibitor was obtained from Aldrich. The pH of the solutions was adjusted by addition

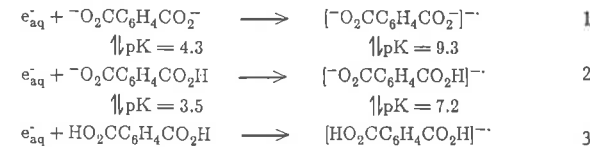
of sulfuric acid, KOH, sodium tetraborate, and sodium phosphates. Solutions were prepared in water which had been purified by a Millipore Milli-Q purification system. All solutions were deoxygenated by bubbling with nitrogen.

3. Results and Discussion

A typical ESR spectrum obtained with terephthalate in continuous photolysis experiments is shown in Fig. 1. The solutions used contained 10 mM of the acid and 1.3 M 2-propanol. The group of five lines in the center is from the anion radical (monoanion at pH 6.7, trianion at pH 13, see below). The two widely spaced 9-line groups (triplet of triplets) are from the CHD formed by net addition of a hydrogen atom at the 1-position. The hyperfine constants of this type of radical are so characteristic [10] that there is no doubt about the identification of the species and isomer. At pH 6.7 the lines of the two species are of comparable intensity and the lines of the CHD show moderate CIDEP with the lines in the high-field group several times more intense than those in the low-field group. At pH 13, the lines of the anion radical are much more intense and the low-field lines of the CHD are now in emission.

A wide variety of compounds gave similar spectra in steady-state spectra as shown in Tables I to III. These include not only the aromatic acids but also some corresponding esters, an imide and an anhydride as studied in 2-propanol rather than in water, and the tricyano compound. Clearly the formation of the CHD is a common reaction.

The equilibria for acid dissociation of terephthalic acid and for the reduction product are given in equations 1-3.



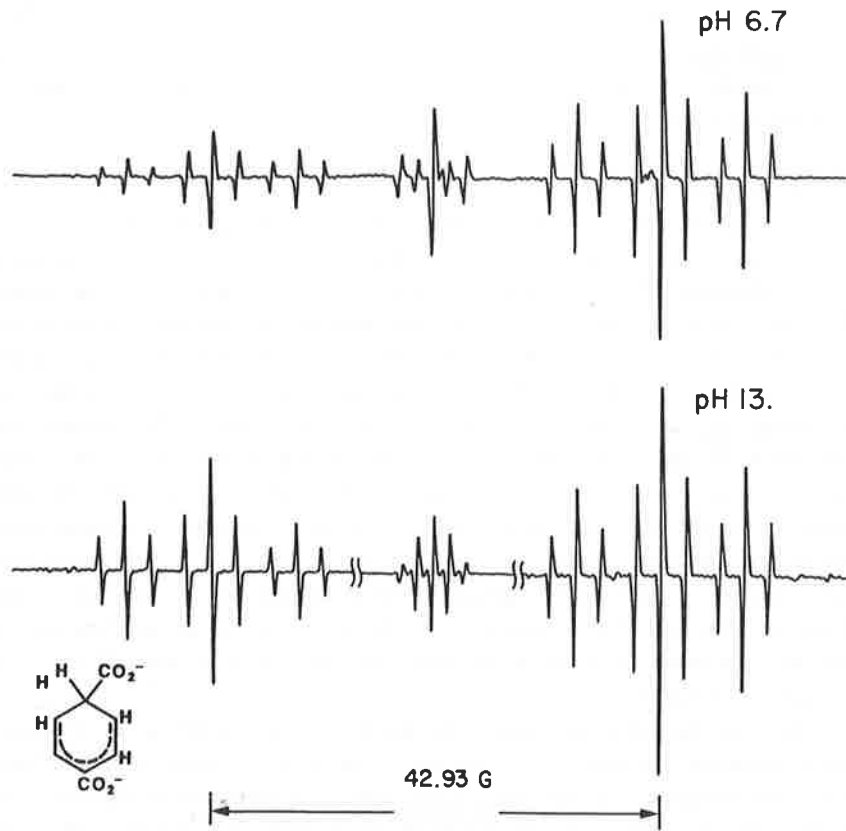


Figure 1. ESR spectra taken during continuous photolysis of aqueous solutions of 10 mM terephthalate containing 1.3 M 2-propanol. The two outer line groups are from the cyclohexadienyl radical which is shown. Note that the low field lines in the pH 13 experiment are in *emission* rather than absorption. The lines in the center are from the anion radical. The gain in the center of the lower spectrum is lower by a factor of 10.

TABLE I : ESR PARAMETERS OF CYCLOHEXADIENYL RADICALS
DERIVED FROM BENZENE CARBOXYLIC ACIDS

Compound	T _{eff*}	I.D. No.	Radical	Hyperfine Constant (Gauss)						<i>g</i> factor
				<i>a</i> ₅ ^H	<i>a</i> ₁ ^H	<i>a</i> ₂ ^H	<i>a</i> ₃ ^H	<i>a</i> ₄ ^H	<i>a</i> ₅ ^H	
<chem>O=C1=CC(=O)C=C1</chem>	6	I	<chem>O=C1=CC(=O)C=C1</chem>	44.51	8.06	2.35--		2.35	8.06	2.00316
<chem>O=C1=CC(=O)C=C1</chem>	6	II	<chem>O=C1=CC(=O)C=C1</chem>	44.98	8.94	2.69	13.02	2.69	8.94	2.00288
<chem>O=C1=CC(=O)C=C1</chem>	6	III	<chem>O=C1=CC(=O)C=C1</chem>	42.93	8.16	2.39--		2.39	8.16	2.00316
<chem>O=C1=CC(=O)C=C1</chem>	6	IV	<chem>O=C1=CC(=O)C=C1</chem>							7.63 2.00296
<chem>O=C1=CC(=O)C=C1</chem>	5	V	<chem>O=C1=CC(=O)C=C1</chem>							2.43-- 2.00330

TABLE II : ESR PARAMETERS OF CYCLOHEXADIENYL RADICALS
DERIVED FROM BENZENE CARBOXYLIC ESTER AND TRICYANO BENZENE

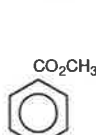
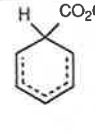
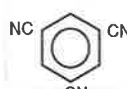
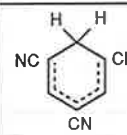
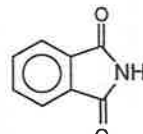
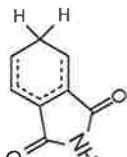
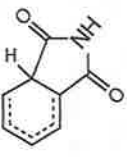
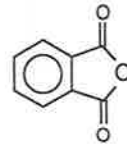
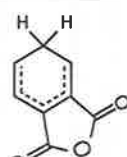
Compound	$T_{\pi\pi^*}$	I.D. No.	Radical	Hyperfine Constant (Gauss)						g factor
				a_6^H	a_1^H	a_2^H	a_3^H	a_4^H	a_5^H	
	S	VI		43.83	7.95	2.28	0.85 (CH ₃)	2.28	7.95	2.00341
	S	VII		47.54	9.17	2.79	13.25	2.79	9.17	2.00276
	S	VIII		41.20	0.96 (CN)	2.61	1.62 (CN)	2.61	0.96 (CN)	2.00302

TABLE III : ESR PARAMETERS OF CYCLOHEXADIENYL RADICALS
DERIVED FROM BENZENE CARBOXYLIC IMIDE AND ANHYDRIDE

Compound	$T_{\pi\pi^*}$	I.D. No.	Radical	Hyperfine Constant (Gauss)						g factor
				a_6^H	a_1^H	a_2^H	a_3^H	a_4^H	a_5^H	
	A	IX		41.33	6.78	0.22 (NH)	0.82 (NH)	2.23	8.76	2.00325
	A	X		54.47	0.35 (NH)	4.11	11.75	2.39	7.64	2.00301
	A	XI		43.30	7.63	---	---	1.98	8.13	2.00305

All experiments were performed above pH 6.7 so the starting material in all cases is the terephthalate dianion. The reaction mechanism for terephthalate involves reaction of the triplet state of the acid anion as shown by optical laser photolysis studies on terephthalate [11]. The terephthalate ion absorbs strongly at 265 nm so it can be studied at low concentration (1 mM) or can be excited by 308 nm at higher concentrations like 40 mM. Sensitization by acetone which absorbs weakly at 308 nm is also possible. A large number of experiments were carried out under a variety of conditions and the most pertinent are summarized here. The triplet of terephthalate has a strong absorption at 320 nm and a lifetime of at least 60 μ s at 1mM terephthalate and near neutral pH. The spectrum of the triplet remains the same from pH 6.7 to 13 and is not dependent on the mode of formation by direct excitation or sensitization. The terephthalate triplet lifetime in the presence of 10% 2-propanol by volume (1.3 M) is about 6 μ s at pH 13. The optical absorption by the CHD is not evident because it absorbs near 350 nm with a much weaker absorption ($\epsilon \sim 3000 \text{ M}^{-1} \text{ cm}^{-1}$) than the anion radical ($\epsilon=30000$). The reaction scheme is given in equations 4-7.

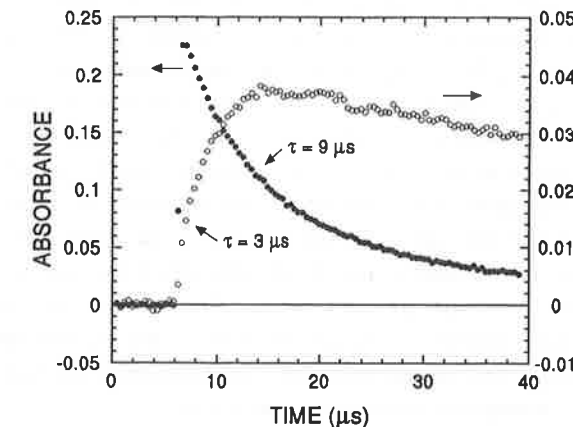
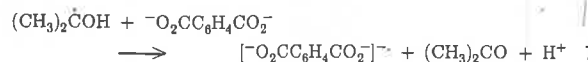
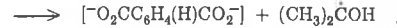
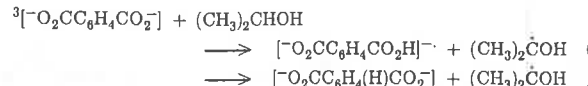
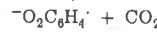
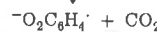
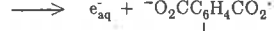
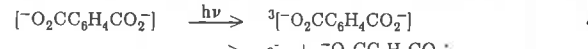


Figure 2. Triplet decay at 320 nm (left scale) and anion growth at 520 nm (right scale) for 10 mM terephthalate and 1.4 M acetone at pH 13.0.

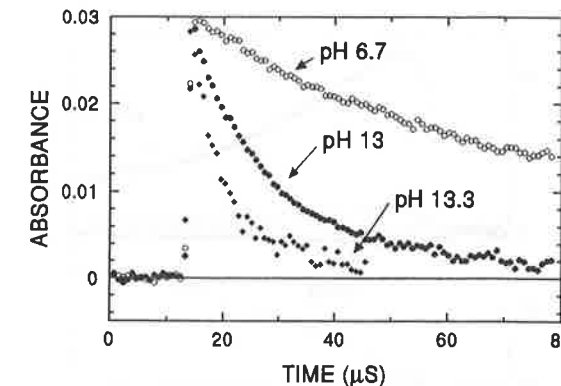


Figure 3. Triplet decay measured at 320 nm for 1 mM terephthalate in the presence of 2.5 M methanol.

The rate constant for energy transfer from acetone triplet to terephthalate is $1.3 \times 10^9 \text{ M}^{-1} \text{ s}^{-1}$. The reduction of terephthalate by $(\text{CH}_3)_2\dot{\text{C}}\text{O}^-$ has a rate constant of about $1 \times 10^7 \text{ M}^{-1} \text{ s}^{-1}$ which is dependent on the ionic strength. The corresponding reaction by $(\text{CH}_3)_2\dot{\text{C}}\text{OH}$ (pK_a 12.0) is considerably slower. Kinetic traces showing the decay of the triplet and the formation of the anion radical are shown in Fig. 2. In this case, no 2-propanol was included so the source of the hydrogen atom is not clear but may involve the acetone. (Some anion radical is also formed in solutions containing only terephthalate. In part, this reaction is the result of a small yield of photoionization of the terephthalate when excited at 265 nm.) The effect of base on the reaction of the triplet is shown in Fig. 3 where methanol was the hydrogen donor. The decay rate of the triplet increased on going to pH 13 and increased further at pH 13.3.

To further understand the observed behavior, time-resolved ESR studies were carried out using a Lumonics HyperEX-400 laser at 308 nm and the direct detection ESR spectrometer previously used for pulse radiolysis experiments. Large signals of the CHD

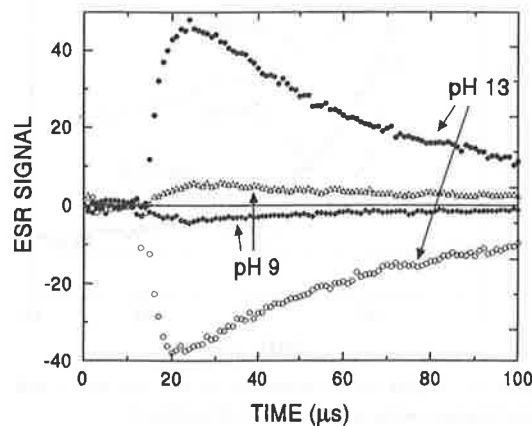


Figure 4. Time profiles of the ESR lines at the centers of the low- and high-field subgroups of the CHD spectrum from 10 mM terephthalate solution containing 1.4 M acetone and 1.3 M 2-propanol.

were found with terephthalate only when alcohols such as ethanol and 2-propanol were used as hydrogen donors and then only in basic solution above about pH 12. If tetrahydrofuran or sodium borohydride were the donors, little CHD radical was formed and increasing the pH had little effect. (It is clear from continuous illumination experiments that some reaction occurs as the lines of the CHD are seen along with those belonging to the radical from the donor.) At neutral pH, where the acid is still present as the dianion, little CHD is found. Typical curves are shown in Fig. 4 at two pH values. The growth of the ESR signal for the cyclohexadienyl radical occurs over about 6 μs and so is clearly limited by the relaxation time and the radical does not have a large initial magnetization. The effect of pH is illustrated in more detail in Fig. 5. Here the central line of the anion radical is shown as well as the central line of the high-field group of the CHD. The signal of the CHD increases somewhat from pH 11.4 to 12.2 and increases much more in going to pH 13.0. Similar behavior has been seen with methanol and ethanol. (Note the increased rate of decay of the triplet at high pH in Fig. 3 also.) It is clear that the reaction of the triplet with the alcohol also involves base. Based on the constancy of the spectrum of the triplet over this pH range, there is no evidence for a change in the structure of the triplet. The reason for the involvement of base is not clear.

The formation of two products from these acids is interpreted in terms of the spin densities of the triplet state which, for the dimethyl ester, has been shown to have a quinoid structure [13]. In terephthalate triplet, there will be spin density mainly on the oxygens and the 1 and 4 carbons of the ring. Addition of hydrogen from the donor can occur at those positions. These reactions must occur by parallel reactions of the triplet, because radiolysis studies show that the anion radical does not protonate on carbon in these time scales. Reaction at the oxygen will be like that in typical ketones. The reaction at a ring carbon is like that seen by Sakaguchi et al. [2,3] for xanthone.

The time-resolved ESR signal of the anion radical showed very unusual behavior. At neutral pH (monoanion radical) the ESR line at the center of the spectrum showed an emission which

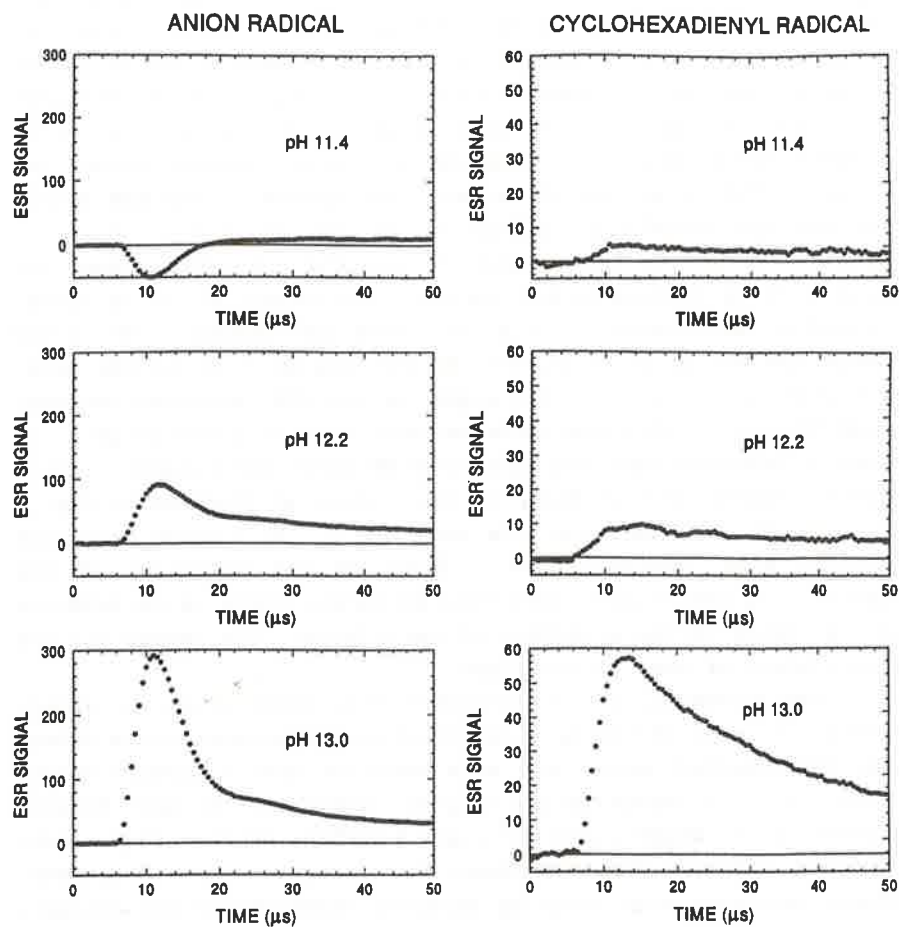


Figure 5. ESR time profiles for 10 mM terephthalate, 1.4 M acetone and 1.3 M 2-propanol.

lasted for about 10 μ s and then converted to absorption as shown in Fig. 5. At pH 12.2 and 13, the anion radical (trianion here) gave a positive signal which seems to have a two-part decay. To help understand this behavior, experiments were then carried out in which the physical quencher β -hydromuconic acid at 10mM was added. Under these conditions the triplet lifetime is only about 1 μ s. The emissive signal was of the same amplitude and decayed to a small positive signal after 30 μ s. At low microwave power, this decay represents the relaxation of the magnetization acquired in the short period that the triplet was present. The observed period of about 10 μ s matches that obtained in modulation experiments [1]. To help show that the magnetization is acquired rapidly, experiments were also carried out under these conditions but with high microwave power. The resultant curves for the anion radical and the CHD are shown in Fig. 6. The Torrey oscillations for the anion are direct evidence that the magnetization is formed quickly. The lack of any such effect for the CHD (which has a similar spin relaxation time) shows that the magnetization for that radical is developed more slowly as a result of radical-radical encounters and the normal radical pair mechanism. Experiments at pH 13 gave the same result for the anion with the important exception that the initial signal was positive. Thus there is a positive polarization present when the radical is formed at high pH.

The origin of the emissive polarization is not clear. Several explanations are possible. Because the lines of the anion are close to the center of the spectrum, a net polarization by a mechanism such as the triplet mechanism is likely. However, the slow formation of the anion (at least the majority of it) over a period of roughly 6 μ s (as shown by the optical results, see Fig. 2) allows relaxation of any polarization of the triplet. For the polarization to arise from the radical-pair mechanism, the second radical would have to have a very different g factor. An alternative comes from the fact that some of the anion may be formed from electrons produced by photoionization. If the electrons were polarized then that polarization would be transferred to the anion. This explanation is unlikely because the emission is still present when an great excess of acetone, a

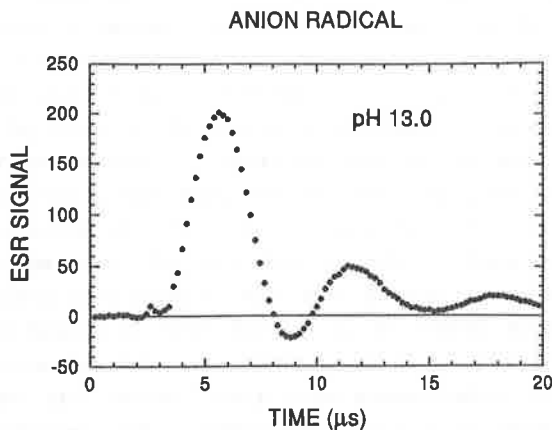


Figure 6(a). ESR time profile of the central line of the anion radical with 10 mM terephthalate, 1.4 M acetone, 1.3 M 2-propanol, and 5 mM β -hydromuconic acid at high microwave power.

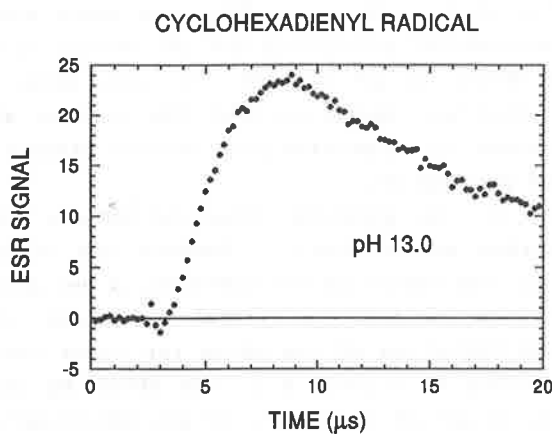


Figure 6(b). ESR time profile of the central line of the high-field group of the CHD under the same conditions as Fig. 6a.

good reactant for the electron, is present. Another possibility might involve two photon photochemistry and the fact that the triplet absorbs strongly at 308 nm. If the triplet were converted to anion radical during the laser pulse, then any triplet mechanism polarization would not have time to relax. The laser dose dependence was studied and some evidence for a greater-than-linear increase in emission intensity was found. The argument against this explanation is that the emission does not seem to depend on whether the terephthalate absorbs directly, producing the triplet within the laser pulse, or is sensitized, in which case the triplet formation is delayed until after the laser pulse is over. A final explanation is polarization by anion radical-terephthalate triplet encounters as described by Blättler et al. [14]. The relatively long triplet lifetime in these experiments would favor such interactions. The fact that the amplitude of the emission is not markedly decreased when a quencher is used may argue against this mechanism also. All in all this last explanation may be correct, but further work is needed to make it clear.

Any explanation for the change in the sense of the polarization for the anion radical between neutral and basic solution is dependent on the explanation for the polarization itself. Several things must be done to answer these questions. A more careful study by optical absorption of the formation of the anion radical is necessary. For example, most of the anion is formed over a period of time and no polarization by triplet mechanism is likely. However, it is necessary to show that there is not a parallel path from the triplet which rapidly forms a small amount of anion and can carry triplet mechanism polarization to the anion. The changes with pH suggest that the exact structure of the triplet may change. However, the experiments done to date do not show any difference in the absorption by that species and so one is forced to conclude that no changes occur. Resonance-enhanced Raman studies of the triplet will be done to use this much more sensitive method to answer this question.

4. Conclusion

The results reported here clearly show the formation of two

types of products by parallel reactions of the triplet of aromatic carboxylic acids with hydrogen donors. A wide variety of aromatic compounds undergo these reactions, including acids esters, amides, anhydrides and cyanobenzenes. The yield of cyclohexadienyl radicals is larger from alcohols than other hydrogen donors such as tetrahydrofuran and is greatly enhanced in the presence of base. The polarization of the cyclohexadienyl radicals is the result of the normal radical-pair mechanism but the magnitude is not known because the yield of the radicals is not known. The source of the initial polarization of the anion radicals is not known.

Acknowledgment

The work described herein was supported by the Office of Basic Energy Sciences of the Department of Energy. This is Contribution No. NDRL-3395 from the Notre Dame Radiation Laboratory.

References

- [1] A. S. Jeevarajan and R. W. Fessenden, *J. Phys. Chem.*, 93 (1989), 3511.
- [2] Y. Sakaguchi and H. Hayashi, *J. Phys. Chem.*, 90 (1986), 550.
- [3] Y. Sakaguchi, H. Hayashi, H. Murai, and Y. J. I'Haya, *J. Am. Chem. Soc.*, 110 (1988), 7479.
- [4] H. Hayashi, Y. Sakaguchi, H. Murai, and Y. J. I'Haya, *J. Phys. Chem.*, 90 (1986), 4403.
- [5] P. B. Ayscough, T. H. English, G. Lambert, and A. J. Elliot, *Faraday Trans. I*, 73 (1977), 1302.
- [6] H.-K. Roth, S. Hoernig, and P. Wuensche, *Polymer Photochem.*, 4 (1984), 409.
- [7] H. F. Davis, H. J. McManus and R. W. Fessenden, *J. Phys. Chem.* 90 (1986), 6400.
- [8] R. W. Fessenden, J. P. Hornak, and B. Venkataraman, *J. Chem. Phys.* 74 (1981), 3694.
- [9] V. Nagarajan and R. W. Fessenden, *J. Phys. Chem.*, 89 (1985), 2330.
- [10] K. Eiben and R. H. Schuler, *J. Chem. Phys.*, 62 (1975), 3093.
- [11] Studies done in conjunction with D. Weir.
- [12] L. Qin, G. N. R. Tripathi, and R. H. Schuler, *J. Phys. Chem.*, 93 (1989), 5432.
- [13] D. R. Arnold, J. R. Bolton, and J. A. Pederson, *J. Am. Chem. Soc.*, 94 (1972), 2872.
- [14] C. Blättler, F. Jent, and H. Paul, *Chem. Phys. Lett.*, 166 (1990), 375.

ELECTRON SPIN POLARIZATION BY A RADICAL-TRIPLET PAIR MECHANISM

Cyrill Blättler and Henning Paul

Physikalisch-Chemisches Institut, Universität Zürich, CH-8057 Zürich, Switzerland

Abstract

Transient alkyl radicals and triplet state molecules are generated simultaneously in solution by laser flash irradiation. Investigations of CIDEP of the radicals by time-resolved ESR spectroscopy demonstrate triplet state molecules to induce emissive ESR polarizations. The phenomenon is termed radical-triplet pair mechanism (RTPM) and attributed to triplet state quenching by radicals as well as to quartet-doublet mixing and splitting in radical-triplet encounters.

1. Introduction

CIDEP of transient radicals in solution is usually interpreted in terms of two main mechanisms (1). One is the triplet mechanism (TM) which occurs if radicals are formed from a triplet state precursor with non-equilibrium sublevel populations (2). The other is the radical pair mechanism (RPM). There, the polarization is built up in reencounter sequences of spin correlated radical pairs. It results from mixing and splitting of the pairs triplet and singlet spin states by the hyperfine and exchange interaction, respectively (3). The TM causes the whole ESR spectrum of the radicals to appear initially in emission (E) or enhanced absorption (A). The RPM produces a multiplet type polarization with usually E on the low-field and A on the high-field side of the spectrum.

Here we present evidence for an additional polarization mechanism which is observed if the radical sample contains triplet state molecules. It resembles the RPM for F-pairs but occurs during encounters of triplets with radicals and, therefore, may be termed radical-triplet pair mechanism (RTPM). The RTPM seems to generate a net polarization of the entire ESR spectrum of the radicals. It probably results from quartet-doublet mixing and splitting due to the zero-field splitting and the exchange interaction, respectively. In addition, doublet pair spin states are filtered out by triplet quenching. In fact, the ESR polarization thus created is just the counterpart of the magnetic field dependent component of triplet quenching by radicals (4).

2. Experimental

Our experimental arrangement for time-resolved ESR measurements after laser flash photolytic radical generation has been described previously (5,6). It comprises an excimer laser (XeCl, 308 nm, 20 ns pulse width, \approx 30 mJ/pulse on sample

surface) and a CW ESR detection system with response time \approx 60 ns (direct detection without field modulation). After deoxygenation the sample solutions are exposed to laser irradiation while flowing through a flat quartz cell (0.6 mm optical path length) inside the ESR cavity. Steady state ESR spectra are recorded on a conventional spectrometer (100 kHz field modulation) during irradiation of the sample with a Xe/Hg 1 kW short arc lamp.

Here we investigate the ESR polarizations of benzyl radicals in the presence of optically excited anthracene, naphthalene, or benzil molecules. Studies were performed at $T = -90^\circ\text{C}$ in 1,2-epoxy propane. All solutions contained 64 mM di-benzyl-ketone for photolytic radical generation and anthracene, naphthalene, or benzil in concentrations 9 mM, 80 mM, and 10 mM, respectively. Thus, for all solutions a total optical density of 1.0 was achieved, 0.4 in the ketone and 0.6 in the additive. All chemicals were purchased in their purest commercially available form and used as supplied.

The photochemistry of di-benzyl-ketone is well known (7,8). After singlet excitation it crosses within a few nanoseconds to the triplet state which undergoes α -cleavage in less than 1 ns into $\text{C}_6\text{H}_5\text{CH}_2\dot{\text{O}}$ and benzyl radicals $\text{C}_6\text{H}_5\dot{\text{C}}\text{H}_2$. At $T = -90^\circ\text{C}$ the acyrladical decarbonylates into CO and benzyl radicals with rate $k_D = 5800\text{ s}^{-1}$ (9,10).

3. Results

The upper part of fig.1 shows a steady state ESR spectrum of benzyl radicals recorded during continuous UV irradiation of a di-benzyl-ketone solution. With the spectrometer settings used the resonances of the acyl counterradicals are not visible. Two arrows mark a high- and low-field line positioned symmetrically to the centre of the spectrum, which have been investigated time-resolved after laser flash photolysis. The results are given in the lower part of fig.1 for three different systems.

Fig.1a shows the time dependencies of the high-field (h) and the low-field (l) resonance amplitude after laser flash irradiation of a solution containing only di-benzyl-ketone. In addition, the sum $s = h + l$ is given, which eliminates the anti-symmetric E/A multiplet polarization and thus reflects twice the net polarization. Under our conditions this net polarization is a weak absorption. Its time dependence has been discussed elsewhere (11,12) and is no matter of concern at this place. Fig.1b and 1c give time profiles of the same resonances as well as their sum, which are observed for solutions containing anthracene (1b) or benzil (1c). Obviously, the net polarization changes to weak and strong emission, if anthracene and benzil, respectively, are present. Investigations of several other benzyl radical resonances show the admixtures to induce net emission only and no additional multiplet polarization.

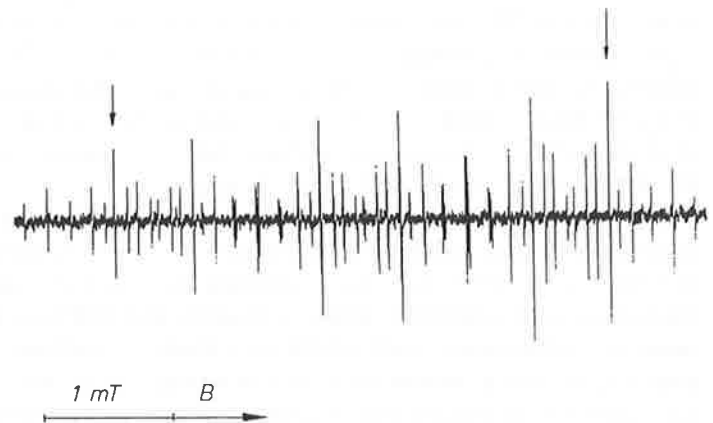


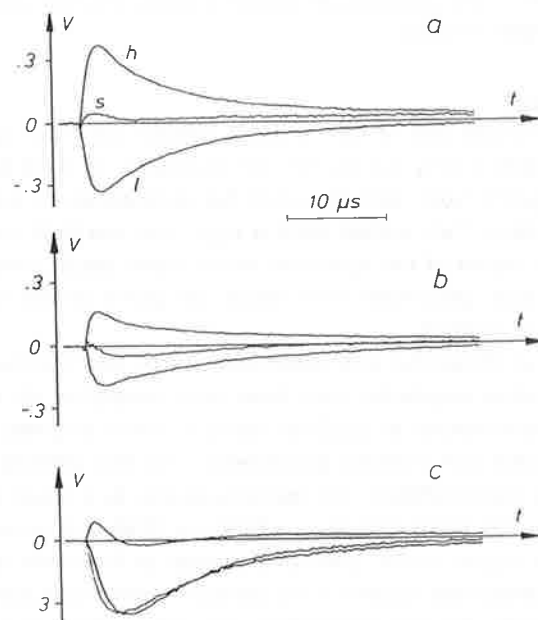
Figure 1

Upper part:

Steady state ESR spectrum of benzyl radicals.

Lower part:

Time profiles of a benzyl radical high-field (h) and low-field (l) resonance and sum $s = h + l$. Irradiation of solutions containing only dibenzylketone (a) and added anthracene (b) or benzil (c).



Similar experiments with other radical systems show the same effect, i.e. production of emission if the radicals are generated by UV irradiation of solutions containing naphthalene, anthracene, or benzil (13).

In order to obtain a rough measure for the size of the effect we have determined the sum $s = h + l$ and the difference $d = h - l$ of the high- and low-field resonance amplitudes at times t_m where s shows maximum emission. The difference d yields twice the RTPM multiplet polarization which should be about proportional to the square of the radical concentration (14). Thus, the ratio s/\sqrt{d} measures the net polarization per unit radical concentration. The results obtained for the benzyl radical systems are compiled in the first columns of table I. For discussion, the last two columns contain the zerofield splitting parameters D of the anthracene, naphthalene, and benzil triplet states with references.

Table I: RTPM polarizations of benzyl radicals and ZFS parameters

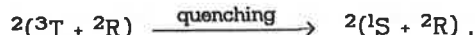
Additive	$t_m(\mu\text{s})$	s/\sqrt{d}	$D(\text{cm}^{-1})$	Ref.
None		> 0		
Anthracene	4.1	- 3.1	0.07	(15)
Naphthalene	3.3	- 4.4	0.10	(15)
Benzil	3.8	- 19.0	- 0.13	(16)

4. Discussion

For explanation of the emissive polarization of the radical electron spin system in the presence of anthracene, naphthalene, or benzil we note that all three additives absorb at $\lambda = 308 \text{ nm}$ and thus are excited simultaneously with the ketone during the laser flash. After intersystem crossing they form triplet states with lifetimes in the millisecond range (15).

We suppose that the observed emissive electron spin polarization originates from encounters of the radicals with those triplet state molecules. It is well known that excited triplet states are quenched by ground state radicals, either by energy transfer or via enhancement of intersystem crossing in radical-triplet pairs (4, 17,18). In order to show that this quenching process can also generate electron spin polarization of the radicals on the μs timescale in qualitative agreement with experiment we consider a simple static model:

Upon encounter a triplet molecule and a radical may form either a quartet or a doublet pair spin state. We assume that the doublet encounters undergo triplet quenching,



and that the radicals leave those encounters unpolarized. The remaining quartet pair states experience radical-triplet interactions altering the spin state populations with time. The relevant high-field spin Hamiltonian,

$$\mathcal{H} = \omega(S_{Rz} + S_{Tz}) - 2J S_R S_T + S_T D |S_T|.$$

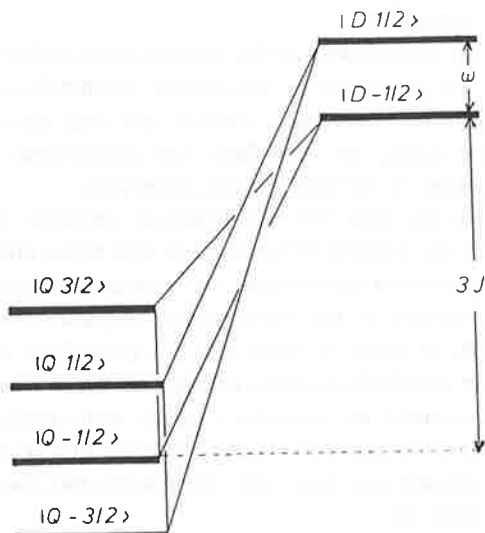
$$\mathcal{H}_0 \quad \mathcal{H}_1$$

consists of Zeeman splitting ($g_R = g_T$ is assumed for the g-factors), exchange interaction, and zero-field splitting (ZFS). The energy levels of \mathcal{H}_0 are given in fig. 2. Our choice of the exchange interaction brings the quartet to $-J$ and the doublet to $2J$. As indicated, the ZFS mixes within the $|Q 3/2\rangle$, $|Q -1/2\rangle$, $|D -1/2\rangle$ as well as within the $|Q -3/2\rangle$, $|Q 1/2\rangle$, and $|D 1/2\rangle$ states.

Employing second-order perturbation theory we have calculated the evolution of the spin state populations in interaction representation from

$$\frac{d}{dt} \rho(t) = \frac{i}{\hbar} [\rho(t), \mathcal{H}_1]$$

Figure 2
Energy level diagram of a radical-triplet pair with exchange ($3J$) and Zeeman (ω) splitting. States connected with each other are mixed by ZFS.



with initial condition that at $t=0$ the doublet substates are empty and the quartet substates are equally populated. For simplicity we assumed $S_T \parallel D \parallel S_T - D(S_T^2/3)$, i.e. a triplet molecule with ZFS parameters $E=0$ and D along a molecular ζ -axis. Furthermore, the exchange interaction J as well as the ζ -axis orientation were considered to be static quantities.

For the orientation $\zeta \parallel z$ the calculation yielded the radical spin polarization $\langle S_{Rz} \rangle(t) = \text{Tr}(\rho(t) S_{Rz}) = 0$, i.e. no polarization. However for $\zeta \perp z$ the result is

$$\begin{aligned} \langle S_{Rz} \rangle(t) &= -\frac{D^2 J}{24 \omega} \{ (2\omega + 3J)^{-2} (1 - \cos(2\omega + 3J)t) + (2\omega - 3J)^{-2} (1 - \cos(2\omega - 3J)t) \\ &\quad - 2(3J)^{-2} (1 - \cos(3Jt)) \} \approx \frac{1}{72} \omega J D^2 t^4 + \dots \end{aligned}$$

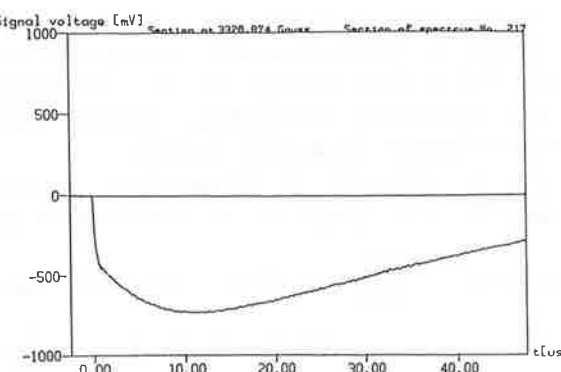
Thus, our crude static model predicts an electron spin polarization of the radicals with the following qualitative features: a) The polarization should be independent of the sign of D . This agrees with experiment since anthracene and naphthalene possess positive D -values whereas benzil has a negative one. b) If J remains constant the polarization should increase with D^2 . In fact, the observed emissions are the more pronounced the larger the $|D|$ values are (compare s/\sqrt{d} and D in tab. I). c) The spin polarization should be emission if $J > 0$. This also agrees with experiment in that a lower quartet than doublet energy of the radical-triplet pair is in accord with Hund's rule.

Although the static model can explain some of the basic features of the RTPM polarization, investigations of the size of the effect and its dependence on parameters like solvent, temperature, and viscosity have to take into account the time dependencies of $J(t)$ and $\mathcal{H}_1(t)$, the evolution of radical-triplet pair spin states, before quenching occurs, and the fact, that often triplet quenching by radicals is not a diffusion controlled process (13).

As described, the RTPM will often induce qualitatively similar electron spin polarizations as does the TM, e.g. net emission. Thus, care has to be taken in interpreting such polarizations. As an example, fig. 3 shows the time dependent signal of benzilketyl radicals after laser flash irradiation of benzil in 2-propanol at $T = -50^\circ\text{C}$. Obviously, it starts with a rapidly rising emission followed by a slowly rising one. This can be explained by partial formation of the species from some higher triplet state, populated during the laser flash via a successive two photon process (5,19), followed by the slow classical photoreduction of the lowest benzil triplet state with 2-propanol (20). The initial emission might be due to the TM and/or to fast transfer of triplet polarization to the ketyl radicals (21). Since any triplet polarization relaxes within nanoseconds the slowly rising emission must be due to the RTPM, induced as long as there are triplet benzil molecules present.

Figure 3

Time dependent ESR amplitude
of $C_6H_5CO\dot{C}(OH)C_6H_5$ after
laser flash irradiation of benzil
in 2-propanol at $T = -50^\circ C$.



Diffusional Aspects of Spin Selective Reactions; Fundamental Quantities and Relations

J. Boiden Pedersen

Fysisk Institut, Odense Universitet,
DK-5230 Odense M, Denmark

Abstract

The reencounter formalism combined with results from the theory of diffusion controlled reactions is used to obtain closed form expressions for the spin dependent recombination probability for selected systems. The expressions are valid for 3-dimensional diffusion in an arbitrary potential and for varying size of the reaction region.

1 Introduction

Magnetic field and spin effects on radical reactions are well known to arise from a combination of a spin selective reaction (usually just singlet pairs react) and quantum mechanical mixing of states. The spin selective reaction occurs when the radicals are close together and may often be taken to be local in space. The mixing of states is more efficient for longer distances since the exchange interaction will tend to prevent the mixing. The understanding of the importance of the consecutive reencounters of the radicals in media in which the radicals may diffuse represented a major step towards a complete and quantitative description.

The quantitative calculation of CIDNP and CIDEP is usually performed by solving the Stochastic Liouville equation (SLE) numerically by using a finite difference technique [1], [2] and [3]. For time independent quantities such as CIDNP and CIDEP polarization this may be conveniently done by a Laplace transformation of the SLE. Time dependent solutions may also be obtained although the calculations may be computationally demanding [4]. The advantage of this approach is its ability to accurately represent an isotropic continuous diffusion in an arbitrary potential and to take full account of any r -dependent operator. The disadvantage is

References

- (1) L.T. Muus, P.W. Atkins, K.A. McLauchlan, and J.B. Pedersen, Ed., "Chemically Induced Magnetic Polarization", D. Reidel Publ. Co., Dordrecht-Holland, 1977, and references cited therein.
- (2) S.K. Wong, D.A. Hutchinson, and J.K.S. Wan, *J. Chem. Phys.* **58** (1973) 985.
- (3) F.J. Adrian, *J. Chem. Phys.* **54** (1971) 3918.
- (4) U.E. Steiner and T. Ulrich, *Chem. Rev.* **89** (1989) 51, and references cited therein.
- (5) F. Jent, H. Paul, and H. Fischer, *Chem. Phys. Letters* **146** (1988) 315.
- (6) F. Jent and H. Paul, *Chem. Phys. Letters* **160** (1989) 632.
- (7) P.S. Engel, *J. Am. Chem. Soc.* **92** (1970) 6074.
- (8) W.K. Robbins and R.H. Eastman, *J. Am. Chem. Soc.* **92** (1970) 6076.
- (9) L. Lunazzi, K.U. Ingold, and J.C. Scaiano, *J. Phys. Chem.* **87** (1983) 529.
- (10) N.J. Turro, I.R. Gould, and B.H. Baretz, *J. Phys. Chem.* **87** (1983) 531.
- (11) A.I. Grant and K.A. McLauchlan, *Chem. Phys. Letters* **101** (1983) 120.
- (12) N.J. Turro, M.A. Paczkowski, M.B. Zimmt, and J.K.S. Wan, *Chem. Phys. Letters* **114** (1985) 561.
- (13) C. Blättler, F. Jent, and H. Paul, *Chem. Phys. Letters* **166** (1990) 375.
- (14) J.B. Pedersen, *J. Chem. Phys.* **59** (1973) 2656.
- (15) S.L. Murov, *Handbook of Photochemistry*, Marcel Dekker, New York 1973, and references cited therein.
- (16) Y. Teki, T. Takui, and M. Hirai, *Chem. Phys. Letters* **89** (1982) 263.
- (17) O.L.J. Gijzeman, F. Kaufman, and G. Porter, *J. Chem. Soc., Faraday Trans. II* **69** (1973) 727.
- (18) H. Hiratsuka, S. Rajadurai, P.K. Das, G.L. Hug, and R.W. Fessenden, *Chem. Phys. Letters* **137** (1987) 255, and references cited therein.
- (19) M. Mukai, S. Yamauchi, and N. Hirota, *J. Phys. Chem.* **93** (1989) 4411.
- (20) B.M. Monroe, *Adv. Photochem.* **8** (1971) 77.
- (21) T. Imamura, O. Onitsuka, and K. Obi, *J. Phys. Chem.* **90** (1986) 6741.

that of any numerical method, i.e. the fundamental dependences may be difficult or impossible to extract from the numerical results.

Another calculation scheme is the reencounter scheme which is based on the physical picture of visualizing the relative diffusive motion of the radicals as a series of reencounters. Using this method the ultimate reaction probability for a radical pair can be expressed by M_i and M_o , the quantum mechanical propagators for the spin evolution averaged respectively over the time spent in the reaction zone and the first reencounter time (first passage time). This picture divides space into two separate regions: (i) a small reaction zone where the reaction takes place and (ii) the surroundings where there is no reaction of the radical pairs except for spin independent scavenging processes. All r -dependent quantum mechanical operators such as the exchange interaction and the operator for the spin dependent reaction are assumed to be of short range and to be active in the reaction zone only. It is often necessary to employ some approximation to the r -dependence of these operators. Outside the reaction zone the quantum mechanical operators are independent of the distance between the radicals r and so is the propagator. In a basis diagonalizing the outside propagator the matrix elements of M_o are equal to $\tilde{R}(i\omega_{ij})$ where \tilde{R} is the characteristic function of the first arrival time (or reencounter time). The transition frequencies ω_{ij} are the differences between the eigenvalues of the free pair Hamiltonian, i.e. the sum of the Hamiltonians of the two individual radicals. All information about the diffusion process is contained in the characteristic function \tilde{R} and accurate analytic solutions which are well suited to radical pair reactions have been obtained [5]. The advantage of this approach is that it gives rise to analytic solutions and that the effect of various aspects of the diffusion process can be identified. The disadvantage is that a general r -dependence of the operators cannot be treated exactly.

It is shown that a combination of the reencounter picture and the theory of diffusion controlled reactions can be used to obtain analytic results for the spin dependent recombination probability. These results permit a direct investigation of the effect of various aspects of diffusion, e.g. the interradical potential, an r -dependent diffusion coefficient, and scavenging reactions.

The paper starts with a discussion of the theory of diffusion controlled reactions with special emphasis on the general aspects and relations and the analytical solutions that are particularly useful in the theory of spin dependent reactions. The general reencounter formalism is then introduced and several approximations are discussed. Finally the formalism is applied to selected systems.

2 Diffusion controlled reactions

The theory of diffusion controlled reactions in continuous media is usually based on the Smoluchowski equation which for a spherically symmetric, 3-dimensional system is

$$\frac{\partial P(r,t)}{\partial t} = D \frac{1}{r^2} \frac{\partial}{\partial r} \left[r^2 \gamma(r) \left(\frac{\partial P}{\partial r} + \frac{1}{kT} \frac{dV}{dr} P \right) \right] \quad (1)$$

The potential energy of interaction between the particles is denoted V , D is the bulk diffusion coefficient, and the relative diffusion coefficient

$$\gamma(r) = D(r)/D \quad (2)$$

is assumed to be nonzero and to approach unity as $r \rightarrow \infty$. In the simplest case the reaction of the particles is assumed to take place when the particles are in contact at a contact distance d only. If all particles that encounter at d react the reaction is said to be *diffusion controlled*. This is described by the absorption boundary condition

$$P(d,t) = 0 \quad (3)$$

A *partially diffusion controlled* reaction is one in which not every encounter leads to reaction. This situation is described by the radiation boundary condition

$$D(d) \left[\frac{\partial P}{\partial r} + \frac{1}{kT} \frac{dV}{dr} P \right]_{r=d} = h P(d,t) \quad (4)$$

which is equivalent with the introduction of a sink term

$$-h\delta(r-d)P(r,t) \quad (5)$$

into the Smoluchowski equation. The limit $h \rightarrow \infty$ is the diffusion controlled limit.

2.1 General relations

The quantity of interest for a recombination process is the rate of recombination which for a pair of particles with initial separation r_0 (and in the absence of scavengers) is

$$R(t, r_0) = -\frac{\partial}{\partial t} \int P(r, t | r_0) d^3r \quad (6)$$

where $P(r, t | r_0)$ is the solution to the Smoluchowski equation that satisfies the initial condition $\delta(r - r_0)/(4\pi r^2)$.

If the initial separation of the particles is a distribution $P_0(r_0)$ rather than a single initial separation then the rate of recombination is given by superposition

$$R(t) = \int R(t, r_0) P_0(r_0) d^3 r_0 \quad (7)$$

For a normalizable initial distribution $P_0(r_0)$ the rate of recombination is called geminate recombination and is denoted $R(t)$. If on the other hand the initial distribution is a Boltzmann distribution extending over all space then the rate of recombination is called the time dependent rate constant for bulk recombination and it is denoted

$$K(t) = \int R(t, r_0) e^{-\beta V(r_0)} d^3 r_0 \quad (8)$$

where $\beta = 1/kT$. This equation can be rewritten to the simpler equation [6,7]

$$K(t) = -4\pi D(d) d^2 e^{-\beta V(d)} R'(t) \quad (9)$$

where

$$R'(t) = (\partial R(t, r)/\partial r)_{r=d} \quad (10)$$

Thus instead of calculating $K(t)$ by an integration of $R(t, r)$ over r it can be obtained by a simple differentiation.

The kinetic equation for a recombination reaction of "classical" particles is

$$\frac{dn}{dt} = -R(t)n - K(t)n^2 \quad (11)$$

The first term describes the rate of disappearance of initially correlated pairs and the second term describes the bulk recombination of initially uncorrelated pairs. This equation implies that $R(t)$ and $K(t)$ varies on a short time scale and $n(t)$ on a long time scale. On the short time scale $R(t) \rightarrow 0$, as $t^{3/2}$ in 3-d, and $K(t) \rightarrow K$, the steady state constant, for $t \rightarrow \infty$.

In general both $R(t)$ and $K(t)$ depend on the rate by which the radicals form a product when they encounter. This is described above by a microscopic rate constant h either in the form of a radiation boundary condition, Eq.(4) or identically by a sink term, Eq.(5). The complication introduced by this extra dependence can be eliminated by the use of the following general relations [6] that show that the general case can be calculated from the diffusion controlled quantity:

$$\tilde{R}(s, r, h) = \frac{\tilde{R}(s, r)}{1 - \tilde{R}'(s)D(d)/h} = \tilde{R}(s, r)\tilde{\Lambda}(s, h) \quad (12)$$

$$\tilde{K}(s, h) = \frac{\tilde{K}(s)}{1 - \tilde{R}'(s)D(d)/h} = \tilde{K}(s)\tilde{\Lambda}(s, h) \quad (13)$$

where tilde indicates the Laplace transformed quantity with variable s . The latter form of the relations have an obvious interpretation as a product of a diffusion controlled rate and a probability of reaction. This is particularly evident in the $t \rightarrow \infty$ limit. The ultimate probability of recombination is equal to

$$\int_0^\infty R(t, r, h) dt = \lim_{s \rightarrow 0} \tilde{R}(s, r, h) = p\Lambda \quad (14)$$

which can be interpreted as the probability that the members of a pair meet for the first time

$$p = \tilde{R}(0, r) \quad (15)$$

multiplied by the total probability Λ that they react either during this encounter or during one of the subsequent reencounters before they diffuse apart never to meet again;

$$\Lambda \equiv \tilde{\Lambda}(0, h) \quad (16)$$

The steady state rate constant can similarly be written as

$$K = \lim_{t \rightarrow \infty} K(t) = \lim_{s \rightarrow 0} s\tilde{K}(s, h) = K_D\Lambda \quad (17)$$

where $K_D = \lim_{s \rightarrow 0} s\tilde{K}(s)$ is the diffusion controlled rate constant. This equation can be interpreted as the rate of which the members of a pair meet for the first time multiplied by the total probability that they react either during this encounter or during one of the subsequent reencounters before they diffuse apart never to meet again.

2.2 Approximate solutions

Exact solutions to the Smoluchowski equation, Eq.(1), are known only for free diffusion and for the $t \rightarrow \infty$ or identically the $s \rightarrow 0$ limit. There has therefore been many attempts to obtain approximate solutions. In this section the most accurate approximate solutions which are useful for the theoretical description of spin dependent recombination processes are reviewed. In order to simplify the notation an effective distance is introduced as

$$r_{eff} \equiv rf^*(r) \equiv \left(\int_r^\infty \frac{\exp(V(x)/kT)}{x^2 \gamma(x)} dx \right)^{-1} \quad (18)$$

When there is no potential energy $V(r)$ between the particles $d = r_{eff}$. Also $r_{eff} < d$ for repulsive forces, $r_{eff} > d$ for attractive forces, and r_{eff} deviates the more from d the larger the range of $V(r)$ is. For long times or identically for small values of the Laplace transform variable s the most accurate expression is [5]

$$\tilde{R}(s, r)_1 = \exp\left(-\sqrt{\frac{s}{D}}(r - d)\right) \frac{d_{eff}}{r_{eff}} \left\{ 1 + \sqrt{\frac{s}{D}} [r - d - r_{eff} + d_{eff}] \right\} \quad (19)$$

Two alternatives to this expression are

$$\tilde{R}(s, r)_2 = \frac{d_{eff}}{r_{eff}} \exp \left[-\sqrt{\frac{s}{D}} (r_{eff} - d_{eff}) \right] \quad (20)$$

$$\tilde{R}(s, r)_3 = \frac{d_{eff}}{r_{eff}} \left[1 - \sqrt{\frac{s}{D}} (r_{eff} - d_{eff}) \right] \quad (21)$$

The last expression is clearly useful only for small values of s since large values may result in negative values of \tilde{R} . The two other expressions have a much larger range of applicability. The second expression is perhaps the most convenient one since it is formally identical to the free diffusion result with the distances d and r replaced by the effective distances d_{eff} and r_{eff} . However, the first expression has been shown [8] to be the most accurate one and should therefore be used. Even for the pathological case of a Coulomb potential does it give useful results with a relative error smaller than 1% for $s = 0.1$ and 3% for $s \simeq 1$. All three approximations are exact for $s = 0$.

In order to be able to calculate the partially diffusion controlled quantities we need an expression for $\tilde{R}'(s)$. Any of the above three expressions yield

$$\tilde{R}'(s) = -\frac{e^{V(d)\beta} d_{eff}}{\gamma(d)} \frac{d_{eff}}{d^2} \left[1 + \sqrt{\frac{sd_{eff}^2}{D}} \right] \quad (22)$$

From this expression and Eq.(9) it follows that the diffusion controlled rate constant is equal to

$$\tilde{K}(s) = 4\pi D d_{eff} \left[1 + \sqrt{\frac{sd_{eff}^2}{D}} \right] \quad (23)$$

It is possible to add higher order corrections of order s and $s^{3/2}$ to this expression [9]. Interestingly these higher order corrections have only been obtained by a method [9] where $\tilde{K}(s)$ is calculated directly rather than from $\tilde{R}(s)$. The probability of reaction can be written as

$$\hat{\Lambda}(s, h) = \frac{h\tau}{1 + h\tau + \sqrt{sd_{eff}^2/D}} \quad (24)$$

where the reaction time τ is given by

$$\tau^{-1} = \left(\frac{D}{d^2} \right) e^{+\beta V(d)} d_{eff} \quad (25)$$

Note that the dimension of τ is TL^{-1} , the inverse of h .

In the theory of spin dependent recombination processes one needs expressions for $\tilde{R}(s)$ with a *complex* argument s ; in the theory of diffusion controlled reactions of classical particles only real values of the Laplace variable are of interest. The above expressions are given below in convenient forms for complex arguments. Note that the ultimate probability of reencounters

$$p = \tilde{R}(0, r) = d_{eff}/r_{eff} \quad (26)$$

Let the complex argument s be given as

$$s \equiv k + i2Q \quad (27)$$

and introduce the following definitions

$$z_{\pm} \equiv \frac{1-p}{p} \left(\frac{d_{eff}^2}{2D} \right)^{\frac{1}{2}} \left[\sqrt{k^2 + 4Q^2} \pm k \right]^{\frac{1}{2}} \quad (28)$$

$$z_{\pm}^0 \equiv \frac{1-p_0}{p_0} \left(\frac{d^2}{2D} \right)^{\frac{1}{2}} \left[\sqrt{k^2 + 4Q^2} \pm k \right]^{\frac{1}{2}} \quad (29)$$

where p_0 is the reencounter probability for free diffusion, i.e.

$$p_0 = d/r. \quad (30)$$

We also need the dimensionless quantity

$$A \equiv 1 - \frac{1-p}{p} \frac{p_0}{1-p_0} \frac{d_{eff}}{d} \quad (31)$$

which is zero for free diffusion. We write the real and imaginary part of $\tilde{R}(s)$ separately and use an index 1, 2, 3 to indicate the approximation. The most accurate expression yields

$$\Re \tilde{R}(s, r)_1 = p e^{-z_+^0} \cos(z_-^0) \left[1 + A(z_+^0 + z_-^0 \tan(z_-^0)) \right] \quad (32)$$

$$\Im \tilde{R}(s, r)_1 = -p e^{-z_+^0} \sin(z_-^0) \operatorname{sgn}(Q) \left[1 + A(z_+^0 + z_-^0 / \tan(z_-^0)) \right] \quad (33)$$

where sgn is the sign function.

Expression 2 which is formally equivalent with the free diffusion expression gives

$$\Re \tilde{R}(s, r)_2 = p e^{-z_+} \cos(z_-) \quad (34)$$

$$\Im \tilde{R}(s, r)_2 = p e^{-z_+} \sin(z_-) \operatorname{sgn}(Q) \quad (35)$$

and the simple expression 3 which is applicable only for very small values of the argument becomes

$$\Re \tilde{R}(s, r)_3 = p(1 - z_+) \quad (36)$$

$$\Im \tilde{R}(s, r)_3 = -p z_- \operatorname{sgn}(Q) \quad (37)$$

It may appear that only the diffusion controlled $\tilde{R}(s)$, as given above, is needed in the theory of spin dependent recombination as this is quantity needed to calculate the average propagator M_o . However, the continuous diffusion model is an approximation that is useful for

trajectories much longer than a typical molecular diameter. If shorter trajectories are important the discrete jump aspects of the diffusion must be taken into account. It has been suggested [10] that this can be incorporated into the continuous description by using the expression for the partially diffusion controlled quantity $\tilde{R}(s, r, h)$ with $h = d\nu/4$, where ν is the jump frequency, instead of the diffusion controlled quantity. As noted above, cf. Eq.(12), a partially diffusion controlled quantity can be derived from the corresponding diffusion controlled quantity by the use of $\tilde{R}'(s)$ which for a complex argument can be written as

$$\tilde{R}'(s) = -\frac{1}{\tau D(d)} \left[1 + \frac{p}{1-p} (z_+ + iz_- \operatorname{sgn}(Q)) \right] \quad (38)$$

where τ is given in Eq.(25). The Laplace transform of the probability of reaction, which is used in the conversion of a diffusion controlled quantity to a partially diffusion controlled quantity, cf. Eq.(12), is equal to

$$\Lambda(s) = \frac{h\tau}{1 + h\tau + (z_+ + iz_- \operatorname{sgn}(Q))p/(1-p)} \quad (39)$$

3 The reencounter formalism

3.1 The reencounter picture of translational diffusion

The idea of visualizing the relative diffusion of two particles as a series of reencounters has proved extremely useful for the development of the theory of CIDNP. The picture was used extensively by Noyes [11] in a treatment of classical reaction kinetics and it was introduced into the CIDNP theory by Adrian [12].

Let d denote the distance of closest approach between two particles and let r_0 be a characteristic distance, of order d , defined such that the particles can be said to be in "contact" in the region $d < r < r_0$. Reaction is allowed in this region of space only. The complete diffusion-reaction process may now be visualized as follows: The particles are initially in contact (first encounter) where they may react with probability λ ; the particles that do not react will separate by diffusion (i.e. their relative distance becomes greater than r_0); a fraction p of the separated radicals will return to $r = d$ (reencounter) after a diffusive excursion; a fraction λ of these reacts; etc. These reencounter cycles continue until all radicals have reacted or until only a negligible fraction of particles is left to reencounter.

The probability of reaction at the first encounter plus all subsequent reencounters is then

$$\Lambda = \lambda + \lambda p(1-\lambda) + \lambda p^2(1-\lambda)^2 + \dots$$

$$= \frac{\lambda}{1-p(1-\lambda)} \quad (40)$$

since the fraction λ reacts at the first encounter; of the remaining $(1-\lambda)$ the fraction p reencounters and of these the fraction λ reacts, i.e. $\lambda p(1-\lambda)$ reacts during the first reencounter; etc. Of the three parameters: λ , p and Λ only the latter can be measured directly. The other parameters are introduced for convenience and should be eliminated at the end of any calculation. However, one may think of relating p to a "contact volume". Suppose the reaction takes place at $r = d$ only and that for some reason the particles need to have a relative separation larger than r_0 before they can be considered separated and can start a reencounter cycle. This could be caused by a potential barrier to the diffusion motion. Then p is simply the probability of reaching d from the initial separation r_0 . For three dimensional continuous diffusion p is given by the above expression Eq.(26). In 2-dimensions $p = 1$ unless the effect of scavengers are taken into account [13].

3.2 Reencounter treatment of spin selective reactions

Within the RPM only the electron and nuclear spin degrees of freedom are considered and the use of the spin density matrix ρ is convenient for a theoretical description. The equation of motion for ρ is given by

$$\frac{\partial \rho}{\partial t} = [-i\mathcal{H}(r)^x - K(r) + R]\rho(t) \quad (41)$$

where the three superoperators between brackets describe spin interactions, recombination of the pair, and spin relaxation and/or scavenging of the radicals. The superoperator \mathcal{H}^x is defined by its action on any operator A :

$$\mathcal{H}^x A = [\mathcal{H}, A] \quad (42)$$

where $[\cdot, \cdot]$ is the commutator symbol. The spin Hamiltonian $\mathcal{H}(r)$, which is given in angular units (rad/s), can be written as

$$\mathcal{H}(r) = \mathcal{H}_A + \mathcal{H}_B - J(r) \left(\frac{1}{2} + 2\vec{S}_A \cdot \vec{S}_B \right) \quad (43)$$

where \mathcal{H}_A and \mathcal{H}_B are the spin Hamiltonians for the isolated radicals A and B. Usually these are considered the angular averaged of the hyperfine and Zeeman interactions. The last term represents the exchange interaction between the two radicals and depends parametrically upon their relative distance.

The superoperator $K(r)$ is introduced phenomenologically; the general features of it are that it is non zero only for $r \simeq d$, the distance of closest approach, and that it acts on the

electron spin degrees only. Two forms of $K(r)$ have been used. These are:

$$K(r)\rho = \frac{1}{2}k(r)[P_S, \rho]_+ \quad (44)$$

$$K(r)\rho = k(r)P_S\rho P_S, \quad (45)$$

when only singlet pairs are allowed to react. In these equations $[,]_+$ indicates the anticommutator and P_S is the singlet projection operator. The function $k(r)$ can be interpreted as the microscopic rate constant for the relaxation process that leads to a bonding state at the distance r . The differences and similarities between the two forms of $K(r)$ become more evident by considering their matrix representations, using the S-T basis. Note that the matrix representation of a superoperator requires four indices since it operates on operators which require two indices. Both forms of $K(r)$ lead to a diagonal matrix-representation. The former expression for $K(r)$ leads to

$$K(r)_{kk} = \begin{cases} k(r) & \text{for } k = SS \\ k(r)/2 & \text{for } k = (ST_i \text{ or } T_iS) \\ 0 & \text{otherwise} \end{cases} \quad (46)$$

while the latter yields

$$K(r)_{kk} = \begin{cases} k(r) & \text{for } k = SS \\ 0 & \text{otherwise} \end{cases} \quad (47)$$

It is seen that both forms of $K(r)$ have the same effect on the singlet diagonal elements, but the first form has an effect on the off-diagonal elements ρ_{ST_i} , too.

Spin relaxation is represented by R and for example a Redfield description may be used. This term can also include scavenging of the radicals by simply letting R equal $-k_S$ (i.e. the negative of the pseudo first order rate constant for scavenging) multiplied by the identity operator.

Complications in solving the equation of motion for ρ arise from the time dependence of r , which is caused by the diffusion of the radicals. However, the r -dependence of the Hamiltonian is due to the exchange interaction and this is non-negligible only for $r < r^*$; where r^* is a characteristic exchange distance, which may arbitrarily be defined by

$$J(r^*) = 10^8 \text{ rad/s} \quad (48)$$

where the numerical value is typical for a hyperfine interaction. Since $J(r)$ decays very fast this definition of r^* is rather insensitive to the value at the right hand side.

The reencounter picture is now introduced and the term average refers to the stochastic description of the relative motion of the two radicals. The average density matrices just before and just after the n 'th reencounter are designated by $\rho(n)$ and $\rho(n)'$, respectively. Since the equation of motion is a first order differential equation in time the following relations can be obtained:

$$\rho(n)' = M_i\rho(n) \quad (49)$$

$$\rho(n) = M_o\rho(n-1) \quad (50)$$

where the matrices M_i and M_o are the time dependent solutions averaged over the time spent respectively in and outside the exchange region. Since the change of the density matrix at the n 'th reencounter is

$$\rho(n)' - \rho(n) = (M_i - 1)\rho(n) \quad (51)$$

it follows that the fraction of radical pairs $F(n)$ that reacts during the n 'th reencounter is

$$F(n) = \text{Tr}[(1 - M_i)\rho(n)]. \quad (52)$$

The total fraction of radical pairs reacted is obtained by summing $F(n)$ over all reencounters n . This leads to:

$$F = \text{Tr} \left[\sum_{n=0}^{\infty} (1 - M_i)(M_o M_i)^n \rho(0) \right] \quad (53)$$

which, may be summed to

$$F = \text{Tr} \left[(1 - M_i)(1 - M_o M_i)^{-1} \rho(0) \right] \quad (54)$$

This general relation is independent of the specific diffusion model and of the exact form of the superoperators.

3.3 Approximations

Under certain conditions one can approximate the general expression and obtain simpler formulae which are useful for an investigation of the various dependences.

3.3.1 The reaction volume approximation

A calculation of the average quantity M_i is difficult for a general situation. Fortunately, the important part of a calculation of F is the M_o -determination and the reencounter summation. The simplest approximation for M_i is the reaction volume approximation which neglects all

superoperators except $K(r)$ in a finite reaction volume extending from d to r . The actual size of the reaction region in which single-triplet mixing is suppressed is important except for small magnetic interactions and low viscosity solvents.

Within this approximation M_i is simply equal to $\langle \exp(-Kt) \rangle$ where the average over contact times is performed by a Poisson distribution. Since K is diagonal in the S-T representation this is easily done. In accordance with the classical reencounter picture define the following two matrices

$$\lambda \equiv 1 - M_i; \quad (55)$$

$$\Lambda \equiv \lambda [1 - p(1 - \lambda)]^{-1} \quad (56)$$

These matrices are diagonal in the singlet-triplet representation with matrix elements

$$\lambda_{kk} = \begin{cases} \lambda & \text{for } k = SS \\ \frac{\lambda/2}{1-\lambda/2} & \text{for } k \in SS^\perp \text{ or } S^\perp S \\ 0 & \text{otherwise} \end{cases} \quad (57)$$

$$\Lambda_{kk} = \begin{cases} \frac{\lambda}{1-p(1-\lambda)} & \text{for } k = SS \\ \frac{\lambda/2}{1-\lambda/2-p(1-\lambda)} & \text{for } k \in SS^\perp \text{ or } S^\perp S \\ 0 & \text{otherwise} \end{cases} \quad (58)$$

where $|S^\perp\rangle$ indicates any vector in the orthogonal complement to $|S\rangle$, i.e. any vector in the subspace spanned by the triplet states. These two expressions are based on the former of the two forms for the operator $K(r)$. The matrices corresponding to the latter form of $K(r)$ is obtained from the above by setting the matrix elements equal to zero for $k \in SS^\perp$.

Introduction of Λ instead of M_i in the general expression leads to

$$F = \text{Tr} \left\{ \Lambda \left[1 + \frac{p\mathbf{1} - M_o}{1-p} (1 - \Lambda) \right]^{-1} \rho(0) \right\} \quad (59)$$

which is a convenient form for many purposes, e.g. expansions and limits.

3.3.2 The reaction surface approximation

In the limit where the extend of the reaction (or contact) region, i.e. $r_0 - d$, approach zero the recombination of the particles takes place on the surface of a sphere with radius d . This situation is in fact identical to the familiar use of boundary conditions in the theory of diffusion controlled reactions, cf. Eqs.(3) and (4).

The relevant equations for this situation can be obtained by letting $r \rightarrow d$ or identically $p \rightarrow 1$ in the above general expressions. However, some care has to be taken. The exact equation (54) for F expressed by M_i and M_o is not useful since both M_i and M_o depends on p . On the other hand the alternative exact expression Eq.(59) for F in terms of Λ and M_o are convenient since the value of Λ is considered an experimentally observed value which should not be changed. Thus only the average of the outside propagator M_o depends on the value of r . If we define

$$M' \equiv \lim_{p \rightarrow 1} \frac{p\mathbf{1} - M_o}{1-p} \quad (60)$$

then the following expression is obtained

$$F = \text{Tr} \left\{ \Lambda [1 + M'(1 - \Lambda)]^{-1} \right\} \rho(0) \quad (61)$$

which is exact when the recombination takes place on the surface of a sphere.

The calculation of M' proceeds as follows. Let the eigenvalues of the superoperator of the free radicals, i.e. $-i\mathcal{H}^x + \mathcal{R}$, be denoted $k_{ij} + i\omega_{ij}$. In a basis diagonalizing this superoperator the average propagators M_o and M' will also be diagonal with the corresponding matrix elements equal to

$$(M_o)_{ij,ij} = \tilde{R}(k_{ij} + i\omega_{ij}, r) \quad (62)$$

$$(M')_{ij,ij} = \tilde{L}(k_{ij} + i\omega_{ij}) \quad (63)$$

where the function $\tilde{L}(s)$ is expressible in terms of the previously introduced function $\tilde{R}'(s)$ as

$$\tilde{L}(s) \equiv 1 - \tilde{R}'(s)/\tilde{R}'(0) \quad (64)$$

Inserting the above expressing, Eq.(22), for $\tilde{R}'(s)$ gives

$$\tilde{L}(s) = \sqrt{\frac{s d_{eff}^2}{D}} \quad (65)$$

which shows that most of the details of the diffusion process have disappeared. For a complex argument $k + i2Q$ the function $\tilde{L}(s)$ can be written explicitly as

$$\tilde{L}(k + i2Q) = \sqrt{\frac{s_+ d_{eff}^2}{D}} + i \text{sgn}(Q) \sqrt{\frac{s_- d_{eff}^2}{D}} \quad (66)$$

where

$$s_\pm \equiv \left[\sqrt{k^2 + 4Q^2} \pm k \right]^{\frac{1}{2}} \quad (67)$$

3.3.3 Limit of slow diffusion or small magnetic interactions

If the diffusion is fast or the energy differences ω_{ij} of the spin system are small such that $\omega_{ij}\tau_d \ll 1$, where τ_d is a characteristic time for the diffusion process, then $M_o \simeq p\mathbf{1}$. If this is the case, or alternatively if the radicals are very reactive $\Lambda \simeq 1$, then one can approximate the inverse matrix by a series expansion. To first order one obtains

$$F = \text{Tr} \left\{ \Lambda \rho(0) - \Lambda \frac{p\mathbf{1} - M_0}{1-p} (\mathbf{1} - \Lambda) \rho(0) \right\} \quad (68)$$

which by use of any of the above forms of Λ can be directly evaluated to

$$F = \left(\Lambda - \Lambda(1-\Lambda) \frac{p - (M_o)_{SS,SS}}{1-p} \right) \rho(0)_{SS} + \Lambda \sum_{k \in S^\perp} \frac{(M_o)_{SS,kk}}{1-p} \rho(0)_{kk} \quad (69)$$

The scalar quantity Λ is equal to the classical probability of reaction and this is also equal to the SS,SS-element of Λ . If the triplet states are equally populated initially, i.e. $\rho(0)_{kk}$ is independent of k , then this expression can be simplified even further to

$$F = [\Lambda - \Lambda(1-\Lambda)F_{app}^*] \rho(0)_{SS} + \Lambda F_{app}^* (1 - \rho(0)_{SS}) \quad (70)$$

where

$$F_{app}^* \equiv \frac{p - (M_o)_{SS,SS}}{1-p} \quad (71)$$

In the derivation of this result we have used a sum rule [14] for the matrix elements of M_o . Several points should be emphasized. The equation is independent of the details of the diffusive motion and of the magnetic interactions; it only requires one of the conditions $\omega_{ij}\tau_d \ll 1$ or $\Lambda \simeq 1$ be satisfied. The equation is also independent of which of the two forms of the recombination operator $K(r)$ is being used. This remarkably simple equation shows that that spin dependent recombination probability can be expressed in terms of just two parameters: the reactivity parameter Λ and an efficiency parameter for the singlet-triplet mixing F_{app}^* . It is quite surprising that in order to calculate F^* only a single matrix elements of M_0 is needed, $(M_o)_{SS,SS}$.

4 Selected Applications

4.1 High field CIDNP

Outside the contact region where the exchange interaction can be neglected the pair Hamiltonian is equal to the sum of the Hamiltonians of the individual radicals, i.e.

$$\mathcal{H} = Q(S_{az} - S_{bz}) + E(S_{az} + S_{bz}) \quad (72)$$

where the parameters Q and E are half the sum and difference of the Larmor frequencies of the individual radicals, i.e.

$$\begin{aligned} \frac{E}{Q} &= \frac{1}{2}(g_a \pm g_b)\beta_e \hbar^{-1} B_0 + \frac{1}{2} \left(\sum_{j \in a} A_j M_j \pm \sum_{k \in b} A_k M_k \right) \end{aligned} \quad (73)$$

The matrix representation of \mathcal{H} and the propagator is easily obtained. One finds

$$\begin{Bmatrix} \rho_{ST_0} - \rho_{T_0S} \\ \rho_{ST_0} + \rho_{T_0S} \\ \rho_{SS} - \rho_{T_0T_0} \\ \rho_{SS} + \rho_{T_0T_0} \end{Bmatrix} (t) = \begin{Bmatrix} \cos(2Qt) & 0 & i \sin(2Qt) & 0 \\ 0 & 1 & 0 & 0 \\ i \sin(2Qt) & 0 & \cos(2Qt) & 0 \\ 0 & 0 & 0 & 1 \end{Bmatrix} \rho(0) \quad (74)$$

The M_o matrix is the above propagator averaged over the reencounter probability density $R(t)$. In the same matrix representation one finds that [15]

$$M_o = \begin{Bmatrix} c & 0 & is & 0 \\ 0 & p & 0 & 0 \\ is & 0 & c & 0 \\ 0 & 0 & 0 & p \end{Bmatrix} \quad (75)$$

where c and s are the cosine and sine transformed of $R(t)$

$$c \equiv \int_0^\infty \cos(2Qt) R(t) dt \quad (76)$$

$$s \equiv \int_0^\infty \sin(2Qt) R(t) dt \quad (77)$$

More generally these quantities may be expressed as the real and imaginary parts of the characteristic function $\tilde{R}(s)$

$$c = \Re \tilde{R}(k_s + i2Q) \quad (78)$$

$$s = -\Im \tilde{R}(k_s + i2Q) \quad (79)$$

where we have included scavenging, with a first order scavenging rate constant k_s , for generality. It now follows immediately that

$$(M_o)_{SS,SS} = \frac{p + c}{2} \quad (80)$$

and thus

$$F_{app}^* = \frac{1}{2} \frac{p - c}{1 - p} \quad (81)$$

Insertion herein of one of the approximate expressions c , Eqs.(32) – (37), and expansion of the results for $z_{\pm} \ll 1$ lead to

$$F_{app}^* = \frac{1}{2} \left(\frac{d_{eff}^2}{2D} \right)^{1/2} \left[(k_s^2 + 4Q^2)^{1/2} - k_s \right]^{1/2} \quad (82)$$

For negligible scavenging this expression reduces to

$$F_{app}^* = \frac{1}{2} \left(\frac{Qd_{eff}^2}{D} \right)^{1/2} \quad (83)$$

while for fast scavenging

$$F_{app}^* = \frac{1}{4} \left(\frac{k_s d_{eff}^2}{D} \right)^{1/2} \frac{Q^2}{k_s^2} \quad (84)$$

The square root dependence of F_{app}^* on Q is characteristic of 3-dimensional free diffusion and is obtained as well by approaches that include a single reencounter only. The independence of p is a result of the inclusion of all reencounters. Note that a scavenging reaction may enhance the Q -dependence of F^* from a square root to a quadratic dependence. However, an enhanced Q -dependence is accompanied by a reduction of the magnitude of F^* .

This limiting behaviour was also found numerically in [2]. To this order of approximation there is no difference between the three expressions for the recombination probability. A space dependent diffusion coefficient is formally equivalent to a potential and is therefore also covered by the above comments.

An exact analytic solution may also be obtained from the reencounter expression. The solution depends on the form of the recombination operator being used, unlike the case for the approximate result, but the dependence is weak, see below. When the operator affecting only the singlet diagonal term of the density matrix is used one obtains [16] the following simple relations

$$F = \frac{\Lambda F^*}{1 + F^*(1 - \Lambda)} [\rho(0)_{T_0 T_0} - (1 - \Lambda)\rho(0)_{SS}] + \Lambda\rho(0)_{SS} \quad (85)$$

where

$$F^* = \frac{(c_0 - c)(1 + c_0) - (c_0^2 - c^2 - s^2)}{2(1 - c_0)^2 + (c_0 - c)(3 - c_0) - (c_0^2 - c^2 - s^2)} \quad (86)$$

and the quantities c and s are defined in Eqs.(78) and (79) and

$$c_0 \equiv c(Q = 0) = \Re \tilde{R}(k_s) \quad (87)$$

Explicit expressions for c and s valid for 3-d continuous diffusion in an arbitrary potential are given in Eqs.(32) – (37). Note that this expression for F^* appears to deviate from that in [16]. This is caused by the present definitions of s and c which are equal to p times the former

definitions. If there is negligible scavenging then $k_s = 0$ and $c_0 = p$. This expression is sensitive to the difference between the two approximate expressions for $\tilde{R}(s)$ and larger deviations are found for larger values of Qd^2/D .

An exact calculation of F^* for the *surface reaction* case may be obtained by following the procedure outlined above, cf. Eqs.(60) – (61). The resulting expression for F^* is

$$F^* = \frac{x_+ + x_+^2 + x_-^2}{2 + 3x_+ + x_+^2 + x_-^2} \quad (88)$$

where

$$x_{\pm} \equiv \left(\frac{s_{\pm} d_{eff}^2}{D} \right)^{1/2} \quad (89)$$

and s_{\pm} is defined in Eq.(67).

The exact analytic expression depends on the form of the recombination operator $K(r)$ being used. However, the actual numerical differences between the two expressions are very small. The largest difference is found for highly reactive radicals ($\Lambda = 1$) to be of the order of 20 % for $Qd_{eff}^2/D \approx 1$; for values of Qd_{eff}^2/D or Λ smaller than 0.5 the difference is insignificant. There is also an effect of including the exchange interaction in the propagator M_i and again the effect is largest and of order 20 % for $Qd_{eff}^2/D \approx 1$ but it is rather insensitive to the value of Λ .

4.2 Effect of paramagnetic impurities

Mints and Pukhov [17] have previously studied the influence of paramagnetic impurities on magnetic effects in radical reactions. They obtained an analytic solution to the stochastic Liouville equation for free diffusion using the approximation that the recombination takes place on a reaction surface only. Since this problem appeared to be ideally suited to the reencounter formalism we [14] have repeated the calculation but for an arbitrary diffusion model and for a reaction volume of finite size.

The averaged propagator M_o is reasonably easy to obtain since the matrix representation of \mathcal{H}^x can be transformed to block diagonal form with a size of 2. After averaging and back transformation one finds that

$$(M_o)_{SS,SS} = \frac{a_1 + 2a_2 + p}{4} \quad (90)$$

and then by application of Eq.(71) that the approximate mixing parameter F_{app}^* is equal to

$$F_{app}^* = \frac{3p - a_1 - 2a_2}{4(1 - p)} \quad (91)$$

where

$$a_1 = \tilde{R}(4\alpha, r) \quad (92)$$

$$a_2 = \Re \tilde{R}(2\beta + i\Omega, r) \quad (93)$$

$$a_3 = \Im \tilde{R}(2\beta + i\Omega, r) \quad (94)$$

and α , β , and Ω are as defined by Mints and Pukhov, i.e.

$$\alpha = \frac{1}{4} (1/T_1^{(1)} + 1/T_1^{(2)}) \quad (95)$$

$$\beta = \frac{1}{2} (1/T_2^{(1)} + 1/T_2^{(2)}) \quad (96)$$

$$\Omega = (g_2 - g_1)\beta H_0/2\hbar \quad (97)$$

The real and imaginary parts of the characteristic function $\tilde{R}(s, r)$ have been given above for 3-dimensional diffusion in an arbitrary potential, Eqs.(32) – (35). Since F for arbitrary reactivity is expressed in terms of F_{app}^* by Eq.(70) an approximate calculation is easily performed.

An exact calculation can also be performed analytically and involves 4 by 4 matrix operations. The complete results are given elsewhere [14]. Here we illustrate the results by displaying the resulting equations for very reactive radicals (i.e. $\lambda = 1$):

$$\begin{aligned} F = \rho(0)_{SS} &+ \frac{a_1 - 2a_2 + a_1 a_2 + p(1 - 2a_1 + a_2)}{4 - 3a_1 - 2a_2 + a_1 a_2 - p(3 - 2a_1 - a_2)} \rho(0)_{T_0 T_0} \\ &+ \frac{-a_1 + a_1 a_2 + p(1 - a_2)}{4 - 3a_1 - 2a_2 + a_1 a_2 - p(3 - 2a_1 - a_2)} (\rho(0)_{T_- T_-} + \rho(0)_{T_+ T_+}) \end{aligned} \quad (98)$$

References

- [1] J. Boiden Pedersen and J. H. Freed. *J. Chem. Phys.*, 58:2746, 1973.
- [2] J. Boiden Pedersen and J. H. Freed. *J. Chem. Phys.*, 61:1517, 1974.
- [3] J. H. Freed and J. Boiden Pedersen. *Adv. in Mag. Res.*, 8:1, 1976.
- [4] K. Tominaga, S. Yamauchi, and N. Hirota. *Chem. Phys. Lett.*, 179:35, 1991.
- [5] J. Boiden Pedersen and P. Sibani. *J. Chem. Phys.*, 75:5368, 1981.
- [6] J. Boiden Pedersen. *J. Chem. Phys.*, 72:3904, 1980.
- [7] V. Gösele. *Chem. Phys. Lett.*, 69:332, 1980.
- [8] J. E. Larsen and J. Boiden Pedersen. *J. Comp. Phys.*, 49:458, 1983.
- [9] P. Sibani and J. Boiden Pedersen. *Phys. Rev. Lett.*, 51:148, 1983.
- [10] K. Razi Naqvi, K. J. Mork, and S. J. Waldenström. *J. Phys. Chem.*, 84:1315, 1980.
- [11] R. M. Noyes. *J. Chem. Phys.*, 22:1349, 1954.
- [12] F. J. Adrian. *J. Chem. Phys.*, 53:3374, 1970.
- [13] M. Tachiya. *J. Chem. Phys.*, 70:238, 1979.
- [14] L. Lolle and J. Boiden Pedersen. *In preparation*.
- [15] J. Boiden Pedersen. *Chem. Phys. Lett.*, 52:333, 1977.
- [16] J. Boiden Pedersen. *J. Chem. Phys.*, 67:4097, 1977.
- [17] R. G. Mints and A. A. Pukhov. *Chem. Phys.*, 87:467, 1984.

Formation of Novel Radicals from the $\pi\pi^*$ Triplet States of Aromatic Ketones

Hisaharu Hayashi, Masatoshi Igarashi, Yoshio Sakaguchi,
Molecular Photochemistry Laboratory, The Institute of Physical and Chemical
Research, Wako, Saitama 351-01, Japan
and Y. J. THaya
Department of Applied Physics and Chemistry, The University of Electro-
Communications, Chofu, Tokyo 182, Japan

Abstract

In the photochemical hydrogen abstraction reactions of aromatic ketones, we have found the formation of novel radicals such as cyclohexadienyl-type, benzyl-type, and α -keto alkyl radicals with the aid of a time-resolved ESR technique. These radicals can be produced through the reactions of the lowest $\pi\pi^*$ triplet states of the ketones, which have been believed to be much less reactive than their lowest $n\pi^*$ ones.

1. Introduction

In the course of the studies of magnetic field effects on photochemical reactions in solution [1, 2], we have carried out CIDEP and CIDNP studies on such reactions as to be influenced by external magnetic fields. In 1985, we found a peculiar CIDEP spectrum due to a cyclohexadienyl-type radical in the reaction of triplet xanthone with triethylgermane (Et_3GeH) in an SDS micelle as shown in Fig. 1 [3]. This was not only one of the earliest observation of so-called "spin-correlated radical pairs" [4] but also the first report on the formation of non-ketyl radicals in the hydrogen abstraction reactions of triplet ketones.

We have also found the formation of cyclohexadienyl-type radicals in the reactions of acetophenone and 2-acetonaphthon [5] and that of benzyl-type ones in flavones [6]. We have found that these novel radicals can be formed with "hydride-type" hydrogen donors such as Et_3GeH and tri-n-butylstannane (Bu_3SnH) through the $\pi\pi^*$ triplet states of aromatic ketones.

Since the lowest $n\pi^*$ and $\pi\pi^*$ triplet states of chromone locate close to each other, we also tried to study its reaction with Bu_3SnH in 2-propanol with the aid of a time-resolved ESR technique [7].

2. Experimental section

The laser flash photolysis-ESR apparatus and the flow system of the sample solutions were similar to those described elsewhere [3-6]. A Varian E-109 X-band ESR spectrometer of the University of Electro-Communications was used for time-

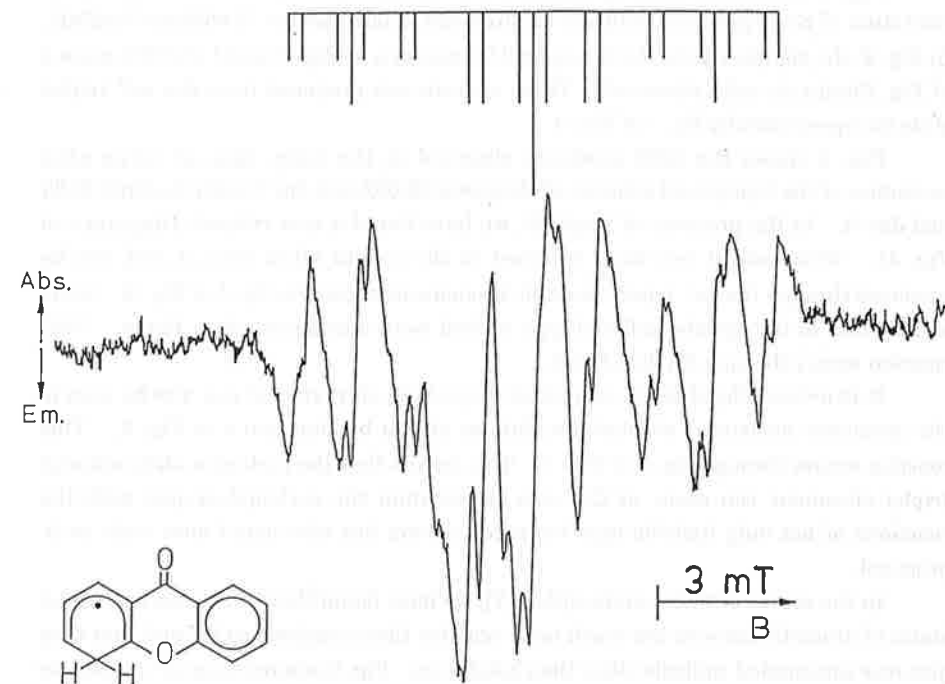


Fig. 1. CIDEP spectrum observed at 1.5 μs after excitation of the SDS micellar solution containing xanthone and Et_3GeH [3].

resolved measurements without field modulation. The solutions employed were bubbled with pure nitrogen gas prior to the measurement. A Lumonix EX510 excimer laser (XeCl , $\lambda=308\text{nm}$) was used as an exciting light source. All time-resolved ESR spectra were measured at room temperature with a time width of $0.2\text{ }\mu\text{s}$.

3. Results and discussion

Fig. 2 shows the ESR spectrum observed at the delay time of $1.2\text{ }\mu\text{s}$ after excitation of the 2-propanol solution of chromone (0.002 mol dm^{-3}) without Bu_3SnH . In Fig. 2, the signals due to the 2-propanol (Diagram a of Fig. 2) and ketyl (Diagram b of Fig. 2) radicals were observed. These radicals are produced from the $n\pi^*$ triplet state as represented by Eq. 1 of Fig. 3.

Fig. 4 shows the ESR spectrum observed at the delay time of $1.2\text{ }\mu\text{s}$ after excitation of the 2-propanol solution of chromone (0.002 mol dm^{-3}) with Bu_3SnH (0.04 mol dm^{-3}). In the presence of Bu_3SnH , we have found a new radical (Diagram c of Fig. 4). This radical has been assigned to the α -keto alkyl radical and can be produced through the $\pi\pi^*$ triplet state of chromone as shown by Eq. 4 of Fig. 3. Weak signals due to the cyclohexadienyl-type radical were also observed in Fig. 4. This reaction occurs through Eq. 6 of Fig. 3.

It is noteworthy that the signals of this α -keto alkyl radical can also be seen in the spectrum measured without Bu_3SnH as shown by Diagram c in Fig. 2. This reaction occurs through Eq. 2 of Fig. 3. This means that the hydrogen abstraction of triplet chromone can occur at C-atoms rather than the carbonyl-oxygen with the reactions of not only hydride-type hydrogen donors but also usual ones such as 2-propanol.

In the course of these studies [3,5,6,7], we have found that the lowest $n\pi^*$ triplet states of aromatic ketones are much more reactive than imagined so far and that they give new unexpected radicals other than ketyl ones. Fig. 5 summarizes our results for the formation of novel radicals such as cyclohexadienyl-type, benzyl-type, and α -keto alkyl ones from $n\pi^*$ triplet states of aromatic ketones.

In fig. 6, the mechanism for giving such novel radicals is shown. Usual hydrogen donors such as 2-propanol can be called “proton-type” ones, where the hydrogen atom to be abstracted is positively charged compared to the connecting atom. Thus, the hydrogen atom should be close to the carbonyl-oxygen which is negatively charged in the ground state. Since the oxygen atom is the most reactive in the lowest $n\pi^*$ triplet state of an aromatic ketone, it can easily abstract the hydrogen, forming a ketyl radical.

On the other hand, special hydrogen donors such as Et_3GeH , Bu_3SnH , and sodium borohydride can be called “hydride-type” ones, where the hydrogen atom to be

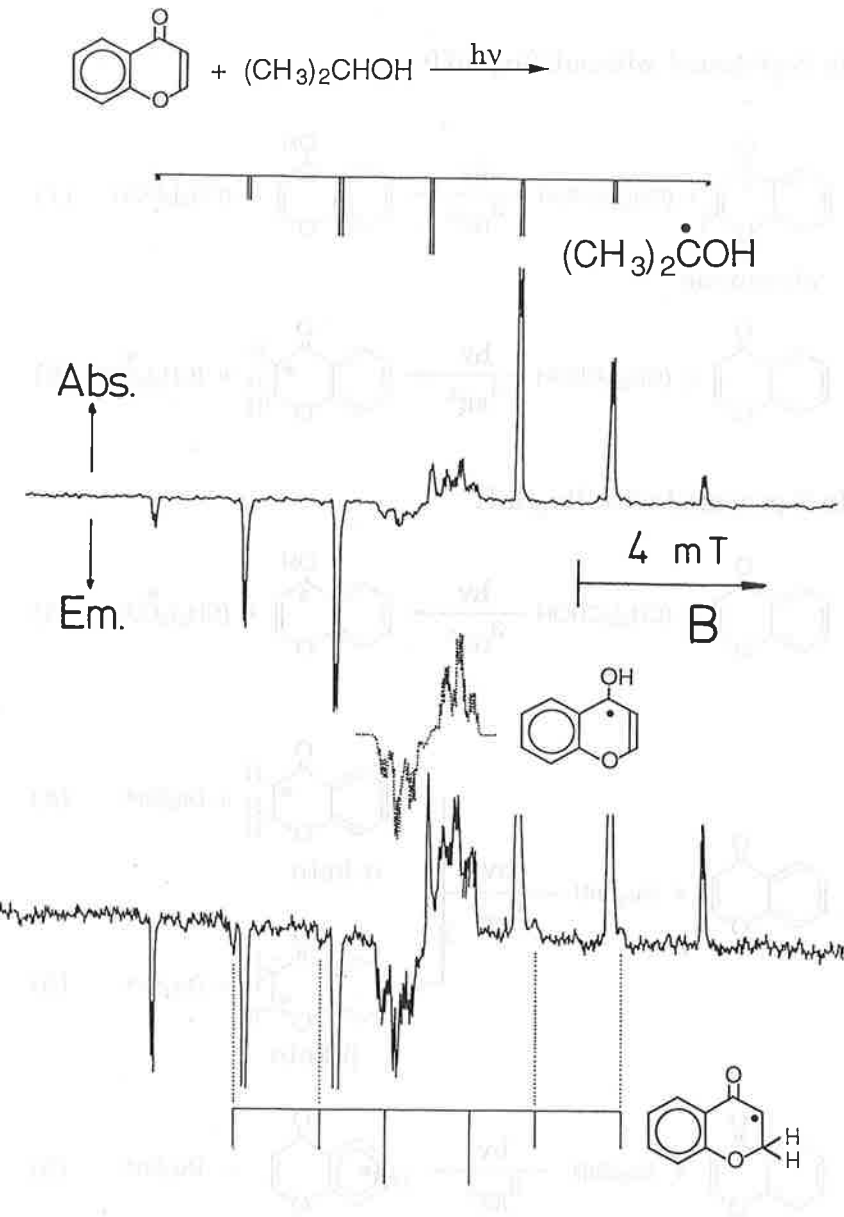
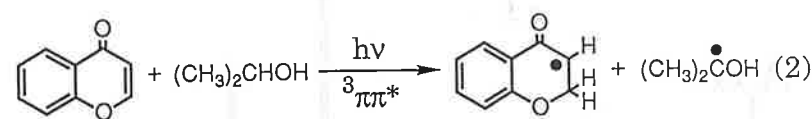
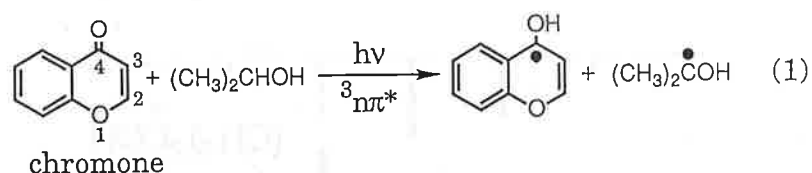


Fig. 2. CIDEP spectra observed at $1.2\text{ }\mu\text{s}$ after excitation of the 2-propanol solution containing chromone [7].

In 2-propanol without Bu_3SnH



In 2-propanol with Bu_3SnH

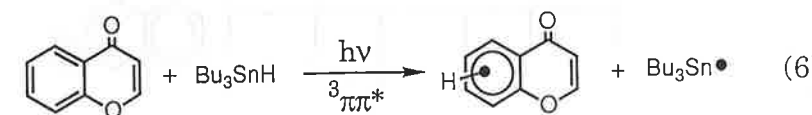
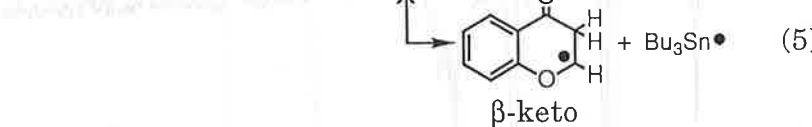
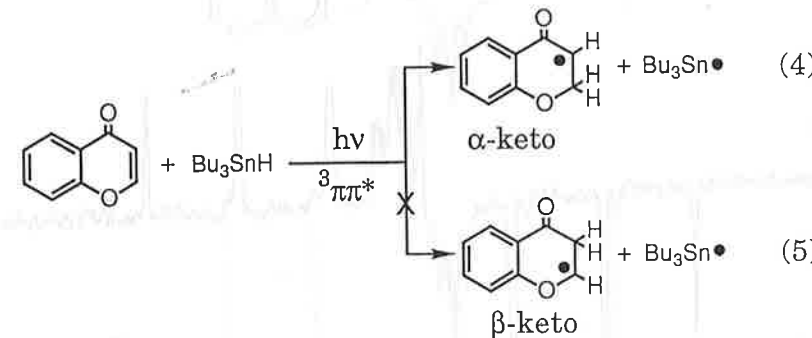
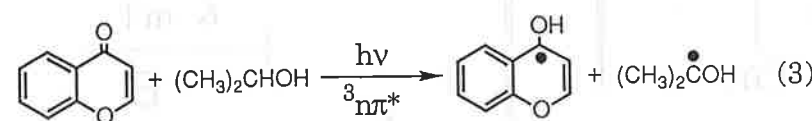


Fig. 3. Reaction schemes of triplet chromone with and without Bu_3SnH in 2-propanol.

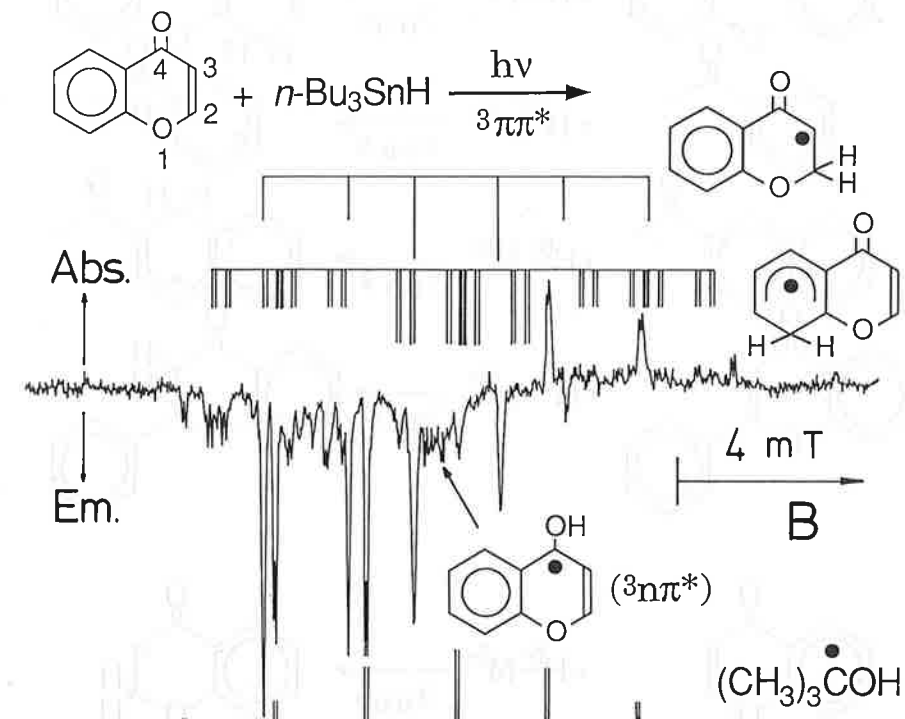


Fig. 4. CIDEP spectrum observed at $1.2 \mu\text{s}$ after excitation of the 2-propanol solution containing chromone and Bu_3SnH [7].

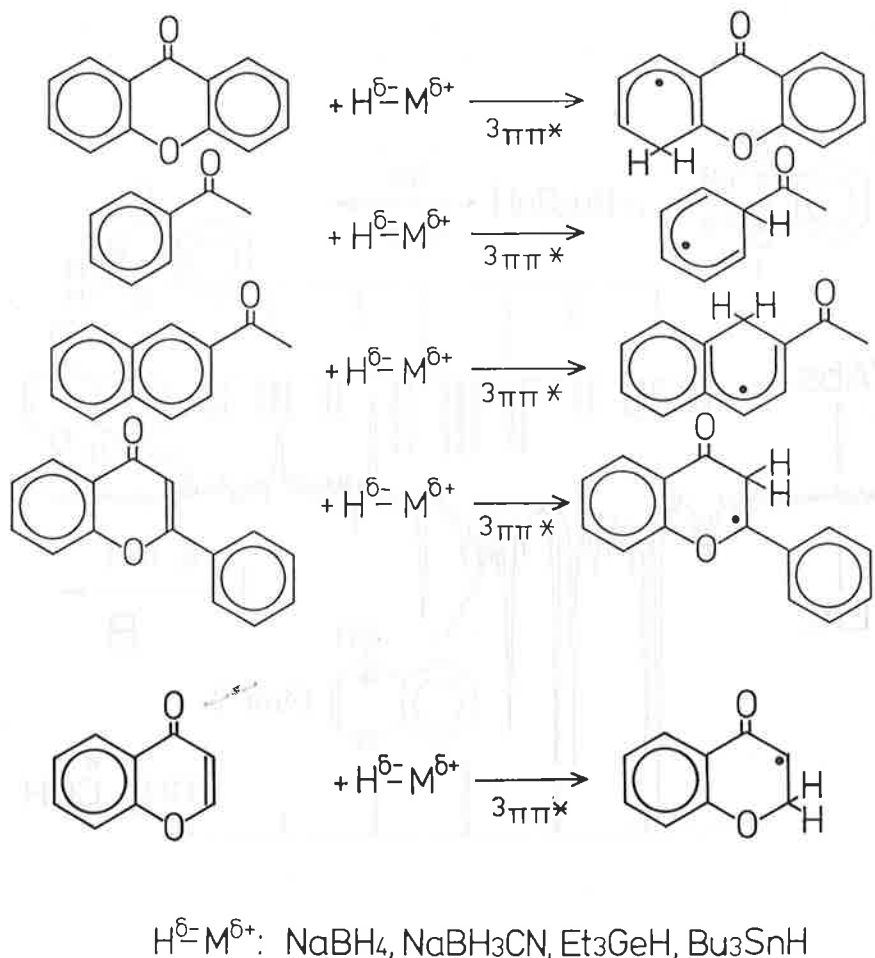


Fig. 5. Summary of our results for the formation of novel radicals from $\pi\pi^*$ triplet states of aromatic ketones. Here, main reactions are only shown.

As far as we know, this is the first report of all these three kinds of radicals formed from the same aromatic ketone under different conditions. These three kinds of radicals have been confirmed by ESR spectra and quantum chemical calculations. The radical formed from the aromatic ketone with the lowest energy triplet state ($3\pi\pi^*$) is a cyclohexadienyl radical, which has been reported previously.¹⁰ The radical formed from the aromatic ketone with the intermediate energy triplet state ($3n\pi^*$) is a non-ketyl radical, which has also been reported previously.¹¹ The radical formed from the aromatic ketone with the highest energy triplet state ($3\pi\pi^*$) is a ketyl radical, which has not been reported previously.

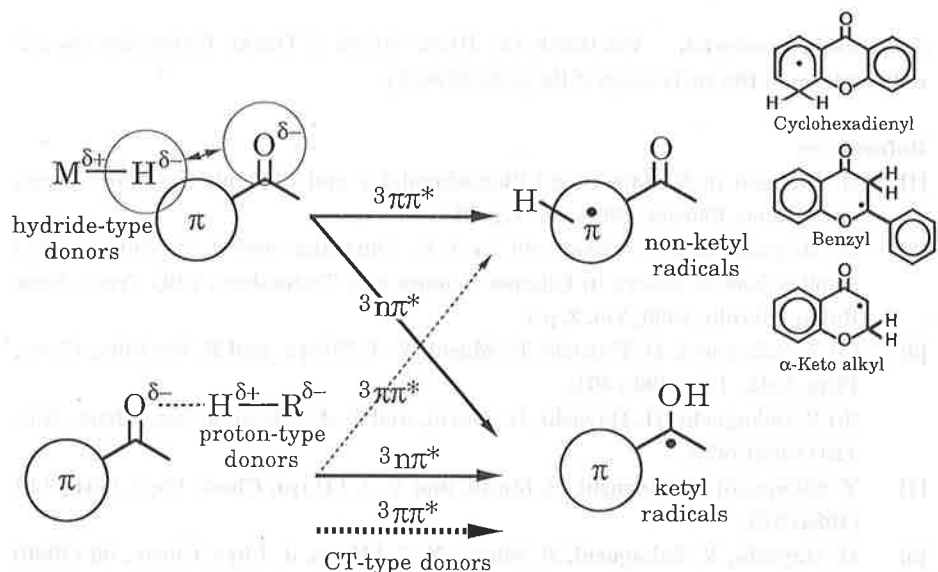


Fig. 6. Mechanism for giving novel radicals from $\pi\pi^*$ triplet states of aromatic ketones.

abstracted is negatively charged compared to the connecting atom. Thus, the hydrogen atom should be repelled from the carbonyl oxygen, but should be attracted to carbon atoms in the π -conjugated system. The reactivity of the carbonyl-oxygen of the $\pi\pi^*$ triplet state is so strong that it can abstract even the hydrogen of an "hydride-type" hydrogen donor. On the other hand, the reaction through the lowest $\pi\pi^*$ one should occur at the carbon-atoms to which the hydrogen is attracted. It is noteworthy that such a novel reaction of the $\pi\pi^*$ triplet state can occur not only with hydride-type hydrogen donors but also with proton-type ones such as 2-propanol.

Acknowledgement. We thank Dr. Hisao Murai of Osaka University for his collaboration at the early stage of the present study.

References

- [1] H. Hayashi in F. Rabek (ed.) Photochemistry and Photophysics, CRC Press, Boca Raton, Florida, 1990, Vol. 1, p.59.
- [2] H. Hayashi and Y. Sakaguchi in J.-P. Fouassier and J. F. Rabek (eds.) Applications of Lasers in Polymer Science and Technology, CRC Press, Boca Raton, Florida, 1990, Vol. 2, p.1.
- [3] (a) Y. Sakaguchi, H. Hayashi, H. Murai, Y. J. I'Haya, and K. Mochida, Chem. Phys. Lett., 120 (1985) 401;
 (b) Y. Sakaguchi, H. Hayashi, H. Murai, and Y. J. I'Haya, J. Am. Chem. Soc., 110 (1984) 7479.
- [4] Y. Sakaguchi, H. Hayashi, H. Murai, and Y. J. I'Haya, Chem. Phys. Lett., 110 (1984) 275.
- [5] H. Hayashi, Y. Sakaguchi, H. Murai, Y. J. I'Haya, J. Phys. Chem., 90 (1986) 4403.
- [6] Y. Sakaguchi, H. Hayashi, H. Murai, and Y. J. I'Haya, J. Phys. Chem., 90 (1986) 6416.
- [7] M. Igarashi, Y. Sakaguchi, H. Hayashi, and Y. J. I'Haya, Chem. Phys. Lett., 181 (1991) 187.

CIDEP of benzil

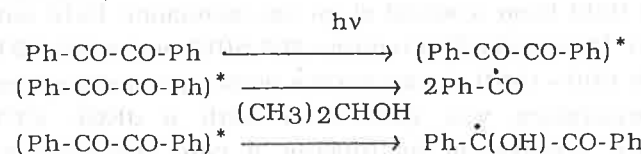
Masahiro Mukai, Seigo Yamauchi[†] and Noboru Hirota
 Department of Chemistry, Faculty of Science
 Kyoto University, Kyoto 606 (Japan)

Abstract

Photolysis of benzil in 2-propanol gives emissive CIDEP signals which are assigned to benzoyl and benzil ketyl radicals. The signal of the benzoyl radical decays very quickly, but the ketyl signal shows a slow rise and then decays slowly. Possible mechanisms to produce the slow rise are examined. The time profile of the ketyl signal is strongly dependent on the temperature, the concentration of benzil and the excitation laser power. The time profiles are simulated on the assumption that the slow rise components are due to the free pair RPM. Good agreements were obtained between the observed and the simulated time profiles.

1. Introduction

Transient radicals detected by TREPR (time-resolved EPR) in the photolysis of benzil in 2-propanol are benzoyl and ketyl radicals. They are considered to be produced by the following reactions,



The CIDEP spectra of both radicals observed immediately after the laser excitation show net emissions (E pattern). There are two possibilities for the net polarization pattern, a radical pair mechanism (RPM) involving a S-T₀ mixing (ST₀M) with different g values of pair radicals and a triplet mechanism (TM). Δg is zero for the formation of the benzoyl radical and is too small to produce a large polarization for the ketyl radical. Consequently the TM was considered to be responsible for the observed emissive polarization. However, the emissive polarization cannot be explained on the basis of the reactions from the lowest excited triplet (T_1) state of benzil, because absorptive signals are expected

from the polarities of the triplet spectra of benzil in rigid media. It was also found that the signal intensities are proportional to the square of the laser power. These observations led us to propose that the reactions take place from higher excited triplet states via two-photon processes.¹⁾ In the present work we have studied time-profiles of the CIDEP signals in detail. We have found that in addition to the signals observed immediately after the photolysis there is a slow rising component in the ketyl signal. In this paper we focus our attention to this slow component.

2.Experimental

Benzil (Nacalai Tesque) was recrystallized from ethanol several times and zone refined extensively. 2-propanol (wako) of spectrograde was used without further purification. Concentrations of benzil in solutions were $10^{-2} \sim 10^{-3}$ M. The solutions were deaerated by blowing nitrogen gas and flowed in a quartz tube of 2.5 mm i.d. at a rate of 0.3 ml/min. The TREPR signals were detected without field modulation with a JEOL-FE3X EPR spectrometer using an excimer laser (Lumonics HE440UBB with a XeCl fill). The spectra were taken at $0.4 \sim 0.8 \mu\text{s}$ after the laser excitation by feeding an output of a modified preamplifier of a microwave unit to a PAR 160 boxcar integrator. The time profile of the transient EPR signal was obtained by subtracting a ghost signal at an off-resonance field from a signal at an on-resonance field with a transient recorder (Kawasaki Electronica MR 50E) and a HP 9816 computer. Normally 600~1000 decay curves were accumulated and averaged. The temperature was controlled with a JEOL VT3A variable temperature cryosystem by flowing a cold nitrogen gas through a quartz dewar.

3.Results and discussion

Fig.1 shows the CIDEP spectrum of benzil in 2-propanol. The spectrum consists of the superposition of the spectra of the benzoyl and ketyl radicals. The time profiles of the CIDEP signals are shown in Fig.2. The benzoyl radical signal decays very quickly with a decay rate constant of $2 \times 10^6 \text{ s}^{-1}$ presumably because of a very fast spin lattice-relaxation time, but the decay of the ketyl signal is very slow. The rise of the ketyl signal consists of two

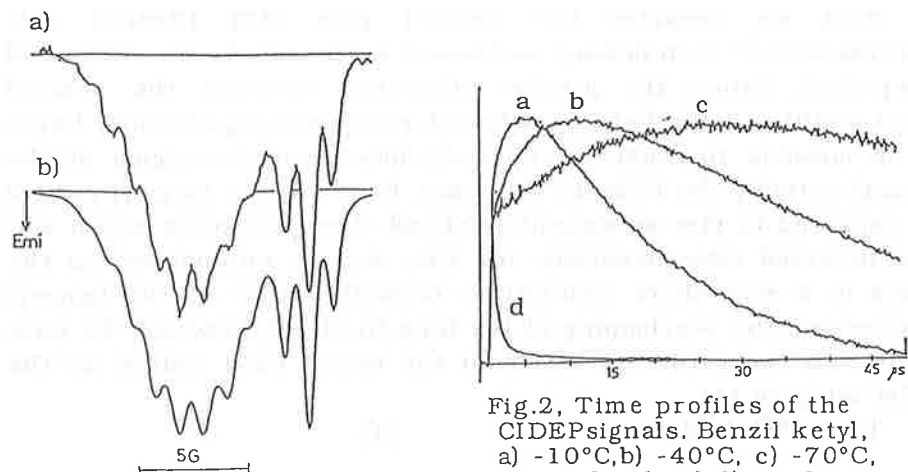


Fig.1, CIDEP spectrum of benzil in 2-propanol
a) observed, b) simulated

Fig.2, Time profiles of the CIDEP signals. Benzil ketyl,
a) -10°C, b) -40°C, c) -70°C,
benzoyl radical d), under
nitrogen bubbling

components, a fast one completing within $0.2 \mu\text{s}$ and a slow one. The fast rise is not very sensitive to the temperature, but the slow rise as well as the decay are very dependent on the temperature as shown in Fig.2. The two component rise becomes quite evident at lower temperatures. We now try to clarify the mechanism to produce this slow rise and decay.

It was recently suggested by Blättler et al.²⁾ that such a slow rising polarization might be produced by the encounter between the radical and triplet molecule (Radical Triplet pair mechanism, RTPM). We first consider this possibility. Since this mechanism requires the presence of a relatively long-lived triplet state, we have compared the CIDEP signals under nitrogen and oxygen bubbling conditions. The triplet state of benzil is quenched effectively by oxygen and the triplet lifetime under oxygen bubbling conditions becomes 0.2 and $0.3 \mu\text{s}$ at -10 and -40°C, respectively. However, the time profiles of the ketyl signals under oxygen bubbling conditions still show slow rising components as under nitrogen bubbling conditions though the rise times as well as the signal intensities are reduced considerably. This observation seems to indicate that the RTPM cannot account for the slow rising polarization entirely, though it may contribute partly.

Next we consider the free(F-) pair RPM (Radical pair mechanism).³⁾ Both benzoyl and benzil ketyl radicals are stable and long-lived. Since the g-value difference between the benzoyl ($g=2.0009$) and the ketyl ($g=2.0046$) radicals is significantly large, it is possible to obtain a relatively large emissive signal of the benzil ketyl by the RPM. In this case, however, the benzoyl radical was expected to give an absorptive signal. The absorptive signal was not detected experimentally, but this may be rationalized on the basis of a very short spin-lattice relaxation time of the benzoyl radical and the overlapping of the long-lived ketyl radical. We have simulated the CIDEP spectrum of the benzil ketyl radical by the RPM using eq (1)

$$P_{la} \propto \text{sign}(Q_{ab}) \sqrt{|Q_{ab}|} \quad (1)$$

$$Q_{ab} = \frac{1}{2} \left\{ (g_1 - g_2) \mu_B B + \left(\sum_i A_{1i} m_{1i} - \sum_j A_{2j} m_{2j} \right) \right\}$$

Here P_{la} is the polarization of the ketyl radical at the nuclear spin state a . Q_{ab} was calculated using the corresponding g values and hyperfine splittings of the benzoyl and ketyl radicals. The simulated spectrum is shown in Fig.3 together with the spectrum observed at 20μs after photolysis at -40°C. The agreement between the observed and the simulated spectra is considered to be satisfactory.

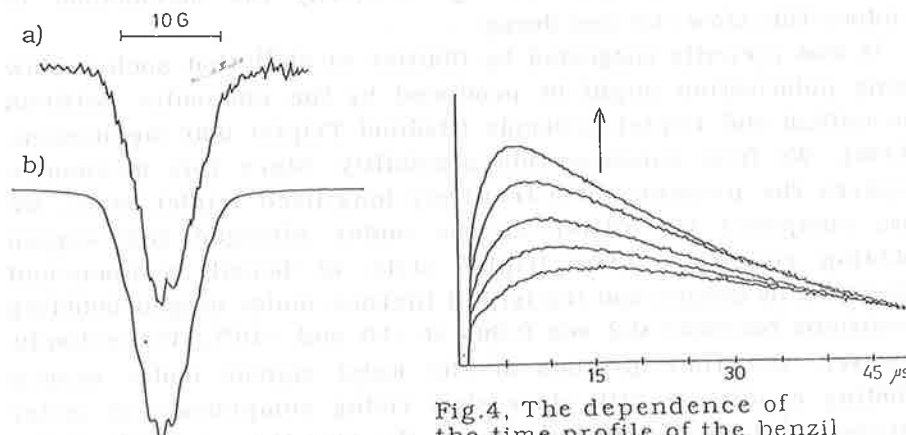


Fig.3. Spectrum of the benzil ketyl at a longer time (-40°C)
a) observed at $t=20\mu s$
b) simulated by the RPM

The time profile of the CIDEP signal of the benzil ketyl radical is extremely temperature dependent as seen from Fig.2. It also depends on the concentration of benzil and the excitation laser power. The power dependence is shown in Fig.4. These dependences show that the slow rising component depends on the radical species produced by the excitation of benzil. We have tried to simulate these time profiles on the basis of the F-pair RPM. The time dependence of the signal intensity for the F-pair polarization is given by eq (2) under the assumption, $T_2=T_1$, $\omega_1^2 T_1 \ll 1$ and the second order decay of the radical,^{4,5)}

$$M_y^f(t) = A \frac{KT_1^2}{(1+n_0 Kt)^2} n_0^2 \left[1 - \left(\frac{t}{T_1} + 1 \right) \exp \left(- \frac{1}{T_1} t \right) \right] \quad (2)$$

where n_0 is the concentration of the radical.

The initial rise and decay of the fast component is given by

$$M^0(t) = B n_0 \left\{ \exp \left(- \frac{t}{T_1} \right) - \exp(-kt) \right\} \quad (3)$$

The overall time profile is given by the sum of $M^0(t)$ and $M_y^f(t)$. Simulated time profiles shown in Fig.5 were obtained by making A/B , K , n_0 , k and $1/T_1$ adjustable parameters. It is seen that the observed time profiles are reproduced reasonably well by the simulation.

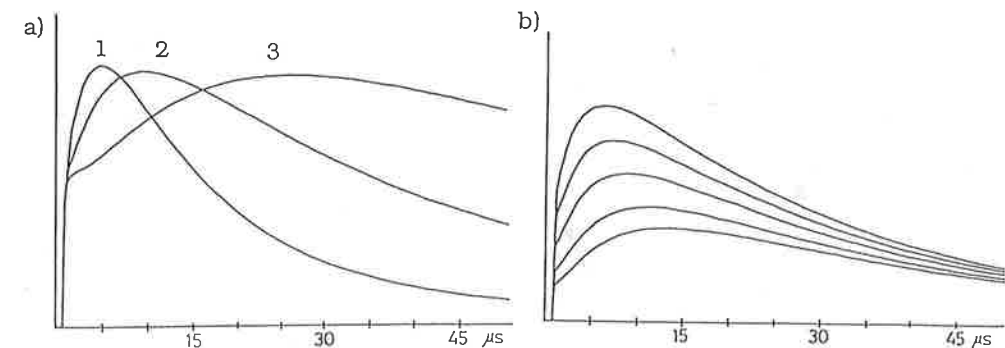


Fig.5 Simulations of the time profiles of (a) the temperature dependence with $k=0.1\mu s$ $n_0=0.7$ (1) $A/B=3$ $K=0.65$ $T_1=8\mu s$ (2) $A/B=1.3$ $K=0.35$ $T_1=22$ and (3) $A/B=0.8$ $K=0.1$ $T_1=40$ and (b) the laser power dependence with $A/B=2.3$ $K=1$ $k=0.1\mu s$ $T_1=20\mu s$, $n_0=0.2, 0.27, 0.4, 0.54$ and 0.7 from bottom to top.

The temperature dependence of the time profile given in Fig.2 is reproduced by changing K and T₁. The power dependence is explained in terms of the change in n₀. Then the observed time profiles seem to be explained satisfactorily on the basis of the F-pair RPM.

In conclusion we think that the F-pair RPM is most likely to be the main mechanism to produce the slow rising emissive polarization observed in the photolysis of benzil.

References

- (1) M.Mukai,S.Yamauchi and N.Hirota,J.Phys.Chem.93(1989)4411
- (2) C.Blättler,F.Jent and H.Paul,Chem.Phys.Lett.166(1990)375
- (3) F.J.Adrian,J.Chem.Phys.54(1971)3918
- (4) J.B.Pedersen,J.Chem.Phys.59(1973)2656
- (5) N.C.Verma and R.W.Fessenden,J.Chem.Phys.65(1976)2139

+ present address

Institute for Chemical reaction Science,
Tohoku University, Sendai 920, Japan

Electron Spin Polarization

Generated in Singlet-Doublet and Triplet-Doublet Systems

Kinichi Obi and Akio Kawai

Department of Chemistry, Tokyo Institute of Technology,
Ohokayama, Meguroku, Tokyo 152, Japan

ABSTRACT

Electron spin polarization was observed in the singlet-doublet and triplet-doublet systems by time resolved ESR. A + A/E pattern CIDEP was generated on radical in singlet-doublet systems, whereas E + E/A pattern CIDEP was generated in triplet-doublet systems. These two types of CIDEP generation was interpreted by doublet and quartet precursor RTPM's, respectively.

1. INTRODUCTION

Just after the pulsed photoirradiation, many kinds of short lived excited molecules and intermediate species coexist interacting with each other and play an obscure but important role in photophysical and photochemical processes. Several kinetic studies have been reported on the quenching of the lowest excited singlet (S_1) or triplet (T_1) state with free radicals, but its detail is not revealed yet. ESR method has an advantage to investigate the paramagnetic species but is not applied to study the excited state quenching with free radical except for a few works.^{1,2)} Time resolved ESR detects CIDEP which is generated through the magnetic interaction between paramagnetic species. We applied CIDEP to the study of quenching process of excited molecules with radicals and found out new mechanisms of CIDEP generation in the excited molecule-radical interaction.

2. EXPERIMENTAL

A conventional X-band ESR spectrometer (Varian E-112) was used to measure TR-ESR spectra. Transient ESR signals obtained without field modulation were transferred to a boxcar integrator (Stanford SR-250) for spectrum measurements or a transient memory (Iwatsu DM-901) for CIDEP decay profiles. The excitation light source was a XeCl excimer laser (Lambda Physik LPX 100). The sample solution was deaerated by bubbling of nitrogen gas and flowed through a quartz flat cell (0.5 mm interior space) in ESR cavity.

3. RESULTS AND DISCUSSION

Fig.1 shows the time resolved ESR spectra of various molecule-TEMPO (*2,2,6,6-tetramethyl-1-piperidinyloxy*) systems. Spin polarized TEMPO was observed with E+E/A pattern in benzophenone and acetone systems. On the contrary, A+A/E pattern was observed in the coronene and fluoranthene systems. E and A mean emission and absorption, respectively.

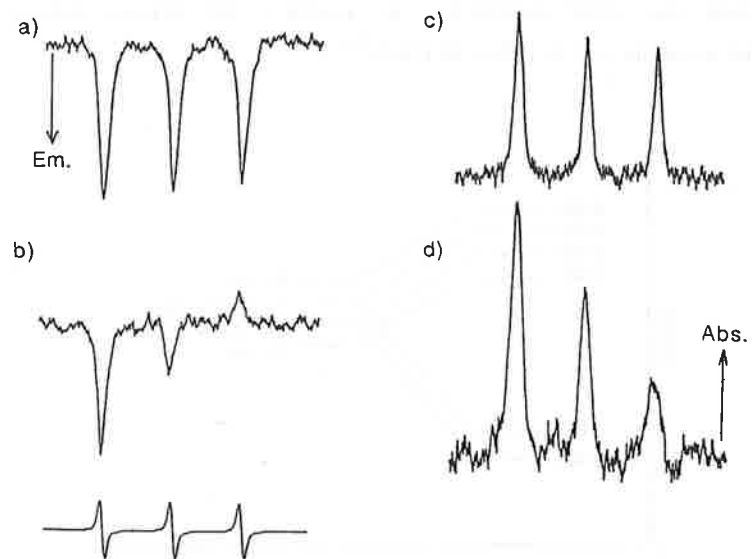


Fig.1 Time resolved ESR spectra obtained in TEMPO and a) benzophenone, b) acetone, c)coronene, d) fluoranthene mixture in benzene solution. Spectra were observed at 1 μ s after 308 nm laser excitation.

Paul and his coworkers reported²⁾ the net emissive CIDEP on radicals by radical triplet pair mechanism (RTPM), but in our systems, not only net emissive CIDEP but also E/A, A and A/E patterns of CIDEP were obtained. We observed CIDEP in many excited molecule-TEMPO systems and summarized the results as follows.

<Systems>	<CIDEP pattern>
Case 1. molecules with long lived S_1 state and radical	A + A/E
Case 2. molecules with high yield of T_1 state and radical	E + E/A

To explain the CIDEP generation, we consider the triplet-radical pair potential assuming $J < 0$ as shown in fig.2.³⁾

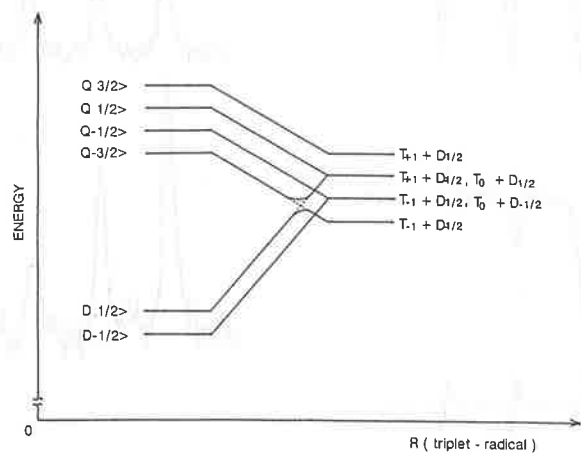


Fig.2 potential of triplet molecule and radical pair.

First, we discuss the net polarization. The $|Q-3/2\rangle$ and $|D1/2\rangle$ states show avoided crossing due to the zfs interaction of triplet molecule. As Paul suggested, doublet states of triplet-radical pair vanished owing to the quenching of T_1 state with radicals. Hence, during the course of dissociation of the pair, net emissive CIDEP is generated on radical, which is observed as the case 2 signal. On the other hand, if the radical quenches the S_1 state molecule, doublet states of triplet-radical pair are generated due to S_1-T_1 enhanced intersystem crossing. This initial condition of triplet-radical pair is opposite to that in above mechanism, and hence produces the net absorptive CIDEP on radical with the same mechanism. This is consistent with experimental results in case 1.

We obtained two types of RTPM's from above discussion and these mechanisms are expected to operate simultaneously in a system where the rate of S_1-T_1 ISC is comparable with that of enhanced ISC. An good example of such a case is naphthalene ($k_{ISC}=10^6\text{ s}^{-1}$). Fig.4 shows decay profiles of triplet-TEMPO systems. In case of the 1-chloronaphthalene-TEMPO system, emissive CIDEP is observed throughout the profiles, which is typical type of quartet precursor RTPM. On the other hand, in time profile of the naphthalene-TEMPO system, phase of CIDEP is absorption for the first $0.4 \sim 0.8\text{ }\mu\text{s}$ and is turned to emission after $0.8\text{ }\mu\text{s}$ which is continued to end of its decay. This phase turning is interpreted by the switching of the CIDEP generation mechanism from doublet precursor RTPM to quartet one with time. In early gate time, doublet precursor RTPM is dominant because the S_1 state of naphthalene is first quenched by radicals and forms the doublet spin states of radical-triplet pair. In later stage, radicals encounter the triplet state of naphthalene and quartet spin states survive in triplet-radical pair during triplet quenching, which results in emissive CIDEP signal observed in later gate time. To confirm this mechanism, we added 1,3-pentadiene to the naphthalene-TEMPO

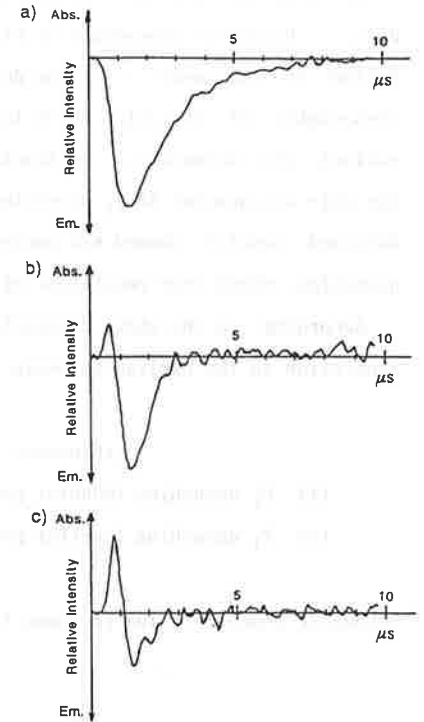


Fig.4 Decay profile of CIDEP signal in a)1-chloronaphthalene-TEMPO, b)naphthalene-TEMPO and c) b)+1,3-pentadiene. Concentration of TEMPO is $6 \times 10^{-4}\text{ M}$.

Secondly, we interpret the hyperfine dependence of CIDEP in the T_1 -radical pair. Hyperfine dependence of CIDEP is explained by the $|Q\pm 1/2\rangle - |D\pm 1/2\rangle$ mixing in the none J region due to hyperfine interaction followed by reencounter of the pair, which is the similar to S- T_0 mixing mechanism of radical pair mechanism. We simulated the spectra assuming initial state of the pair was quartet in T_1 quenching, doublet state in S_1 quenching, and $J<0$. Obtained results showed E/A pattern in T_1 quenching and A/E pattern in S_1 quenching, which were consistent with the experimental results.

According to the above discussion, we concluded the general rule of CIDEP generation in the excited molecule-radical interaction as follows.

<Process>	<CIDEP pattern>
(1) S_1 quenching (doublet precursor RTPM)	A + A/E
(2) T_1 quenching (quartet precursor RTPM)	E + E/A

Schematic representation is shown in fig.3 for both RTPM's.

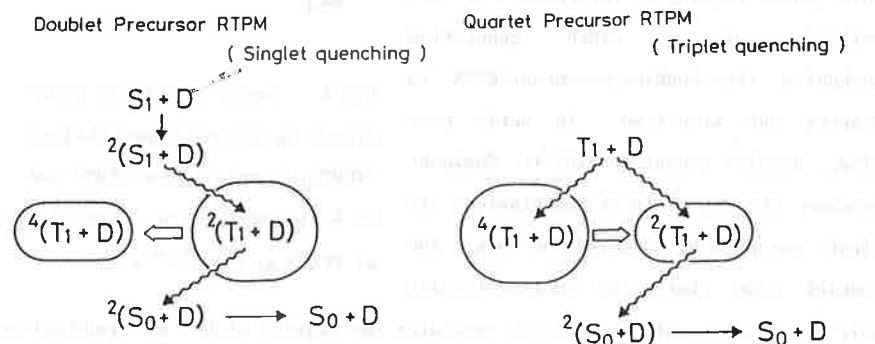


Fig.3 Schematic representation of both RTPM's.

system as a triplet quencher. Decay profile of this system is shown in fig.4-c. The absolute intensity is not calibrated but the relative intensity of emissive signals is reduced in this decay profile, which is interpreted by reduction of quartet precursor RTPM signal due to quenching of triplet naphthalene. Hence, the switching mechanism is confirmed by the phase turning of the CIDEP signal in the naphthalene-TEMPO system.

<REFERENCES>

- 1) T. Imamura, O. Onitsuka, and K. Obi, J. Phys. Chem. **90**, 6741 (1986).
- 2) C. Blättler, F. Jent, and H. Paul, Chem. Phys. Lett. **166**, 375 (1990).
- 3) A. Kawai, T. Okutsu and K. Obi, J. Phys. Chem. in press.

CIDEP Studies on the Photoinduced Electron Transfer Reactions from Metalloporphyrins to Quinone

Seigo Yamauchi, Toru Ueda, Minoru Satoh, Kimio Akiyama, Shozo Tero-Kubota, Yusaku Ikegami and Masamoto Iwaizumi
Institute for Chemical Reaction Science, Tohoku University,
Sendai 980, Japan.

Abstract

The photoinduced electron transfer reactions in the systems of Zn and Mg tetraphenylporphyrins(TPP) and 1,4-benzoquinone(BQ) were investigated by means of a time-resolved EPR(TREPR) technique and deuteration of the compounds. Three kinds of reaction intermediates, the porphyrin cation, the quinone anion and their ion pair were definitely assigned with the EPR parameters. By observing these three species effects of a solvent, a salt and an axial ligand on the reaction were analyzed. The effects were also found to be dependent on a central metal from the results of the systems of ZnTPP-BQ and MgTPP-BQ.

1. Introduction

A time-resolved EPR (TREPR) technique is very useful for assignment and structural analysis of reaction intermediates in comparison with a transient absorption technique. In the photoinduced electron transfer reactions of the metalloporphyrin-quinone systems, the intermediate species have been observed by transient EPR. The porphyrin anions and quinone cations were observed by TREPR[1], and the anion and the ion pair by FTEPR[2]. We here report the first simultaneous observations of the anion, the cation, and these ion pair in solution by means of TREPR. We also examine effects of a solvent, a salt, an axial ligand, and a central metal on the reaction.

2. Experimental section

TPP-d₂₀ was synthesized originally from toluene-d₈ following the published procedure[3]. BQ-d₄ was synthesized from phenol-d₈. The typical concentrations of the deaerated samples are 1×10^{-4} M for ZnTPP and MgTPP, 1×10^{-2} M for BQ, 0.1M for the salt, and 1~2M

for the axial ligand in alcohol solutions. The S₁ states of metalloporphyrins were excited by using an excimer laser(Lumonics HE-420) pumped dye laser(Lumonics Hyper Dye 300) at 585 or 561nm. Transient EPR signals detected with an EPR spectrometer (Varian E-109E) was amplified by a home-made fast amplifier and was fed into a boxcar integrator(NF EX531). Detailed descriptions of the TREPR system were reported previously[4].

3. Results and Discussion

The CIDEP spectra observed at room temperature in 2-butanol (BuOH) are shown in Figure 1. The nine peaks($g = 2.0025$ and $a_N = 1.60$ G) observed at 1 μ s after the laser pulse are definitely assigned to those of ZnTPP-d₂₀⁺. An another set of nine peaks($g = 2.0040$, $a_D = 0.36$ G) at 2 μ s is assigned to that of BQ-d₄⁻. The polarization of the spectra shows an absorption(A) of the microwave and is dominated by the triplet mechanism(TM). At -5.5°C the contribution of the radical pair mechanism(RPM) appears and the peak of the ion pair is observed as shown in Figure 2. From an analysis of the splitting of the E and A peaks the ion pair is assigned to the solvent separated ion pair(SSIP)[5]. The contact ion pair(CIP) is not observed by TREPR.

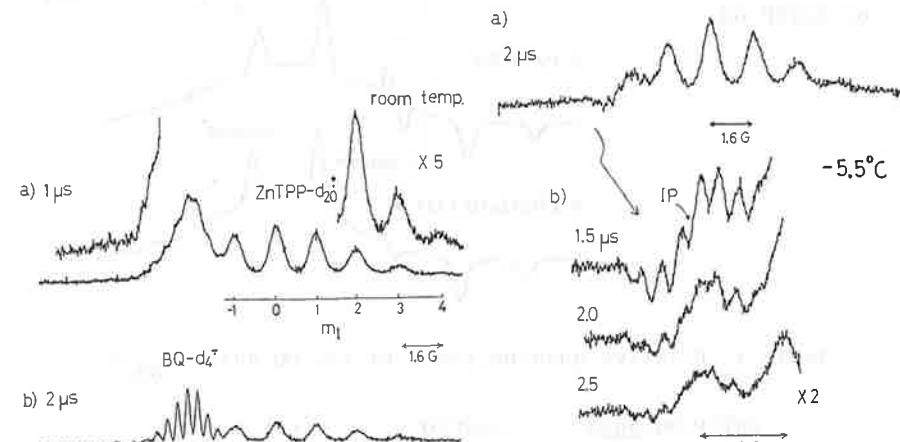


Figure 1

TREPR Spectra of ZnTPP-d₂₀⁺-BQ-d₄⁻ in BuOH

Figure 2

The peak of the pair decays faster($<0.5\mu s$) than those ($2\sim 5\mu s$) of the isolated ions. The decay rate of the deuterated ion pair is very similar to that of the hydrated ion pair ($ZnTPP^+ \dots BQ^-$). This fact indicates that the decay of the ion pair is not mostly controlled by a spin-lattice relaxation process but by a dynamics of the pair[6].

Effects of a solvent, an axial ligand and a salt on the CIDEP spectra were examined as shown in Figure 3. The yields of the BQ^- anion (ϕ_{BQ^-}) are summarized in Table 1. The ion yield increases with increasing a polarity of the solvent and increases also with ligation of pyridine and addition of the salt. More importantly, it is found that the yield of ion pair also increases with ligation of pyridine or increasing the solvent polarity as analogous to those of the ions, and that the yield of the ion pair decreases with addition of the salt in contrast to the increases of the ions (Figure 3).

Figure 3

Effects of an axial ligand and a salt on ZnTPP-BQ

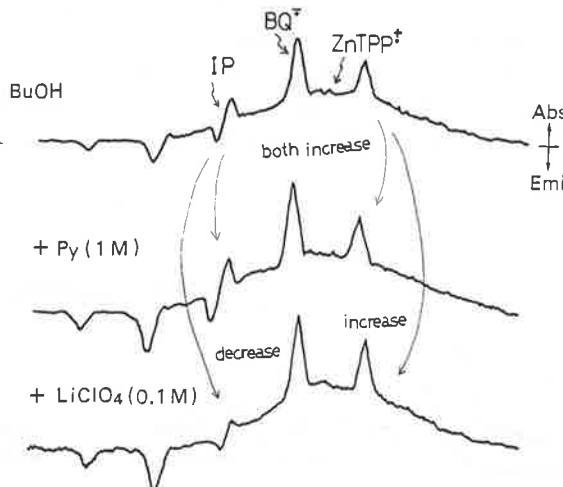
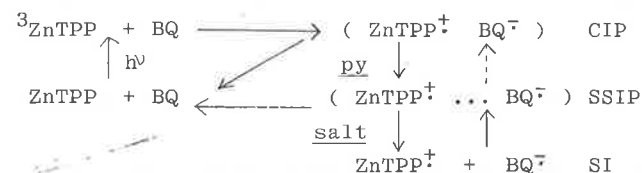


Table 1 Relative quantum yield of the BQ^- anion (ϕ_{BQ^-})

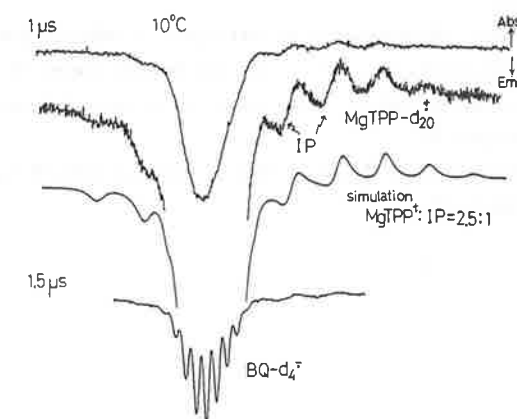
<u>ZnTPP-BQ/BuOH</u>	<u>+LiClO₄</u>	<u>+Py</u>
1	1.91	1.63
<u>MgTPP-BQ/BuOH</u>	<u>+LiClO₄</u>	<u>+Py</u>
1	1.37	1.26

On the basis of these results the mechanism of the photoinduced electron transfer reaction is summarized in the following[7].



The CIDEP spectra of $MgTPP-d_{20}^- BQ-d_4^-$ in $BuOH$ are shown in Figure 4. Three kinds of intermediate species, $MgTPP-d_{20}^+(g = 2.0023, a_N = 1.68G)$, $BQ-d_4^-(g = 2.0040, a_D = 0.36G)$, and their ion pair, could be again definitely assigned due to their sharp peaks of the deuterated compounds. The decay time of the pair is found to be longer for $MgTPP-BQ$ than that for $ZnTPP-BQ$, though the absolute value for $MgTPP$ is difficult to be obtained. The effects of the axial ligand and the salt are summarized in Table 1.

Figure 4
TREPR spectra
of $MgTPP-d_{20}^- BQ-d_4^-$ in $BuOH$



For the two points the results are different from the $ZnTPP$ system. 1) The contribution of TM is weaker and 2) the effects of both the axial ligand and the salt are less remarkable in the $MgTPP$ system. The first point is interpreted by the fact that the electron transfer from ${}^3MgTPP^*$ is slower than that from

ZnTPP [8]. The second point is interpreted by the stronger interactions between 3d orbitals of Zn (3d¹⁰) and the nonbonding orbital of the ligand, and/or 3d¹⁰ and the orbitals of the porphyrin ring due to close proximity of these orbitals[9].

References

- [1] H.van Willigen, M.Vuolle, and K.P.Dinse, J.Phys.Chem., 93 (1989)2441.
- [2] a)M.Puschau, A.Zahl, K.P.Dinse and H.van Willigen, J.Chem. Phys., 90(1989)3153. b)A.Angerhofer, M.Toporowicz, M.K. Bowman, J.R.Norris, and H.Levanon, J.Phys.Chem., 92(1988) 7164.
- [3] L.A.Dust and E.W.Gill, J.Chem.soc.C, (1970)1631.
- [4] K.Akiyama, A.Kaneko, S.Tero-Kubota, and Y.Ikegami, J.Am.Chem. Soc, 112(1990)3297.
- [5] a)G.L.Closs, M.D.E.Forbes, and J.R.Norris, J.Phys.Chem., 91(1987)3592. b) D.A.Hunter, P.J.Hore, and K.A.McLauchlan, Chem.Phys Lett., 135(1987)307.
- [6] K.Tominaga, S.Yamauchi, and N.Hirota, J.Chem.Phys., 92(1990) 5175.
- [7] H.Seki, M.Hoshino, H.Shizuka, J.Phys.Chem., 93(1989)3630.
- [8] M.K.Bowman, In L.Kevan and M.K.Bowman(ed.), Modern Pulsed and Continuous-Wave Electron Spin Resonance, John Wiley & Sons, 1990,pp.1.
- [9] M.Zerner and M.Gouterman, Theor.Chim.Acta, 4(1968)44, 8(1967)26.

CIDEP Measurement in Low Magnetic Field

Masahide Terazima*, Shin-ichi Hayakashi, and Tohru Azumi

Department of Chemistry, Faculty of Science,
Tohoku University, Aoba-ku, Sendai 980,Japan

*) present address; Department of Chemistry, Faculty of Science,
Kyoto University, Kyoto, 606, Japan

Abstract;

Chemically induced dynamic electron polarization (CIDEP) is investigated in low magnetic field by using a L band EPR spectrometer. The CIDEP spectrum of acetone in 2-propanol shows emission/absorption (E/A) pattern with net absorptive polarization in the X band region at room temperature. While, CIDEP spectrum in the L band region shows E/A pattern with net emissive polarization. The magnetic field dependence of the net polarization and the mechanism of the S-T₁ polarization are investigated in detail from the polarization pattern.

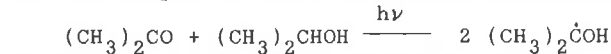
1. Introduction

During the last two decades, chemically induced dynamic nuclear and electron spin polarization (CIDNP and CIDEP, respectively) have been useful method to elucidate the mechanism and the intermediate species of photochemical reactions. In order to obtain further information on the intermediate radical pairs, magnetic field dependence of the polarization have sometimes used in the CIDNP method.¹⁻³ For that kind of experiment, a sample transfer method has been frequently applied; nuclear polarization is created at various magnetic field and then the sample is transferred to another constant magnetic field under which the nuclear polarization is measured. The key point of this method is that the spin-lattice relaxation time of nuclear spin is usually very long (an order of seconds). On the other hand, since the spin-lattice relaxation time of electron spin is about six orders magnitude shorter than that of the nuclear spin, the sample transfer method is very hard to be applied for CIDEP. Therefore, there have been no report on the magnetic field dependence of CIDEP and the information on the

intermediate radical pair by the CIDEP method has been limited. In order to elucidate the CIDEP mechanism in detail, we investigate CIDEP at low magnetic field by using an L band EPR spectrometer.

Our L band CIDEP experiment demonstrates that the S-T₋ polarization can be studied even at room temperature in nonviscous solvent. Moreover, the detailed mechanism of S-T₋ polarization can be investigated by analyzing the polarization in the second-order splittings.

We choose acetone in 2-propanol photochemical reaction system for the sample of the L band-CIDEP measurement.



The reaction scheme and the polarization mechanism of this system at the X band region has been extensively studied.⁴⁻⁸

2. Experiment

An L band ESR spectrometer (JEOL ES-LB) was used for the measurement of the L band CIDEP spectrum. A cavity of the spectrometer is a loop gap resonator type (diameter~14 mm) with three stripe type windows to allow light irradiation. The resonance frequency was ~1.5 GHz.

3. Results

Fig.1 depicts the CIDEP spectrum observed at 1.5 μ s after the laser irradiation in the X band

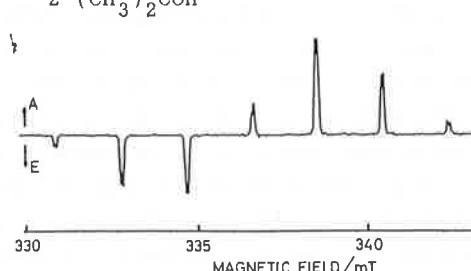


Fig.1

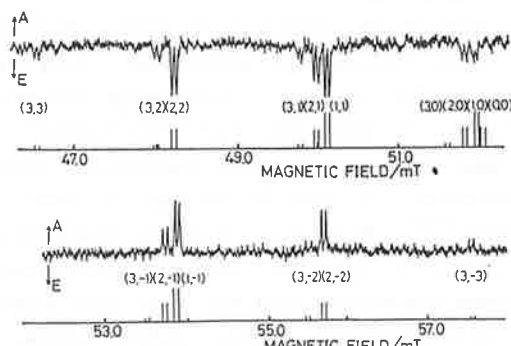


Fig.2 Upper part: The observed CIDEP spectrum in the L band region. Lower part: The calculated magnetic field and the relative intensities of hyperfine structure based on the second-order splittings by the methyl proton under Boltzmann population condition.

region ($\omega \sim 9.18$ GHz, $B_0 \sim 330$ mT) at room temperature. The feature of this spectrum is very similar to that reported previously.⁴⁻⁸ The CIDEP spectrum shows emission in the low field side and enhanced absorption in the high field side with net absorptive character (E/A* pattern). The E/A polarization comes from the ST₀M and the net absorptive polarization is explained by TM.⁸

$$P = a P_{ST_0} + b P_{TM} + c P_{ST} \quad (1)$$

Fig.2 depicts the CIDEP spectrum in the L band region ($\omega \sim 1.44$ GHz, $B_0 \sim 50$ mT) under the same conditions as those of the X band CIDEP measurement. There are two distinguished features compared with the X band CIDEP spectrum. First, the dominant polarization is still E/A pattern but the net polarization is emission at this magnetic field. Second, each hfs due to the methyl protons splits clearly to several peaks besides the splitting due to the hydroxyl proton. The further splitting can be explained by the second-order hyperfine splittings of the methyl protons. The stick spectrum at the lower part of the CIDEP spectrum (Fig.2) depicts the calculated hfs positions and the expected intensities of these hfs under the Boltzmann population distribution condition.⁹ The agreement of the magnetic field between the observed and calculated hfs is quite good. These hfs are denoted by the set of the total (I) and the total z component of the nuclear-spin angular momentum of the methyl protons (m) as shown in Fig.2.

4. Discussion

According to the CIDEP theory, the polarization due to TM is proportional to the external magnetic field under the fast tumbling conditions ($\omega\tau_2 \ll 1$, where τ_2 is the rotational correlation time),¹⁰ which is usually satisfied in a nonviscous solution at room temperature. Therefore, the contribution of TM is expected to decrease about factor ~0.15 as the magnetic field decrease from 330 mT to 50 mT. On the other hand, the polarization of ST₀M is predicted to be inverse proportion to the magnetic field.^{9,12} Concerning ST₀M, since the intermediate radical pair consists of the same kethyl radicals in this reaction system, the difference of the g values is zero ($\Delta g = 0$). Therefore, the magnetic field dependence of the ST₀M polarization is predicted to be insensitive to the external magnetic field.¹¹ Based on these consideration, the opposite net polarization in the X and L band regions is interpreted

as the decrease of the TM polarization (~ 0.15) and the increase of the ST_M polarization (~ 6.6) by changing the magnetic field from 330 mT to 50 mT.

Recently, Buckley and McLauchlan have separated the ST_M into two parts;⁷ hyperfine dependent (ST_M-d) and hyperfine independent (ST_M-i) parts. ST_M polarization arises from the mutual flip-flop of electron spin and nuclear spin through the non-zero matrix element

$$|\langle S, I, m-1 | A S_I | T_-, I, m \rangle|^2 = A^2 [I(I+1)-m(m-1)] \quad (2)$$

where A denotes hfcc. In this matrix element, the nuclear spin which plays a role in the S-T_- interaction can belong to either the observed radical or the counter radical because the electron spin is coupled to any of the nuclei of the radicals during the period of the S-T_- mixing. The hyperfine dependent part of the ST_- polarization appears when the nuclear spin which participates in the S-T_- interaction belongs to the observed radical. In this case, the efficiency of the ST_M is determined by the magnitude of the non-zero matrix element (eq.(2)) and it depends on the set (I,m) of each hyperfine lines. While, the hyperfine independent part comes from the S-T_- interaction using the nuclear spin of the observed and the counter radicals. Fig.3 also depicts the relative intensity of the polarization pattern due to TM, ST₀ and ST_M-d. Here, the ST_M polarization due to the hydroxyl proton is neglected because the polarization due to small hfcc of the hydroxyl proton (0.06 mT) is expected to be very small compared to that of the methyl protons (1.88 mT). Buckley and McLauchlan have observed the CIDEP spectrum of propanolyl radical in the same reaction system at low temperature in the X band region and concluded that the hyperfine-independent contribution is dominant.⁷ However, the clear distinction of ST_M-d and ST_M-i in the X band CIDEP spectrum seems to be difficult because each hfs of the same m are mixed together. On the other hand, the hyperfine lines of different (I,m) are expected to show very different polarization pattern depending upon the mechanism (ST_M-d or ST_M-i) (Fig.3). Thus, the L band CIDEP spectrum is expected to be suitable to distinguish ST_M-d and ST_M-i.

The observed L band CIDEP spectrum is tried to reproduce by using the polarization due to ST₀, TM, and ST_M-d, or ST_M-i for ST_M (eq.(1)). We neglect the contribution of TM (b=0).

Fig.4 shows the observed and calculated spectrum based on eq.(1) with ST_M-d and ST_M-i for P_{ST_-}, and b=0. When ST_M-d is used for P_{ST_-}, the observed spectrum can be reproduced with a:c=1:0.20~0.25. When ST_M-i is the origin of the ST_M polarization, the calculated spectrum with a:c=1:0.15~0.2 is reasonably similar to the observed CIDEP spectrum (Fig.3). At the first glance, both of the calculated spectra seem to reproduce the observed one well and the difference between these spectra seems minor. The minor polarization intensities difference comes from the small contribution of ST_M in the spectrum. By the closer examination, however, we can notice several differences in these spectra. First, the intensity of (1,-1) is very similar to that of (2,-2) in the ST₀+ST_M-d spectrum. On the other hand, the intensity of (2,-2) is predicted to be larger than that of (1,-1) by ST₀+ST_M-i. The observed spectrum shows the similar intensities between (1,-1) and (2,-2) peaks. Second, the difference is specially significant in the central region (m=0) because there is no

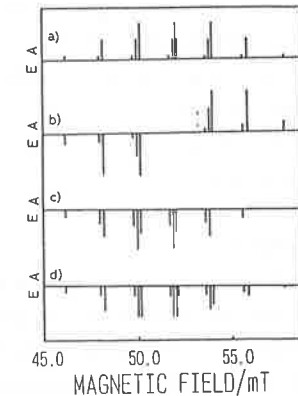


Fig.3 Calculated spectra in the L band region for each hfs of (I,m).

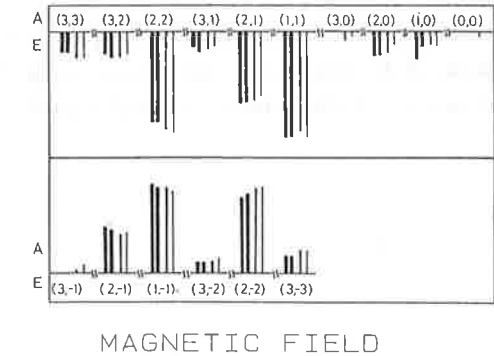


Fig.4 The intensities of the observed CIDEP spectrum in the L band region (thick bars), the calculated ones by using eq.(1) and ST_M-d for ST_M (middle thick bars), and ST_M-i for ST_M (thin bars).

contribution of ST₀M at these peaks. In ST_M-d spectrum, the (0,0) peak is missing. On the other hand, (2,0) and (3,0) peaks are very weak in the ST_M-i spectrum. The observed spectrum shows rather intense peaks at (1,0) and (2,0) and no peak is observed at the expected magnetic field for (0,0). Based on these differences, we conclude that the ST_M-d for ST_M polarization is more reasonable to explain the observed CIDEP spectrum.

References

1. Spin polarization and magnetic effects in radical reactions.
Edited by Y.N.Molin (Elsevier, Amsterdam, 1984).
2. Chemically induced magnetic polarization. Edited by L.M.Muus,
P.W.Atkins, K.A.McLauchlan, J.B.Pedersen(Reidel,Dordrecht,1977).
3. Kaptein,R.;der Hollander,J.Ä.J.Am.chem.Soc.,1972,94,6269.
4. Wong,S.K.;Chui,T.M.;Bolton,J.R.J.Phys.Chem.,1981,85,12.
5. Basu,S.;Grant,A.J.;McLauchlan,K.A.Chem.Phys.Lett.,1983,
94,517.
6. Thurnaner,M.C.;Chui,T.M.;Trifunac,A.D.Chem.Phys.Lett.,1985,
116,543.
7. Buckley,C.D.;McLauchlan,K.A.Chem.Phys.Lett.,1987,137,86.
8. Tominaga,K.;Yamauchi,S.;Hirota,N.J.Phys.Chem.,1986,90,2367;
J.Chem.Phys.,1988,88,553.
9. Fessenden,R.W.J.chem.Phys.,1962,37,747.
10. Atkins,P.W.;Evans,G.T.Mol.Phys.,1974,27,1633.
11. Adrian,F.J.J.Chem.Phys.,1972,57,5107.

Formation Mechanism of Spin Polarized Solvated Electron in Photoionization.

Hisao Murai and Keiji Kuwata,

Department of Chemistry, Faculty of Science, Osaka University,
Toyonaka, Osaka 560 (Japan)

Abstract

The spin polarized solvated electrons were observed in the photolysis of two different systems. The first system is mono-photonic ionization of *N,N,N',N'-tetramethyl-p-phenylenediamine* (TMPD) in alcoholic media. In this system, a very characteristic spectrum of the radical ion pair and that of solvated electron with CIDEP appeared. It is concluded that the photoionization takes place via the excited singlet state of TMPD and the radical-ion pair possesses a positive Δ -value. The second system is bi-photonic electron ejection from aromatic carbonyl compounds through the interface of SDS micellar aggregation. In this system, the emissively spin polarized hydrated electron was observed in the photolysis. The spin-lattice relaxation rate of the hydrated electron was about 10-fold faster than that reported previously. It is tentatively concluded that the spin polarized hydrated electron is formed through the consecutive excitation of the lowest excited triplet state of aromatic carbonyls.

1. Introduction

Most ESR studies on the solvated electron are limited to the reports of radiation chemistry. Only a few reports on the solvated electron formed in photoionization are available¹⁻². Concerning the spin polarized solvated electron, the study on the radiolysis of aqueous solutions containing several ion species has been reported in which the quenching to the triplet state of products has been postulated³. ESR studies provide unique information about the interaction of the photo-ejected electron and solvent molecule (and/or counter cation radical) from the data such as the g-factor, spectral line shape and the spin relaxation time.

In the present report, new CIDEP studies on photoionization of organic compounds and the formation of the spin polarized solvated electron concerning two different systems will be given. In the first system, mono-photonic ionization of *N,N,N',N'*-tetramethyl-*p*-phenylenediamine (TMPD) in alcoholic media and the formation of the radical ion pair are focused. The second one is the bi-photonic electron ejection from aromatic carbonyls in micellar systems and the formation mechanism of the spin-polarized hydrated electron is presented.

2. Experimental

An X-band ESR spectrometer was modified for the time-resolved ESR measurements (time-resolution of *ca.* 60 ns). A combined system of a transient wave-memory, Iwatsu DM-901, and a 16 bit micro-computer, NEC PC-9801VX, was used to detect the spin polarized transient paramagnetic species. A boxcar integrator was also used to record the CIDEP spectra. In the first system, a nitrogen-gas laser ($\lambda = 337$ nm) of 5 mJ/pulse output-power was mainly used for the excitation of TMPD, and excimer lasers (XeF: $\lambda = 351$ nm, 60 mJ/pulse, and XeCl: $\lambda = 308$ nm, 100mJ/pulse) were also employed. Throughout the experiment, the concentration of TMPD was between 5.0×10^{-3} and 2.0×10^{-2} M (mol dm⁻³), and 2-propanol was mainly used as the solvent. In the second system, an excimer laser (XeCl: $\lambda = 308$ nm) was used for the excitation. The concentrations of xanthone (or other carbonyls) and SDS in distilled water were 2.0×10^{-3} and 1.0×10^{-1} M, respectively. In both systems, the solutions were deoxygenated by bubbling with pure nitrogen gas prior to the time-resolved ESR measurements. The CIDEP measurements were carried out using a flat flow cell at lowered temperature (0 - -6°C) in the first system, and at room temperature in the second one.

3. Results and Discussion

1) TMPD in alcohols²

In the photolysis of TMPD in 2-propanol, absorptive time-resolved ESR signals were observed. This signal was weak and its peak position shifted gradually to the lower field direction by delaying the observation time and finally settled at the field of

$g = 2.0020$. In order to clarify this novel phenomenon, the experimental run with lowered temperature was carried out. Fig. 1(a) shows the time-resolved ESR spectra of some paramagnetic species at several observation times after laser Em. excitation at -2°C. Immediately after a laser pulse, a broad E/A polarized spectral pattern appeared. This E/A pattern gradually became narrower and some strong total absorptive component grew up along with the disappearance of the E/A

pattern component. Finally, the absorptive peak reached to $g = 2.0020$ position which was almost identical with that of the solvated electron reported in the radiolysis of methanol⁴. The superposition of two independent signals was the cause of the apparent peak shift observed at room temperature.

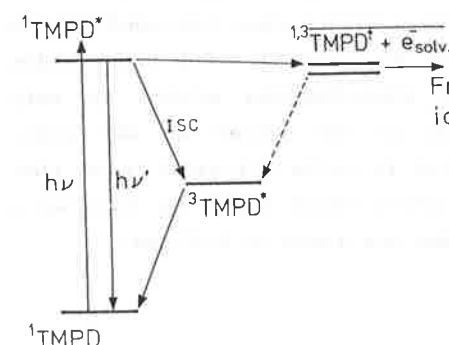
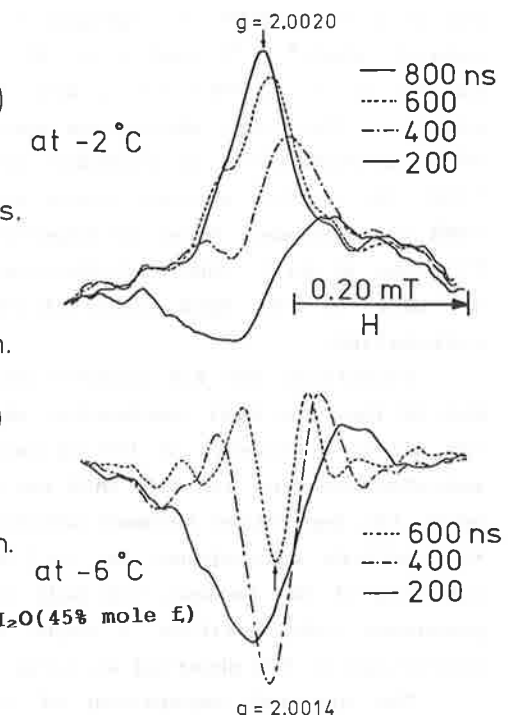


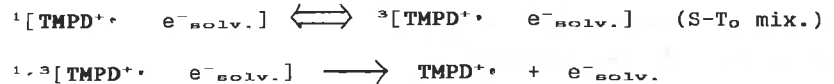
Fig. 2. Energy diagram of photoionization process of TMPD.

The rise and the decay of the total absorptive signal strongly depend upon the microwave power. This indicates that the absorptive signal is mainly due to the spin polarization induced probably by the S-T mixing as a geminate pair of the solvated electron and the TMPD cation radical. The photoejection of an

electron from TMPD in 2-propanol takes place from the excited singlet state^{5,6,7)} (see Fig. 2). Since the g-factor of TMPD cation ($g = 2.0034$) is a bit larger than that of solvated electron, the total absorption spectrum leads to the postulation of a positive value of exchange interaction (J). The ionization from the singlet excited state of TMPD is also proved by the FDMR (fluorescence detected magnetic resonance) technique made by Trifunac et al⁶). The contribution of the excited triplet state of TMPD to the spin polarization seems unlikely on careful examination.

Concerning the E/A pattern observed immediately after laser excitation, the most persuasive explanation of this spectrum is the direct appearance of the exchange interaction^{8,9)} between the solvated electron and the TMPD cation. In theory of the radical pair, the separation between emissive and absorptive peaks of the E/A pattern corresponds to $2xJ$ at a particular time. This spectrum of the radical ion pair is also explained by a singlet precursor with positive J value which is consistent with the conclusion of RPM observed at later observation time.

The apparent separation of the peaks in the E/A pattern gradually decreases, ranging 0.2-0.05 mT along with delaying (>100 ns) the observation time. The total absorption pattern grows up with the decrease of the E/A pattern. This indicates that the transient time region of the S-To mixing after the decrease of the exchange interaction of radical ion pair is observed in this particular system. It is known that the separation of the radicals from the geminate cage followed by the reencounter must take place for the S-To mixing. The observation of a positive J value in these photochemical system is very scarce, but it is not surprising in the system of the ionic radical pair in which the situation is quite different from that of the ordinary neutral radical pairs which react by forming a covalent bond. The reaction schemes are given as follows:



Recent careful experiments showed that the intensity ratio of the enhanced absorptin to the E/A pattern slightly altered by changing the light intensity. This implies that there still exists some contribution of the unknown nonlinear mechanism.

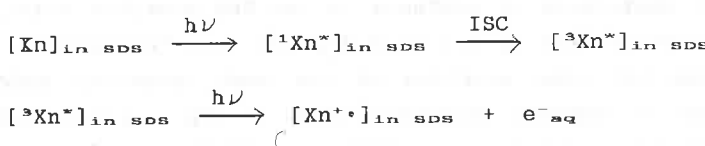
The addition of a large amount of water (higher than 0.3 mole fraction) to the solution drastically changed the spin polarization from an enhanced absorption to a net emission, and also changed the g-factor as shown in Fig. 1(b). The shift of the resonant field is explained by the increased contribution of the hydration which was reported previously⁴. The net emissive polarization may be explained by the increase of the contribution of TM (triplet mechanism) under the environment of much higher solvent polarity by the addition of water. The time-resolved ESR study of the lowest excited triplet state of TMPD showed that the intersystem crossing induced the population to the upper sublevels. An independent experiment of photooxidation reaction of TMPD with high concentration of maleic anhydride showed strong emissive polarization by TM. Therefore the TM spin polarization of TMPD must be emissive. The detailed analysis is now under way.

2) Xanthone in SDS micellar solution

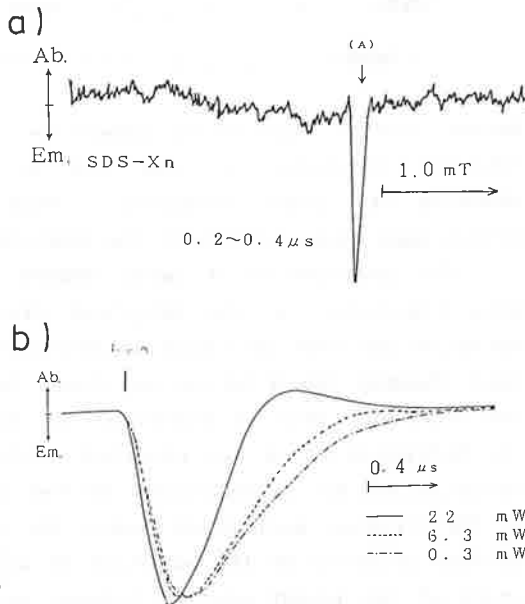
Fig. 3(a) shows the time-resolved ESR spectrum observed in the laser photolysis of xanthone in the SDS micellar solution at the observation time of 0.2 to 0.4 μ s at room temperature. Fig. 3(b) shows the time profiles of the peak intensity under the conditions of various microwave power. The g-factor of this sharp emissive signal is 2.0003 (± 0.00015) which is almost identical with that of the hydrated electron reported previously¹. Some other CIDEP signals superposed on the spectrum of the solvated electron are too weak to be assigned. This indicates that the hydrogen abstraction reaction from an SDS molecule which occurs in other carbonyls such as benzophenone is very slow. According to the light intensity dependence of the ESR signal, the hydrated electron is produced through biphotonic

process as shown in Fig. 4. The signal of the hydrated electron was easily quenched by the addition of Cu^{2+} ion, and the quenching rate ($3 \times 10^{10} \text{ M}^{-1}\text{s}^{-1}$) was in good agreement with that reported before¹⁰.

These results lead to the conclusion that xanthone is photoionized through the two photon processes in an SDS micelle and the electron is quickly ejected to the aqueous circumstance through the interface of the SDS micelle. The cause of the emissive spin polarization may be explained by the fast intersystem crossing followed by photoionization in the second excitation of the spin polarized triplet state. It is known that the intersystem crossing of the photo-excited xanthone to its lowest excited triplet state is 10^{11} s^{-1} and the emissively polarized triplet state is produced efficiently.



Both the g-factor and the quenching rate by Cu^{2+} indicate that the electron ejected from the SDS micellar aggregate exists under the aqueous circumstance. However, the direct observation of the decay time of the spin polarized signal of the solvated electron as the low microwave power limit was $0.7 \mu\text{s}$. This value corresponds to the spin-lattice relaxation time of the hydrated electron. But this relaxation is about 10-fold faster than that



reported in the photolysis of an aqueous solution of $\text{Na}_2\text{SO}_3^{11}$. It is not clear whether this discrepancy is due to the difference of the observation time region (immediately after photolysis or thermally equilibrated) or the difference of the aqueous circumstances between those two systems. When the other aromatic carbonyl compounds, benzophenone and anthrone (known to provide emissively polarized TM in photochemistry) were employed, the spin polarized hydrated electrons with an emissive character but different intensities were observed. These photoionization processes of aromatic carbonyls in SDS micelles may be the same, namely, fast intersystem crossing followed by a second excitation takes place.

As shown in the present report, the time-resolved ESR method is very suitable and useful to investigate solvated electrons formed in the photoionization. The spin polarized solvated electrons provide unique and important information concerning the ionization processes and/or the environment of the electrons.

Acknowledgment

We are grateful to Mr. N. Ishiwata for his earnest help and reliable data analysis especially for the micellar system.

References

- [1] A. S. Jeevarajan and R. W. Fessenden, *J. Phys. Chem.*, **93** (1989) 3511.
- [2] Preliminary report; H. Murai and K. Kuwata, *Chem. Phys. Letters*, **164**(1989) 567.
- [3] R. W. Fessenden and N. C. Verma, *J. Am. Chem. Soc.*, **98** (1976) 243.

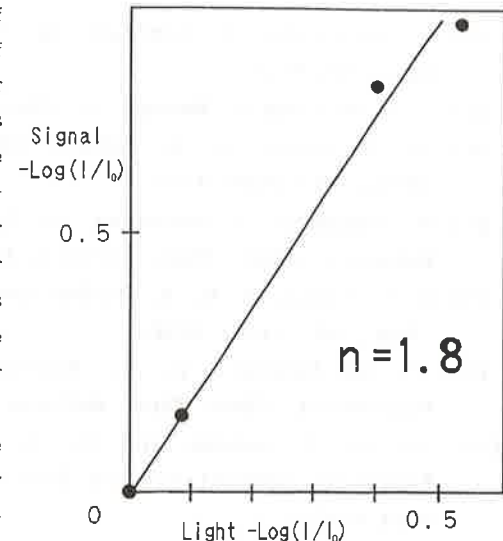


Fig.4. Light intensity dependence of signal intensity of e^-_{aq} .

- [4] H. Shiraishi, K. Ishigure and K. Morokuma, *J. Chem. Phys.*, **88** (1988) 4637.
- [5] Y. Hirata and N. Mataga, *J. Phys. Chem.*, **89** (1985) 4031.
- [6] L. T. Percy, M. G. Bakker and A. D. Trifunac, *J. Phys. Chem.*, **93** (1989) 4393.
- [7] Y. Tanimoto, T. Watanabe, R. Nakagaki, M. Hiramatsu and S. Nagakura, *Chem. Phys. Letters*, **116** (1985) 341.
- [8] G. L. Closs, M. D. E. Forbes and J. R. Norris, Jr., *J. Phys. Chem.*, **91** (1987) 3592.
- [9] C. D. Buckley, D. A. Hunter, P. J. Hore and K. A. McLaughlan, *Chem. Phys. Letters*, **135** (1987) 307.
- [10] J. W. T. Spinks and R. J. Woods, "An Introduction to Radiation Chemistry" 2nd Edition, John Wiley & Sons, New York (1976).

Investigation of Novel Radical Pair Interaction: Ionic System and Micellar System.

Hisao Murai, Hidekazu Honma, Natsuo Ishiwata and Keiji Kuwata
Department of Chemistry, Faculty of Science, Osaka University,
Toyonaka, Osaka 560, Japan

Abstract

Two different systems of special radical pair were studied by the aid of a time-resolved ESR technique. The first system is the photooxidation reaction of *N,N,N',N'*-tetramethyl-*p*-phenylenediamine (TMPD) with maleic anhydride in alcoholic media. In this system, the emissively polarized anion radical of maleic anhydride was observed through the reaction of the excited triplet state of TMPD. Under the low concentration condition of maleic anhydride, the emissive TM-like polarization is explained by the S-T-1 mixing of the radical ion pair. The Coulombic interaction may be the cause of the restrained molecular motion which induces the S-T-1 mixing. In the second system, the hydrogen abstraction reactions of photoexcited xanthone from phenol derivatives in SDS micellar solution were investigated. In this system, metastable radical pair having the E/A-like phase alternation was observed. These spectra were well simulated by assuming the quick relaxation between middle two mixed states. The radical pair survives a few μ s without changing the spectral pattern. This long-lived radical pair interaction may be due to the confined motion of these radical pair in the micellar environment.

1. Introduction

Recent development of CIDEP studies is clarifying the details of the important radical-pair interactions which work in the initial steps of chemical reaction. These interactions are also known to be the cause of the external magnetic field effects on chemical reaction. The investigation of radical pair interactions, however, has not been completed yet. In this report, quite novel phenomena of radical pair interactions observed by the aid of a time-resolved ESR technique will be

given concerning two independent systems. First system is the photooxidation of *N,N,N',N'*-tetramethyl-*p*-phenylenediamine (TMPD) with maleic anhydride (MA), and an ionic interaction between two geminate radicals is presented. In the second system, new information of radical pair formed in the photoreaction of xanthone (Xn) with phenol derivatives in well known SDS micelles is presented. In the former system, the contribution of the enhanced S-T₋₁ mixing is postulated. In the latter system, the fast relaxation between middle two mixed levels of the spin correlated radical pair and stabilization of the radical pair due to the large J -value in an SDS micelle are postulated. In both systems, the exchange interaction may play an important role.

2. Experimental

A DC detected X-band time-resolved ESR spectrometer and a boxcar integrator (or a transient wave memory combined with a computer) were used for the CIDEP measurements. In the first system, an excimer lasers (XeF: $\lambda = 351$ nm and XeCl: $\lambda = 308$ nm) were used for the light source. The concentration of TMPD was 1.2×10^{-2} M. The concentration of MA was varied from 5×10^{-4} to 3×10^{-2} M. 2-Propanol was mainly used as the solvent. In the second system, an excimer laser (XeCl: $\lambda = 308$ nm) was used for the excitation. The concentrations of Xn and SDS in distilled water were 1×10^{-3} M and 5×10^{-2} M, respectively. Under this concentration condition, about 1.4 xanthone molecules (simple average) are designed to be solubilized in an SDS micelle. As the phenol derivatives (1×10^{-3}

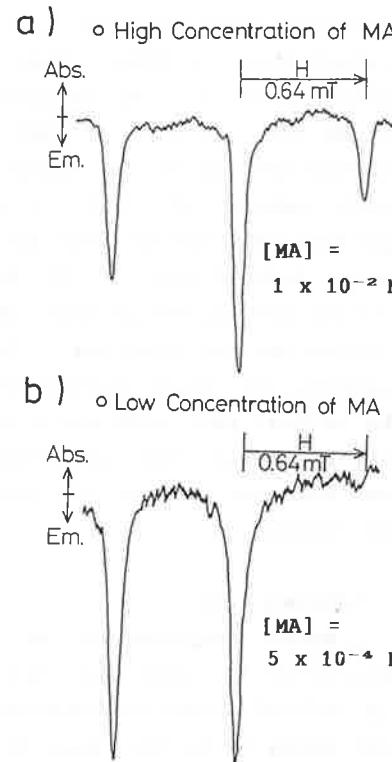


Fig. 1. trESR spectra of MA^- in 2-PrOH at room temperature.

M), 2,6-di-*t*-butylphenol (DTBP), 2,4,6-tri-*t*-butylphenol (TTBP) and 2,6-di-*t*-butyl-*p*-cresol (DTBC) were employed.

3. Results and Discussion

1) Enhanced S-T₋₁ Mixing of Radical Ion Pair¹

Fig. 1a shows the CIDEP spectrum observed in the photolysis of TMPD in the presence of the high concentration of MA (1.0×10^{-2} M) in 2-propanol. This spectrum is assigned to the anion radical of MA, and the polarization pattern is explained by the superposition of an E/A pattern of the RPM (S-T₀ mixing) on the emissive TM. It is concluded that this reaction takes place via the excited triplet state of TMPD as shown in Fig. 2 and the following equations:

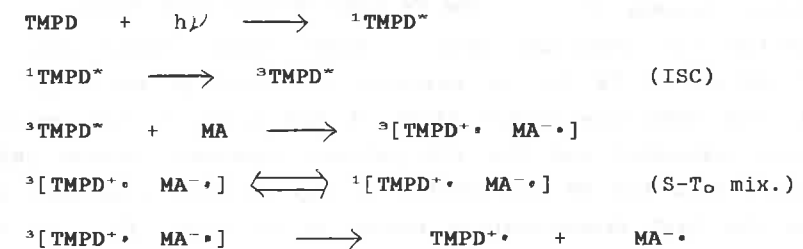


Fig. 1b shows the CIDEP spectrum observed under the condition of the low concentration of MA (5×10^{-4} M). As shown in this figure, the low and middle resonant field lines show

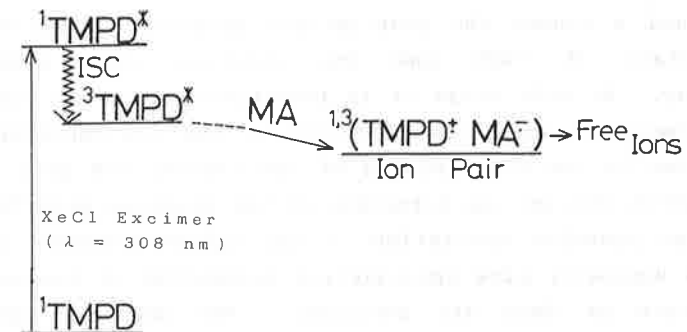


Fig. 2. Energy diagram of photooxidation of TMPD with MA.

almost the same intensity, while the highest one almost disappears or shows a weak E/A shape. Under the low concentration region of MA (2×10^{-3} - 5×10^{-4} M), the polarization pattern did not alter, and the rise of the signal depended on the concentration of MA, probably because it reflected the reaction rate. Under these conditions, the contribution of TM to the emissive component is unlikely. In fact, the semi-logarithmic plots of the ratio of the emissive TM-like component and the E/A pattern component versus $[MA]^{-1}$ indicate that the TM contributes to the emissive component only under the high concentration region of MA (Fig. 3). In this analysis, an approximated empirical equation was used instead of the Stern Volmer-type one.

$$\frac{I_{TM}}{I_{RPM}} = \left(\frac{I_{TM}}{I_{RPM}} \right)_0 \exp\{-T_1^{-1}/k[MA]\}$$

where T_1 and k denote the spin-lattice relaxation time of the triplet state of TMPD and the reaction rate constant, respectively. At this stage it is tentatively proposed that the emissive component under the condition of the low concentration of MA is due to the S-T₋₁ mixing of the radical ion pair. The other possibilities of the formation of the emissive polarization such as the possible excitation of the charge transfer complex and/or the unusually slow spin-lattice relaxation of the excited triplet state of TMPD are excluded. The observed spectral pattern may be explained by the superposition of the emissive S-T₋₁ mixing component and the E/A pattern of the S-T₀ mixing. In this case, the S-T₋₁ mixing is thought to be hyperfine

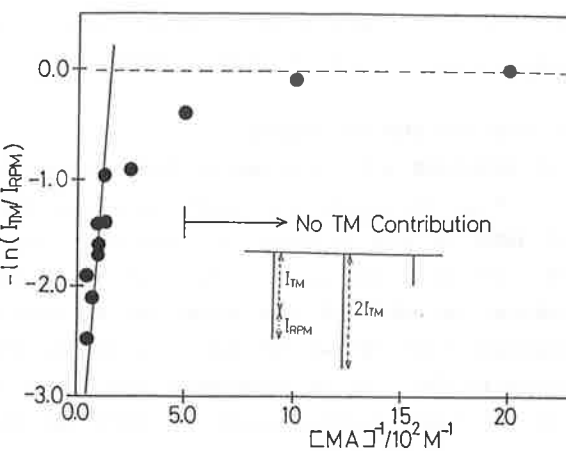


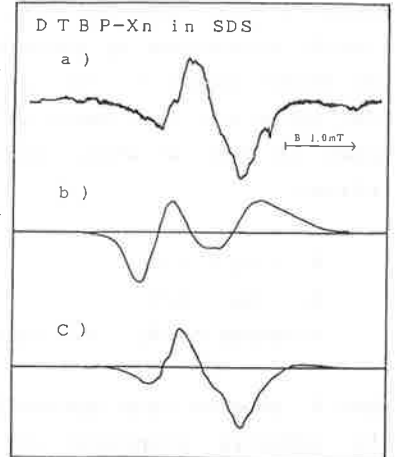
Fig. 3. Concentration dependence of the TM contribution (see text).

independent because of the complex hyperfine structure of the TMPD cation radical.



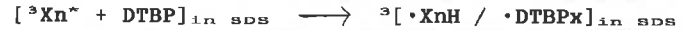
The S-T₋₁ mixing may be enhanced by the Coulombic interaction of the geminately formed ion radicals. It should be noted that in this particular ionic system the S-T₋₁ mixing occurs even under the conditions of small hfc values of radicals, the ordinary non-viscous solvent, and also room temperature. As far as we know, this report is the first example of the S-T₋₁ mixing enhanced by the Coulombic force of the radical ion pair observed as the CIDEP by using

Fig. 4. Observed and simulated trESR spectra of radical pair (DTBP/Xn in SDS).



2) Special Radical Pair in an SDS Micelle

Fig. 4(a) shows the trESR spectrum of radical pair observed in the photolysis of xanthone and DTBP in an SDS micelle in aqueous solution. The observed spectrum shows E/A alternating hyperfine structure which implies the formation of the spin correlated radical pair. In this system, Xn is thought to react exclusively with DTBP to form metastable radical pair in the micelle.



where $\cdot\text{XnH}$ and $\cdot\text{DTBPX}$ denote xanthone ketyl radical and di-t-butylphenoxy radical, respectively. Fig. 5(a) shows the time-resolved ESR spectrum observed in the case of xanthone and DTBC in an SDS micelle in aqueous solution. Similar alternating hyperfine structure was observed. TTBP also worked similarly but

the intensity was very weak.

There are two distinct points which are newly discovered in these systems. (1) the signal decayed for a few μ s with keeping the same spectral pattern. (2) The calculation trial of these spectra by the ordinary assumption of radical pair^{2,3)} failed as shown in Figs. 4(b) and 5(b). The unusual spectrum shape (2) was finally reproduced by introducing quick relaxation between middle two mixed states to the calculation as shown in Figs. 4(c) and 5(c) where a slight emissive component was added. The scheme is shown in Fig. 6 where the quick relaxation is introduced as follows:

$$N_1 = N_4 = 1/3$$

$$N_2 = N_3 = 1/6$$

$$(instead of N_2 = (1/3)\cos^2\theta, N_3 = (1/3)\sin^2\theta)$$

Here N_i denotes each sublevel ($|i\rangle$) of the radical pair. Whether the emissive component of the radical pair is due to the contribution of the TM or that of the S-T₋₁ mixing is not clear at this stage. The phenomenon (2) in an SDS micelle is very similar to that reported in the system of methylene linked biradicals⁴). This fast relaxation must have something to do with the exchange interaction between two spins and/or the small separation between the middle two mixed states.

It is noteworthy that the radical pairs in micelles reported so far show the conversion of the spectrum to the normal S-T₀ mixing (an E/A pattern)^{5,6}), while no S-T₀ mixing appears in this system. The preservation of the spectral pattern (1) implies that the diffusional motion of these particular radical pair systems is anomalously slow in the restrained environment probably because of the

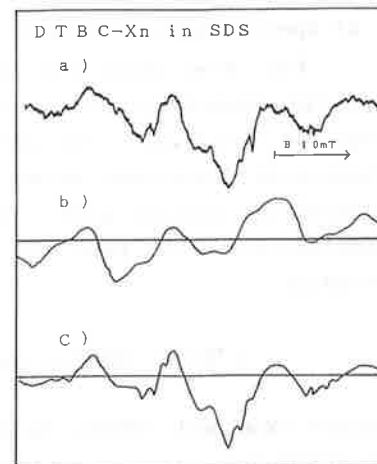


Fig.5. Observed and simulated trESR spectra of radical pair (DTBC/Xn in SDS).

existence of bulky t-butyl groups. The decay of the signal may reflect the spin-lattice relaxation of these particular system under the magnetic field.

4. conclusion

Both in the ionic system and in the micellar system, the exchange interaction may play an important role in the S-T₋₁ mixing and/or the formation of the metastable radical pair. In former system, the Coulombic interaction may enhance the confined conditions which induces the S-T₋₁ mixing. In the latter system, the micellar environment restrains the molecular motion of the radical pair with bulky alkyl groups. It prolongs the interaction of the radical pair. The relaxation of the middle two state of the spin correlated radical pair becomes very fast in this particular system.

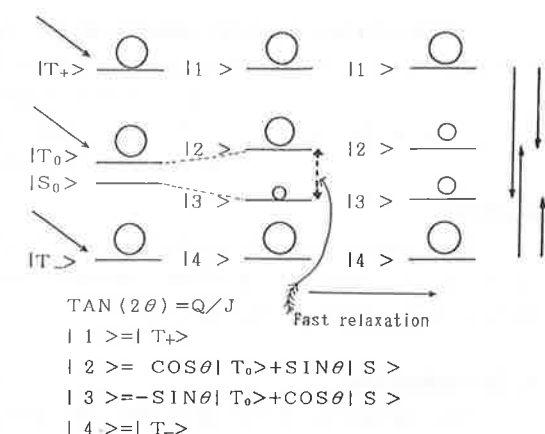


Fig.6. Schematic energy diagram of the proposed model of the spin correlated radical pair.

References

- [1] H. Honma, H. Murai and K. Kuwata, Preliminary report appeared in 29th ESR symposium at Tokyo (1990).
- [2] G. L. Closs, M. D. E. Forbes and J. R. Norris, Jr., *J. Phys. Chem.*, **91** (1987) 3592.
- [3] C. D. Buckley, D. A. Hunter, P. J. Hore and K. A. McLauchlan, *Chem. Phys. Letters*, **135** (1987) 307.
- [4] M. Terazima, K. Maeda, T. Azumi, Y. Tanimoto, N. Okada and M. Itoh, *Chem. Phys. Letters*, **164** (1989) 562.
- [5] Y. Sakaguchi, H. Hayashi, H. Murai and Y. J. I'Haya, *Chem. Phys. Letters*, **110** (1984) 275
- [6] Y. Sakaguchi, H. Hayashi, H. Murai, Y. J. I'Haya and K. Mochida, *Chem. Phys. Letters*, **120** (1985) 401.

Stimulated nuclear polarization and related phenomena
 R.Z.Sagdeev, E.G.Bagryanskaya, I.V.Koptyug, Yu.P.Tsentalovich and
 A.V.Yurkovskaya
 The Institute of Chemical Kinetics and Combustion,
 Novosibirsk (USSR)

Abstract

The paper reports results of SNP and flash-CIDNP studies of short-lived radical species (radical pairs localized in micelles, biradicals, triplet molecules).

1. Introduction

The recently developed SNP [1] and time-resolved CIDNP [2] techniques show high sensitivity and, at the same time, allow one to obtain quantitative information on radical intermediates (kinetics of their transformation, ESR spectrum).

The SNP method is based on the resonance mw-field effect on the singlet-triplet conversion in the RP. The resonance mw-field induced S-T transitions in RP selectively with respect to nuclear spin orientation, which leads to nuclear spin polarization in radical reaction products. The SNP technique with ^{13}C detection, we have recently developed [3], turned out to be extremely helpful in investigating the dynamics of exchange interaction of RP in micelles and short-lived biradicals.

Flash-CDNP method is essentially a pulse excitation followed by pulse NMR detection of CIDNP effects with variable time delay between them. The time resolution we have achieved is 50 ns.

2. Results and discussion

2.1 RP in micelles. We have studied [4] photolysis reaction of dibenzylketone and α -methyldesoxy benzoin in SDS micelles. The SNP signal intensity in the photolysis in micelles appeared to be several hundreds of times higher than that for homogeneous solution that allowed us to work with natural abundance of ^{13}C . Splitting in SNP spectra in micelles coincides within experimental accuracy with reported hfi constants for free radicals. Thus, the mean exchange interaction in micelles is small (a few oersteds), which is consistent with results of other authors [5]. The SNP line width is more than three times higher than the mw-field amplitude. The SNP theory has been developed [6] for radical

pairs in micelles, which is based on the numerical solution of the stochastic Liouville equation including distance-dependent exchange interaction for a model of a microreactor [7]. The exchange interaction parameters ($J(r)=J_c \exp(-(r-R)/\lambda)$) have been optimized by means of comparison of calculations and experimental field dependencies of CIDNP and mw-field amplitude dependencies of SNP line width. The optimal values obtained are $J_c = -7 \times 10^9$ rad/s, $\lambda = 0.5 \text{ \AA}$. The relatively small value of J_c is apparently due to the anisotropy of exchange interaction.

2.2 SNP in biradicals. General regularities of SNP formation in short-lived flexible biradicals, arising in photolysis of cycloalkanones in the series from cyclodecanone to cyclotridecanone [8], have been studied experimentally in our previous works. However, to obtain quantitative information on the exchange interaction in biradical and on other parameters, one should compare experimental data with calculation. To do this, a realistic model has been constructed, based on the solution of the stochastic Liouville equation (SLE). This allows one to take into account the exchange interaction dependence on separation of radical centers, the modulation of exchange interaction by biradical chain motion, as well as mixing of the singlet state with all the three triplet levels. The polarization value was found using numerical solution of SLE [9]. The character of spectrum is mainly determined by relative values of the external field and exchange interaction and is less affected by other parameters [10], which allows one to determine the parameters of exchange interaction.

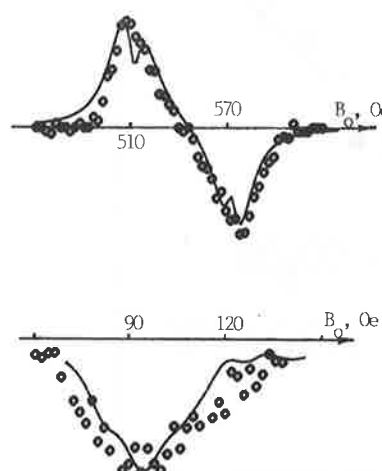


Fig. 1. The experimental (circles) and calculated (lines) SNP spectra of the biradical, detected by carbonyl (a) and α -carbon (b) of d_4 -cyclododecanone at mw-frequency of 1531 MHz and 308 MHz, respectively.

308 MHz, respectively. Calculated spectra are presented in the same figures. The splitting in the spectrum of fig.1a is half as much as corresponding hfi constant, which is commonly explained by the presence of considerable exchange interaction. Calculations have shown however that fast biradical decay from the singlet state results in the same splitting decrease in SNP (RYDMR, ESR) spectra [11].

2.3 CIDNP kinetics in biradicals. The escape in the bulk is a concurrent channel for geminate recombination of RP. In this case the amplitude of nuclear polarization in geminate recombination of RP is known to increase monotonously with decreasing diffusion coefficient, or increasing in-cage lifetime. For biradicals, where RP partners are coupled by polymethylene chain, this channel is absent - products of biradical disproportionation and recombination are in-cage and times of geminate evolution are of hundreds of nanoseconds.

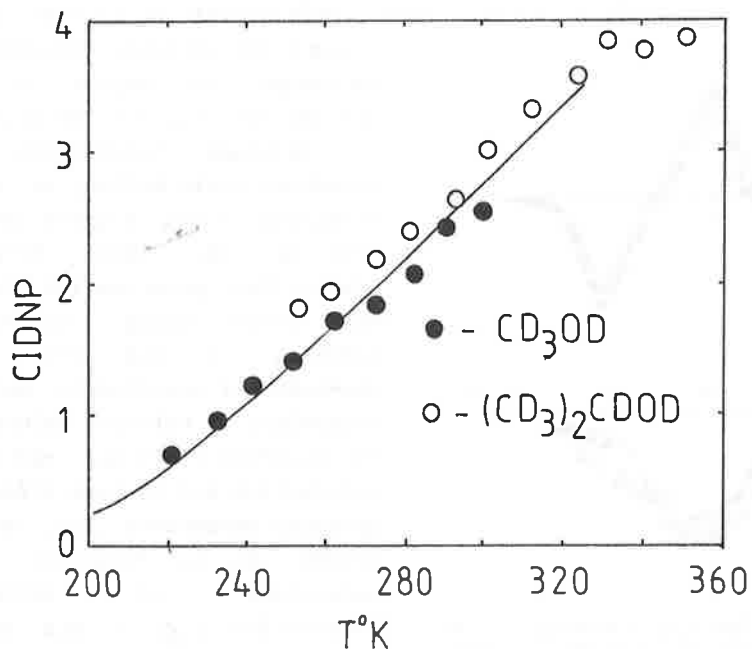


Fig.2. Temperature dependence of CIDNP intensity of cyclododecanone in different alcohols.

We have obtained [12] the kinetic curve of nuclear

polarization in recombination of acyl-alkyl biradicals formed in photolysis of cycloalkanones. CIDNP has been shown to have a maximum 160 ns after the laser pulse. The influence of viscosity, temperature, and diffusion coefficient on CIDNP amplitude in different alcohols (deuterated methanol, isopropanol, n-butane, and cyclohexanol) has been studied in a wide temperature range (220-420 K) [13]. It has been shown that, unlike in normal RP, CIDNP in biradicals decreases monotonously with decreasing diffusion coefficient and temperature.

Model calculations have been performed of CIDNP kinetics in geminate recombination of biradical, including variations of the conformational distribution of polymethylene chain with temperature. The calculations are based on the solution of the SLE for density matrix by means of the Fourier transform with the subsequent reconstruction of the time dependence $\rho(t)$. Hfi with four protons of the alkyl end and exchange interaction dependent on the distance between radical centers, modulated by biradical ends motion, are taken into account. Quantitative agreement with experiment has been obtained for diffusion dependencies of CIDNP kinetics in biradicals with the use of the exchange interaction parameters obtained in simulations of SNP experiments.

2.3 Triplet lifetime measurements and two-photon processes. Flash-CIDNP can also be used for studying the kinetic behavior of triplet molecules. The triplet lifetime is traditionally determined from the Stern-Volmer dependence of product yield on quencher concentration. Since geminate polarization is formed independently in each radical pair, its amplitude is directly proportional to the number of RP and it is described by the Stern-Volmer dependence

$$\frac{\text{CIDNP}(0)}{\text{CIDNP}(C_q)} = 1 + k_q C_q \tau$$

where k_q - the quenching rate constant, C_q - the quencher concentration. We have used this technique for measuring the lifetimes of the triplet states of some aliphatic ketones [14].

It should be noted that in excitation of molecules by laser light of high intensity, of importance are double-quantum processes caused by absorption of the second photon during the laser pulse. In this case highly excited triplet states of great

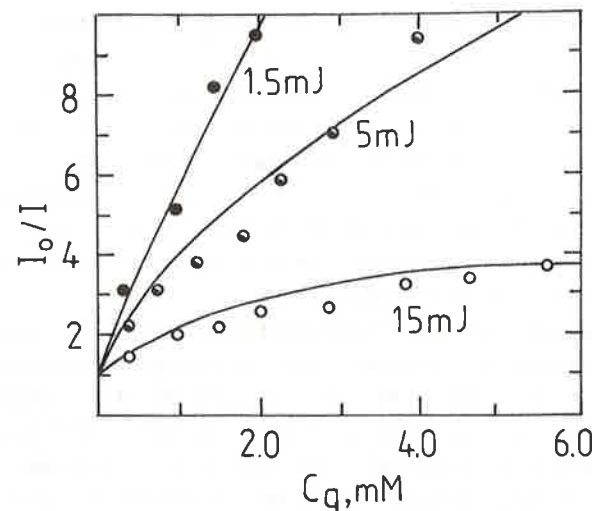


Fig.3. Stern-Volmer plots of geminate CIDNP in the 2-butanone photolysis for different laser energy.

reactivity are formed, whose kinetic behavior can be considerably different from that of usual triplets. Stern-Volmer dependencies here become essentially nonlinear. Based on the analysis of Stern-Volmer dependencies of CIDNP for different laser pulse energies, one can obtain quantitatively the triplet lifetime and the contribution of two-photon processes in the photolysis. The similar results were obtained by direct measurement of time dependences of geminate CIDNP for different laser energy in these reactions [14].

When photolysis of highly excited states occur in another way than it does in one-photon processes, the use of flash-CIDNP allows easy distinguishing between these two pathways. The intensities of polarized geminate products formed in two-photon and single-photon reactions depend differently on laser energy. E.g., in the photolysis of acetone in isopropanol, it has been shown that methane results from a two-photon process and enol from a single-photon one, the intensity ratio increasing linearly with laser pulse energy (fig.4). The use of quencher also allows one to distinguish efficiently between contributions to CIDNP formation from single- and double-photon reactions. Since the

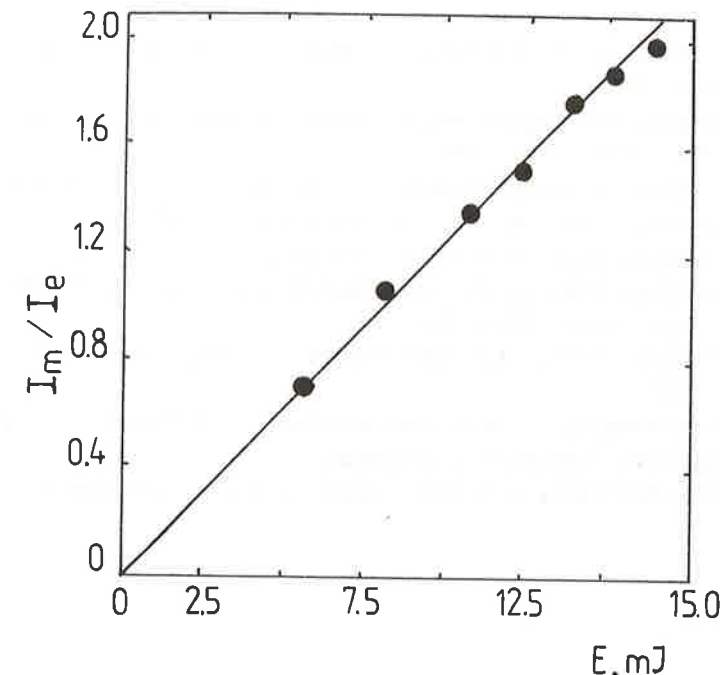


Fig.4. The ratio of CIDNP intensities of methane and enol vs laser power during acetone photolysis in isopropanol.

Lifetimes of highly excited states are as a rule several orders of magnitude shorter than the lifetimes of normal triplets, the quencher affects only the single-photon reactions.

References

- [1] R.Z.Sagdeev and E.G.Bagryanskaya, Pure and Appl.Chem. 62 (1990) 1547.
- [2] G.L.Closs, R.J.Miller and O.D.Redwine, Acc.Chem.Res. 18 (1985) 196.
- [3] I.V.Koptyug, E.G.Bagryanskaya and R.Z.Sagdeev, Chem.Phys. Letters 163 (1989) 503.
- [4] E.G.Bagryanskaya, V.F.Tarasov et al, Zh.Chem.Phys. (Russian), in press.
- [5] G.L.Closs, H.D.E.Forbes and J.R.Norris, J.Chem.Phys. 91 (1987) 3592.
- [6] I.A.Shrob, V.F.Tarasov and E.G.Bagryanskaya, Chem.Phys., in

press.

- [7] V.F.Tarasov, A.L.Buchachenko, V.F.Maltzev and J.Russ, Phys.Chem. 55 (1981) 1921;
- [8] I.V.Koptyug, E.G.Bagryanskaya, Yu.A.Grishin and R.Z.Sagdeev, Chem. Phys. 145 (1990) 375.
- [9] I.V.Koptyug, E.G.Bagryanskaya, N.N.Lukzen, A.B.Doctorov and R.Z.Sagdeev, Chem. Phys., submitted for publication.
- [10] I.V.Koptyug, Ph.D. Thesis, Novosibirsk, 1991.
- [11] I.V.Koptyug, N.N.Lukzen, E.G.Bagryanskaya and A.B.Doctorov, Chem. Phys. Lett. 175 (1990) 467.
- [12] Yu.P.Tsentalovich, A.V.Yurkovskaya et al, Chem.Phys. 139 (1989) 307.
- [13] A.V.Yurkovskaya, Yu.P.Tsentalovich, N.N.Lukzen and R.Z.Sagdeev, Chem.Phys., in press.
- [14] Yu.P.Tsentalovich, A.V.Yurkovskaya et al, in preparation.

Determination of the Enhancement Factor of CIDNP in the Photochemical α -Cleavage of Ketones

Tomomi Sakata, Masahide Terazima, and Tohru Azumi

Department of Chemistry, Faculty of Science, Tohoku University, Sendai 980 (Japan)

Abstract

The enhancement factor of CIDNP in the photolysis of dibenzyl ketone is measured. The Boltzmann population corrected enhancement factor ϵ was -2.88×10^{-3} . We conclude that nearly 80 percent of the α -cleavage takes place in the singlet state.

The determination of the enhancement factor of CIDNP is very important in understanding the mechanism of photochemical reactions. In this paper, we wish to point out that qualitative analysis of the sign of the CIDNP polarization alone may sometimes lead to an erroneous conclusion. Let us illustrate how it is important to determine the enhancement factor by taking the photochemical α -cleavage of dibenzyl ketone (DBK),



as an example.

Figure 1 shows the NMR spectra measured (a) before the light irradiation and (b) during the light irradiation. The CIDNP signal for the benzyl protons of DBK (the recombination product) at 3.7 ppm is emissive, and the CIDNP signal for the methylene proton of dibenzyl (escaped product) at 2.9 ppm is absorptive. By application of the Kaptein rule, the precursor is predicted to be the triplet state, and this prediction agrees with the results of numerous studies reported so far. Complication arises, however, if reaction occurs from both triplet and singlet states. We should note that the enhancement factor of CIDNP greatly differs between the singlet precursor and the triplet precursor.

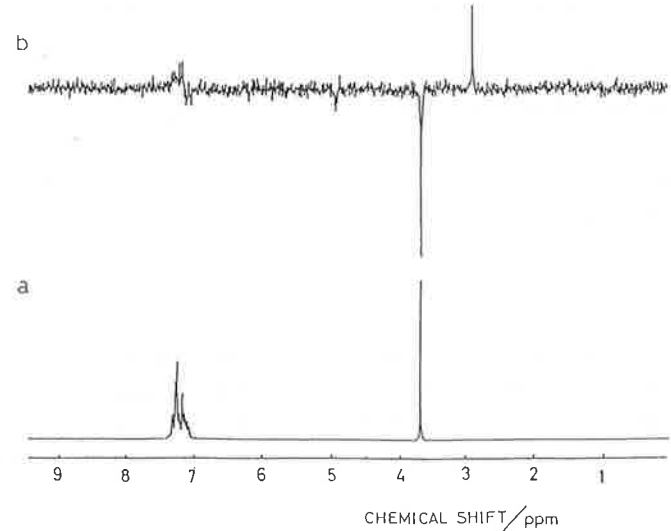


Figure 1. NMR spectra of DBK at room temperature (a) before light irradiation and (b) during the irradiation under the conditions of $P_{\text{sat}} = P_{\text{obs}} = 12.0 \mu\text{s}$, $\tau = 0.50 \text{ s}$, and $\tau_{\text{obs}} = 1.50 \text{ s}$.

Sometimes the absolute magnitude of the enhancement factor for the triplet precursor can be several orders of magnitude larger than that for singlet precursor. In order to avoid such misdetermination of the reaction precursor, not only the sign but also the magnitude of the enhancement factor of CIDNP should be analyzed with the aid of theoretical values.

Experimental determination of the enhancement factor is, however, very difficult. First of all, the observed CIDNP intensity is affected by relaxation and thus this effect should be properly taken into account. Second, in the present DBK photophysics case, the recombination product is chemically identical species with the reactant, and thus the amount of DBK produced by the reaction is hard to determine.

In this paper, the first difficulty was overcome by utilizing the saturation recovery pulse sequence, $(P_{\text{sat}} - \tau - P_{\text{obs}} - t_{\text{obs}})_N$, proposed by Lawler and Barbara.¹ The

second difficulty was overcome by the temperature dependence method to be outlined below. The observable physical quantities are (a) CIDNP intensity I of DBK, (b) decrease of the NMR intensity $-\delta I_e$ of DBK by the light irradiation, and (c) the consumption rate constant K of DBK. From kinetic consideration we obtain the following expression

$$\frac{1}{K} = \left(\frac{-\delta I_e}{I} \right) \frac{1}{k_{\text{exc}} E} \frac{1}{k_{\text{exc}}}$$

where k_{exc} is the rate constant which represents the efficiency of the creation of the radical pair by the light irradiation. Thus we expect that the plot of $1/K$ versus the $(-\delta I_e)/I$ ratio obtained at various temperatures should become a straight line and the slope/intercept ratio of this straight line can yield the enhancement factor E or the Boltzmann population corrected enhancement factor $\varepsilon = (g_N \mu_N B / 2kT)E$. The experimentally obtained plots are shown in Figure 2.

We indeed obtained a rather good straight line, and this observation supports several underlining assumptions made in developing the above kinetics.

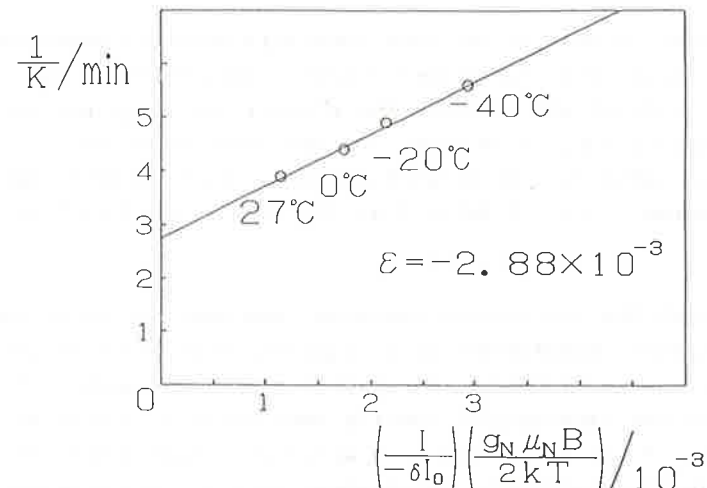


Figure 2. Plot of $1/K$ versus $(I / -\delta I_e) (g_N \mu_N B / 2kT)$

The ϵ value determined from Figure 2 is -2.88×10^{-3} . This value does not depend on the concentration of DBK in the 0.01 - 0.06 M range.

We are also able to obtain the quantum yield of the recombination (Φ_c) of DBK after the photocleavage reaction by the formula $\epsilon[\Phi_c/(1-\Phi_c)] = I/(-\delta I_e)(g_N\mu_N B/2KT)$. The results are shown in Table 1.

Table 1. Temperature dependence of the quantum yield of the recombination (Φ_c) of DBK after the photocleavage reaction.

Temp.	Φ_c
- 40 °C.	0.505
- 20 °C.	0.422
0 °C.	0.381
27 °C.	0.283

In order to analyze the experimentally obtained enhancement factor, ϵ values were calculated theoretically based on the theory of Pedersen and Freed.² The theoretical value for the triplet precursor ϵ_T is -0.2237. On the other hand, the theoretical value for the singlet precursor ϵ_S is a very small positive value. ($\epsilon_S = 5.5 \times 10^{-4}$ at 27°C, $\epsilon_S = 3.75 \times 10^{-4}$ at -40°C.)

Although the qualitative features (the emissive polarization and temperature independence of ϵ) suggests that the precursor of the photocleavage of DBK is the triplet state, the quantitative analyses of the experimental results encounters difficulties in two points. First difficulty is a great discrepancy between the observed and the calculated enhancement factor. The calculated ϵ value for the triplet precursor is two orders magnitude as large

as the experimental value (-2.88×10^{-3}). The second difficulty is that the yield of cage product (Φ_c) exceeds 1/3 below 0 °C. (Table 1). Since the photoreaction occurs in the high magnetic field (2.349T), only the T_0 state of the radical pair can mix with the S state. In such a case, Φ_c for the triplet precursor should be less than 1/3. We might be able to conceive of the following five possibilities for the origin of the discrepancies between the experimental results and theoretical expectation in ϵ and Φ_c . a) Participation of the spin-lattice relaxation of individual radical which composes the radical pair, b) participation of the spin-orbit coupling (SOC) in the radical pair state, c) regeneration of DBK from free radicals, d) Overhauser effect, and e) participation of the singlet precursor.

Having examined these five possibilities very carefully, we have finally reached the conclusion that the possibility e) is most likely. From the examination of the data, we conclude that nearly 80 % of the reaction takes place from singlet excited state. This conclusion was also supported by the triplet sensitizer experiments.

References

- [1] Lawler, R. G.; Barbara, P. F. J. Magn. Res. 1980, 40, 135.
- [2] Pedersen, J. B.; Freed, J. H. J. Chem. Phys. 1972, 61, 1517.

Temperature Dependence of the Magnetic Field Effect of the CIDNP in the Photocleavage of Cycloalkanone.

Naotoshi Suzuki, Kiminori Maeda, Qing-Xiang Meng,
Kouei Suzuki, Masahide Terazima[†], Tohru Azumi.

Department of Chemistry, Faculty of Science, Tohoku University, Sendai 980, Japan

[†] Present address: Department of Chemistry, Faculty of Science, Kyoto University, Kyoto, Japan

We measured the temperature effect of the effective J value of the biradical generated from photocleavage of cyclodecanone with using the magnetic field effect of CIDNP. The effective J value increases as higher temperature. We simulated the magnetic field effect of CIDNP with the stochastic Liouville equation. From this result we conclude that the temperature effect of effective J value is caused by the temperature dependence of the distribution function of interradical distance.

1. Introduction

Biradicals generated from the Norrish type I reaction of cycloalkanone have been well investigated. In this system the biradical chain dynamics is connected with the spin dynamics through the exchange integral J . So the interradical distance is very important for the reaction of biradicals.

Wang et al. reported the temperature dependence of the biradical lifetimes in the substituted cycloalkanone, and discuss the mechanism of intersystem crossing from Arrhenius plots¹. This temperature dependence is caused by the temperature dependence of the mean end to end distance of the biradical. Recently we found an evidence of the shrinking of the intermediate biradicals in the polymethylene linked systems through the simulation of the radical pair CIDEP spectrum². Staerk et al. recently reported the temperature dependence of the magnetic field effect on reaction yield of radical ion pair

linked with polymethylene chain³. The peak position of magnetic field effect curve shifts to the higher field at the higher temperature. They explained the temperature dependence of this magnetic field effect as due to motional shift rather than the shrinking of the end-to-end distance.

In this work, we measured the magnetic field effect (MFE) of CIDNP on the photocleavage of cyclodecanone in various temperatures, and determined the effective J value of the biradicals in each temperature from the peak position of the MFE of CIDNP. We simulated this curve with a stochastic Liouville equation⁴, and discuss the cause of the temperature effect.

2. Experimental

We used sample flow system in order to measure the magnetic field effect of CIDNP. The solution have to be transferred from quartz cell in the variable magnetic field to the NMR probe before nuclear polarization relaxes to thermally equilibrated polarization. The measurement is performed at -9, 4, 23, 40 °C.

3. Results and Discussion

The NMR spectrum before and during light irradiation of cyclodecanone are shown in Fig.1. All peaks of spectrum are emissive. This fact indicate that S-T₁ mixing mainly contributes to the intersystem crossing.

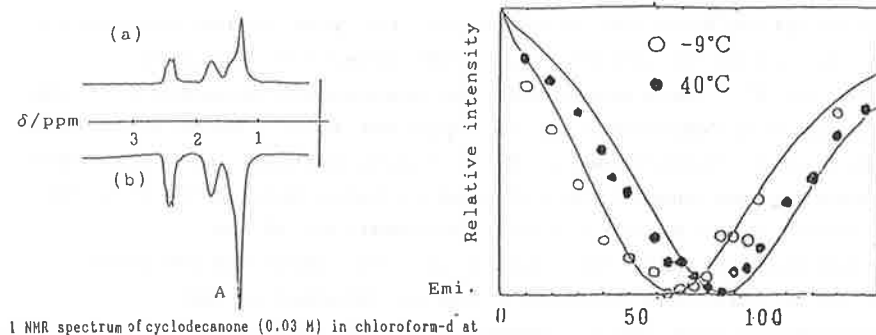


Fig 1 NMR spectrum of cyclodecanone (0.03 M) in chloroform-d at room temperature: (a) before the light irradiation, (b) during the light irradiation in the magnetic field $B=80\text{mT}$. Fig 2 The temperature dependence of MFE on CIDNP of cyclodecanone at -9°C and 40°C, solid curve is simulation spectrum with parameters shown in Table 2.

We observed the temperature dependence of magnetic field effect on CIDNP signal of peak A marked in Fig.1. The temperature dependence of MFE of CIDNP of cyclodecanone is shown in Fig.2. The peak position of the MFE curve shifts to higher field at higher temperature. When the exchange interaction is negative and relatively large compared with the hyperfine interaction, T-S mixing plays the most important role. The maximum T-S mixing and the maximum nuclear polarization must arise in the field when the T-S mixing appear in resonance. So the effective exchange integral J_{eff} is related with the magnetic field B_{max} which cause resonance in T-S mixing, as

$$g\mu_B B_{\text{max}} = 2J_{\text{eff}}$$

Therefore we can obtain the effective $|J_{\text{eff}}|$ value from the peak position of MFE of CIDNP. The effective exchange integral J thus determined at various temperatures are shown in Table.1. The effective J value increases as temperature increases.

In order to clarify the cause of the shift of the MFE curve, we simulated this curve with the stochastic Liouville equation proposed by Kanter et al. We examine the temperature dependence of the diffusional motion and that of the distribution of interradical distance. The diffusional motion of biradical is discussed by the restricted diffusion model. With the neglected the activation energy of C-C bond rotation, the effective diffusion constant D' is related with the viscosity of solvent by Einstein-Stocks equation. The effective diffusion constant D' is varied from 7.6×10^{-5} (-9°C) to 15.1×10^{-5} (40°C). If the temperature dependence of the distribution function is neglected, the peak in the calculated the MFE curve is independent of the effective diffusion constant D' . This means that the temperature dependence of the distribution function plays an important role. The distribution function is calculated by the following method. The only three conformations around the C-C bond is taken into account in the polymethylene chain. The all conformations of the polymethylene chain are counted up. The distribution function at an interradical distance r can be obtained at any temperature from the Boltzmann factor of individual

conformations. The results show that temperature dependence of the mean interradical distance r_{av} is small, but none the less meaningful.; $r_{\text{av}}(40^{\circ}\text{C}) \approx 9.15\text{\AA}$, $r_{\text{av}}(-9^{\circ}\text{C}) \approx 9.29\text{\AA}$. We simulate the MFE of CIDNP with this distribution function. Parameters shown Table.2 can fit the experimental MFE curve. Therefore we conclude that the shift of J_{eff} with temperature is caused by temperature dependence of distribution function.

Table 1 The temperature dependence of the exchange integral J determined from MFE of CIDNP of cyclodecanone.

$J_{\text{eff}} / \text{mT}$	
-9°C	33
4°C	36
22°C	39
40°C	42

Table 2 The parameter used for simulation of MFE of CIDNP.

$J_0 / \text{rad} \cdot \text{s}^{-1}$	0.65×10^{15}
$\alpha / \text{\AA}^{-1}$	1.43
$D' / \text{cm}^2 \cdot \text{s}^{-1}$	
(-9°C)	7.6×10^{-5}
(4°C)	9.4×10^{-5}
(22°C)	12.0×10^{-5}
(40°C)	15.1×10^{-5}

1. Wang,J.;Doubleday,C.;Turro,N.J. J. Am. Chem. Soc. 1989, 111, 3962
2. Maeda,K.;Terazima,M.;Azumi,T.;Tanimoto,Y. J. Chem. Phys. 1991, 95, 197
3. Staerk,H.;Busmann,H.G.;Kuhnle,W.;Treichel,R. J. phys. Chem. 1991, 95, 1906
4. Kanter,F.J.J.;Hollander,J.A.;Huizer,A.H.;Kaptein,R. Mol. phys. 1977, 34, 857

CIDNP and CIDEP Studies on Intramolecular Hydrogen Abstraction Reaction of Polymethylene linked System.

Kiminori Maeda, Naotoshi Suzuki, Qing-Xiang Meng, Kouei Suzuki, Masahide Terazima[†], Tohru Azumi.

Department of Chemistry, Faculty of Science, Tohoku University, Sendai 980, Japan.

Yoshifumi Tanimoto

Department of Chemistry, Faculty of Science, Hiroshima University, Hiroshima 730, Japan.

Abstract

Intramolecular hydrogen abstraction reaction of a polymethylene linked xanthone and xanthene is investigated by using low field chemically induced dynamic nuclear polarization (CIDNP) and chemically induced dynamic electron polarization. The exchange integral J between the two terminal radicals of the system is obtained from the simulation process by using the spin-correlated radical pair CIDEP theory. The magnetic field effect of the CIDNP is simulated with the stochastic Liouville equation, and the effective exchange integral J between the two terminal radicals is determined from the peak position. The determined J values are much longer than those obtained by the CIDEP method. The differences of the J values obtained from CIDEP and CIDNP is discussed.

1. Introduction.

Intramolecular hydrogen abstraction reaction of a polymethylene linked xanthone and xanthene ($XO-(n)-XH_2$ n=3,6,12) has been investigated by using the transient absorption, and the effect of the exchange interaction has been suggested from the magnetic field effects of the biradical lifetime.¹⁾ But it is difficult to measure the exact value of the exchange integral with using the optical methods. In this study, the exchange integral J between the two terminal radicals of the polymethylene linked system is obtained from both of the simulation of the radical pair CIDEP spectrum and the magnetic field effect of the low field CIDNP respectively. Further we compare the observed J values obtained from the low field CIDNP and the spin correlated CIDEP method.

[†]) Present address: Department of Chemistry Faculty of Science, Kyoto University, Kyoto, Japan.

1) Tanimoto, Y.; Takashima, M.; Hasegawa, K.; Itoh, M. *Chem. Phys. Lett.* 1987, 137, 330.

2. Experimental.

CIDEP studies were carried out on an Ar-bubbled solution by using a flow system and an excimer laser (XeCl, 308nm) as a light source. The CIDEP apparatus and flow systems of the solution were similar to those reported by Akiyama et al.²⁾ In the measurement of magnetic field dependence of CIDNP, the photoreaction was carried out in a JEOL RE-1X magnet, and the CIDNP spectrum was measured at high field in a JEOL FX-100 NMR spectrometer. The sample was transferred from the ESR magnet to the NMR magnet by using a flow system. The solution was deoxygenated by the nitrogen bubbling method. Chloroform-d was used for the solvent and the concentration was about 0.025M.

3. Results and discussion.

The CIDEP spectrum of $XO-(12)-XH_2$ at -60°C is shown in Figure 1. This CIDEP spectrum cannot be interpreted either by the conventional radical pair mechanism or by the triplet mechanism and can be simulated based on the spin correlated radical pair CIDEP mechanism. In the

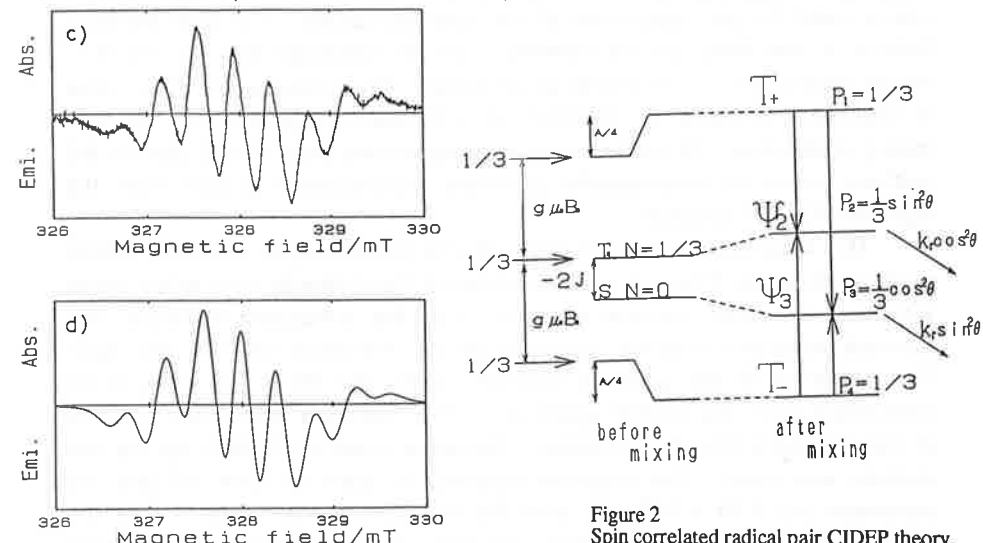


Figure 2
Spin correlated radical pair CIDEP theory.

Figure 1
a) The CIDEP spectrum of $XO-(12)-XH_2$ at -60°C.
Delay time is 1μs. b) Simulation spectrum.

2) Akiyama,K.;Tero-Kubota, S.; Ikegami, Y.; Ikenoue,T. *J. Phys. Chem.* 1985, 89, 339.

simulation process of this CIDEP, we used the spin correlated CIDEP theory shown in Figure 2 modified with (a) the fast population relaxation between the central S-T₀ mixed state,³⁾ (b) the contribution from the triplet mechanism, and (c) hyperfine line dependent line width.⁴⁾ We changed J value as the fitting parameter and simulate the observed spectrum. The observed spectrum can be reproduced well with $-0.0 > J > -0.18$ mT. Figure 1 b is an example of the simulation spectrum with $J=-0.1$ mT, $\alpha=6.5 \times 10^{-3}$. The finite value of α means that the triplet mechanism exists in the spin correlated radical pair CIDEP spectrum. The agreement between the calculated and observed CIDEP is very good. From the simulation the effective J value of the intermediate biradical is determined for the three different polymethylene chains.

The low field CIDNP spectrum of XO-(3)-XH₂ below 25mT shows total emission pattern. In Figure 3, the spectrum measured at 5mT is depicted for example. The pattern is totally different from that measured in high magnetic field (2.5T) reported previously. The spectrum in high field is satisfactorily explained by the S-T₀ mixing mechanism and the Kaptein's rule is used for the assignment of the observed peaks. The total emission feature in low field, on the contrary, can be explained well by the S-T₀ mixing mechanism. In the biradical system, the exchange integral J value is significant because of restriction of interradical diffusion and the S-T₀ mixing is effective. In ref.3 we have assigned the peak at 4.5 ppm to the methine proton of intramolecular geminate recombination product from the high field CIDNP spectrum.

The magnetic field dependence of the CIDNP signal intensity of this peak is shown in Figure 4. We simulated the magnetic field effect curve with the stochastic Liouville method. For the simulation spectrum, the reported hyperfine coupling constants of the individual radicals are used. The difference of the g values between XO_H and XH is too small to be determined from the CIDEP spectrum in the hydrogen abstraction reaction of free xanthone from the xanthene. The same g value (2.00331) for the two radicals was used. The hyperfine coupling constant A=1.264 mT and the parameter $J_0=-9.48 \times 10^8$ mT⁵⁾ from the literature and $a = 1.80 \text{ \AA}^{-1}$ as the fitting parameter. The effective diffusion constant calculated from the solvent viscosity 5×10^{-5} is used for the effective diffusion constant D'.

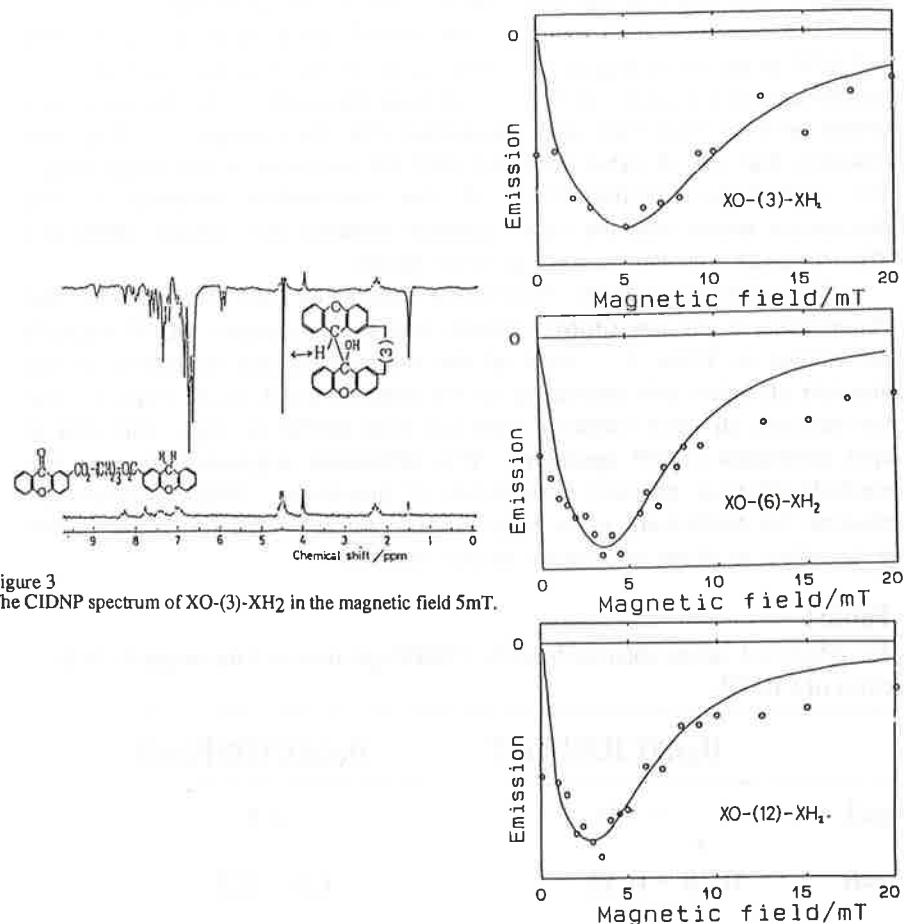


Figure 3
The CIDNP spectrum of XO-(3)-XH₂ in the magnetic field 5mT.

Figure 4
Magnetic field effect of CIDNP intensity.
(a) XO-(3)-XH₂, (b) XO-(6)-XH₂, (c) XO-(12)-XH₂.

³⁾ Terazima, M.; Maeda, K.; Azumi, T.; Tanimoto, Y.; Okada, N.; Itoh, M. *Chem. Phys. Lett.* 1989, 164, 562.

⁴⁾ Maeda, K.; Terazima, M.; Azumi, T.; Tanimoto, Y. *J. Phys. Chem.* 1991, 95, 197.

⁵⁾ Kanter,F.J.J. ;Sagdeev, R. Z. ;Kaptein,R. *Chem.Phys.Lett.* 1978, 58, 334.

We used the kinetic parameter $k_r = 1.0 \times 10^8 \text{ s}^{-1}$ and $k_s = 1.0 \times 10^6 \text{ s}^{-1}$. They are almost the same with the other work and the curve of the magnetic field effect is not sensitive to such kinetic parameters.

The magnetic field effect of the CIDNP polarization in XO-(n)-XH_2 ($n=3, 6, 12$) is shown in Figure 4. The curve of the magnetic field effect is normalized by the peak intensity. The peak positions of the magnetic field effects shift to high field with decreasing the chain length n . This shift indicates that the $|J|$ value increases with the decrease of the chain length. The probability function $P_0(r)$ of the interradical distance in the equilibrium shows that the mean distance between the radicals (XOH and XH) increases with the increase of chain length.

The $|J_{eff}|$ value of the XO-(n)-XH_2 determined from the magnetic field dependence of the low CIDNP intensity and spin correlated CIDEPE methods are shown in Table 1. Both of the methods show increasing of the absolute $|J|$ value with decreasing of the polymethylene chain length n . But the absolute $|J|$ value observed from low field CIDNP is larger than that of spin correlated CIDEPE spectrum. This difference suggests that the two methods observe different components of biradicals; CIDEPE method can observe the conformers which have longer interradical distance, and CIDNP is sensitive to those of relative shorter distance.

Table 1

The effective J values obtained from the CIDEPE spectrum and the magnetic field effect of CIDNP.

	$ J_{eff} (\text{CIDEPE})/\text{mT}$	$ J_{eff} (\text{CIDNP})/\text{mT}$
$n=3$	~ 7.0	2.5
$n=6$	0.28 ~ 0.38	1.5 ~ 2.5
$n=12$	~ 0.18	1.3 ~ 1.7

From Table 1 $|J_{eff}|$ is shifted to larger value in shorter interradical chain length. Recently Tanimoto et. al. reported the magnetic field effects on the biradical lifetime in this system. They suggested that the chainlength dependence of the biradical lifetime is the effect of the change of the $|J|$ value. Mainly the decay of the biradical is caused by the geminate recombination between the terminal radicals. The geminate recombination products, which shows CIDNP, is formed through the geminate recombination process concerned with the decay of the biradicals. Therefore the $|J_{eff}|$ from CIDNP seems to be better to explain the chainlength dependence of the magnetic field effect of biradical lifetimes. Indeed, the shift of the J value obtained from CIDEPE is so small that it is difficult to explain the result of the transient absorption, but the shift of the $|J_{eff}|$ obtained from CIDNP is larger than that of CIDEPE and more explanable to the chainlength dependence of the magnetic field effect.

Acknowledgment.

We are much indebted to Professor Y.Ikegami, Professor S.Tero-Kubota, and Dr.K.Akiyama of the Chemical Research Institute of Non-Aqueous Solutions, Tohoku University, for allowing us to use their CIDEPE apparatus. We also express our thanks to Fujinomiya Research Laboratories of Juji Photo Film CO., Ltd., for the gift of the sample. The present research was supported by a Grant-in-Aid for Scientific Research (No.62430001) from the Japanese Ministry of Education, Science and Culture.

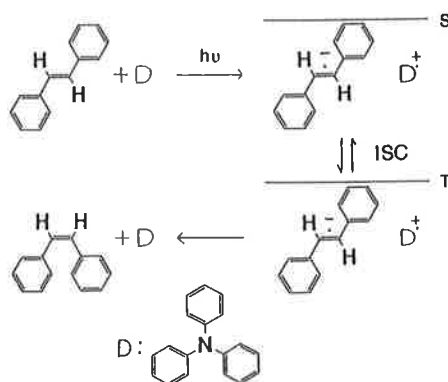
Effect of Coulomb Force on Diffusion as Studied by CIDNP Intensities of Photo-Induced Electron Transfer Reactions of trans-Stilbene

Takafumi Aizawa, Tomomi Sakata, Kiminori Maeda, Tohru Azumi
Department of Chemistry, Faculty of Science, Tohoku University,
Sendai 980, Japan

In order to examine the effect of Coulomb force in the diffusional motion of radicals, the CIDNP intensities of photosensitized trans-stilbene isomerization in various solvents are measured. Theoretical analysis using a stochastic Liouville equation is carried out. As a result, as the solvent permittivity decreases, the yield of the reaction product first increases and then decreases.

1. Introduction

The CIDNP intensity of triphenylamine-sensitized isomerization of trans-stilbene is measured. The CIDNP studies carried out by Kruppa et al. show that this reaction takes place via a radical ion pair.^{1,2)} (Scheme 1) In this case, the effect of Coulomb force between the positive and negative radical components of each radical pair is important in the diffusional motion of radicals. In order to examine the effect of Coulomb force in the diffusional motion of radicals, the solvent polarity effect of the CIDNP intensity is measured. Theoretical analysis using a stochastic Liouville equation including the effect of Coulomb force in the diffusional motion is carried out.



Scheme 1 Reaction scheme of photo-induced electron transfer reactions of trans-stilbene. Triphenylamine is used as a donor. ISC, intersystem crossing, depends on the nuclear spin, so CIDNP is observed at the peak of cis-stilbene.

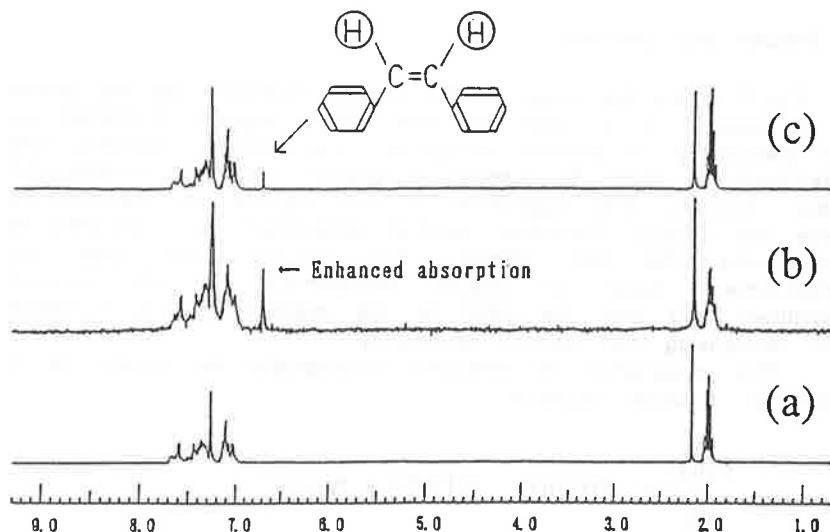


Fig. 1 ¹H CIDNP in trans-cis isomerization of stilbene in the presence of triphenylamine. The enhanced absorption is measured at the peak of cis-stilbene. (a) before irradiation, (b) in the presence of light, (c) after irradiation.

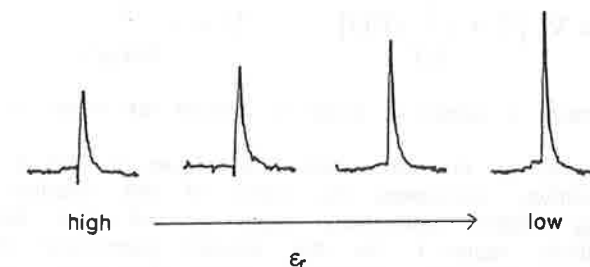


Fig. 2 CIDNP intensities at the peak of cis-stilbene. The CIDNP intensity gets large as the solvent permittivity decreases.

2. Experimental

The CIDNP intensities (enhanced absorption for cis-stilbene, see Fig. 1) are measured in solvents of various permittivities. The sample is mixture of 0.02M trans-stilbene and 0.02M triphenylamine. We change the solvent permittivity by varying the mixing ratio of acetonitrile-d₃ ($\epsilon_r=37.5$) and benzene-d₆ ($\epsilon_r=2.28$).

3. Results and discussion

Fig. 2 shows the effect of the solvent permittivity on the proton of cis-stilbene. It is clear that the CIDNP intensity increases as the permittivity of solvent decreases. The CIDNP intensities are determined by both the amount of product and the enhancement factor; however, this experiment is not capable of distinguishing these two factors. Therefore, another experiment was designed to discriminate the two effects. The results show that the enhancement factor is almost independent of the solvent permittivity and only the yield of the reaction product increases with decreasing the solvent permittivity.

This observation is analyzed theoretically by means of a stochastic Liouville equation,

$$\frac{\partial \rho(t)}{\partial t} = -iH^x \rho(t) + D\Gamma \rho(t) + K\rho(t)$$

where $\rho(t)$ is the spin density matrix of the radical pair, H^x is the spin Hamiltonian, K is the reaction operator, and Γ is the diffusion operator. The diffusion operator is expressed as follows:

$$\Gamma = \nabla \cdot [\nabla + (\frac{1}{kT}) \nabla U] \quad U = -\frac{e^2}{4\pi\epsilon_0\epsilon_r r}$$

The second term is added in order to include the effect of Coulomb force.

The results of the calculation are shown in Fig. 3. As the solvent permittivity decreases, the yield of the reaction product first increases (higher permittivity region), and then decreases (lower permittivity region). As the solvent permittivity decreases, the effect of Coulomb attractive force increases. In higher permittivity region as the solvent permittivity decreases the probability of reencounter increases. As a result the yield increases. In lower permittivity region as the solvent permittivity decreases the probability of intersystem crossing decreases. So the yield decreases.

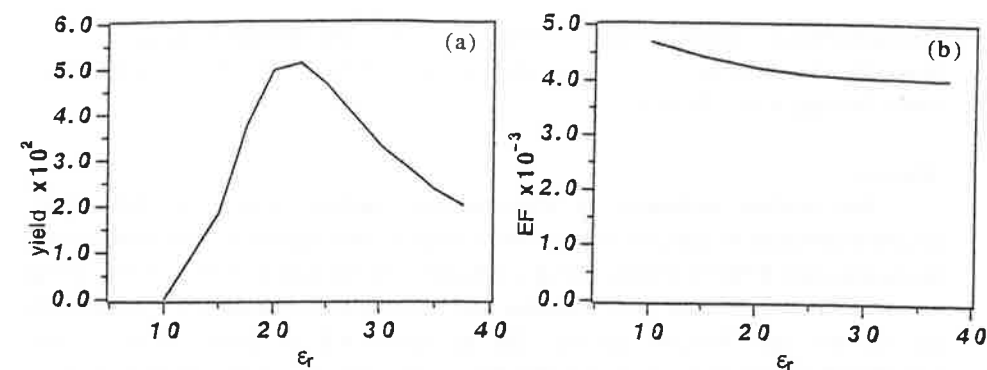


Fig. 3 The results of the calculation. (a) the yield of the reaction product, (b) enhancement factor

The behavior observed experimentally is in accord with theoretical calculations in higher permittivity region. In this region the increase of the probability of reencounter at higher permittivity is more important than the suppression of the probability of intersystem crossing. The Coulomb force affects more to increase the probability of reencounter than to suppress the probability of intersystem crossing.

In conclusion Coulomb force between radicals affects the diffusional motion of radicals. In the present system by the effect of Coulomb force the yield of the reaction product increases as the permittivity of solvent decreases.

References

- 1) T. V. Leshina, S. C. Belyaeva, V. I. Maryasova, R. Z. Sagdeev and Yu. N. Molin, Chem. Phys. Lett., 75, 438(1980).
- 2) A. I. Kruppa, O. I. Mikhailova and T. V. Leshina, Chem. Phys. Lett., 147, 65(1988).

Photo-Induced Electron Transfer Reaction Between Hexamethyldisilane and Quinones as Studied by a CIDNP Technique

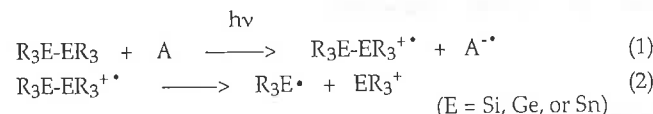
Masanobu Wakasa, Masatoshi Igarashi, Yoshio Sakaguchi, and Hisaharu Hayashi
Molecular Photochemistry Laboratory, The Institute of Physical and Chemical Research,
Wako, Saitama 351-01 (Japan)

Abstract

The reaction mechanism of photo-induced electron transfer reactions from hexamethyldisilane to quinones in chloroform solution was studied at room temperature by means of a CIDNP technique. With irradiation, the formation of the corresponding mono- and di-trimethylsilyl hydroquinones and trimethylsilyl chloride was confirmed by GC, GC-MS, and ^1H NMR spectra. The absorptive CIDNP phase of the mono-trimethylsilyl hydroquinone indicates that this reaction precursor is the triplet radical ion pair of the hexamethyldisilane cation radical and quinone anion radical, and that the former radical reacts with the latter prior to the fission of its Si-Si bond.

1. Introduction

The σ -bonds between group 14 elements (Si-Si, Ge-Ge, Sn-Sn etc.) have rather low ionization potentials [1,2]. These values are close to those of carbon-carbon π -bonds, not of their σ -bonds. For this advantage, these compounds ($\text{R}_3\text{E-ER}_3$) have been widely used as electron donors. The photo-induced electron transfer between group 14 element compounds and electron acceptors have been studied for interests in the reaction mechanism and the synthetic chemistry during last decade [3-10]. After the photo-initiated electron transfer to the acceptor, the resultant cation radical ($\text{R}_3\text{E-ER}_3^{+ \cdot}$) is considered to decompose quickly to a couple of group 14 element centered radical ($\text{R}_3\text{E}^{\bullet}$) and cation ($\text{ER}_3^{+ \cdot}$) type species. (eqs.(1) and (2))



However, there has been no report elucidating clearly the existence of the reaction intermediates for eqs.(1) and (2). In addition, almost all reports use nitriles like cyanobenzenes and cyanoethylenes as electron acceptors. There are few experiments with other electron acceptors [11-13].

In the present paper, we used quinones instead of nitriles as electron acceptors, and carried out the photo-induced electron transfer reactions of hexamethyldisilane with high potential quinones; 1,4-benzoquinone (BQ), chloro-1,4-benzoquinone (MCQ), 2,5-

dichloro-1,4-benzoquinone (2,5-DCQ), 2,6-dichloro-1,4-benzoquinone (2,6-DCQ), and tetrachloro-1,4-benzoquinone (TCQ). On the bases of the laser-photolysis studies, CIDNP spectra and product analysis, we shall discuss the reaction intermediate and mechanism [14].

2. Results and discussion

The chloroform solution of hexamethyldisilane ($\text{Me}_3\text{Si-SiMe}_3$) and quinones in quartz photolysis cell was irradiated with a 1-kW high pressure mercury lamp after bubbling pure nitrogen gas at room temperature for 10 min. The reaction products were analyzed by GC and GC-MS. The main products were dichloro-4-trimethylsiloxyphenols (1's, HQSiMe_3), dichloro-1,4-bis(trimethylsiloxy)benzenes (2's, $\text{Me}_3\text{QSiMe}_3$) and trimethylsilyl chloride (3).



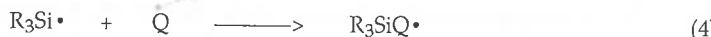
The typical product yields obtained for the reaction of $\text{Me}_3\text{Si-SiMe}_3$ (273 mM) and 2,5-DCQ (252 mM) were 32.1 % (1a), 10.2 % (2a), and 50.4 % (3) based on the amount of consumed $\text{Me}_3\text{Si-SiMe}_3$. Fig. 1 shows the NMR spectrum of $\text{Me}_3\text{Si-SiMe}_3$ (50 mM) and 2,5-DCQ (100 mM) in CDCl_3 after irradiation for 10 min. Here, the signals of the starting compounds were observed at 0.04 ppm (methyl-H of $\text{Me}_3\text{Si-SiMe}_3$) and at 7.16 ppm (ring-H of 2,5-DCQ). Several new signals appeared in the course of the irradiation with the concomitant decrease of the starting ones. The signals at 0.16, 4.38, and 7.40 ppm were assigned to the methyl-H, hydroxyl-H, and ring-H of product 1a, respectively. The signals at 0.29 and 6.86 ppm were assigned to the methyl-H and ring-H of product 2a. The signal at 0.46 ppm was assigned to methyl-H of product 3.

The hydroxyl-H of 1a is not deuterium as shown in Fig. 1. The products of this reaction in CHCl_3 and in CDCl_3 were analyzed by GC-MS. The mass spectrum of 1a formed in CDCl_3 showed the same parent m/e peak ($\text{M}^+ 250$) observed in CHCl_3 [15]. Accordingly, the hydroxyl-H of 1a as a final product is concluded not to be deuterium but to be hydrogen. In addition, the strong CIDNP signal of hydroxyl-H, as described later, stands against the formation of deuterated 1a and the following D-H exchange by the contaminated H_2O in CDCl_3 . Consequently, the hydrogen of the solvent is not introduced to 1a.

When 2,6-DCQ, MCQ, and BQ were used, the products were similar to those observed for the reaction of 2,5-DCQ. In the case of TCQ, $\text{Me}_3\text{Si-SiMe}_3$ was decreased during the irradiation, but 1 could not be observed. This may be due to the instability of 1 ($n=4$) or due to some different reaction paths.

In order to clarify further the reaction intermediates and reaction precursor, transient absorption spectra studies were carried out. Nanosecond transient absorption spectra measurements were performed on the chloroform solution of $\text{Me}_3\text{Si-SiMe}_3$ and 2,5-DCQ using fourth harmonic pulse of a Nd: YAG laser as an exciting light source. The time-resolved absorption spectra observed at delay times of 100 ns and 9 μs after excitation are shown in Fig. 2 (a). The spectra of this figure have three absorption peaks (A-C). The time dependence of the transient absorbance ($a(t)$) of each absorption peak is also shown in Fig. 2 (b).

As shown in Fig. 2 (b), the $a(t)$ curves of peaks A and B decay more slowly than that of peak C. Both peaks A and B can safely be assigned to be the 2,5-DCQ anion radical because the spectral shapes and the peak position agree well with those of BQ and TCQ anion radicals in literature [16]. Careful examination of the peak A shows that this is composed of the two components (lifetime, $\tau > 20 \mu\text{s}$, $\tau < 2 \mu\text{s}$, respectively). The former is reasonably assigned to that of the 2,5-DCQ anion radical. What is the latter carrier of the shorter lived transient? On the basis of the reaction products and the position of the absorption band, an plausible intermediate is trimethylsiloxyphenoxyl radical ($\text{Me}_3\text{SiQ}^\bullet$). Then, we tried to generate it by another reaction route, as shown in eqs. (3) and (4), and measured the transient absorption spectrum of it.



The observed spectrum of $\text{R}_3\text{SiQ}^\bullet$ agrees well with those as shown in Fig. 2 (a). Accordingly, the shorter lived species at peak A may be assigned to $\text{Me}_3\text{SiQ}^\bullet$. The peak C can safely be assigned to be the T-T absorption of 2,5-DCQ because of the lifetime and the peak position.

Here, we would like to construct the reaction scheme. Since the light was selectively absorbed by quinone (Q) in the initial stage of the reaction, the triplet excited state of Q (${}^3\text{Q}^*$) should be generated immediately after its intersystem crossing. The triplet radical pair of $\text{Me}_3\text{Si-SiMe}_3^{+}\cdot$ and $\text{Q}^{-}\cdot$ is formed by electron transfer from $\text{Me}_3\text{Si-SiMe}_3$ to ${}^3\text{Q}^*$.

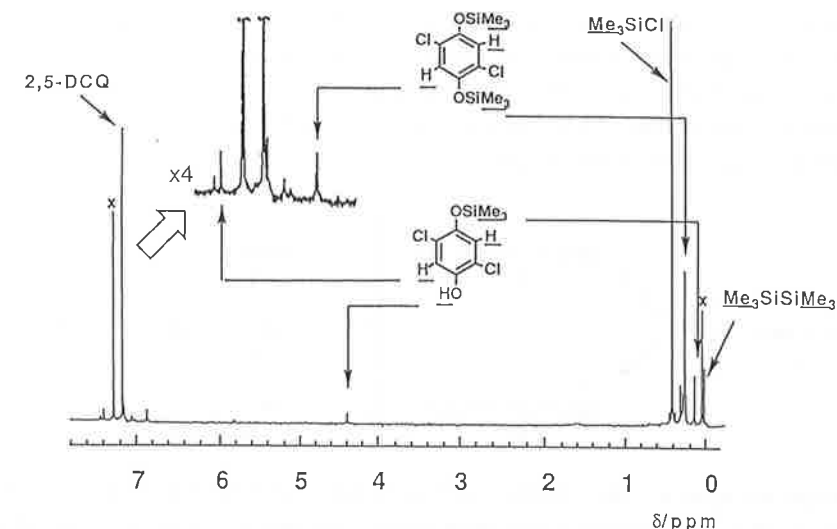
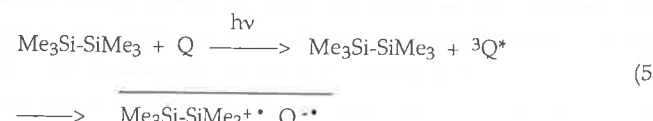


Fig. 1 ${}^1\text{H}$ NMR spectrum of $\text{Me}_3\text{Si-SiMe}_3$ (50 mM) and 2,5-DCQ (100 mM) in CDCl_3 after irradiation for 10 min. The signals denoted by x are due to hexamethyldisiloxane (0.07 ppm) and CHCl_3 (7.27 ppm). Hexamethyldisiloxane is a minor contamination of $\text{Me}_3\text{Si-SiMe}_3$.

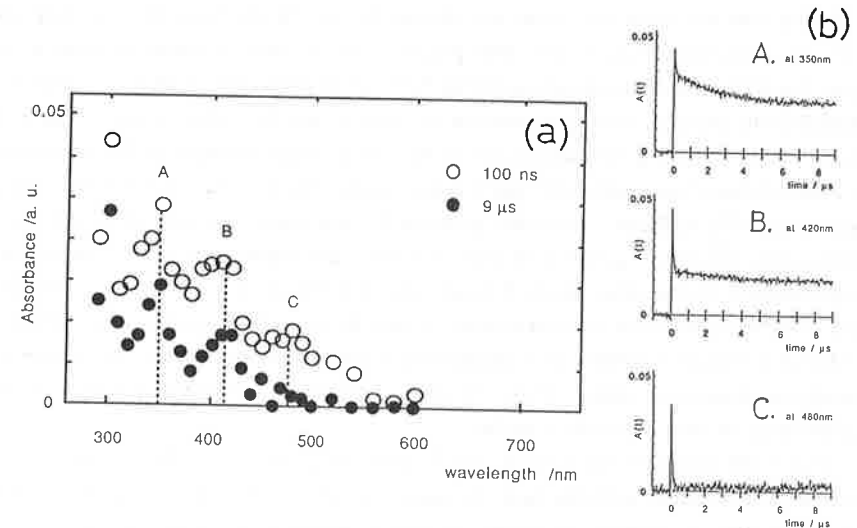
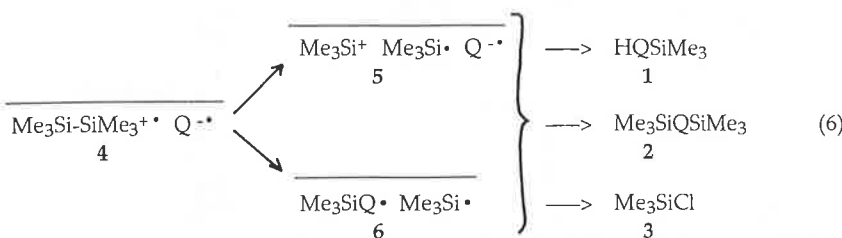


Fig. 2 (a) Transient absorption spectra of $\text{Me}_3\text{Si-SiMe}_3$ and 2,5-DCQ in chloroform at delay time of 500 ns and 9 μs after excitation. (b) $A(t)$ curves at 350, 420, and 480 nm.

The absence of CT absorption band eliminates the direct charge separation from the singlet excited state of the complex. The products **1**, **2**, and **3** are produced by succeeding reactions. Since **1** and **2** are mono- and di-trimethylsilyl adducts of quinones, the Si-Si bond fission of $\text{Me}_3\text{Si}-\text{SiMe}_3^{+}$ is necessary. This bond fission is considered to occur either by itself or by reaction as shown in eq.(6).



The initial radical pair **4** of $\text{Me}_3\text{Si}-\text{SiMe}_3^{+}$ and $\text{Q}^{\cdot-}$ can be transformed to radical pair **5** of $\text{Me}_3\text{Si}^{\cdot}$ and $\text{Q}^{\cdot-}$ by spontaneous Si-Si bond fission. The radical pair **6** of the trimethylsiloxyphenoxyl radical ($\text{Me}_3\text{SiQ}^{\cdot}$) and $\text{Me}_3\text{Si}^{\cdot}$ can be formed by the reactive fission of $\text{Me}_3\text{Si}-\text{SiMe}_3^{+}$ with $\text{Q}^{\cdot-}$.

At the initial stage, radical pairs are all in solvent cages. The formation of **1**, **2**, and **3** can occur either in the cage or after the separation of the component radicals from the pair. To elucidate the reaction scheme, we should classify the products into "in-cage" and "out-of-cage" reaction products. For this purpose, we scavenged escaping radicals by oxygen. The CDCl_3 solution containing $\text{Me}_3\text{Si}-\text{SiMe}_3$ (12.5 mM) and 2,5-DCQ (50 mM) was irradiated in the presence and in the absence of oxygen, and the yields of **1a** and **2a** were analyzed by ^1H NMR. The formation rates of **1a** and **2a** under nitrogen at the early stage were $0.154 \text{ mM min}^{-1}$ and $0.089 \text{ mM min}^{-1}$, respectively. On the other hand, those under oxygen were $0.122 \text{ mM min}^{-1}$ and $0.047 \text{ mM min}^{-1}$. The formation rate of **2** was much suppressed by oxygen compared with that of **1**. Thus, **2** is attributable to an "out-of-cage" reaction product. On the other hand, **1** is considered to be an "in-cage" reaction product. Since **3** is not included in the initial reactions, **3** must be an "out-of-cage" reaction product. The CIDNP technique is suitable to determine the reaction path, since this reaction includes a radical pair at its initial stage. Then, we tried to measure the CIDNP spectra to decide the importance of radical pairs **4**, **5**, and **6**.

The NMR spectra of $\text{Me}_3\text{Si}-\text{SiMe}_3$ (12.5 mM) and 2,5-DCQ (50 mM) in CDCl_3 were measured on irradiation with the high pressure mercury lamp. Those obtained before, during, and after irradiation are shown in Fig. 3. Several new signals were observed during irradiation. Among them, the signals at 4.38, 6.65, 7.40 and 7.44 ppm disappeared after irradiation as shown in Figs. 3-(b) and (c). Since the signals at 4.38 and 7.40 ppm are assigned to **1a** as observed in Fig. 1, these signals are ascribed to the enhanced

absorption (A) signals due to CIDNP. The yield of **1a** in $4\text{sec} \times 32$ irradiation is so small that the signal for hydroxyl-H and ring-H of **1a** is not observed in Fig. 3-(c). The polarization of hydroxyl-H is about ten times larger than that of ring-H. The other two signals are not assigned to the main products and will not be discussed further. No polarization was observed for the signals due to **2a** and **3**.

The CIDNP measurements were also carried out with other quinones. 2,6-DCQ gave the same A polarization of ring-H and hydroxyl-H like 2,5-DCQ. MCQ gave also A phase of hydroxyl-H of **1**, but its polarization was too weak to observe that of ring-H. When BQ was used, we could not observe any CIDNP signal. This may be due to the low reactivity of BQ.

The reaction mechanism can be analyzed by Kaptein's CIDNP phase rule [17](eq.(7)):

$$\Gamma = \mu \cdot \varepsilon \cdot \Delta g \cdot \alpha \quad (7)$$

$\Gamma > 0$: Enhanced absorption (A)

$\Gamma < 0$: Emission (E).

Here the parameters μ and ε enter with the following signs:

μ : the initial spin multiplicity of a given radical pair

+ : triplet, - : singlet

ε + : for "in-cage" reaction products - : for "out-of-cage" reaction products.

The parameter Δg is the difference of the g values, the parameter α is hyperfine coupling (hfc) constant of examined H atom.

In the reaction of $\text{Me}_3\text{Si}-\text{SiMe}_3$ and $\text{Q}^{\cdot-}$, we found the A polarization on ring-H and hydroxyl-H of **1**. As mentioned above, the initial reaction proceeds via the triplet radical pair ($\mu > 0$), and **1** is the "in-cage" reaction product ($\varepsilon > 0$). On the other hand, the signs of Δg and α are dependent on the radical pair, which enables us to discriminate the reaction mechanism. The g values and the signs of the hfc for the component radicals in each radical pair in eq.(6) are listed in the Table 1.

We would like to consider the polarization for ring-H first. The expected polarizations of ring-H should be A ($\Gamma > 0$), E ($\Gamma < 0$), and E ($\Gamma < 0$) for **1a** produced from radical pairs **4**, **5**, and **6**, respectively. Since the observed polarization was A, the reaction precursor is the radical pair **4** of hexamethyldisilane cation radical and quinone anion radical rather than the radical pair **5** and **6**. The polarization phase for hydroxyl-H of **1a** can also be consistent with radical pair **4**.

The polarization phase of **1a** derived from radical pair **4** indicates that radical pair **4** has a long lifetime, namely the Si-Si bond fission of $\text{Me}_3\text{Si}-\text{SiMe}_3^{+}$ is not so fast. To get the polarization for hydroxyl-H, the hydrogen must come from the initial radical pair.

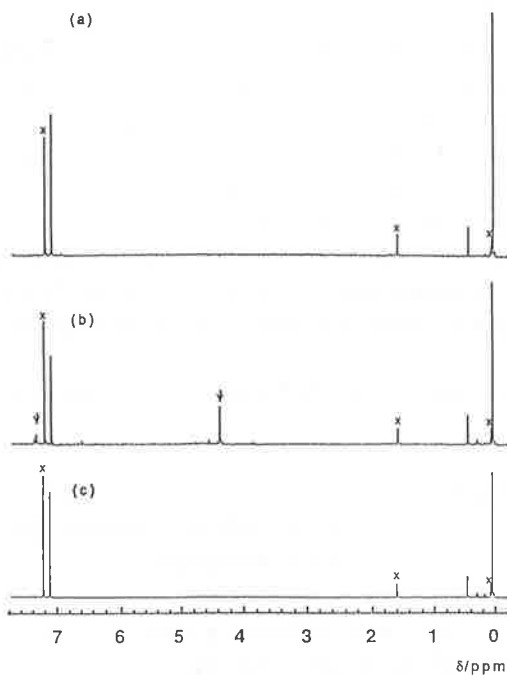


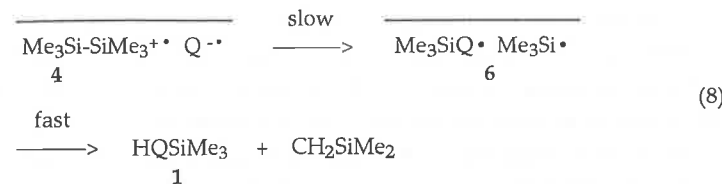
Fig. 3 ^1H NMR spectra of $\text{Me}_3\text{Si}-\text{SiMe}_3$ (12.5 mM) and 2,5-DCQ (50 mM) in CDCl_3 , (a) before, (b) during, and (c) after irradiation. All of them are obtained by 32 times accumulation. Spectra (b) and (c) are obtained by 4sec \times 32 irradiation. The arrows denote the CIDNP signals of **1a**. The signals denoted by x are hexamethyldisiloxane (0.07 ppm), H_2O (1.59 ppm), and $^1\text{CHCl}_3$ (7.27 ppm).

Table 1. The g values and signs of hyperfine coupling constants of component radicals in expected radical pairs.

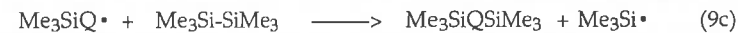
radical	g value [ref.]	the sign of proton hfc [ref.]
$\text{Me}_3\text{Si}-\text{SiMe}_3^{+}\cdot$	2.0075 [18]	+
$\text{Me}_3\text{Si}\cdot$	2.0031 [19]	-
$\text{Q}^{\cdot-}$ Q = 2,5-DCQ	2.0055 [13]	-
2,6-DCQ	2.0053 [13]	-
MCQ	2.0058 [20]	
BQ	2.0050 [13]	-
$\text{R}_3\text{EQ}^{\cdot-}$ Q = 2,5-DCQ	2.0054 ^a [13]	-
2,6-DCQ	2.0053 ^a [13]	
BQ	2.0047 ^a [13]	
t-Bu ₂ Q	2.0046 ^b [12]	

a) R=n-Bu, E=Sn, b) R=Et, E=Si. The g values of $\text{Me}_3\text{SiQ}\cdot$ are expected to be similar to these values.

To generate **1**, the reaction must proceed via radical pair **6**, but the polarization due to radical pair **6** was not observed. The appearance of the polarization due to radical pair **4** instead of radical pair **6** is explained by the "memory effect" [27]. Consequently, the lifetime of radical pair **6** is considered to be short owing to disproportionation.(eq.(8))



Product **2** is formed by "out-of-cage" reaction after the separation of the component radicals from radical pair **6**(eq.(9a)) Consequently, the nuclear polarization on the escaping radicals should be relaxed before the termination reaction.(eq(9b) and (9c))



Product **3** would be generated through several processes. Free $\text{Me}_3\text{Si}\cdot$ is obtained after several steps from the separation of radicals from radical pairs **4**, **5**, and **6**, and the reaction of this free $\text{Me}_3\text{Si}\cdot$ with chloroform generates **3**. (eq.(10)) Therefore, the polarization of **3** is unexpected.



The whole reaction mechanism of the photo-induced electron transfer reaction between $\text{Me}_3\text{Si}-\text{SiMe}_3$ and Q is represented by eqs.(5), (8), (9), and (10).

In conclusion, the reaction mechanism of photo-induced electron transfer reaction from hexamethyldisilane, a group 14 element compound, to halogenated quinone was explained clearly by means of a CIDNP technique. In chloroform solution of hexamethyldisilane and quinone, mono- and di-trimethylsilyl hydroquinones and trimethylsilyl

chloride are formed on irradiation. We have proved that the reaction precursor is the ion radical pair of the hexamethyldisilane cation radical and quinone anion radical. In the formation of mono-trimethylsilyl hydroquinone, the former radical reacts with the latter prior to the fission of its Si-Si bond.

3. Experimental

Apparatus. ^1H NMR spectra and CIDNP spectra were recorded with a JEOL JNM-FX100 FT NMR spectrometer. UV absorption spectra were measured with a Hitachi 320 spectrophotometer and a quartz cell of 1 cm path length. Gas chromatography was performed with a Shimadzu GC-8A equipped with a 2 m 10 % SE30 column. GC-MS spectra were recorded with a JEOL JMS-DX 303 mass spectrometer.

Photolysis. The chloroform solution of hexamethyl-disilane and a quinone was irradiated with a 1-kW high pressure mercury lamp after bubbling pure nitrogen gas. Product 1a: ^1H NMR (δ , CDCl₃) 0.16(s, 9H), 4.38(s, 1H), 7.40(s, 2H); MS(EI, 70eV) m/z(%) 252/250(M⁺, 53, 86), 237(90), 234(100), 202(19), 201(23), 200(43), 199(51), 173(9), 171(17), 141(6), 117(11), 95(37), 93(86), 73(75); HR-MS calcd for C₁₂H₂₀O₂Si₂Cl₂[M⁺]: 249.9984. Found: 249.9983. Product 2a was isolated with GC. ^1H NMR (δ , CDCl₃) 0.29(s, 18H), 6.86(s, 2H); MS(EI, 70eV) m/z(%) 324/322 (M⁺, 79, 100), 309(19), 307(26), 274(32), 272(56), 199(27), 93(51), 73(56); HR-MS calcd for C₁₂H₂₀O₂Si₂Cl₂[M⁺]: 322.0379. Found: 322.0367. Product 3 was identified in comparison with the authentic sample by GC and GC-MS.

Laser-photolysis and CIDNP measurements. The details of the apparatus for laser-photolysis were described elsewhere [28]. NMR spectra were measured before, during (immediately after) and after irradiation. The irradiation of the 1-kW high pressure mercury lamp was focused onto the NMR detecting region of a sample cell through a water filter and quartz lenses. The sampling and the irradiation time were controlled by a DG535 pulse generator (Stanford Research Systems, Inc.) with an electrical shutter. The irradiation period was 4 sec prior to the rf pulse applied. The total interval including the signal sampling was 7.99 sec. Usually, the signal was accumulated 32 times.

4. References

- [1] H. Bock, B. Solouki, "The Chemistry of Functional Groups, The Chemistry of Organic Silicon Compounds", S. Patai and Z. Rappoport, Eds., John Wiley, New York (1989) part 1, p.555.
- [2] K. Mochida, A. Itani, M. Yokoyama, T. Tsuchiya, S. D. Worley, and J. K. Kochi, Bull. Chem. Soc. Jpn., 58 (1985) 2149.
- [3] S. Fukuzumi, C. L. Wong, and J. K. Kochi, J. Am. Chem. Soc., 102 (1980) 2928.
- [4] Y. Nakadaira, N. Komatsu, and H. Sakurai, Chem. Lett., (1985) 1781.
- [5] H. Watanabe, M. Kato, E. Tabei, H. Kuwabara, N. Hirai, T. Sato, and Y. Nagai, J. Chem. Soc., Chem. Commun., (1986) 1662.
- [6] C. L. Tu and P. S. Mariano, J. Am. Chem. Soc., 109 (1987) 5287.
- [7] J. K. Kochi, Angew. Chem. Int. Ed. Engl., 27 (1988) 1227.
- [8] J. P. Dinnocenzo, S. Farid, J. L. Goodman, I. R. Gould, W. P. Todd, and S. L. Mattes, J. Am. Chem. Soc., 111 (1989) 8973.
- [9] S. Kyushin, Y. Ehara, Y. Nakadaira, and M. Ohashi, J. Chem. Soc., Chem Commun., (1989) 279.
- [10] K. Mizuno, K. Nakanishi, J. Chosa, T. Nguyen, and Y. Otsuji, Tetrahedron Lett., 30 (1989) 3689.
- [11] M. T. Craw, A. Alberti, M. C. Depew, and J. K. S. Wan, Bull. Chem. Soc. Jpn., 58 (1985) 3675.
- [12] A. Alberti, S. Dellonte, C. Paradisi, S. Roffia, and G. F. Pedulli, J. Am. Chem. Soc., 112 (1990) 1123.
- [13] S. Kozima, H. Fujita, T. Hitomi, K. Kobayashi, K. Kobayashi, and M. Kawanisi, Bull. Chem. Soc. Jpn., 53 (1980) 2953.
- [14] M. Igarashi, T. Ueda, M. Wakasa, and Y. Sakaguchi, J. Organomet. Chem., in press (1991).
- [15] The H-D exchange of hydroxyl-D in GC-MS column was measured using 4-methoxyphenol-d₁ instead of DQSiMe₃ to be 35.6 %, eliminating the complete H-D exchange during the analysis. If DQSiMe₃ is formed in CDCl₃, its mass spectrum pattern should be different from that in CHCl₃. However, we did not observe such a difference.
- [16] T. Shida, "Physical Sciences Data 34; Electronic Absorption Spectra of Radical Ions", Elsevier, Amsterdam, (1988) p.308, 378.
- [17] R. Kaptein, J. Am. Chem. Soc., 94 (1972) 6251.
- [18] M. C. R. Symons, J. Chem. Soc., Chem. Commun., (1981) 1251.
- [19] J. T. Wang and F. Williams, J. Chem. Soc., Chem. Commun., (1981) 666.
- [20] J. E. Wertz and J. L. Vivo, J. Chem. Phys., 23 (1955) 2441.
- [21] C. Glidewell, J. Chem. Research, (1983) (S)22.
- [22] W. E. Geiger, Jr. and W. M. Gulick, Jr., J. Am. Chem. Soc., 91 (1969) 4657.
- [23] K. Maruyama, H. Furuta, and A. Osuka, Chem. Lett., (1986) 473.
- [24] The signs of the hfc constants of ring-H for 2,5-di-tert-butyl-4-methoxyl phenoxy and 2,5-dimethyl-4-hydroxyl phenoxy radicals are reported to be negative.
- [25,26] The hfc constants for these radicals are similar to those of the n-Bu₃SnQ_. Therefore, the spin distribution is considered to be similar to each other and we can expect that n-Bu₃SnQ_. and hence Me₃SiQ_. has the same negative sign as those radicals.
- [27] R. Kaptein, J. Am. Chem. Soc., 94 (1972) 6262.
- [28] Y. Sakaguchi, H. Hayashi, and S. Nagakura, J. Phys. Chem., 86 (1982) 3177.

Magnetic Field Effects on the Decay Kinetics of Triplet Radical Pairs in Homogeneous and Organized Systems

Peter P. Levin and Vladimir A. Kuzmin

Institute of Chemical Physics, Academy of Sciences of the USSR,
117334 Moscow, USSR

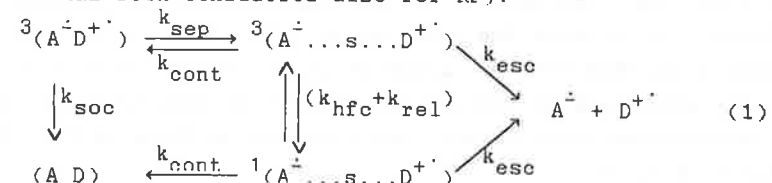
Abstract

The magnetic field effects (MFE) on the decay kinetics of triplet-derived radical ion pairs (RIP) and radical pairs (RP) formed by electron or hydrogen atom transfer from aromatic amines or phenols (D), to the quinones and the ketones (A) in solvents of middle polarity, in viscous solvents, in micellar solutions and on the surface of porous glass, have been studied by transient absorption measurements using the laser flash technique. The time scale of the triplet RIPs and RPs geminate recombination is of the order of 0.01-10 μ s. Two most important pathways of geminate recombination are under discussion: (i) intersystem crossing to the ground state (spin inverted backward electron transfer or intersystem recombination induced by spin-orbit coupling (SOC) in a contact state of the RIPs or RP); (ii) magnetosensitive process with reversible stage of formation of the distance-separated RIP or RP. The interplay of these two routes is controlled by the organization of the environment, by the interaction between the radicals as well as by the radical structure. The comparison of the behavior of similar RIP or RP in different media clarifies the relative importance of different factors.

1. Introduction

The kinetical behavior of geminate triplet-derived RIP and RP in homogeneous and organized media have received considerable attention over the last decade particularly due to the pronounced MFEs, which give the unique possibilities for effecting and controlling radical processes [1-6]. The MFEs give the approach to the dynamics of primary RIP and RP formed in the photochemical processes. It is possible to identify the contact pairs and the separated ones, based upon their different behavior in the magnetic fields. Backward intersystem electron transfer (et) in contact RIP

or intersystem recombination of contact RP due to the SOC are not very sensitive to the external magnetic field, except in the special cases of pairs with the sublevel selective heavy atom enhanced intersystem crossing [7]. The spin-multiplicity change in the separated RP and RIP is brought about by the hyperfine-coupling (HFC) induced coherent spin motion of the unpaired electron spins [1]. The spin conversion due to the HFC is depressed in the magnetic field because of the Zeeman splitting of the triplet sublevels. The interplay of intersystem recombination or et and of the pathway with reversible stage of formation of the distance-separated RIP or RP determines the kinetics of geminate recombination of the triplet RP or RIP and the kinetical MFE. The following kinetic scheme has been considered (here the case of RIP is presented, which is formed by et from D to 3A ; the same type of the scheme has been considered also for RP):



where k_{soc} is the rate constant for spin-inverted et in the contact state of the RIP caused by SOC, k_{sep} is the rate constant for the separation of the contact RIP, k_{cont} is the rate constant of the separated RIP junction to the contact RIP, k_{hfc} and k_{rel} are those for T - S transitions in the separated RIP due to the HFC and the relaxation mechanisms respectively, k_{esc} is the rate constant for separated RIP dissociation into the radicals in the bulk.

MFEs due to the HFC mechanism have been observed in the measurements of the yields of the radical ions as well as products of RIP geminate recombination formed in the charge transfer quenching experiments of the singlet [8] and the triplet [9,10] excited states in liquid homogeneous solutions. Our recent laser photolysis studies of the charge transfer triplet exciplexes (TE) have shown that in nonpolar solvents the only TE decay route is the intersystem crossing from TE to the ground state induced by SOC [10]. There is no MFE. The coulomb attraction does not permit the radical ion components of the TE to separate. However, in polar solvents partial TE dissociation takes place and there is a

reversible stage of distance-separated RIP formation and corresponding MFE. Thus, the MFE in the decay kinetics of the charge transfer TE is strongly dependent on the nature of a solvent. Herewith the MFE in the decay of different charge-transfer TE, i.e. triplet RIP formed by quenching of a quinone or an aromatic ketone in the triplet excited state by triphenylamine (TPA) in 1,1,2,2-tetrachloroethane (TCE) and different alcohols will be discussed.

In homogeneous solvents of the viscosity $\eta \geq 1$ P, it is possible to record the microsecond kinetics of the geminate recombination of the triplet RP without coulomb attraction between the radicals [11]. In the case of triplet exciplexes as well, the most important pathway of the RP decay in viscous solvents is the intersystem recombination induced by SOC in the contact RPs. At the same time, the contribution of the magnetosensitive process may be sufficient to observe the MFEs up to 100%. This contribution goes through a maximum with an increase in η . In this work the triplet RPs were generated by the photoreduction of benzophenone (BP) and its derivatives with phenol, p-cresol or aniline (PhOH, CrOH or PhNH₂) in glycerol.

The decay kinetics of a number of micellized RPs formed in the course of the Norrish type I reactions of ketones [12-16] or intermolecular photoreduction of carbonyl compounds [15,17-20] and dyes [7] have been examined in some details. These time-resolved observations of the magnetic-field-dependent recombination kinetics of the triplet spin correlated RP in micelles reveal the important regularities. The drastically increased RP lifetime in supercage environments enhances the role of the RP spin evolution and allows significant contributions from the interactions and the reaction pathways which are too weak and too slow to be important in a nonviscous homogeneous solution.

The HFC in the separated state of the micellized RP is mainly responsible for the RP spin conversion in the absence of a magnetic field (magnetic field strength $H \ll A_{\text{hfc}}$, where A_{hfc} is the effective constant of the HFC) [12-20]. The interplay of HFC induced spin evolution and diffusional process of the intramicellar encounters should determine the rate of RP recombination in the micelles in zero magnetic field. The rate of triplet-singlet (T-S)

transitions due to the isotropic HFC in zero magnetic field (k_{hfc}) may be evaluated as A_{hfc}/h , which is of the order of $1 \times 10^8 \text{ s}^{-1}$ for ordinary aromatic RP and RIP [1,8]. The frequency of reencounters (k_{dif}) within the supercage is determined by the effective size, the viscosity and the internal order of the microreactor. For most of the commonly used micelles the value of k_{diff} seems to be several times smaller than that of k_{hfc} . The corresponding dependence of the RP recombination rate on the micellar volume is a strong evidence of the intramicellar encounters as the rate-controlling process of the RP recombination within micelle in zero magnetic field [7,20]. One other consequence of fast spin dynamics compared with the spin-allowed recombination is the finding, that the RPs produced from the singlet states show a similar zero-field recombination kinetics as the RPs produced from the triplet states [21].

In the presence of sufficiently high magnetic fields ($H \geq A_{\text{hfc}}$), the $T_{\pm}-S$ transitions in the separated states of the micellized RPs may become the limiting step of RP decay. The magnetic field dependences do not saturate at low H , which is typical for the isotropic HFC mechanism (the saturation is expected to be observed at 10 - 20 mT). The anisotropy-induced spin relaxation as a mechanism of $T_{\pm}-T_0$, S transitions have been involved to account for the delayed magnetic field dependences and the RP kinetics in micelles at $H > A_{\text{hfc}}$ [17,22]. The spin relaxation can be enhanced in the presence of paramagnetic additives, when this source of electronic magnetic spin interacts with the electronic spins of the RP in micelles [20,23,24]. The addition of paramagnetic ions as well as stable free radicals or $^3\text{O}_2$ results in the acceleration of the micellized RP recombination in the magnetic field, while the RP recombination may be insensitive to these paramagnetic species in zero magnetic field.

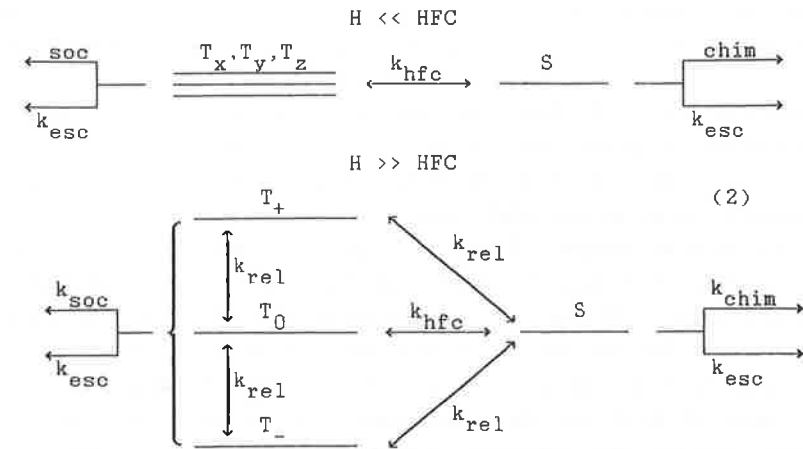
The substantial recombination of RPs in T_{\pm} states can occur even in a very strong magnetic fields $H \gg A_{\text{hfc}}$, if the supercage environments retard diffusive separation sufficiently. When isotropic HFC and relaxation routes of $T_{\pm}-T_0, S$ transitions in micellized RP are suppressed strongly, the intersystem recombination induced by SOC in a contact RP may become the basic pathway for the recombination of these RP, which are produced in T_{\pm}

states. A very pronounced internal heavy atom effect [7,20,25] as well as some external one [20] was observed for the recombination of micellized RP in strong magnetic fields. Recombination at high H accelerates significantly upon substitution of a heavy atom into the aromatic radicals, whilst the acceleration at H = 0 is small. A corresponding decrease in the magnetic field effect was observed.

The values of the rate constants for the intersystem recombination of contact triplet aromatic RP being ordinarily in the range $10^6 - 10^7 \text{ s}^{-1}$, are much smaller than those for the recombination of the singlet contact RP of the active radicals. The main state of the RP in a commonly used nanometer-sized micelles, like micelles of sodium alkyl sulfates, seems to be the separated one. Under this condition, the contribution of the intersystem recombination should be very small in zero magnetic field. The HFC mechanism of intersystem crossing in separated RP is the basic one in RP recombination at $H < A_{\text{hfc}}$ in micelles due to the high k_{hfc} values. But in strong magnetic fields, when HFC and relaxation routes of $T_{\pm} - T_0, S$ transitions in RP are suppressed, the intersystem recombination may become the basic and the only pathway for the recombination of RP in T_{\pm} states.

The present paper deals with the recombination kinetics of model RPs formed by quenching of the triplet excited states of the derivatives of BP or benzoquinone by 4-phenylaniline (PNH_2) or 4-phenylphenol (POH) in aqueous micellar solutions of sodium alkyl sulfates under the external magnetic fields up to 0.45 T. The effects of the reagent and micellar structures, the addition of NaCl to vary the micellar properties, the addition of paramagnetic metal complex as well as $^{3}\text{O}_2$, the influence of iodo- and bromobenzenes as the sources of external heavy atoms have been investigated. The experimental results are discussed in terms of a simple kinetic scheme (2) of first order processes [20], which includes the singlet-triplet transitions in the separated states of RP due to the isotropic hfc (k_{hfc}) and relaxation (k_{rel}), the RP recombination in the singlet state (k_{chim}), the escape of the radicals from the micelle (k_{esc}) and the intersystem recombination process due to the SOC (k_{soc}) in the contact state of the RP.

The behavior of the geminate RP and RIP adsorbed onto the surface of silicate porous glass has similarities with that in the



homogeneous as well as in the micellar solutions. MFEs up to 100% have been observed [26], which is the result of a significant contribution of the recombination route through the separated RP. The pronounced internal heavy atom effect of the same order of magnitude as that for the TE, the RP in viscous solvents and the RP in micelles in high magnetic field, evidences the important role of intersystem recombination or intersystem et. The present paper deals with the RPs formed by quenching of 8,10-anthraquinone (AQ) in the triplet state by TPA, tri(4-bromophenyl)amine (BTPA) or PNH_2 as well as the RP formed by the quenching of BP or 4-bromobenzophenone (p-BrBP) by PNH_2 or POH adsorbed onto optically transparent silicate porous glass with average pore size 8 nm under the external magnetic fields up to 0.24 T.

2. Experimental section

The absorption spectra and decay kinetics of the intermediates were recorded by laser photolysis using a PRA LN-1000 nitrogen laser (337 nm, 1 mJ per pulse) or PRA LN-102 dye laser ($\lambda = 385$ nm), pumped by a PRA LN-1000 nitrogen laser as an excitation source [10,11,20,26]. The kinetic spectrophotometer (8-ns resolution) included an averaging system consisting of a Biomation 6500 waveform recorder coupled to an Apple IIe microcomputer.

Kinetic curves were averaged over 128 laser pulses. In the magnetic field experiments, the sample was placed between two pole pieces of a permanent magnet. The distance between the pole pieces could be varied and at the closest position (16 mm) the magnetic field strength $H = 0.45$ T. The compounds were purified by sublimation or by recrystallization from ethanol. All measurements were conducted at 20°C . Oxygen was removed from the solution by Ar purging or by evacuation on a vacuum pump line.

The concentration of sodium alkyl sulfates in distilled water was equal to 0.1 mol/l, which corresponds to a concentration of micelles near 0.001 mol/l. A concentration of A of the order of 0.001 mol/l for BP and its derivatives or of 0.0001 mol/l for 2,6-diphenyl-1,4-benzoquinone and that of POH or $\text{PNH}_2 \approx 0.005$ mol/l were used in most of the experiments. To avoid the formation of radical anions and neutral 4-phenylanilino radical PNH' , 0.001 mol/l HCl was added to the micellar solutions.

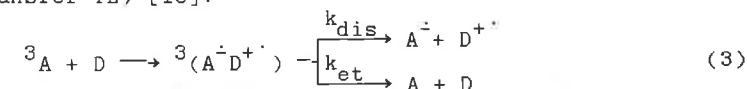
The samples of commercially available $\text{Na}_2\text{O}\text{-B}_2\text{O}_3\text{-SiO}_2$ glass DB-1M 3x4x10 mm in size were pretreated by the standard procedure in an aqueous solution of NaOH and then in an aqueous solution of HCl with subsequent washing in distilled water and drying in vacuum. After this pretreatment the pores with an average size nearer to 8 nm and an internal area $100 \text{ m}^2/\text{cm}^3$ occupied 30% of the internal volume of the remained porous SiO_2 skeleton. The light scattering was small due to the small size of the pores, providing for the optical transparency in the visible and in the near UV region. The samples of porous glass obtained in such a way were saturated with a benzene solution of A and D (concentration of 0.05 mol/l). The solvent was removed by placing the sample under vacuum in a cell, followed by degassing at 1×10^{-3} Torr. Only 1% of porous surface area was covered by A and D under the given conditions. In the experiments with thermal pretreatment, the porous glasses were placed under vacuum at 200°C for 3 days. The A - D coating procedure was made by adsorption of A and D from the gas phase.

3. Results and discussion

3.1. Charge transfer TE in the solvents of middle polarity.

The photoexcitation of A in the presence of tertiary aromatic amines results in et from D to ${}^3\text{A}$ and to the appearance of a RIP

(charge transfer TE) [10]:



The absorption spectra of TE (see the examples on fig. 1) virtually coincide with the superposition spectra of A^{\cdot} (maximum at 440 - 450 nm for p-benzoquinone derivatives [10,27-29]; in the regions 400, 500 and low intensity bands at 700 - 900 nm for AQ and its derivative [10,30]; and in the region 600 - 700 nm for BP and its derivative [10,31]) and D^{\cdot} (maximum at 650 (720) and a smaller one at 550 (560)nm for TPA (BTPA)) [10,28]. The passage from TCE to the alcohols as a solvent results in a blue-shift in the A^{\cdot} absorption band in the TE spectra (fig. 1) due to the H-bond formation [10,30,31]. The effect is most pronounced (the shift on up to 100 nm) for the radical anions of AQ, BP and their derivatives.

The solvents used are polar enough and the disappearance of the transient absorption induced by the laser pulse occurs in two more or less readily distinguishable stages (fig. 2). The fast one is due to the backward et within TE or RIP with the formation of A and D as the final result. The slow stage corresponds to the decay of the radical ions in the bulk of the solvent. Photoconductivity measurements showed free ions in the bulk to be formed simultaneously with the decay of TE - RIP [27]. In terms of the simplest exponential approach, TE gets deactivated (rate constant $k_{\text{TE}} = k_{\text{et}} + k_{\text{dis}}$) by two ways (scheme 3): via backward electron transfer (rate constant k_{et}) and via dissociation to radical ions (rate constant k_{dis}). The yields of A^{\cdot} and D^{\cdot} in the bulk of the solvent $\Phi = k_{\text{dis}}/k_{\text{TE}}$ may be obtained from the ratio of the absorption due to A^{\cdot} and D^{\cdot} free radicals to that of the initial TE immediately after the pulse. The corresponding data are presented in the tables 1 and 2.

In the case of the most polar solvents, namely 1- or 2-propanol and ethanol, the geminate stage of reaction is indistinguishable from the bimolecular second order recombination of the free radical ions in the bulk. The first order rate constants corresponding to the initial slope of the kinetic curves were taken as a measure of the decay rates of the radical ions in these solvents (table 2).

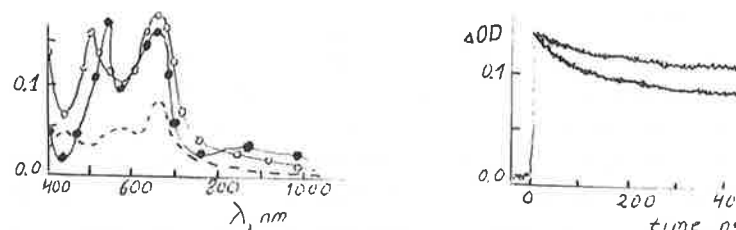


Fig. 1. The absorption spectra of the intermediates formed from 9,10-anthraquinone in the presence of triphenylamine in TCE (●), in tert-butanol (○) and on porous glass (dashed line).

Fig. 2. Decay of the transient absorption at 650 nm for duroquinone - triphenylamine system in benzylalcohol at $H = 0$ (lower curve) and $H = 0.45$ T (upper curve).

Imposition of a magnetic field leads to an increase in the value of Φ and the inhibition of geminate recombination (fig. 2). The increase of Φ corresponds to the decrease of k_{et} , the value of k_{dis} remaining unaffected within $\pm 10\%$. The magnetic field induced change in k_{TE} (Δk) and the value $\alpha = [\Phi(H) - \Phi(0)]/\Phi(0)$, where $\Phi(0)$ and $\Phi(H)$ are the values of Φ at the zero magnetic field and at the magnetic field strength H respectively, are taken as a measure of the magnetic field effect.

The dependences of Δk and α on H may be divided into two stages: a "sharp" one on going from $H = 0$ to $H = 0.01$ T where the main changes of Δk and α take place and a saturated one at $H > 0.2$ T where the magnetic field dependences are close to saturation [10].

The magnetic field effect is particularly tangible for $H < 20$ mT, which is typical for the HFC mechanism. The value of $k_{hfc} \approx 1 \times 10^8$ s $^{-1}$ being the effective HFC in the aromatic radicals is much larger than the k_{et} observed. Therefore, at $H = 0$, the TE decay to the initial reagents in the ground state through the separated RIP is limited by the separation and junction of the RIP, i. e. by the molecular mobility and diffusion in the coulomb field.

In a strong magnetic field, for $H \geq 0.2$ T, k_{TE} and Φ are independent of H . The rate of relaxation due to the g-factor anisotropy and the relaxation due to spin-rotational coupling, which also is determined by g anisotropy is independent of H at

Table 1

Decay rate constants (in 10^6 s $^{-1}$) of triplet exciplexes of different electron acceptors with triphenylamine in 1,1,2,2-tetrachloroethane ($\epsilon = 8.2$; $\eta = 1.84$ cP and $k_{dis}^E = 2 \times 10^6$ s $^{-1}$ at $\sigma = 0.7$ nm). Errors in k_{TE} , Δk and Φ 10%.

Acceptor	Φ	k_{TE}	k_{et}	k_{dis}	Δk	$\alpha, \%$ ($H = 0.45$ T)
BP	0.70	3.3	1.0	2.3	0.4	10
BBP	0.51	5.1	2.5	2.6	1.0	18
1,4-dimethoxy-						
9,10-anthraquinone	0.57	3.3	1.4	1.9	0.7	26
AQ	0.49	5.1	2.6	2.5	1.0	27
duroquinone	0.55	7.8	3.5	4.3	1.4	32
2,6-diphenyl-						
1,4-benzoquinone	0.37	8.2	5.2	3.0	1.6	27
p-fluoraniline	0.35	15	9.7	5.3	1.4	17

Table 2

Decay rate constants (in 10^6 s $^{-1}$) of triplet exciplexes of duroquinone with triphenylamine in different solvents. Errors in k_{TE} , Δk and Φ 10%. (* Values were obtained from the initial slope of the kinetic curves).

Solvent	ϵ	$\eta,$ cP	Φ	k_{TE}	k_{et}	k_{dis}	k_{dis}^E ($\sigma = 0.7$ nm)	Δk	$\alpha, \%$ (0.45 T)
tert-									
amylalcohol	5.8	2.8	0.12	3.7	3.3	0.4	0.03	0.2	5
1-octanol	10.3	11	0.12	5.8	5.1	0.7	2.1	0.9	25
tert-butanol	10.9	3.3	0.49	6.4	3.3	3.1	9.6	0.7	11
benzylalcohol	13.1	5.1	0.62	10	3.8	6.2	18	2.0	25
iso-									
amylalcohol	14.7	3.0	0.73	11	3.0	8.0	55	1.1	11
iso-butanol	17.7	3.9	0.86	13	2	11	90	0.7	4
2-propanol	18.3	1.8	-	-	0.7*	-	220	0.3	-
1-propanol	20.1	2.0	-	-	0.3*	-	270	0.04	-
ethanol	24.3	1.1	-	-	0.5*	-	850	≤ 0.02	-

high magnetic field [7,22]. However, both these and the other mechanisms of the paramagnetic relaxation give the k_{rel} value $1.3 \times 10^5 \text{ s}^{-1}$ for the duroquinone radical anion in the medium with viscosity $\eta \approx 2 \text{ cP}$ at $H = 0.33 \text{ T}$ (the X-band ESR) [32]. This value of k_{rel} is significantly lower than the k_{et} obtained at high H (tables 1 and 2). Hence, the paramagnetic relaxation can contribute, but in most systems only to a small extent in the decay of the TE in high magnetic field.

The bell shape of k_{et} dependence on TE energy, which has been obtained in TCE at high H [10], is an evidence for the direct ${}^3(A^- \cdot D^+) \rightarrow (A D)$ transition induced by SOC in the contact state of the RIP as a main route of TE decay at high H . Thus, according to a scheme 1 in a rough approximation, the value of k_{et} may be offered as $k_{soc} + \Delta k$, where Δk depends on the mutual diffusion of the radical ions in a given medium, e. g. Δk should be the characteristic of the solvent mainly. Indeed, the most part of the experimental values of Δk for the different TE in TCE are in the range $(1.0 - 1.5) \times 10^6 \text{ s}^{-1}$ independent of the nature of the radical ions in the TE (table 1). However, the Δk value for the TE with high energy (benzophenone - D system), for which the very low value of k_{soc} is expected from the bell shaped dependence, is significantly lower than the "normal" Δk value for TCE (table 1). The reason for this deviation may be in the enhanced relative contribution of HFC induced $T_0 - S$ transitions in the separated RIP to the TE decay in the magnetic field. The contribution of the HFC mechanism being relatively small for most of the systems under investigation, we have neglected the role of this mechanism in the decay of the RIP in the T_0 state, though it remains operative in the magnetic field and may be very considerable in a strong H for the systems with low k_{soc} .

The Δk values depend on the nature of the solvent used (table 2). The increase of Δk with the increase of dielectric constant (ϵ) of the alcohol up to $\epsilon = 13$ is caused as per the scheme (1) by the increase of k_{sep} . Further increase of ϵ leads to the Δk decrease due to the retardation of the junction of the radical ions participating in the random wandering. In the most polar ethanol, the probability of the contact of the separated RIP is relatively small and a corresponding small magnetic field effect is observed

(table 2).

For more precise discussion of the dependence of the magnetic field effect on solvent, it is important to cast a glance over the solvent effect on k_{dis} to obtain the conclusions about the mutual diffusion of radical ions in the RIP and TE structure. The dissociation of TE to radical ions is an ion escape process and depends on the ϵ and η of the medium. The value of k_{dis} observed in TCE may be successfully obtained from an Eigen equation:

$$k_{dis}^E = 3RD/\sigma^3[\exp(R/\sigma) - 1] \quad (4)$$

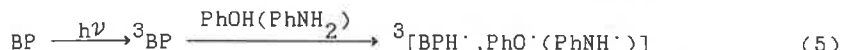
(here $R = e^2/\epsilon kT$ is the Coulomb radius, σ is the formation radius and D is the coefficient of mutual diffusion) using $\sigma = 0.7 \text{ nm}$, which is usually taken for distance in the encounter complex of solvated radical ions [8], and calculating D by the Stoks-Einstein equation as $D = 2kT/3\pi\eta$ (table 1) [10]. However, analogous calculations for alcohols give the k_{dis}^E values, which differ significantly from those observed experimentally (table 2). The dependence of k_{dis} on ϵ is weak relative to that predicted by equation (4) at $\sigma = 0.7 \text{ nm}$. The value σ for tert-amylalcohol, which should be used in eq. (4), is higher than 0.7 nm and seems to increase with the increase of ϵ . This may lead to the enhancement of the RIP separation process. On the other hand, the real coefficients of the mutual diffusion describing the geminate recombination of the RIP are significantly smaller than those predicted by Stoks-Einstein equation due to the interplay of the molecular motions in the cage. This is the reason for the small k_{dis} values observed in most polar alcohols (table 2), where the Coulomb attraction grows feeble and not the σ value but the mutual mobility of the radical ions in the RIP determines the k_{dis} observed. The correlation between the molecular motions in the cage should lead to the retardation of RIP separation.

In general, it should be noted that there are several most important solvent dependent factors, which determine the competition between two different routes of backward electron transfer in triplet exciplexes - radical ion pairs in liquid media. The rate of spin orbital coupling induced intersystem electron transfer in the contact state of a pair is determined by the position of a system on the bell shaped energy gap dependence and by the parameters of this dependence [10]. The probability of

magnetosensitive process, in which the separation of the RIP is followed by its junction, goes through a maximum with the increase of the media polarity.

3.2 MFE in geminate recombination kinetics of triplet RP in glycerol

Photoexcitation of BP in the presence of 1 M PhOH or PhNH_2 initiates the well-known series of processes [11,20,33]



where the brackets enclose the RP. At $[D] = 1 \text{ M}$ the lifetime of ${}^3\text{BP}$ is shorter than the resolution time of the registering system. The well known absorption of the ketyl radicals with characteristic maxima at 540 nm and that of PhO^\cdot or PhNH^\cdot (maximum near 400 nm) [20,33] are registered immediately after the flash. In the presence of HCl the radical cation PhNH_2^+ is observed.

The traces of the radical absorption decay contain the fast component ($t \leq 5 \mu\text{s}$), which corresponds to the RP geminate recombination and the slow component ($t \gg 50 \mu\text{s}$) reflecting the decay of the radicals that have escaped to the bulk (fig. 3). The kinetic data obtained in terms of the simplest exponential approach (scheme 3, $k_{\text{obs}} = k_{\text{rec}} + k_{\text{dis}}$) are presented in table 3.

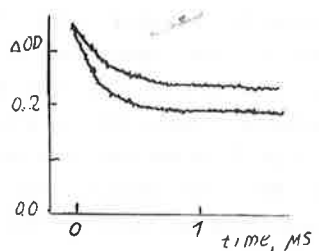


Fig. 3. Decay of the transient absorption of BPH^\cdot at 540 nm for BP - p-cresol system in glycerol at $H = 0$ (lower curve) and $H = 0.34 \text{ T}$ (upper curve)

The MFE is particularly tangible for $H < 20 \text{ mT}$ as well as in the case of TE, typically of the HFC mechanism. However, the field dependences become flat only at $H \geq 0.1 \text{ T}$ which is much in excess of the A_{hfc} for given RPs. This may be due to the relaxation mechanism the details of which will be discussed in the next section.

At high H the only pathway of RP geminate recombination seems to be the SOC-induced intersystem rout. A ponderous argument in

favor of such a mechanism in RP in glycerol is the internal heavy atom effect: k_{rec} increase when a Br atom is introduced into radicals as substituent (table 3) [11].

Table 3
Decay rate constants (in 10^6 s^{-1}) of geminate triplet RP recombination in glycerol

RP	Φ	k_{obs}	k_{rec}	k_{dis}	Φ	k_{obs}	k_{rec}	k_{dis}
							$H = 0$	$H = 0.34 \text{ T}$
$\text{BPH}^\cdot, \text{PhNH}^\cdot$	0.65	5.2	1.8	3.4	0.77	4.8	1.4	3.4
$\text{BPH}^\cdot, \text{PhNH}_2^+$	0.49	7.9	4.0	3.9	0.73	5.3	1.4	3.9
$p\text{-BrBPH}^\cdot, \text{PhNH}^\cdot$	0.37	11	6.9	4.1	0.41	10	5.9	4.1
$p\text{-BrBPH}^\cdot, \text{PhNH}_2^+$	0.34	13	8.6	4.4	0.48	9.2	4.8	4.4
$\text{BPH}^\cdot, \text{PhO}^\cdot$	0.55	6.4	2.9	3.5	0.65	5.2	1.8	3.4
$\text{BPH}^\cdot, \text{CrO}^\cdot$	0.53	4.9	2.3	2.6	0.65	3.8	1.3	2.6
$p\text{-BrBPH}^\cdot, \text{CrO}^\cdot$	0.39	14	8.8	5.2	0.57	13	7.4	5.4

The kinetic scheme (1) may be considered to give a so far most comprehensive description of the MFE for RP in glycerol and to underline the magnetically sensitive stage.

3.3 SOC, HFC and paramagnetic relaxation in micellized triplet RP

Photoexcitation of A in the presence of POH or PNH_2 and HCl in micelles as well as in other media initiates the series of processes according to the scheme (5). The solubility of the given hydrophobic reagents in water is very low. They are localized in a micellar phase, where the RPs are generated via the reaction (5). At the present concentrations of POH or PNH_2 (5 molecules of a quencher per micelle), the lifetime of ${}^3\text{A}$ is shorter than the resolution time of the registering system. The well known absorption of the ketyl radicals with characteristic maxima at 540 - 580 nm or neutral semiquinone radical from 2,6-diphenyl-1,4-benzoquinone (maximum at 400 nm) and that of PO^\cdot (maximum near 520 nm) or PNH_2^+ , with a very intense maxima at 675 nm and another of relatively low intensity at 800 nm [20] are observed immediately after the laser pulse (fig. 4). The lifetime

of ${}^3\text{BP}$ in sodium alkyl sulfate solutions in the absence of a quenchers is ≥ 100 ns and that of the triplet states of benzophenone derivatives or of 2,6-diphenyl-1,4-benzoquinone triplet are 5 - 10 times longer. In the presence of 0.001 mol/l POH or PNH_2 (one molecule of quencher per micelle), the evaluations of ${}^3\text{A}$ lifetimes give the values 20 - 30 ns. It may be safely assumed that, in the presence of 5 molecules of POH or PNH_2 in a micelle, AH^\cdot is formed only via reaction (5).

The traces of the radical absorption decay contain the fast component ($t \leq 5 \mu\text{s}$), which corresponds to the micellized RP recombination and the slow component ($t \gg 50 \mu\text{s}$) reflecting the decay of the radicals that have escaped to the aqueous phase and the lone micellized radicals (fig. 5). The ratios of the absorption due to the escaped and lone radicals to that of initial RP ($\varphi = \text{OD}_\infty/\text{OD}_0$, see table 4) correspond to the contributions of the escape process to the RP decay.

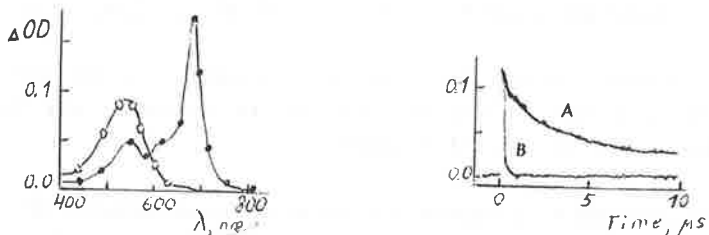


Fig. 4. The absorption spectra of the intermediates formed from BP in aqueous SDS solution in the presence of PNH_2 (0) and POH (0) under laser flash photolysis; recorded immediately after the flash.

Fig. 5. Decay of the transient absorption at 675 nm (BP - PNH_2 system) in aqueous SDS solution H = 0 (B) and H = 0.45 T (A).

At $H = 0$, the fast component fits the monoexponential law with a fair accuracy (k_{obs} at $H = 0 \text{ T}$, see table 4). Imposition of a magnetic field leads to an increase in the value of φ and the inhibition of geminate recombination (fig. 5, table 4). A monoexponential law does not describe the fast component in the magnetic field. The first order rate constants of the second slow part were calculated from the point $\text{OD}_0/2$ (or $2\text{OD}_0/3$ for the few systems with high values of φ) to OD_∞ (k_{obs} at $H = 0.45 \text{ T}$)

Table 4

Contributions of escape process, rate constants (in 10^6 s^{-1}) and relaxation parameters for the recombination of the micellized radical pairs. Errors in k_{obs} , φ 5%.

Acceptor	φ		k_{obs}	k_{chim}	k_{soc}	k_{esc}	τ_c	$ V /\text{g}\beta$
	0 T	0.45 T	0 T	0.45 T	0 T	0.45 T	(ps)	(mT)
sodium decyl sulfate, 4-phenylaniline								
benzophenone	0.05	0.44	11	0.78	41	0.26	0.50	100
2,6-diphenyl-1,4-benzoquinone	0.05	0.19	4.5	0.90	15	0.65	0.23	90
sodium dodecyl sulfate, 4-phenylaniline								
4,4'-dimethoxy-benzophenone	≤ 0.02	0.22	7.9	0.30	30	0.19	0.10	170
4,4'-dimethyl-benzophenone	≤ 0.02	0.15	7.3	0.35	28	0.25	0.08	190
benzophenone	≤ 0.02	0.20	7.1	0.44	27	0.29	0.13	170
benzophenone- d_{10} (in $D_2\text{O}$)	≤ 0.02	0.20	6.3	0.43	24	0.29	0.13	160
benzophenone (+2 mol/l EtOH)	0.07	0.51	10	0.93	37	0.21	0.70	110
benzophenone (+0.4 mol/l NaCl)	0.04	0.32	1.9	0.15	7.1	0.06	0.07	120
4-carboxy-benzophenone	≤ 0.02	0.17	5.8	0.58	21	0.43	0.14	160
4,4'-dichloro-benzophenone	0.05	0.15	7.6	1.6	25	1.2	0.34	190
2-bromo-benzophenone	≤ 0.02	0.03	8.2	4.5	19	4.2	0.2	170
4-bromo-benzophenone	≤ 0.02	≤ 0.02	11	9.1	17	9.0	≤ 0.02	170
2,6-diphenyl-1,4-benzoquinone	0.03	0.09	2.2	0.58	7.1	0.49	0.07	110
sodium tridecyl sulfate, 4-phenylaniline								
benzophenone	≤ 0.02	0.20	4.6	0.33	17	0.21	0.10	200
2,6-diphenyl-1,4-benzoquinone	0.03	0.11	1.8	0.42	5.9	0.34	0.06	130

sodium pentadecyl sulfate, 4-phenylaniline

benzophenone	≤0.02	0.11	4.1	0.30	15	0.23	0.05	220	0.53
2,6-diphenyl-1,4-benzoquinone	≤0.02	0.08	1.5	0.35	5.0	0.28	0.04	150	0.44

sodium decyl sulfate, 4-phenylphenol

benzophenone	0.11	0.37	6.4	1.3	21	0.60	0.68	90	0.44
2,6-diphenyl-1,4-benzoquinone	0.12	0.41	2.9	0.60	9.5	0.24	0.35	70	0.37

sodium dodecyl sulfate, 4-phenylphenol

4,4'-dimethylbenzophenone	0.07	0.31	4.9	0.76	17	0.41	0.34	130	0.44
benzophenone	0.08	0.29	4.7	0.91	16	0.53	0.37	120	0.43
benzophenone-d ₁₀ (in D ₂ O)	0.09	0.29	4.3	0.90	14	0.52	0.37	120	0.36
4,4'-dichlorobenzophenone	0.15	0.40	3.7	0.96	11	0.41	0.54	130	0.42
2-bromo-benzophenone	0.06	0.10	5.0	2.1	13	1.8	0.29	120	0.47
4-bromo-benzophenone	0.04	0.05	6.2	4.2	12	3.9	0.25	120	0.50
2,6-diphenyl-1,4-benzoquinone	0.10	0.34	2.0	0.42	6.6	0.20	0.20	100	0.36

sodium tridecyl sulfate, 4-phenylphenol

benzophenone	0.06	0.23	2.9	0.56	9.8	0.36	0.18	140	0.43
2,6-diphenyl-1,4-benzoquinone	0.14	0.32	1.3	0.39	3.9	0.21	0.17	110	0.36

These rate constants should represent the decay of RPs produced in the T_f states at high magnetic fields. In the cases of the systems PNH₂ - BP and its derivatives without Br- or Cl-substituents, at high magnetic fields, the kinetics of RP recombination in the micelles acquire a pronounced biexponential form (fig. 5): the contribution of the first fast part being close to 30% and the evaluated rate constants being (1-2)×10⁷ s⁻¹.

The magnetic field dependences of k_{obs} and ϕ may be divided approximately into three stages: a "sharp" one (on going from H = 0 to 0.02 T, for most of the systems, k_{obs} decreases by a factor of more than 2); a "gentle" one (0.02 < H < 0.2 T) and a saturated one (H > 0.2 T), where the dependences of k_{obs} and ϕ on H are close to

saturation (see fig. 6).

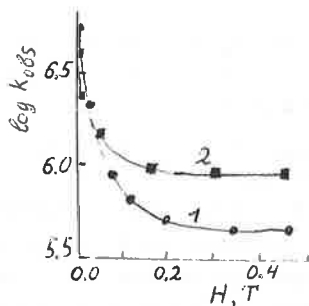
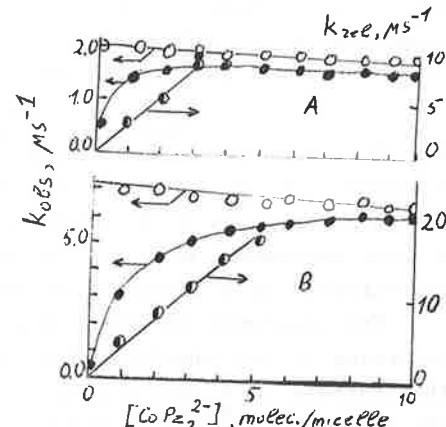


Fig. 6. The dependences of k_{obs} on magnetic field strength for BP - PNH₂ (1) or BP - POH (2) systems in solutions of SDS in H₂O.

Fig. 7. The dependences of the values of k_{obs} on CoPz₂Cl₂ concentration in the absence (0) and presence of a magnetic field 0.45 T (●) for the systems 2,6-diphenyl-1,4-benzoquinone - POH (A) and BP - PNH₂ (B) in aqueous SDS solutions. The dependences of the calculated values of k_{rel} on CoPz₂Cl₂ concentration at H = 0.45 T.

The utilization of the simple scheme (2), described by a system of four first order equations is very useful for the discussion of the experimental results of RP recombination in micelles. The simple monoexponential form of the RP decay kinetics in micellar solutions of sodium alkyl sulfates at H = 0 and a biexponential one at an external magnetic field lends a strong support to the validity of this first order rate constant approach. This system of equations can be easily solved in the limit of k_{hfc} ≫ k_{chim}, k_{soc}, k_{rel} and k_{esc}. The values of k_{chim}, k_{soc} and k_{esc} calculated according to this solution of scheme (2) from the experimental values of k_{obs} and ϕ at H = 0 and those extrapolated to H → ∞ are presented in table 4. The solution of scheme (2) allows the calculation of k_{rel} from the magnetic field dependences of k_{obs} and ϕ [20].

The values of k_{chim} (table 4) for most of the systems are close to that of the first-order rate constant of the intramicellar encounters (k_{dif}). The values of the rate constants for the



diffusion-controlled intramicellar process of pyrene excimer formation in SDS equal to 2×10^7 and $2.6 \times 10^7 \text{ s}^{-1}$ have been reported [34]. The value of k_{dif} may also be estimated by the eq. (6)

$$k_{\text{dif}} = 2kT/\pi\eta R_m^3 \quad (6)$$

Here η is the intramicellar microviscosity and R_m is the radius of a micelle. At $R_m = 2 \text{ nm}$ [35] and $\eta = 10 - 20 \text{ cP}$ [36] for SDS micelles, expression (6) leads to $k_{\text{dif}} = (2-4) \times 10^7 \text{ s}^{-1}$, which is in a good agreement with the values of k_{chim} calculated from the experimental data obtained for the SDS solutions (table 4).

The increase in the chain length of sodium alkyl sulfate according to (6) should be followed by the decrease in k_{dif} due to the increase in R_m and η [35]. One can estimate from data [35] that the values of R_m^3 increase by 2 and 3 times on going from decyl sulfate to tridecyl and pentadecyl sulfates micelles respectively. A corresponding decrease in k_{chim} is observed as well (table 1).

It was estimated that the addition of 2 mol/l EtOH to the SDS aqueous solutions results in the decrease of R_m and η by 1.1 [37] and 1.5 [36] times respectively. As expected from (6), two times increase of k_{dif} is significantly larger than that observed for the k_{chim} in the presence of EtOH, while the qualitative regularity is revealed (table 4).

A qualitative correlation between the SDS micellar properties and the value of k_{chim} is also observed, when they are varied by the addition of NaCl up to 0.4 mol/l. This addition results in the doubling of R_m [35,38] and a three times decrease in η [36]. The observed decrease in k_{chim} upon the addition of 0.4 mol/l NaCl (table 1) is more pronounced than that expected from (6).

In general, it should be mentioned, that the correlation of the kinetic data with microparameters of micellar solutions obtained by the different techniques needs a lot of caution, because of the effects of the change of the shape as well as of the confluence of the micelles. For example, the further increase of the concentration of NaCl ($> 0.5 \text{ mol/l}$) in SDS solutions results in an insignificant decrease of k_{chim} only [20], while a sharp increase in the aggregation number and in the micellar size is observed by the quasielastic light scattering spectroscopy [38]. However, the pyrene fluorescence quenching methods have revealed the saturation value of the aggregation number as 200 at very high

NaCl concentrations [39].

The rate of the intramicellar encounters is not the only factor which determines the values of k_{chim} . A small but noticeable effect of $^{3}\text{O}_2$ on k_{obs} in zero magnetic field observed in several systems (see below) is an evidence of the interplay of the RP diffusion dynamics and spin evolution to some extent [20]. While the relation $k_{\text{hfc}} > k_{\text{chim}}$ is valid, nevertheless a total quasi-spin equilibrium between the S and T spin states of RP is not achieved in time in relatively small SDS micelles. Hence the k_{obs} value at $H = 0$ is sensitive in some extent to the spin balance, which is shifted to the corresponding side by the addition of the paramagnetic species.

Moreover, the values of k_{chim} depends significantly on the chemical nature of the radicals (table 4). This difference in the RP reactivity may be attributed to the anisotropic nature of the intramicellar diffusional dynamics caused by the localization of the radicals of different structure in the different regions of micelles as well as to the steric and chemical effects. The increase of k_{chim} with the increase of the electron-donor strength of ketyl radicals within the first two groups of the RPs evidences the charge transfer nature of the intermediate complex or of the transition state of the RP recombination process (table 4). The presence of this substituent effect reveals that the RP recombination is not totally diffusion controlled and some contribution of the chemical dynamics is also important.

The values of k_{soc} (table 4) for RPs which include radicals without heavy Br substituents, are much lower than that of k_{dif} . It means that the intersystem crossing is the rate determining step of the reaction in high magnetic field. The form of the dependences of k_{obs} on H with a saturation at high H , leads to the conclusion, that k_{soc} , obtained via the scheme in fig. 1, are independent of H . There are two mechanisms of T - S transitions in the separated RP, which are independent of H at high magnetic field: (i) relaxations due to g anisotropy and (ii) spin-rotational coupling [1,7,22]. However, the analysis shows that these mechanisms can hardly have any effect on the decay of the RP in question [11,20]. Both these mechanisms and the relaxation due to HFC anisotropy give the k_{rel} values for ketyls in the medium, with $\eta \approx 10 \text{ cP}$ at $H = 0.33 \text{ T}$ (the

X-range ESR) near 2×10^4 s⁻¹ [40], which is much lower than the k_{soc} obtained (table 4).

If the intersystem crossing occurs in the contact states of micellized RP, then, $k_{soc} = K_c k_{soc}^0$, where K_c is the contribution of contact states and k_{soc}^0 is the rate constant of intersystem recombination of the contact RP (transition from triplet contact RP to the products of recombination). Using the estimation $K_c \approx 0.1$ for SDS, which were obtained from the comparative analysis of the kinetic parameters of RP geminate recombination in SDS and glycerol (in glycerol RP recombination is mainly due to SOC in contact states), a value of $k_{soc}^0 \approx (2 - 5) \times 10^6$ s⁻¹ may be calculated from k_{soc} for RP without heavy atoms. These values of k_{soc}^0 are of the same order of magnitude as the rate constants of SOC-induced intersystem recombination of the biradicals [41,42] and the intersystem et in polar TE. For example, a rate constant 8×10^6 s⁻¹ was obtained for the decay of the triplet ketyl - phenoxy radical [42]. Our recent investigations of analogous contact RP decay kinetics in β -cyclodextrin cavity gave the rate constant of intersystem recombination 1.2×10^7 s⁻¹ [43]. The values in the range $10^6 - 10^7$ s⁻¹ are ordinary for SOC-induced intersystem recombination of contact aromatic RP.

The dependence of k_{soc} on K_c implies the corresponding correlation with the micellar volume. Indeed a tendency to a decrease in k_{soc} with the increase of the chain length of the detergent is observed for most of the systems except BP - PNH₂ (table 4). The lack of unambiguous and pronounced correlation of k_{soc} and R_m^3 unlike that for k_{chim} is not very surprising because of the strong sensitivity of SOC to the space configuration of the radicals in the contact states of the RP, which may be varied significantly with the structure of the micelles.

As expected for the SOC induced processes, k_{soc} increases dramatically after the introduction of a heavy Br atom into the ketyl radical (table 4). Even the introduction of Cl atoms into the system results in an increase in the value of k_{soc} . The heavy Br atom effect is more pronounced in the case of 4-substitution than in that of 2-substitution. This position dependence is in accordance with the amplitude of unpaired electron spin density in 4 and 2-positions of the aromatic ring. The internal heavy atom

effect in micellized RP is of the same order of magnitude as that in polar TE. For Br-containing RPs, the value of k_{soc} becomes even comparable with that of k_{dif} (table 1). It means that the probability of recombination of the contact triplet RP during the lifetime of the encounter complex $p_{soc} = k_{soc}/k_{dif}$ is rather high ($p_{soc} \approx 0.5$ for the system 4-bromobenzophenone - PNH₂). It has to lead to a decrease in the initial yield of RPs, which are generated in the contact state. The corresponding correlation of the radical yield and Br-substitution has been observed in several related systems [7,20] This correlation puts a strong argument in support of the validity of the assumption of the role of intersystem recombination.

The addition of bromobenzene to the SDS micellar solution (up to 0.01 mol/l) of the system BP - PNH₂ has insignificant effect (within 10%) on the lifetime of the corresponding RP in the zero as well as in the high magnetic fields, whilst that of iodobenzene is followed by an increase of k_{obs} at $H = 0.45$ T with k_{obs} at $H = 0$ being unchanged. The slope of the dependence of k_{obs} at $H = 0.45$ T on the content of iodobenzene molecules per one SDS micelle (up to 10) gives the value of the first order quenching rate constant equal to 1.5×10^5 s⁻¹.

The acceleration of the RP intramicellar decay in the presence of iodobenzene in a high magnetic field is the manifestation of an external heavy atom effect. Two quite different mechanisms of this effect may be taken into account: (i) the enhancement of SOC in a some kind of a complex of contact RP with iodobenzene and (ii) the acceleration of the spin relaxation in the separated RP. The value of 1.5×10^6 s⁻¹ may be ascribed to the rate constant of the contact RP quenching by iodobenzene molecules in SDS micelle if $K_c \approx 0.1$. This value is only one order of magnitude smaller than k_{dif} and seems to be too high. The values as small as $10^{-3} - 10^{-4}$ of the diffusion controlled limit have been obtained for the triplet contact radical ion pair quenching by iodobenzene due to the external heavy atom effect. However, the efficiency of this mechanism may be enhanced significantly, when the reactants are localized in the same region of the micelle. The second mechanism, which is due to the modulation of the g factors of the radicals by the encounters with a heavy atom, may be involved as well.

The values $1/k_{\text{rel}}$ depend linearly on H^2 at $H \geq 0.03$ T in accordance with the relaxation theory in terms of the perturbation with exponential correlation function [22], if the off-diagonal matrix element of interaction (V) is independent of H :

$$k_{\text{rel}} = 2\tau_c |V|^2 / \hbar^2 (1 + \omega^2 \tau_c^2) \quad (7)$$

Here τ_c is the rotational correlation time, the frequency $\omega = g\beta H/\hbar$ (g is the mean value of the isotropic g factors of the radicals in RP). The values of τ_c and V obtained from the slopes and the intercepts of the linear fits are presented in table 4. The calculation of k_{rel} according to eq.(7) with the obtained values of τ_c and V (table 1) leads to the values $(2-7) \times 10^4$ s $^{-1}$ at $H = 0.33$ T, which are in coincidence with the values of $1/T_1$ for ketyl radicals from ESR experiments at $\eta = 10$ cP [40]. This conformity is a good proof for the validity of this model.

The values of τ_c obtained are in very good agreement with the τ_c for the free radicals in SDS determined from the ESR experiments [44]. The difference in τ_c for RPs under consideration shows that, as a rule, the rotational mobility of the micellized neutral radicals are higher than that of the radical cations localized on the negatively charged surface of the SDS micelles. The rotational mobility of the radicals is increased with a decrease in the alkyl chain length of the detergent as well as after the addition of EtOH or NaCl due to the decrease of η .

The values of $|V|$ obtained permit one to analyse the contribution of the different mechanisms of relaxation. This analyses leads to a conclusion that, the relaxation due to HFC anisotropy is most important [20,22]. The role of HFC anisotropy may be considered in terms of the simplest model RP, each of the partners of which has a HFC with only one nucleus having the spin 1/2. In this case $|V_{\text{hfc}}| = \Delta A_{\text{hfc}}/6$, where ΔA_{hfc} is the square-root from the sum for the two radicals of the values $(\Delta A_{\text{hfc}}^{\parallel} - \Delta A_{\text{hfc}}^{\perp})^2$ which characterized the HFC anisotropy [20]. The values of $|V|$ obtained (table 1) correspond to $\Delta A_{\text{hfc}}/g\beta = 2.2 - 3.6$ mT which is in a very good agreement with the effective A_{hfc} for aromatic radicals. This coincidence apparently testifies the preferential role of relaxation due to HFC anisotropy. The deuteration of the ketyl leads to a decrease in $|V|$ (table 4) showing the important role of the relaxation based on hfc. The values of $|V|$ for RPs,

containing PO^{\cdot} are smaller than those for RPs with PNH_2^{+} (table 4). The possible reason may be due to an additional source of relaxation due to HFC anisotropy on the N nucleus. The large value of $|V|$ for RPs with PNH_2^{+} in comparison to those with PO^{\cdot} may be the reason for the pronounced difference in the initial part of the corresponding magnetic field dependences (fig. 6).

The saturation of the micellar solutions by air or even by molecular oxygen does not influence or accelerates insignificantly within 10% the values of k_{obs} at $H = 0$ for most of the RPs. The more or less noticeable effect up to 25% is observed for the RPs with the longest lifetimes only, e.g. for the RP of the system 2,6-diphenyl-1,4-benzoquinone - POH [20]. The effect of $^3\text{O}_2$ on the lifetime of the fast component of the decay of micellized ketyl or semiquinone radicals is the same as that for the PO^{\cdot} or PNH_2^{+} and it is due on the whole to an acceleration of the geminate recombination of the RPs in the micelles. The semiquinone radicals of 2,6-diphenyl-1,4-benzoquinone as well as PO^{\cdot} and PNH_2^{+} are not quenched by $^3\text{O}_2$ either in the homogeneous liquid systems or in the aqueous phase of the micellar solution or in the lone state in the micelles. In the case of the ketyl radicals, the lifetime of the slow component of the decay of the corresponding absorption at 540 - 580 nm in $^3\text{O}_2$ saturated micellar solutions is at least one order of magnitude longer than that of the fast one.

At high magnetic fields, a pronounced increase of k_{obs} values are observed in the presence of $^3\text{O}_2$. In $^3\text{O}_2$ saturated micellar solutions, the values of k_{obs} at $H = 0.45$ T becomes close to those at $H = 0$, the magnetic field effects become small. The corresponding second-order rate constants ($k(O_2)$) of the RP quenching by $^3\text{O}_2$ at $H = 0.45$ T are very high. Calculations for the air saturated micellar solutions using a value of 0.28 mmol/l (being equal to the concentration of $^3\text{O}_2$ in air saturated water) give the value of $k(O_2)$ as $(5 - 7) \times 10^9$ l/mol.s.

The magnetic field effect is quenched significantly in the presence of paramagnetic complex CoPz_2Cl_2 (Pz - 3,5-dimethyl-4-ethylpyrazole), which is poorly soluble in water, as the cations of CoPz_2^{2+} are being localized at the micellar interface. The values of k_{obs} at $H = 0$ decrease insignificantly with increase of the metal complex concentration, while those at $H =$

0.45 T increase dramatically (fig. 7). At a concentration of the paramagnetic species corresponding to 10 molecules per one micelle the magnetic field effect becomes negligible.

The interaction of the electronic magnetic spins of the paramagnetic additives with the electronic spins of the RP causes the relaxation of the T_+ states to the T_0 and S states. The fact that the RP decay kinetics at zero field is not affected significantly by the addition of the paramagnetic quencher supports the conclusion about the participation of the separated RPs in the process. The corresponding contribution to the k_{rel} values in high magnetic field may be calculated in terms of the solution of the scheme 2 from the dependences of k_{obs} on the concentration of the paramagnetic species (fig. 7). The slopes of the plots of k_{rel} versus the intramicellar concentration of CoPz_2^{2+} give the values of the quenching rate constants equal to 3.9×10^6 and $2.4 \times 10^6 \text{ s}^{-1}$ for the systems BP - PNH_2 and 2,6-diphenyl-1,4-benzoquinone - POH respectively. This process is only few times slower than the diffusion controlled one. The quenching of the RPs in a high magnetic field by ${}^3\text{O}_2$ seems to be near the diffusion control as well. Whilst the experimental results available are not sufficient for the very definite separation of the contributions of the dipolar relaxation and the spin exchange mechanisms, as it was done for the quenching of the kinetic magnetic field effect in biradicals by paramagnetic metal complexes [45], nevertheless, the very high values of the quenching rate constants for the paramagnetic species (${}^3\text{O}_2$, CoPz_2^{2+} as well as the stable nitroxyl radicals [20]) with very different electronic spin-lattice relaxation times, definitely support the spin exchange mechanism.

In general, the geminate recombination kinetics of the radical pairs produced in the triplet state in the micelles as well as the attendant structural, additive and magnetic field effects are satisfactorily described in terms of a simple kinetic scheme of the first order processes, which includes the singlet-triplet transitions in the separated states of a pair due to the isotropic HFC and relaxation as well as intersystem recombination process due to the spin-orbit coupling in the contact states of a pair (transition from the triplet contact state of the radical pair to the energetic surface of recombination products in the singlet

state). The magnetic field dependence at $0.03 < H < 0.1 \text{ T}$ is conditioned by the decrease in the rate of paramagnetic relaxation, which is mainly due to the anisotropy of the hyperfine interaction. Intersystem recombination is the most important route of the decay of micellized radical pairs produced in T_+ states in very high magnetic fields. The model gives a possibility to determine the relaxation parameters from the magnetic field dependences.

3.4 MFE in recombination kinetics of RP on the surface

Photoexcitation of AQ in the presence of TPA, BTPA or PNH_2 on the surface leads to the RIP formation. At the content of D available on the surface at the present experimental conditions, the lifetime of ${}^3\text{AQ}$ is shorter than the duration of the laser pulse and, immediately after the pulse, the well known absorption of D^+ (fig. 1) is observed. There is also another maximum in the transient absorption spectra at 430 nm (fig. 1), which may be ascribed to the absorption of AQ^- [13]. This maximum is strongly blue-shifted in comparison with those in solution. The quenching of ${}^3\text{BP}$ by POH or PNH_2 on the surface leads to the formation of the same RPs as in micelles.

The oscilloscopic traces of optical density due to the RIP or RP absorption contain the fast component ($t \leq 10 \mu\text{s}$), which corresponds to the RIP geminate recombination, and the slow component ($t \geq 100 \mu\text{s}$) reflecting the decay of the radical-ions that have escaped from the "super cage" on the surface of the channels in porous glass and the lone radical-ions in the "supercages" (fig. 8). Only two exponentials are necessary to fit adequately the fast component. However, the deviation from the monoexponential law is relatively pronounced for AQ - TPA system only. The characteristic feature of this system is the low contribution of the escape process, which is much more important for the other systems (fig. 8). The deviations from the first order law in these systems is masked by the slow component. But even for the system AQ - TPA, this deviation may be neglected in the frame of zero approximation. The k_{obs} values and the contributions of slow component (Φ_{obs}) obtained from the monoexponential approximations for all the systems investigated are presented in table 5.

Table 5

The values of k_{obs} and Φ_{obs} obtained in terms of the monoexponential model and calculated values of k_{rec} and k_{dis} for the recombination of adsorbed radical pairs with and without magnetic field ^{a)} Thermally pretreated glass.

RP	H = 0				H = 0.24 T			
	Φ_{obs}	k_{obs}	k_{rec}	k_{dis}	Φ_{obs}	k_{obs}	k_{rec}	k_{dis}
AQ ^{-·} ,TPA ⁺	7	5.7	5.3	0.4	12	3.8	3.3	0.5
AQ ^{-·} ,TPA ^{+,a)}	2	1.8	1.8	0.04	3	1.4	1.4	0.04
AQ ^{-·} ,BTPA ⁺	27	13	9.5	3.5	35	12	7.8	4.2
AQ ^{-·} ,PNH ₂ ⁺	35	5.4	3.5	1.9	43	4.2	2.4	1.8
BH [·] ,PNH ₂ ⁺	42	5.8	3.4	2.5	54	6.6	3.0	3.6
BBH [·] ,PNH ₂ ⁺	45	17	9.4	7.6	54	17	7.8	9.2
BH [·] ,PO [·]	36	2.3	1.5	0.8	50	1.8	0.8	0.8
BBH [·] ,PO [·]	37	3.5	2.2	1.3	46	3.1	1.7	1.4

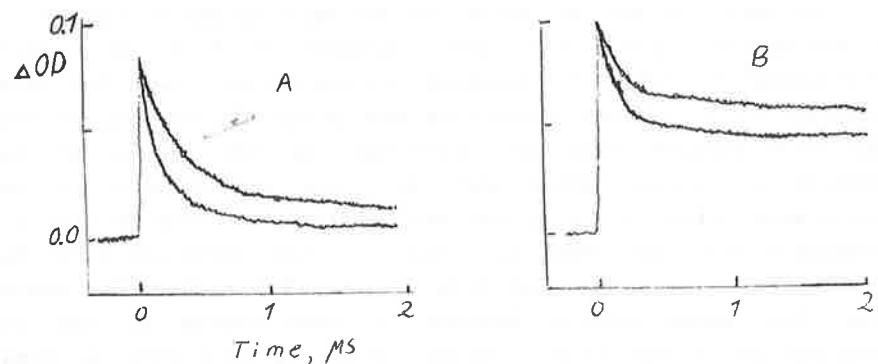


Fig. 8. Decay of the transient absorption at 650 nm due to the adsorbed RIP [AQ^{-·},TPA⁺] (A) and at 675 nm due to the adsorbed RP [BPH[·],PNH₂⁺] (B) at H = 0 (lower curves) and H = 0.24 T (upper curves).

The simplest kinetic description of a RP in terms of the monoexponential model (3) gives the possibility of detailed description of the RP decay processes, which have already been used for the RP in micelles, in viscous media and for charge transfer TE. The values of k_{rec} and k_{dis} calculated from k_{obs} and Φ_{obs} are also presented in table 5.

The SiO₂ surfaces are covered with hydroxyl groups and physisorbed water [46,47]. The estimation based on the data from [47] gives the content of OH groups on the surface of porous glass close to the monolayer. Thus the molecular environment of the adsorbed species should be similar in some extent to that on the surface of water. On the one hand, the fact that the radicals from AQ exist on the surface in the anion form testifies, that the pH of the surface is greater than the pK_a of AQ^{-·} (5.3). On the other hand the cation form of the aniline radicals evidences that the surface is acidic, if we suppose a pK_a value near 7 for the anilino radical. The ketyl radicals (pK_a of BP[·] is equal to 9.2) are in neutral form on the surface all the more. Thus the pH on the surface of the pours is in the range 5.3 - 7.

Polar oxygen and nitrogen containing aromatic and quinoid compounds under the discussion as well as the corresponding excited states and free radicals or radical-ions are bound to the silicate surface via hydrogen bonds with the silanol groups [46,47]. A very significant blue shift of AQ^{-·} absorption band on going from solution (even of solvents with high ability for H-bond formation, e. g. alcohols) to the surface is a direct evidence of the participation of AQ^{-·} in a strong hydrogen bonding on the surface (fig. 1).

The chemical nature of the surface of porous silicate glasses without thermal pretreatment seems to be analogous to that of undried silica gels, where high translational mobilities of aromatic molecules with heteroatoms as well as the corresponding free radicals were established [46,47]. At the present content of A and D on the surface (the evaluated mean distance between A and D is 5 nm), the excited state quenching processes (1) and (2) should be dynamic and proceed with the participation of ³A, due to very fast intersystem crossing ¹AQ → ³AQ or ¹B → ³B. The high contribution of the escape processes to the RP decay also evidences

the significant mobility of the adsorbed radicals. The comparison of the values of the rate constant k_{dis} within the monoexponential model may serve as a measure of the mutual relative radicals mobility as well as a measure of coulomb and other types of interaction between the radicals in RP or RIP. For example, the lower values of k_{dis} for B - POH and AQ - TPA systems than those for B - PNH₂ and AQ - PNH₂ respectively suggest that the mobility of PO[·] and TPA⁺ is lower than that of PNH₂⁺ (table 5).

The noticeable values of k_{dis} even for the triplet RIPs evidences that these RIPs seem to be found in a polar environment which ensures weakening of the coulomb attraction between the radical ions. This feature together with the high mobility of the radicals on the surface provide an easy formation of a distance separated RIP and RP, where magnetosensitive S - T evolution mechanisms are active. On the other hand, high values of cage effect (ϕ being for many systems significantly smaller than unity, see table 5) even for neutral RP, where there is no coulomb attraction, suggests that the adsorbed RIPs are localized in the "super cages" of some kind with a restricted escape. Thus, the distance-separated RP formation from the contact one is a reversible process. These two important features determine the high magnetic field effect observed (table 5), which is somewhat stronger than that for the same RIP and RP in the corresponding solvents of intermediate polarity and of high viscosity. On the other hand, the magnetic field effects observed are much smaller than those in micelles. The most important rout of RIP or RP recombination on the surface should be the intersystem backward et or intersystem recombination in the contact state due to the SOC as it was concluded for TE in solvents of intermediate polarity and triplet RP in viscous media. The k_{rec} values obtained for the surface (table 5) are of the same order of magnitude as those for TE in solution and for RP in glycerol. The dependence of k_{rec} values on the structure of the radicals looks the same as that for liquid systems.

The thermal pretreatment of the porous glass causes a decrease in the values of k_{dis} and k_{rec} (table 5). On thermally pretreated SiO₂ surfaces, the silanol groups are partly replaced by siloxane units which decreases the lateral mobility of adsorbed species

[46,47]. The decrease of the content of water on the surface may result also in the decrease of the polarity of the RP environment. These changes should result in the decrease of the corresponding rate constants and the magnetic field effect as well, which has been observed for the triplet RIP.

In general, the nature of SiO₂ material strongly affects the kinetics of RP decay on the surface. Our preliminary results for RIP of AQ - TPA system on ariosyl gave a slower RIP geminate recombination and a smaller escape and magnetic field effect. In the case of the system B - 2,4,6-trimethylphenol on the silica, the contribution of geminate recombination to the decay of the corresponding RP was very small and the main route for the disappearance of the radicals was the bimolecular recombination on the surface [48].

Imposition of a magnetic field leads to an increase in the value of Φ_{obs} and to the inhibition of geminate recombination for most of the systems studied (fig. 8). A very pronounced increase of Φ_{obs} and a decrease of k_{obs} are observed on going from H = 0 to 0.01 T showing the importance of HFC mechanism. An increase of H in the range H ≥ 0.1 T has no influence on Φ_{obs} and k_{obs} . The only route of the decay of adsorbed RP or RIP arising in T₊ states at high H is the intersystem recombination or intersystem backward et.

As expected for SOC-induced processes, k_{rec} obtained at H = 0 as well as at H = 0.24 T increases after the introduction of heavy Br atoms into one of the radicals in RP or RIP (table 8). The magnetic field effect is relatively small and becomes even negligible in the case of Br-substituted RP or RIP. The internal heavy atom effect in geminate recombination of RP or RIP on the surface resembles that for RP in viscous solvents or for RIP in solvents of intermediate polarity, where the most important route of RP or RIP decay is intersystem recombination or intersystem et in the contact state due to SOC.

The increase in the values of k_{rec} on going from BP to p-BrBP on the surface are close to those obtained for analogous systems in liquid solutions. Nevertheless, it should be mentioned that the internal heavy atom effect in adsorbed RIP of AQ - TPA (BTPA) system is significantly smaller than that in the corresponding contact RIP in liquid solutions. The decay rate constant increases

by a factor of ten on going from ${}^3[\text{AQ}^{\cdot-}, \text{TPA}^{\cdot+}]$ to ${}^3[\text{AQ}^{\cdot-}, \text{BTPA}^{\cdot+}]$ in benzene and by the factor of 50 in the presence of alcohol. However, this discrepancy may be attributed to the strong dependence of SOC on the conformation of the contact RIP. It is very likely, that the spatial configuration of the donor and the acceptor in the contact RIP adsorbed on the surface does not promote the SOC, which is localized in the valence p_z -orbital of the heavy halogen atom (parallel "sandwich" type structure is optimal in this case).

In general, it should be noted that the use of optically transparent porous materials give the opportunity of obtaining a detailed and direct kinetic information about the radical pairs behavior on the surfaces, by resorting to the conventional laser photolysis technique. The geminate recombination of adsorbed RPs has similarities with that of micellized triplet RP as well as with that of triplet RIP in solvents of intermediate polarity and triplet RP in viscous media. Introduction of a heavy atom as a substitute in the radicals leads to acceleration of the geminate recombination; application of an external magnetic field results in retardation. The heavy atom effect shows the contribution of the intersystem backward electron transfer or intersystem recombination in the contact states of a triplet RP due to the spin-orbit coupling. The magnetic field effect is due to the significant contribution of the recombination route through the separated RP, where the hyperfine coupling and relaxation mechanisms of RP spin evolution are active.

References

- [1] K. M. Salikhov, Yu. N. Molin, R. Z. Sagdeev and A. L. Buchachenko, *Spin Polarization and Magnetic Effects in Radical Reactions* (Elsevier, Amsterdam, 1984).
- [2] N.J.Turro and B.Kraeutler, *Acc.Chem.Res.* 13 (1980) 369;
N.J.Turro, *Pure Appl. Chem.* 58 (1986) 1219.
- [3] S.Nagakura and H.Hayashi, *Intern. J. Quantum Chem.* 18 (1984) 571.
- [4] J.C.Scaiano, *Trans. Roy. Soc. Can.* 21 (1983) 133.
- [5] Y.Tanimoto and M.Itoh, in: *Physical organic chemistry 1986*, Vol. 31, ed. M. Kobayashi (Elsevier, Amsterdam, 1987) p. 257.
- [6] U.E.Steiner and T.Ulrich, *Chem. Rev.* 89 (1989) 51.
- [7] T. Ulrich, U. E. Steiner and W. Schlenker, *Tetrahedron* 42 (1986) 6131;
U. E. Steiner and W. Haas, *J. Phys. Chem.* 95 (1991) 1880.
- [8] A. Weller, H. Staerk and R. Treichel, *Faraday Disc. Chem. Soc.* 78 (1984) 271.
- [9] E. Ya. Fedotova, Yu. M. Stolovitskiy and E. L. Frankevich, *Dokl. Phys. Chem.* 254 (1980) 423.
- [10] P.P.Levin and V.A.Kuzmin, *Bull.Acad.Sci.USSR,Div.Chem.Sci.*, 36 (1987)2426; P.P.Levin, P.F.Fluzhnikov and V.A.Kuzmin, *Chem. Phys.*, 137(1989)331; P.P.Levin, P.K.N.Raghavan and V.A.Kuzmin, *Chem.Phys.Letters*, 167(1990)67.
- [11] P.P.Levin, I.V.Khudjakov and V.A.Kuzmin, *Bull.Acad.Sci.USSR, Div.Chem.Sci.*, 35(1986)479; 36(1987)395,918; 37(1988)432; 38(1989)18; *Dokl.Phys.Chem.*, 288(1986)440; *Kinet.Katal.*, 29(1988)326; *Khim.Fiz.*, 8(1989)902; *J.Phys.Chem.*, 93(1989)208.
- [12] N.J.Turro, M.-F.Chow, C.-J.Chung and G.C.Weed, *J.Am.Chem.Soc.* 103 (1981) 4574;
N.J.Turro, M.B.Zimmt and I.R.Gould, *J.Am.Chem.Soc.* 105 (1983) 6347;
I.R.Gould, M.B.Zimmt, N.J.Turro, B.H.Baretz and G.F.Lehr, *J.Am.Chem.Soc.* 107 (1985) 4607;
N.J.Turro, M.B.Zimmt, X.G.Lei, I.R.Gould, K.S.Nitsche and Y.Cha, *J.Phys.Chem.* 91 (1987) 4544.
- [13] N.J.Turro, M.B.Zimmt and I.R.Gould, *J.Phys.Chem.* 92 (1988) 433.
- [14] H.Hayashi, Y.Sakaguchi and S.Nagakura, *Chem.Lett.* (1980) 1149;
H.Hayashi, Y.Sakaguchi, M.Tsunooka, H.Yanagi and M.Tanaka, *Chem.Phys.Letters* 136 (1987) 436;
H.Hayashi, Y.Sakaguchi, M.Kamachi and W.Schnabel, *J.Phys.Chem.* (1987) 3936.
- [15] Y.Sakaguchi, H.Hayashi and S.Nagakura, *J.Phys.Chem.* 86 (1982) 3177.
- [16] J.C.Scaiano and J.-L.Shi, *Chem.Phys.Letters* 173 (1990) 271.
- [17] Y.Sakaguchi, S.Nagakura and H.Hayashi, *Chem.Phys.Letters* 72 (1980) 420; 82 (1981) 213.
Y.Sakaguchi and H.Hayashi, *Chem.Phys.Letters* 87 (1982) 539;
Y.Sakaguchi and H.Hayashi, *J.Phys.Chem.* 88 (1984) 1437;
- [18] J.C.Scaiano and E.B.Abuin, *Chem.Phys.Letters* 81 (1981) 209;

- J.C.Scaiano, E.B.Abuin and L.C.Stewart, *J.Am.Chem.Soc.* 104 (1982) 5673;
- E.B.Abuin and J.C.Scaiano, *J.Am.Chem.Soc.* 106 (1984) 6274;
- J.C.Scaiano and D.J.Lougnot, *J.Phys.Chem.* 88 (1984) 3379;
- C.Evans, K.U.Ingold and J.C.Scaiano, *J.Phys.Chem.* 92 (1988) 1257;
- C.H.Evans and J.C.Scaiano, *J.Am.Chem.Soc.* 112 (1990) 2694.
- [19] Y.Tanimoto and M.Itoh, *Chem.Phys.Letters* 83 (1981) 628;
- Y.Tanimoto, H.Udagawa, Y.Katsuda and M.Itoh, *J.Phys.Chem.* 87 (1983) 3976;
- Y.Tanimoto, H.Udagawa and M.Itoh, *J.Phys.Chem.* 87 (1983) 724;
- Y.Tanimoto, K.Shimizu and M.Itoh, *J.Am.Chem.Soc.* 106 (1984) 7257; *Chem.Phys.Letters* 112 (1984) 217.
- Y.Tanimoto, M.Takashima and M.Itoh, *Chem.Phys.Letters* 100 (1983) 442; *J.Phys.Chem.* 88 (1984) 6053; *Chem.Lett.*(1984)1981;
- Y.Tanimoto, E.Shimada and M.Itoh, *Bull.Chem.Soc.Jpn.* 59 (1986) 3039;
- Y.Tanimoto, M.Takayama, M.Itoh, R.Nakagaki and S.Nagakura, *Chem.Phys.Letters* 129 (1986) 414.
- [20] P.P.Levin and V.A.Kuzmin, *Bull.Acad.Sci.USSR,Div.Chem.Sci.*, 35 (1986)430,1435; 36(1987)691,923; 37(1988)224; *Dokl.Phys.Chem.*, 292(1987)26; *Khim.Fiz.*, 7(1988)909; 8(1989)1034; *Chem.Phys. Letters*, 165(1990)302; *Chem.Phys.* (submitted).
- [21] D.Baumann, T.Ulrich and U.E.Steiner, *Chem.Phys.Letters* 132 (1987) 113.
- [22] H.Hayashi and S.Nagakura, *Bull.Chem.Soc.Japan* 57 (1984) 322.
- [23] Y.Sakaguchi and H.Hayashi, *Chem.Phys.Letters* 106 (1984) 420.
- [24] N.J.Turro, X.G.Lei, I.R.Gould and M.B.Zimmt, *Chem.Phys.Letters* 120 (1985) 397.
- [25] N.J.Turro, C.-J.Chung, G.Jones,II and W.G.Becker *J.Phys.Chem.* 86 (1982) 3677.
- [26] P.P.Levin, I.V.Katalnikov and V.A.Kuzmin, *Bull.Acad.Sci.USSR, Div.Chem.Sci.*, 38(1989)1095; *Khim.Fiz.*, 8(1989)1604; *Chem. Phys. Letters*, 167(1990)73; *Chem.Phys.* (accepted).
- [27] P. P. Levin and V. A. Kuzmin, *Russian Chem. Rev.* 56 (1987) 528.
- [28] E. Amouyal and R. Bensasson, *J. Chem. Soc. Faraday Trans. 1* 73 (1977) 1561.
- [29] H. Kobashi, M. Funabashi, T. Kondo, T. Morita, T. Okada and N. Mataga, *Bull. Chem. Soc. Japan* 57 (1984) 3557.
- [30] K. Hamanoue, T. Nakayama, Y. Yamamoto, K. Sawada, Y. Yuhara and H. Terenishi, *Bull. Chem. Soc. Japan* 61 (1988) 1121.
- [31] J. D. Simon and K. S. Peters, *J. Am. Chem. Soc.* 104 (1982) 6542.
- [32] B. S. Prabhananda and J. S. Hyde, *J. Chem. Phys.* 85 (1986) 6705.
- [33] P.K.Das, W.V.Encinas and J.C.Scaiano, *J.Am.Chem.Soc.* 103 (1981) 4154, 4161.
- [34] A.Malliaris, J.Le Moigne, J.Strum and R.Zana, *J.Phys.Chem.* 89 (1985) 2709; N.J.Turro, M.Okamoto and P.-L.Kuo, *J.Phys.Chem.* 91 (1987) 1819.
- [35] V.Yu.Bezzobotnov, S.Borbely, L.Cser, B.Farago, I.A.Gladkikh, Yu.M.Ostanevich and Sz.Vass, *J.Phys.Chem.* 92 (1988) 5738; S.Borbely, L.Cser, Yu.M.Ostanevich and Sz.Vass, *J.Phys.Chem.* 93 (1989) 7967; A.Rohder and E.Sackmann, *J.Colloid Interface Sci.* 70 (1979) 494.
- P.J. Missel, N.A.Mazer, G.B.Benedek and M.C.Carey, *J. Phys. Chem.* 87 (1983) 1264.
- [36] N.J.Turro and T.Okubo, *J.Am.Chem.Soc.* 103 (1981) 7224; J.Emert, C.Behrens and M.Goldenberg, *J.Am.Chem.Soc.* 101 (1979) 771; W.D.Turley and H.W.Offen, *J.Phys.Chem.* 89 (1985) 2933.
- [37] M.Almgren and S. Swarup, *J.Coll.Interface Sci.* 91 (1983) 256.
- [38] N.A.Maser, G.B.Benedek and M.C.Carey, *J.Phys.Chem.* 80 (1976) 1075; N.A.Maser, M.C.Carey and G.B.Benedek, in: *Micellization, Solubilization, and Microemulsions*, ed. K.L.Mittal (Plenum Press, New York, 1977) p. 359; P.J. Missel, N.A.Mazer, G.B.Benedek, C.Y.Young and M.C.Carey, *J.Phys.Chem.* 84 (1980) 1044.
- [39] J.Chen, T. Su and C.Y.Mou, *J.Phys.Chem.* 90 (1986) 2418.

- [40] K.A.McLauchlan, R.C.Scally and J.M.Wittmann, Mol.Phys. 36 (1978) 1397.
- [41] M.B.Zimmt, C.Doubleday, I.R.Gould and N.J.Turro, J.Am.Chem.Soc. 107 (1985) 6724; M.B.Zimmt, C.Doubleday, and N.J.Turro, J.Am.Chem.Soc. 107 (1985) 6726; 108 (1986) 3618; C.Doubleday, N.J.Turro and J.-F.Wang, Acc.Chem.Res. 22 (1989) 199.
- [42] J.C.Scaiano, W.G.McGimpsey, W.J.Leigh and S.Jakobs, J.Org.Chem. 52 (1987) 4540.
- [43] P.P.Levin, Ya.N.Malkin and V.A.Kuzmin, Chem.Phys.Letters 175 (1990) 74.
- [44] K.Suga, K.Maemura, M.Fujihira and S.Aoyaqui, Bull.Chem.Soc.Japan 60 (1987) 2221; P.Baglioni, M.Ottoviani and G.Martini, J.Phys.Chem. 90 (1986) 5878; N.M.Atherton and S.J.Strach, J.Chem.Soc.Faraday Trans.2 68 (1972) 374.
- [45] J.Wang, K.M.Welsh, K.C.Waterman, P.Fehlner, C.Doubleday and N.J.Turro, J.Phys.Chem. 92 (1988) 3730; Y.Tanimoto, A.Kita, M.Itoh, M.Okazaki, R.Nakagaki and S.Nagakura, Chem.Phys.Letters 165 (1990) 184.
- [46] P. de Mayo, Pure Appl. Chem. 54 (1982) 1623.
- [47] D. Oelkrug, S.Uhe, F. Wilkinson and C. J. Willsher, J. Phys. Chem. 93 (1989) 4551.
- [48] P. P. Levin, L. F. V. Ferreira and S. M. B. Costa, to be published.

MECHANISMS OF SPIN-ORBIT COUPLING DEPENDENT MAGNETIC FIELD EFFECTS IN CHEMICAL KINETICS

U.E. Steiner, D. Baumann, W. Haas, , H.-J.Wolff and D. Bürßner
Fakultät für Chemie, Universität Konstanz,
D-7750 Konstanz, Germany

The mechanisms by which magnetic field effects (MFEs) on chemical kinetics ensue, almost exclusively conform to the following general pattern [1]: A manifold of close lying spin(-orbit) states of a reaction intermediate - usually a pair of reacting species with unpaired spins- is coupled to some reaction channel in a spin-substate selective way, while other non-spin-selective channels may also exist. The magnetokinetic effect is based on a recoupling of the spin substates by a magnetic field and may be detected either directly as a magnetic field dependent decay kinetics of the reaction intermediate or, indirectly, as a magnetic field dependent yield into one of the available reaction channels, that need not be a spin-selective one.

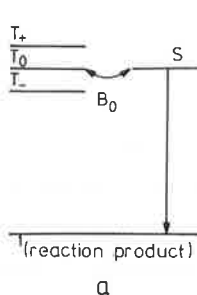
Spin-orbit coupling (SOC) may be involved in such a mechanism in two ways. (i) It may modify the interaction of the reactive components of the intermediate with the external magnetic field and thereby increase the magnetic coupling between the eigenstates of the zero-field Hamiltonian, or (ii) it may be responsible for the reactive coupling of the reaction intermediate to a product channel and thereby cause a sublevel selectivity of this channel.

In our paper three mechanistic cases of such SOC-assisted MFEs (cf. Scheme I) will be specified and experimental examples employing photoinduced electron transfer reactions will be provided for them.

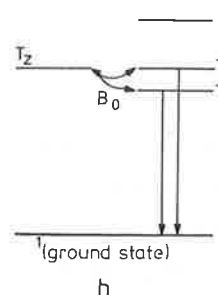
Case (a) of Scheme I is encountered as a feature of the well known radical pair mechanism (RPM). Different SOC in the radicals

SCHEME I

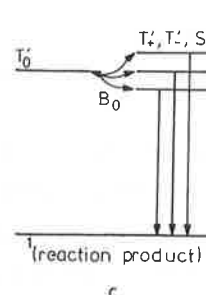
Δg -type
Radical Pair Mechanism



Triplet Mechanism



RPM with strongly
spin-orbit mixed
Kramers doublet

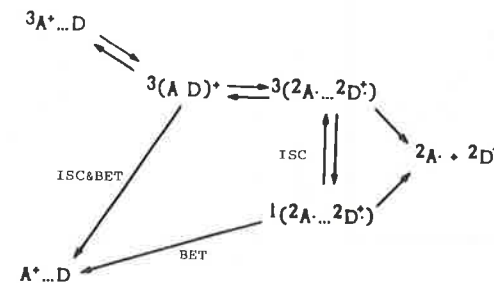


of the pair will cause their g -factors to be different, so that a magnetic field dependent coupling of T_0 and S ensues. This effect, belongs to type (i) of the cases specified above.

Case (b) is a variant of the so-called triplet mechanism (TM). Here we consider an electronically excited reactant with a distinct T_1/S_1 splitting. Spin-substate selective decay of the triplet occurs by intersystem crossing to the singlet ground state. This process is driven by SOC, an interaction which is triplet substate selective. An external magnetic field recouples the zero-field triplet substates and thereby changes the overall decay kinetics and the yield into chemical reaction channels that may be present. In this mechanism the effect of SOC is of case (ii) type.

Regarding case (c) we will show that it is encountered as a hybrid of cases (a) and (b) for redox pairs involving as one component a strongly spin-orbit coupled Kramers doublet species. Here the true singlet spin character cannot be concentrated in one single spin-orbit substate of the pair as in the RPM (a). Therefore, even in zero field, several of the eigenstates of the spin Hamiltonian have a finite reaction probability. The effect of an external magnetic field includes both g -type T_0'/S' mixing and a TM type T' substate mixing.

encounter complex	triplet exciplex	geminate radical pair	free radicals
-------------------	------------------	-----------------------	---------------



SCHEME II

Application of these mechanistic cases (a)-(c) will be demonstrated with experiments utilizing photoelectron transfer reactions with excited triplet species. Transients exhibiting the magnetic field effects are triplet exciplexes and spin-correlated radical pairs (cf. Scheme II). A spin selective reaction channel is provided by fast BET regenerating the singlet ground state reactants. A spin-independent chemical channel is the formation of free radicals.

Cases (a) and (b) apply to the reaction of excited dye triplets, like methylene blue, with heavy atom substituted electron donors like p-I-aniline, where the heavy atom substituent provides the strong SOC required to maximize magnetokinetic effects of this type. Figure 1 shows examples of results with this system. The initial field dependence of the free radical yield is due to the TM in triplet exciplexes formed as primary reaction products, whereas the high-field part is due to the g -type RPM. The observed magnetic field dependence can be quantitatively reproduced by the two mechanisms and the characteristic kinetic parameters of the triplet exciplexes with lifetimes in the 20-50 ps region can be obtained (cf. ref [2]).

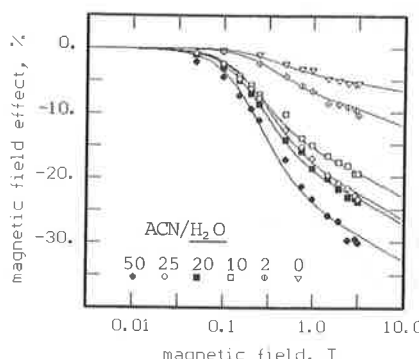


Figure 1. (left) Magnetic field dependence of free radical yield from electron transfer between p-I-aniline and methylene blue triplet in acetonitrile/water solvent mixtures.

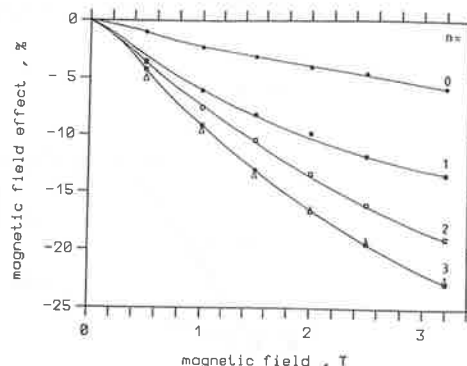


Figure 2 (right) Magnetic field dependence of methylviologen radical yield in the quenching of photoexcited complexes $[\text{Ru}(\text{bpy})_n(\text{dce})_{3-n}]^{++}$.

Case (c) applies to the reaction of photoexcited Ru(II)-tris-chelate complexes with the electron acceptor methylviologen [3-5]. As an example the MFEs with the series of $\text{Ru}(\text{bpy})_n(\text{dce})_{3-n}^{++}$ ($\text{bpy} = \text{bipyridyl}$, $\text{dce} = 4,4'\text{-dicarboethoxy-bpy}$) is shown in Fig.2.

The magnetic field dependent yield of free radicals can be modelled quantitatively on the basis of a Stochastic Liouville Equation (SLE) solved numerically for the 4-state spin density matrix of the ($\text{Ru}^{\text{III}}\text{..MV}^+$) redox pair. In particular this SLE properly takes into account the strongly SOC-mixed nature of the Ru^{III} Kramers doublet and the fast spin relaxation in this species, induced by SOC modulation through uncorrelated vibrational motions of the ligands. A striking correlation between the spin relaxation data obtained from analysis of the magnetokinetic effect (cf. Figure 3) and the linewidths in paramagnetic $^1\text{H-NMR}$ spectra of $\text{Ru}(\text{bpy})_3^{+++}$ and $\text{Ru}(\text{phen})_3^{+++}$ is pointed out. In fact it appears that the magnetokinetic effect in the photoelectron transfer reaction of transition metal complexes can provide independent information on the electron spin motion in paramagnetic redox states of these com-

plexes in liquid solutions which hitherto has been only indirectly accessible through paramagnetic NMR. Both methods may benefit from each other through this complementarity.

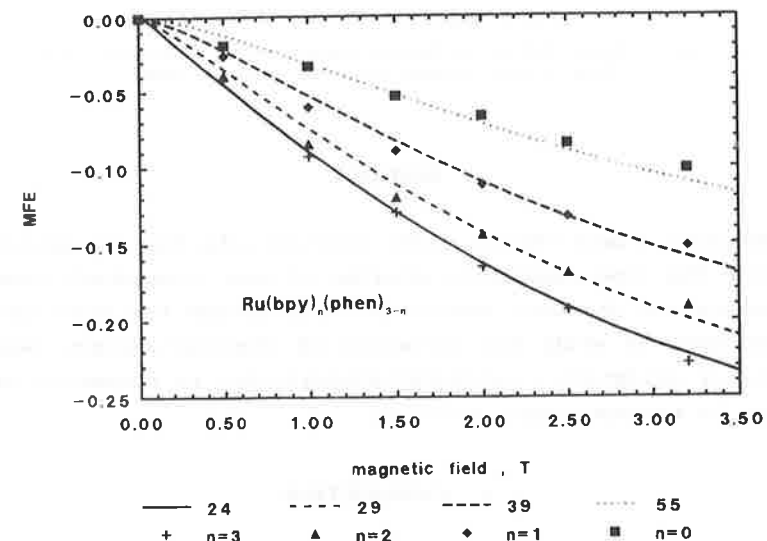


Figure 3. Magnetic field dependence of methylviologen radical yield in the quenching of photoexcited complexes $[\text{Ru}(\text{bpy})_n(\text{phen})_{3-n}]^{++}$. The curves are obtained from theoretical model calculations with parameter sets differing only in the rate constant (k_a) of spin-flip transitions in the Ru^{III} complexes. Values assigned refer to k_a and are in units of 10^9 s^{-1} .

References

- [1] U.E. Steiner and T. Ulrich, Chem. Rev. **89** (1989) 51; U.E. Steiner and H.-J.Wolff, in J.J.Rabek and G.W. Scott, Eds., CRC Series, Photochemistry and Photophysics Vol. IV, in press
- [2] U.E. Steiner and W.Haas, J.Phys.Chem. **95** (1991) 1880
- [3] U.E. Steiner, H.-J.Wolff, T. Ulrich and T. Ohno, J.Phys.Chem. **93** (1989), 5147
- [4] U.E. Steiner and D. Bürßner, Z.Physik.Chem. N.F. **169** (1990) 159
- [5] H.-J.Wolff and U.E.Steiner, Z.Physik.Chem. N.F. **169** (1990) 147

Magnetic Field Effects in Luminol Chemiluminescence

Michael M.Triebel, Andrew K.Morozov, Maxim M.Totrov,
and Eugine L.Frankevich

Institute of Energy Problems of Chemical Physics, Academy of Sciences, USSR
117334, Moscow, Leninsky prospekt. 38, build. 2, USSR

ABSTRACT

Magnetic field effects (MFE) provide with the new possibilities for the time resolution studies of some elementary steps of spin dependent chemical reactions. This method has been used in present work to study the mechanism of chemiluminescent reaction of luminol oxidation (3-aminophthalhydrazide) by potassium ferricyanide in aqueous alkali solution.

I. INTRODUCTION

Along with the well-known pulse technique the method of phase fluorometry is used for measuring the lifetime of the luminescent state [1]. This method is based on measuring the phase shift in between the sine modulated light exciting the sample and sine modulated luminescence intensity. The phase shift is brought about by the finite lifetime of the excited state of molecules, relaxation of which is accompanied by luminescence. Application of this method can be spread to studying the mechanisms of chemical reactions for the purpose of detecting and investigating the intermediate active particles only. If these reactions are initiated by some external action, for example by light or other radiation intensity of which can be modulated. In other cases different pulse methods are used for time resolution, for instance "stop-flow" or "temperature jump" techniques. In pulse studies the information about particular elementary steps of complex processes can be obtained from mathematical treatment of signal if the initiation step of the reaction is not a limiting one.

Magnetic field effects (MFE) provide with the new possibilities for the time resolution studies of some elementary steps of

spin dependent chemical reactions. This technique is based on the concept that modulation of the rate constants of certain elementary processes by external magnetic field can bring about the phase shift in between the modulated intensity of magnetic field and modulated yield of reaction products. The phase shift is obvious in case intermediate particles are formed in between the magnetosensitive step and the product registered during the reaction, the inverse value of their lifetime being comparable with the modulation frequency of the rate constant of magnetosensitive step.

This method has been used in present work to study the mechanism of chemiluminescent reaction of luminol oxidation (3-aminophthalhydrazide) by potassium ferricyanide in aqueous alkali solution.

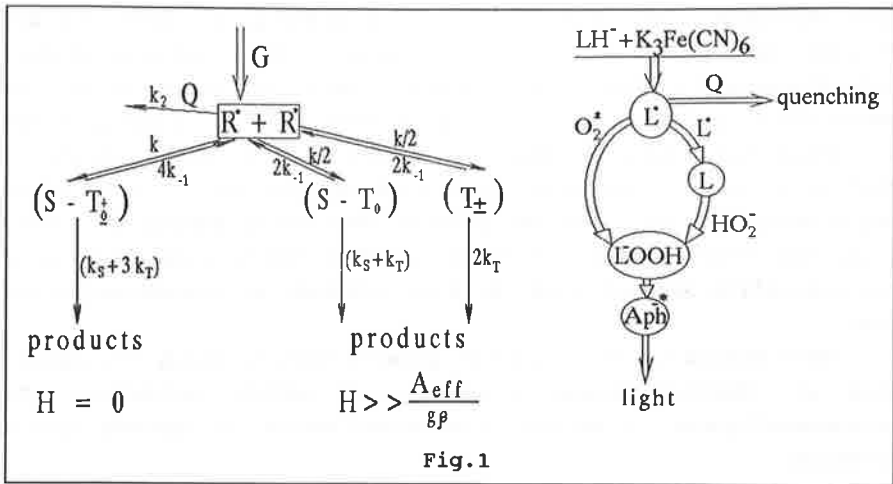
Reactions with luminol participation are widely used for analytical purposes and also for studying the mechanisms of transformation of chemical bond energy into electronic excitation energy of molecules.

The basic result of studying the reactions with luminol participation [2,3] is the conclusion that the necessary condition of chemiluminescence (CL) generation is the presence of luminol radicals, L^{\cdot} , in the system. Interaction of L^{\cdot} with superoxide ion O_2^{\cdot} results in formation of unstable peroxide compound, $LOOH$. The latter decomposes to form electronic excited anion of aminophthalic acid, $(Ap^-)^{\cdot}$, a light emitter.

A big rise in CL intensity is observed if hydrogen peroxide, H_2O_2 , is present in the system and reacts with the immediate product of luminol radicals recombination, diazoquinone L . As a result of this reaction electronic excited anion of aminophthalic acid, (Ap^-) , is also formed.

It is a fact that luminol radicals can be obtained by photolysis or radiolysis of luminol solution, and also by using various oxidants. At the same time owing to the small steady-state concentrations of L^{\cdot} there is no direct experimental evidence of L^{\cdot} participation in CL generation. Magnetic effects method makes it possible to distinguish the elementary steps with luminol radicals participation and to study them with time resolution.

Fig.1a shows a simplified scheme of CL reaction mechanism of luminol oxidation and also the structural formulae and notation of the particles adopted in this work.



METHODOLOGY

1. Variations in the rate of radical recombination under the effect of magnetic field.

Luminol radicals formed during the reaction can participate in the three main processes:

- Interaction with superoxide ion. As a result light emitters, (Ap^-) , are formed.
- Interaction with some radical quenchers, Q . As a result CL is not generated.
- Recombination with each other. As a result light emitters, (Ap^-) , are formed only if H_2O_2 participate in the reaction with recombination products.

Consider a general case of recombination of certain R' radicals in magnetic field. There is a strict quantum-mechanical treatment of this process in literature. Below we give a simplified analysis of mechanism of magnetic field effect in a pair of radicals proved sufficient for understanding the phenomena observed by the authors when studying luminol CL.

Collision of two radicals R' in solution produces with equal probabilities the pairs in the four basis spin configurations: the singlet $S(^{\uparrow\downarrow})$ and three triplet, $T_+(^{\uparrow\uparrow})$, $T_0(^{\uparrow\downarrow})$, $T_-(^{\downarrow\downarrow})$ (see Fig.1b). In the absence of external magnetic field all the four states can be mixed as a result of hyperfine interaction (HFI) of

the spins of electrons and radical nuclei participating in recombination, and form as if a single state with statistic weight 4, populated at the rate of $k[R]^2$ which decomposes with the rate constant of $(k_s + 3k_T - 4k_{-1})$. Here the notations of the rate constants of the following processes are used: k_T refers to the radical recombination; k_s and k_T to the formation of products from singlet and triplet pair states, respectively; k_{-1} to scattering of radicals from pairs (this process is spin independent).

In an external magnetic field H , T_+ and T_- state energies change while S and T_0 state energies remain unaffected. When Zeeman energy of the interaction of radical spins with external magnetic field ($g\beta H$) exceeds that of HFI, the states, T_+ and T_- are completely separated in energy from T_0 . Thus in a sufficiently strong magnetic field there are two mixed states $(S - T_0)$ and two unmixed ones, T_+ and T_- . Since the two unmixed states are practically indistinguishable as concerns chemical activity in the absence of exchange interaction, all ensemble of spin states can be reduced to two states, $(S - T_0)$ and (T_{\pm}) , each with statistical weight 2.

The effect of external magnetic field consists in the fact that the spin system of recombining pairs transforms from a single mixed state $(S - T_0)$ with statistic weight 4 to two independent states, $(S - T_0)$ and (T_{\pm}) with different product formation rate constants, $(k_s + k_T)$ for $(S - T_0)$ and $2k_T$ for (T_{\pm}) , or different products.

At $H = 0$ the concentration of radicals and the populations of spin states are described by the system of kinetic equations:

$$\frac{dR}{dt} = G - 4k_{-1} [S - T_0] - [k]^2 R^2 - k_2 [Q] R \quad (1.1)$$

$$\frac{d[S - T_0]}{dt} = k [R]^2 - (4k_{-1} + k_s + 3k_T) [S - T_0] \quad (1.2)$$

In case of a strong field when Zeeman energy sufficiently exceeds that of HFI the following system of equations is valid

$$\frac{d[R]}{dt} = G + 2k_{-1} [(S - T_0) + (T_{\pm})] - k [R]^2 - k_2 [Q] [R] \quad (1.3)$$

$$\frac{d[S-T_0]}{dt} = \frac{1}{2} k [R]^2 - (2k_{-1} + k_s + k_T) [S - T_0] \quad (1.4)$$

$$\frac{d[T_{\pm}]}{dt} = \frac{1}{2} k [R]^2 + 2(k_T + k_{-1}) [T_{\pm}] \quad (1.5)$$

The following notations are used here $[R]$ is the concentration of radicals, $[S-T_0]$, $[S - T_0^+]$, $[T_{\pm}]$ - are the concentrations of radical pairs in the corresponding spin state, $k_2[Q][R]$ is the overall rate of all radical reactions, which unlike the recombination, are first order by $[R]$, G is the rate of radical formation.

Solving these systems of equations under the conditions that spin states are populated during much less time as compared to the radical lifetime, gives for both cases

$$\frac{d[R]}{dt} = G - k[R]^2 - k_2[Q][R] \quad (1.6)$$

where at $H = 0$ radical recombination rate constant

$$k = \frac{k (k_s + 3k_T)}{4k_{-1} + k_s + 3k_T} \quad (1.7)$$

and for the field H considerably exceeding the hyperfine one

$$k = \frac{k (k_s k_{-1} + 2k_s k_T + 2k_T^2 + 3k_T k_{-1})}{2(2k_{-1} + k_s + k_T)(k_T + k_{-1})} \quad (1.8)$$

Equations (1.7) and (1.8) easily yield the maximum relative change in the radical recombination rate constant in magnetic field

$$\frac{\Delta k}{k} = \frac{k_{-1} (k_s - k_T)^2}{2(2k_{-2} + k_s + k_T)(k_{-1} + k_T)(k_s + 3k_T)} \quad (1.9)$$

Negative sign in the right part of (1.9) shows that magnetic

field decreases the radical recombination rate constant.

2. The effect of magnetic field on the concentration of free radicals.

Change in the recombination rate constant will result in the change in the steady-state concentration of radicals. In fact, solving Eq.(1.6) for a steady state has the form

$$[R] = \frac{k_2 Q}{2k} \left[\sqrt{1 + \frac{4kG}{(k_2 Q)^2}} - 1 \right] \quad (1.10)$$

Since $\Delta k/k$ is usually a small quantity of the order of 10^{-3} , after differentiating Eq.(1.10) by k and dividing the result by Eq.(1.10) we have

$$\frac{\Delta[R]}{[R]} = \frac{1}{2} \left(\frac{a}{\sqrt{1+a^2}} - 1 \right) \frac{\Delta k}{k} \quad (1.11)$$

where $a = k_2 Q / \sqrt{4kG}$.

Equations (1.9) and (1.11) show that magnetic field cannot change the concentration of radicals if the rate constants of the product formation in the singlet and triplet recombination channels, k_s and k_T , are equal. If the quantity a grows, according to Eq.(1.11) magnetic field effect on the concentration of radicals weakens because the multiplier at $\Delta k/k$ tends to zero. If that quantity approaches zero, the relative change in radical concentration tends to its maximum value

$$\frac{\Delta[R]}{[R]} = \frac{1}{2} \frac{\Delta k}{k} \quad (1.12)$$

Equation (1.11) shows that the ratio $\Delta[R]/[R]$ can be changed during the experiment either by changing the quencher Q , and therefore the constant k , or by changing its concentration, Q , or the concentration of the initial substances, that is the quantity G , the rate of radical formation.

3. Modulation of the recombination rate of radicals by magnetic field and determination of radical lifetime.

In case of the sine modulation of the radical recombination rate constant by magnetic field at a cyclic frequency ω , equation (1.6) has the form

$$\frac{d[R]}{dt} = G - (k + \Delta k \sin \omega t)[R]^2 - k_2[Q][R] \quad (1.13)$$

Solution to this equation at $G = \text{const}$ and $\Delta k \ll k$

$$[R] = [R]_0 \left(1 + \frac{\Delta[R]}{[R]} \sin(\omega t - \varphi) \right) \quad (1.14)$$

where $[R]_0$ is determined from Eq.(1.10), and $\Delta[R]/[R]$ and φ from Eqs.(1.15) and (1.16), respectively

$$\left(\frac{\Delta[R]}{[R]} \right)_\omega = \left(\frac{\Delta[R]}{[R]} \right)_{\omega=0} \left(1 + \omega^2 \tau^2 \right)^{-\frac{1}{2}} \quad (1.15)$$

$$\varphi = \arctg \omega \tau \quad (1.16)$$

If the yield of reaction products is proportional to the concentration of radicals, sine modulation of the radical recombination rate constants by magnetic field will result in sine modulation of reaction product yield at the same frequency (see Eqs. (1.14)-(1.16)).

Thus the amplitude of the system response to the sine modulated external magnetic field decreases as modulation frequency grows and a phase shift is observed in between the modulating field and the change in the reaction product yield. The quantity

$$\tau = \left(4KG + k_2^2 [Q]^2 \right)^{-1/2} \quad (1.17)$$

has the dimension of time, and $\left(\frac{\Delta[R]}{[R]} \right)_{\omega=0}$ makes the sense of MFE quantity at zero frequency, i.e. in a d.c. magnetic field.

The quantity of τ has the sense of effective lifetime of radicals under conditions of their recombination and quenching determined by magnetomodulational method. Using the experimentally measured value of the phase shift, φ , and knowing the cyclic frequency of magnetic field modulation, ω , enables one to obtain the radical lifetime from magnetic field effect:

$$\tau = \frac{\operatorname{tg} \varphi}{\omega} \quad (1.18)$$

The method of vector diagram is used by the authors for the analysis of amplitude, frequency and phase characteristics of MFE (Fig.2). The angle is determined by the phase shift of MFE, and the vector module, C , is proportional to the quantity of MFE at the given frequency. MFE has the maximum, $\left(\frac{\Delta[R]}{[R]} \right)_{\omega=0}$ in d.c. field ($\omega=0$), the phase shift being equal to zero. As frequency grows, so does the phase shift tending to 90° in the limit with the vector module, C , approaching zero.

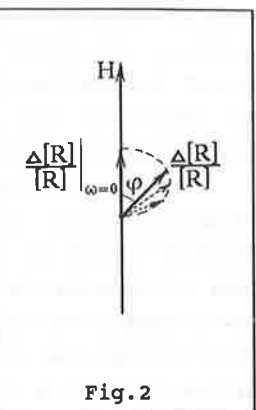


Fig.2

II. EXPERIMENTAL

To study intermediate radical processes in the CL reactions of luminol oxidation we made a flow system. Its scheme is shown in Fig.3.

Solution of luminol and potassium ferricyanide in aqueous alkali (0.1 M NaOH) were introduced continuously through the mixer M into optical cell C . Mixing the reagents in the mixer took less than 0.1 s. The time interval between mixing and passing the flow thorough the observation zone was 0.3 s which corresponded to the CL kinetic curve maximum for the reaction studied within the working range of concentrations. The inlet system

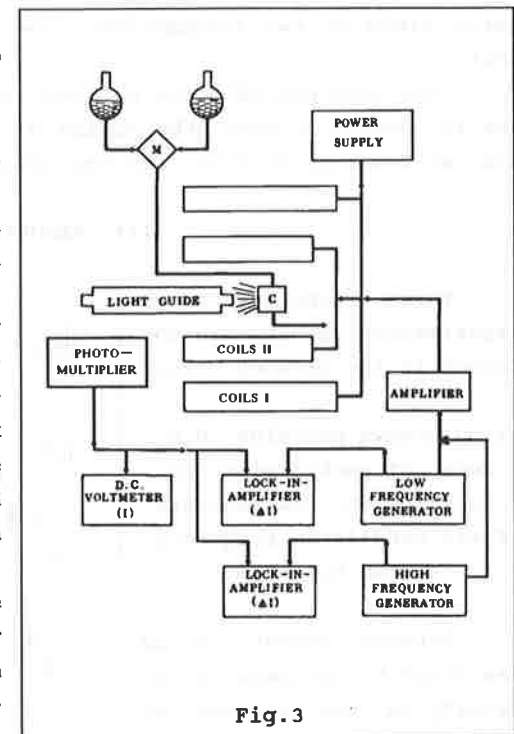


Fig.3

ensured consumption of equal amounts of reagent solution with the accuracy not worse than 1 % by volume and stability of the light signal during the experiment time (150 s) within 1.5% of the maximum intensity. The flow part of the unit was made of inert materials having no effect on the reaction.

The optical cell was situated within the gap between the Helmholtz coils. One pair of coils, I, produced a d.c. magnetic field $H \leq 3500$ Oe. The other one created a a.c. field with amplitude of several Oe within the frequency range (40 Hz - 100 kHz). Power supply to coils II was from low and high frequency generators through the corresponding amplifiers. The CL light was transmitted through a light guide to a photoelectron multiplier protected from scattered magnetic fields by a special screen. The signal was then fed into a registration system with two channels. The first one registered the signal I proportional to the total CL intensity, the second channel, a lock-in detection system, permitted to register simultaneously two signals I proportional to the variable components of the CL intensity modulated by the magnetic field at two frequencies, low (40-300 Hz) and high (1-100 kHz).

The unit provided the possibility to register the changes in the CL intensity under the action of the external magnetic field with an accuracy of $5 \cdot 10^{-5}$ of the total CL intensity.

III. RESULTS

Three groups of basic experimental results are obtained in the present work:

1. Hydrogen peroxide, H_2O_2 , does not participate in CL reaction. Low magnetic field modulation frequency (below 0.5 kHz).

External magnetic field was found to increase CL intensity in the absence of hydrogen peroxide, H_2O_2 ,

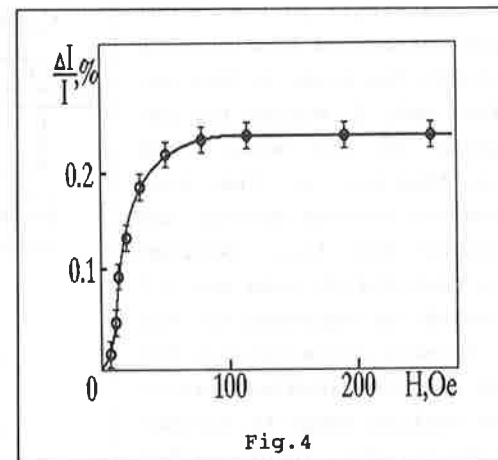


Fig. 4

, i.e. the sign of magnetic effect (MFE) is positive. The dependence of relative CL intensity variations, $\Delta I/I$, on external magnetic field strength, H , is shown in Fig.4. The same MFE only for a wider range of H is given in Fig.5 as a dependence of MFE derivative, $\frac{d}{dH} \frac{\Delta I}{I}(H)$, on magnetic field strength, H . The MFE is seen to have a step-like form with a half - saturation field of about 15 Oe, which remains unchanged up to 3500 Oe.

The value of MFE was found to decrease monotonically reaching the value of the signal noise at ω of about 200 Hz (Fig.6) with increasing the magnetic field frequency, ω .

The phase shift, φ , was found to occur in between the sine

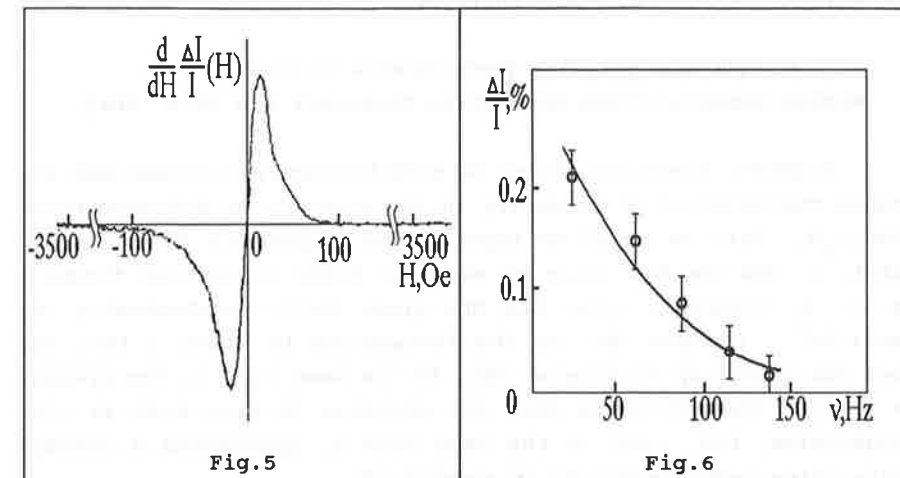


Fig. 5

Fig. 6

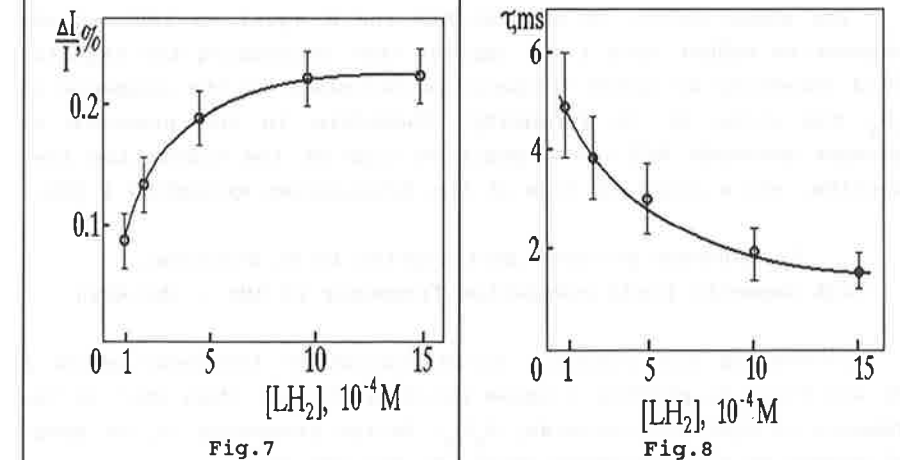


Fig. 7

Fig. 8

modulated magnetic field strength, H , and sine modulated CL intensity. It proved to increase by a tangential law with the growth of the field modulated frequency, ω , tending in the limit to $\varphi = 90^\circ$. Amplitude of the modulated component of CL intensity approaches zero.

The values of MFE and the phase shift, φ , were found to depend on the concentration of reagents (luminol, potassium ferricyanide, oxygen, OH^-). Increasing the concentration of these substances, except for oxygen, increased the MFE value (a typical plot is shown in Fig.7) and decreased the phase shift. Increasing oxygen concentration decreased the MFE value and practically did not affect that of the phase shift, φ .

2. Hydrogen peroxide participates in CL reaction.

Medium magnetic field modulation frequency (up to 8 kHz).

Magnetic field was found to simultaneously increase and decrease the value of CL intensity in the presence of hydrogen peroxide, H_2O_2 . This is based on experimental dependence of the phase shift, φ , and the MFE value on magnetic field modulation frequency, ω . As frequency grows the MFE phase shift monotonically exceeds 90° , reaches 180° at the frequencies of about 1 kHz, and does not change up to several kHz. At the same time in the presence of H_2O_2 the MFE value does not decrease to zero even at high frequencies, but, like is the case with φ , approaches a steady-state value unchangeable up to several kHz.

The phase shift, in between MFE and H equal to 180° at the frequencies higher than 1 kHz implies that increasing the magnetic field intensity at these frequencies decreases in the presence of H_2O_2 the value of CL intensity. Therefore in the presence of hydrogen peroxide MFE has a positive sign at low modulation frequencies, and a negative sign at the frequencies exceeding 1 kHz.

3. Hydrogen peroxide participates in CL reaction.

High magnetic field modulation frequency (8 kHz - 100 kHz)

Increasing the magnetic field modulation frequency above 8 kHz was found to produce a phase shift, φ , higher than 180° in the presence of hydrogen peroxide, H_2O_2 . At the frequency, ω , of several dozens of kHz the phase shift, φ , exceeds 270° .

The value of phase shift was found to decrease with increasing H_2O_2 concentration, however remaining higher than 180° for the magnetic field modulation frequencies exceeding 8 kHz.

DISCUSSION

OF THE MECHANISM OF FREQUENCY-PHASE DEPENDENCE OF MFE IN CL REACTION OF LUMINOL

Like in the previous section we shall arrange the discussion matter here into the three parts:

1. Hydrogen peroxide, H_2O_2 , does not participate in CL reaction. Low magnetic field modulation frequency (below 0.5 kHz).

The dependence obtained of a relative CL intensity variations on magnetic field intensity (Fig.4 and Fig.6) is typical of the interaction of radicals at a spin dependent rate when spin state mixing of a pair of radicals is controlled by the hyperfine interaction mechanism.

Since the experimental value of MFE half-saturation field of 15 Oe corresponds to effective hyperfine infraction in radicals and close to the expected one for luminol radical L^{\cdot} the latter is one of the most probable participants of magnetosensitive process resulting in altering the CL intensity in magnetic field. Either the ions of iron, or the molecule or radical of oxygen could serve as a paramagnetic "partner" of luminol radical. Molecules containing iron atoms usually have spin relaxation time of $T_1 \sim 10^{-10}$ s and therefore cannot determine magnetic field effects in weak fields. In fact the lifetime of a pair of radicals in our case

$$t > 1/\omega_{\text{HFI}} = h/g\beta H = 3 \cdot 10^{-10} \text{ s}$$

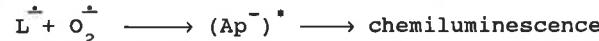
where ω_{HFI} is the effective HFI frequency.

Oxygen molecule is known to be triplet in the ground state and therefore one should expect for the pair "luminol radical plus oxygen molecule" MFE of a different shape from the obtained one (Fig.4).

For MFE observed oxygen radical is not a suitable "partner" of luminol radical in a pair of interacting paramagnetic par-

ticles. This is confirmed by MFE positive sign in the absence of H_2O_2 . In fact magnetic field is known to decrease recombination rate of radicals. Therefore the effect of magnetic field on recombination rate of the pair ($L^- - O_2^+$) could result in decreasing the CL intensity. But this contradicts the experimental data.

So, MFE most probably occurs in recombination of luminol radicals L^- , with each other. It should be emphasized that this process competes with that of interaction of L^- and superoxide ion O_2^+ . External magnetic field decreases recombination rate of luminol radicals, L^- responsible for diazoquinone L^{\ddagger} (Fig.1) formation, and therefore decreases decay rate of L^- in the channel not leading to the light generation in the absence of H_2O_2 . So the rate of the competing reaction



increases in magnetic field.

Thus positive MFE can be accounted for in the given reaction in the absence of H_2O_2 .

Amplitude-frequency dependence and MFE phase shift are connected with the value of effective lifetime of luminol radical L^- . In fact, while recombination rate constant of radicals L^- changes practically simultaneously with magnetic field, the concentration of radicals L^- changes in magnetic field with certain characteristic delay time, τ called effective lifetime of radicals L^- . As soon as the rate of CL generation is proportional to concentration L^- , alteration of CL intensity in magnetic field occurs with delay τ . According to Eq.(1.18) the value of τ determines the MFE phase shift experimentally measured. Amplitude-frequency dependence of MFE is satisfactorily described by Eq.(1.15). As magnetic field modulation frequency, ω , increases the concentration of radicals L^- has not enough time to change completely. As a result the value of MFE decreases.

Similar to phase fluorometry technique the method of phase MFE makes it possible to determine effective lifetime of intermediate active particles both from the amplitude-frequency MFE dependence and from the difference of phases in between sine modulated magnetic field strength H , and chemiluminescence intensity I .

The frequency dependence of magnetic field effect value, $\frac{\Delta I}{I}(\omega)$, for CL reaction in the absence of hydrogen peroxide (Fig.6)

is described by Eq. (1.15). Linearizing it in appropriate coordinates enables to determine the value of τ . The same value of τ is obtained by Eq.(1.16) from the phase shift measurements of MFE. The coincidence of the values of τ obtained from amplitude frequency dependence and phase shift of MFE is indicative of the presence of a limiting step in the reaction in which participate long-lived particles of only a single type.

Eq.(1.17) shows that the value of τ is dependent of the concentration of the substances participating in CL reaction. For the concentrations $[LH_2] = 10^{-3}$ M, $[K_3Fe(CN)_6] = 5 \cdot 10^{-4}$ M, $pH = 13$ and equilibrium at atmospheric pressure $[O_2] = 2 \cdot 10^{-4}$ M the value of effective lifetime of luminol radicals $\tau = 2.4 \pm 1.5$ ms.

The possibility of using the concentration dependencies of MFE (Fig.7) and τ (Fig.8) to study the mechanism of CL reaction under study will be discussed below.

It should be noted that determination of the value of τ from amplitude frequency dependence of MFE is more cumbersome and less accurate. The reason is the necessity of determination of the value of MFE, i.e. relative alteration of chemiluminescence intensity $\left(\frac{\Delta I}{I}\right)_{\omega=0}$ in a d.c. magnetic field ($\omega=0$). It is impossible to measure this value directly because of small values of MFE that require employing lock-in detection technique. The value can be only obtained by extrapolation of amplitude - frequency dependence of MFE to $\omega=0$. To find τ a phase shift of MFE was mainly used in the present work.

2. Hydrogen peroxide participates in CL reaction.

Medium magnetic field modulation frequency (up to 8 kHz).

Diazoquinone L^{\ddagger} formed as a result of recombination of luminol radicals L^- is known to interact with deprotonized form of hydrogen peroxide, HO_2^- . This reaction leads to the formation of luminol hydroperoxide, (L^-OOH) , an immediate precursor of light emitter (Fig.1). In both CL generation channels:

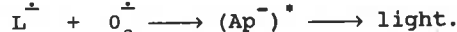
channel 1 - through interaction of luminol radicals L^- with superoxide ion O_2^+ ;

channel 2 - through formation of L diazaquinone light emitter is the same, namely electronically excited anion of aminophthalic acid, $(Ap^-)^*$ [3].

With the magnetic field modulation frequency of up to 8 kHz

the particles L and L⁻OOH do not reveal themselves and so modulated CL intensity in the second channel lags 180° behind magnetic field in phase. Therefore increasing magnetic field strength brings about a decrease in CL intensity. Negative sign of MFE in the second channel is due to decreasing the recombination rate constant of radicals L⁻ in the magnetic field.

At the same time generation of CL is observed in the first channel in the presence of H₂O₂. The reason is the same, i.e. decreasing the recombination rate of radicals L⁻ in the magnetic field increases the rate of the competing reaction,



Accordingly the sign of MFE in the first channel is positive. On account of long lifetime of luminol radicals MFE is characterized by a phase lag in the first channel and a decrease in amplitude with increasing modulation frequency.

Therefore two MFE are observed simultaneously at low modulation frequencies (up to 0.5 kHz) in the presence of H₂O₂. To analyze the superpositions of those MFEs observed in experiment it is advisable to make use of the vector diagram of MFEs shown in Fig.9. Amplitude of vector \bar{A} is determined from the experimental value of the total MFE measured at a low modulation frequency. Angle θ is the phase shift of the total MFE obtained experimentally. An amplitude of the vector \bar{B} is determined from the negative (turned about with respect to the field vector \bar{H}) MFE in the second channel of light generation. An amplitude of the vector \bar{C} and angle φ are determined by the value and phase of MFE in the first channel of light generation and cannot be measured in experiment. Increasing the modulation frequency up to 1 kHz decreases the amplitude of vector \bar{C} to zero. Therefore MFE measured in experiment within the frequency range from 1 kHz to 8 kHz determines vector \bar{B} . It should be emphasized that vector \bar{B} is unchangeable at all modulation frequencies up to 8 kHz. So the amplitude and angle θ of vector \bar{A} and the amplitude of vector \bar{B} are obtainable from experiment. The vector diagram (Fig.9) shows that amplitude \bar{C} and phase of MFE in the first channel of light

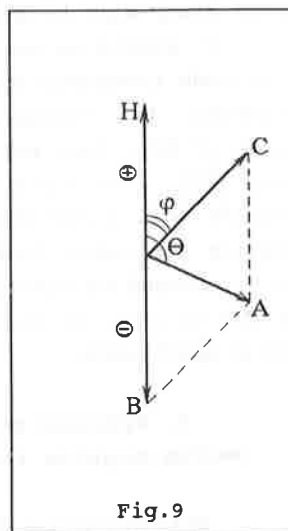


Fig.9

generation can be obtained from the following equations

$$C^2 = A^2 + B^2 + 2AB \cdot \cos \theta \quad (1.19)$$

$$\tan \varphi = \frac{\sin \theta}{\frac{B}{A} + \cos \theta} \quad (1.20)$$

The possibility of dividing the MFEs in the two light generation channels enables to study the concentration dependencies of those MFE values as well as the values of effective lifetime of intermediate active particles in both channels. Dependencies of the modules of MFEs H and C on the magnetic field strength demonstrated similarity with each other and with MFE shown in Fig.4. Half-saturation fields of those MFEs coincided as well. This is indicative of the fact that all the phenomena studied are caused by the magnetic field effect on one and the same radical pair.

3. Hydrogen peroxide participates in CL reaction.

High magnetic field modulation frequency (8 kHz - 100 kHz).

At frequency exceeding 8 kHz and in the presence of H₂O₂ the lifetimes τ_1 and τ_2 of diazoquinone L and hydroxyperoxide L⁻OOH, respectively, begin affecting the amplitude-frequency and phase dependencies of MFE in the second channel of light generation. It should be noted that with such high modulation frequencies MFE is fully suppressed in the first channel and there is only MFE in the second channel (vector \bar{B} , Fig.10). At frequency lower than 8 kHz the phase shift for that MFE is 180°. At higher frequencies the phase shift, α (Fig.10), exceeding 180° is the total of the phase shifts on L and L⁻OOH :

$$\alpha = \arctg(\omega \tau_1) + \arctg(\omega \tau_2) \quad (1.21)$$

The values of τ_1 and τ_2 can be easily obtained from measuring at two different modulation frequencies and solving the system of equations of the type (1.21). For hypothetical case of N successively arranged particles responsible for comparable phase shifts this procedure can be obviously repeated as many times as required. If the lifetime of one of those hypothetical particles is much longer than that of the rest (a limiting step) this very particle

DISCUSSION OF CONCENTRATION DEPENDENCIES OF MFEs AND LIFETIME OF LUMINOL RADICALS.

We would consider first the mechanism of the reaction under study without hydrogen peroxide participation. Substitute arbitrary radicals R for luminol radicals L^{\cdot} in Eq.(1.11)

$$\frac{\Delta[L^{\cdot}]}{[L^{\cdot}]} = \frac{1}{2} \left(\frac{a}{\sqrt{1+a^2}} - 1 \right) \frac{\Delta k}{k} \quad (1.22)$$

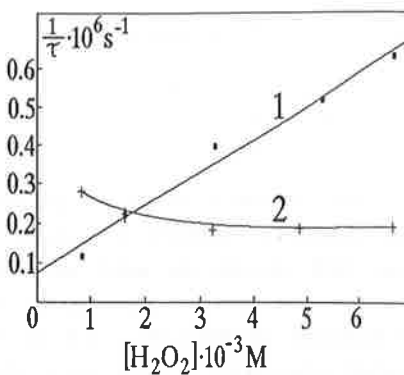
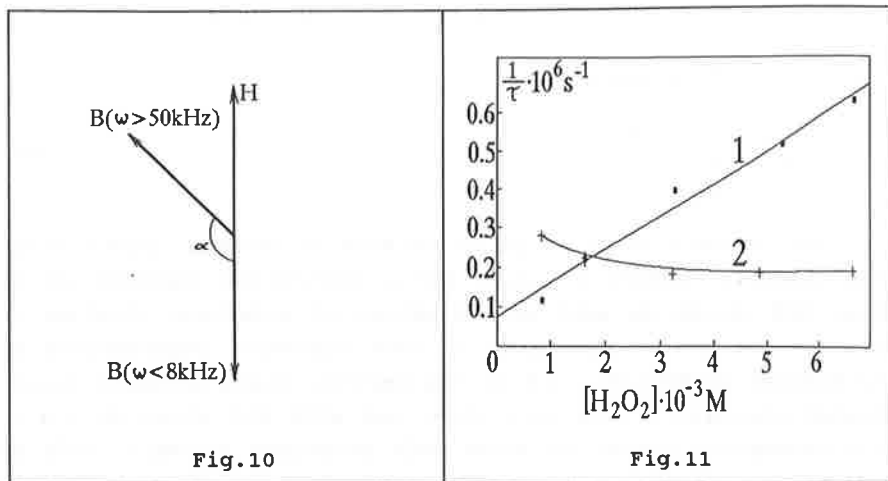
where $a = \frac{k_2 \cdot \theta}{\sqrt{4kG}}$ is a parameter characterizing the relation of the rates of linear and quadratic decay of radicals L^{\cdot} .

Dependence of the MFE value on the rate, G, of radicals, L^{\cdot} , formation and total rate of all reactions of these radicals, $k[\theta][L^{\cdot}]$, being the first order in $[L^{\cdot}]$ contrary to recombination, is determined by the following multiplier

$$S = \frac{1}{2} \left(\frac{a}{\sqrt{1+a^2}} - 1 \right) \quad (1.23)$$

In a steady-state case (continuous flow and fixed interval between mixing and observation) the value of G depends on the concentration of initial reagents: luminol $[LH_2]$, potassium ferricyanide $[Fe^{3+}]$ and pH $[OH^-]$

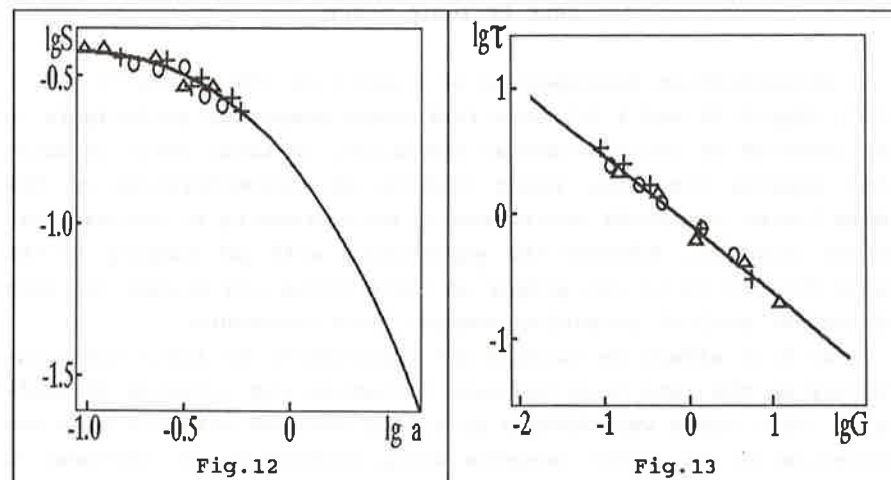
Calculated dependence of multiplier S value characterizing magnetic field effect is shown in Fig.12 as a solid line. Symbols



alone will determine the phase shift measured in experiment.

Measuring at the concentration of hydrogen peroxide $[H_2O_2] = 10^{-3} M$ yielded the values of $\tau_1 = 2 \mu s$ and $\tau_2 = 5 \mu s$. An attempt of formal introduction of a third particle into reaction scheme in the second channel as well as measuring the phase shifts at three different frequencies gave the value of $\tau_3 = 0$. This means that no other particles exist in that channel except for diazoquinone and hydroperoxide with the lifetime inverse value comparable with modulation frequency of MFE in the frequency range up to 100 kHz.

The scheme of reaction (1) shows that at high concentration of hydrogen peroxide diazoquinone L decays in the reaction of pseudo-first order. Therefore the lifetime of diazoquinone should be dependent of H_2O_2 . Experimental dependence of $\frac{1}{\tau}$ vs H_2O_2 is shown in Fig.11. The value of the rate constant of the interaction between diazoquinone and deprotonized hydrogen peroxide obtained from this dependence, $k = 10^8 M^{-1}s^{-1}$, is twice as high as that determined by pulse radiolysis technique [3]. Diazoquinone is known to decay not only in interaction with H_2O_2 but also in the reaction with OH^- not shown in Fig.1. The evidence is the crossing of curve 1 with the y axis in Fig 10 when extrapolating this dependence to $H_2O_2 = 0$. This interaction can be accounted for and the rate constant of this reaction can be measured from the dependence of τ_1 vs pH.



$\Delta, \alpha, +, -$ stand for the experimental values of MFES dependent or concentrations $[LH_2]$, $[K_3Fe(CN)_6]$ and pH , respectively. As a result of displacing the calculated curve in logarithmic coordinates, i.e. choosing parameter a , a good coincidence was obtained between calculated curve and experimental points provided that the rate of radical formation

$$G \sim [LH_2] \cdot [Fe^{3+}] \cdot [OH^-]^2 \quad (1.24)$$

If (1.24) is observed a good coincidence is also obtained between the calculated dependence of the value of effective lifetime of luminol radicals, τ , on concentration $[LH]$, $[K_3Fe(CN)_6]$, pH and experimental data (Fig.I3). Experimental concentration dependencies of the value of τ conform to the following relationship

$$\tau = [LH_2]^{1/2} [Fe^{3+}]^{-1/2} [OH^-]^{-1} \quad (1.25)$$

Calculated dependence of τ on reagent concentrations can be obtained from Eq.(1.17). Experimental dependence (1.25) has the form, $\tau \sim G^{1/2}$. This corresponds to the maximum magnetic effect, $k_2^2[\theta]^2 \ll 4kG$. It follows that radicals L^\cdot mainly decay in the reaction second-order in their concentrations and are formed in the reaction which rate corresponds to (1.24). The second-order reaction of luminol radicals, L^\cdot , decay is the magnetosensitive recombination of radicals.

ROLE OF IONIC FORCE

Concentration dependencies of G and τ on $[LH_2]$, $[Fe^{3+}]$ and $[OH^-]$ (Eqs.1.24 and 1.25) show that these compounds participate in the reaction of luminol radical formation. If ionic force in solution remains constant, power factors of concentrations of the above listed compounds correspond to stoichiometry of radical formation reaction. However the experiments with pH varying in the range from 12 to 13 can affect an ionic force and change the rate of luminol radical formation changing rate constants.

To this effect we carried out experiments on ionic force influence on the rate G of radicals formation and lifetime of radicals. Ionic force was changed by adding NaCl to solution with the concentration of other reagents being unchanged. An increase in ionic force was found to be accompanied by a linear increase in

the rate of radicals L^\cdot formation, G. Fig.I4 shows that the lifetime, τ , of radicals decreases with increasing the ionic force by the law $1/\sqrt{I}$, where I is the value of ionic force proportional to the full concentration of ions in solution. It should be pointed out that alterations in ionic force are mainly determined by the concentration $[OH^-]$ at high pH and comparably low concentrations of other reagents used in the work.

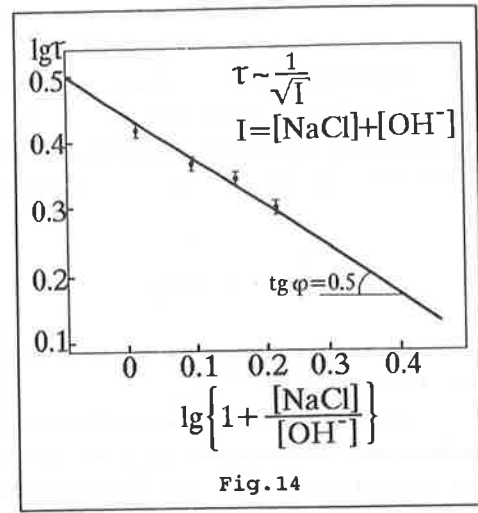
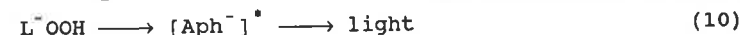
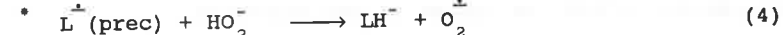
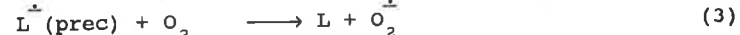
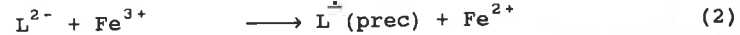


Fig.14

Therefore it leads to conclude that concentration dependence of G on $[OH^-]$ in Eq.(1.24) is explained by the fact that τ first order is due to the direct $[OH^-]$ participation in generation of L^\cdot (reaction 1 in the scheme below), and one more order is due to the effect of $[OH^-]$ on ionic force and hence on the reaction rate of L^\cdot formation (for example reaction 2 in the scheme below). The dependence of τ on $[OH^-]$ (Eq.1.25) can be explained in a similar manner.



*Reactions (4) and (9) take place only when H_2O_2 is present.

THE ROLE OF OXYGEN

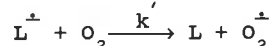
For the reaction under consideration the reaction rate of luminol radicals with oxygen is of importance. It was found that the lifetime remained unchanged with oxygen concentration varying within 10^{-4} to 10^{-3} M. This is possible if

$$\tau \ll \frac{1}{k_2 [O_2]} \quad (1.26)$$

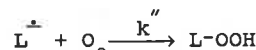
The result obtained is in a good agreement with that given in [3], $k \approx 5.5 \cdot 10^2 \text{ M}^{-1} \text{ s}^{-1}$.

The value of MFE proved to be more sensitive to oxygen concentration. Increasing $[O_2]$ within the mentioned range decreased the relative change in chemiluminescence intensity $\Delta I/I$ by a factor of 1.4. According to Eq.(1.22) and Fig.12 this corresponds to the change in $a=k[Q]/\sqrt{4kG}$ from 0.14 to 0.43, i.e. $a \sim Q \sim [O_2]^{1/2}$. It follows that the quenchers of luminol radicals, L^\cdot , are not the molecules of oxygen but the products of oxygen transformation. This is most probably superoxide ion, O_2^\cdot .

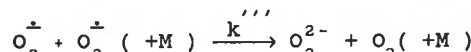
It should be emphasized that the experimental values of a and CL intensity are proportional to $[O_2]^{1/2}$. We would try to account for the role of oxygen in CL generation under supposition that superoxide ion is formed in the reaction



and hydroxyperoxide, $L^\cdot OOH$, is formed in the reaction



To explain the dependence of CL intensity and the rates of radical quenching, k_q , on oxygen concentration (each being proportional to $[O_2]^{1/2}$) it is necessary to make a supposition that quadratic decay of superoxide ion



The dependence of chemiluminescence intensity, I , on the rate

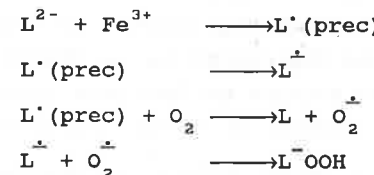
of radical formation, G , and oxygen concentration is determined via the expression

$$I_{CL} \sim [L^\cdot OOH] \sim k'' [L^\cdot] [O_2^\cdot] \sim k'' [L^\cdot] \left[\frac{k' [L^\cdot] [O_2]}{k'''} \right]^{1/2}$$

with $[L^\cdot] \sim G^{1/2}$, we have $I_{CL} \sim G^{3/4} [O_2]^{1/2}$.

Experiment gives a different relationship, $I_{CL} \sim G^{1/2} [O_2]^{1/2}$.

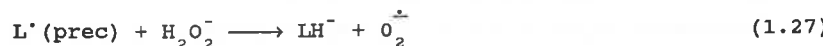
This demonstrates that O_2^\cdot is formed in the reaction of oxygen with the particles which concentration changes proportional to G but not $G^{1/2}$, like is the case with luminol radicals. As far as superoxide ion can be formed only in the reaction of oxygen with a certain radical, a hypothetical radical has to be introduced, $L^\cdot(\text{prec})$. The latter is a short-lived precursor of radical L^\cdot responsible for the formation of O_2^\cdot . We would suppose that the following reactions takes place



Then chemiluminescence intensity, $I_{CL} \sim G \cdot [O_2]^{1/2}$ and $a \sim [O_2]^{1/2}$, i.e. a good agreement with the experimental data is observed.

The experimental data obtained from the reaction with hydrogen peroxide, H_2O_2 , participation also testify to the existence of $L^\cdot(\text{prec})$. It was found that H_2O_2 not only increased chemiluminescence intensity but also affected the lifetime of radicals L^\cdot : at low $[H_2O_2]$ the value of τ increases, at high $[H_2O_2]$ it is slowly falling (Fig.15). Increasing the concentration of other reagents decreases τ , like is the case with the reaction without H_2O_2 . Eq.(I.17) shows that if quadratic recombination of radicals L^\cdot is the basic channel of their decay, an increase in τ is only possible as a result of decreasing the value of the rate of radicals L^\cdot formation, G . The change in the value of G was measured in experiment by photometric technique during the time of flow moving from the mixer to the observation zone. The reason was to under-

stand the role of a possible reaction $\text{Fe}^{3+} + \text{H}_2\text{O}_2$ which could lead to consumption of Fe^{3+} and as a result to decreasing G. The change in G was only several per cent. Therefore the change in G at this step cannot produce the changes in τ observed in experiment (Fig.15). The authors ascribe the changes in τ to the reaction of deprotonized form of hydrogen peroxide with radical $\text{L}'(\text{prec})$



The decay of $\text{L}'(\text{prec})$ in the reaction with HO_2^- results in decreasing the value of the rate of radicals L^{\cdot} formation G, and as a consequence in increasing the lifetime τ . Such a conclusion approves the introduction of radical $\text{L}'(\text{prec})$ as a precursor of radical L^{\cdot} and excludes any speculations as to its formation in the reaction going in parallel with L^{\cdot} formation. Radicals L^{\cdot} are less active than $\text{L}'(\text{prec})$, more long-lived, and decay mainly in magnetosensitive recombination process on each other, as well as in the reaction with O_2^{\cdot} . The use of a two-step process of luminol radical formation enables to describe the concentration dependence of the lifetimes of radicals L^{\cdot} . The authors believe that reaction (1.27) is the main process of O_2^{\cdot} generation in the presence of H_2O_2 . The rate of transformation of $\text{L}'(\text{prec})$ into L^{\cdot} is apparently rather high. Hence the concentration of $\text{L}'(\text{prec})$ is low. That is why the reactions of the type: $(\text{L}^{\cdot} + \text{L}'(\text{prec}))$ or $(\text{L}'(\text{prec}) + \text{L}'(\text{prec}))$ are of little importance. Low reactivity of secondary radicals L^{\cdot} as concerns all particles with the exception of O_2^{\cdot} makes it possible for the radicals to be accumulated up to the concentration when their recombination $(\text{L}^{\cdot} + \text{L}^{\cdot})$ becomes the main decay channel. This is the low chemical activity of radicals L^{\cdot} that permits to observe MFE even in such a low viscous liquid as water.

The results of studying MFE of chemiluminescence reaction of luminol oxidation by potassium ferricyanide are summed up in the scheme of reaction mechanism in Fig.15.

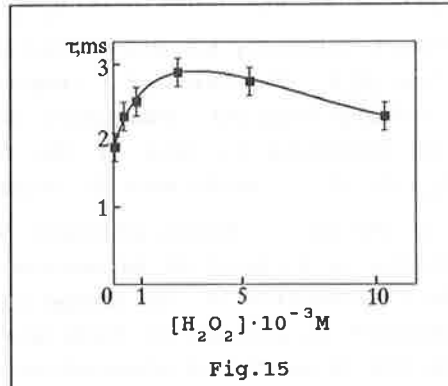


Fig.15

The scheme suggested can, in particular, explain an increase in the lifetime of radicals L^{\cdot} in the range of low concentrations of hydrogen peroxide (Fig.15). At low concentrations of H_2O_2 the process of decreasing the rate of radicals L^{\cdot} generation, G, in reaction (4) dominates. According to Eq.(1.17) this leads to increasing τ . Further increase in $[\text{H}_2\text{O}_2]$ results in here unstudied reactions which products quench radicals L^{\cdot} . This is displayed in a slow decrease τ in Fig.15.

References:

1. Zakowicz, J.R. Principles of Fluorescence Spectroscopy, (1983), Plenum Press, N.Y.
2. Baxendale, J.H. Pulse Radiolysis Study of the Chemiluminescence of Luminol. *J.Chem.Soc., Faraday Trans. I*, **69** (1973), 1665-1677.
3. Merenyi, G., Lind, J. and Eriksen, T.E. *J.Bioluminescence and Chemiluminescence*, **5** (1990), 53-56.

Temperature Dependence of Lifetime of Chain-Linked Biradicals in the Absence and Presence of a Magnetic Field

Yoshifumi Tanimoto

Department of Chemistry, Faculty of Science, Hiroshima University, Naka-ku, Hiroshima 730 (Japan)

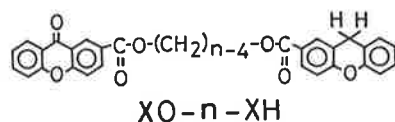
Abstract

With increasing temperature, lifetime of chain-linked triplet biradicals composed of xanthone ketyl and xanthenyl radicals decrease, reach a minimum at 270–300 K and then increase slightly at zero field. This anomaly may be resulted from the difference in the temperature dependence of the rate constants of chain motion and end-to-end recombination reaction. In the presence of a magnetic field (0.6 T), the spin-lattice relaxation is the rate controlling step in the deactivation of triplet biradicals.

1. Introduction

Studies of the magnetic field effects on the dynamics of chain-linked biradicals are of great interest in order to clarify the role of spin motion and chain motion in their reaction [1]. In the previous papers [2–5], we reported how a distance between two radical centers affects magnitude of magnetic field effects on the biradical lifetime at room temperature.

In the present paper, we studied temperature dependence of lifetime of triplet biradicals generated from the xanthone-xanthene-linked system in the absence and presence of a magnetic field by laser flash photolysis.



2. Experimental section

Syntheses of bifunctional chain molecules, α -(xanthone-2-carbonyloxy)- ω -(xanthene-2-carbonyloxy)alkanes (XO-n-XH , $n=7, 10, 12, 16, 20$), were described elsewhere [4]. Here, n represents the

number of linkers ($-\text{CH}_2-$, $-\text{CO}-$, $-\text{O}-$). Spectrograde ethylacetate was used as supplied. Sample solutions were deaerated by repeated freeze-pump-thaw cycles.

Transient absorptions were measured by using a nitrogen gas laser (337 nm) as an exciting light source. Transient signals on a digital oscilloscope were fed into a microcomputer for analysis. Details were described elsewhere [4]. Temperature of sample solutions was controlled by flowing cold nitrogen gas or hot water in the sample holder.

Decay curves of the biradical absorption intensity monitored at 345 nm was expressed with a single exponential function in the usual sense. Lifetime of biradicals were, thus, defined as the lifetime calculated under the single exponential approximation. Simulation of the decay curves was carried out by numerical integration of differential rate equations with the Runge-Kutta-Gill method [6].

3. Results and discussion

3.1 In the Absence of a magnetic field

Upon laser excitation of XO-16-XH in ethyl acetate, the excited triplet XO chromophore undergoes hydrogen abstraction from XH at the other end of the chain, generating the triplet biradical ($^{\bullet}\text{XOH-16-X}^{\bullet}$) composed of a xanthone ketyl radical (XOH^{\bullet}) and a xanthenyl radical (X^{\bullet}) [4].

Figure 1 shows temperature dependence of the lifetime of $^{\bullet}\text{XOH-16-X}^{\bullet}$. At zero field, the dependence may be divided into two regions at about 270 K. In the high temperature region, the lifetime becomes slightly longer with increasing temperature, in marked contrast to the lifetime in the low temperature region. Interestingly, analogous temperature dependence of the lifetime were observed in other biradicals, $^{\bullet}\text{XOH-n-X}^{\bullet}$.

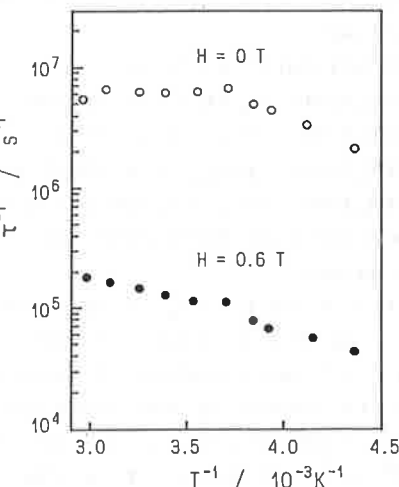
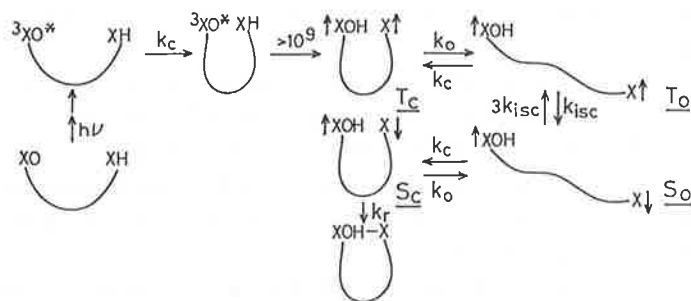


Fig. 1. Temperature dependence of the lifetime τ of $^{\bullet}\text{XOH-16-X}^{\bullet}$.



Scheme 1. Reaction pathways of XOH-16-XH.

(n=7, 10, 12, 20).

In the chain-linked systems, decay rate of a biradical is considered as the functions of chain motion, spin motion and end-to-end recombination reaction rate, when an intermolecular process is negligibly slow. Thus an attempt was made to analyze the decay curves of transient signal of 'XOH-16-X' within a framework shown in Scheme 1. Here, T_c is the triplet biradical in the closed form, T_o the triplet one in the open form, S_o the singlet one in the closed form, and S_c the singlet one in the closed form. k 's are the rate constants of the respective process. The rate equations for the 'XOH-16-X' biradical are as follows:

$$d[{}^3\text{XO}^*]/dt = -k_c [{}^3\text{XO}^*] \quad (1)$$

$$d[T_c]/dt = -k_o [T_c] + k_c ({}^3\text{XO}^* + [T_o]) \quad (2)$$

$$d[T_o]/dt = -(k_c + k_{isc}) [T_o] + k_o [T_c] + 3k_{isc} [S_o] \quad (3)$$

$$d[S_o]/dt = -(3k_{isc} + k_o) [S_o] + k_{isc} [T_o] + k_o [S_c] \quad (4)$$

$$d[S_c]/dt = -(k_o + k_r) [S_c] + k_o [S_o] \quad (5)$$

Observed time dependence $I(t)$ of the biradical concentration can be given;

$$I(t) \propto [T_c] + [T_o] + [S_o] + [S_c] \quad (6)$$

In the present calculation, k_c was estimated from the rate of the biradical formation which was determined from the growth curves of the transient signal at low temperatures. The rate constant, k_{isc} , was used a theoretical value ($k_{isc} = 3.8 \times 10^8 \text{ s}^{-1}$) evaluated from the hyperfine coupling constants of component radicals [4] and was assumed to be temperature-independent. Simulation of decay curves was carried out for the two unknown parameters, k_o and k_r , by numerically solving the

differential equations (1)-(5). In the calculation, k_o and k_r were varied from 10^8 to 10^{11} and from 10^7 to 10^{11} s^{-1} , respectively. Temperature dependence of k_o and k_r calculated for 'XOH-16-X', as well as that of observed k_c , are shown in Fig. 2. Analogous temperature dependence of rate constants were obtained for other biradicals (Table 1). k_r 's are temperature-independent. On the other hand, k_c and k_o depend strongly on temperature (about 3 kcal/mol), which is comparable to the energy for the conformational change of a methylene chain [7].

Anomaly in the temperature dependence of the lifetime at zero field (Fig. 1) is clearly explained by the temperature dependence of the rate constants shown in Fig. 2 and Table 1, though the present analysis is rather crude. The observed lifetime are chiefly determined by the rate constants associated with S_c . In the low temperature region (< 270 K), the order of rate constants is $k_c < k_o < k_r$. The lifetime change is attributable mainly to k_c , since the

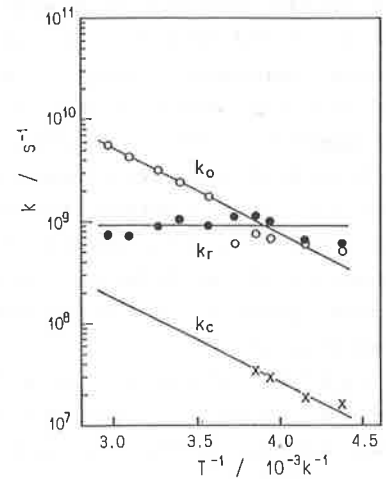


Fig. 2. Temperature dependence of k_o , k_c , and k_r .

Table 1. Rate constants-temperature relationship:

$$\log k = A - \Delta E/RT$$

n	a)		k_o		k_r	
	A	$\frac{\Delta E}{\text{kcal/mol}}$	A	$\frac{\Delta E}{\text{kcal/mol}}$	A	$\frac{\Delta E}{\text{kcal/mol}}$
7	12.4 ± 0.1	5.5 ± 0.1	13.7 ± 0.2	5.4 ± 0.2	8.8 ± 0.1	0.0 ± 0.1
10	11.4 ± 0.2	4.2 ± 0.2	13.0 ± 0.2	4.6 ± 0.3	8.8 ± 0.0	0.0 ± 0.0
12	11.7 ± 0.5	4.6 ± 0.5	12.9 ± 0.2	4.6 ± 0.3	8.8 ± 0.0	0.0 ± 0.0
16	10.6 ± 0.1	3.7 ± 0.1	12.1 ± 0.4	3.7 ± 0.5	9.0 ± 0.3	0.0 ± 0.5
20	11.1 ± 0.6	4.1 ± 0.9	12.3 ± 0.6	4.1 ± 0.9	9.1 ± 0.2	0.4 ± 0.3

a) Estimated from the growth curve of the transient signal,

recombination rate (k_r) is faster than the dissociation rate (k_o) in S_c . On the other hand, in the high temperature region, the order of the rate constants becomes $k_c < k_r < k_o$. Thus, the net fraction of the recombination reaction $k_r/(k_r + k_o)$ in S_c decreases with increasing temperature, though the overall rate is still mainly controlled by the slowest process, k_c . This may result in the slight increase in the biradical lifetime in the high temperature region.

3.2 In the presence of a magnetic field In the presence of a magnetic field (0.6 T), the lifetime of ·XOH-16-X· is about 8 μ s at room temperature, which is about 50 times longer than that at zero field as shown in Fig. 1. The lifetime change caused by the magnetic field is so drastic that the biradical lifetime at 0.6 T is most probably controlled by spin-conversion process. In order to clarify whether the spin relaxation is the rate-controlling process in the presence of a magnetic field, the temperature dependence of the lifetime at 0.6 T was analyzed with the theoretical equation (7) for the temperature dependence of the relaxation time [8]:

$$1/\tau = \gamma^2 |H_{loc}|^2 \tau_c / (1 + \omega^2 \tau_c^2) \quad (7)$$

Here, τ_c is the correlation time and ω the Larmor frequency. As shown in Fig. 3, the observed data exhibit the linear relationship as expected from eq. 7. A radius of a rotating molecule and a locally fluctuating field $|H_{loc}|$ were obtained to be 0.35 nm and 1.3 mT, respectively. This indicates that rotational motion of X· and/or ·XOH group is the origin of the spin-lattice relaxation in ·XOH-16-X· at 0.6 T. The observed $|H_{loc}|$ agrees qualitatively with a crude theoretical value (0.5 mT). Analogous results were obtained from the analysis of the temperature dependence of biradical lifetime of ·XOH-12-X· and

·XOH-20-X·.

Acknowledgements The author expresses his thanks to Prof. M. Itoh, Kanazawa University, and Prof. M. Hayashi, Hiroshima University for their kind support during the study. He thanks Dr. M. Okazaki, Governmental Industrial Research Institute, Nagoya, for helpful discussions and suggestions. He also thanks Fujinomiya Research Laboratories, Fuji Photo Film Co. Ltd. for the gift of the sample. This work was supported by Grant-in-Aid for Scientific Research from the Ministry of Education, Science and Culture.

References

- [1] For a review, see: Y.Tanimoto, in Council of Scientific Research Integration(ed.), Trends in Physical Chemistry, Research Trends, Trivandrum, 1990, Vol.1, p.79.
- [2] Y.Tanimoto, M.Takashima, M.Uehara, M.Itoh, M.Hiramatsu, R.Nakagaki, T.Watanabe and S.Nagakura, Chem.Lett., 1985, 15. Y.Tanimoto, M.Uehara, M.Takashima, M.Itoh, M.Hiramatsu, R.Nakagaki, T.Watanabe and S.Nagakura, Bull.Chem.Soc.Jpn., 63(1990)2164.
- [3] Y.Tanimoto, N.Okada, M.Itoh, K.Iwai, K.Sugioka, F.Takemura, R.Nakagaki and S.Nagakura, Chem.Phys.Lett., 136(1987)42. Y.Tanimoto, K.Hasegawa, N.Okada, M.Itoh, K.Iwai, K.Sugioka, F.Takemura, R.Nakagaki and S.Nagakura, J.Phys.Chem., 93(1989)3586.
- [4] Y.Tanimoto, M.Takashima, K.Hasegawa and M.Itoh, Chem.Phys.Lett., 137(1978)330. Y.Tanimoto, M.Takashima and M.Itoh, Bull.Chem.Soc.Jpn., 62(1989)3923. Y.Tanimoto, A.Kita, M.Itoh, M.Okazaki, R.Nakagaki and S.Nagakura, Chem.Phys.Lett., 165(1990)184.
- [5] Y.Tanimoto, N.Okada, S.Takamatsu and M.Itoh, Bull.Chem.Soc.Jpn., 63(1990)1342.
- [6] K.Yamaoka, Microcomputer Analysis of Pharmacokinetics, Nankodo, Tokyo, 1984.
- [7] M.Sisido and K. Shimada, J.Am.Chem.Soc., 99(1977)7785.
- [8] A.Carrington and A.D.McLachlan, Introduction to Magnetic Resonance, Harper & Row, New York, 1967.

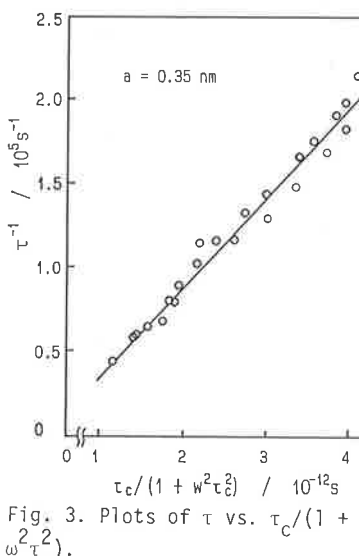


Fig. 3. Plots of τ vs. $\tau_c/(1 + \omega^2 \tau_c^2)$.

Intermediates for Photoisomerization of Aromatic Olefins in the Presence of Electron Acceptors as Studied by Magnetic Field Effects

Kazuhiro Naitoh, Takahisa Oguchi, Ryoichi Nakagaki,[†] Tatsuo Arai, Hirochika Sakuragi,* Katsumi Tokumaru, and Saburo Nagakura[†]
Department of Chemistry, University of Tsukuba, Tsukuba, Ibaraki 305, Japan
[†]Institute for Molecular Science, Myodaiji, Okazaki 444, Japan

The efficiency of isomerization of *trans*-2-(3,3-dimethyl-1-butenyl)naphthalene (*t*-BN) in the presence of electron acceptors was reduced by an magnetic field in polar solvents such as acetonitrile. This effect together with laser flash photolysis studies indicates that the precursor of isomerization is the BN triplet arising from intersystem crossing of a singlet radical pair consisting of a *t*-BN cation and an acceptor anion. The external magnetic field effect was employed to estimate the contribution of ion radical pairs to the isomerization of *t*-BN in the presence of *p*-dicyanobenzene in various solvents. The contribution of radical ions decreases with decreasing polarity of solvents, but the quantum yield for isomerization through radical ions reaches a maximum value at a medium dielectric constant (ϵ) of 8.9 of dichloroethane. The *t*-BN triplet was produced most efficiently almost through an exciplex in chloroform ($\epsilon = 4.8$) among the employed solvents.

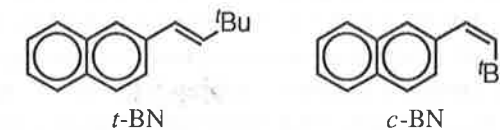
1. Introduction

Photoinduced electron transfer reactions have recently been receiving much attention [1–5] and some reports have appeared on the photoisomerization of olefins induced by electron transfer [6–15]. Electron-accepting sensitizers such as cyanoaromatics (singlet), quinones (triplet), and triphenylpyrylium salts (singlet and triplet) are frequently used to generate olefin radical cations, which undergo isomerization unimolecularly or bimolecularly (through addition and elimination), or give olefin triplets through reverse electron transfer with sensitizer anion radicals; the olefin triplets are well-known intermediates for isomerization.

Direct observation of intermediates by laser flash photolysis (LFP) and measurements of magnetic field effects (MFE) upon reaction efficiency under steady illumination are diagnostic tools for elucidating the mechanisms for electron-transfer induced isomerization of aromatic olefins [16–20]. For example, MFE studies showed that 9,10-dicyanoanthracene (DCA)-sensitized isomerization of stilbene proceeds through the stilbene cation radical [15] and that the key intermediate for pyrene-sensitized isomerization of *trans*-stilbene [18] is the olefin triplets generated by reverse electron transfer between initially produced ion radicals; however, the

reports on the magnetic field effect upon photoisomerization are limited [7,12,18,20,21].

Quenching of olefins in excited states with electron acceptors in polar solvents may generate radical pairs which are precursors of geometrical isomerization of the olefins. We have found that the excited singlet state of *trans*-2-(3,3-dimethyl-1-but enyl)naphthalene (2-NpCH=CHBu^t, *t*-BN) is efficiently quenched by electron acceptors such as dicyanobenzenes (DCB) and dimethyl terephthalate (MT) to afford the *cis* isomer (*c*-BN) in various solvents ranging from nonpolar benzene to polar acetonitrile [22]. We have demonstrated that the precursor of *t*-BN isomerization in acetonitrile is the olefin triplet arising from intersystem crossing of a singlet radical pair [12]. In benzene, however, the quenching was accompanied by emissions ascribable to exciplexes between *t*-BN and the acceptors at the longer wavelength regions, suggesting that the isomerization in nonpolar solvents proceeds through the olefin triplet generated from the exciplexes [22].



In order to clarify the reaction intermediates and their contribution to the isomerization in various solvents, we employed LFP and MFE on the isomerization quantum yield on steady irradiation.

2. Experimental

A mixture of *c*-BN and *t*-BN was synthesized by the condensation of dimethylpropanal with the ylide prepared from 2-naphthylmethyltriphenylphosphonium bromide and butyllithium in ether. Pure *c*-BN and *t*-BN were separated by column chromatography. *t*-BN was crystallized from ethanol. Dimethyl terephthalate-*d*10 (MT-*d*10) was prepared by refluxing terephthalic acid-*d*4 in methanol-*d*3 in the presence of sulfuric acid. MT and MT-*d*10 were crystallized from ethanol. *o*-, *m*-, and *p*-DCB were also crystallized from ethanol. Tetrahydrofuran and propionitrile were distilled before use. Benzene, chloroform, dichloromethane (Dotite Luminazol), 1,2-dichloroethane (Dotite Spectrozol), and acetonitrile (Merck) were used as received. All sample solutions were deaerated by several freeze-pump-thaw cycles or bubbling with argon before irradiation.

Absorption spectra were measured on a U-3200 Hitachi or a JASCO 660 spectrophotometer and fluorescence spectra were measured on a Hitachi MPF-2A or a

Hitachi F-4000 spectrofluorimeter. Fluorescence lifetimes were measured with a Horiba NAES-1100 time-resolved spectrofluorometer (single photon counting). The excitation light was obtained from a hydrogen-arc lamp through a 330-nm band pass filter and the emission was collected and passed through a monochromator (Horiba SGM-111).

Laser flash photolyses were performed with 308-nm laser pulses from an excimer laser (Lambda Physik EMG-50E) as an exciting light source and a xenon flash lamp (EG&E FX-200) as a probe light, or with 337-nm laser pulses from a nitrogen laser (Lambda Physik EMG-101) as an exciting light source and a pulsed xenon arc (Wacom KXL-151) as a monitoring light source. The details of the apparatus for laser flash photolysis have been described elsewhere [20,23].

Sample solutions in quartz cells were placed between the pole pieces of an electromagnet (Tokin SEE-9) and irradiated with UV light from an Ushio 500-W xenon lamp filtered by a combination of Toshiba glass filters (UV-25, UV-31, UV-D33S) or from a 300-W xenon lamp (ILC LX-300F) filtered by a combination of glass filters (Toshiba UV-25, UV-32, UV-D33S, and IRA-25S), which correspond to the excitation of *t*-BN. A high-performance liquid chromatograph (Waters 590 or 600 Multisolvent Delivery System) equipped with an LC spectrophotometer (Waters 481 or 490 Programmable Multiwavelength Detector) was used for analyses of reaction mixtures.

3. Results and Discussion

3.1. Isomerization quantum yield

Irradiation of *t*-BN (0.01 M) at 313 nm in various solvents afforded *c*-BN with varying quantum yields ($\Phi_{t \rightarrow c}^0$), as shown in Table 1. The isomerization was assumed to proceed mainly on the singlet manifold since the quantum yield was not affected by triplet quenchers such as ferrocene. In the presence of electron acceptors such as *p*-DCB and MT, the isomerization quantum yield ($\Phi_{t \rightarrow c}$) decreased remarkably in acetonitrile, but increased noticeably in benzene, with increasing acceptor concentration to approach the limiting quantum yields ($\Phi_{t \rightarrow c}^\infty$), as shown in Fig 1. The $\Phi_{t \rightarrow c}^\infty$ values for *t*-BN in the presence of *o*-, *m*-, *p*-DCB, and MT in various solvents are summarized in Table 1, where K_{SV} ($= k_q \tau^0$) represents the Stern-Volmer constant for the quenching of the excited singlet *t*-BN by a quencher (Q); $\Phi_{t \rightarrow c}$ in the presence of *p*-DCB decreased also in propionitrile, but increased in chloroform and THF, with increasing *p*-DCB concentration. Since *t*-BN fluorescence (lifetime $\tau_0 = 63$ ns in acetonitrile) was effectively quenched by the acceptors employed (Table 1; rate constants $k_q = 1.4 \times 10^{10}$ and $1.2 \times 10^{10} \text{ M}^{-1} \text{ s}^{-1}$ for *p*-DCB

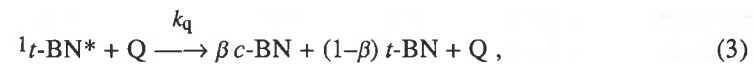
and MT, respectively, in acetonitrile) and no ground-state interactions between the reactants were detected by absorption spectroscopy, $\Phi_{t \rightarrow c}$ can be expressed as

$$\Phi_{t \rightarrow c} = \beta + (\alpha - \beta) / (1 + K_{SV}[Q]), \quad (1)$$

by assuming that the isomerization takes place both without interaction,



and with interaction,



with the quencher Q. α and β are equal to $\Phi_{t \rightarrow c}^0$ and $\Phi_{t \rightarrow c}^\infty$, respectively.

The interaction of the excited singlet *t*-BN with the acceptors results in the formation of exciplexes in nonpolar solvents, as confirmed by emissions in the longer wavelength region. In polar solvents, however, an electron transfer from the *t*-BN singlet to the acceptors is assumed to be a favorable process from energetic considerations based on Rehm-Weller's equation [24],

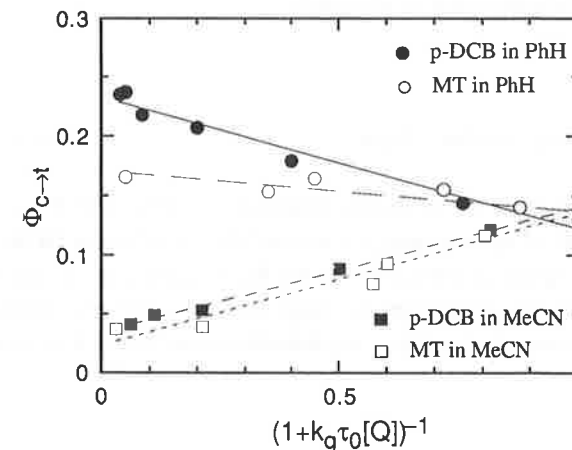


Fig. 1. Acceptor concentration dependence of the isomerization quantum yield.

Table 1. Isomerization quantum yields of *t*-BN in the absence and presence of electron acceptors in various solvents

Solvent	Acceptor	ϵ ^{a)}	K_{SV} ^{b)}	$\Phi_{t \rightarrow c}^0$ ^{c)}	$\Phi_{t \rightarrow c}^\infty$ ^{d)}
Benzene	MT	2.28	370	0.13	0.17
	<i>o</i> -DCB		470		0.16
	<i>m</i> -DCB		71		0.11
	<i>p</i> -DCB		540		0.23
Chloroform	<i>p</i> -DCB	4.81	200	0.14	0.29
Tetrahydrofuran	<i>p</i> -DCB	7.58	560	0.13	0.20
Dichloromethane	<i>p</i> -DCB	8.93	400	0.19	0.18
1,2-Dichloroethane	<i>p</i> -DCB	10.4	230	0.19	0.14
Propionitrile	<i>p</i> -DCB	27.2	690	0.15	0.05
Acetonitrile	MT	37.5	780	0.14	0.02
	<i>o</i> -DCB		830		0.05
	<i>m</i> -DCB		540		0.06
	<i>p</i> -DCB		870		0.04

a) Dielectric constants of the solvents. b) Stern-Volmer constants for quenching of the *t*-BN excited singlet by acceptors. c) Isomerization quantum yields of *t*-BN in the absence of acceptors. d) Isomerization quantum yields of *t*-BN in the presence of an infinitely high concentration of acceptors.

$$\Delta G^\circ = E_{\text{ox}} - E_{\text{red}} - e_0^2/\alpha\epsilon - E_{0,0}, \quad (4)$$

where E_{ox} and E_{red} indicate the oxidation potential of *t*-BN (1.55 V vs. SCE) and the reduction potential of the acceptor (-1.64 for MT, -1.62 for *o*-DCB, -1.60 for *p*-DCB, and -1.92 V (peak potential) for *m*-DCB), respectively, as determined in acetonitrile, $E_{0,0}$ is the singlet excitation energy of *t*-BN (3.63 eV, estimated from its fluorescence spectrum), and $e_0^2/\alpha\epsilon$ is a coulombic term (0.06 eV in acetonitrile).

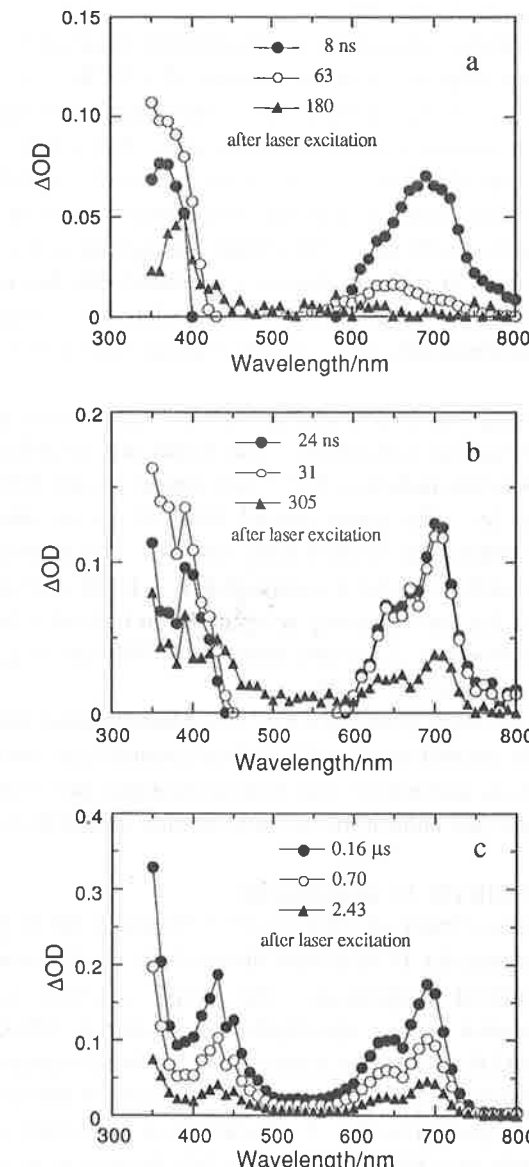


Fig. 2. Transient Absorption spectra observed on excitation of *t*-BN in the presence of *p*-DCB in chloroform (a), dichloromethane (b), and acetonitrile (c).

3.2. Transient absorption spectra

The transient absorption spectra were measured by irradiating *t*-BN (3×10^{-3} mol dm $^{-3}$) with 337-nm laser pulses in the presence of *p*-DCB (5×10^{-2} mol dm $^{-3}$) in deaerated solutions, as shown in Figs. 2a-c. The sample concentrations were controlled so that more than 90% of the excited singlet *t*-BN was quenched by the acceptor. In chloroform (Fig. 2a) a broad band appeared around 700 nm and decayed in the shorter time range. The decay of this band was accompanied by the build-up of a band around 400 nm. The former absorption is ascribable to the exciplex of *t*-BN with *p*-DCB since its lifetime is identical with that of the exciplex emission. The latter band can be ascribed to *t*-BN triplets by comparison with the spectrum measured independently [25]. Similar transient absorption spectra were observed in benzene.

The transient absorption spectra of the *t*-BN/*p*-DCB system in acetonitrile were measured under similar conditions. The bands due to *p*-DCB anion (*p*-DCB $^-$) [26] and *t*-BN cation radical (*t*-BN $^+$) [27] appear around 340 and 600–750 nm, respectively (Fig. 2c). The bands around 400–500 nm are identified as the superposition of absorptions due to both ionic species. The transient absorption spectra of *t*-BN in acetonitrile in the presence of MT, *o*-DCB, and *m*-DCB can be ascribed to *t*-BN $^+$ and the corresponding acceptor anion radicals [28]. The cation radical *t*-BN $^+$ was detected in dichloromethane (600–750 nm, Fig. 2b) and 1,2-dichloroethane in the presence of *p*-DCB.

These observations show unambiguously that photoinduced electron transfer takes place between the excited singlet *t*-BN and the ground-state electron acceptors in polar solvents such as acetonitrile and dichloromethane; however, in nonpolar solvents such as benzene and chloroform no ionic species were detected.

3.3. Magnetic field effects in acetonitrile

Daeaerated solutions (5 ml) of *t*-BN (2×10^{-4} M) and *p*-DCB (9×10^{-3} M) in acetonitrile were irradiated for 15 min with filtered light ($\lambda \geq 310$ nm) from a 500-W xenon lamp at ambient temperature. The sample solutions were examined before and after irradiation using a spectrophotometer and an HPLC apparatus to determine the initial and final concentrations of *t*-BN. The disappearance yields of *t*-BN ($\Phi(H)/\Phi(0)$) at various applied magnetic fields relative to that at the zero magnetic field strength are plotted in Fig. 3. Under these irradiation conditions the light was absorbed only by *t*-BN; *p*-DCB and *c*-BN formed were not practically excited. The reaction was attained to 40–50% *t*-BN conversion, but side products were negligible, providing good reliability in determining the relative disappearance yields. Figure 3 clearly shows that the relative yield is reduced at the field

strengths lower than 1 kG and reached a nearly constant value (≈ 0.86) at the higher strength region.

A similar magnetic field effect was observed on irradiation of deaerated acetonitrile solutions of *t*-BN and MT with the filtered light. The reaction efficiency of *t*-BN decreased similarly with increasing magnetic field strength and was saturated at a nearly constant value ($\Phi(H)/\Phi(0) \approx 0.94$, Fig 3). In this system, however, the effect is smaller than that observed in the *t*-BN/DCB system. A similar but much smaller magnetic field effect (at most $\Phi(H)/\Phi(0) \approx 0.97$) was observed when *t*-BN was irradiated with perdeuterated MT (MT-*d*₁₀) in acetonitrile under similar conditions to those employed for the *t*-BN/MT system.

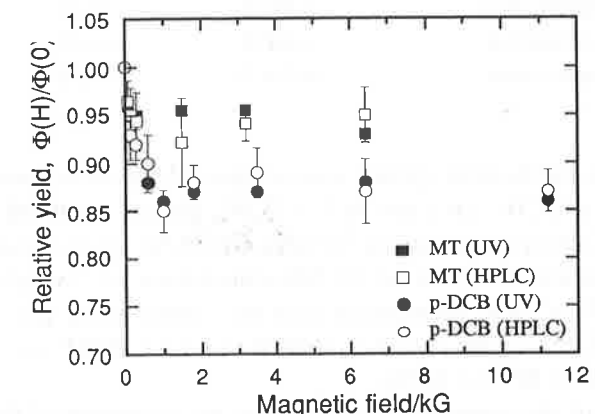


Fig. 3. Relative disappearance yields of *t*-BN in the presence of acceptors at various magnetic field strengths.

In another series of experiments deaerated solutions (3 ml) of *t*-BN (2×10^{-4} mol dm $^{-3}$) and DCB's (5×10^{-2} mol dm $^{-3}$) in acetonitrile were irradiated for 10–20 min with filtered light ($\lambda \geq 330$ nm) from a 300-W xenon lamp at ambient temperature. The concentrations of *c*-BN produced were determined after irradiation using an HPLC apparatus. The conversion was controlled at 6–8%. The asymptotic $\Phi(H)/\Phi(0)$ values are listed in Table 2.

The hyperfine interaction B_i between the nuclear spins I_k and the unpaired electron spin in each component radical is governed by the isotropic hyperfine coupling constants, a_{ik} , and can be expressed by [29,30]

$$B_i = (\sum a_{ik}^2 I_k (I_k + 1))^{1/2}. \quad (5)$$

Table 2. Asymptotic $\Phi(H)/\Phi(0)$ values at the high magnetic field in isomerization of *t*-BN in the presence of electron acceptors in various solvents

Solvent	Acceptor	$\Phi(H)/\Phi(0)$
Benzene	<i>p</i> -DCB	≈ 1
Chloroform	<i>p</i> -DCB	≈ 0.98
Tetrahydrofuran	<i>p</i> -DCB	≈ 0.90
Dichloromethane	<i>p</i> -DCB	≈ 0.87
1,2-Dichloroethane	<i>p</i> -DCB	≈ 0.84
Propionitrile	<i>p</i> -DCB	≈ 0.79
Acetonitrile	<i>p</i> -DCB	≈ 0.67
Acetonitrile	<i>o</i> -DCB	≈ 0.67
Acetonitrile	<i>m</i> -DCB	≈ 0.53

The B_i values for the ionic species were computed by using reported a_{ik} for *o*-[31,32], *m*- [32], *p*-DCB^{·-} [31], and MT^{·-} [33,34], and a_{ik} estimated for *t*-BN⁺, according to McConnell's equation ($a_k^H = 22.5\rho_k$ G) [35,36] where the odd-electron densities, ρ_k , were obtained from LCAO MO calculations for 2-vinylnaphthalene cation radical [37] (a small contribution from the *t*-butyl group was neglected): $B(p\text{-DCB}^{\cdot-}) = 4.7$, $B(o\text{-DCB}^{\cdot-}) = 6.3$, $B(m\text{-DCB}^{\cdot-}) = 10.4$, $B(\text{MT}^{\cdot-}) = 3.2$, $B(\text{MT}-d_{10}^{-}) = 0.80$, and $B(t\text{-BN}^+) = 6.9$ G.

Comparison of the computed B_i values with the magnitude of the magnetic field effect observed for the above acceptors indicates that the hyperfine interaction plays a major role in the present case. The $B_{1/2}$ values defined by [30]

$$\Phi(B_{1/2}) = \frac{1}{2}[\Phi(0) - \Phi(\infty)] \quad (6)$$

were estimated as 11–18 G by substituting the above B_i values into

$$B_{1/2} = 2(B_1^2 + B_2^2)/(B_1 + B_2). \quad (7)$$

This is consistent with the facts that the isomerization yield was decreased by application of remarkably low magnetic fields and that the effect was saturated at higher fields.

3.4. Magnetic field effects in various solvents

Deaerated solutions (3 ml) of *t*-BN (2×10^{-4} mol dm⁻³) and *p*-DCB (5×10^{-2} mol dm⁻³) in various solvents were irradiated for 10–20 min with filtered light ($\lambda \geq 330$ nm) from a 300-W xenon lamp at ambient temperature. The yield of *c*-BN ($\Phi(H)/\Phi(0)$) at various applied magnetic fields relative to that at the zero magnetic field strength are plotted in Figs. 4a and 4b. These figures show that the relative yields of *c*-BN are reduced, except for the case of benzene as solvent, at the field strengths lower than 1 kG and reached nearly constant values at the higher strength region. The effect of magnetic field on isomerization quantum yield arises from the hyperfine interaction in radical pairs. The asymptotic $\Phi(H)/\Phi(0)$ values estimated from Fig. 4 are summarized in Table 2.

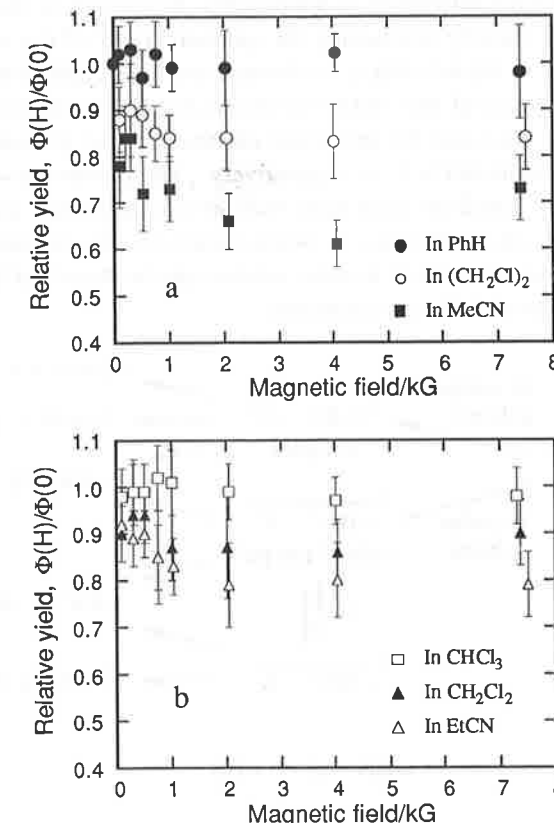
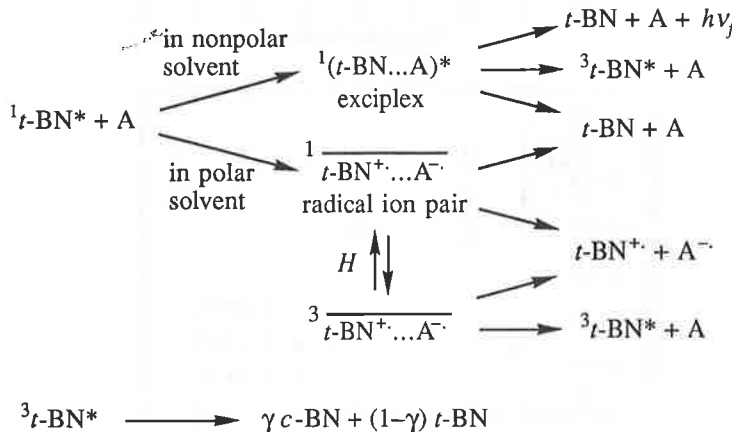


Fig. 4. Relative yields of *c*-BN formation in various solvents in the presence of *p*-DCB at varying magnetic field strengths.

3.5. Intermediates and their contribution to isomerization

In the presence of electron acceptors in polar solvents such as acetonitrile the isomerization quantum yield $\Phi_{t \rightarrow c}$ is lower than that in their absence, but still remains at a finite value even when the excited singlet *t*-BN are completely quenched. The laser flash photolysis indicates that the quenching of the excited singlet *t*-BN by DCB's and MT affords singlet radical pairs consisting of a *t*-BN cation and an acceptor anion (Scheme 1, in polar solvent). These radical pairs undergo either reverse electron transfer to give the starting materials or intersystem crossing into triplet radical pairs. The reverse electron transfer in the triplet pairs generates the triplet state of *t*-BN, a rational precursor of isomerization. The triplet *t*-BN decays to ground-state *c*-BN and *t*-BN in a nearly 1:1 ratio ($\gamma \approx 0.5$) [25,38]. The intersystem crossing between singlet S_0 and triplet T_+, T_- states induced by the hyperfine interaction is appreciably diminished in the presence of high magnetic fields thereby attenuating the quantum yield of the triplet radical pair. The population of triplet *t*-BN is exothermic since the triplet energy of *t*-BN and the energy of the radical pair can be estimated as 52 [25] and 76–78 kcal/mol (from the difference between the measured electrochemical potentials of *t*-BN ($E(D^+/D)$) and acceptors ($E(A/A^-)$), respectively. The possibility of isomerization from *t*-BN can be ruled out since *trans*-stilbene cation radicals are reported to be more stable than, and inefficient in isomerization to, the *cis* cation radicals. Thus, the isomerization mechanism in polar solvents can be described by Scheme 1, where the olefin triplet is the key intermediate.



Scheme 1

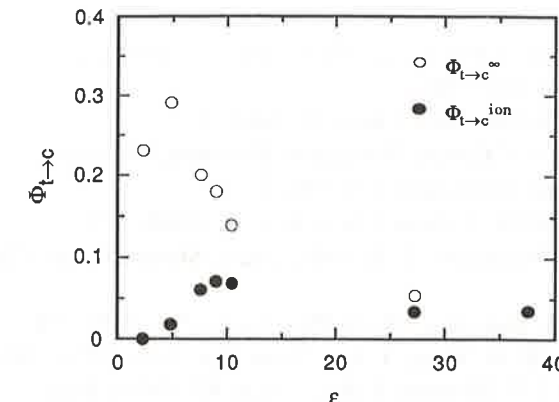


Fig. 5. Contribution of ionic intermediates (•) to the isomerization of *t*-BN in the presence of *p*-DCB (○) in various solvents.

In the *t*-BN/*p*-DCB system the largest magnetic field effect was observed in acetonitrile, and the effect was reduced in the order of acetonitrile, propionitrile, 1,2-dichloromethane, dichloromethane, and benzene. In benzene neither magnetic field effect was observed, nor radical ions were detected in laser flash photolysis though the *t*-BN fluorescence was effectively quenched and a weak exciplex emission was detected. Thus, in nonpolar solvents the isomerization is assumed to proceed through *t*-BN triplets generated from collapse of the exciplex between *t*-BN and the acceptor (Scheme 1, in nonpolar solvent).

It can be reasonably assumed that the isomerization proceeds exclusively through radical ions in acetonitrile. Accordingly, the asymptotic $\Phi(H)/\Phi(0)$ values at the high magnetic field in various solvents relative to that in acetonitrile correspond to contributions of the ionic intermediates to the isomerization in the respective solvents. Figure 5 shows plots of the total quantum yields for isomerization ($\Phi_{t \rightarrow c}^{\infty}$) and quantum yields due to ionic intermediates ($\Phi_{t \rightarrow c}^{ion}$) estimated using the asymptotic values. These results show that the contribution of radical ions decreases with decreasing polarity of solvents, but that $\Phi_{t \rightarrow c}^{ion}$ reaches a maximum value at a medium dielectric constant of 8.9 of dichloroethane. Taking into account the fact that the isomerization quantum yield of *t*-BN in the presence of electron acceptors decreases with increasing solvent polarity (Table 1), it can be concluded that the isomerization proceeds through *t*-BN triplets generated from the interactions of *t*-BN singlets with the acceptors, and that the efficiency of triplet formation decreases with increasing polarity of the solvent by switching of the precursors of *t*-BN triplets from exciplexes to radical ion pairs.

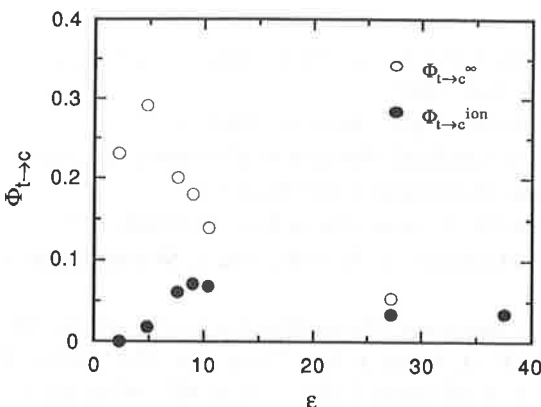


Fig. 5. Contribution of ionic intermediates (\bullet) to the isomerization of *t*-BN in the presence of *p*-DCB (o) in various solvents.

In the *t*-BN/*p*-DCB system the largest magnetic field effect was observed in acetonitrile, and the effect was reduced in the order of acetonitrile, propionitrile, 1,2-dichloromethane, dichloromethane, and benzene. In benzene neither magnetic field effect was observed, nor radical ions were detected in laser flash photolysis though the *t*-BN fluorescence was effectively quenched and a weak exciplex emission was detected. Thus, in nonpolar solvents the isomerization is assumed to proceed through *t*-BN triplets generated from collapse of the exciplex between *t*-BN and the acceptor (Scheme 1, in nonpolar solvent).

It can be reasonably assumed that the isomerization proceeds exclusively through radical ions in acetonitrile. Accordingly, the asymptotic $\Phi(H)/\Phi(0)$ values at the high magnetic field in various solvents relative to that in acetonitrile correspond to contributions of the ionic intermediates to the isomerization in the respective solvents. Figure 5 shows plots of the total quantum yields for isomerization ($\Phi_{t \rightarrow c}^\infty$) and quantum yields due to ionic intermediates ($\Phi_{t \rightarrow c}^{\text{ion}}$) estimated using the asymptotic values. These results show that the contribution of radical ions decreases with decreasing polarity of solvents, but that $\Phi_{t \rightarrow c}^{\text{ion}}$ reaches a maximum value at a medium dielectric constant of 8.9 of dichloroethane. Taking into account the fact that the isomerization quantum yield of *t*-BN in the presence of electron acceptors decreases with increasing solvent polarity (Table 1), it can be concluded that the isomerization proceeds through *t*-BN triplets generated from the interactions of *t*-BN singlets with the acceptors, and that the efficiency of triplet formation decreases with increasing polarity of the solvent by switching of the precursors of *t*-BN triplets from exciplexes to radical ion pairs.

References

- [1] M. A. Fox and M. Chanon, ed., Photoinduced electron transfer, Parts A-D (Elsevier, Amsterdam, 1988).
- [2] R. S. Davidson, *Advan. Phys. Chem.* 19 (1983) 1.
- [3] D. Creed and R. A. Caldwell, *Photochem. Photobiol.* 41 (1985) 715.
- [4] M. A. Fox, *Advan. Photochem.* 13 (1986) 237.
- [5] G. J. Kavarnos and N. J. Turro, *Chem. Rev.* 86 (1986) 401.
- [6] G. G. Aloisi, U. Mazzucato, J. B. Birks, and L. Minuti, *J. Am. Chem. Soc.* 99 (1977) 6340.
- [7] H. Hayashi and S. Nagakura, *Chem. Phys. Letters* 53 (1978) 201.
- [8] D. R. Arnold and P. D. Wong, *J. Am. Chem. Soc.* 101 (1979) 1894.
- [9] F. D. Lewis and J. T. Simpson, *J. Phys. Chem.* 83 (1979) 2015.
- [10] G. Gennari, G. Cauzzo, G. Galiazzo, and M. Folin, *J. Photochem.* 14 (1980) 11.
- [11] B. K. Adams and W. R. Cherry, *J. Am. Chem. Soc.* 103 (1981) 6904.
- [12] H. Sakuragi, R. Nakagaki, T. Oguchi, T. Arai, K. Tokumaru, and S. Nagakura, *Chem. Phys. Letters* 135 (1987) 325.
- [13] T. Oguchi, T. Arai, H. Sakuragi, and K. Tokumaru, *Bull. Chem. Soc. Jpn.* 60 (1987) 2395.
- [14] Y. Kuriyama, T. Arai, H. Sakuragi, and K. Tokumaru, *Chem. Letters* (1988) 1193.
- [15] Y. Kuriyama, T. Arai, H. Sakuragi, and K. Tokumaru, *Chem. Letters* (1989) 251.
- [16] Yu. N. Molin, ed., Spin polarization and magnetic field effects in radical reactions (Elsevier, Amsterdam, 1984).
- [17] I. R. Gould, N. J. Turro, and M. B. Zimmt, *Advan. Phys. Org. Chem.* 20 (1984) 1.
- [18] T. V. Leshina, K. M. Salkhov, R. Z. Sagdeev, S. G. Belyaeva, V. I. Maryasova, P. A. Purtov, and Yu. N. Molin, *Chem. Phys. Letters* 70 (1980) 228.
- [19] S. G. Boxer, C. E. D. Chidsey, and M. G. Roelofs, *Ann. Rev. Phys. Chem.* 34 (1983) 389.
- [20] R. Nakagaki, M. Hiramatsu, T. Watanabe, Y. Tanimoto, and S. Nagakura, *J. Phys. Chem.* 89 (1985) 3222.
- [21] A. Gupta and G. S. Hammond, *J. Chem. Phys.* 57 (1972) 1789.
- [22] T. Oguchi, T. Arai, H. Sakuragi, and K. Tokumaru, *Bull. Chem. Soc. Jpn.* 60 (1987) 2395.
- [23] H. Furuuchi, T. Arai, Y. Kuriyama, H. Sakuragi, and K. Tokumaru, *Chem. Phys. Letters* 162 (1989) 211.
- [24] D. Rehm and A. Weller, *Isr. J. Chem.* 8 (1970) 259.
- [25] T. Arai, H. Sakuragi, K. Tokumaru, Y. Sakaguchi, J. Nakamura, and H. Hayashi, *Chem. Phys. Letters* 98 (1983) 40.
- [26] A. Ishitani and S. Nagakura, *Theoret. Chim. Acta* 4 (1966) 236.
- [27] T. Shida, Electronic absorption spectra of radical ions (Elsevier, Amsterdam, 1988).
- [28] M. Yamamoto, M. Ohoka, K. Kitagawa, S. Nishimoto, and Y. Nishijima, *Chem. Letters* (1973) 745.
- [29] K. Schulten and P. G. Wolynes, *J. Chem. Phys.* 68 (1978) 3292.
- [30] A. Weller, F. Nolting, and H. Staerk, *Chem. Phys. Letters* 96 (1983) 24.
- [31] A. Carrington and P. F. Todd, *Mol. Phys.* 6 (1963) 161.
- [32] P. H. Reinmuth and G. K. Fraenkel, *J. Am. Chem. Soc.* 85 (1963) 683.
- [33] M. Hirayama, *Bull. Chem. Soc. Jpn.* 40 (1967) 2234.
- [34] J. Voss, W. Schmueser, and K. Schlapkohl, *J. Chem. Res. (S)* (1977) 144.
- [35] J. R. Bolton, in Radical ions, eds. E. T. Kaiser and L. Kevan (Interscience, New York, 1968) p.1.
- [36] J. E. Wertz and J. R. Bolton, Electron spin resonance, elementary theory and practical applications (McGraw Hill, New York, 1972) p. 96.
- [37] C. A. Coulson and A. Streitwieser, Jr., Dictionary of π -electron calculations (Pergamon Press, New York, 1965) p. 20.
- [38] T. Arai, H. Sakuragi, and K. Tokumaru, *Chem. Letters* (1980) 1335.

An Application of Spin Trapping to the Study of Magnetic Field Dependent Chemical Reactions.

Masaharu Okazaki*, Kazumi Toriyama, and Yutaka Tai.

Government Industrial Research Institute, Nagoya, Hirate, Kita-ku, Nagoya, 462, Japan.

Takeshi Shiga

Department of Physiology, School of Medicine, Osaka University, Yamadaoka, Suita, 565, Japan.

ABSTRACT

The yield of the spin adduct of SDS radical during the photoreduction of quinones in SDS micellar solution was modulated by the ESR transitions of the semiquinone radical as well as the SDS radical, which constitute the transient radical pair of this reaction system. This observation is a direct evidence for the radical pair model of this kind of magnetic field dependent reactions. The apparatus has been improved for the study of time dependent phenomenon using a XeCl excimer laser and a pulsed microwave system, which are controlled with a pulse programmer and a personal computer. This new apparatus allows us to detect the microwave field effect at high powers without the dielectric heating for an aqueous micellar system as well as to observe the time dependencies of the phenomena. In the photoreduction of anthraquinone in SDS micellar solution, spin adduct yield decreased due to the ESR transition of anthrasemiquione to almost one half of the original value (under B_0 of 334 mT) at the microwave power of 16 W. This large microwave effect suggests that this technique can be practically applicable to control the reaction path. From the dependence of the spin adduct yield on the microwave pulse length it was revealed that the microwave effect has a lag time of about 500 ns after the laser excitation.

1. Introduction

Although the magnetic field dependent yield of a chemical reaction has been interpreted with the radical pair model[1,2], it is rare that both the component radicals of the pair were detected as functions of the external magnetic field. Since the magnetic field effect appears strongly in photo-reduction of quinones or ketones in the micellar solutions[3,4], we tried to detect the SDS radical by spin trapping whose counter part, the semiquinone radical, had been already detected as a function of the magnetic field [5].

As the result[6], a very large magnetic field effect was detected on the yield of SDS radical escaped from the micelle. To confirm the radical pair mechanism and to get into details of the phenomenon, however, only the observation of both the transient radicals as the functions of magnetic field is still insufficient. A detailed theoretical curve fitting of the magnetic field effect or some direct confirmation should be needed for that.

In the previous studies, we showed that irradiation of microwave at X-band under the magnetic field at around 330 mT decreased the yield of the spin adduct of SDS radical in the above reaction system and the effect as a function of magnetic field traced the ESR spectra of both the semiquinone radical and the SDS radical. This method, which we call "product yield detected ESR", enabled us to observe the ESR spectra of the transient radical pair through measuring the spin adduct yield. This is a direct evidence for the radical pair model of this kind of magnetic field dependent reactions, because the yield of one of the escaped radical (SDS adduct) decreased by the spin flip of either of the component radicals of the pair.

In the present study, we would like to show our recent results with our newly constructed apparatus to extend the above experiment to the time dependent observation as well as to the high microwave-field region without the dielectric heating. As the results: (1) We achieved more than 40 % decrease in the yield of the spin adduct of SDS radical by inducing the ESR transition of anthrasemiquione radical in the photo-reduction of anthraquinone in SDS micellar solution. This large microwave effect suggests that this method may be used to control chemical reactions in a practical base which have the radical pair as the intermediates. (2) It is clari-

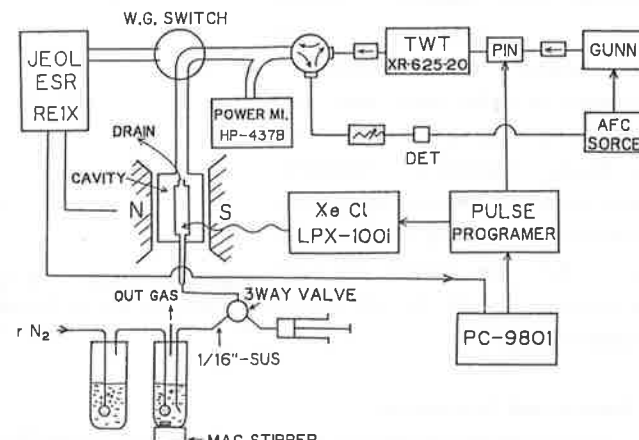


Figure 1. Schematic diagram of the apparatus to observe PYESR spectrum.

fied that the dependence of the spin adduct yield on the microwave pulse length is useful to elucidate the dynamics of the radical pair.

(3) Dependence on the microwave strength can be obtained in a wide range of power without the dielectric heating even for an aqueous micellar system.

2. Experimental

Figure 1 shows a schematic diagram of our new apparatus. Well deoxygenated sample solution is charged into a quartz flat cell with a flow system (made of stainless steel) and is irradiated with an XeCl excimer laser (Lambda Physik, LPX-105i) under the various magnetic field. The sample solution is also irradiated with a pulsed microwave from a TWT amplifier (Keltec Florida XR 625-20) at an arbitrary timing with photo-irradiation. Duration of the microwave pulse can be changed from 10 nsec to 40 μ sec in units of 0.2 nsec using a pulse programmer (Iwatsu SY8220). The AFC circuit is used only in a CW experiment with photo-irradiation using a ultra-high pressure mercury lamp (Usio UD500H). The spin adduct yield is measured by the conventional ESR method after switching the connection of the cavity from the TWT amplifier to the original ESR system (JEOL RE-1X). All these instruments are controlled with a personal computer (NEC PC9801 DS).

Anthraquinone was obtained from Tokyo Kasei Kogyo and recrystallized from ethanol. Sodium dodecyl sulfate and 3,5-dibromo-4-nitrosobenzene-sulfonate (a spin trap) were used as supplied from Nakarai Chemicals and Sigma Chemical Company, respectively. Experiments were performed at ambient temperatures (ca. 27 °C). The sample solution was buffered with 50 mM sodium phosphate at pH 6.0.

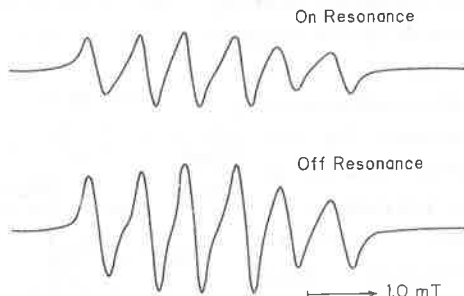


Figure 2. Effect of the ESR transition of anthra-semiquinone on ESR spectrum of the spin adduct of SDS radical.

3. Results and Discussion

Figure 2 shows the ESR spectra of the spin adduct in an UV-irradiated SDS (0.2 M) micellar solution of anthraquinone (0.1 mM) with simultaneous irradiation of a microwave pulse of 10 μ sec at 9.39 GHz at the resonance magnetic field for the semiquinone radical (334.7 mT; lower) or at a magnetic field off-resonant for both the intermediate radicals (330 mT; upper). The

microwave power was about 16W. Since the ESR spectrum indicates that the trapped radical has one alpha-proton ($a_H=0.76$ mT), it is safely assigned to the SDS radical as in the previous study[7]. The observed reduction in the spin-adduct yield is about 45% which is the maximum resonant-microwave effect ever observed.

Figure 3 shows the reduction in the spin-adduct yield due to microwave irradiation as a function of the magnetic field. The stick diagram shows the expected ESR lines from both the SDS radical and the semiquinone radical. As mentioned in the previous studies, this coincidence of the stick diagram with the observed "PY-ESR spectrum" indicates that

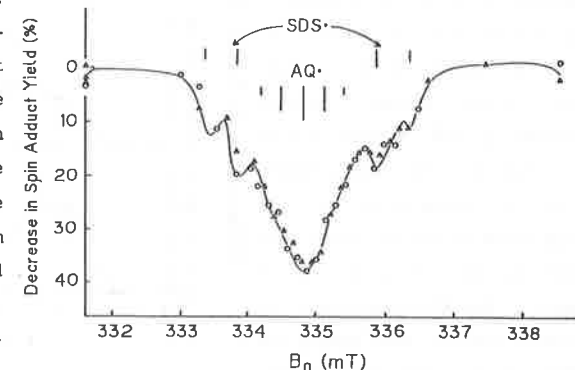


Figure 3. PY-ESR spectrum for UV-irradiated 0.1 mM anthraquinone solution of 0.2 M SDS micellar solution.

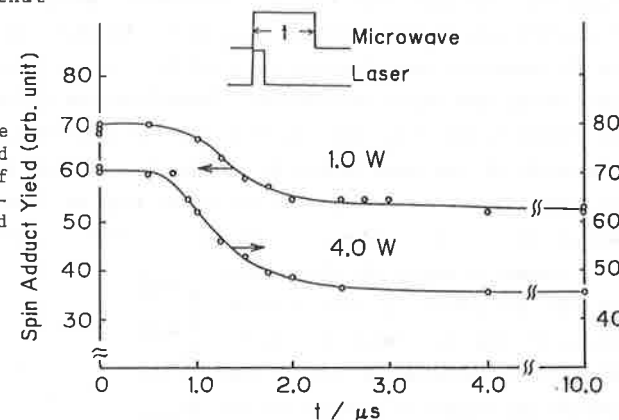


Figure 4. Dependence of spin adduct yield on the duration of laser pulse at microwave power of 1.0 and 4.0 W.

microwave-induced spin-flip of one of the component radicals of the transient radical pair modulates the spin state of the radical pair from the initial triplet state to the singlet state, from which the cage product is efficiently formed. (thus the spin adduct decreases.) In other words, the yield of escaped SDS radical accumulated as the spin adduct decreases by the spin-flip of either the SDS radical or the semiquinone radical. This is a direct evidence for the radical pair theory of this kind of magnetic field dependent chemical reactions. As an extension of this technique, isotope

enrichment was demonstrated in a previous study [8] by selective induction of one of the ESR transitions of the intermediate SDS(D) and SDS(H) radicals in the same type of reaction [8].

Figure 4 shows the dependence of spin adduct yield on the duration of the microwave pulse at two microwave powers (peak value; 1.0 W, upper; 4.0 W, lower). The microwave effect appears after the lug time of about 500ns and saturates at about 3.0 μ sec. The differentials of these curves are shown in Figure 5. The lug times for the two microwave powers are the same each

other but the peak positions are different. Scaino et al.[9] measured the concentration of benzophenone radical in the photoreduction of benzophenone in SDS micellar solution and reported that it becomes the maximum about 500 nsec after the laser excitation. Therefore, we consider that the lug time in Figure 4 and 5 is the lug time for the appearance of the radical pair. The shift of the peak position at higher microwave power may indicate that it takes less time for spin inversion at high microwave field. The detailed analysis of these curves are now in progress.

Figure 6 shows the dependence of the decrease in spin-adduct yield on the microwave strength. With weak microwave field the effect increases in proportion to the square of the field (or proportional to the microwave power), and it saturate with the further increase of the field. This tendency was already predicted in a theoretical calculation of PYESR spectra [7].

This phenomenon may be classified as one of the "RYDMR" experiments,

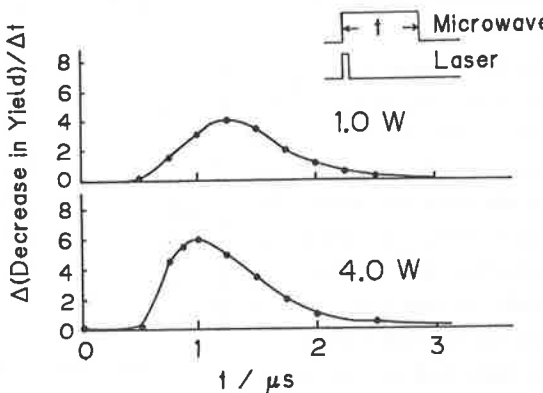


Figure 5. Derivative of the two curves in Figure 4.

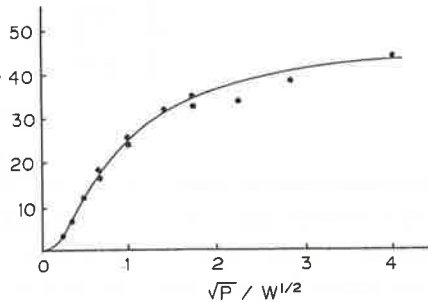


Figure 6. Decrease of spin adduct yield as a function of square root of the theoretical calculation of PYESR microwave power

where fluorescence from a transient species is monitored [10]. In the present experiment, on the other hand, the yield of the final stable product is measured.

Acknowledgement

Dr. Ryusei Konaka and Dr. Sigeru Sakata of Sionogi Research Laboratory are gratefully acknowledged for supplying a spin trapping reagent of dimethylnitrosobenzenesulfonate and various helpful discussions.

4. References

- (1) P.W. Atkins and T.P. Lambert, Ann. Rep. Prog. Chem., 72A, 67 (1975).
- (2) R.Z. Sagdeev, Yu.N. Molin, K.M. Salikhov, V. Leshina, M.A. Kamha, and S.M. Shein, Org. Magn. Reson., 5, 603 (1973).
- (3) N.J. Turro and B. Kraeutler Acc. Chem. Res. 13, 369 (1980).
- (4) Y. Sakaguchi and H. Hayashi, J. Phys. Chem., 88, 1437 (1984).
- (5) M. Okazaki, S. Sakata, R. Konaka, and T. Shiga, J. Am. Chem. Soc., 107, 7214 (1985).
- (6) M. Okazaki and T. Shiga, Nature 323, 240 (1986).
- (7) M. Okazaki, S. Sakata, R. Konaka, and T. Shiga, J. Chem. Phys., 86, 6792 (1987).
- (8) M. Okazaki, T. Shiga, S. Sakata, R. Konaka, and K. Toriyama, J. Phys. Chem., 92, 1402 (1988).
- (9) J.C. Scaino, E.B. Abuin, and L.C. Stewart, J. Am. Chem. Soc., 104, 5673 (1982).
- (10) A.I. Grant, K.A. McLauchlan, and S.R. Nattrass, Mol. Phys. 55, 557 (1985).

External magnetic field effects on bichromophoric photochemistry

Ryoichi Nakagaki

Faculty of Pharmaceutical Sciences, Kanazawa University,
Kanazawa, Ishikawa 920 (Japan)

Abstract

We have studied magnetic field effects upon photochemistry involving biradical intermediates where both of radical species are bonded at the terminal ends of a methylene chain. Two kinds of photochemistry have been employed to produce biradical species. The first is homolytic photocleavage of cycloalkanones and the magnetic field effects are measured on the decay rates for biradicals derived from cyclic ketones. The second is photoinduced intramolecular electron transfer or hydrogen atom transfer between a nitro-aromatic chromophore and anilino group, and the magnetic field effects are observed on reaction yields of cage and escape photoredox products. Magnitude of magnetic field effects are found to be dependent on the chain length linking the two radical sites.

\downarrow The Magnitude of J in Biradicals

Biradicals containing stable nitroxides have been extensively studied by means of ESR spectroscopy [1]. The following three situations have been observed:

- (1) $J \gg a$ for small r ,
- (2) $J \approx a$ for intermediate r , and
- (3) $J \ll a$ for large r , where the exchange interaction (J) decreases approximately exponentially with respect to the inter-radical distance (r), and the hyperfine interaction (a_N) between the electronic spin and nuclear magnetic moments of ^{14}N is rather independent of r .

One of the necessary conditions for observing magnetic field

effects is that the exchange interaction must be negligibly small in comparison with the hyperfine interaction, namely, $J \ll a$. Therefore, it is anticipated that external magnetic fields have some effects on dynamical behavior and chemical reaction yields of long-chain biradicals.

2 Magnetic Field Effects on Decay Rates for Biradical Intermediates

2,2-Diphenylcycloalkanones undergo the Norrish type I process. The resultant biradical consists of acyl and diphenylalkyl radicals. Scheme 1 illustrates the reaction intermediates and the end products derived from 2,2-diphenylcycloalkanones. The transient absorption due to diphenylalkyl moiety at 335nm was monitored by means of nanosecond laser flash photolysis. The lifetime of biradical intermediates were determined by analyzing the absorbance change at 335nm. The ratio (k^H/k^O) of decay rate constant in the presence and the absence of magnetic fields have been plotted as a function of the field strength in Figure 1.

Photochemical bond cleavage takes place in the $n-\pi^*$ triplet state. Therefore, a triplet biradical is initially prepared. The lifetime of triplet biradical is elongated on application of an external magnetic field because the hyperfine coupling mechanism is of dominant importance and the intersystem crossing rate is reduced in the presence of the magnetic field.

3 Magnetic Field Effects upon Reaction Yields

[a] Formation of Cage and Escape Products

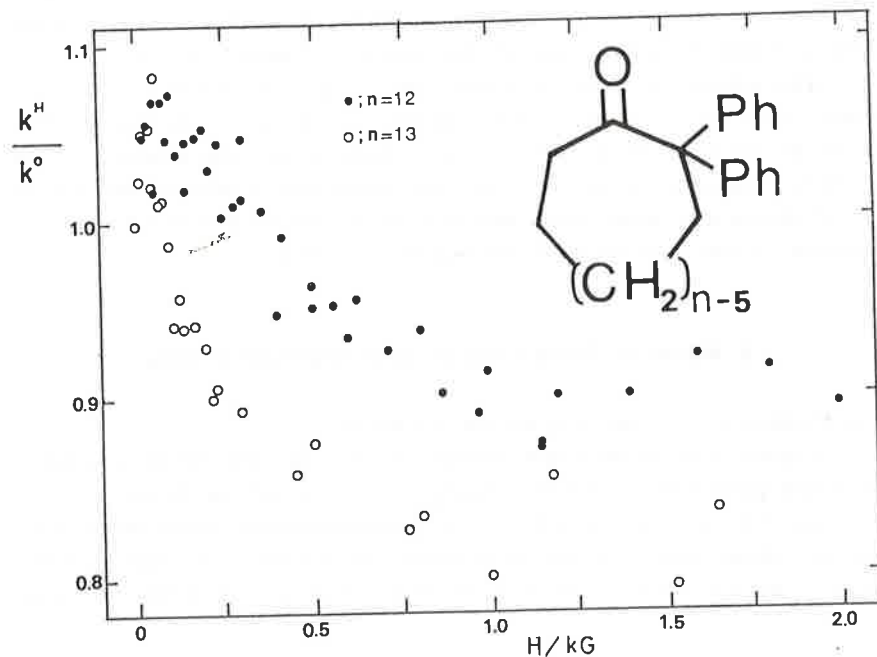
Figure 2 describes the formation of cage and escape products upon the photolysis of $\text{O}_2\text{N}-4-\text{C}_{10}\text{H}_6-1-\text{O}(\text{CH}_2)_n-\text{NH}\text{C}_6\text{H}_5$ [2,3].

Two distinct processes in the bichromophoric photochemistry for the naphthoxyl series have been identified. A cage process is an intramolecular oxidative dealkylation of alkylanilines

coupled with nitro to nitroso deoxygenation. An escape process is bimolecular photoredox reaction where the nitro to nitroso reduction in the first molecule is associated with the oxidative dealkylation of the second molecule.

An external magnetic field (0.64T) has conspicuous effects on the product distribution for photo-redox reactions. Figure 3 shows the product distribution in terms of percentages in the absence and presence of the magnetic field. At the particular chain length of 8, the cage product is dominant in the zero field, while the escape process predominates under the magnetic field. These findings clearly show that the external magnetic field can be applied for controlling reaction yields or selecting a favorable reaction pathway from others.

Figure 1 Magnetic Field Effects upon the Decay Rates



Chain Length and Magnetic Field Effects

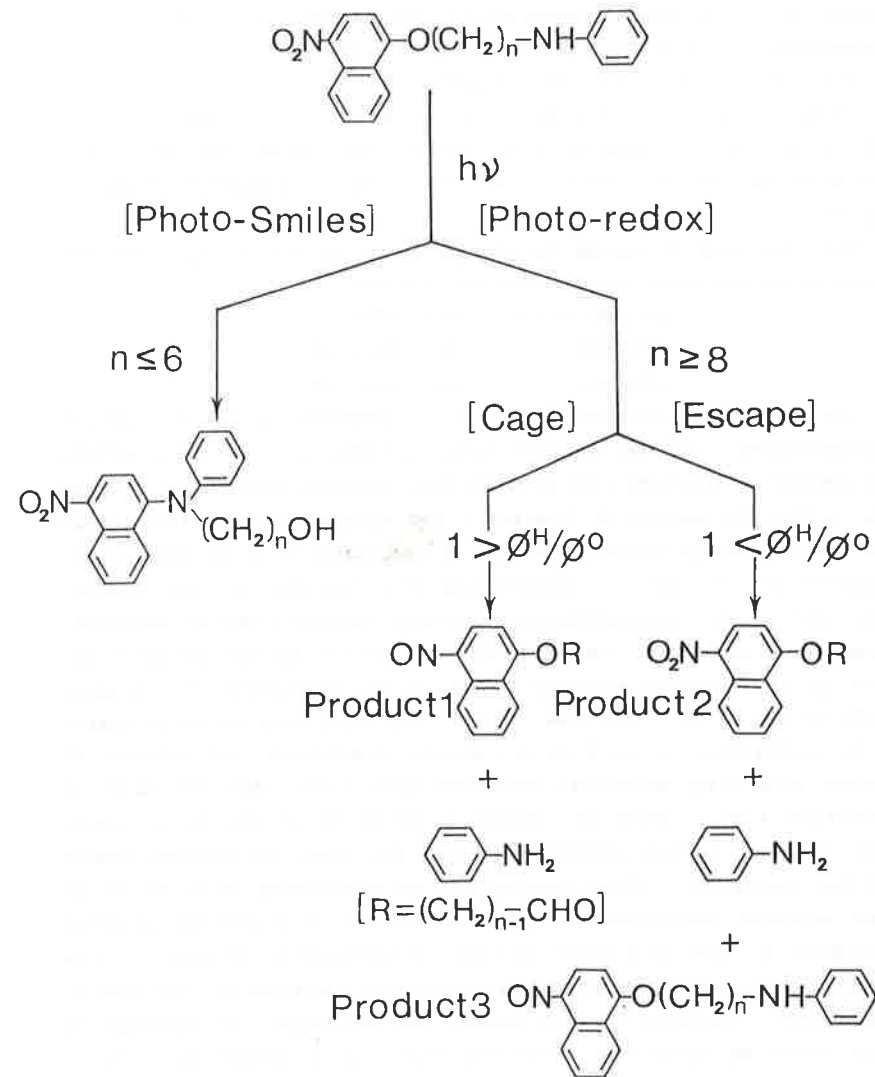


Figure 2 Chain Length and Magnetic Field Effects on Bichromphoric Photochemistry

[b] Disappearance of the Starting Species

We have observed external magnetic field effects upon disappearance of the starting compound on the steady state photolysis. The magnetic field effect parameter R has been determined by HPLC as $R = \{I(0,0) - I(t,H)\} / \{I(0,0) - I(t,0)\}$, where $I(0,0)$ denotes the peak area in the chromatogram recorded before UV-irradiation and $I(t,X)$ refer to the peak area in the chromatogram recorded after photolysis in the presence of X Tesla. The irradiation time is shown by t.

The observed R values for $C_6H_5NH-(CH_2)_{12}-O-1-C_{10}H_6-4-NO_2$ in several solvents were summarized as follows:

acetonitrile	$R=1.00 \pm 0.02$
benzene	$R=0.96 \pm 0.04$
ethanol	$R=0.79 \pm 0.09$.

The nature of the escape process depends on the period of UV-irradiation. At the earlier stage of photolysis the starting nitro-aromatic species reacts with the triplet biradicals. This leads to the formation of Product 2 and Product 3. As the steady state photolysis proceeds, Product 3 can compete with the starting material in radical scavenging process due to the higher reactivity of nitroso-aromatic molecule toward radical species. It has been observed that nitrosobenzene is preferentially attacked by hydrocarbon radicals even in the presence of a higher concentration of nitrobenzene [4]. If the starting nitro-aromatic species continues to work as a radical scavenger, the amount of consumed starting material may increase with the increase in irradiation time. When an ethanolic solution of the nitro-naphthoxyl derivative was photolyzed, the decrease in disappearance yield was observed. This finding can be explained in terms of an escape process involving Product 3. In the bimolecular process of triplet biradicals with radical scavengers, Product 3 may preferentially react as a radical quencher instead of the starting species. Therefore, this causes the decrease in consumption of the starting material. The two reaction pathways are illustrated in Figure 4.

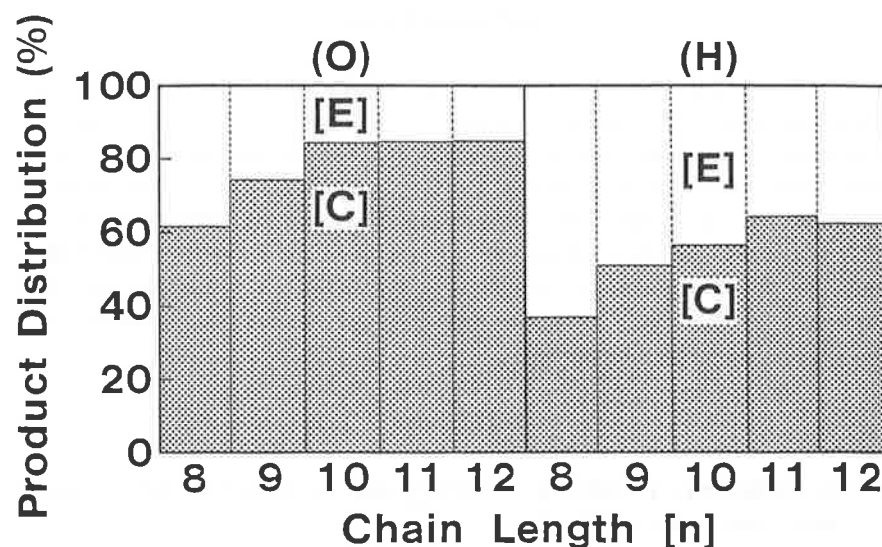


Figure 3 Magnetic Field Effects on Product Distribution

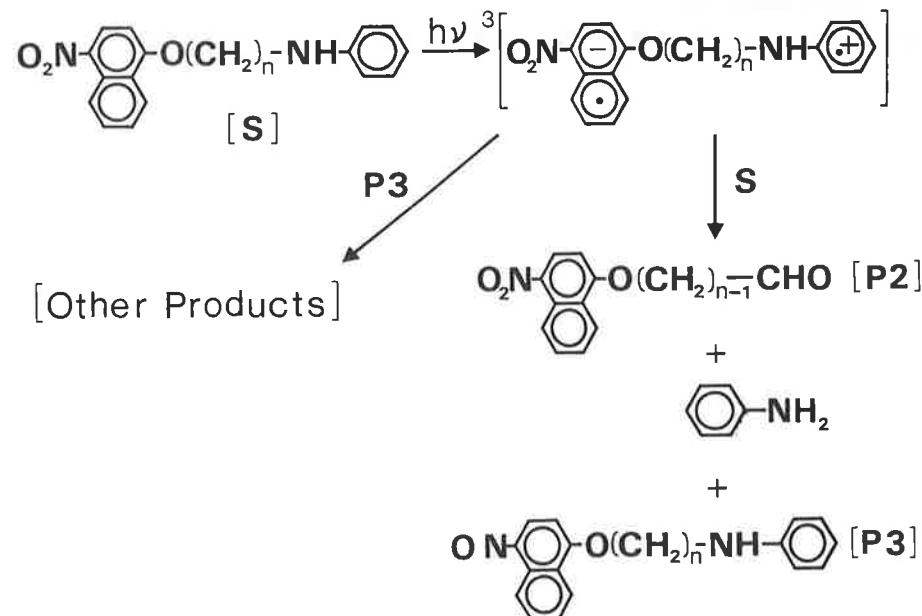


Figure 4 Bimolecular Escape Processes

4 Acknowledgement

The author thanks Professor S. Nagakura for his continuing encouragement and support. Thanks are also due to Professors Y. Tanimoto, K. Mutai, and H. Sakuragi for their valuable suggestion and discussion. This work was partly supported by a Joint Studies Program of Institute for Molecular Science on "Magnetic Field Effects upon Dynamic Behavior of Excited Species", (1985-1988) and the Grant-in-Aid for Scientific Research on Priority Area No. 02230228 (1990-1991) from the Ministry of Education, Science, and Culture, Japanese Government.

References

- [1] A. Nakajima, H. Ohya-Nishiguchi, and Y. Deguchi, Bull. Chem. Soc. Jpn., 45 (1972) 713.
- [2] R. Nakagaki, K. Mutai, M. Hiramatsu, H. Tukada, and S. Nagakura, Can. J. Chem., 66 (1988) 1989.
- [3] R. Nakagaki, K. Mutai, and S. Nagakura, Chem. Phys. Lett., 154 (1989) 581.
- [4] S.K. Wong and J.K.S. Wan, Can. J. Chem., 51 (1973) 753.

Laser Flash Photolysis Studies of the Magnetic Field Effects on the Bifunctional Chain Molecules Containing Benzophenone and N,N-Diethylaniline

Yoshifumi Tanimoto, Yoshihisa Fujiwara, Akinori Saegusa, and Michiro Hayashi
Department of Chemistry, Faculty of Science, Hiroshima University, Naka-ku, Hiroshima 730 (Japan)

Abstract

The external magnetic field effect (MFE) on the intramolecular photoreaction of the bifunctional chain molecules, α -(4-benzoyl)phenoxy- ω -(4-N,N-diethylamino)benzoyloxyalkane (BP-n-DEA, n=6-11) were studied by laser flash photolysis. The lifetimes of biradicals generated intramolecularly increase remarkably as increasing the external magnetic field. This phenomenon was explained in terms of the hyperfine and relaxation mechanism. The dependence of MFE on the number (n) of the linkers suggested that the effective degeneracy between triplet and singlet biradicals occurs at n>9.

1. Introduction

Since about a decade, using transient absorption spectroscopy, a lot of investigations of external magnetic field effect (MFE) on typical photo-induced reactions of hydrogen abstraction and electron transfer of aromatic carbonyl compounds have been continued irrespective of intra- and intermolecular reaction systems. Once radicals are generated intramolecularly, they come to behave just like an intramolecular biradical existing in equilibrium between triplet and singlet states if they could keep a proper interradical distance during the deactivation time. Recently, excellent investigations of MFE in xanthone-(CH₂)_n-xanthene (n=2-12), Ar-(CH₂)₁₂-xanthene (Ar = anthraquinone-4-carbonyloxy, 4-benzoylphenoxy, and 4-acetylphenoxy) and benzophenone-O-(CH₂)_n-O-diphenylamine (n=2-16) systems by means of laser flash photolysis have been reported by Tanimoto et al [1,2]. They have shown significant MFE by fixing the intramolecular interradical distance with an aliphatic chain such as a methylene. In addition, in the case of an ionic biradical system,

phenanthrene-(CH₂)_n-dimethylaniline has become an object for research of MFE in intramolecular electron-donar-acceptor systems [3,4]. All compounds have shown the same conclusion of large MFE which has been interpreted in terms of the hyperfine(hf)-relaxation mechanism. Nakagaki et al. [5] have also reported MFE on a photo-redox reaction of N-[{(p-nitrophenoxy)alkyl]amines, and suggested the significance of the chain length toward MFE. In this study we will explore MFE on photoreaction of bifunctional molecules, α -(4-benzoyl)phenoxy- ω -(4-N,N-diethylamino)benzoyloxyalkanes (BP-n-DEA, n=6-11) in order to make prudent consideration for the mechanism of external MFE on the biradical reaction dynamics.

2. Experimental section

Materials. The synthesis of BP-n-DEA (n=6-11) consists of the following two steps, n being the number of linkers. : Firstly, the intermediate, 1-(4-benzoyl)phenoxy-n-bromoalkane was prepared by stirring p-hydroxybenzophenone and 1,n-dibromoalkane in dimethylformamide (DMF) containing sodium hydride at room temperature. Secondly, the objective BP-n-DEA was synthesized by condensation of the intermediate and N,N-diethylaminobenzoic acid under a aqueous basic condition including tetrabutylammonium bromide. Then, BP-n-DEA was purified by means of column chromatography. The sample solution (10^{-3} - 10^{-4} M) for laser flash photolysis was deaerated by several freeze-pump-thaw cycles.

Laser flash photolysis. An N₂ laser (337 nm, fwhm=10 ns) and a xenon flash lamp equipped with a synchronously operated electro-motive shutter were used as exciting and monitoring light sources, respectively. Transient absorption spectra and the time profiles obtained with a monochromator-photomultiplier-stragescope system were analyzed by a microcomputer. Magnetic field (MF) (< 1 T) was applied with an electromagnet. The details were described elsewhere [1].

3. Results and discussion

Transient absorption spectra were measured for the purpose of recognizing the absorption band of radical intermediates directly concerned with MFE. Figure 1 shows the typical transient absorption spectra of BP-11-DEA in DMF solvent obtained

upon 337 nm photoexcitation at room temperature. Taking account of spectral data so far reported in literatures, both two remarkable absorption bands (λ_{max} 350 and 560 nm) are ascribed to BP neutral ketyl radical, exhibiting that a hydrogen abstraction reaction of the lowest triplet state BP from DEA leading to a biradical takes place, though the absorption spectrum of the aliphatic DEA neutral radical, probably located at an ethyl moiety, is not apparently obtained in the uv and visible wavelength region measured from 350 to 700 nm in the present stage. Here, let us consider the reaction scheme (see Reaction Scheme). Since there is no absorption of BP at exciting wavelength (337 nm), DEA is firstly excited. Secondly, it is conceivable that the triplet BP is yielded within a laser pulse as a result of the triplet-triplet energy transfer from the triplet DEA. The generated triplet BP gives rise to hydrogen abstraction from ethyl groups leading the triplet intramolecular biradical because the fact that no triplet-triplet absorption band of BP is observed in a few nanosecond time scale suggests this abstraction comes about intramolecularly. The intermolecular reaction rate constant controlled by diffusion is estimated at 10^{-5} - 10^{-7} s⁻¹ from low concentration of the samples and that with a DMF solvent might be also very small. After triplet-to-singlet intersystem

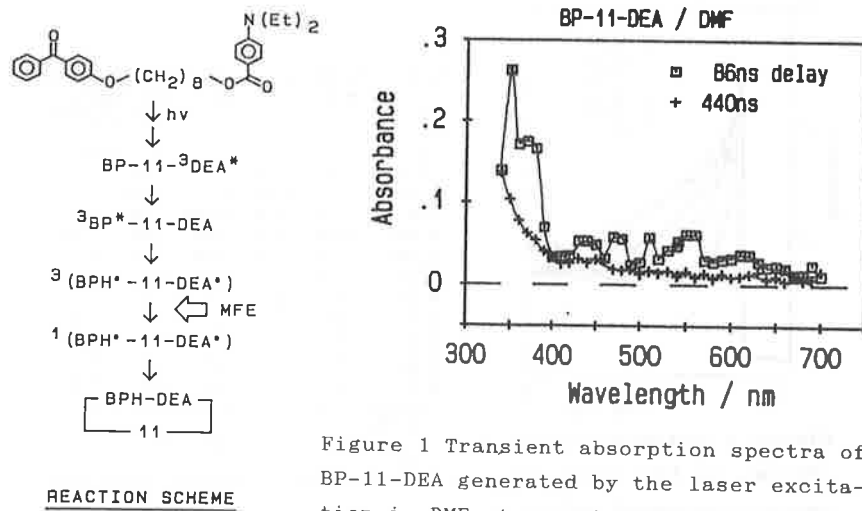


Figure 1 Transient absorption spectra of BP-11-DEA generated by the laser excitation in DMF at room temperature.

crossing (ISC), the singlet biradical mainly forms a final cyclic product as shown in Reaction Scheme. Time profiles of the absorption bands of BP ketyl radical rise immediately after laser excitation and decay within 1 μ s at zero MF, indicating that the hydrogen abstraction reaction takes place rapidly in a nanosecond time domain as described precedently and the resulting biradical is likely to deactivate relatively fast through reactions such as an intramolecular recombination reaction. No detectable absorption band of the other neutral and/or ionic radicals is observed may predict no electron transfer in this system compared with benzophenone-diphenylamine chain linked system reported previously [2].

Figure 2 depicts decay curves of transient absorption (360 nm) of BP ketyl radical at several MFs. Each curve consists of two components of relatively short and extremely long lifetimes, as the most clearly at zero MF. Judging from the fact of the unchanged absorption spectra during appearance of the former component just since laser excitation, the short lifetime seems to be definitely responsible for the biradical, while the latter is tentatively ascribed to a permanent by-product due to the free radicals diffused because the absorption spectrum ($\lambda_{\text{max}} < 350$ nm) at 440 ns delay time is distinctly different from that of BP ketyl radical. The lifetimes in a series of chain length (n) of

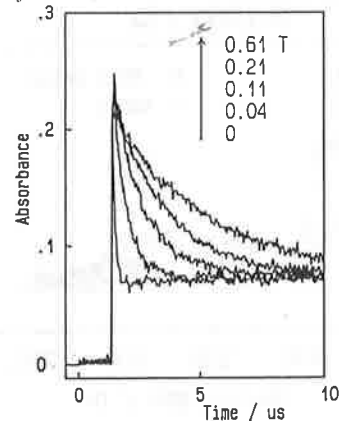


Figure 2 Magnetic field effects on the transient absorption decay curves monitored at 360 nm.

Table Lifetime (μ s) of the Biradicals Generated from BP-n-DEA in DMF at Room Temperature

B (T)	n				
	6	7	9	11	13
0.0	0.62	0.14	0.084	0.084	0.12
0.036	0.89	0.61	0.48	0.56	0.62
0.070	1.3	0.70	0.66	0.80	1.1
0.11	1.7	1.0	0.88	1.1	1.1
0.14	2.2	1.2	1.1	1.4	1.9
0.21	2.8	1.6	1.6	2.1	2.4
0.36	3.2	2.4	2.3	2.7	2.6
0.48	3.3	2.8	2.5	3.0	3.1
0.58	3.7	2.9	2.8	3.5	3.8
$\tau(0.58)$					
$\tau(0)$					

biradicals were therefore calculated after subtracting a long lifetime component, as listed in Table. Thus, the quantum efficiency of $T \rightarrow S$ ISC process, affected by MF, of the biradical was investigated using the initial absorption decay behavior. The other absorption bands in a full range measured shows a single-exponential decay as well and similar MFE to shown in Figure 2. It is noteworthy that the biradical lifetime increases anomalously along with increasing the magnitude of MF, though the rise is constantly fast regardless of MF.

Figure 3 shows conspicuous MFE in the biradical lifetimes of all compounds as a function of the magnitude of MF (0-0.58 T). The magnitude of maximum MFE surprisingly reaches up to more than 40 times in n=11 at 0.58 T. The mechanism of MFE can be interpreted in terms of the hf-relaxation mechanism. According to hf-relaxation mechanism, hf-induced triplet-to-singlet ISC occurs among nearly degenerated states at zero MF. The ISC rate is decelerated by Zeeman splitting of triplet sublevels. In high MFs, on the other hand, MFE is interpreted in accordance with that relaxation process from T_+ and T_- levels to T_0 in fast dynamic equilibrium with S is hindered because of the Zeeman splitting. As increasing MF, Tanimoto et al. [2] have reported temporary decrease of the biradical lifetime in benzophenone-O-

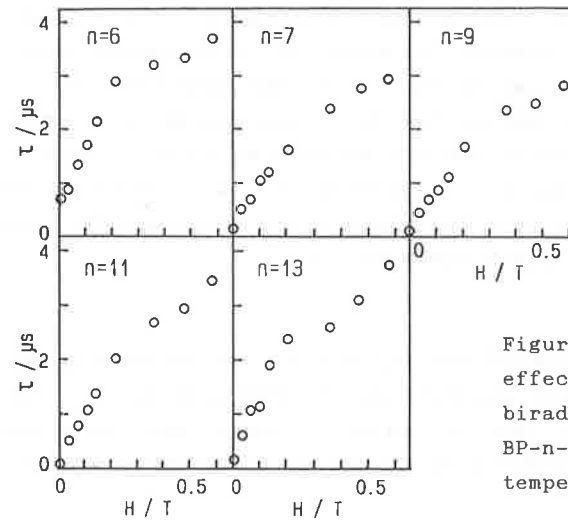


Figure 3 Magnetic field effects on the lifetimes of biradicals generated from BP-n-DEA in DMF at room temperature.

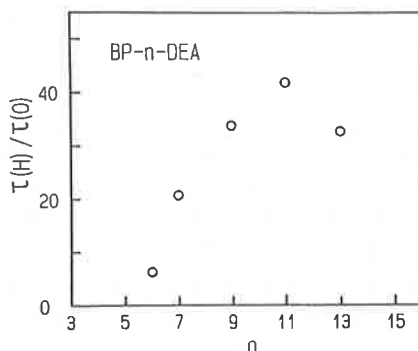


Figure 4 Chain length (n) dependence of the lifetime ratio $\tau(H)/\tau(0)$ of the biradicals generated from BP- n -DEA in the presence and absence of a magnetic field ($H=0.58$ T).

$(\text{CH}_2)_2\text{-O-diphenylamine}$ compound, suggesting T_{-S} level crossing. However, such a dip is not obtained in any present chain molecules shown in Figure 3.

The chain length (n) dependence of the biradical lifetime ratio ($\tau(H)/\tau(0)$) in the presence ($H=0.58$ T) and absence of MF is given in Figure 4. It makes clear the dependence of MFE on the chain number. It's noteworthy that the magnitude of MFE is increasing together with n , and saturating at around $n=11$. Since the triplet-singlet energy gap of biradicals is closely related to electron exchange interaction ($2J(r)=A\exp(-\alpha r)$) dependent on the interradical distance (r), the longer the interradical distance is, the smaller the splitting energy is and the more easily the degeneracy of the two states can occur. Hence, the MFE on lifetimes can be interpreted to have tendency to increase in proportion to the chain length (n) and saturate when $n>11$ where $2J(r)$ may be nearly equal to zero.

4. Conclusion

This study has introduced the significant MFE on the typical photoreaction of hydrogen abstraction of benzophenone. The maximum magnitude of the MFE is extremely large and therefore the good reaction yield induced by MF may be expected considera-

bly. Moreover, the investigation about dependence of MFE on the chain length linking each terminal reaction chromophores has predicted the possibility of controlling reactions strongly associated with the triplet-singlet degeneracy. The results obtained in this study is in good agreement with those of xanthone-xanthene ($n>10$), benzophenone-diphenylamine ($n>8$) and phenanthrene-dimethylaniline ($n>10$) linked systems [1-4] though no MF dependence attributable to the T_{-S} level crossing was measured in contrast to a benzophenone-diphenylamine system. This discrepancy might be responsible for the difference in the structure of the respective terminal groups (-O- or -COO-) of the chain.

Acknowledgement

This work was supported by Grant-in-Aid for Scientific Research from the Ministry of Education, Science and Culture.

References

- [1] Y. Tanimoto et al., Bull. Chem. Soc. Jpn., 62, 3923 (1989).
- [2] Y. Tanimoto et al., Bull. Chem. Soc. Jpn., 63, 1342 (1990).
- [3] Y. Tanimoto et al., Chem. Phys. Lett., 136, 42 (1987).
- [4] Y. Tanimoto et al., J. Phys. Chem., 93, 3586 (1989).
- [5] R. Nakagaki et al., Chem. Phys. Lett., 134, 171 (1987).

Magnetic Field Effects on Photoinduced Electron-Transfer and the Succeeding Processes in Phenothiazine-Viologen Linked Compounds Incorporated into Cyclodextrin

Taku Matsuo, Hiroshi Nakamura, and Hiroaki Yonemura

Department of Chemical Science and Technology, Faculty of Engineering, Kyushu University, Hakozaki, Fukuoka 812(Japan)

Abstract

Laser-induced electron-transfer in phenothiazine-viologen linked compounds afforded highly active radical pairs, when the linked compounds were incorporated into the cavity of either α - or β -cyclodextrin. Remarkable magnetic field effects on the radical decay rate were observed, and it was ascribed to Zeeman splitting of triplet sublevels of the radical pair. Spectroscopic evidences were provided to indicate that the spacer between phenothiazine and viologen units is in extended conformations, and the magnetic field effect was explained in terms of the relaxation mechanism. In zero-magnetic field, the radical decay rate was appreciably reduced with decrease of the spacer chain length. Increased singlet-triplet energy separation in the linked compounds with shorter spacer was suggested to be responsible for the reduced decay rate.

1. Introduction

Photosynthesis in the nature is initiated by photoinduced electron-transfer to afford a geminate radical pair in thylakoid membranes. Dynamic behaviors of various radical pairs in solutions have vividly been elucidated by virtue of magnetic field effects on the reaction kinetics [1]. In contrast to the mobile radical pairs in solutions, molecular motions of the radical fragments in thylakoid membranes are strongly hindered due to extremely high viscosity of the surrounding microenvironment. The restricted motions of the radical pair should affect reaction kinetics as revealed by investigation of the magnetic field effects. Model systems of the immobilized radical pairs could be obtained, if the radical components are bound to each other either by covalent bonding or by compartmentalization into relatively rigid matrices such as organized molecular assemblies. In fact, porphyrin-viologen linked compounds afforded photogenerated geminate radical pairs, and the radical decay rates were remarkably affected by external magnetic fields as expected [2,3]. In addition, the radical decay rate at zero magnetic field was found to increase with the length of spacer between porphyrin and viologen moieties [4]. These observations were explained on the basis of

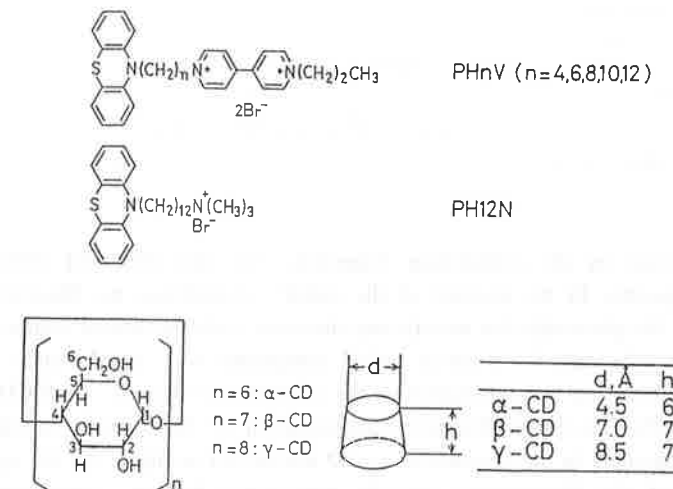
Zeeman splitting of triplet sublevels of the radical pairs and variation of the triplet-singlet energy separation with the interradical distance [2].

Donor-acceptor linked compounds, as represented by porphyrin-viologen pairs, are useful model systems for the study of photoreaction center in artificial photosynthesis. However, the studies have always been plagued with the flexibility of the spacer chain. A novel method to solve the problem was developed by complexing the donor-acceptor linked compound with cyclodextrins (abbreviated to CD) [5,6]. The study has been extended to cover wider range of donor-acceptor linked compounds with various spacer chain-lengths. In the present paper, photodynamic behaviors of phenothiazine-viologen linked compounds complexed with CD are investigated.

2. Experimental section

The phenothiazine-viologen linked compounds, as well as the amphiphilic phenothiazine, were synthesized according to standard procedures. Concentration of the phenothiazine unit was kept to 0.1 mM in all experiments. Cyclodextrin concentration was 2 mM in each case.

For laser photolysis, solutions containing the linked compound in a quartz cell (3.5 cm optical path length) with water jacket (25 °C) was deoxygenated by passing argon streams. The cells were placed in the gap of an electromagnet with 8 cm polepieces, and irradiated with Lambda Physik EMG-100 series XeF excimer laser (351 nm, 10 Hz, 5 mJ/pulse) or with a Quantel YG-571-10 Nd-YAG laser (355 nm, 10 Hz, 60 mJ/pulse).



3. Results and discussion

3-1. Structural Characterization of Phenothiazine-Viologen Linked Compounds Complexed with CD

Phenothiazine-viologen linked compounds were examined to elucidate the effect of spacer chain length on the photodynamic behaviors. An amphiphilic phenothiazine derivative with a trimethyl ammonium group was studied as a reference compound. Three types of CD were used to study the effect of pore size on the complexing behaviors of the phenothiazine-viologen linked compounds. Photogenerated radical pairs could be observed when either α - or β -CD was combined with phenothiazine-viologen pair separated by a relatively long spacer ($n=8$ or above). Proton NMR spectra of the corresponding solutions revealed relevant factors, which control complexation between the linked compound and CD. When D_2O solution contained phenothiazine-viologen linked compound with the relatively longer spacer, distinct signals due to phenothiazine and viologen moieties in the complexed species were observed apart from the free species. Equilibrium constants for the stable 1:1 complexes, as evaluated from the NMR signals, are listed in Table 1. As to γ -CD, the NMR spectra indicated that the complex and the free species are exchanging rapidly in NMR time scale. Even with α - or β -CD, no stable complex was found either if the linking spacer was short: $n=4$ and 6 for α -CD, and $n=4, 6$, and 8 for β -CD.

Table 1.
Equilibrium constants for the stable 1:1 complex between the phenothiazine-viologen linked compound and α -CD as evaluated from NMR spectra

Compound	PH4V	PH6V	PH8V	PH10V	PH12V
$K(M^{-1})$	---	---	2.2×10^3	4.5×10^4	4.4×10^4

The difference in the complexing behaviors was also observed with the fluorescence spectra. In the absence of the stable complexes, no fluorescence emission from the phenothiazine moiety was observed with the linked compounds in the aqueous solutions. For a given linked compound with appropriately long spacer, the fluorescence was intensified on the addition of either α - or β -CD but not with γ -CD [5]. The effects of spacer chain length on the fluorescence spectra of the linked compounds in the presence of α -CD are shown in fig. 1. As the spacer length increased, the fluorescence intensity approached that of corresponding

emission from the reference compound without viologen unit. It is clear that the singlet excited state of the linked compound is easily quenched by the interaction with the linked viologen unit in the aqueous solutions. Formation of stable complexes with CDs is suggested to suppress the quenching process. The suggestion could also be confirmed by the measurement of fluorescence lifetime: PH12N(0.1 mM)- α -CD(2 mM), 2.3 ns; PH12V (0.1 mM)- α -CD(2 mM), 1.6 ns; PH10V(0.1 mM)- α -CD(2 mM), 1.2 ns; and PH8V (0.1 mM)- α -CD(2 mM), 0.7 ns.

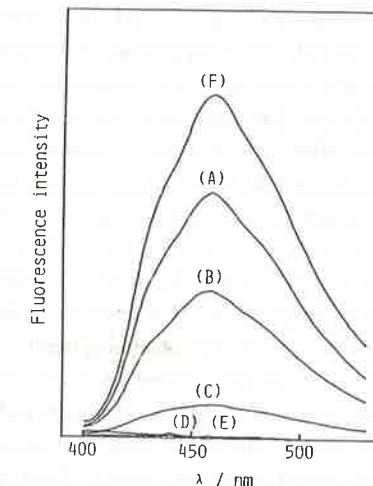


Fig. 1. Effects of α -CD (2 mM) on the fluorescence intensity of the phenothiazine-viologen linked compound as excited at 320 nm (25 °C): (A) PH12V, (B) PH10V, (C) PH8V, (D) PH6V, and (E) PH4V. The spectrum for PH12N is included as the reference (F).

The above spectroscopic observations are explained on the basis of a CD complex structure as shown in fig. 2. The suggested structure was further confirmed by analyzing NOESY spectra of the complex obtained with a 400 MHz NMR spectrometer.

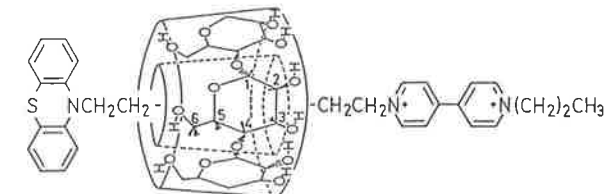


Fig. 2. The suggested structure of PH12V- α -CD complex.

3-2. Radical Pair Generation and the Decay on Laser Excitation of the Stable CD Complexes

Laser excitation of the phenothiazine-viologen linked compounds afforded a pair of viologen cation radical (λ_{max} , 603 nm) and phenothiazine cation radical (λ_{max} , 520 nm)[5], only if the linked compound formed stable CD complexes. In the case of α -CD complexes, the transient absorption due to the viologen cation radical showed sharp decrease at first and turned into extremely slow-decaying, second component as shown in fig. 3 for three different linked compounds in the absence of magnetic field. The time profile of the slow-decaying, second component indicates that the radicals are disappearing via bimolecular processes in this time domain. The quickly decaying, first component followed first-order reaction kinetics, which indicates that intramolecular process is responsible for disappearance of the viologen cation radical. Rate constants (k_d) for the first order decay process could be evaluated from the decay curves after subtracting the contribution of the slow-decaying, second component. It is clearly observed that intramolecular decay process in PH8V is much slower than those in the linked compounds with longer spacer (PH10V and PH12V). The effect of spacer chain length on the k_d -values at zero magnetic field is extremely interesting. Since the spacer chain is in extended conformation, the observed trend is most likely caused by variation of the triplet-singlet energy separation ($-2J$) with the interradical distance as pointed out in the case of porphyrin-viologen linked compounds [2] (fig.5). In other words, the results suggested that the increased triplet-singlet energy separation ($-2J$) for the linked compound with a short spacer is responsible to the decrease in k_d -value at zero magnetic field. For large triplet-singlet separation, either hyperfine-coupling or Δg in the radical-pair may not provide efficient means for enhancing intersystem-crossing processes.

One should also notice that the yield of viologen cation radical increases with the increase of the spacer chain length (fig. 3). This is in good agreement with the trend observed with the fluorescence intensity in fig. 1. The increment of fluorescence intensity, however, is not linearly correlated to that of viologen cation-radical concentration.

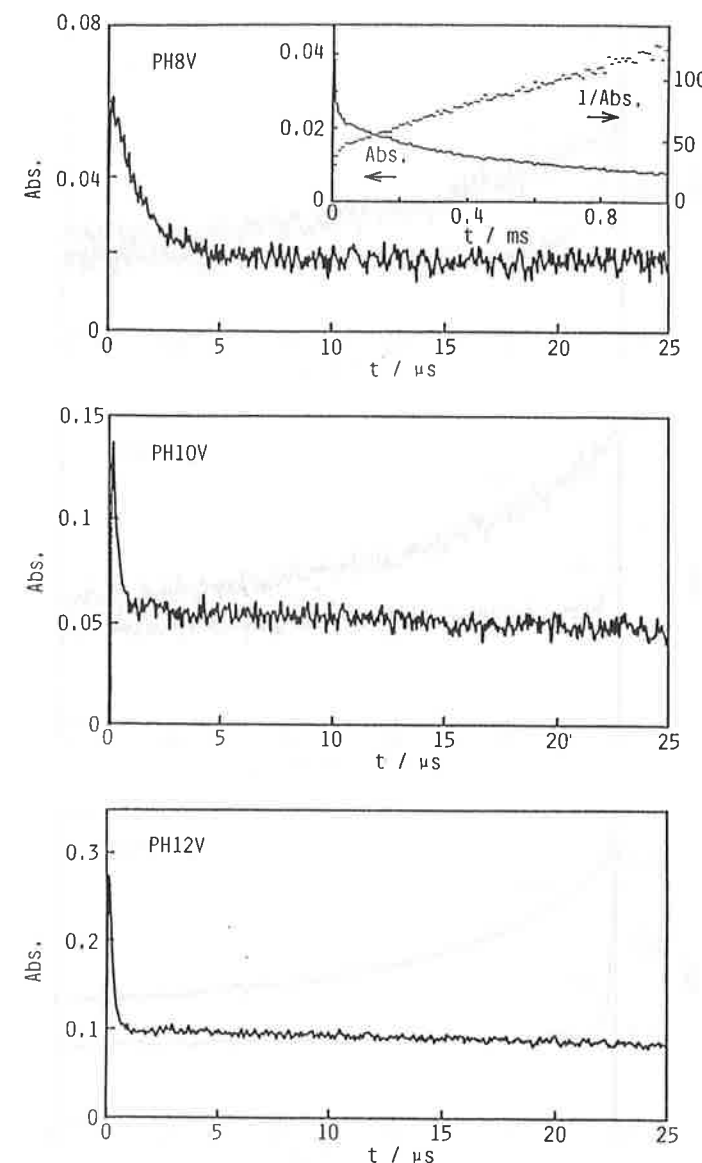


Fig. 3. Decay profiles of transient absorption due to viologen cation radical detected at 603 nm for PH8V, PH10V, and PH12V. The time profile of the slow-decaying, second component for PH8V is shown in the inset at the top.

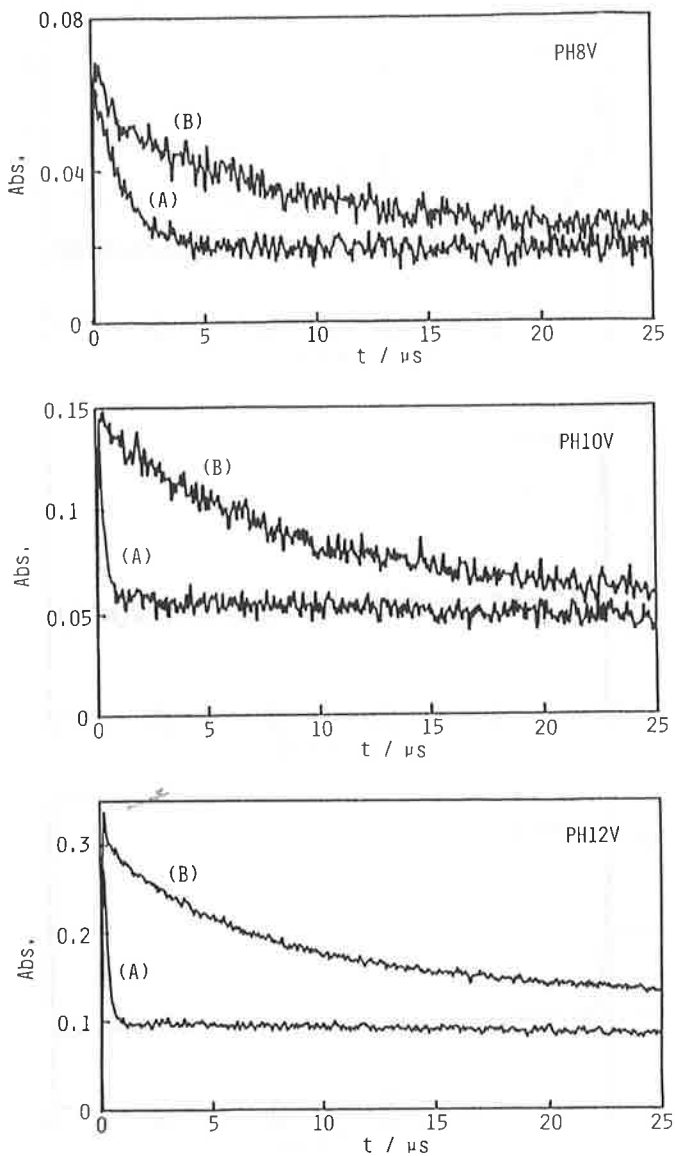


Fig. 4. EMFES on the transient absorption at 603 nm on laser excitation of the linked compounds complexed with α -CD: (A) zero magnetic field, and (B) 1 T.

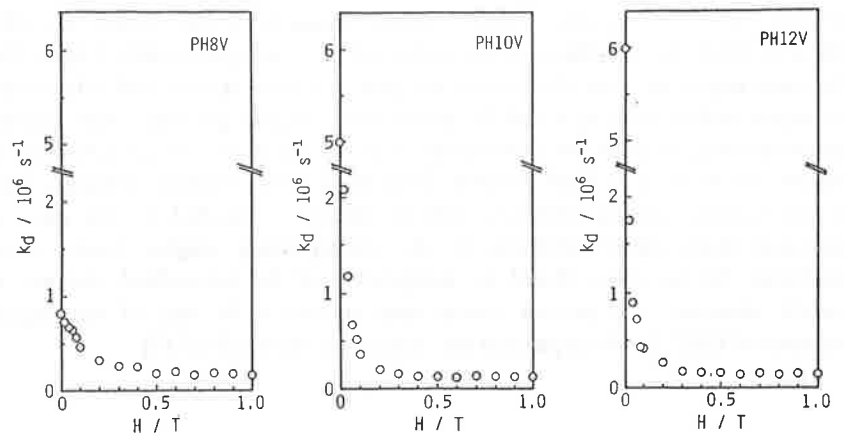


Fig. 5. EMFES on the decay rate constant (k_d) for the short-living, first component on laser excitation of the linked compound.

The rapid decay of the radical at the initial part of the transient absorption was remarkably suppressed in the presence of external magnetic fields. The external magnetic field effects (abbreviated to EMFES) for the three phenothiazine-viologen linked compounds (0.1 mM) in the presence of α -CD (2 mM) are shown in fig. 4. In each case, the radical concentration just after the laser pulse was not affected but the decay rate was reduced considerably. The decay rate constant (k_d) for the short-living, first component decreased with the increase of external magnetic fields and reached a plateau region at above 0.3 T (fig. 5). In the absence of external magnetic field, the k_d -value for the linked compound with the shortest spacer (PH8V) is smaller than those for the corresponding compound with longer spacer (either PH10V or PH12V) by an order of magnitude. Consequently, EMFES are more pronounced in the linked compounds with longer spacers. The k_d -values at the plateau region for the three linked compounds agree with each other in spite of the difference in the spacer chain-length. All of these characteristics in EMFES are exactly the same as observed with porphyrin-viologen linked compounds [4]. Since the spacer chains are forced to be in extended conformations in the core of α -CD, the data in fig. 5 are assured to represent general example of interradical

distance effects on k_d -values under various magnetic fields. Under the high magnetic fields, the k_d -values became independent of the spacer chain length. The preceding papers have established that the photogenerated species under discussion are triplet radical pairs [2,4 and 5]. Intersystem crossing processes thus become rate-determining step for the radical pairs to decay via reverse electron-transfer as indicated by k_4 in fig. 6. High magnetic fields induce large Zeeman splitting so that the intersystem crossing processes will be simply controlled by the rates of relaxation from triplet sublevels to the corresponding singlet. Under these conditions, the k_d -values should be independent of the interradical distance as actually observed. The present system thus appears to be one of the typical examples of EMFES, which proceed via "Relaxation Mechanism" [7].

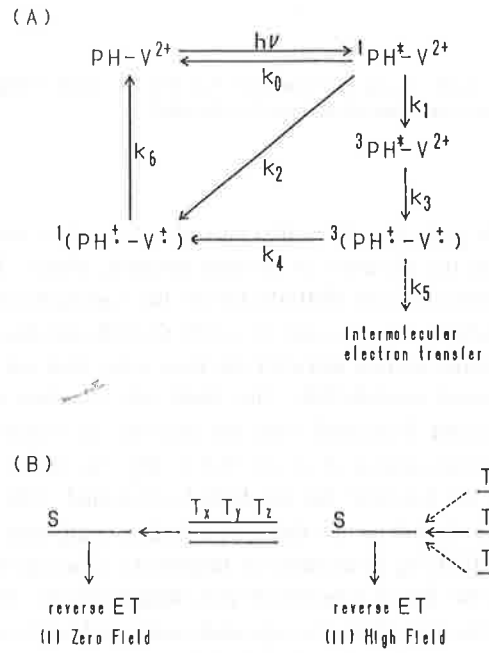


Fig.6. Schematic presentation of phenomena relevant to EMFES on the decay rate of geminate radical pair as obtained by laser excitation of the linked compounds: (A) photoinduced electron-transfer and the succeeding process, and (B) two extreme modes of radical decay via intersystem crossing at degenerated S-T levels

3-3 Contribution of Intermolecular Electron-Transfer Process as Revealed by Inspection of EMFES

In the case of α -CD complexes of the linked compounds, EMFES on the quickly-decaying, first component were accompanied by the increase of long-living, second component as shown in fig. 4. The long-living component decayed via second-order reaction kinetics. Rather different phenomena were observed with the β -CD complexes. The quickly-decaying, first components were affected by EMFES in exactly the same manner as in the case of α -CD complexes. The long-living, second component, however, did not increase at all even at 1 T (fig.7).

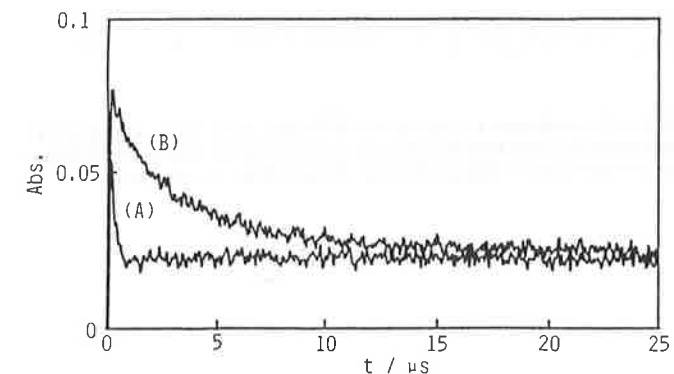


Fig. 7. EMFES on the transient absorption at 603 nm on laser excitation of PH12V complexed with β -CD: (A) zero magnetic field, and (B) 1 T.

Spectroscopic analyses indicated that phenothiazine moiety of the linked compounds are capable of complexing with another β -CD with an equilibrium constant of an order of 10^3 M^{-1} . On the other hand, no 1:2 complex was observed with α -CD. The reason may be easily understood as due to the difference in the pore size of the two CDs: phenothiazine unit can be incorporated into β -CD pore (7.0 \AA) but not into α -CD (4.5 \AA). On the basis of these observations, the long-living, second components observed with the linked compound- α -CD complex are ascribed to the contribution of intermolecular electron-transfer reaction as shown in fig. 8. It should be noticed that the intermolecular electron-transfer becomes important if the lifetime of the linked radical pair is extended by EMFES up to a few μs time domain. In the case of β -CD complexes, however, electron-transfer to the phenothiazine cation radical encapsulated by β -CD from the

neighboring linked-compound seems to be too slow to take place in this time-domain.

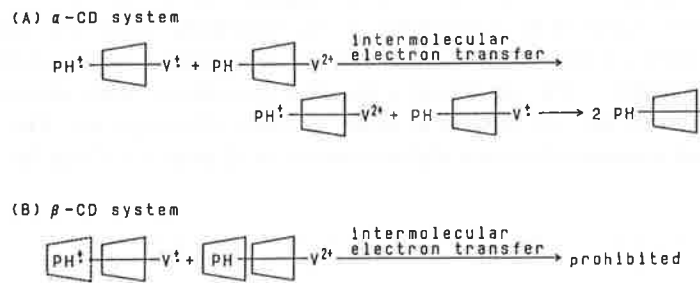


Fig. 8. Reaction schemes to explain the difference between α - and β -CD in intermolecular electron transfer processes involving photogenerated linked radical pair and unexcited phenothiazine-viologen linked compounds.

References

- [1] H. Hayashi in J.F. Rabek (ed.) Photochemistry and Photophysics, CRC Press, Boca Raton, 1990, Vol. 1, p.59. U.E. Steiner and T. Ulrich, Chem. Rev. 89 (1989) 51.
- [2] A. Uehata, H. Nakamura, S. Usui and T. Matsuo, J. Phys. Chem. 93 (1989) 8197.
- [3] V.Y. Shafirovich, E.E. Batova and P.P. Levin, Chem. Phys. Letters 172 (1990) 10.
- [4] H. Nakamura, A. Uehata, A. Motonaga, T. Ogata and T. Matsuo, Chem. Letters (1987) 543.
- [5] H. Yonemura, H. Nakamura and T. Matsuo, Chem. Phys. Letters 155 (1989) 157.
- [6] H. Yonemura, H. Saito, S. Matsushima, H. Nakamura and T. Matsuo, Tetrahedron Letters 30 (1989) 3143.
- [7] H. Hayashi and S. Nagakura, Bull. Chem. Soc. Jpn. 57 (1984) 322.

4. Concluding Remarks

The remarkable EMFES on the k_d -values for photogenerated radical pairs of phenothiazine-viologen linked compounds are ascribed to Zeeman splitting of triplet sublevels in the radical pairs just as in the case of porphyrin-viologen linked compounds. By virtue of tight complexation with either α - or β -CD, phenothiazine-viologen linked compounds with extended spacer chain afforded novel means to study the effect of interradical distance on the k_d -values. In future, elucidating in details the role of spin interaction in the radical pair complexed with CD may lead to bring a break through in the system design and reation control of charge separation in artifical photosynthesis.

Acknowledgment

The authors are grateful to Center of Advanced Instrumental Analysis, Kyushu University, and Mr. Hide Saito for the measurement of ^1H NMR by a 400 MHz spectrometer. Financial support from the Ministry of education, Science and Culture (Grants in Aid for Scientific Research No.01603023, No.02203119 and No.02453080) is deeply appreciated.

Paramagnetic Ion Quenching of the Magnetic Field Effect in the Photochemical Reaction of Naphthoquinone in Micelles

Yoshio Sakaguchi and Hisaharu Hayashi

Molecular Photochemistry Laboratory, The Institute of Physical and Chemical Research, Wako, Saitama 351-01 (Japan)

Abstract

By means of the time-resolved ESR and transient optical absorption spectroscopies, the effect of paramagnetic transition metal ions on the photochemical reaction of naphthoquinone in micelles was investigated in the absence and presence of external magnetic fields below 1 T, and was compared with that of lanthanoid ions. The paramagnetic transition metal ions accelerated the recombination of the generated radical pair. The enhancement of the disappearance of the CIDEP signals of the component radicals by the paramagnetic lanthanoid and transition metal ions shows that the relaxation of the electron spin of the component radical in a pair is a key process of the magnetic field effect on the reactions in micellar solutions or those of long-lived radical pairs, which is a strong evidence for "relaxation mechanism" proposed by us.

1. Introduction

The external magnetic field effect on chemical reactions is one of the most dramatic presentations of the magnetic interactions between chemical species. Although the magnetic interactions of paramagnetic and diamagnetic species are much smaller in magnitude than their electric ones, even an ordinary magnetic field below 1.5 T can have great influence on the rate and yield of various reactions through radical pairs and biradicals [1-3]. Applying micellar solutions as reaction environments, we observed the magnetic field effects on the reaction rates of benzophenone and naphthoquinone derivatives [4-6]. The induced changes were much larger than those in homogeneous solutions. These reactions also showed clear magnetic isotope effects, that is induced by the magnetic interaction among the electron spins and nuclear spins [7]. We extended the studies of magnetic-field and magnetic-isotope effects under magnetic fields larger than the magnitude of the hyperfine interaction of the component radicals (up to 1.34 T), where we found the absence of the saturation in the magnetically induced changes [8, 9]. This observation contradicted with the established mechanisms such as hyperfine mechanism and Δg mechanism [1-3, 10]. We explained this anomalous phenomenon by

"relaxation mechanism" which introduces the magnetic field dependence of the relaxation of the electron spins of radical pairs [8, 11].

To clarify the importance of the electron spin relaxation, we tried to measure the dynamic behavior of the electron spins of the radicals with a time resolved ESR (TRESR) technique [12]. We exhibited the correspondence between the relaxation rate of the electron spin polarization observed by TRESR and the recombination rate of the radical pairs observed by TROA at the magnetic field (0.34 T) of the X-band ESR spectrometer. The following two acceleration experiments confirmed the relaxation mechanism: We investigated the effect of paramagnetic lanthanoid ions [13], and Okazaki *et al.* investigated the effect of the microwave resonant to the ESR transitions of the component radicals [14]. Both experiments enhanced the recombination of triplet radical pairs by scrambling the electron spins of the pairs as the relaxation mechanism predicts.

Our experiments using lanthanoid ions were rather simple and easy to apply to other systems. Turro *et al.* [15], Basu *et al.* [16], and recently Tanimoto *et al.* [17] investigated the effects of lanthanoid ions. In the present paper [18], we investigate the effects of another series of paramagnetic metal ions, transition metal ions, on the magnetic field effects of naphthoquinone in micelles and compare these results with those of lanthanoid ions [13] to elucidate the mechanism of electron spin relaxation by these ions.

2. Experimental

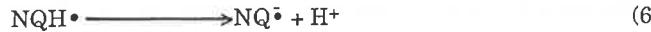
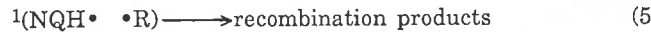
1,4-Naphthoquinone (NQ) was repeatedly recrystallized from petroleum benzine. Sodium dodecyl sulfate (SDS, Wako) was purified by repeated recrystallization from ethanol-methanol mixture. Cetyltrimethylammonium chloride (CTAC, Kodak) and Brij 35 (TCI) were used as received. Water was deionized and distilled. All metal chlorides were purchased commercially and were used as received. $K_3Fe(CN)_6$ (Wako) was used as received.

For the TROA experiments, samples were prepared under nitrogen atmosphere, filled in quartz cells, and closed with rubber septa. Laser photolysis measurements were performed at room temperature by using the fourth harmonic (266nm, pulse width 5ns) of a Quanta-Ray DCR-1 or DCR-11 Nd:YAG laser as the exciting light source. The laser photolysis apparatus and measuring system were similar to those published elsewhere [9, 19]. Magnetic fields were provided by a Mitsubishi 6MA-EM1275A electromagnet. The strength of the magnetic field was measured by an F. W. Bell 9200 Gaussmeter. The lowest magnetic field generated by cancelling the residual field of the electromagnet was less than 2×10^{-4} T. Hereafter the experiments under the lowest magnetic field are denoted as those in the absence of a magnetic field.

For the TRESR experiments, samples were bubbled with nitrogen. The measurements were performed at room temperature by using a Molelectron UV24 nitrogen gas laser (337.1 nm) as the exciting light source. The experimental apparatus and measuring system were similar to those published elsewhere [20, 21].

3. Results and discussion

In the previous papers, we showed that the photochemical reactions of NQ in micelles occurred as follows [9, 20];



The formation of naphthoquinone radical ($\text{NQH}\cdot$) and naphthoquinone anion ($\text{NQ}\cdot^-$) is identified by the TROA method [9]. The alkyl radicals ($\cdot \text{R}$) formed from micellar molecules, $\text{NQH}\cdot$, and radical pair of them are identified by the TRESR method [12]. The process (3), which corresponds to the triplet-singlet (TS) conversion of the generated radical pair is sensitive to external magnetic fields and paramagnetic ions through the relaxation mechanism [2, 3, 8, 11].

Figures 1 and 2 show the decay of TROA of $\text{NQH}\cdot$ at 380 nm for SDS (sodium dodecyl sulfate, 80mM) micellar solutions of NQ (0.4mM) containing a metal ion, Sc^{3+} and Mn^{2+} (0~1mM), respectively [18]. At first, let us consider the results without metal ions. The time profile of the transient optical absorbance, $I(t)$, is composed of a fast decay component and a constant (or a very slow decay) one in the observed time scale (less than 8 μs). This nearly constant component corresponds to the escaping radical, which decays with a rate constant smaller than $3 \times 10^4 \text{ s}^{-1}$. The decaying part corresponds to the recombination process of the generated radical pair, reactions (3)-(5). In the presence of a magnetic field, the decay becomes slower and the constant component becomes larger [9]. This observation reflects the inhibition of the recombination of the radical pair by the external magnetic field and the subsequent enhancement of the escaping radicals by it. We also measured the decay of the CIDEP signals of $\text{NQH}\cdot$ and $\cdot \text{R}$ and found that the CIDEP decay agreed well with the decay of the TROA signal, which indicates that both decay curves correspond to the electron spin relaxation of the generated radical pair. Therefore, these magnetic field effects can successfully be interpreted by the relaxation mechanism [11].

To clarify the importance of the electron spin relaxation in the magnetic field of chemical reactions, we investigated the effect of paramagnetic lanthanoid ions

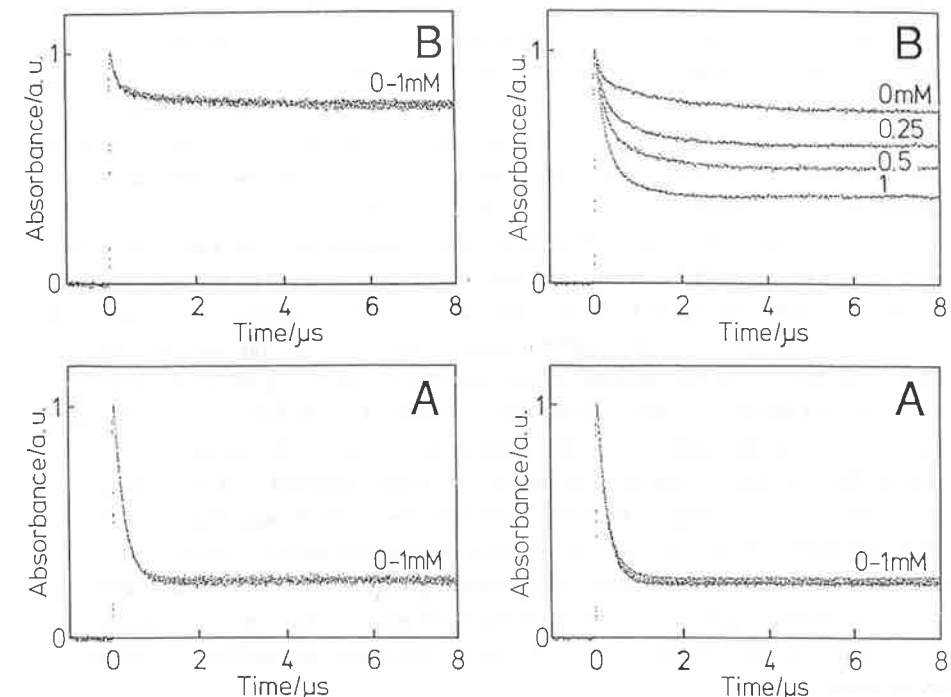


Figure 1. The decay of the transient absorbance, $I(t)$, observed at room temperature at 380nm in the (A) absence and (B) presence of a magnetic field of 1T for micellar SDS solutions containing Sc^{3+} of $0\sim 1 \times 10^{-3} \text{ mol dm}^{-3}$, respectively. All $I(t)$ curves are overlapped with one another.

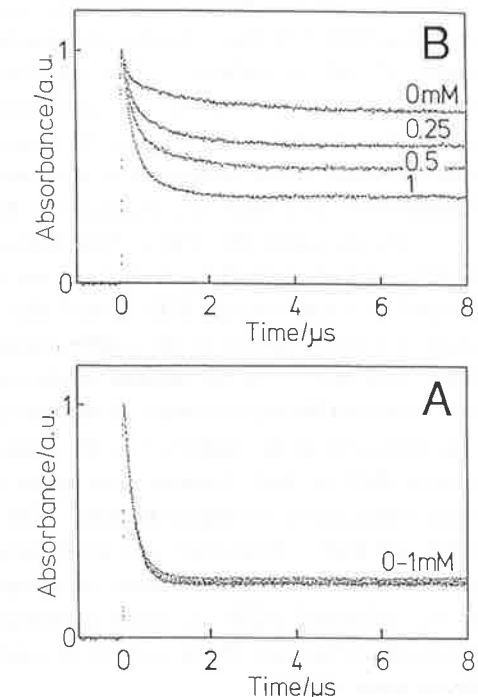


Figure 2. The decay of the transient absorbance, $I(t)$, observed at room temperature at 380nm in the (A) absence and (B) presence of a magnetic field of 1T for micellar SDS solutions containing Mn^{2+} of $0\sim 1 \times 10^{-3} \text{ mol dm}^{-3}$, respectively.

[13], and found that these paramagnetic ions including Gd^{3+} reduced the yield of the escaping $\text{NQH}\cdot$ in the presence of a magnetic field but that the diamagnetic La^{3+} and Lu^{3+} did not reduce it. We considered this effect to be due to the enhanced relaxation of the electron spin by the paramagnetic lanthanoid ions. In the present study, we investigate the effects of paramagnetic transition metal ions. The direct measurement of the relaxation of electron spin by paramagnetic metal ions using TRESR is the best method to elucidate the effects by these ions.

We measured the effects of lanthanoid and transition metal ions (Lu^{3+} , Gd^{3+} , Mn^{2+} , and Cu^{2+} , $0\text{--}2 \times 10^{-3}$ mol dm $^{-3}$) on the CIDEP decay curves in the reaction of NQ (1×10^{-3} mol dm $^{-3}$) in the SDS (8×10^{-2} mol dm $^{-3}$) micellar solution. Figure 3A-3C show the decay curves of the $\text{NQH}\cdot$ signal in the absence and presence of Lu^{3+} , Gd^{3+} , and Mn^{2+} . In the absence of the metal ions, the decay of the CIDEP signal was slow and the signal almost disappeared in $6\text{--}8 \mu\text{s}$. The decay rate of the signal was measured to be $\sim 5 \times 10^5 \text{ s}^{-1}$ in the absence of the ions. The more the concentration of Gd^{3+} or Mn^{2+} became, the faster the signal decayed and the smaller the initial intensity of the signal became. The behavior of Cu^{2+} was similar to those of Gd^{3+} and Mn^{2+} . Since Gd^{3+} and Mn^{2+} have no chemical activity toward $\text{NQH}\cdot$, this enhancement of the CIDEP decay is explained by the acceleration of the relaxation of the polarized $\text{NQH}\cdot$ by these paramagnetic ions. On the other hand, Lu^{3+} changed neither the decay nor the intensity indicating negligible contribution of heavy atom effect.

Consequently, the basic assumption is proved; the paramagnetic metal ion enhances the TS conversion of radical pairs through the electron spin relaxation. This result also indicates the essential equivalence of the effects of Gd^{3+} (lanthanoid ions) and Mn^{2+} (transition metal ions). The decrease of the initial intensity with the addition of paramagnetic metal ions is also a reflection of the enhanced relaxation. Since our TRESR equipment has insufficient time resolution, the faster decay cannot be traced by our apparatus. Thus, its real shape was rounded and the initial intensity was reduced instead. Although the TRESR technique provides direct information on the electron spin, the decay of the CIDEP signal is governed by multiple factors: electron spin relaxation, disappearance of radicals, radical pair polarization, and system response. Therefore TRESR was applied only for a qualitative test and we used the laser TROA instead of TRESR in order to evaluate the effects of each metal ions.

With the aid of the nanosecond laser TROA technique, we investigated the dynamic behavior of the reactions of the aqueous micellar solution of SDS (8×10^{-2} mol dm $^{-3}$) containing NQ (4×10^{-4} mol dm $^{-3}$) and metal chloride ($0\text{--}1 \times 10^{-3}$ mol dm $^{-3}$) in the absence and presence of a magnetic field up to 1 T. The decay curves of the transient absorbances, $I(t)$'s, of $\text{NQH}\cdot$ containing Sc^{3+} or Mn^{2+} ($0\text{--}1 \times 10^{-3}$ mol dm $^{-3}$)

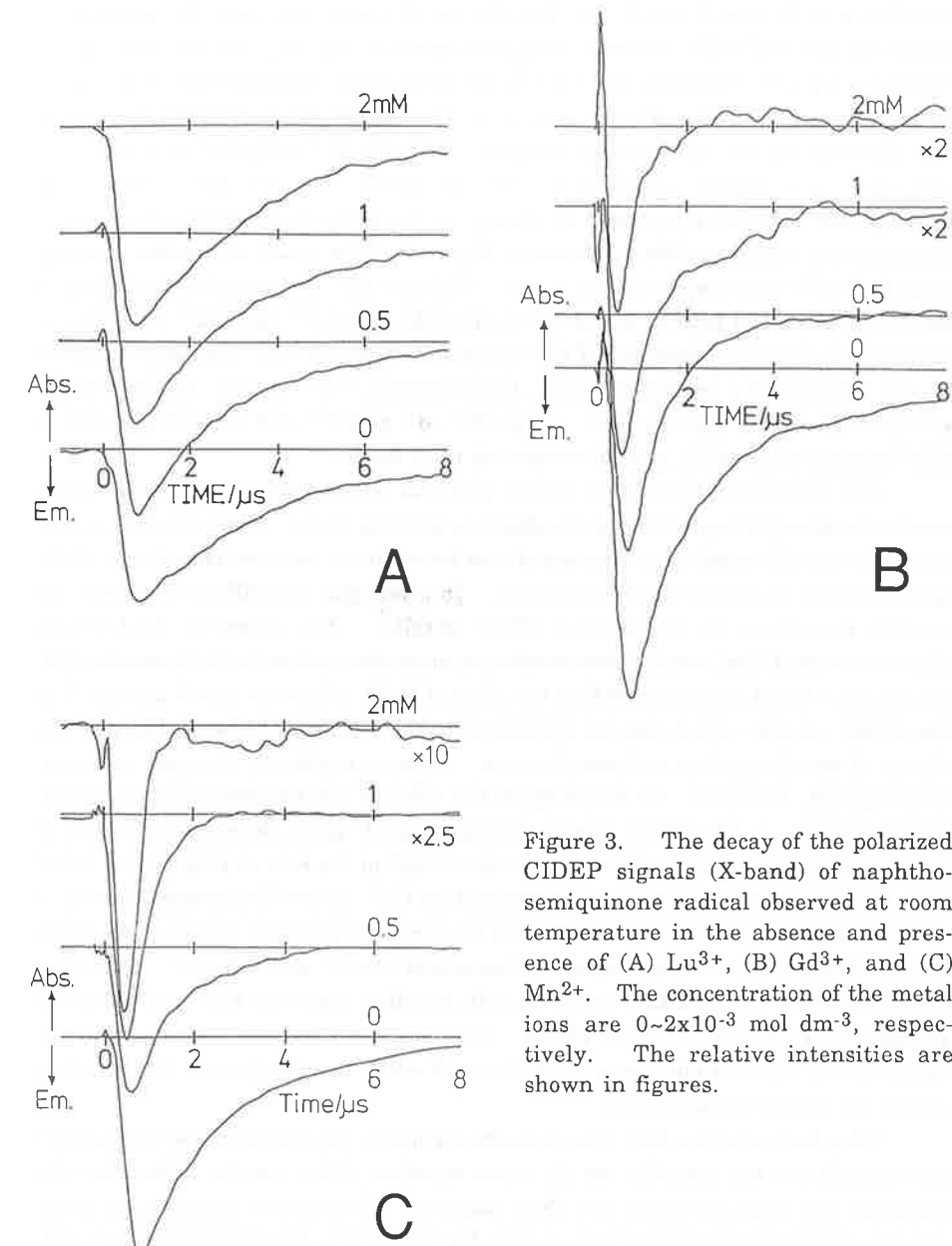


Figure 3. The decay of the polarized CIDEP signals (X-band) of naphtho-semiquinone radical observed at room temperature in the absence and presence of (A) Lu^{3+} , (B) Gd^{3+} , and (C) Mn^{2+} . The concentration of the metal ions are $0\text{--}2 \times 10^{-3}$ mol dm $^{-3}$, respectively. The relative intensities are shown in figures.

are shown in Figures 1 and 2. In the absence of a magnetic field, the addition of paramagnetic Mn^{2+} (d^5) caused no change as shown in Fig. 2A. On the other hand, in the presence of a magnetic field of 1 T, the yield of the escaping radical decreased and the rate of recombination increased as the concentration of Mn^{2+} increased. The effects on the $I(t)$ curves by paramagnetic Cr^{3+} (d^3), Fe^{2+} (d^6), Co^{2+} (d^7), and Ni^{2+} (d^8) ions were similar to that observed with Mn^{2+} (d^5). On the contrary, the diamagnetic Sc^{3+} (d^0) ion caused no change on the curves both in the absence and presence of a magnetic field as shown in Figure 1. The result of another diamagnetic Zn^{2+} (d^{10}) was similar to that of Sc^{3+} . The Cu^{2+} (d^9) ion caused the oxidation of the escaping radical both at 0 and 1 T in the rate of 2.7×10^7 mol dm $^{-3}$ s $^{-1}$. On the other hand, the initial decrease of the escaping radicals by Cu^{2+} was only observed in the presence of a magnetic field. Consequently, Cu^{2+} can be included in the group of other paramagnetic ions. Since Ti^{3+} (d^1) and V^{3+} (d^2) reacted with NQ in SDS micelles in the dark, we did not study them further.

The interaction between a radical pair and paramagnetic species is considered to be strongly dependent on the distance between them. Since the pair is dissolved inside of a micelle and the metal ions locate at its exterior, the charge of the micelle seems to control their separation. To investigate the effects of charge, we studied the effects in the cationic CTAC micelle. The magnetic field effects observed in the CTAC micelle were similar to those observed in the SDS micelle [10]. On the other hand, we could not find the effect of Mn^{2+} or Ni^{2+} ($0-1 \times 10^{-3}$ mol dm $^{-3}$) in the CTAC micelle, which can be attributed to the repulsion between the positive charge of micelle surface and metal cation. Using a negatively charged paramagnetic species, $Fe(CN)_6^{3-}$, we found again the effect of the paramagnetic ion in the CTAC micelle. In the CTAC micelle, the ferricyanide anion decreased the yield of the escaping radical and further oxidizes the radical in the rate of 1.0×10^8 mol $^{-1}$ dm 3 s $^{-1}$. This behavior is similar to that observed for Cu^{2+} in the SDS micelle which is a set of opposite charge for the micelle and the ion. In the SDS micelle, this anion simply oxidized the escaping radical in the rate of 7.2×10^7 mol $^{-1}$ dm 3 s $^{-1}$. The similarity between the oxidation rates in both micelles indicates that the oxidation process occurs mainly in water phase. On the other hand, the quenching of the magnetically induced change is only observed when the charges of the quencher and of the micelle are attractive.

This fact indicates that this quenching effect occurs between the radical pair in a micelle and the quencher on the water interface of the micelle. This fact also indicates that this interaction is a short-range one. It is noteworthy that all investigated paramagnetic metal ions except for $Fe(CN)_6^{3-}$, are high-spin aquo complexes. On the quenching effect, there is no difference between low- and high-spin complexes. We investigated also the low-spin diamagnetic complex, such as

$Co(NH_3)_6^{3+}$, $Fe(CN)_6^{4-}$, and $Ni(CN)_4^{2-}$, but these compounds induced troubles in the reaction system, such as precipitation of the surfactants or reduction of NQ. At least, we found no quenching effect by $Co(NH_3)_6^{3+}$ in the Brij 35 micelle.

In order to compare the quenching abilities of paramagnetic metal ions, we should directly measure their quenching rates. As described in the previous papers [9], the $I(t)$ curves observed in the presence of a magnetic field are described by the summation of three exponential decay curves. The nearly constant part of these components corresponds to disappearance of the escaping radical. The remaining decaying part can be analyzed by a combination of two exponential curves. The slower one corresponds to the relaxation from the T_{+1} and T_{-1} states to the T_0 and S states. The fastest one should be correspond to the reaction from T_0 via S. Both of the decay rate constants can be dependent on the magnetic field and the concentration of paramagnetic ions. The rate of the faster one is so large that the dependence on the field or ions cannot be determined with sufficient accuracy. For the slower components, we obtained the rates in several good conditions, but in the other cases the analysis of the second component was also very difficult owing to the long term fluctuation of the monitor light.

Instead of the direct analysis of the quenching rates, we chose the yield of escaping radicals as the measure of the rates by paramagnetic ions. By a simplified quenching scheme, the concentration dependence of the inverse of the yield of an escaping radical indicates the quenching rate. We know this scheme is too simplified for the micellar solutions and for the system including three independent triplet sublevels. These simplified values, however, can safely be applied to the comparison of the relative quenching rates since the kinetic scheme of the quenching by the paramagnetic ions are common. The correlation factor obtained by the analysis of the data in the presence of 0, 2.5, 5, and 10×10^{-4} mol dm $^{-3}$ paramagnetic ions was more than 0.995 for each relative rate. This value seems tolerable.

In Figure 4, we plotted the relative quenching rates of the employed transition metal ions in the presence of a magnetic field of 0.1 and 1 T. The average of the relative quenching rates of Gd^{3+} at 0.1 and 1 T is set to one in order to compare the present results with those of lanthanoid ions. Since the change of the yield of the escaping radical is much larger at 1 T than that at 0.1 T, the scatter between the obtained results at 1 T is smaller than that at 0.1 T. The quenching rates of Cu^{2+} and Ni^{2+} obtained by the analyses of $I(t)$ curves are 6.5 (6.1) $\times 10^8$ and 7.8 (7.5) $\times 10^8$ mol $^{-1}$ dm 3 s $^{-1}$ in the presence of a magnetic field of 0.1 (1) T, respectively. Therefore the units, the quenching rate of Gd^{3+} in Figs. 4 and 5, may be accepted to be about 6×10^8 mol $^{-1}$ dm 3 s $^{-1}$. These quenching rates are about ten times larger than those of oxidation by Cu^{2+} or $Fe(CN)_6^{3-}$.

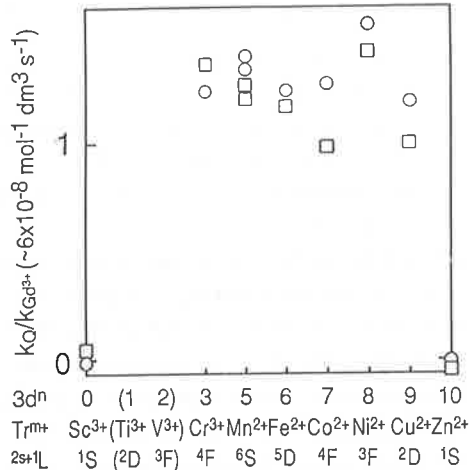


Figure 4. Relative quenching rate for the yield of escaping naphthoquinone radical radical by transition metal ions observed at 0.1 T (open square) and 1 T (open circle). Along the abscissa are shown the number of 3d electrons of each ions, its symbol, and electronic state. The unit is the averaged quenching rate of Gd^{3+} at 0.1 T and 1 T ($\sim 6 \times 10^8 \text{ mol dm}^{-3} \text{ s}^{-1}$)

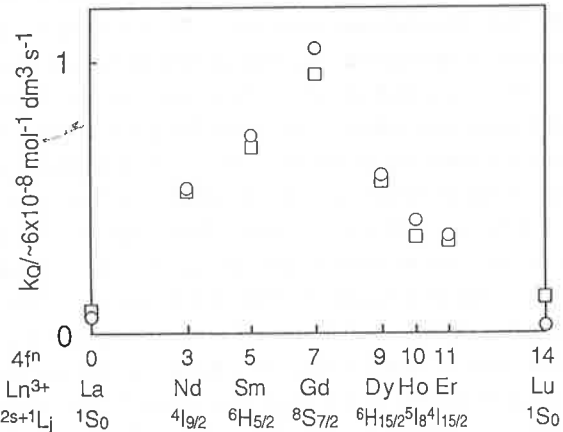


Figure 5. Relative quenching rate for the yield of escaping naphthoquinone radical radical by lanthanoid ions observed at 0.1 T (open square) and 1 T (open circle). Along the abscissa are shown the number of 4f electrons of each of the trivalent ions, its symbol, and electronic state [13]. The unit is the averaged quenching rate of Gd^{3+} at 0.1 T and 1 T ($\sim 6 \times 10^8 \text{ mol dm}^{-3} \text{ s}^{-1}$)

In Figure 5, those for lanthanoid ions are shown [13]. The comparison of these figures shows that the values obtained for the transition metal ions are relatively constant in contrast to those obtained for the lanthanoid ions. The former values are larger than the largest value among the lanthanoid ions, *i.e.* the rate of Gd^{3+} . The paramagnetic properties of transition metal ions arise from their *outer* 3d orbitals which induce many varieties on chemical and physical properties. On the other hand, those of lanthanoid ions arise from their *inner* 4f orbitals, which are chemically inert. The observed larger quenching rates of the transition metal ions can be expected, but the absence of the variety among them cannot. The triply charged Cr^{3+} has no larger efficiency than the other doubly charged ions. The ionic radii are largest for Mn^{2+} (83 pm) and smallest for Cr^{3+} (61.5 pm), which have no appreciable differences in the quenching rates. The differences of the reduction and oxidation potentials induced several effects on the reaction itself, but no correlation between the quenching rates and those potentials was found.

In the previous paper [13], we attributed the effect of lanthanoid ions to the electron spin relaxation, which was confirmed in the present study with the aid of TRESR. We gave, however, no detailed mechanism, since we could not find the mechanism explaining the observed dependence on the numbers of the electron spin. Basu *et al.* introduced Heisenberg exchange interaction to explain these dependences [16]. Tanimoto *et al.* denied it and introduced the dipole-dipole interaction [17], but this interaction was discarded by Basu *et al.* owing to the different dependence on lanthanoid ions. In our opinion, therefore, the mechanism for the quenching by lanthanoid ions still remains unclear. On the other hand, Tanimoto *et al.* suggested the exchange interaction for the quenching by a Cu^{2+} complex [22].

In the case of the dipole-dipole interaction, the quenching rate by Gd^{3+} should be much larger than those by the transition metal ions since Gd^{3+} has the largest magnetic moment. Consequently, the dipole-dipole interaction does not explain the present results for the transition metal ions. Molin *et al.* derived theoretically the rate of spin exchange of a radical by paramagnetic species [23]. Their analyses can be applied to the present result at the view point of the exchange interaction. According to their analyses, the rate of spin exchange (k_{ex}) is complicated but it can be classified into the following four extreme cases: L) The electron spin relaxation time of the radicals and the quencher is longer or comparable to the interaction time of the radicals and the quencher. L-1) In the case of weak exchange interaction limit ($J\tau_c < 1$),

$$k_{\text{ex}} = (2/3)s_Q(s_Q+1)J^2\tau_c^2k_d.$$

L-2) In the case of strong exchange interaction limit ($J\tau_c > 1$),

$$k_{\text{ex}} = (2/3)s_Q(s_Q+1)/(s_Q+1/2)^2k_d.$$

S) The electron spin relaxation time of the quencher is much shorter than that of the radicals and the interaction time. S-1) In the case of weak exchange interaction limit,

$$k_{\text{ex}} = (1/3)s_Q(s_Q+1)J^2(T_{1Q}+T_{2Q})\tau_c k_d.$$

S-2) In the case of strong exchange interaction limit,

$$k_{\text{ex}} = k_d.$$

Here, J is the magnitude of the exchange interaction between the radical and the quencher. τ_c is the correlation time of the system. s_Q is the spin quantum number of the quencher. T_{1Q} and T_{2Q} are electron spin relaxation times of the quencher. k_d is the diffusion controlled limit rate. In these equations, the steric factor for the interaction is neglected. To apply this mechanism to evaluate the quenching rates (k_Q) of a radical pair by the paramagnetic metal ions [17], the derived rate should be doubled for the interaction with two radicals in a pair, $k_Q = 2k_{\text{ex}}$.

In micellar solutions, the correlation time τ_c should be longer than the usual solutions [11]. This is a prominent nature to characterize the magnetic field effect in micellar solutions. In usual solutions, the paramagnetic transition metal ions should be separated into the above two classes, L and S, depending on their electron spin relaxation time compared to the correlation time τ_c . In micellar solutions, the electron spin relaxation times of the paramagnetic transition metal ions are considered to be shorter than τ_c , because the ions tend to stick to the micellar surface. Thus, the condition S seems to hold for all transition metal ions. The weak interaction case, S-1), requires very large dependence on s_Q , which does not explain our results. Therefore we take S-2), the strong interaction case. Even if we neglect τ_c , the conditions L-1) and L-2) cannot explain the absence of the dependence on s_Q in the observation. In the case S-2), the quenching rates by all paramagnetic transition metal ions should be the same. This prediction agrees well with the observed values shown in table 1. In this case, the quenching rates (k_Q 's) of all paramagnetic transition metal ions should be $2k_d$, twice of the diffusion controlled limit rate. The k_d value in water is about $7 \times 10^9 \text{ mol}^{-1} \text{ dm}^3 \text{ s}^{-1}$. This value is, however, ten times larger than those observed.

This discrepancy may be avoided by considering the diffusion of the charged species on the water interface of the micelle. The radius of the micelle seems too large for the strong exchange interaction if the radicals locate at the center of the micelle. NQ seems as hydrophilic as benzophenone. Consequently NQ is considered to locate near water interface as found in the case of benzophenone [24, 25]. The radical pair of NQH^\bullet and R^\bullet also seems to move around there. In this case, the strong exchange interaction between the radicals and a transition metal ion is expected and the metal ion which attaches to the other end of the micelle sphere must diffuse there to quench the radical pair through the exchange interaction. By

assuming that the k_d on the surface of the SDS micelle to be about one tenth of that in water, the observed results are rational as a whole, though we cannot estimate theoretically this rate at this stage. The absence of the difference between the triply charged Cr^{3+} and other doubly charged ions might invoke another problem with this assumption.

In conclusion, we investigated the effects of transition metal ions on the electron spin relaxation of the radical pair generated by the reaction of NQ in micelles by means of the TRESR and TROA techniques. The diamagnetic ions, Sc^{3+} and Zn^{2+} , showed no effect. On the other hand, the paramagnetic transition metal ions, *i.e.* Cr^{3+} , Mn^{2+} , Fe^{2+} , Co^{2+} , Ni^{2+} , and Cu^{2+} , enhanced the electron spin relaxation with larger rates than that of Gd^{3+} , the strongest quencher among the lanthanoid ions. In contrast to the results of lanthanoid ions, the quenching abilities of transition metal ions are almost the same. The dipole-dipole interaction between the radicals and paramagnetic metal ions cannot interpret the obtained results. In the case of the large exchange interaction with the fast relaxation of the quencher, the quenching rates of all ions attain a common maximum rate. This condition explains the observed results by assuming the relatively slow diffusion process of the ion on the micelle surface.

Acknowledgement

We are indebted to Professor Yasumasa J. IHaya and Dr. Hisao Murai of the University of Electro-Communications for their kindness in allowing us to have their time-resolved ESR apparatus at our disposal.

References

- [1] U. E. Steiner and T. Ulrich, Chem. Rev. 89 (1989) 51.
- [2] H. Hayashi and Y. Sakaguchi, in: Applications of Lasers in Polymer Science and Technology, Vol. 2, eds. J.-P. Fouassier and J. F. Rabek (CRC Press, Boca Raton, 1990) p. 1.
- [3] H. Hayashi, in: Photochemistry and Photophysics, Vol. 1, ed. J. F. Rabek (CRC Press, Boca Raton, 1990) p.59.
- [4] Y. Sakaguchi, S. Nagakura and H. Hayashi, Chem. Phys. Letters 72 (1980) 420.
- [5] H. Hayashi, Y. Sakaguchi and S. Nagakura, Chem. Letters (1980) 1149.
- [6] Y. Sakaguchi, H. Hayashi and S. Nagakura, J. Phys. Chem. 86 (1982) 3177.
- [7] Y. Sakaguchi, S. Nagakura, A. Minoh and H. Hayashi, Chem. Phys. Letters 82 (1981) 213.
- [8] Y. Sakaguchi and H. Hayashi, Chem. Phys. Letters 87 (1982) 539.
- [9] Y. Sakaguchi and H. Hayashi, J. Phys. Chem. 88 (1984) 1437.

- [10] Y. Sakaguchi, H. Hayashi and S. Nagakura, Bull. Chem. Soc. Jpn. 53 (1980) 39.
- [11] H. Hayashi and S. Nagakura, Bull. Chem. Soc. Jpn. 57 (1984) 322.
- [12] Y. Sakaguchi, H. Hayashi, H. Murai and Y. J. I'Haya, Chem. Phys. Letters 110 (1984) 275.
- [13] Y. Sakaguchi and H. Hayashi, Chem. Phys. Letters 106 (1984) 420.
- [14] M. Okazaki, S. Sakata, R. Konaka and T. Shiga, J. Chem. Phys. 86 (1987) 6792.
M. Okazaki and T. Shiga, Nature 323 (1986) 240.
- [15] N. J. Turro, X. Lei, I. R. Gould and M. B. Zimmt, Chem. Phys. Letters 120 (1985) 397.
- [16] S. Basu, L. Kundu, and M. Chowdhury, Chem. Phys. Letters 141 (1987) 115. S. Basu, D. Nath, and M. Chowdhury, J. Lumin. 40/41 (1988) 252.
- [17] Y. Tanimoto, A. Kita, M. Itoh, M. Okazaki, R. Nakagaki and S. Nagakura, Chem. Phys. Letters 165 (1990) 184.
- [18] Some preliminary results are reported in; Y. Sakaguchi, H. Hayashi, H. Murai and Y. J. I'Haya, 25th Symposium on Photochemistry 1984, Okayama Japan.
- [19] H. Hayashi and S. Nagakura, Bull. Chem. Soc. Jpn. 53 (1980) 1519.
- [20] Y. Sakaguchi, H. Hayashi, H. Murai, Y. J. I'Haya and K. Mochida, Chem. Phys. Letters 120 (1985) 401.
- [21] H. Murai, Y. Sakaguchi, H. Hayashi and Y. J. I'Haya, J. Phys. Chem. 90 (1986) 113.
- [22] J. S. Hyde and T. J. Sarna, J. Chem. Phys. 68 (1978) 4439.
- [23] Yu. N. Molin, K. M. Salikov and K. I. Zamaraev, Spin Exchange, (Springer, Berlin, 1980).
- [24] J. H. Fendler, E. J. Fendler, G. E. Infante, P.-S. Shih and L. K. Patterson, J. Amer. Chem. Soc. 97 (1974) 89.
- [25] R. Breslow, S. Kitabatake and J. Rothbard, J. Amer. Chem. Soc. 100 (1978) 8156.

Magnetic Field Effects in Photoinduced Electron-Transfer in Porphyrin-Viologen Systems

Taku Matsuo, Hiroshi Nakamura[†], and Hiroaki Yonemura

Department of Chemical Science and Technology,
Faculty of Engineering, Kyushu University, Fukuoka 812, Japan

Abstract:

Magnetic field effects on photo-induced electron transfer in porphyrin-viologen pairs as donor-acceptor pairs were examined. The life time was appreciably extended in the presence of external magnetic fields. Remarkable magnetic field effects on the reverse electron transfers were observed, when the porphyrin and viologen were kept a close distance by the method of (1) covalently bonding or (2) compartmentalization by the use of AOT reversed micelles. These magnetic field effects were well elucidated by relaxation mechanisms between the triplet sublevels of the radical pairs. This was confirmed by experiments with the use of lanthanide ions. CIDEP spectra could also provide useful information for analyzing this mechanisms.

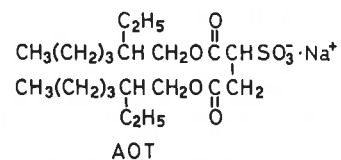
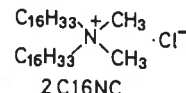
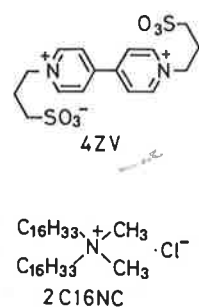
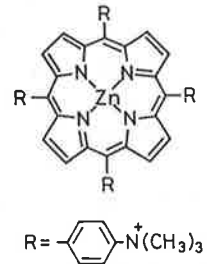
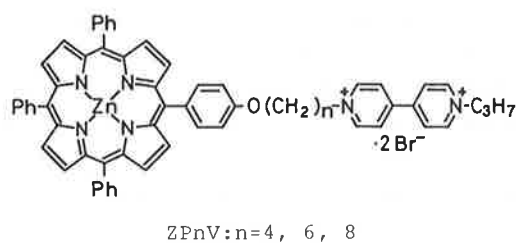
1. Introduction

Photoinduced-electron transfer reactions are the first steps of the photoreaction center of the photosynthesis of the plants. In these reactions, the microenvironment of the thylakoid membrane plays a significant role for the generation of the active redox pairs and the charge separation. In our previous study, appropriately designed donor and acceptor systems combined with molecular assemblies were investigated as a model of the thylakoid membrane, and the formations of active redox pairs from the donor-acceptor linked system were controlled by microenvironment such as molecular bilayers [1].

In this study, following porphyrin-viologen linked compounds

[†] Present address: Department of Chemistry, Faculty of Science, Hokkaido University, Sapporo 060, Japan

and unlinked pairs were examined as donor-acceptor pairs for photoinduced electron transfer experiments. The photo-induced electron transfer from a donor (zinc tetraphenylporphyrin:ZP) to an acceptor (viologen:V) were found to afford triplet radical pairs, and consequently the reverse electron transfer reactions of this triplet radical pairs were affected by an External Magnetic Field (EMF) [2-4]. The interactions between the electron spins of the radical pairs were also investigated by CIDEP spectra in aerosol OT (AOT) reversed micellar solutions of the donor-acceptor systems.



2. Experimental section

Materials:

The linked compounds (ZPnV: n=4, 6, and 8) were used for linked donor-acceptor systems. For unlinked donor-acceptor systems in AOT reversed micelles, a water soluble porphyrin (ZTAP) or an amphiphilic porphyrin (ZPnA) was used as donors, and zwitter ionic viologen (4ZV) was used as an acceptor.

Measurement of transient absorption:

The AOT (0.1 M) reversed micellar (isooctane) or aqueous acetonitrile solution of linked compound ZPnV (0.1 mM) or ZTAP-4ZV were prepared in quartz sample tubes (3.5 cm optical path length) with water jacket (25 °C), and they were placed between the gap of an electromagnet (0-1.4 T) pole pieces. The sample was irradiated by a laser (Xe-F excimer laser: 351 nm or YAG-Dye laser: 565 nm), and the decay of transient absorption due to radical pair was measured.

Measurement of time resolved ESR (CIDEP):

The AOT reversed micellar solution prepared as above was taken into a ESR sample tube (O.D.=5 mm), and was degassed by freeze-pump and thaw method. The sample was irradiated by YAG-Dye laser (565 nm; 8 ns) and the time resolved ESR spectra were measured by a combination of ESR spectrometer without field modulation, a wave memory.

3. Results and discussion

Photogenerated radical pairs were observed with the porphyrin viologen linked compound (ZPnV: n=4, 6, and 8) on the laser excitation in the aqueous acetonitrile solutions or in the molecular bilayers of DHAC [2]. Typical time profile of the decay was shown in Figure 1. This decay curve was consisted with two components, fast decaying and slow decaying components. The fast decaying component was disappeared within 5 μs, and followed a first-order kinetics, which could be attributed to an intramolecular reverse

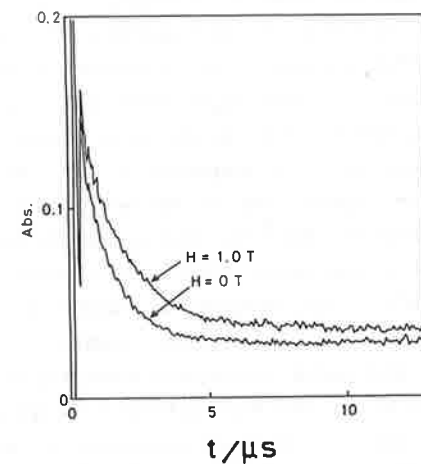


Figure 1. Decay of transient absorption (640 nm) on the laser photolysis of ZP4V in aq.-acetonitrile (50% w/w).

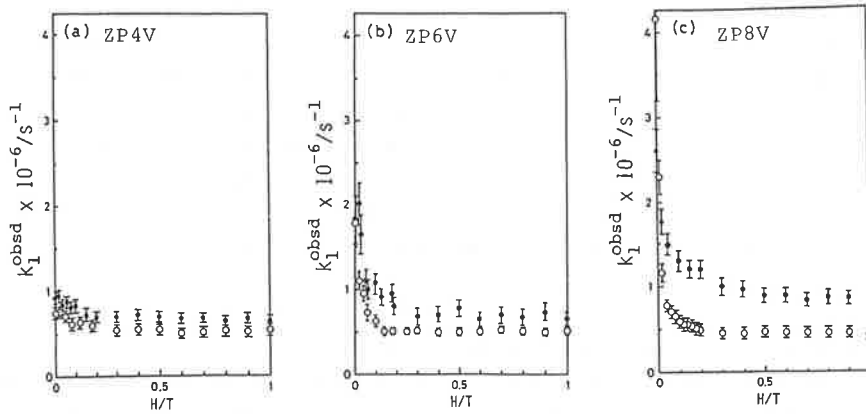


Figure 2. EMFEs on the rate of reverse electron transfer in the photogenerated radical pairs of ZPnV in aq.-acetonitrile (●) and DHAC (○).

electron transfer of linked donor-acceptor system. The slow component which survived up to a few ms time region could be ascribed to an intermolecular process.

The first-order decay rate constants (k_d) was strongly reduced in the presence of external magnetic fields (EMF) as shown in Figure 2. The k_d -values rapidly decreased with the increase of EMF, and reached asymptotic values at EMF above ca. 0.2 T. The k_d -values at zero magnetic field increased with the spacer methylene chain length, while these asymptotic values did not show so much difference by the spacer methylene length. These trends became more clear when ZPnV was incorporated into molecular bilayers of (DHAC). The asymptotic values of the rate were almost independent on the spacer methylene length.

The above described remarkable external magnetic field effects (EMFEs) on the radical-pair decay rates was further investigated by the use of reversed micelles to elucidate the cause of EMFEs [5]. decay rates of the radical pairs obtained with two porphyrin-viologen linked compounds (ZP4V and ZP6V) were examined. The porphyrin moiety of the linked compounds was fixed to the wall of the reversed micelles, while water-soluble viologen moiety was

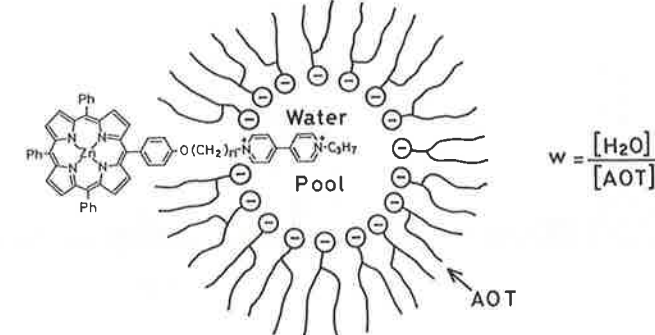


Figure 3. Schematic presentation of trapped ZPnV in reversed micelles.

confined to the water pool (Figure 3). General features of the EMFEs observed with the reversed micellar systems were identical to those in the DHAC molecular bilayers.

Effects of lanthanide ions on the decay rate of the radical pairs provided extremely useful information to elucidate the origin of EMFEs. Laser-induced radical pairs were examined in the presence of three different lanthanide ions (La^{3+} , Dy^{3+} , and Gd^{3+}) in the water pool of the reversed micelles. The results are summarized in Figure 4 or ZP4V. In the presence of high EMF (>0.5 T), the decay rates considerably increased on the addition of either Dy^{3+} ($S=5/2$ and $J=15/2$) or Gd^{3+} ($S=J=7/2$), while no effect was observed with La^{3+} ($S=J=0$). These data clearly indicate that the radical pairs decay faster in the presence of lanthanide ions with higher spin multiplicities (i.e. higher paramagnetism). Exactly the same lanthanide ion effects were observed with the radical pairs for ZP6V at 0.5 T (Figure 5).

The above observations strongly indicate that the EMFEs are originated from Zeeman splitting of triplet sublevels of the radical pairs. The spin flipping relaxation from the triplet sublevels to singlet state of the radical pairs appears to be the rate determining step, which has been well known as Relaxation Mechanism of EMFEs [6].

In the absence of EMF, the lanthanide ions affected the radical decay process for ZP4V and ZP6V in entirely different manner. As

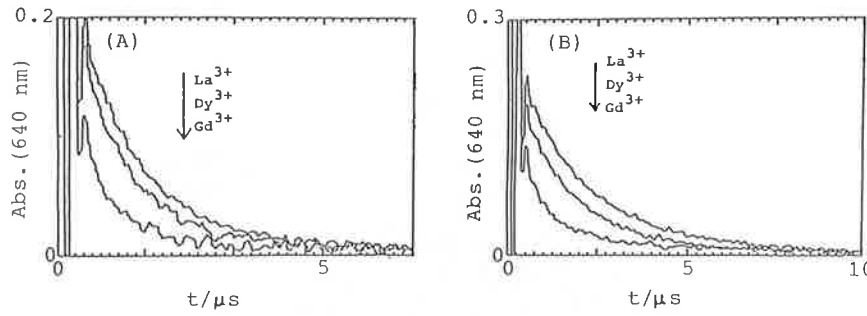


Figure 4. Effects of lanthanide ions on the decay rates of radical pairs for ZP4V at (A) 0T and (B) 0.5 T.

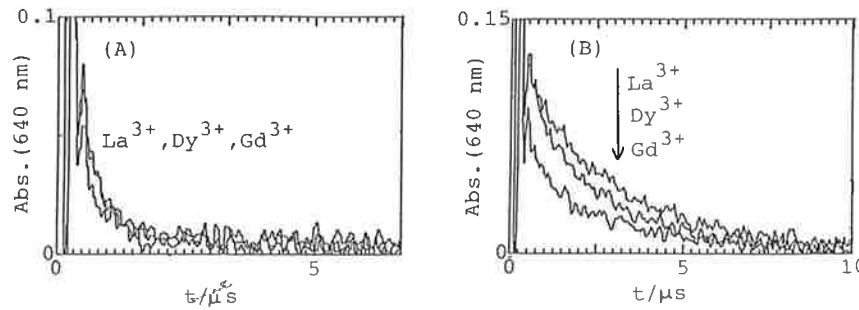


Figure 5. Effects of lanthanide ions on the decay rates of radical pairs for ZP6V at (A) 0T and (B) 0.5 T.

to ZP4V, the decay rate of the radical pair was affected by the three lanthanide ions to almost the same extent as observed at high EMF. In the case of the radical pair generated from ZP6V, however, the decay rate was hardly affected at 0 T. The most important difference between ZP4V and ZP6V is the fact that the radical pair generated from ZP6V decayed much faster than those from ZP4V at 0 T. This is related to the difference in the spacer methylene chain lengths between the porphyrin and viologen moieties. On

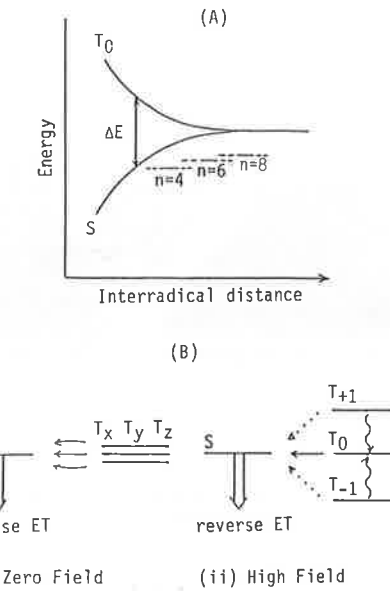


Figure 6. Schematic presentation of phenomena relevant to EMFEs on the decay rate of photogenerated geminate radical pairs: (A) variation of singlet-triplet energy separation with interradical distance, (B) two extreme case of radical decay via intersystem crossing at S-T levels.

going from ZP4V to ZP6V, the spacer methylene chain length increases by two units, and an electron spin exchange interaction (ΔE) in the radical pair is expected to decrease accordingly. When ΔE approaches zero, the singlet and the triplet energy levels of the radical pair become degenerated to each other. In this extreme case, the intersystem crossing from the triplet to singlet is expected to proceed easily via hyperfine coupling- and/or Δg -mechanisms. Consequently, the rate will not be appreciably affected by paramagnetic ions such as Gd^{3+} . The relevant factors for EMFEs are shown in Figure 6.

The transitions between T_{+1} , T_0 and T_{-1} correspond to the ESR transition, and they can be measured by time resolved ESR technique (CIDEP). These CIDEP spectra of these systems have not only information of the individual radical but also the interaction between

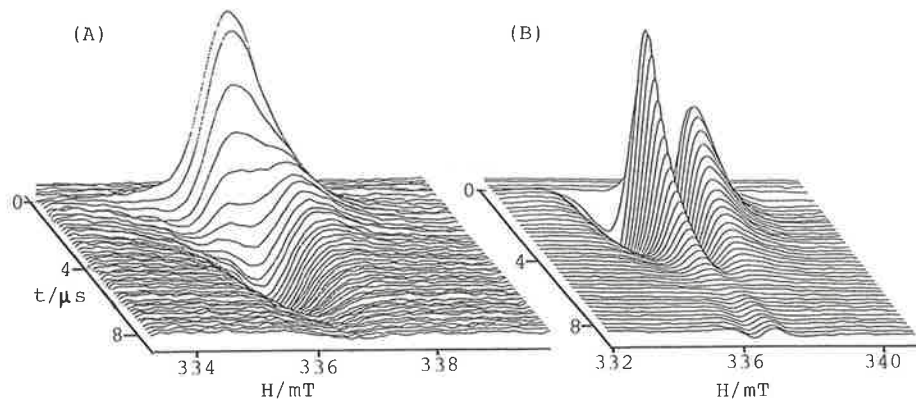


Figure 7. CIDEP spectra of linked compound ZPnV in reversed micelles (AOT w=40). (A) n=4, (B) n=8.

spins of the radical pair.

The CIDEP spectra of the radical pair of the linked compound ZPnV were obtained in AOT reversed micellar solution (Figure 7). The spectrum of ZP4V gave an absorption type at early stage and then it changed to an emission spectrum. This suggested that the initial polarization of the radical pair come from Triplet Mechanism, and the polarization of T_{-1} decreased probably by S-T $_{-1}$ mixing. The spectra of ZP6V and ZP8V were E/A/E/A pattern which was quite different from those of n=4. These difference may be caused by a change of interactions between the electron spins of the radical pair, and it may reflect on the EMFE of these systems.

While, in case of unlinked system (ZTAP-4ZV) of AOT reversed micelle showed considerably different spectra from ZPnV case. Only absorption pattern was obtained at large water pool size (w=40), but it resembled to a spectrum of ZP4V at early stage, however the time dependence of it was completely different from each other. On the other hand, quite different spectrum was obtained at small water pool size (w=5) (Figure 8), and this spectrum rather resembled to those of ZP6V and ZP8V. Since the small water pool might make the distance between ZTAP and 4ZV short, these results of unlinked system were opposit to those of linked system. Thus, the mechanism of these CIDEP spectrum may not be the same as those of linked system.

Any way, these phenomena may be caused by relaxations of excited triplet state of zinc porphyrin before forward electron transfer and also by interactions of electron spins of the radical pair, which govern the EMFEs of these electron transfer reactions.

References

- [1] H. Nakamura, A. Motonaga, T. Ogata, S. Nakao and T. Matsuo, Chem. Lett., (1986) 1615.
- [2] H. Nakamura, A. Uehata, A. Motonaga, T. Ogata, and T. Matsuo, Chem. Lett., (1987) 543.
- [3] S. Usui, H. Nakamura, T. Ogata, A. Uehata, A. Motonaga, and T. Matsuo, Chem. Lett., (1987) 1779.
- [4] S. Usui, A. Uehata, H. Baba, H. Nakamura, and T. Matsuo, Nippon Kagaku Kaishi, (1989) 1477.

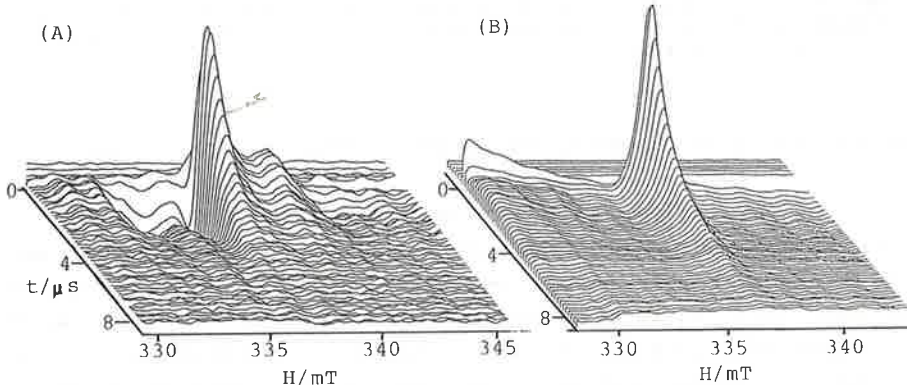


Figure 8. CIDEP spectra of unlinked system (ZTAP-4ZV) in reversed micelles. (A) w=5, (B) w=40.

- [5] A. Uehata, S. Usui, H. Nakamura and T. Matsuo, *J. Phys. Chem.*, 93 (1989) 8198.
[6] H. Hayashi and S. Nagakura, *Bull. Chem. Soc. Jpn.*, 57 (1984) 322.

Applications of Electron Spin Echo Spectroscopy to Location Control of Alkylphenothiazine Derivatives in Photoinduced Charge Separation Across Vesicles, Micelles and Reverse Micelle Interfaces

Larry Keván

Department of Chemistry, University of Houston
Houston, Texas 77204-5641 (USA)

Abstract

The efficiency of photoinduced charge separation across surfactant interfaces of micelles and vesicles depends in part on the location of electron donors and acceptors relative to the interface. Achievement and assessment of control of such location by the addition of pendant alkyl chains to donors and acceptors is shown to be achievable. The net photoionization efficiency can be measured by electron spin resonance of radical ions in frozen surfactant solutions. Assessment of relative locations of radical ions with respect to a surfactant interface has been achieved by analysis of electron spin-echo modulation from deuterium in deuterated water at the interface.

Results for a series of positive, neutral and negatively charged alkylphenothiazine derivatives in vesicle, micelle and reverse micelle surfactant assemblies of different interface charge are discussed. Controlling factors involve the alkyl chain length of the electron donors, the relative charge of the surfactant assembly interface versus that of the electron donor derivative, and the degree of molecular order in the interface. Secondary factors include alkyl chain bending, photoinduced radical conversion and back electron transfer.

I. Introduction

Surfactant systems such as vesicles, micelles and reverse micelles can be used to achieve and control molecular compartmentalization. The compartmentalization of photoionizable molecules is being used as model systems for artificial photosynthesis to achieve net photoinduced charge separation and hence the storage of light energy. One broad approach to enhance the photoionization efficiency in such systems is to modify the surfactant assembly interface and also to some extent its interior structure. Control factors for interface modification include the polar headgroup type of the

surfactant, the charge of the surfactant, the alkyl chain length of the surfactant, the interface charge density, the ionic strength of the interface which can be varied by added salts and by specific complexation of counterions by crown ethers and the incorporation of surface active additives such as salts, alcohols and cholesterol. These aspects have been studied intensively in this laboratory by various electron magnetic resonance methods [1] applied to micelles [1-48] and vesicles [1,8,20,28,29,40,44,45,49-67].

The complementary approach to control the net photoionization efficiency in surfactant assemblies is to add variable length alkyl chains to the photoactive molecules acting as electron donors or acceptors [44]. The idea is to use the interactions that form surfactant assemblies to control the location of a photoionizable or photoreducible moiety of a surfactant type molecule where alkyl chains of variable length are attached to such photoactive moieties. Initial work dealing mostly with photoreduction of alkylmethylviologens in surfactant assemblies of various types has demonstrated achievement of such location control by this approach [28,35,64,67].

In this review we will summarize results on a series of alkylphenothiazine derivatives which undergo monophotonic photoionization in surfactant assemblies. The focus is on how the interaction of the interface charge with the charge on the photoionizable molecule modulates alkyl chain length effects.

2. Experimental Section

The photoionizable compounds used include four classes of alkylphenothiazine derivatives as shown in Figure 1 with their associated abbreviations. These include phenothiazine alkylsulfonates with a negative charge, phenothiazine alkyltrimethylammonium bromides with a positive alkyl charge and alkylphenothiazines which are neutral. In addition, a negative sulfonate group has been attached directly to the phenothiazine moiety to form alkylphenothiazine sulfonates which have a polar headgroup at the phenothiazine moiety. These are somewhat analogous to the neutral alkylphenothiazines in that they both have only one polar center in the molecule. The synthesis of these various derivatives has been described [66,68,69].

The surfactants used to form the micelle, vesicle and reverse micelle assemblies are summarized in Figure 2. Note the contrasting interface charges from the surfactant headgroups. All of these surfactants are commercially

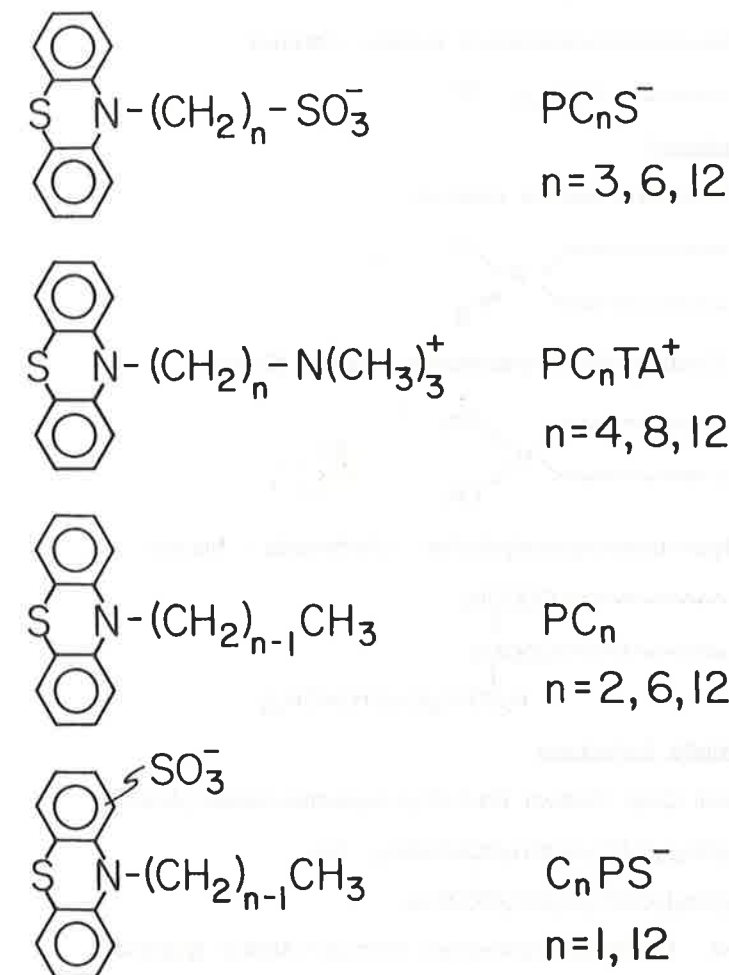


Figure 1. Alkylphenothiazine derivatives and abbreviations.

Micelle Surfactants

SDS - Sodium Dodecyl Sulfate (Anionic)

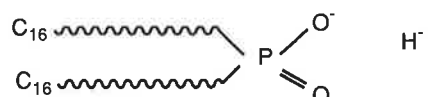


DTAB - Dodecytrimethylammonium Bromide (Cationic)

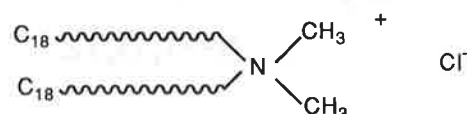


Vesicle Surfactant

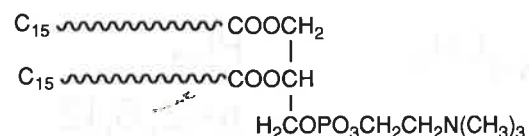
DHP - Dihexadecylphosphate (Anionic)



DODAC - Dioctadecyldimethylammonium Chloride (Cationic)

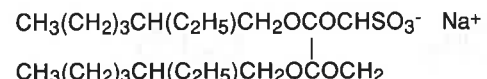


DPPC - Dipalmitoylphosphatidylcholine (Zwitterionic = Neutral)



Reverse Micelle Surfactants

AOT - Aerosol Octyl (Sodium Bis-2-ethylhexylsulfosuccinate) (Anionic)



CTAB/C_nOH - Cetyltrimethylammonium Bromide/n-Alcohol (Cationic)

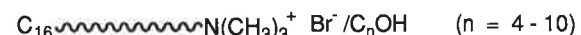


Figure 2. Surfactants used with abbreviations

available from Aldrich, Eastman Kodak and Sigma companies.

The net photoionization efficiency is measured by electron spin resonance of the phenothiazine cation radicals generated by photolysis. These studies are carried out in frozen solutions so that the photoproduced cations are stable and the net photoionization yield can be easily measured by electron spin resonance. The use of the frozen solution also allows weak electron-nuclear dipolar interactions to be measured by electron spin echo modulation patterns which provide an approach to measuring small distance changes of the phenothiazine moiety from the surfactant assembly interfaces. In all cases the surfactant assemblies are prepared in deuterated water and the electron spin echo modulation associated with the phenothiazine cation radicals is due to interactions with deuterium in water at the interface.

It has been found most effective to analyze the modulation in terms of the normalized deuterium modulation depth at the first minimum in the modulation pattern versus the interpulse time. The absolute modulation depth from the unmodulated electron spin echo decay curve at the first minimum in the modulation pattern is normalized by dividing by the distance from the unmodulated decay curve to the baseline [12]. The normalized modulation depth has been found to be quite reproducible and intercomparable between different systems, and thus is a convenient quantitative method of distinguishing locations in analogous series of surfactant assembly systems. The normalized deuterium modulation depth is a function of both the distance and number of surrounding deuterium nuclei about the paramagnetic species out to a distance of about 0.6 nm. However, in the systems to be discussed here the differences in the normalized deuterium modulation depth are largely due to different distances of interaction and will be so interpreted.

Since the exploitation of electron spin echo modulation requires solid systems, the surfactant assemblies are rapidly frozen in order to make such analysis possible. This also allows the electron spin resonance doubly integrated intensity of the photoproduced cation to serve as a measure of the net photoionization efficiency. Numerous studies have shown that in relatively rapidly frozen aqueous solutions the micellar and vesicular structure is in fact retained. Some seven different types of experiments have shown support for the retention of the surfactant assembly structures for aqueous solutions [44]. Not only can micellar structure be directly detected in frozen micellar solutions by electron microscopy, but similar aggregation numbers, that is the number of

surfactant molecules making up the micelles, are directly measured in both liquid and frozen micellar solutions by luminescence quenching methods. Also, it has been possible to measure partition coefficients of surface active molecules between the micellar interface and the bulk phase in both liquid and frozen solutions. The values have been found to be the same which also supports the retention of micellar structure in the frozen systems. Thus quite an extensive body of evidence indicates unambiguously that the micellar and vesicular structure is retained in the relatively rapidly frozen aqueous solutions described in this work.

Electron spin resonance measurements were carried out at 77 K with a Bruker ESP 300 spectrometer. The electron spin echo measurements were made with a home-made spectrometer using 40 ns excitation pulses [70].

The preparation of the vesicle and micellar solutions has been described [39,66]. Photoirradiation of the samples were carried out at 77 K for 10 minutes with a 300 W xenon lamp and suitable filters for a wavelength range centered at 310 nm.

3. Results and Discussion

General Aspects

No electron spin resonance spectrum is observed from the alkylphenothiazine derivatives in the surfactant assemblies before photoirradiation. After irradiation with wavelengths longer than 300 nm these samples turn pink which is characteristic of the alkylphenothiazine radical cations. Also, an ESR singlet is observed with a g factor of 2.005 to 2.006 which is characteristic of alkylphenothiazine radical cations. In some cases, particularly with longer alkyl chain lengths, weak ESR lines are seen on either side of the intense phenothiazine radical cation singlet. These weak lines have been identified as due to surfactant secondary alkyl radicals formed by photoinduced radical conversion of the phenothiazine radical [64]. At long irradiation times the surfactant alkyl radicals totally dominate the ESR spectrum. In general, this photoinduced radical conversion increases the net photoionization yield because electron back reactions don't occur to the alkyl radical. Also, the efficiency of the radical conversion increases with the alkyl chain length of the phenothiazine derivative so that this process is more noticeable for longer alkyl chains. This is a complicating side effect which is

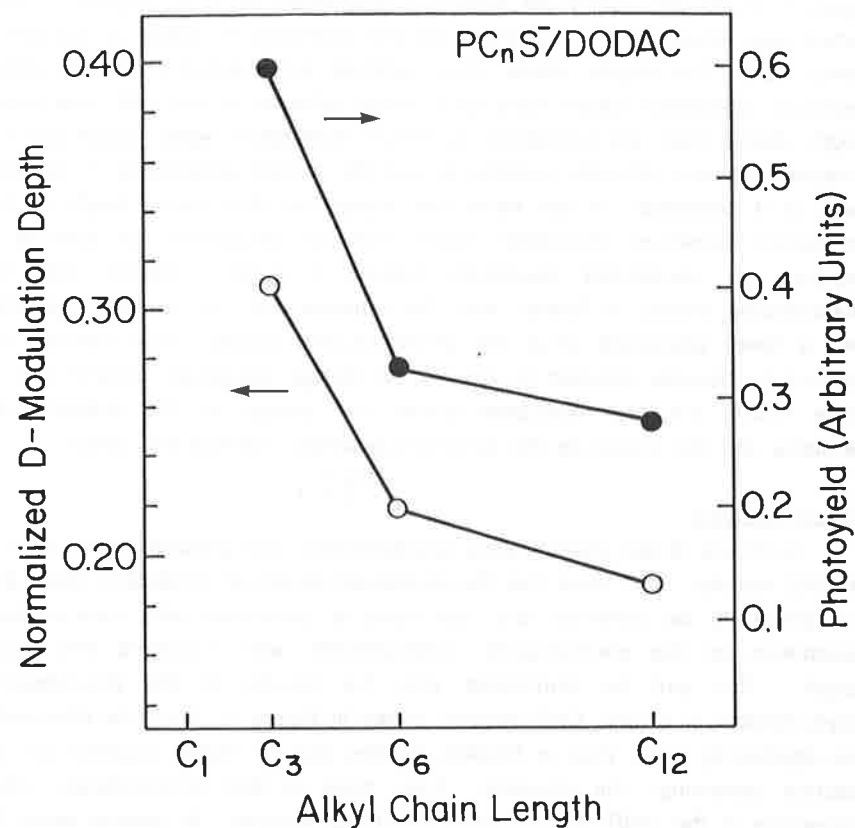


Figure 3. Normalized deuterium modulation depth and photoyield versus alkyl chain length for the PC_nS-/DODAC cationic vesicle system.

ignored here by doubly integrating the entire ESR spectrum to obtain relative photoyields.

The major results are displayed for easy interpretation in plots as in Figure 3 where the normalized deuterium modulation depth is plotted on one vertical axis versus alkyl chain length and the photoyield is plotted on the other vertical axis. This display readily shows whether the photoyield and normalized deuterium modulation depth have the same or different trends with alkyl chain length. Recall that the normalized deuterium modulation depth values can be compared between different systems as can the relative photoyields. In general, there is a correlation in the trend with increasing alkyl chain length of the normalized deuterium modulation depth and the photoyield. In essence, a decrease in normalized deuterium modulation depth indicates that the phenothiazine moiety is further from the interface and this normally correlates with a lower photoyield since the photoproduced electron must traverse the interface to become solvated to achieve net charge separation. Several sets of these results are now discussed where the charge on the phenothiazine derivative and the charge on the surfactant assembly interface are varied.

Vesicle Systems

In Figure 3 the phenothiazine alkylsulfonates are photoionized in cationic DODAC vesicles. It is seen that the normalized deuterium modulation depth and the photoyield do correlate and the trend is consistent with more interface penetration for the phenothiazine alkylsulfonate with increasing alkyl chain length. This can be contrasted with the results of the phenothiazine alkylsulfonates in anionic DHP vesicles shown in Figure 4. Here the photoyields are significantly lower than in DODAC vesicles due to charge repulsion on the electron traversing the interface. Also, there is less photoinduced radical conversion in the DHP vesicles than in DODAC vesicles. In general when the interface is negative it is more difficult for the electron to traverse it and the net yields are lower. The normalized deuterium modulation depth does show an alkyl chain length effect however there is little alkyl chain effect on the photoyield because the negative surface charge flattens out the effect.

Figures 5 to 7 give analogous results for the positively charged phenothiazine alkyltrimethylammonium compounds in vesicles of different interface charge. Figure 5 shows results in cationic DODAC vesicles where the normalized deuterium modulation depth does not show a monotonic trend with

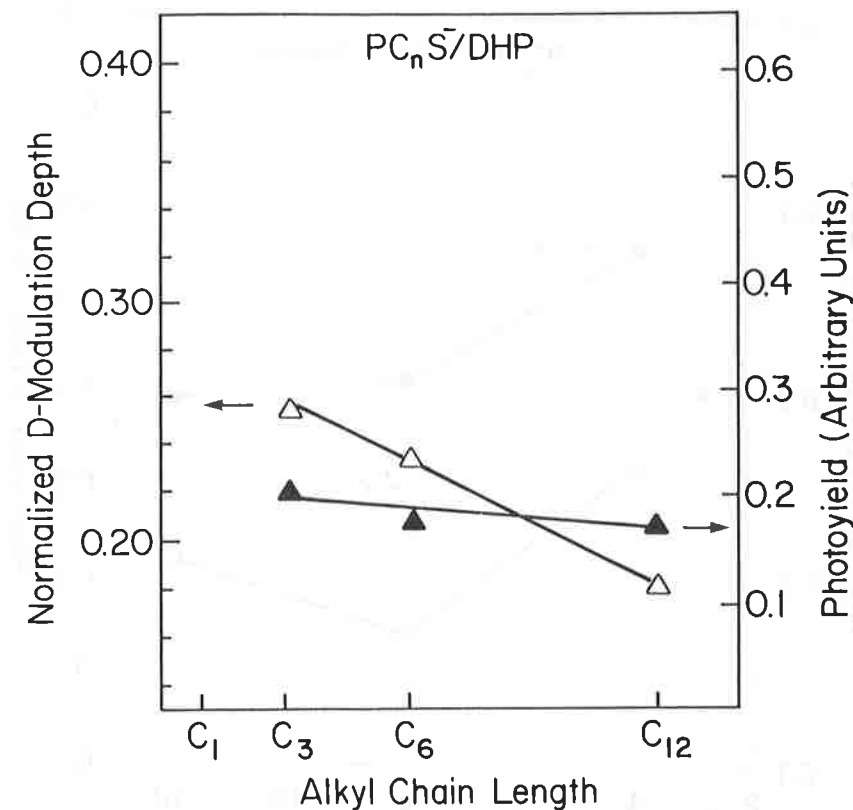


Figure 4. Normalized deuterium modulation depth and photoyield versus alkyl chain length for the $\text{PC}_n\text{S}^-/\text{DHP}$ anionic vesicle system.

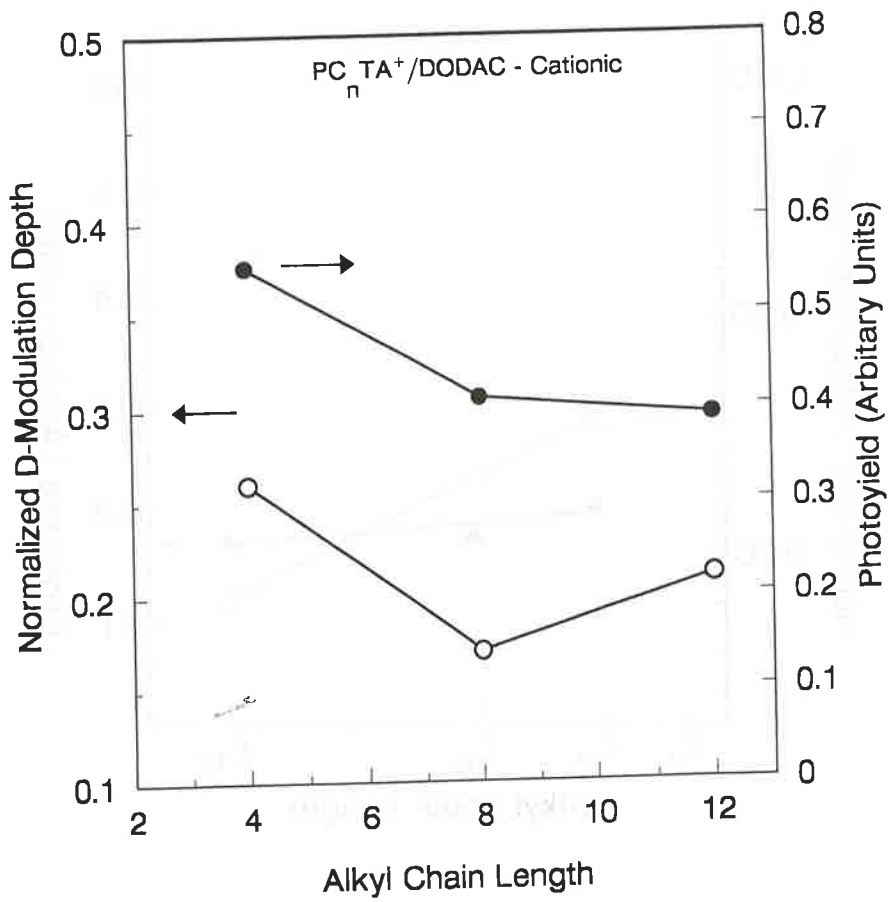


Figure 5. Normalized deuterium modulation depth and photoyield versus alkyl chain length for the PC_nTA^+ /DODAC cationic vesicle system.

alkyl chain length but shows a minimum for C_8 with somewhat of an increase for C_{12} . This is characteristic of alkyl chain bending and indicates that the cationic alkyl phenothiazine derivative shows more chain bending than does the anionic derivative in cationic DODAC vesicles. The photoyields somewhat reflect this.

Figure 6 for the phenothiazine trimethylammonium compounds in the anionic DHP vesicles shows an even more dramatic chain bending effect. Here the normalized deuterium modulation depth actually monotonically increases with increasing alkyl chain length indicating increasing chain bending. The normalized deuterium modulation depth and the photoyield do still correlate since the photoyield increases modestly with increasing alkyl chain length. However, the photoyield is relatively low due to the negative surface charge of the anionic vesicle.

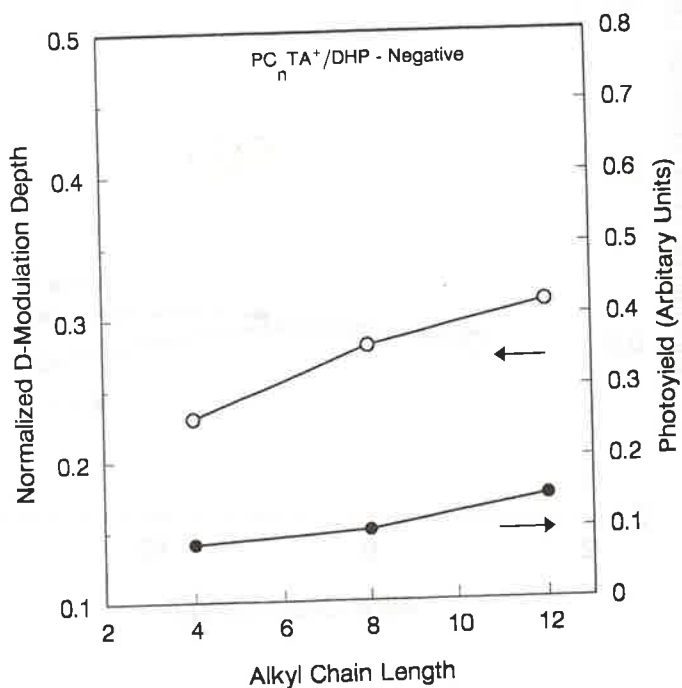


Figure 6. Normalized deuterium modulation depth and photoyield versus alkyl chain length for the PC_nTA^+ /DHP anionic vesicle system.

Figure 7 shows results for PC_nTA^+ in the nominally neutral (actually zwitterionic) DPPC vesicle system. Here, both the normalized deuterium modulation depth and the photoyield show little effect due to increasing alkyl chain length. The expected alkyl chain length effect seems to be counterbalanced by more alkyl chain bending and the net result is little change as shown.

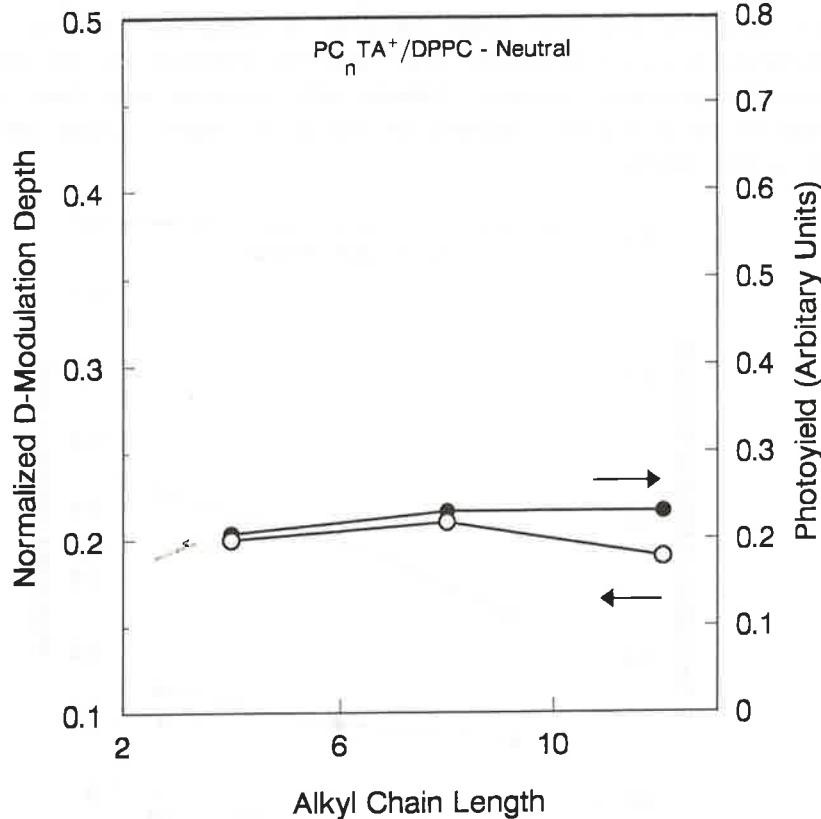


Figure 7. Normalized deuterium modulation depth and photoyield versus alkyl chain length for the PC_nTA^+ /DPPC neutral vesicle system.

These results can be summarized by the schematic diagram of the relative location of the alkylphenothiazine derivatives relative to DODAC and DHP vesicle interfaces in Figure 8. Two features are to be noted. First, the

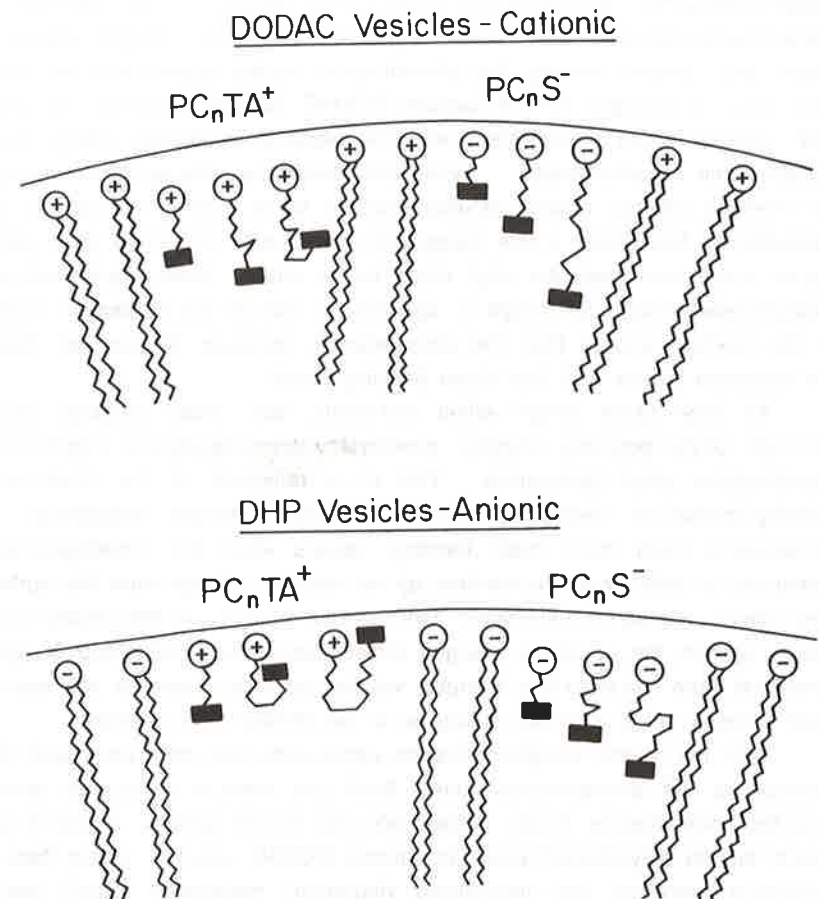


Figure 8. Schematic of the location of PC_nTA^+ and PC_nS^- molecules in cationic DODAC and anionic DHP vesicles. The rectangle is the phenothiazine moiety.

position of the phenothiazine moiety shown by a rectangle relative to the interface is given by the normalized deuterium modulation depth results and second the charge effects, or electrostatic repulsion and attraction effects between the surfactant interface charge and the charge on the alkylphenothiazine derivative are taken into account. In general, the phenothiazine alkylsulfonates show significant alkyl chain length effects with longer alkyl chains forcing the phenothiazine moiety deeper into the vesicle. This effect is stronger for the cationic DODAC vesicles than for the anionic DHP vesicles which is consistent with the negative headgroup charge on the phenothiazine alkylsulfonates. When this headgroup charge is the same as the interface charge, charge repulsion occurs which pushes the phenothiazine alkylsulfonate headgroup a little deeper into the vesicle and more chain bending occurs which minimizes the alkyl chain length effect. When the phenothiazine alkylsulfonate headgroup charge is opposite to that of the surfactant molecule or the interface charge then the photoionizable molecule fits securely between the surfactant chains and less chain bending occurs.

An alkyl chain length effect still exists, but chain bending becomes dominant for the positively charged trimethylammonium headgroup attached to the phenothiazine alkyl compounds. This is a reflection of the much bulkier trimethylammonium headgroup relative to the sulfonate headgroup. And consequently much more chain bending occurs when the trimethylammonium headgroup is held near the interface by an opposite charge from the surfactant alkyl chains, namely in the anionic DHP vesicle system. In the cationic DODAC vesicle system the positively charged trimethylammonium headgroup is repelled somewhat from the positively charged vesicle interface. There is still significant chain bending but it is not as strong as in the anionic DHP vesicles.

With the neutral alkylphenothiazine compounds the most polar part of the molecule is the phenothiazine moiety itself and there is no charge center to force the phenothiazine moiety deeper into the vesicle system. Figure 9 shows results for the alkylphenothiazines in cationic DODAC vesicles. Again there is a correlation between the normalized deuterium modulation depth and the photoyield. There is little difference in penetration between the C₂ and C₆ alkyl chains, but there is substantially more penetration into the vesicle for the C₁₂ alkyl chains. In contrast, Figure 10 shows that for the alkylphenothiazines in the anionic DHP vesicles there is some increase in penetration going from the C₂ to C₆ chains but no more penetration for a C₁₂ chain. This is a

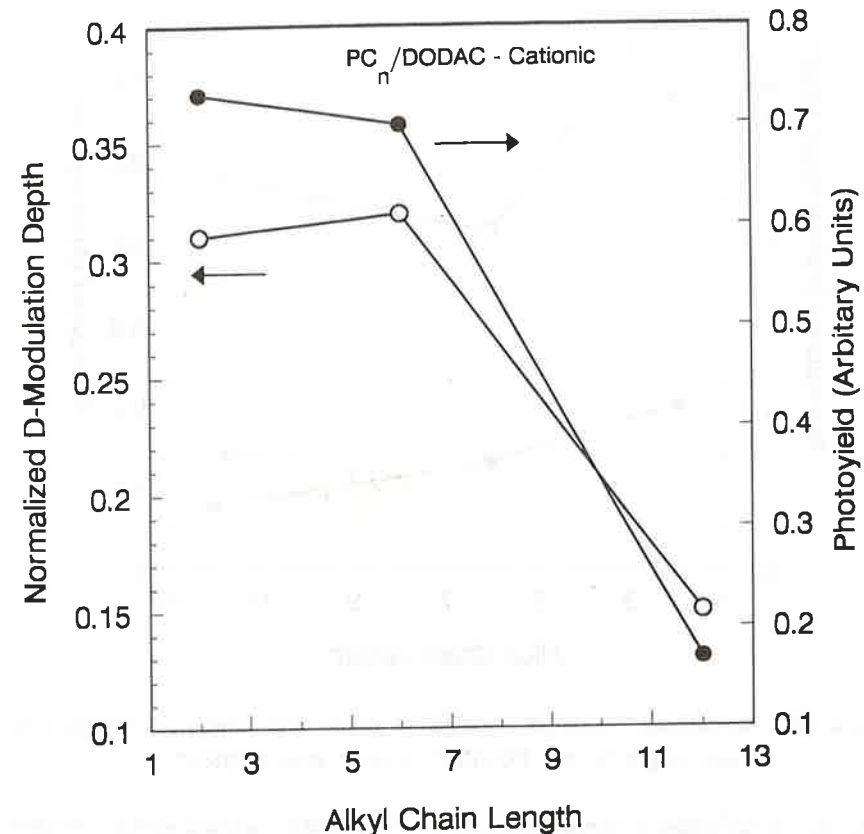


Figure 9. Normalized deuterium modulation depth and photoyield versus alkyl chain length for the PC_n/DODAC cationic vesicle system.

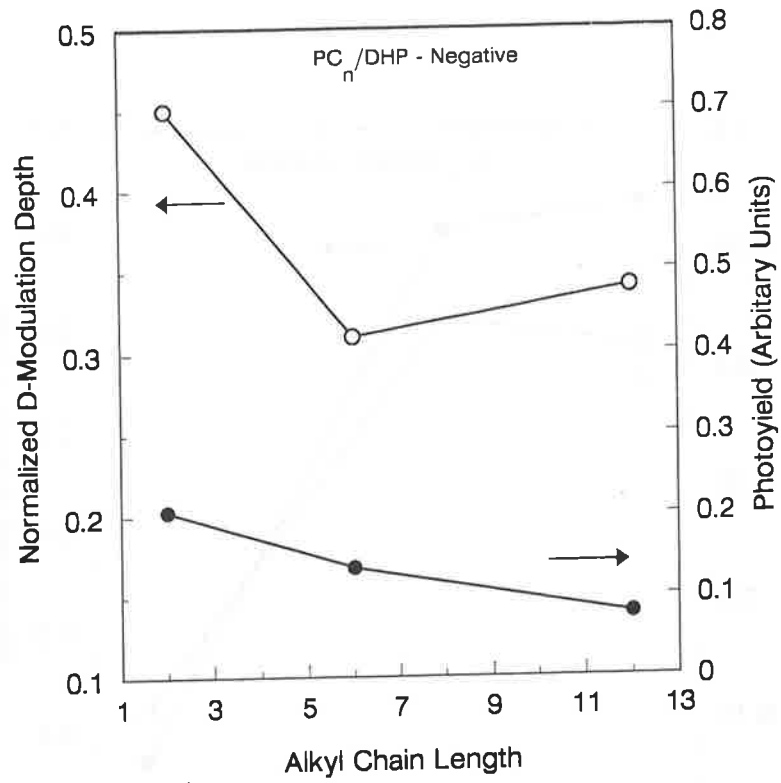


Figure 10. Normalized deuterium modulation depth and photoyield versus alkyl chain length for the PC_n/DHP anionic vesicle system.

reflection of the different surface packing of the DODAC vesicles versus the DHP vesicles. The bulkier dimethylammonium headgroups for the DODAC vesicles give a looser alkyl chain packing and looser surface packing than in the DHP vesicles. Thus the alkylphenothiazines penetrate more easily into the looser packed DODAC vesicles than into the more tightly packed DHP vesicles.

Somewhat similar results are found for the alkylphenothiazine sulfonates in which the sulfonate group is attached to the phenothiazine moiety to form a bulky negatively charged polar headgroup. This bulky charged headgroup makes penetration into the interface more hindered but the C_nPS^- compounds penetrate a little more into a more loosely packed DODAC vesicle than into a more tightly

packed DHP vesicle. Figure 11 shows a schematic diagram of the PC_n and C_nPS^- surfactants in DODAC and DHP vesicles. It illustrates a significant alkyl chain length effect for the alkylphenothiazines but little or no alkyl chain length effect for the alkylphenothiazine sulfonates. There is more penetration for both types of molecules, but more significantly for the alkylphenothiazines, into the DODAC vesicles than into the DHP vesicles.

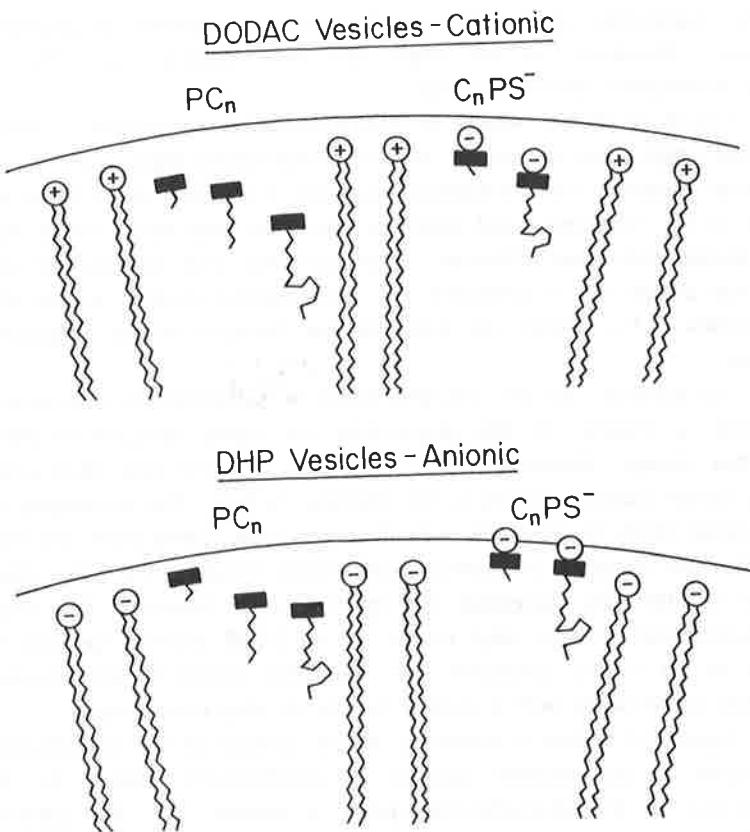


Figure 11. Schematic of the location of PC_n and C_nPS^- molecules in cationic DODAC and anionic DHP vesicles. The rectangle is the phenothiazine moiety.

Micelle Systems

Now let us consider photoionization of the alkylphenothiazine derivatives in micelle assemblies. It must be remembered that the internal disorder of the alkyl chains is much greater in micellar systems than in vesicular systems. It is also true that the interface structure is more disordered in micelles than in vesicles and is sometimes described as a thicker headgroup region because of the disorder of the headgroups at the interface. Thus, in general one expects greater penetration and smaller alkyl chain length effects in micelles versus vesicles. However, as we shall see this depends upon the particular alkylphenothiazine derivative used.

Figure 12 shows results for phenothiazine alkylsulfonates in anionic SDS micelles. Again the normalized deuterium modulation depth and the photoyield correlate. However the normalized deuterium modulation depth trend with alkyl chain is not monotonic and indicates significant alkyl chain length bending of the alkylphenothiazine sulfonates. This contrasts with vesicles for the same interface charge but is consistent with more internal disorder of the alkyl chain in micelles. The yields are relatively low because of the negative surface charge.

In contrast, for the alkylphenothiazine sulfonates in the cationic DTAB micelles in Figure 13 the photoyields are higher because of the positive interface charge. However, there appears to be very little alkyl chain length effect on the location relative to the interface surface. The normalized deuterium modulation depth is quite low indicating significant penetration into the micelle interface but because of significant alkyl chain bending the alkyl chain length effect is effectively cancelled out by the chain bending. The increase in photoyield with longer alkyl chains in the DTAB micellar systems does not seem to be clearly consistent with the other overall trends developed and requires further study with a greater number of alkyl chain lengths.

Figure 14 shows a schematic of the location of the phenothiazine alkylsulfonates in the micellar systems. A predominant feature is that the penetration of the phenothiazine group is greater into the cationic DTAB micellar system than into the anionic SDS micellar system. This is probably not so much an effect of interface charge as it is of the bulkier headgroup of the DTAB micelles thus leading to more interface penetration. The same trend is observed with the alkylphenothiazine sulfonates as also shown schematically. In

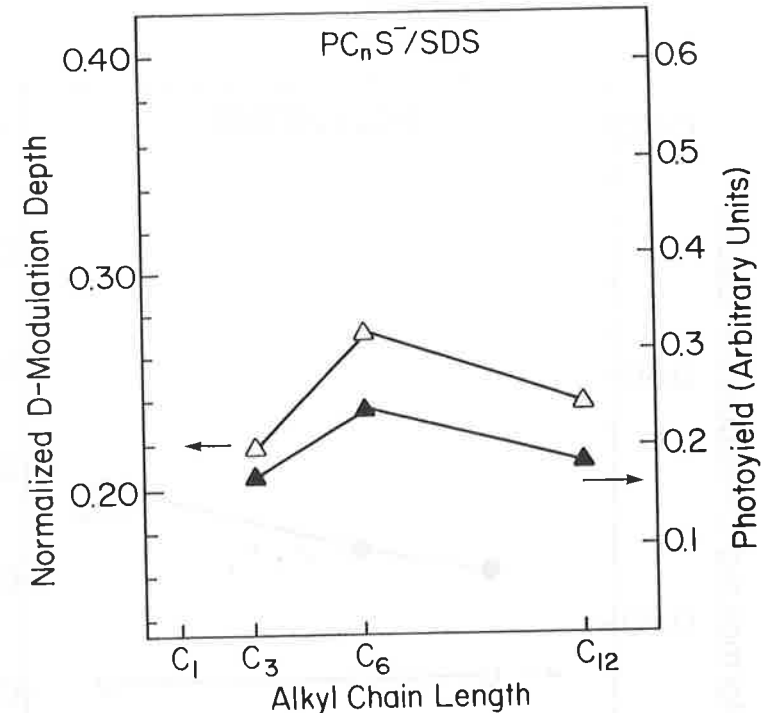


Figure 12. Normalized deuterium modulation depth and photoyield versus alkyl chain length for the $\text{PC}_n\text{S}^-/\text{SDS}$ anionic micelle system.

other words, these molecules also penetrate more deeply into the DTAB micellar interface than into the SDS micellar interface.

Results for the neutral alkylphenothiazine molecules in DTAB and SDS micelles are shown in Figures 15 and 16. In both cases there is a significant alkyl chain length effect. It is in the opposite direction than is typically encountered in vesicle systems, but there is a good correlation between the normalized deuterium modulation depth and the photoyield. In the SDS micellar system the normalized deuterium modulation depth is higher than in the DTAB micellar system thus indicating less penetration into the SDS interface. This is consistent with the results found for the phenothiazine alkylsulfonates in the micellar systems. The normalized deuterium modulation

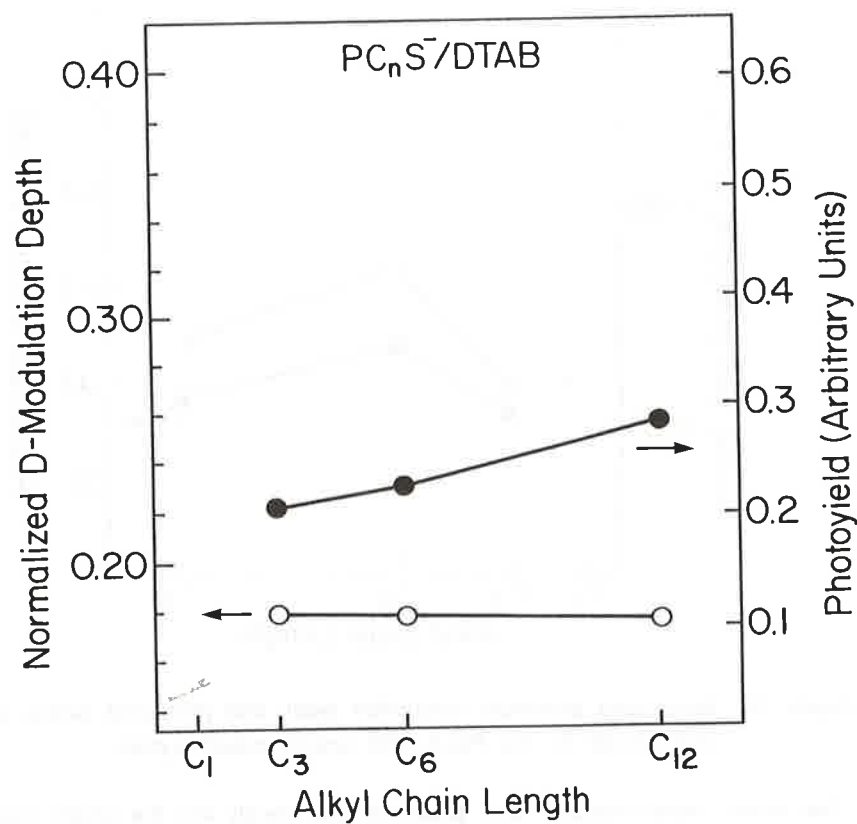


Figure 13. Normalized deuterium modulation depth and photoyield versus alkyl chain length for the $\text{PC}_n\text{S}^-/\text{DTAB}$ cationic micelle system.

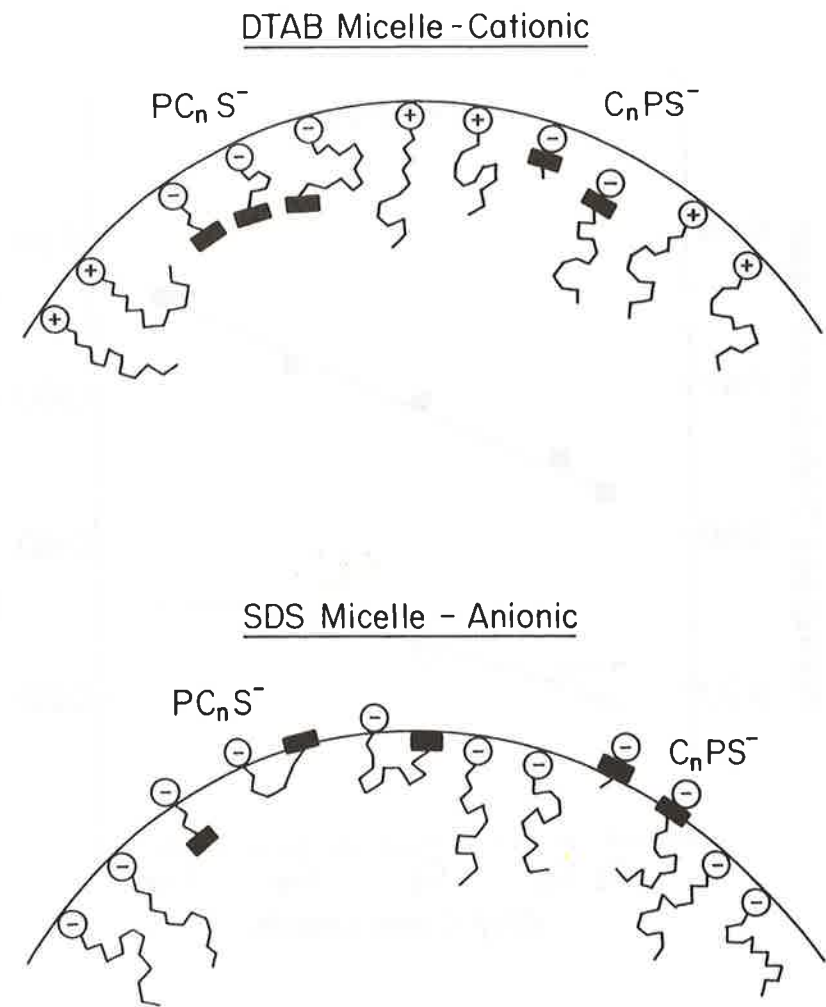


Figure 14. Schematic of the location of PC_nS^- and C_nPS^- molecules in cationic DTAB and anionic SDS micelles. The rectangle is the phenothiazine moiety.

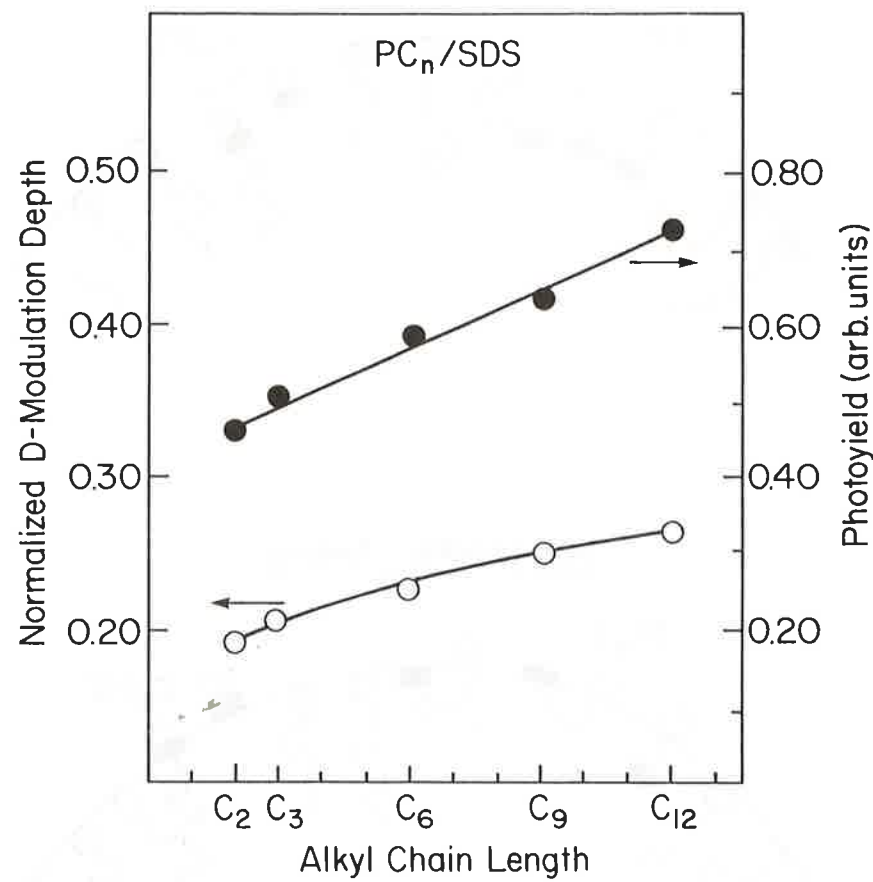


Figure 15. Normalized deuterium modulation depth and photoyield versus alkyl chain length for the PC_n/SDS anionic micelle system.

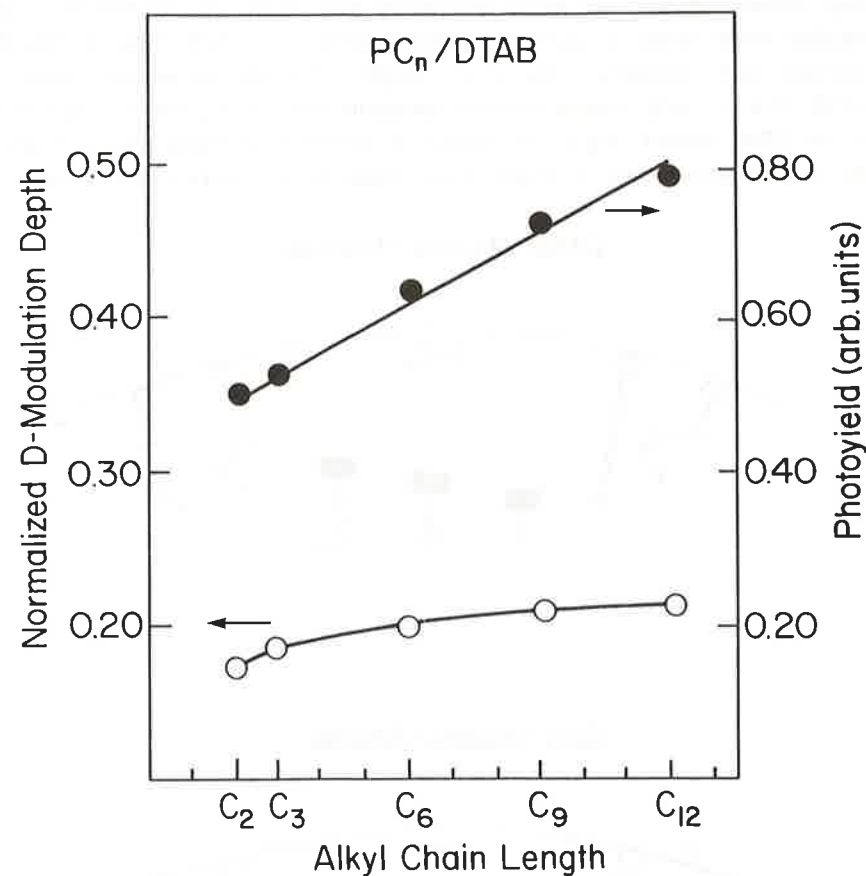


Figure 16. Normalized deuterium modulation depth and photoyield versus alkyl chain length for the PC_n/DTAB cationic micelle system.

depth shows decreasing penetration with increasing alkyl chain length for the phenothiazine moiety. This presumably reflects steric pressure of the longer alkyl chains against the highly disordered alkyl chains in the interior of the micelles which tends to push the phenothiazine moiety further out toward the interface with increasing alkyl chain length. The photoyields are higher in DTAB than in SDS micellar systems consistent with the positive surface charge in the DTAB system. Figure 17 shows a schematic of these results in which the phenothiazine moiety is shown to get closer to the interface with a longer

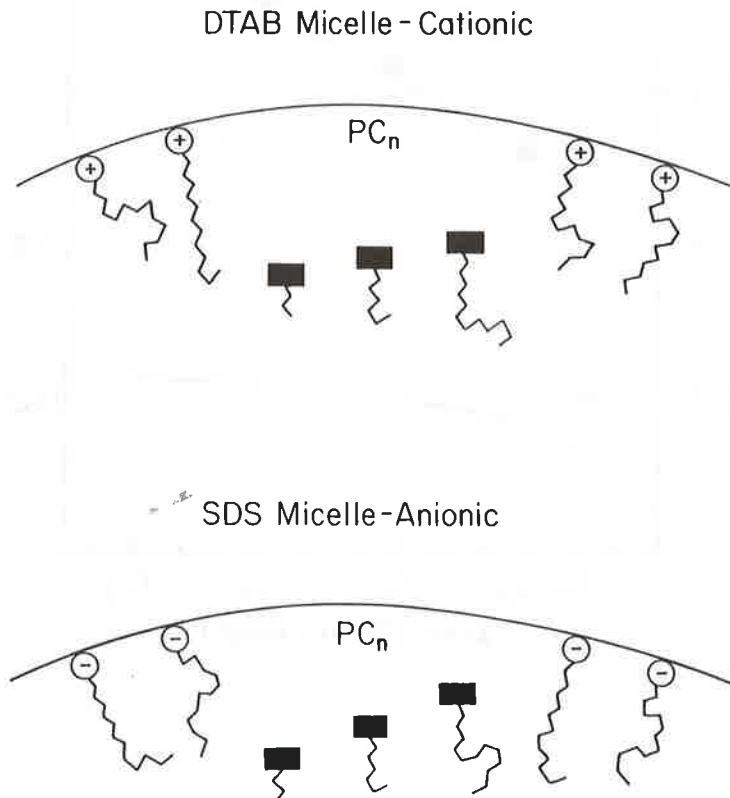


Figure 17. Schematic of the location of PC_n molecules in cationic DTAB and anionic SDS micelles. The rectangle is the phenothiazine moiety.

alkyl chain and to penetrate more deeply into the DTAB micellar interface than into the SDS micellar interface. It should also be noted that the greater penetration into the DTAB micelles by the alkylphenothiazine derivatives is consistent and analogous to the greater penetration into the DODAC vesicles by the alkylphenothiazine derivatives. In the vesicle systems this is interpreted as being associated with looser alkyl chain packing due to the bulkier headgroup in DODAC vesicle systems. The same argument can be used for the DTAB micellar system which has the bulky trimethylammonium headgroup and which may lead to looser alkyl chain packing. Thus there is a pleasing consistency between the overall trends and results in the vesicle versus the micellar systems.

Reverse Micelle Systems

Finally, we consider two reverse micellar systems. Reverse micellar systems are formed in an alkane solvent such as isoctane with a polar water pool in the center and the polar headgroups toward the center of the reverse micelle rather than in the opposite direction as in normal micelles. Figure 18 shows a schematic of two reverse micellar systems, the anionic AOT system and the cationic CTAB/ C_6OH system. The anionic AOT system is the most popular reverse micellar system studied. CTAB alone forms normal micelles but with a sufficient amount of an alcohol cosurfactant it forms reverse micelles. The alcohol acts to lower the interfacial tension between the water and the organic phase and it partitions between the nonpolar organic phase and the water. About 10 volume percent of a 1-alcohol with a C_4 chain or longer is used in this cationic reverse micelle system.

Figure 19 shows the photoyield versus alkyl chain length of the phenothiazine alkylsulfonate compounds. It is seen that the photoyield decreases somewhat as the alkyl chain increases. This is consistent with what has been seen before mainly in vesicle systems. In fact, the trend in the cationic reverse micelle system is similar to the trend in the cationic DODAC vesicle systems. In this case the alkyl chains of the phenothiazine alkylsulfonates are largely extended. The trend looks similar to that for the anionic AOT system which is also similar to that in anionic DHP vesicles.

An anomalous finding is that the photoyield is greater in the anionic AOT than in the cationic CTAB/ C_6OH reverse micelle systems. In all other cases in normal micelle systems and in vesicle systems the photoyields are greater in

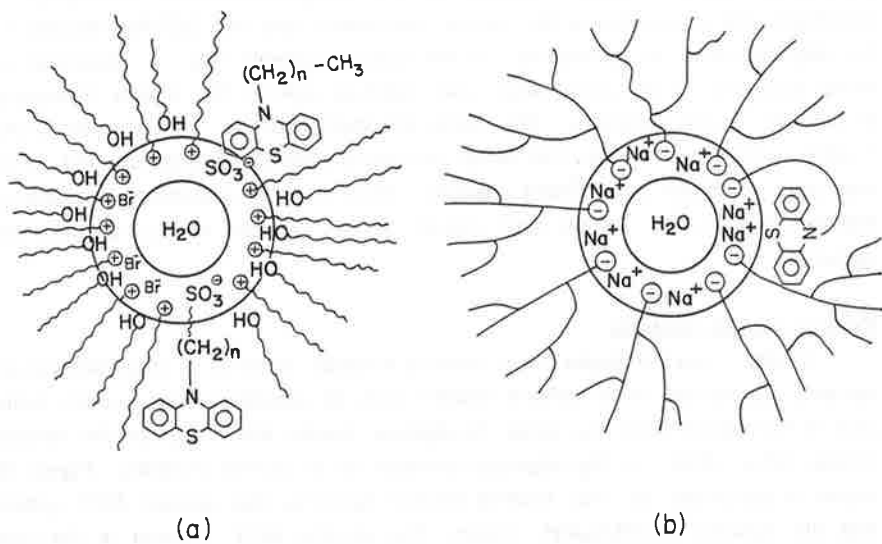


Figure 18. (a) Schematic of CTAB/ C_4OH reverse micelles with PC_nS^- and C_nPS^- molecules and (b) AOT reverse micelles with PC_nS^- molecules.

cationic than in anionic surfactant assemblies. This reversal for anionic AOT reverse micelle systems can be explained if the alkyl chains of the phenothiazine alkylsulfonates are significantly bent. This would bring the phenothiazine group closer to the interface and increase the photoyield. Thus the relatively high photoyield implies that significant alkyl chain bending occurs in the anionic AOT reverse micelle system. This is shown schematically in Figure 18 in which the photoionizable molecule has largely extended alkyl chains in the CTAB/ C_4OH cationic reverse micelle system and largely bent alkyl chains in the AOT anionic micelle system. The branched surfactant chains also

lead to a less ordered environment which promotes alkyl chain bending for the photoionizable molecule. The same charge on the interface and on the phenothiazine alkylsulfonate also induces a headgroup repulsion which promotes

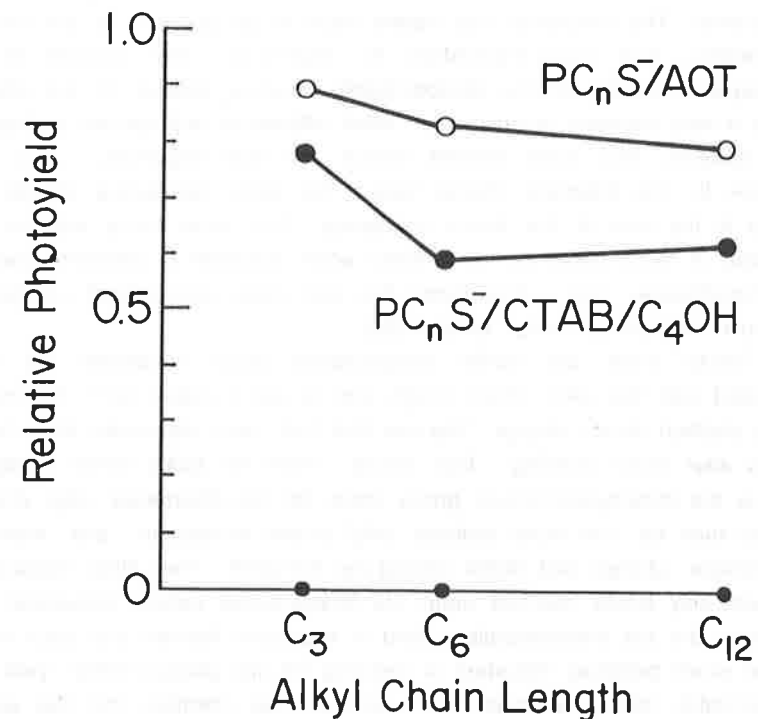


Figure 19. Relative photoyield versus alkyl chain length for PC_nS^- molecules in anionic AOT and cationic CTAB/ C_4OH reverse micelles.

alkyl chain bending. Thus, in some sense, the reverse micelle systems seem somewhat more analogous to vesicle systems of the same interface charge than they do to normal micelle systems.

4. Conclusions

The results reviewed here show that location control of electron donors is possible near surfactant assembly interfaces by the addition of variable length alkyl chains. This conclusion has largely been made possible by the utilization of electron spin echo modulation for monitoring the location of the paramagnetic moiety of the photoionizable molecule relative to the interface. This is a very sensitive technique for small differences in distances and location.

However, two other control factors are also important. The most important is the interface charge versus the donor headgroup charge. The second is the size of the donor headgroup. This latter factor has not been discussed in much detail but is a factor when sulfonate is attached directly to the phenothiazine ring. This factor has also been encountered previously in ruthenium tris(bipyridyl) alkyl systems [35].

Finally there are some complications which modulate the trends associated with the alkyl chain length and to some extent with the interface versus electron donor charge. The one that has been discussed most here is due to alkyl chain bending. This occurs more for bulky donor headgroups such as the trimethylammonium group, more for the disordered alkyl chains in micelles than for the more ordered alkyl chains in vesicles, and more when the interface charge and donor charge are the same. Two other complications that were only briefly touched upon are photoinduced radical conversion which can affect the net photoionization yield in a positive fashion and back electron transfer which becomes important in reducing the net photoionization yield if the photoionizable moiety extends much outside the interface into the aqueous phase. This latter complication has been only found to be important when the sulfonate group is attached directly to the phenothiazine moiety.

Acknowledgment

This research was supported by the Division of Chemical Sciences, Office of Basic Energy Sciences, Office of Energy Research, U.S. Department of Energy.

References

- [1] Larry Kevan in M.A. Fox and M. Chanon (eds.), *Photoinduced-Electron Transfer Part B: Experimental Techniques and Medium Effects*, Elsevier, Amsterdam, 1988; pp. 329 - 384.
- [2] P. A. Narayana, A.S.W. Li and L. Kevan, *J. Am. Chem. Soc.*, 103 (1981) 3603.
- [3] L. Kevan, P.A. Narayana and A.S.W. Li, *J. Photochem.*, 17, (1981) 180.
- [4] P. A. Narayana, A.S.W. Li and L. Kevan, *J. Phys. Chem.*, 86 (1982) 3.
- [5] P. A. Narayana, A.S.W. Li and L. Kevan, *J. Am. Chem. Soc.*, 104 (1982) 6502.
- [6] P.A. Narayana and Larry Kevan, *Photochem. Photobiol.*, 37 (1983) 105.
- [7] L. Kevan, A.S. W. Li and P.A. Narayana in A. Zewail (ed.), *Photochemistry and Photobiology*, Harwood Academic Publishers, New York, 1983, Vol. 2, pp. 1071-1082.
- [8] L. Kevan, in S.V. Szokolay (ed.), *Solar World Congress*, Pergamon Press, Oxford, 1984, Vol. 3, pp. 2028-2032.
- [9] A.S.W. Li and L. Kevan, *Radiat. Phys. Chem.*, 24 (1984) 441.
- [10] E. Szajdzinska-Pietek, R. Maldonado, L. Kevan and R.R.M. Jones, *J. Am. Chem. Soc.*, 106 (1984) 4675.
- [11] A. Plonka and L. Kevan, *J. Chem. Phys.*, 80 (1984) 5023.
- [12] R. Maldonado, L. Kevan, E. Szajdzinska-Pietek, and R.R. M. Jones, *J. Chem. Phys.*, 81 (1984) 3958.
- [13] A. Plonka and L. Kevan, *J. Phys. Chem.*, 88 (1984) 6348.
- [14] R. Maldonado, E. Szajdzinska-Pietek, L. Kevan, R.R.M. Jones, *Faraday Discuss. Chem. Soc.*, 78 (1984) 165.
- [15] E. Szajdzinska-Pietek, R. Maldonado, L. Kevan, R.R.M. Jones and M.J. Coleman, *J. Am. Chem. Soc.*, 107 (1985) 784.
- [16] E. Szajdzinska-Pietek, R. Maldonado, L. Kevan, S.S. Berr and R.R.M. Jones, *J. Phys. Chem.*, 89 (1985) 1547.
- [17] R. Arce and L. Kevan, *J. Chem. Soc. Faraday I*, 81 (1985) 1025.
- [18] A. Plonka and Larry Kevan, *J. Phys. Chem.*, 89, 2087 (1985).
- [19] A. Plonka and L. Kevan, *J. Chem. Phys.*, 82 (1985) 4322.
- [20] N. Ohta and L. Kevan, *J. Phys. Chem.*, 89 (1985) 2415.
- [21] E. Szajdzinska-Pietek, R. Maldonado, L. Kevan and R.R.M. Jones, *J. Am. Chem. Soc.*, 107 (1985) 6467.
- [22] R.R.M. Jones, R. Maldonado, E. Szajdzinska-Pietek and Larry Kevan, *J. Phys. Chem.*, 90 (1986) 1126.

- [23] E. Szajdzinska-Pietek, R. Maldonado, L. Kevan and R.R.M. Jones, *J. Colloid Interface Sci.*, 110 (1986) 514.
- [24] I. Hiromitsu and L. Kevan, *J. Phys. Chem.*, 90 (1986) 3088.
- [25] R. Maldonado, E. Szajdzinska-Pietek, L. Kevan and R.R.M. Jones in K.L. Mittal and P. Bothorel (eds.), *Surfactants in Solution*, Plenum Press: New York, 1986, Vol. 4, pp. 253 - 261.
- [26] P. Baglioni and L. Kevan, *J. Phys. Chem.*, 91 (1987) 1516.
- [27] P. Baglioni and L. Kevan, *J. Phys. Chem.*, 91 (1987) 2106.
- [28] M.J. Colaneri, L. Kevan, D.H.P. Thompson and J.K. Hurst, *J. Phys. Chem.*, 91 (1987) 4072.
- [29] L. Kevan in S. Terol (ed.), in *Proceedings of the 1986 International Congress on Renewable Energy Sources*, C.S.I.C., Madrid, 1987, Vol. II, pp. 936-941.
- [30] A.S.W. Li and L. Kevan, *Arabian J. Sci. Engin.*, 13 (1988) 157.
- [31] P. Baglioni and L. Kevan, *J. Chem. Soc. Faraday Trans. I.*, 84 (1988) 467.
- [32] E. Rivara-Minten, P. Baglioni, and L. Kevan, *J. Phys. Chem.* 92 (1988) 2613.
- [33] P. Baglioni, E. Rivara-Minten and L. Kevan, *J. Phys. Chem.* 92 (1988) 4726.
- [34] Piero Baglioni and L. Kevan, *Prog. Colloid Polym. Sci.*, 76, 183 - 187 (1988).
- [35] Michael J. Colaneri, Larry Kevan and Russ Schmehl, *J. Phys. Chem.*, 93 (1989) 397.
- [36] Piero Baglioni, Elisabeth Rivara-Minten and Larry Kevan, *J. Phys. Chem.*, 93 (1989) 1570.
- [37] Thomas Wolff and Larry Kevan, *J. Phys. Chem.*, 93 (1989) 2065.
- [38] Piero Baglioni, Roberta Bongiovanni, Elisabeth Rivara-Minten and Larry Kevan, *J. Phys. Chem.*, 93 (1989) 5574.
- [39] Piero Baglioni, Ming Hu and Larry Kevan, *J. Phys. Chem.*, 94 (1990) 2586.
- [40] Larry Kevan, *Radiat. Phys. Chem.*, 36 (1990) 181.
- [41] Piero Baglioni, Enzo Ferroni and Larry Kevan, *J. Phys. Chem.*, 94 (1990) 4296.
- [42] L. Kevan and P. Baglioni, *Pure Appl. Chem.* 62 (1990) 275.
- [43] Ming Hu and Larry Kevan, *J. Phys. Chem.*, 94 (1990) 5348.
- [44] L. Kevan, *Intl. Rev. Phys. Chem.*, 9 (1990) 307-328 (1990).
- [45] L. Kevan, *Radiat. Phys. Chem.*, 37 (1990) 629.
- [46] Chris Stenland and Larry Kevan, *Radiat. Phys. Chem.*, 37 (1990) 423.
- [47] H. Nakamura, P. Baglioni, L. Kevan and T. Matsuo, *J. Phys. Chem.*, 95, (1991) 0000, in press.
- [48] P. Baglioni, H. Nakamura and L. Kevan, *J. Phys. Chem.*, 95 (1991) 3856-3859.
- [49] K. Madden, L. Kevan, P.D. Morse and R.N. Schwartz, *J. Phys. Chem.*, 84 (1980) 2691.
- [50] K. Madden, L. Kevan, P.D. Morse and R. Schwartz, *J. Am. Chem. Soc.*, 104 (1982) 10.
- [51] A.S.W. Li and L. Kevan, *J. Am. Chem. Soc.*, 105 (1983) 5752.
- [52] N. Ohta and L. Kevan, *J. Phys. Chem.*, 89 (1985) 3070.
- [53] N. Ohta, M. Narayana and L. Kevan, *J. Chem. Phys.*, 83 (1985) 4382.
- [54] I. Hiromitsu and L. Kevan, *J. Am. Chem. Soc.*, 109 (1987) 4501.
- [55] T. Hiff and L. Kevan, *Photochem. Photobiol.* 48 (1988) 553.
- [56] I. Hiromitsu and L. Kevan, *J. Phys. Chem.* 92 (1988) 2770.
- [57] T. Hiff and L. Kevan, *J. Phys. Chem.*, 92 (1988) 3982.
- [58] Marie-Pierre Lanot and Larry Kevan, *J. Phys. Chem.*, 93 (1989) 998.
- [59] Thomas Hiff and Larry Kevan, *J. Phys. Chem.* 93 (1989) 1572.
- [60] Thomas Hiff and Larry Kevan, *J. Phys. Chem.*, 93 (1989) 2069.
- [61] Thomas Hiff and Larry Kevan, *J. Phys. Chem.*, 93 (1989) 3227.
- [62] I. Hiromitsu and L. Kevan, *J. Phys. Chem.*, 93 (1989) 3218.
- [63] Marie-Pierre Lanot and Larry Kevan, *J. Phys. Chem.*, 93 (1989) 5280.
- [64] M. Sakaguchi and L. Kevan, *J. Phys. Chem.*, 93 (1989) 6039.
- [65] Thomas Hiff and Larry Kevan, *Colloids and Surfaces*, 45 (1990) 185.
- [66] M. Sakaguchi, M. Hu and L. Kevan, *J. Phys. Chem.*, 94 (1990) 870.
- [67] M. Sakaguchi and L. Kevan, *J. Phys. Chem.*, 95 (1991) 0000, in press.
- [68] Y. S. Kang, P. Baglioni, H.J.D. McManus and L. Kevan, *J. Phys. Chem.*, 95 (1991) 0000, in press.
- [69] Peter Bratt, Young Soo Kang, Larry Kevan, Hiroshi Nakamura and Taku Matsuo, *J. Phys. Chem.*, 95 (1991) 0000, in press.
- [70] T. Ichikawa, L. Kevan and P.A. Narayana, *J. Phys. Chem.*, 83 (1979) 3378.

New Aspects of Photo-induced Chemical Reactions Studied by FT-EPR

Klaus-Peter Dinse, Gerhard Kroll, Marc Plüschauf

Institut für Physik, Universität Dortmund, W-4600 Dortmund 50,

Otto-Hahn-Strasse

and

Dieter Beckert, Zentralinstitut für Isotopen- und Strahlenforschung,

Permoserstraße 15, D-7050 Leipzig, Germany

Abstract

Utilizing Fourier-transform EPR, photo-initiated electron and proton transfer has been studied in the system anthraquinone/4-Methyl-2,6-di-tert-butylphenol in 2-propanol. The resulting superposition of anthrasemiquinone and hydroxy-anthroxy radical spectra spinpolarized by the triplet mechanism of CIDEP could be fully analyzed with respect to generation, interconversion and decay. For the first time clear evidence for a two-step sequential electron/proton transfer was found with magnetic resonance techniques. Using improved relative time synchronization for the interrogating microwave and the photo excitation pulse, the build-up and decay kinetics of the Coulomb-coupled metastable radical pair Zn-tetraphenylporphyrin/benzoquinone was studied in different solvents. The kinetic data could be interpreted invoking solvent screening of the Coulomb potential as dominating the temperature dependence of the kinetic constants.

1. Introduction

The investigation of radical pairs and of the "cage effect" of solvated reaction partners seems to be crucial for the description of chemical reactions in solution. Obviously, such an investigation has to cover many orders-of-magnitude in time resolution, starting in the ps domain for a survey of molecular relaxation processes, and also covering the quasi-static ms range for a description of final reaction channels. Magnetic resonance (MR) techniques have been developed to follow kinetics down to the 10 ns level [1-5]. This time resolution is sufficient for a direct observation of photo-initiated, diffusion-controlled electron transfer reactions, if the scavenger concentration is less than 10^{-2} M. The great advantage of MR is given by its spectral resolution, enabling the unambiguous identification of radicals involved in the reaction. This spectral resolution in combination with time resolution is obtained by using Fourier-transform EPR (FT-EPR), i.e., by monitoring the free induction decay (FID) of the system after a single microwave pulse, time-labeling the radicals. Therefore FT-EPR can

be envisaged as a perfect stroboscopic method, enabling the observation of the intensity/time profile (including phase) of individual hyperfine components (hfcs), even in the case of partially overlapping spectra from different reaction products.

The ability to detect also the phase of individual hfcs is important because "dispersive" admixtures have been identified as characteristic for biradical-like spectra and can thus be used as a "fingerprint" for the existence of an exchange- or dipolar-coupled spin hamiltonian. Increasing the time resolution of FT-EPR to the 10 ns limit, the observation of the creation and decay of metastable radical pairs even in homogeneous, isotropic solvents could be monitored in detail, allowing the determination of the coupling potential.

Considering the high spectral resolution of FT-EPR, only limited by T_2 and the spectral density of hfcs, it is possible to investigate photo-induced chemical reactions with multiple reaction channels. As an example, triplet quenching of anthraquinone by alcohols and/or phenols can occur via electron or hydrogen transfer, resulting in anthrasemiquinone ($AQ^{\cdot-}$) radical ions or hydroxy-anthroxy (AQH^{\cdot}) neutral radicals, respectively. It was the aim of this investigation to follow the kinetics of these reactions in detail and to search for evidence of a two-step sequential electron/proton transfer after diffusion-controlled encounter of the reactants.

2. Method and materials

The experiments were performed with a home-built FT-EPR apparatus [2]. The timing of the pulse programmer is synchronized with respect to the laser pulse by two different methods, depending on the delay time. For delays ≥ 350 ns, a trigger pulse generated by a fast photodiode is directly used to initiate the pulse program for the microwave pulse and various gates. For shorter delays, the rather large set-up delay of the TWT gate necessitates the use of the electric discharge pulse of the excimer laser as time reference for the microwave pulse. Because of a noticeable jitter between this discharge pulse and the actual light pulse, this simple method can lead to a timing error (jitter and drift) in the order of 10 - 30 ns, resulting in unrepeatable results for the fast build-up rate constants. Although the jitter can be minimized by running the excimer laser under stable discharge conditions for an extended time, we rather chose to exclude the jitter by using a coincidence circuit, allowing accumulation of data only if the relative delay of light and microwave pulses is within a preset time window of 6 ns. Either light of the excimer laser (308 nm) with pulse energy of 10 mJ or of the dye laser (≈ 580 nm) with pulse energy

2 mJ was used for optical excitation.

Triplet quenching of anthraquinone (AQ, 5×10^{-4} M) in 2-propanol (~50 ml) with 4-Methyl-2,6-di-tert-butylphenol (DTBPH, 0.1 M) was investigated at room temperature in a flow system in order to avoid solute depletion. AQ, DTBPH and 2-propanol were used without further purification. High-purity nitrogen was used to remove the oxygen and to drive the solvent flow. ZnTPP/DQ was investigated in carefully evacuated sample tubes of appr. 2 ml, as described elsewhere [2, 3].

3. Results and discussion

3.1 Investigation of the Anthraquinone/4-Methyl-2,6-di-tert-butylphenol photo-redox system

Figure 1 shows the EPR spectrum calculated from two phase-orthogonal FID's for a laser/microwave pulse delay of 10 μ s. The experimental data have been completed in the time domain with respect to missing points in the dead time interval using a LP routine of order 350 [8]. This method of

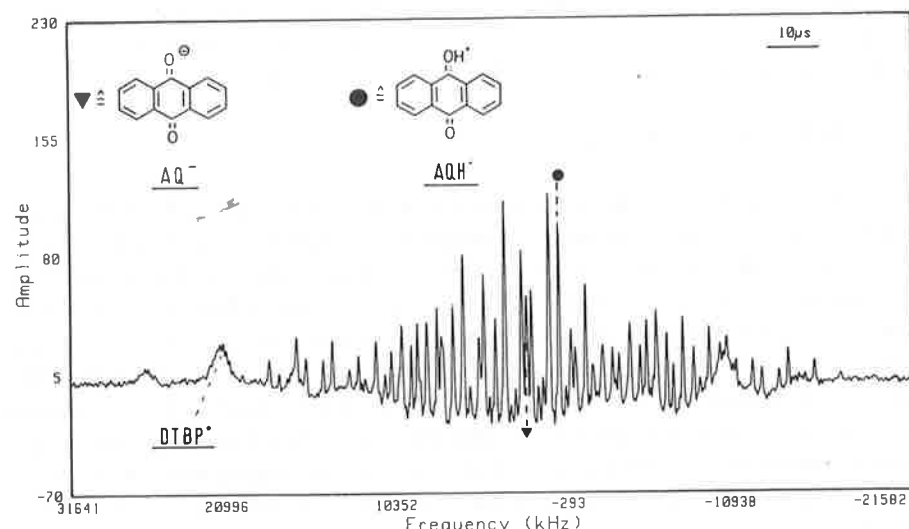
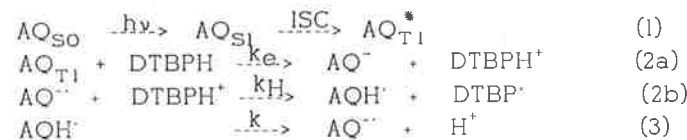


FIGURE 1

Room temperature EPR signal obtained 10 μ s after photo-reduction of AQ in 2-propanol with 0.1 M DTBPH as triplet quencher. Hyperfine lines indicated were used for selective monitoring of AQ⁻ and AQH⁺ intensities. The analysis of the spectra by simulation will be discussed elsewhere [9].

hybridization of experimental and calculated data leads to a noticeable improvement of the baseline, which was essential for the evaluation of single-line intensities. The spectrum could be fully analyzed by assuming a superposition of AQ⁻, AQH⁺ and DTBPH⁺ spectra. Owing to the high spectral density of the AQH⁺ spectrum, most lines overlap with the exception of two prominent lines marked in the figure. The intensity profile of both characteristic lines could be followed over the full delay range of 10 ns to 100 μ s. As can be seen in fig. 2, the signals of both radicals rise sharply in less than 1 μ s, followed by a slow decay of the dominating AQH⁺ signal to zero, whereas the AQ⁻ signal gains intensity by a rate similar to the AQH⁺ decay rate, approaching finally its absorptive Boltzmann value. Under high time resolution (not shown here), both signals show a fast initial rise with time constant 30(10) ns, which can be identified with the spectrometer response time.

The observed intensity/time profile of both radicals could fully be explained by considering the following reaction scheme:



In (2) the electron and proton donor is DTBPH and DTBPH⁺, respectively. In this scheme, the excited AQ triplet allows immediate electron transfer after diffusion-controlled encounter with the DTBPH quencher. The resultant change in pK of AQ⁻ initiates a subsequent proton transfer. This additional charge transfer normally opens the separation channel for the neutral radical products. The finite escape probability for the primary AQ⁻ radical before neutralizing proton transfer describes the coupling of (2a) and (2b). Finally, proton equilibrium with the solvent leads to the AQ⁻ "end product", stable on a time scale of 1 ms. (The repetition rate of the laser was reduced to 2 Hz to allow for a complete decay of all paramagnetic species in the cavity.) A sequential two-step electron/proton transfer can be identified unambiguously by the observation of a fast component in the build-up of the emissive AQ⁻ signal.

The time profile of both radicals could be modelled by approximating the multi-level spin systems by a five-level system. Here the photo-polarized AQ^{*} is described by one level (because of a predominant triplet mechanism (TM), one level is sufficient for a description of the radical precursor), whereas each radical is described by a two-level spin system. Spin polar-

ization originating from TM is modelled by defining population rates $k_{AOH^{\cdot}}$ and $k_{AQ^{\cdot-}}$ for both levels with a ratio $k(\text{upper})/k(\text{lower}) = p$, in which p is the limiting TM polarization under conditions of vanishing spin relaxation and chemical decay. Proton equilibration is taken as spin-conserving, i.e.,

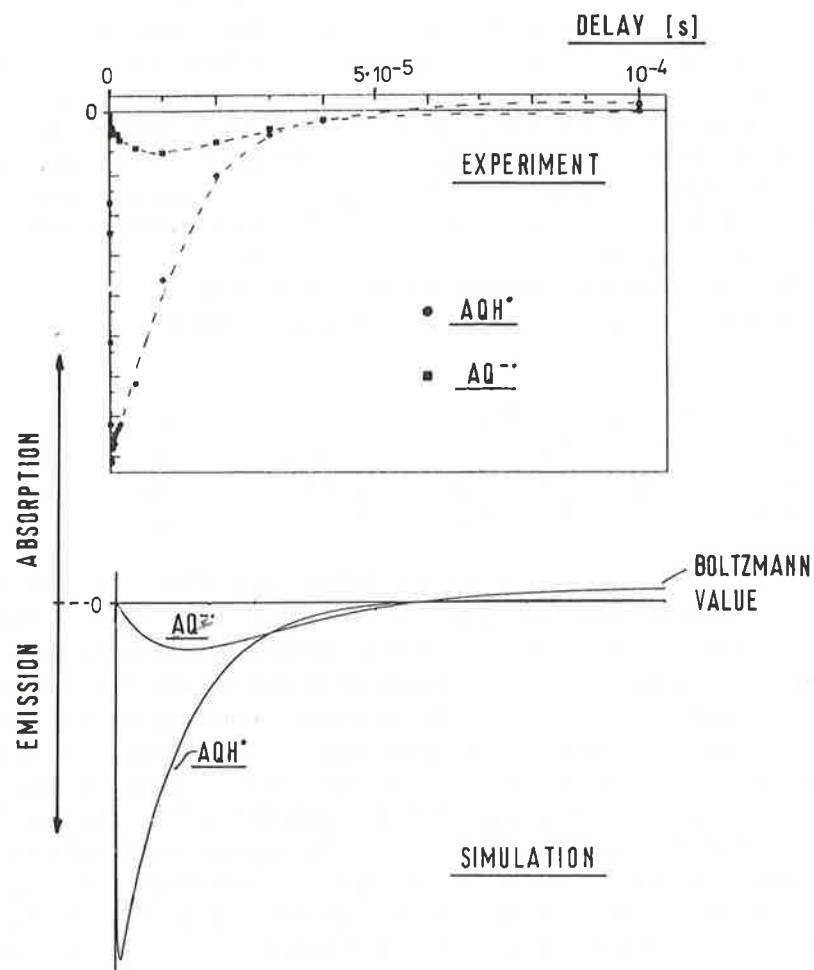


FIGURE 2

EPR intensities in the coupled $AQ^{\cdot-}$ and AOH^{\cdot} system. Most of the $AQ^{\cdot-}$ intensity visible in this figure results from the comparatively slow proton equilibrium reaction with the solvent. Data used for the simulation are given in the text.

the two rate constants k , connecting the upper and lower spin sublevels, are taken as equal. Finally, spin-lattice relaxation of both radicals was also included. The resulting set of 5 coupled differential equations was solved *analytically*, allowing a convenient modelling of the EPR signals as function of the various rate constants.

Excellent agreement with the experimental data was obtained with the following set of constants: $T_1(AQH^{\cdot}) = T_1(AQ^{\cdot-}) = 16 \mu\text{s}$, $k = 2.5 \times 10^4 \text{ s}^{-1}$, $k_{AOH^{\cdot}} = 4 \times 10^7 \text{ s}^{-1}$ and finally defining an escape probability $f = 0.03$ for the initially generated $AQ^{\cdot-}$. The observed $k_{AOH^{\cdot}}$ is limited by the response function of the spectrometer. The diffusion-limited rate constant for the primary electron transfer step is estimated as $3 \times 10^8 \text{ s}^{-1}$ [11], which cannot be observed in our experiment. The fast build-up of $AQ^{\cdot-}$, generated by escape from the primary radical pair, is measured as $\geq 4 \times 10^7 \text{ s}^{-1}$. Considering the escape probability $f = 0.03$, we can derive a lower limit for the second step proton transfer rate $k_H \geq 1.2 \times 10^8 \text{ s}^{-1}$.

3.2 Investigation of the metastable radical pair in the Zn-tetraphenylporphyrin/benzoquinone photo-redox system

First experiments using ZnTPP with duroquinone (DQ) as electron acceptor have been successfully interpreted with a model of a Coulomb-coupled metastable radical pair (RP) [6]. The use of the dispersive signal component as measure for the momentaneous concentration of the RP necessitates a high-precision determination of the phase of each hfc, in particular if the dispersive admixture is small. Such conditions are frequently met in low-viscosity solvents, allowing for a fast temperature-activated separation of the RP. The determination of the phase of each line with a precision of ≤ 2 degrees was performed with a two-step routine. In a first step, using a non-iterative LPSVD [8] routine, the number of signal components was determined in combination with the respective parameters for frequency and damping. Secondly, these parameters were used as starting values for a non-linear fit in the time domain, utilizing the VARPRO [10] routine. The calculated intensity and phase parameters for each hfc as a function of the delay time Δt between laser and microwave pulse was finally used for a projection of the complex signal intensity on the absorptive and dispersive axes, taking the phase limit ($\Delta t \rightarrow \infty$) as absorptive reference. Figure 3 shows the dispersive signal component as a function of Δt of each hfc in BQ^{\cdot} at 244 K. As expected, the amplitude uncertainty is largest for the $|M_1| = 2$ hfcs, although all lines show qualitatively the same time dependence. The rise time of the dispersive components were found equal within error limits with the electron transfer rates, deduced

from the absorptive components with higher precision. Those rates range from $7.3(7) \times 10^6 \text{ s}^{-1}$ at 244 K to $23(1) \times 10^6 \text{ s}^{-1}$ at 292 K and are found to scale linearly with $(\eta/T)^{-1}$ within the quoted errors.

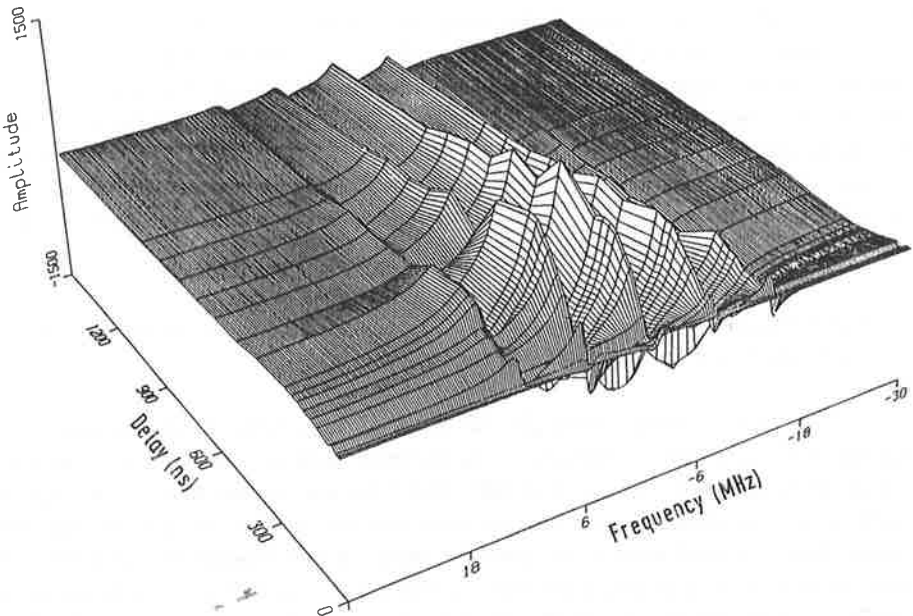


FIGURE 3

Dispersive signal amplitude in the ZnTPP/BQ system at 244 K.

If the escape rates are evaluated in the model of Shushin modified according to ref. 6, a binding potential of 0.10 (1) eV is deduced. Taking into account the dielectric constant of 2-propanol, ranging from 29 at 244 K to 20 at 290 K, the unshielded binding potential is calculated as 2.5(3) eV. This value is noticeably smaller than the potential of the RP in ethanol, consistent with the expectation of increased spatial separation owing to the increased volume of the solvent molecules.

4. Conclusion

Although the spin-correlated RP cannot be observed directly with FT-EPR, its presence at short time after the photo-initiated charge transfer can be monitored with high time resolution. For the RP in 2-propanol the binding potential used for modelling the metastable pair in its solvent cage is reduced to $u(r_C) \approx 4 \text{ kT}$, close to the limit of validity of Shushin's model. Further reduction of $u(r_C)$ would lead to a breakdown of the central assumption that the temperature-activated fluctuation Δ of the equilibrium distance r_C is negligible compared with the escape distance l . Under such conditions, RP separation by unhindered translational diffusion would be undistinguishable, a situation expected for 2-propanol at still lower temperatures.

High spectral resolution analysis of the triplet quenching of AQ with DTBPH gave clear evidence for a sequential two-step electron/proton transfer. Although both individual processes are faster than the response time of the spectrometer, the fast initial rise of EPR signals from both radicals AQ^\cdot and AQH^\cdot is unambiguous proof for a finite escape probability of the initially generated AQ^\cdot radical. Obviously, this escape probability will be influenced by deuteration of the DTBPH scavenger. Anticipating that the transition state involved in the proton abstraction reaction invokes C-H bond stretching, the proton transfer rate should be reduced by approximately a factor of 2 [7], being easily detectable by a corresponding increase of the concentration of initially generated AQ^\cdot radicals.

Acknowledgments

We gratefully acknowledge financial support of the Deutsche Forschungsgemeinschaft, as well as helpful discussions with H. van Willigen (Boston).

References

1. T. Prisner, O. Dobbert, K.-P. Dinse, and H. van Willigen, *J. Amer. Chem. Soc.*, 110 (1988) 1622
2. M. Plüscha, A. Zahl, K.-P. Dinse, and H. van Willigen, *J. Chem. Phys.*, 90 (1989) 3153
3. A. Angerhofer, M. Toporowics, M.K. Bowman, J.R. Norris, and H. Levanon, *J. Phys. Chem.*, 92 (1988) 7164
4. J. Gorcester and J.H. Freed, *J. Chem. Phys.*, 88 (1988) 4678
5. A. Schweiger, *Angew. Chemie* 103 (1991) 223

6. G. Kroll, M. Plüschauf, K.-P. Dinse, and H. van Willigen, J. Chem. Phys., 93 (1990) 8709
7. G. Porter, S.K. Dogra, R.O. Loutfy, S.E. Sugamori, R.W. Yip, J. Chem. Soc. Faraday Trans. I (1973) 1462
8. H. Barkhuysen, R. de Beer, W.M.M. Bovee, D. van Ormondt, J. Magn. Reson. 61 (1985) 465
9. Paper in preparation.
10. G.H. Golub, V. Pereyra, J. Numer. Anal. 10 (1973) 413
11. D. Beckert, G. Schneider, Chem. Phys. 116 (1987) 421.

**Electron Spin Echo Study of CIDEP in Photolysis
of di-t-butyl Ketone at Low Temperatures**

P.P.Borbat, A.D.Milov and Yu.N.Molin.
Institute of Chemical Kinetics and Combustion,
630090, Novosibirsk, USSR

Abstract

Electron spin echo was used to study CIDEP of t-butyl radicals in toluene and 2-propanol. The cross-relaxation was found to be effective at low-temperature and to have significant influence on the observed kinetics of CIDEP decay. Computer simulations allowed us to estimate the rates of cross-relaxation transitions and the magnitude of nuclear polarization.

I. Introduction.

At short times, the radicals produced in a pulse very frequently show transient ESR spectra that differ significantly in magnitudes and phases from the equilibrium ones. This phenomenon is known as the chemically induced dynamic electron polarization (CIDEP) [1] or, more generally, as the electron spin polarization (ESP), two main mechanisms accounting for the majority of its observations.

The first is triplet mechanism (TM) [2]. It operates in the fast reactions of the spin-polarized triplet molecules, some part of the triplets polarization is left in the escaping radicals. This results in emissive (E) or absorptive (A) ESR spectra with normal line intensity ratios, the sign being determined by the sign of zero field splitting value D.

The second, known as the radical-pair mechanism (RPM), is responsible for the so-called multiplet CIDEP that is due to the singlet-triplet (ST) mixing in the geminate spin-correlated radical pairs (RP) or in the F-pairs formed by diffusing radicals. This mixing depends on the particular nuclear spin states of radicals forming RP that makes ESP non-uniform across the spectrum. For RP composed of radicals *a* and *b*, the polarizations are a function of quantity $Q_{ab}\alpha(\omega_a - \omega_b)$, where ω_a ,

ω_b are the Larmor frequencies of the radicals in the given nuclear states m_a, m_b . The $S T_0$ mixing in both the triplet RP and F-pairs gives the E/A type of spectra with abnormal line intensity ratios, emissive low-field and absorptive high-field halves, for singlet RP one observes the A/E polarization. The $S T_-$ mixing originates when radicals, composing a pair, diffuse apart and the S term crosses T_- . This results in slightly asymmetrical net emissive spectra with specific line intensity ratios and is observed noticeably for high viscosity.

It was recently found the TM and RPM are not responsible for all observed ESP patterns, and other phenomena such as polarization of biradicals [3] and of RP itself [4-6] cause each line in spectrum to have EA polarization. The net emissive polarization mechanism was proposed [7] and found in the quenching triplets of duroquinone [8], antraquinone [9] and benzophenone [10] by stable radicals and also in quenching of the benzil and some other triplets by short-lived radicals [11]. On a longer time-scale other mechanisms are found also to determine ESP pattern [30,31].

The tools for the study of the ESP in a microsecond domain are based today on a broad band cw time-resolved ESR detection (TRESR) [12]. The pulsed in essence techniques, such as the electron spin echo (ESE) [13] and Fourier transform ESR [14,15] are also used and bring their specific advantages.

It was also realized that for certain conditions in some radicals, in particular, those which have large hf constants, the cross-relaxation (CR) arising from modulation of the isotropic or anisotropic hf interactions by molecular motion might transform CIDNP into ESP or vice versa. This may cause inversion of the intial multiplet CIDEP from E/A in A/E on a longer time scale, provided nuclear polarization in radical is not small compared to CIDEP and CR is sufficiently fast [16,17]. For radicals with hf as large as 20 G both of these conditions

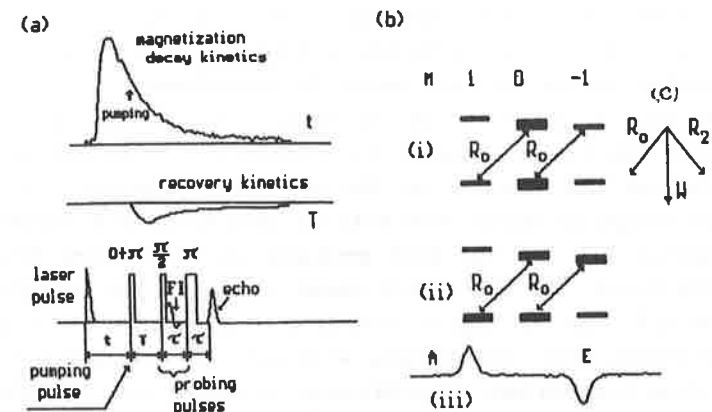


Fig.1. The scheme of the ESE kinetic technique (a) and diagram illustrating conversion of CIDNP to ESP (b), filled rectangles reflects the populations of a radical with two equivalent nuclei with $I=1/2$. R_0 and R_2 correspond to the cross-relaxation transitions with changing of the total electron and nuclear spin magnetic numbers to be equal $\Delta m=0$ and $\Delta m=2$, respectively, W is responsible for the spin-lattice relaxation (c). The resulting A/E ESR spectrum is shown below (iii).

may be well fulfilled. The mechanism of sign reversal is illustrated in fig.1b for the simplest case of the radical having two equivalent nuclei with $I=1/2$ and a positive hf constant. It is clear from the diagram how the R_0 transitions, governed by scalar CR mechanism, convert the initial CIDNP of EA type in radical (i) into A/E ESP (ii) (for triplet RP this E/A polarization means excess of the radicals with antiparallel α and β nuclear spins).

Using the TRESR technique it was found that the inversion of the sign of multiplet CIDEP is sure to occur at least for the 2-propylketyl and t-butyl radicals but is visible at high radical concentrations [18-20]. The photolysis of acetone in 2-propanol for different temperatures has also been studied by ESE [21] and time resolved NMR techniques [22]. The ESE studies show that at temperatures below 220K, the initial E/A

polarization of 2-propylketyl radicals transforms to the A/E at 10 μ s after the laser flash. This behavior has been explained by the existence of a sufficiently high multiplet nuclear spin polarization in the radical which is transformed into electron spin multiplet polarization by means of CR due to scalar relaxation mechanism caused by rotation of methyl groups. Time-resolved NMR studies on the sign of multiplet effect in cage and escape products show both of them to be A/E contrary to the expected E/A for the bulk products as it follows from the Kaptein's rules. The NMR result seems to be in some disagreement with the ESR ones but may be referred to high magnetic field of NMR experiment. This discrepancy will not be discussed further.

At room temperature in nonviscous solvents the CR rates are believed to be slow enough to provide marked influence on ESP. Thus, special conditions, for example, implying a sufficiently fast spin exchange to quench initial E/A polarization, should be found to obtain the ESP sign reversal [19]. Lowering the temperature and/or increasing viscosity the CR rates may be sufficiently increased and become comparable with spin-lattice relaxation rate τ . So, as previously [22], we have used the ESE technique to study the CIDEP of t-butyl radicals on the subject of the CR role, especially, at low-temperatures.

In ESE, the magnetization of the radicals created by a photolytic pulse is detected via sequence of microwave pulses forming the spin-echo or free induction (FI) signals that gives a time profile of radical magnetization whose time behavior is determined by various sources. The variety of reasons determine the ESP time evolution on a long time scale and so it is important to search for suitable methods to separate them. The possibility of changing CIDEP by influencing magnetization in a desired way is constructive and yet has been exploited in TRESR experiments to study electron exchange [23] and also in ESE investigations on spin-lattice relaxation times of short-lived radicals [24] and in ESE two-dimensional FT experiments on unstable radicals as well [15].

2. Experimental.

t-Butyl radicals were produced upon photolysis of the solutions, containing vol 1% of di-t-butyl ketone in toluene or 2-propanol, using a home-built XeCl laser running at up to 4Hz repetition rate. Solutions were circulating in a closed cycle gas-lift system, pure Ar being used both as carrier gas and oxygen remover. The quartz flow cell having inner dimensions of 3x3x15 mm was placed inside a quartz dewar tube mounted in a TE₁₀₂ cavity of the ESE spectrometer [25].

Temperature was monitored using a thermocouple placed into the cell 2 cm above the illuminated region and found to be stable in the limit of 0.5K. The lowest temperature achieved was 180K for 2-propanol and 150K for toluene. For solutions under study, lowering the temperature from ambient to the lowest achieved with the given solution results in the decrease of the flowing rate from 2 to 0.1 ml/min due to the increase of the viscosity. Heating of the solution was measured not to exceed 1K in the worst case, i.e. the slowest flow, the maximum repetition rate and full photon flux up to 60 mW. To attenuate light pulse calibrated filters was placed in a light path.

A typical ESE experimental procedure shown in fig.1a implies the application of narrow microwave pulses at different delays after the laser pulse with subsequent detection of the primary echo or FI signals to obtain magnetization time-profile of the desired spectral region. The ESE signal recorded in a field sweep mode gives the ESE detected ESR spectrum with a certain delay after radical creation.

There is another method which implies the application of the additional "pumping" microwave pulse to change magnetization of the chosen spectral region in a suitable manner. This pulse is set at a fixed delay t relative photolytic pulse and after a certain period of time T probing pulses are as usual used to detect the echo or FI signals. The last procedure is used to discern the polarization sources operating on a longer timescale and already not buried under the large initial polarization. In its simplest form, the method used may be referred to as "dynamic recovery technique" [24]. All other experimental details were the same as those described previously [21].

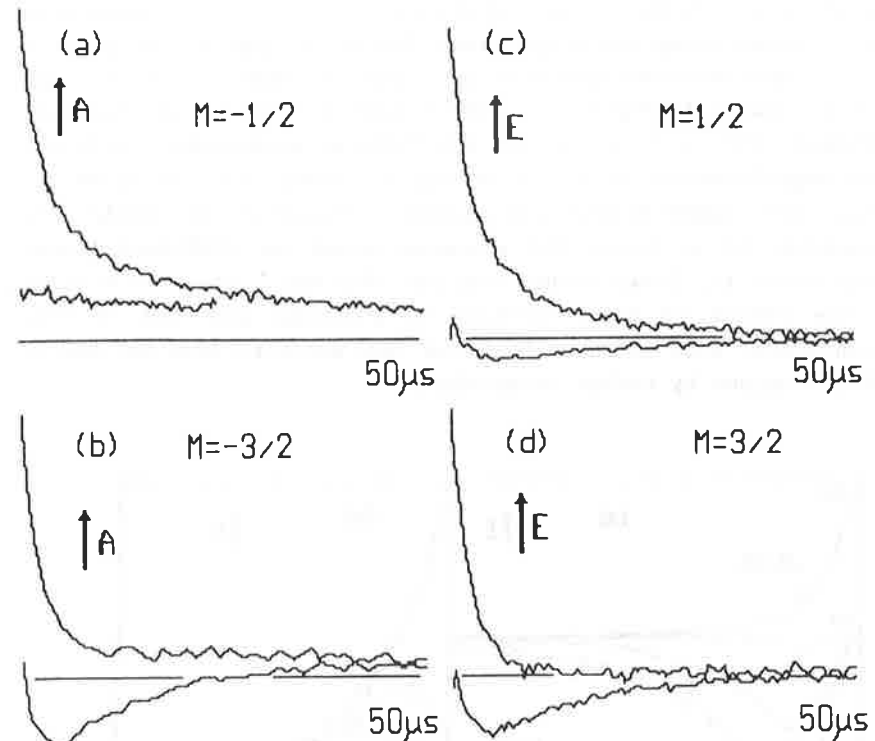
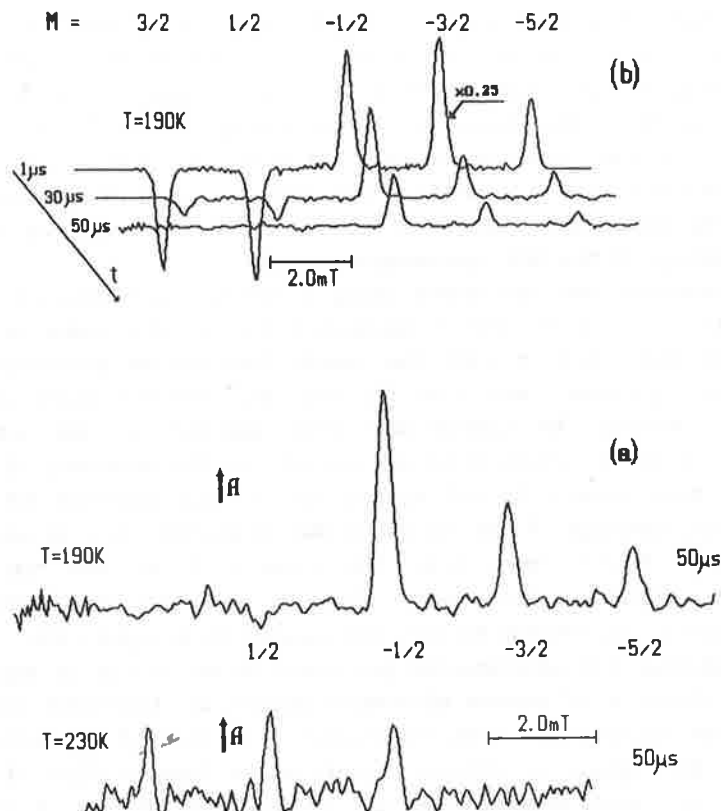


Fig.3. Time-profiles of the four centre lines of t-butyl radical in toluene for 159K in common with corresponding recovery kinetics.

Fig.2. The central part of t-butyl radical spectrum recorded at different temperatures (a) and delays from laser pulse (b), using toluene as solvent.

3. Results.

In fig2(a) the ESE spectra of t-butyl radical in toluene for 190K and 230K are plotted for delays of 50 μ s. It is clearly seen that for higher temperature the spectrum is indicative of the A^*/E polarization while for the lower temperature it obviously shows E/A^* . This is in agreement with the previous studies [19].

The central part of spectrum for the set of delays taken at 190K plotted in the fig.2b clearly shows that the spectrum shape

undergoes marked distortion with time. In fig.3 the time profiles are shown for the lines with $m=\pm 1/2, \pm 3/2$ in common with the corresponding recovery curves for a 90° pumping pulse. For $m=\pm 5/2$ the recovery kinetics are close to that for $m=\pm 3/2$ and are not given in figure. The behavior of decay and recovery kinetics for the lines (note, ESE signals, we measured, reflects the magnetization of the secondary splitted lines as a whole) that are symmetricaly positioned relative to centre of spectrum, if to forget for a moment about the different levels they relax to, looks rather similar. For the lines with $m = \pm 1/2$, the effect of sign reversal in recovery kinetics is less pronounced. Both of these features are expected from ESP due to CR determined by scalar relaxation.

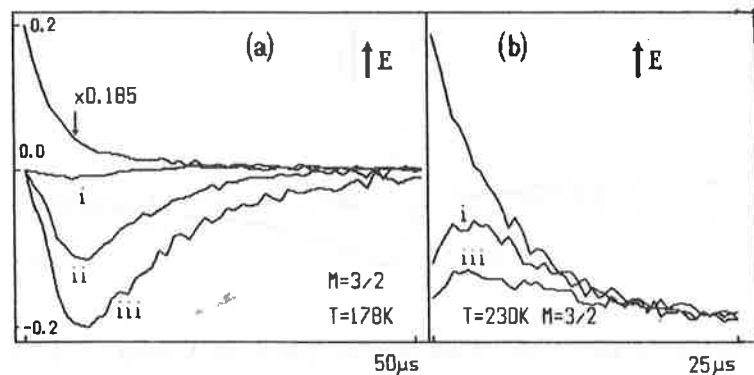


Fig.4. Recovery time-profiles of t-butyl radical in toluene normalized to the initial unperturbed amplitude for (a) 178K and (b) 230K, recorded for different levels of light flux
 (i) - light unattenuated;
 (ii),(iii) - attenuated to 60% and 36% respectively.

For higher temperatures, the F-pair polarization overlaps and prevents the sign reversal in the recovery kinetics (fig.4b). The decrease in the light intensity makes the contribution of F-pairs to diminish thus isolating the CR effect as it is seen in fig.4a. This result points to the fact that CR is very effective indeed at this temperature in t-butyl radical so as for $(\text{CH}_3)_2\text{COH}$. Unfortunately, the F-pair polarization in

toluene is not low in experimental conditions and decays slowly for low temperatures thus overcoming A/E, created as believed in transfer of nuclear polarization, and preventing the sign reversal (fig.3). Polarization transfer occurs within a shortened time interval and is masked by the large initial and F-pairs polarizations.

It is of interest to compare the results for the two above solvents. In fig.5, the results for toluene and 2-propanol are presented for 156K and 182K, respectively. For these temperatures, the viscosities are believed to be close as follows from the similarity of the spectra (For toluene, the spectrum is shown in fig.6 and may be reproduced satisfactorily if we suppose CIDEP enhancement to obey the dependence on Q of the type $Q^{0.5} \cdot a \cdot Q$ [32]). In 2-propanol, in contrast to toluene, the F-pairs seem to produce no considerable polarization at 182K and thus its E/A signal is overcomed by the nuclear polarization

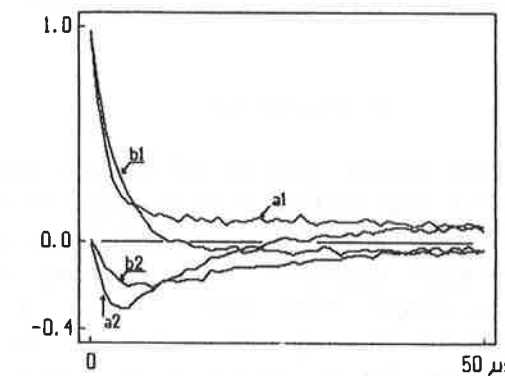


Fig.5. Time profiles of line with $m=-3/2$ of t-butyl radical in toluene at 156K (a1) and that for $m=3/2$ line of t-butyl radical in 2-propanol at 182K (b1); both with corresponding recovery kinetics (a2,b2) obtained with 90° pumping pulse. Kinetics for $m=3/2$ are shown inverted relative to these for $m=-3/2$.

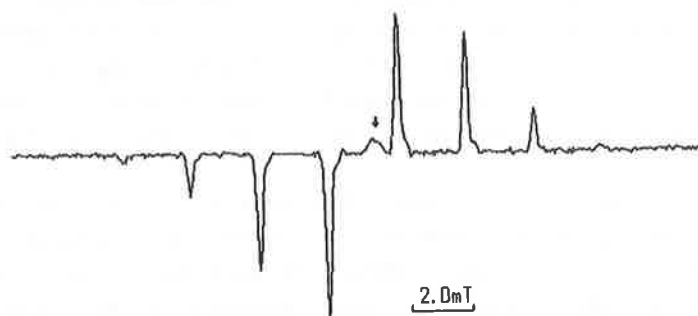


Fig.6.The spectrum of t-butyl radical in toluene at 155K.

transferred *via* CR. From recovery kinetics CR in 2-propanol is visible to be some slower than in toluene thus being operative at the times where large initial polarization decays to a great extent.

4. Discussion

The shape of the central portion of the spectrum clearly indicates that except spin-lattice relaxation an extra mechanism exists on a longer timescale in a sufficiently wide temperature region. This mechanism manifests itself in changing of the spectrum shape at longer time scale (fig.2) and also in substantially different time dependences for the intensities of lines with different m [fig.3]. The second is strongly confirmed by the recovery method. The recovery kinetics proved to be different for $m=\pm 1/2$ and $m=\pm 3/2$.

For estimating of the CR rates by computer simulations, we accept a simple model in which the spectral densities for fluctuating hf constants are the same for n equivalent nuclei with $I=1/2$, that results in two different CR rates R_0 and R_2 , for transitions with Δm equal 0 and 2 respectively. For this model we may write the following set of equations for populations of radical energy levels

$$\begin{aligned} \dot{D}_m(t) = & -\left(\frac{n}{2} k_d + 2W\right) D_m - \frac{1}{2} k_s (a_{m+1} D_{m+1} + b_{m-1} D_{m-1}) - \\ & - \frac{1}{2} k_d (a_m S_m + a_{m+1} S_{m+1} - b_{m-1} S_{m-1} - b_m S_m) \\ \dot{S}_m(t) = & -\frac{1}{2} k_s (a_m S_m - a_{m+1} S_{m+1} + b_m S_m - b_{m-1} S_{m-1}) - \\ & - \frac{1}{2} k_d (a_m D_m - a_{m+1} D_{m+1} - b_{m-1} D_{m-1} - b_m D_m) \\ a_m = & n/2+m, \quad b_m = n/2-m, \quad K_s = R_0 + R_2, \quad K_d = R_0 - R_2 \end{aligned} \quad (1)$$

Here D_m S_m are the differences and sums of populations of the upper and lower energy levels corresponding to the given nuclear spin magnetic number m . Initial ESP and nuclear populations were taken in form $D_m(0)=P_e E_m \varepsilon_{em}$, $S_m(0)=E_m(1-\alpha \varepsilon_{nm})$. Here E_m is the intensity of m -th line in equilibrium spectrum, P_e and α characterize the magnitude of polarization enhancement for the electron and nuclei respectively. Factors, responsible for the dependence on m of the polarization enhancement for electron and nuclear spins, are ε_{em} and ε_{nm} respectively. The first is calculated from the initial spectrum while the second for the pair. of t-butyl and acyl radicals is supposed to be proportional $|m|^{0.5}$ as follows from the existing theories for at least non viscous solvents [26-28]. F-pairs are included in (1) in common with equilibrium spectrum as the constant addendum $F_m = E_m(1+F \cdot \varepsilon_{em})$.

Calculations show that when one of the CR transitions is more effective than the other, the decay of transferred magnetization becomes much slower than in the case of comparable R_0 and R_2 . Satisfactory fitting of the recovery curve shown in fig.6 is achieved with the set of parameters listed therein. Of course, these values are very approximate since, first, we have

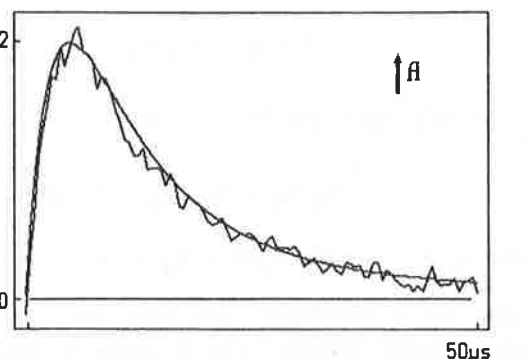


Fig.7. Recovery of $m=3/2$ line of the t-butyl radical in toluene at 159K normalized to the initial unperturbed decay kinetics and fitting to it using $R_0=0.015\mu\text{s}^{-1}$, $R_2=0.0075\mu\text{s}^{-1}$, $\alpha=0.1$, $P_e=20$, $F=0.6$, $W=0.067\mu\text{s}^{-1}$.

three greatly unknown parameters α , R_0 and R_2 , and, second, the distribution of nuclear populations ε_{nm} for the conditions of high viscosity is not clear. But it may be not unexpected that CIDNP tends to diminish at high viscosity. As has already been mentioned [16] in the case when nuclear polarization is less than a certain value (of the order of electron polarization) the sign reversal could take place in nuclear rather than in electron spins manifold and CR manifests itself only in slowing of electron polarization decay and making it to be nonexponential and hyperfine dependent.

5. Conclusions

We found that the cross-relaxation becomes very efficient for t-butyl radical at low temperature in toluene so as in 2-propanol. This is contrary in some extent to TRESR results [19] in sense of CR inefficiency for low temperatures. Even for

temperature as low as 159K the F-pairs contribute sufficiently in toluene to prevent the sign reversal. This is not unexpected because the reported recombination constant for t-butyl radicals is $9.8 \cdot 10^9 \text{ dm}^3 \text{ mol}^{-1} \text{ s}^{-1}$ at 218K [29]. It is also obvious that the observed kinetics in fig.3(a-d) are determined not only by the initial CIDNP transfer but also by the second term in equations (1) which is responsible for the differential relaxation of CIDEP itself. In what extent the above-mentioned mechanism influences recovery kinetics could be determined from pulsed electron double resonance experiment.

Acknowledgement

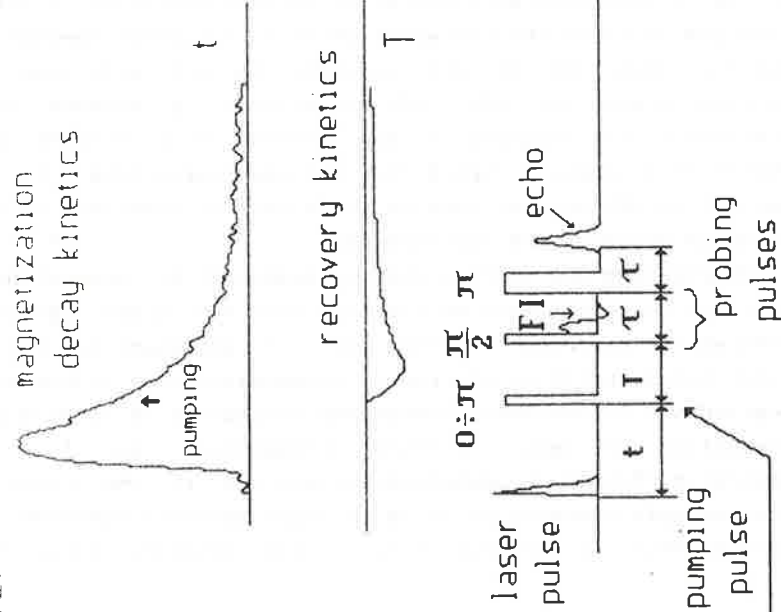
The authors thank H.Paul for kindly supplied di-t-butyl ketone and for communication of results prior publication.

References.

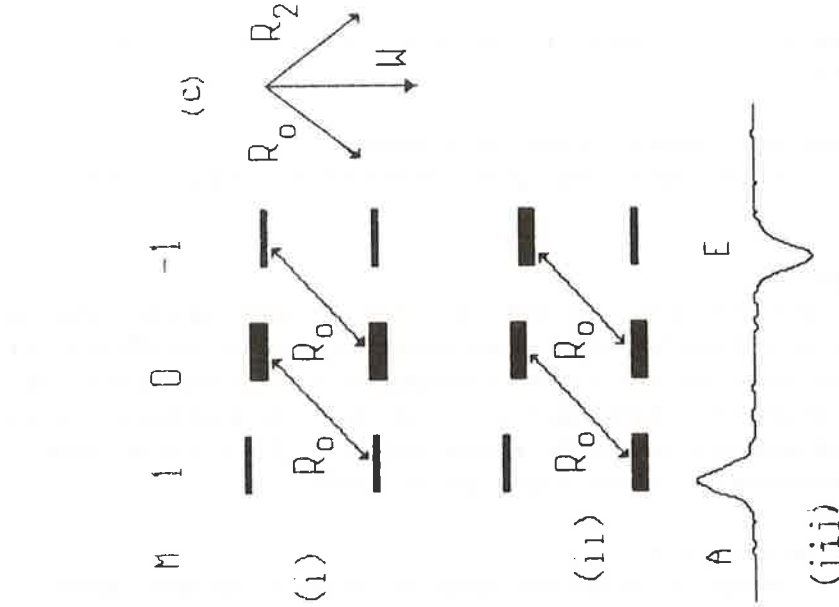
1. L.T.Muus, P.W.Atkins, K.A.McLauclan and J.B.Pedersen, eds. *Chemically Induced Magnetic Polarization* (Reidel, Dordrecht, 1977).
2. S.K.Wong, D.A.Hutchinson and J.K.S.Wan, *J.Chem.Phys.* 58(1973)985.
3. G.L.Closs and M.D.E.Forbes, *J.Am.Chem.Soc.* 109(1987)6185.
4. G.L.Closs, M.D.E.Forbes and J.K.Norris, *J.Phys.Chem.* 91(1987)3592
5. C.D.Buckley, D.A.Hunter, P.J.Hore and K.A.McLauchlan, *Chem.Phys.Lett.* 135(1987)307.
6. K.Tominaga, S.Yamauchi and N.Hirota, *J.Chem.Phys.* 88(1988)553.
7. M.C.Thurnauer and D.Meisel, *Chem.Phys.Lett.* 92(1982)343.
8. P.P.Borbat and Yu.D.Tsvetkov, *Dokl.Phys.Chem.* 278(1984)865.
9. P.P.Borbat, unpublished.
10. T.Imamura, O.Onitsuka and K.Obi, *J.Phys.Chem.* 90(1986)6741.
11. C.Bittler, F.Jent, and H.Paul, *Chem.Phys.Lett.* 166(1990)375.
12. K.A.McLauchlan and D.G.Stevens, *Mol.Phys.* 57(1986)223.
13. A.D.Trifunac, J.R.Norris and R.G.Lowler, *J.Chem.Phys.* 71(1979)4380.

14. G.L.Millhauser, J.Freed, *J.Chem.Phys.* 81(1984)37.
 15. M.K.Bowman, Workshop on "Electron Spin Echo Spectroscopy",
 March 29-31, 1988, Amsterdam.
 16. V.I.Valyaev, Yu.N.Molin and R.Z.Sagdeev, Cross-Relaxation
 in the Chemically Induced Spin Polarization Experiment.
 Preprint 21, Institute of Chemical Kinetics and Combustion.
 Novosibirsk (1987) [in Russian].
 17. V.I.Valyaev, Yu.N.Molin, R.Z.Sagdeev, P.J.Hore,
 K.A.McLauchlan and J.K.Simpson, *Mol.Phys.* 63(1988)891.
 18. F.Jent,H.Paul,K.A.McLauchlan and D.G.Stevens,
 Chem.Phys.Lett. 141(1987)443.
 19. F.Jent and H.Paul, *Chem.Phys.Lett.* 160(1989)632.
 20. L.T.Muus, *Chem.Phys.Lett.* 160(1989)17.
 21. P.P.Borbat, A.D.Milov and Yu.N.Molin, *Chem.Phys.Lett.*
 164(1989)330.
 22. A.V.Yurkovskaya, Yu.P.Tsentalovich and R.Z.Sagdeev,
 Chem.Phys.Lett. 171(1990)406.
 23. S.Basu, K.A.McLauchlan and A.J.D.Ritchie, *Chem.Phys.Lett.*
 105(1984)447.
 24. D.M.Bartels, A.D.Trifunac and R.G.Lowler, *J.Chem.Phys.*
 83(1985)2704.
 25. A.G.Semenov, M.D.Shirov, V.D.Zhidkov, V.E.Khmelinskii
 and E.D.Dvornicov, Coherent Spectrometer of Electron
 Spin Echo, Preprint (in Russian), Institute of Chemical
 Kinetics and Combustion, Novosibirsk (1979).
 26. J.B.Pedersen and J.H.Freed, *J.Chem.Phys.* 61(1974)1521.
 27. K.M.Salikhov, Yu.N.Molin, R.Z.Sagdeev and A.L.Buchachenko,
 Spin Polarization and Magnetic Effect in Radical Reaction,
 (Akad mia Kiad , Budapest, 1984).
 28. A.I.Shushin, *Chem.Phys.* 144(1990)212.
 29. John E.Bennet, John A.Eyre, C.Peter Rimmer and Raymond
 Summers, *Chem.Phys.Lett.* 26(1974)69.
 30. K.A.McLauchlan and N.J.K.Simpson,
 Chem.Phys.Lett. 154(1989)550.
 31. K.A.McLauchlan and D.G.Stevens, *J.Chem.Phys.* 87(1987)4399.
 32. K.A.McLauchlan and D.G.Stevens, *J.Magn.Reson.* 63(1985)473.

(a)



(b)



Application of Pulsed EPR Spectroscopy to the Study of Radical Reactions

Tsuneki Ichikawa and Hiroshi Yoshida

Faculty of Engineering, Hokkaido University, Sapporo, 060 Japan

Abstract

Electron spin echo (ESE)-detected EPR spectrum has been found to be a powerful way of discriminating overlapping EPR spectra by utilizing the difference of paramagnetic relaxation rates. The ESE technique has been applied on alkyl radicals generated from normal and branched alkanes by γ -irradiation at 77 K for elucidating the mechanism of radical reactions in solids.

1. Introduction

Ambiguity in the EPR identification of organic radicals in solids arises from line broadening due to distribution of hyperfine coupling constants (hfcc). The distribution is caused by the dynamic and the static distortion of radical conformation. If several radical species coexist in a solid sample and their EPR spectra overlap with each other, it is very difficult to differentiate and identify the EPR spectrum of each radical specimen. The computer simulation of the spectrum is not effective as is expected, since the hfcc of, especially, β protons is very sensitive to the location of the protons with respect to the orbital of a singly-occupied electron and ranges from 0 to 4 mT. Thus, it is not an easy task to study radical reactions in organic solids by applying EPR spectroscopy.

Overlapping EPR spectra can be examined by separating them into each component with an electron spin echo (ESE) spectroscopy based on the difference in the rate of paramagnetic relaxation [1,2]. Paramagnetic relaxation is categorized into transverse and longitudinal relaxations. Transverse relaxation is induced by the fluctuation of spin precession frequencies that is called spectral diffusion. Longitudinal relaxation is the recovery of electron spin energies at an on-resonant spectral position, and is induced either by the flop of on-resonant spins by energy transfer

or by the diffusion of on-resonant spins to off-resonant spectral region and concomitant diffusion of off-resonant spins into the on-resonant spectral region. The latter process is also categorized as spectral diffusion. For organic radicals spectral diffusion is mainly induced by the time fluctuation of hfcc due to thermal motion of the radicals, so that the diffusion rate is sensitive to the geometrical structure of the radicals. The ESE spectroscopy detects the magnetization of unrelaxed on-resonant spins as a function of a waiting time after the excitation. The overlapping spectra is therefore differentiated into each component by measuring the intensity of ESE signals while sweeping the external field very slowly. The relaxation rates reflect the motion of radical species in the matrices, so that the ESE method is also useful for understanding the relation between molecular motion and radical reaction.

The present work summarizes our recent results on radical reactions in solids obtained by the application of the ESE spectroscopy.

2. Experimental Section Fig. 1 shows the sequence of microwave pulses used for the measurement of transverse and longitudinal relaxations. The transverse relaxation was observed by measuring the intensity $E(t_2)$ of two-pulse ESE signals as a function of the time interval τ between the first and the second pulses. Since the transverse relaxation takes place between the first pulse and the time of the ESE observation, $t_2=2\tau$ is the time interval for the transverse relaxation. To observe the longitudinal relaxation, the total magnetization of on-resonant spins under the thermal equilibrium was first detected at a fixed τ by the two-pulse method.

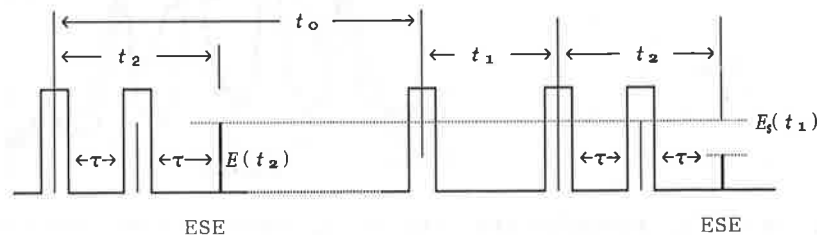


Fig.1. Sequences of microwave pulses used for the measurement of transverse and longitudinal relaxation.

After time t_0 , enough for complete relaxation of the spin system, a saturation pulse was applied to saturate the on-resonant spins. Then, after time t_1 , the total magnetization was detected by the two-pulse method. The difference in the ESE intensity with and without the saturation pulse, $E_s(t_1)$, is equal to the amount of the longitudinally unrelaxed spins at t_1 after the saturation pulse. The EPR spectra of $E(t_2)$ and $E_s(t_1)$ were obtained by sweeping the external magnetic field very slowly while fixing t_2 and t_1 . The spectra thus obtained will be designated as t_2 and t_1 -dependent EPR spectra.

3. Results and Discussion

Comparison of CW and ESE-detected EPR spectra. The shape of an ESE-detected EPR spectrum is not necessarily the same as that of the corresponding CW EPR spectrum. An extreme case is the EPR spectrum of 1-hydroxyethyl radical in a γ -irradiated ethanol matrix at 77 K.[3] As is shown in Fig. 2, the CW EPR spectrum of the radical is composed of five lines due to hyperfine interactions with one α proton and three β protons of a methyl group. The hyperfine interaction depends on the location of the β protons with respect to the p orbital of the unpaired electron. However, the observed hyperfine coupling constant is the same for all the β protons because of quick rotation of the methyl group in the time scale of

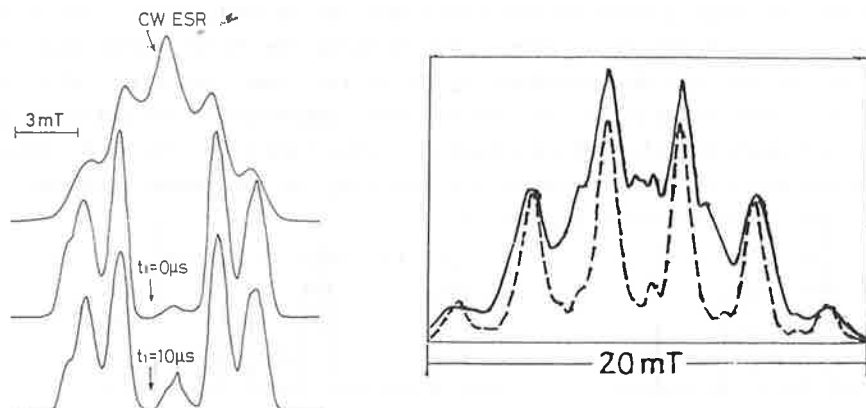


Fig. 2. CW and t_1 -dependent EPR spectra of hydroxyethyl radical at 77 K of γ -irradiated n-hexane single crystal at $t_1=1$ and 50 μ s.

the CW EPR measurement. On the other hand, the ESE-detected EPR spectrum is composed of four lines due to the hyperfine interactions with three β protons of the spin state $\pm(1/2, 1/2, 1/2)$ and one α proton of the spin state $\pm 1/2$. The rotation of the methyl group with the nuclear spin state other than $\pm(1/2, 1/2, 1/2)$ causes the fluctuation of the hyperfine interactions. The rotation is not fast enough to average out the fluctuation of the hyperfine interaction but is fast enough to induce the complete phase relaxation between the time of the excitation and the detection. The 1-hydroxyethyl radicals with the methyl protons of the spin state other than $\pm(1/2, 1/2, 1/2)$ is therefore not observed by the ESE-detected EPR.

The resolution enhancement of an EPR spectrum is occasionally observed on the ESE-detected EPR spectrum. An example is alkyl radicals in n-hexane (Fig. 3). Two types of secondary alkyl radicals are known to be generated and stabilized in γ -irradiated n-alkane crystals at 77 K. They are the penultimate alkyl radical with the unpaired electron on a carbon second to the end of the carbon chain and the internal alkyl radical with the unpaired electron on a carbon farther than the second one. The irradiated crystals show the overlapping CW EPR spectra of these radicals. On the other hand, the ESE-detected EPR show the spectrum of the penultimate radical. This difference arises from the fast paramagnetic relaxation of the penultimate radical induced by time fluctuation of the EPR spectrum, or spectral diffusion. The spectral diffusion of the penultimate radical are much faster than the internal one, because the bending motion of the C-CH-C bond, the source of the fluctuation of α and β proton hyperfine couplings, is faster for the penultimate radical. The resolution of the ESE-detected EPR spectrum increases with the time of longitudinal relaxation, which implies that the relaxation is slower for the spins near the peak of the spectrum. The resolution enhancement is caused by the spectral diffusion. When an EPR spectrum is broadened due to the dynamic change of the spectrum, the relative intensity of the spectrum is proportional to the lifetime of the spins staying at the observed spectral position. The longitudinal relaxation due to the spectral diffusion is therefore slower for the spins near the peak of the spectrum.

Selectivity of alkyl radical formation by tunneling C-H hydrogen abstraction. Several types of alkyl radicals are expected to be formed and stabilized in γ -irradiated solid alkanes. For example, five types of alkyl radicals are expected to be formed from 2-methylpentane by the scission of a C-H bond. Numbering the main chain carbons from the end of the shortest main chain for the unpaired electron, these are expressed as Me(2)R(1), Me(2)R(2), Me(2)R(3), Me(4)R(2) and Me(4)R(1). The values of m and n in Me(m)R(n) denote the location of the main chain carbons possessing the methyl group and the unpaired electron, respectively. The CW EPR spectra of these radicals are similar, since the proton hyperfine coupling constants are not much different. The identification of the radicals can be achieved more clearly by utilizing the difference of the paramagnetic relaxation rates. Fig. 4 shows the longitudinal relaxation of these radicals at 77 K in deuterated methanol. The relaxation rate decreases with increasing the intramolecular distance between the radical carbon and the terminal one. The main process of the longitudinal relaxation is therefore spectral diffusion due to the molecular motion of β protons with respect to the p orbital of the unpaired electron.

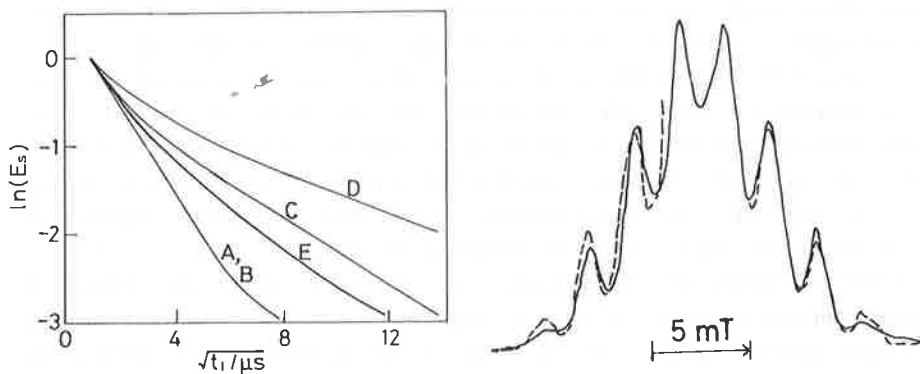


Fig. 4. Longitudinal relaxation of (A) Me(2)R(1), (B) Me(4)R(1), (C) Me(4)R(2), (D) Me(2)R(3), and (E) Me(2)R(2) radicals in deuterated methanol at 77K.

Fig. 5. t_1 -dependent EPR spectra at 77 K for (—) γ -irradiated neat 2-methylpentane and of (--) Me(4)R(2) radical in deuterated methanol at $t_1=0$ and 50 μ s.

A longer carbon chain is more difficult to move than the shorter one, so that the rate of spectral diffusion decreases with increasing length of chains attaching to the radical carbon. The free rotation of the methyl β protons does not cause the longitudinal relaxation.

Since the relaxation rates are not the same for these radicals, it is possible to extract the spectral components from the overlapping spectrum by measuring the t_1 -dependent EPR spectra. Figure 5 shows the t_1 -dependent EPR spectra for neat 2-methylpentane at 1 week after γ -irradiation. The relative shape of the spectrum does not depend on t_1 , which implies that only one type of the radical remains in the sample. The remaining radical is obviously the Me(4)R(2) radical with 8 EPR lines. The spectrum of alkyl radicals generated from 2-methylpentane in deuterated methanol by the abstraction of C-H hydrogen by deuterium atoms agrees with that of the Me(4)R(2) radical. Although the primary alkyl radicals are observed after the irradiation, they gradually convert to the Me(4)R(2) radical by the abstraction of penultimate secondary C-H hydrogen. The formation of the internal secondary radical and the tertiary radical is prohibited at 77 K. The hydrogen abstraction proceeds by quantum-mechanical hydrogen tunnelling process, since C-D deuterium abstraction is much slower than C-H hydrogen abstraction. The selective formation of secondary penultimate radical is also observed for another branched alkanes.

Contrary to the selectivity in solids, the selectivity of alkyl radical formation in alkane liquids simply depends on the strength of the C-H bonds. The tertiary C-H bond is the weakest, so that a considerable amount of the tertiary radicals are generated from branched alkanes even the number of the tertiary C-H bonds is the smallest.

Although a considerable amount of internal radicals are generated from protiated solute n-alkanes by γ -irradiating deuterated n-alkane crystals at 77 K, only penultimate secondary radicals, 1-methylalkyl radicals, are generated from the solutes in the glassy matrices of deuterated alcohols. The yield of the solute radicals is more than 20 % of the total radical yield even the solute concentration is less than 2 %. The formation of the

solute radicals therefore proceeds by the quantum-mechanical tunneling of C-H hydrogen.

The difference of the selectivity between the crystal and the glass matrices arises from the effect of solid phases on a specific molecular motion assisting the tunneling of C-H hydrogen. The tunneling rate is determined not only by the activation energy for the abstraction but also by the easiness of molecular motion assisting the hydrogen abstraction. In the glassy matrix, a sp^3 \leftrightarrow ($sp^2 + p$) umbrella motion assisting the abstraction of the C-H hydrogen is slower for the tertiary and the inner carbons than the penultimate secondary carbons, because three carbon chains for the tertiary carbon and two carbon chains for the inner carbon prevent the umbrella motion. The rates of the tertiary and the inner secondary radical formation are therefore slower than that of the penultimate radical formation even the activation energies are lower than and the same as that for the penultimate secondary carbon, respectively. In a crystalline solid all the carbon atoms in a molecule are on the molecular plane. The crystal has a structure close to a layered one. The accordion motion of the C-C chain is therefore easy to take place in the crystal. Since the accordion motion causes the change of sp^3 \leftrightarrow ($sp^2 + p$) for all the carbons, the tunneling C-H hydrogen abstraction also takes place on the internal carbons.

The viscosity of alkane liquids is too low to prevent the molecular motion, so that the selectivity of alkyl radical formation simply follows a classical law; the reaction rate increases with decreasing the activation energy.

References

- [1] Ichikawa, T. *J. Phys. Chem.*, 1988, 92, 1431
- [2] Ichikawa, T.; Yoshida, H. *J. Phys. Chem.*, 1988, 92, 5684
- [3] Ichikawa, T.; Yoshida, H. *J. Phys. Chem.*, 1990, 94, 949

Effect of Electron Spin Diffusion on Electron Spin Echo Decay

Vadim V. Kurshev* and Tsuneki Ichikawa

Faculty of Engineering, Hokkaido University, Sapporo, 060 (Japan)

The effect of electron spin flip-flop on two- and 2+1 pulse electron spin echo decay due to instantaneous diffusion was studied on hydrogen atoms in γ -irradiated quartz. The observed decay was slower than the theoretical one including no spin flip-flop, and the discrepancy was increased with the concentration of the hydrogen atoms. Comparison of the theoretical and the experimental decay rates revealed that the main factor diminishing the effect of instantaneous diffusion is not direct flip-flop between on-resonant spins, but the fluctuation of the local magnetic fields for on-resonant spins due to flip-flop of adjacent spin pairs.

Dipole-dipole (d-d) interactions between paramagnetic centers in solids induce the phase relaxation of electron spins which can be detected as the decay of an electron spin echo (ESE) envelope. The investigation of the ESE decay allows one to evaluate physical parameters in various spin relaxation processes and to obtain information concerning the motion and the spatial arrangement of paramagnetic centers (1-2). One of the most powerful methods for this purpose is to analyze the ESE decay due to instantaneous diffusion (ID) mechanism, since ID is created by perturbation of spin coupling by microwave pulses and therefore artificially controllable relaxation process. A novel pulse sequence suitable for extracting ID has recently been invented (3). In this method, called 2+1 pulse ESE, additional ID is induced by strong microwave pulse inserted between the first labelling pulse and a refocusing pulse, and the decay of a two pulse ESE envelope due to the additional ID is measured as a function of the time interval between the first and the additional pulses.

The analytical expression for the 2+1 ESE decay is easily obtained by neglecting a flip-flop term, $S_{+-}S_-$, in the Hamiltonian of d-d interaction. Although the flip-flop is expected to give a

* On leave from Institute of Chemical Kinetics & Combustion, Novosibirsk, 630090 (USSR)

significant effect on ID, most of theoretical and experimental works did not take it into consideration. For clarifying the applicability of the two and 2+1 pulse ESE method to the study of d-d interaction, it is therefore necessary to know the effect of the flip-flop on the ESE decay due to the ID mechanism.

Experiments with a hydrogen atoms stabilized at 77K in γ -irradiated quartz glass shows the effect of electron flip-flops on the manifestation of d-d interactions in ESE decay, Fig.1. The

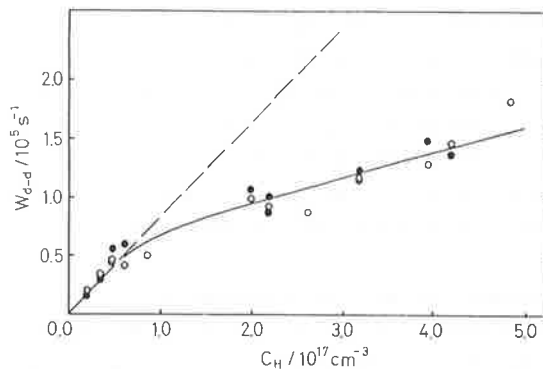


Fig.1. Strength of d-d interaction estimated from (○) two and (●) 2+1 pulse ESE decay under the assumption of no flip-flops. The real strength is shown with a broken line.

dependence of the dipole broadening of ESR line on the concentration of hydrogen atoms estimated from two and 2+1 pulse ESE decays deviates from linear, predicted by stochastic theory (4).

The effect of the flip-flop can be divided into two categories: direct and indirect effects. The direct effect is due to the flip-flop between an observed spin and its partner one. The indirect effect is due to the flip-flop between a pair of spins near an observed spin. The flip-flop of the pair of spins causes the spectral diffusion of the observed spin through the change of the local magnetic field. Since the spectral diffusion is faster for spin groups with stronger d-d interactions, the average d-d interaction for the ESE-detected spin group decreases with increasing time τ between the labelling and the refocusing pulses. Therefore, if the observed ID is analyzed by using a theory including no flip-flop term, it gives a weaker d-d interaction and a longer spin-spin distance than real ones.

Exact calculations of density matrix evolution revealed unimportance of direct effect on the ESE decay both in two and 2+1 pulse methods. The influence of flip-flop interaction of observed spins linearly increase with a concentration of paramagnetic centers

as well as effect of ID mechanism. Therefore the relative effect of direct interaction does not increase, and it is important only for a very short initial time interval of ESE decays.

The indirect effect is induced by interaction between many particles. Instead of solving a density matrix for spin groups under multiple d-d interactions, we treat a pair case in which an observed spin interacts with a partner spin without flip-flop but the partner spin flip-flops with another spins with the rate of $2W$. Provided the flip-flop rate is the same for all the spins, the decay kinetics of identical spins under the random spatial distribution is given by

$$E(2\tau) = E_{ID}(2\tau)E_{SD}(2\tau)E_o(2\tau) \quad (1)$$

where $E_{ID}(2\tau)$ and $E_{SD}(2\tau)$ denote the ESE decay due to ID and spectral diffusion by the d-d interaction, respectively; $E_o(2\tau)$ is the decay due to other reasons. E_{ID} and E_{SD} can be represented as

$$E_{ID}(2\tau) = \exp[-\sin^2(\theta/2)\gamma^2\hbar CD_A(2W\tau)\tau]; \quad (2)$$

$$E_{SD}(2\tau) = \exp[-\gamma^2\hbar CD_B(2W\tau)\tau]$$

where θ is the angle of spins turn by refocussing pulse, γ is hyromagnetic ratio, C is the concentration of hydrogen atoms,

$$D_A(x) \approx 5.07/(1 + 1.08x^{1/2} - 2.04x + 2.51x^{3/2}); \quad (3)$$

$$D_B(x) \approx 2.53x/(1 + 0.25x^{1/2} + 0.63x^{3/2})$$

The decay kinetics in 2+1 pulse ESE is given by

$$E(2\tau, \tau') \approx \exp[-\sin^2(\phi/2)\cos\theta\gamma^2\hbar CD_A(2W\tau')\tau'] \quad (4)$$

where ϕ is the angle of spins turn by additional pulse.

It can be seen from Eqs.(3,4) that the increase of x ($= 2W\tau$) causes the deviation of the ID decay kinetics from the exponential function and the decrease of the decay rate. Assuming 10 % accuracy for the observed decay rate, the flip-flop term is negligible only if $x < 0.02$. The ESE decay due to ID is very sensitive to the flip-

flop. The flip of only one of 50 spins gives the observable effect. The flip-flop also accelerates the ESE decay due to spectral diffusion.

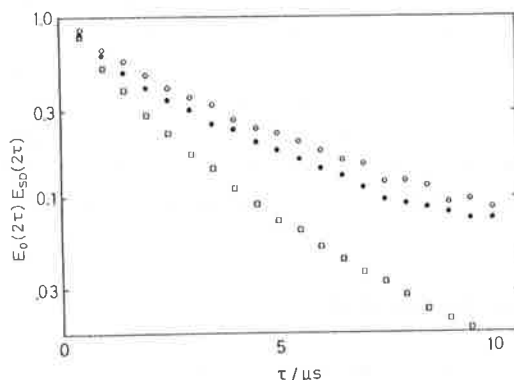


Fig.2. Two pulse ESE decay of hydrogen atoms in γ -irradiated at 77 K quartz due to spectral diffusion.

The concentrations of the hydrogen atoms are (○) 1.3, (●) 2.6, and (□) $4.85 \times 10^{17}/\text{cm}^3$.

Fig.2 shows the experimental dependence of $E_0(2\tau)E_{SD}(2\tau)$, two-pulse ESE decay without ID, on the spin concentration. The increase of the decay rate indicates that the indirect effect is the main source of diminishing the effect of ID on the ESE decay.

The result of this work can be resumed as follow. Flip-flops between electron spins diminish the effect of instantaneous diffusion on two and 2+1 pulse ESE envelope decays even if the longitudinal relaxation is much slower than the phase relaxation. The main mechanism diminishing the effect of instantaneous diffusion is not the direct flip-flop of observed spins but the flip-flop of spin pairs adjacent to them. A theory including no flip-flop term is not applicable to the analysis of observed ESE decay kinetics if the microwave power-independent phase relaxation rate depends on the spin concentration.

References

- [1] K.M.Salikhov, S.A.Dzuba, and A.M.Raitsimring, J. Magn. Reson. 42 (1981) 255.
- [2] M.Romanelli and L.Kevan, J. Magn. Reson. 91 (1991) 549.
- [3] V.V.Kurshev, A.M.Raitsimring, and Yu.D.Tsvetkov, J. Magn. Reson. 81 (1989) 441.
- [4] A.Abragam, "The Principles of Nuclear Magnetism", Clarendon, Oxford, 1961.

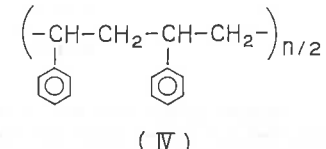
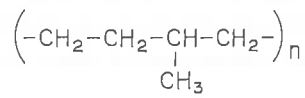
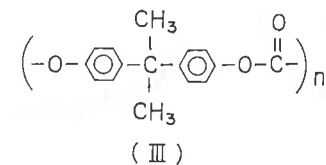
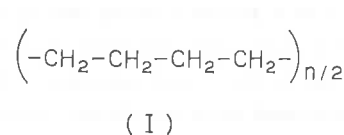
An ODESR Study on Charge Recombination Process in X-ray irradiated Polymers
Yutaka Tai, Masaharu Okazaki, and Kazumi Toriyama
Government Industrial Research Institute, Nagoya,
Hirate, Kita-ku, Nagoya, 462, Japan

ABSTRACT

The Fluorescence-detected ESR (ODESR) spectrum and the magnetic field dependence on the recombination fluorescence were observed for X-ray irradiated polymers doped with pyrene, including low density polyethylene, polystyrene, and poly carbonate. Fluorescence spectra were also observed for the X-ray irradiated as well as the UV-irradiated polyethylene and polystyrene. In the case of polyethylene, a saturated polymer, the charge hopping occurs mainly between the doped pyrenes. This process, which is activated thermally, was interpreted in the same way as in the previous study on ethylene-propylene rubber. On the other hand, in polystyrene which includes benzene ring on the polymer chain charge hopping occurs between aromatic molecules including benzene residues and the doped pyrenes. An exciton-like excited state was postulated in the recombination process to explain a broad dip in the magnetic field dependence on the recombination fluorescence. This dip was assigned to the reduction in fluorescence due to level crossing of the singlet to a triplet sublevel. Only a small part of the fluorescence was thermally activated in this case, which probably be due to the stiffness of the polymer which does not allow the aromatic rings to change the mutual orientation.

1. Introduction

Characteristic features of the radiation chemical reactions, especially in inhomogeneous materials including biological systems, will be clarified



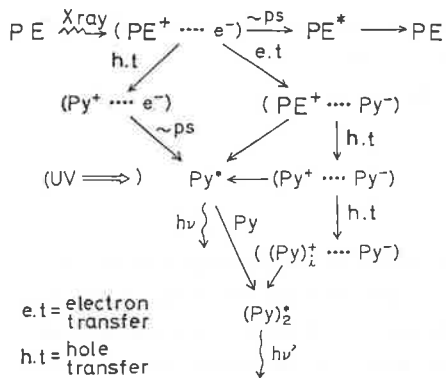


Figure 1. Proposed charge recombination mechanism in the irradiated saturated polymer doped with pyrene.

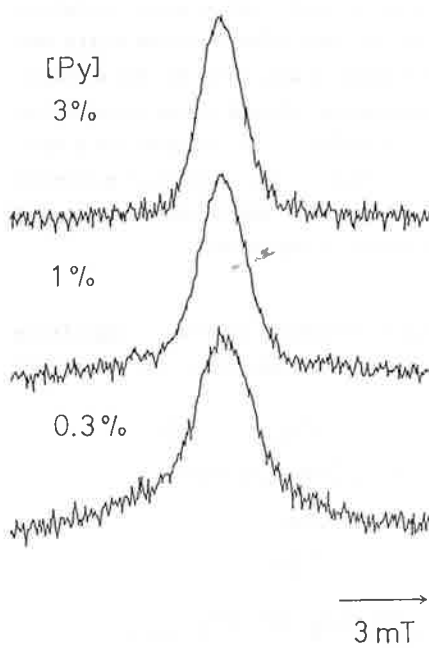


Figure 2. ODESR spectrum for low density polyethylene doped with pyrene at 303K.

only after a detailed analysis of the charge migration and the recombination processes. Therefore, a detailed knowledge about these processes is indispensable for the development of radio-resistive plastics for the nuclear- as well as the cosmoindustry. The fluorescence detected ESR technique [1-3] is potentially a very powerful technique in studying this field. Molin et al.[4] applied this technique to detect the free hole and the free electron in the irradiated systems and obtained the mobility of these charges in the liquid state from the linewidth of the ODESR spectrum. We also applied this technique to investigate the charge recombination process in squalane [5,6] as well as in ethylene-propylene copolymer (II; EP-rubber)[7]. The latter study is the first ODESR study in plastics and clarified the basic charge migration process in the saturated polymer. The mechanism [7] is shown in Figure 1 which includes the following steps. [In this case PE in the figure should read as EP-rubber]

(1) At a pyrene concentration as high as 1.0 %, the charges hop mainly between the doped pyrenes. This is confirmed with the ODESR line shape that contains no broad component due to polymer-derived cation at the pyrene concentration more than 1.0 wt%.

(2) At temperatures higher than 290 K, not only the electron but the hole can hop between the pyrene molecules. This

is evidenced by the excess excimer fluorescence in the X-ray excited system compared with the system irradiated with UV-ray [6].

(3) The charge hopping process is thermally activated. Temperature at which the ODESR amplitude is the maximum value shifts towards lower temperatures for the sample at higher pyrene concentrations. This is another evidence for the charge hopping between the solute pyrenes.

In the present study we applied the same techniques mentioned above to the study on charge migration and recombination process in low density polyethylene (I) doped with pyrene. Since the stiffness of polyethylene is considerably higher than that of EP-rubber, this system is suitable to confirm the above mechanism. Besides, we extended the study to aromatic polymers, i.e. polystyrene (III) and polycarbonate (IV), doped with pyrene and discussed the role of aromatic groups on the polymer chain in the charge recombination process. As shown in the scheme the polystyrene molecule has phenyl groups as the pendant group while the polycarbonate molecule has them in the main chain. In these systems the magnetic field effect on the fluorescence intensity has two phases, one is a sharp increase and the other is a broad dip at around 60 mT followed by a gradual increase of the fluorescence. The latter broad component was explained as being due to the level crossing between the singlet and the triplet levels of an exciton-like excited state which has a exchange interaction of some 60 mT.

2. Experimental

Pyrene was obtained from Tokyo Kasei Kogyo and purified with the zone-

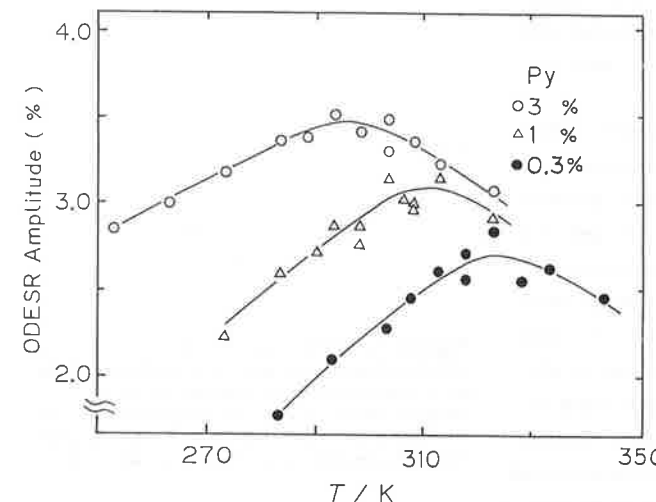


Figure 3. Temperature dependence of the ODESR amplitude for low density polyethylene doped with pyrene at three concentrations.

melting method. Low density polyethylene from Mitsubishi Petroleum Co. (as a gift), polystyrene from General Science Co., and polycarbonate from Aldrich Chemicals were used as supplied. Polymer samples were kneaded with pyrene at 463 K and molded with a Mini-molder from CSI Inc. into a rod of o.d. 4.0 mm. ODESR and fluorescence spectrum were observed with an apparatus described elsewhere [5].

3. Results and Discussion

3-1. Low Density Polyethylene

Figure 2 shows the ODESR spectrum for low density polyethylene doped with pyrene at three concentrations, 0.3, 1.0, and 3.0 wt%. At the lowest pyrene concentration, the ODESR spectrum contains a broad component which is assigned to a cation derived from polyethylene itself as in the same way of the previous study. Since the ODESR spectrum for the system with pyrene concentration higher than 1.0 wt% consists of mainly pyrene ion signals, the charges reside mainly on the doped molecules and thus hop only between the pyrenes.

Figure 3 shows the ODESR amplitudes as the functions of temperature for three pyrene concentrations, 0.3, 1.0 and 3.0 wt%. When the temperature is raised, the ODESR amplitude increases, then comes to the maximum value, and finally decreases. The temperature at which the ODESR amplitude becomes the maximum value shifts higher, when the pyrene concentration is decreased,

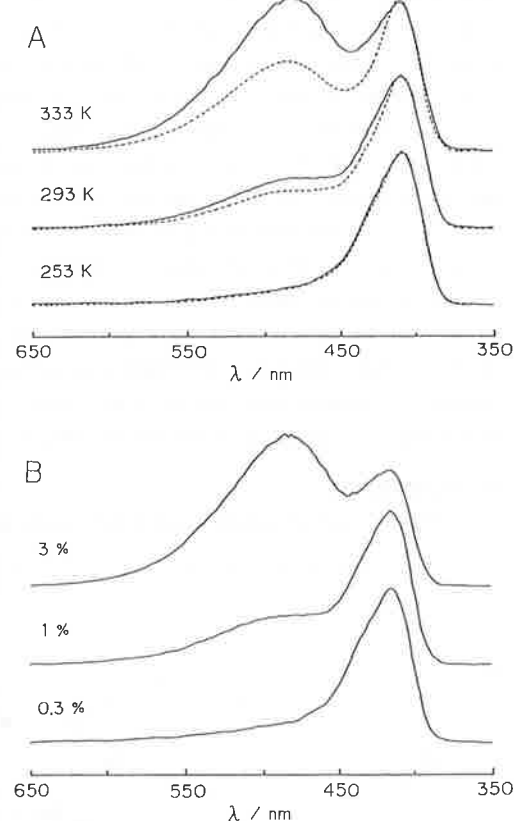


Figure 4. Fluorescence spectra for pyrene-doped low density polyethylene. A: temperature dependence for 1.0 % sample, with X-ray irradiation (solid) or UV-excitation (dotted). B: dependence on pyrene concentration at 293K.

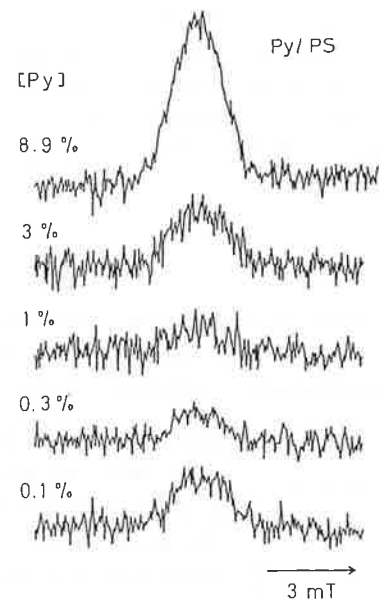


Figure 5. ODESR spectrum for polystyrene doped with pyrene at various concentrations. The observations were made at an ambient temperature.

monotonously with the increase of the temperature. This sharpening of the linewidth upon warming the sample is naturally assigned to rapid averaging of the local field (mainly from hyperfine interaction) due to hopping of the radical center.

Figure 4 shows the fluorescence spectrum of this system at various temperatures for the 1.0 % sample (A) and the concentration dependence at 293K. The peaks at around 400 and 500 nm are due to the monomer and the excimer, respectively. Upon warming the sample the excimer peak increases regardless of the excitation method. This result indicates that excimer formation is accelerated by reorientation and translational diffusion of the doped pyrenes. At a high temperature ($>293\text{K}$) and a concentration ($>1.0\%$) the relative height of the excimer peak of solid spectrum in [A], obtained with X-ray irradiation, is considerably higher than that of the dotted spectrum, obtained with UV-excitation. This excess excimer fluorescence in the X-ray excited system can be explained with the hole hopping from a pyrene to a cluster of pyrenes which

The decrease of the ODESR amplitude at a lower temperature (than the optimum temperature) can be explained with the loss of spin correlation during the recombination time. On the other hand, the decrease of it after the maximum amplitude when the sample temperature is raised further is assigned to the decrease of the probability of spin-flip by the microwave field due to a shortened recombination time. It is well known that ODESR amplitude as the function of microwave field saturates [8] when $B_1 \gg 1/\tau$. Therefore, the recombination time for each systems at the temperature for the maximum ODESR signal would be equal each other, if the same spin relaxation parameters are postulated. This means that with increasing the pyrene concentration the charge hopping rate increases and thus the recombination time decreases. This interpretation is confirmed by the fact that the ODESR linewidth decreases

stabilizes the hole resulting a oligomer cation [6,7], if the electron migration rate is higher than that of hole. This is neutralized later by recombination with the electron and the excimer is preferentially formed. From the present results, with referring to the former study on EP-rubber[7], we generalized the charge recombination mechanism shown in Figure 1 for all the polyolefin system doped with aromatic molecules.

3-2. Polystyrene & Polycarbonate

Figure 5 shows the ODESR spectrum of polystyrene doped with pyrene at the concentration of 0.1, 0.3, 1.0, 3.0, and 8.9 wt%. The spectrum does not show a broad shoulder even if the pyrene concentration is reduced to 0.1 %.

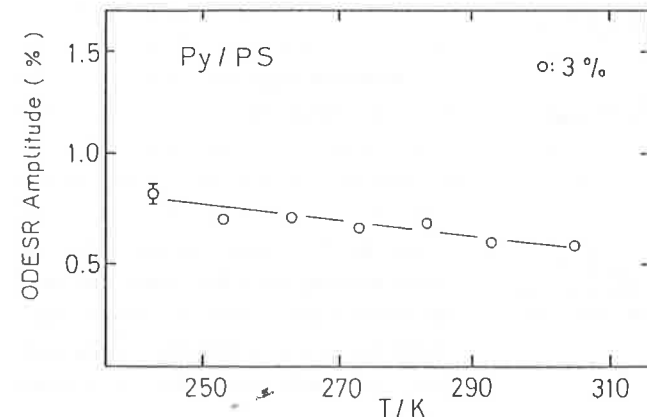


Figure 6. ODESR amplitude for polystyrene doped with pyrene at 3.0 % as a function of temperature.

chain. It is also noteworthy that the intensity becomes minimum at the concentration of 1.0%. ODESR amplitude for the polystyrene system as a function of temperature is shown in Figure 6. Compared with the polyethylene case, the intensity is less than one half even at the highest pyrene concentration. In addition, it does not depend on temperature very much and there is no maximum in our experimental temperature range (243-303K). These facts indicates that the recombination time is so long that most of the spin coherence is lost when the ion pair recombines.

The general slow hopping of the charges in polystyrene may be related with the fact that polystyrene is so hard that the dissolved pyrene molecules can not reorient to accelerate the charge hopping between them. The small temperature dependence can be explained with the small freedom of the pyrenes.

This fact indicates that the charges hop only between the aromatic molecules even at a low concentration of pyrene in contrast to the case of polyethylene or EP-rubber. Therefore the charges must reside in the pendant phenyls but not in saturated carbons in the main

At the concentration of 1.0 % the average separation between the pyrenes is about 35 Å which may be too long for the electron to tunnel with one step. At 0.1 % the average separation becomes more than 70 Å. In this case there may be only one pyrene on the course of charge recombination, thus we can put the charge migration from pyrene to pyrene out of consideration. This is the reason that the ODESR increases again with decreasing the pyrene concentration from 1% to 0.1 %.

Figure 7 shows the magnetic field dependence of the recombination fluorescence for the system of polystyrene and polycarbonate. The most interesting feature is that the magnetic field dependence is apparently composed of two phases, one is a sharp increase of the fluorescence which saturates over the magnetic field of about 50 mT and the other is a broad dip at around 60-150 mT followed by the gradual increase which does not saturate even over 500 mT. The sharp magnetic field effect becomes minimum at the concentration of 1.0 % in parallel with the ODESR intensity. This component is due to the ion pair with a long life-time, which is the main contributor to both the ODESR signal and this sharp magnetic field effect. The cause of the dip is naturally attributed to the level crossing between a triplet sublevel and the singlet level of

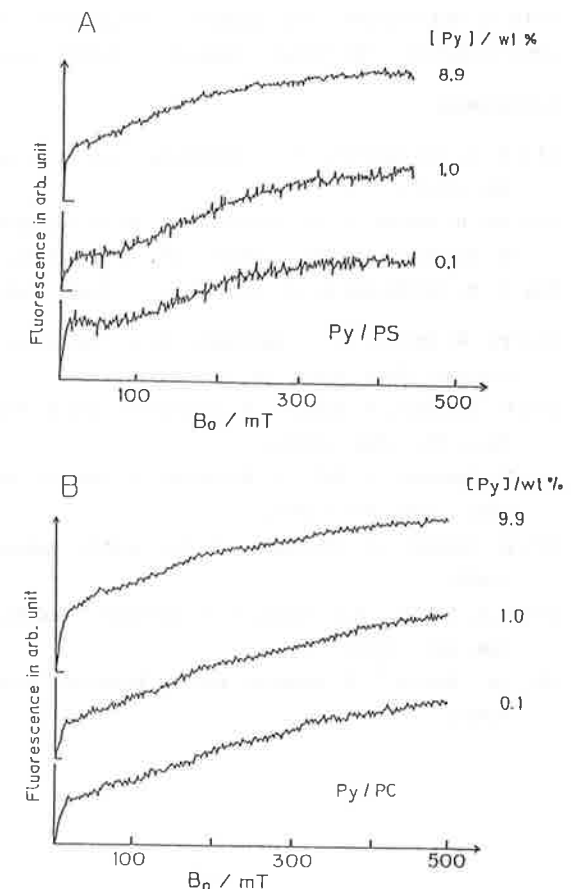


Figure 7. Magnetic field dependences of the recombination fluorescence for X-ray irradiated low density polyethylene (A) and polystyrene (B) doped with pyrene at various concentrations.

the geminate pair. The exchange interaction of 60–150 mT may correspond to a separation of less than 10 Å[9]. We tentatively assign this metastable state as an excited state like exciton, which needs some energy to recombine to yield the excited pyrene.

Because this dip appears most clearly for the 0.1 % sample, the ion pair which contributes this broad component must be composed of pyrene cation and the electron in polystyrene. The molecular structure of polystyrene shows that every third phenyl is coplanar, thus the electron may be able to delocalize. The magnetic field effect for polycarbonate shows the same tendency. The broad component, however, does not show a distinct dip.

5. Reference

- [1] E. L. Frankevich, A. I. Pristupa, and V. I. Lesin, *Chem. Phys. Lett.*, **47**, 304 (1977).
- [2] Yu. N. Molin, O. A. Anisimov, V. M. Grigoryants, V. K. Molchanov, and K. M. Salikhov, *J. Phys. Chem.*, **84**, 1853 (1980).
- [3] J. P. Smith and A. D. Trifunac, *J. Phys. Chem.*, **85**, 1645 (1981).
- [4] Yu. N. Molin, O. A. Anisimov, V. I. Melekhov, and S. N. Smirnov, *Farad. Discuss. Chem. Soc.*, **78**, 289 (1984).
- [5] M. Okazaki, K. Nunome, K. Matsuura, and K. Toriyama, *Bull. Chem. Soc. Jpn.*, **63**, 1396 (1990).
- [6] M. Okazaki, Y. Tai, R. Nakagaki, K. Nunome, and K. Toriyama, *Chem. Phys. Lett.*, **166**, 227 (1990).
- [7] M. Okazaki, K. Toriyama, Y. Tai, and K. Nunome, *Appl. Magn. Reson.*, **1**, 213 (1990).
- [8] M.N. Lukzen, V.O. Saik, O.A. Anisimov, and Yu.N. Molin, *Chem. Phys. Lett.*, **118**, 125 (1985).
- [9] A. Weller, H. Sraerk, and R. Treichel, *Discuss. Farad. Soc.*, **78**, 271 (1984).

EPR and ODMR Studies of the Phosphorescent States of trans-2,2'-Bipyridine, Metal-Free cis-2,2'-Bipyridine and $[\text{Zn}(\text{bpy})]^{2+}$

Mikio Yagi

Department of Physical Chemistry, Faculty of Engineering,
Yokohama National University, Tokiwadai, Hodogaya-ku,
Yokohama 240, Japan

Bruce D. Schlyer and August H. Maki

Department of Chemistry, University of California, Davis,
CA 95616, USA

Abstract

Using a 2-propanol-water ($i\text{-PrOH-H}_2\text{O}$) mixture as a host, EPR spectra have been observed for the lowest excited triplet (T_1) states of trans-2,2'-bipyridine (trans-bpy) and metal-free cis-bpy at 77 K. The zero-field splitting (ZFS) parameters and sublevel kinetics were determined for the T_1 states of trans-bpy, metal-free cis-bpy and $[\text{Zn}(\text{bpy})]^{2+}$ in $i\text{-PrOH-H}_2\text{O}$ at 1.2 K by a zero-field optically detected magnetic resonance technique. The ZFS E parameter is sensitive to the conformational change of bpy, while the triplet sublevel kinetics are sensitive to both the conformational change and to the metal complex formation with Zn^{2+} .

1. Introduction

2,2'-bipyridine (bpy) is a typical bidentate chelating agent for metal ions. The photophysics and photochemistry of bpy complexes are under active investigation. The lowest excited triplet (T_1) states of bpy complexes have been studied through optically detected magnetic resonance (ODMR) [1–3] and time-resolved EPR (TREPR) [2,4] experiments. The T_1 states of organometallic complexes of nd^{10} configuration, such as Zn^{2+} and Cd^{2+} with bpy have been thought to possess $^3\pi\pi^*$ type T_1 states. The nature of the T_1 state of $[\text{Zn}(\text{bpy})]^{2+}$ may usually be explained by a small perturbation of bpy by Zn^{2+} . During the course of the TREPR studies, however, a remarkable change in the anisotropy of the triplet sublevel populating rates has been observed for $[\text{Zn}(\text{bpy})]^{2+}$ [5].

The geometry of bpy is remarkably changed upon coordination with a metal ion. The trans and cis conformations are possible in

bpy, as shown in Fig. 1. The ground-state (G-state) molecule has the trans conformation in solutions [6,7] and in the crystalline state [8]. The T₁ state bpy has been considered for many years to have the trans conformation in ethanol [9], in Shpol'skii matrices [3,10] and in a single crystal of durene [11] at low temperatures. On the other hand, the stable conformation of bpy in its metal complexes is apparently cis. It is difficult to determine whether the observed change in the sublevel populating rates is due to the intrinsic effect of the coordination to Zn²⁺ or the effect of the conformational change. The lack of data on metal-free cis-bpy leaves the question open.

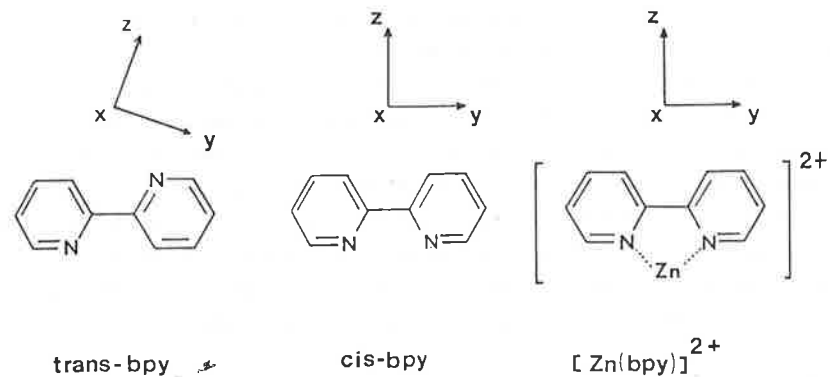


Fig. 1. Molecular structures and coordinate systems chosen for trans-bpy, cis-bpy and [Zn(bpy)]²⁺.

Recently, the T₁ state EPR spectra of a metal-free cis-bpy have been observed in mixtures of water with various alcohols at 77 K [12]. In the present work, we have observed the EPR and ODMR signals from bpy using a 2-propanol-water (i-PrOH-H₂O) mixture as a host. We have been able to observe EPR and ODMR signals of the T₁ states of trans-bpy, cis-bpy and [Zn(bpy)]²⁺ in these solvent mixtures. The separate effects of conformation and Zn²⁺ coordination on the zero-field splitting (ZFS) parameters and sublevel kinetics of bpy are discussed.

2. Experimental Section

Sample solutions of bpy were prepared at concentration of 5 × 10⁻⁴ mol dm⁻³. Solutions of the complexes were prepared by addition of Zn(ClO₄)₂·6H₂O (2.5 × 10⁻² mol dm⁻³) and bpy (5 × 10⁻⁴ mol dm⁻³) to i-PrOH-H₂O (2:3, v/v).

For the EPR measurements, samples were excited using a Canrad-Hanovia 1 kW Xe-Hg arc lamp through 5 cm of distilled water and a Toshiba UV-D33S glass filter. The EPR spectra were measured at 77 K by a JEOL-FE1XG spectrometer. The experimental setup for the EPR measurements is the same as that reported previously [13].

For the ODMR measurements, the excitations were carried out at 303 nm using an Osram 100 W high pressure mercury arc lamp through an 11 cm NiSO₄ solution filter and a 10 cm Jobin Yvon H10 monochromator. Emission passed through a Corning WG-345-2 glass filter and a 1 m McPherson model 2051 monochromator was detected by an EMI 9789QA photomultiplier tube. Details of the ODMR measurements have been described previously [14].

3. Results and Discussion

Two sets of the T₁ state EPR spectra of bpy were observed in i-PrOH-H₂O and in a stretched poly(vinyl alcohol) (PVA) film at 77 K. Assuming molecular planarity in the T₁ state, the principal axes (x,y,z) of the ZFS tensor were taken to be as shown in Fig. 1. For cis-bpy with the C_{2v} symmetry, the y-axis is taken to be parallel to the long in-plane molecular axis, while for trans-bpy with the C_{2h} symmetry, the y-axis should not be parallel to the long in-plane molecular axis. Using such a difference in the direction of the principal axes of the ZFS tensor relative to the molecular axes, two sets of the EPR spectra observed in the stretched PVA film can reasonably be assigned to the trans and cis conformers [13].

The EPR signals observed in i-PrOH-H₂O (3:2, v/v) are different from those observed in i-PrOH-H₂O (2:3, v/v). The former signals can be reasonably assigned to the trans conformer, because their resonance fields are almost the same as those for the trans conformer observed in the stretched PVA film. On the other hand, from the similarity of the resonance fields between bpy in i-PrOH-H₂O (2:3, v/v) and the cis conformer observed in the stretched PVA film, bpy is expected to have the cis conformation in i-PrOH-H₂O (2:3, v/v) at 77 K.

The EPR signals assigned to the cis conformer of metal-free bpy should not be attributed to signals from the complex with Zn^{2+} , which results from the contamination of polar solvents with traces of Zn^{2+} as shown in the fluorescence experiments of bpy [15]. The reasons for this assignment are as follows:

(1) the observed T_1 state lifetime of the cis conformer in i-PrOH-H₂O (2:3, v/v) at 77 K is 0.95 s, while that of the Zn^{2+} complex is 1.18 s in the same solvent at the same temperature;

(2) the resonance fields of the EPR $\Delta M_S = \pm 1$ transitions of the cis conformer are slightly different from those of the Zn^{2+} complex;

(3) the intensity ratio of EPR signal for the cis conformer to that for the trans conformer depends on solvent composition; in the ranges from 10 to 20 wt% of i-PrOH and from 54 to 100 wt% of i-PrOH, only one set of the trans conformer signals was observed. The last phenomenon suggests that the EPR signals assigned to cis-bpy should not be attributed to the formation of aggregates of bpy in i-PrOH-H₂O.

The phosphorescence spectra of bpy and $[Zn(bpy)]^{2+}$ complex were measured at 4.2 K and are shown in Fig. 2. The T_1 state lifetimes obtained from the decay of the phosphorescence at 4.2 K are listed in Table 1.

Each ODMR measurement was made by monitoring the apex of the first band of the phosphorescence (428 nm for trans-bpy, 429 nm for cis-bpy and 423 nm for $[Zn(bpy)]^{2+}$). The ODMR slow-passage signals of $[Zn(bpy)]^{2+}$ are shown in Fig. 3. All three of the ODMR slow-passage signals were observed from the phosphorescence of the trans-bpy and $[Zn(bpy)]^{2+}$. On the other hand, the T_z-T_x transition signal of cis-bpy was too weak to be observed. This transition was observed, however, by the microwave induced delayed phosphorescence (MIDP) experiment [16]. The obtained ZFS parameters are listed in Table 1. Here, the ZFS parameters D and E are defined to be $D = -3X/2$ and $E = (Z-Y)/2$. The D values and lifetimes suggest that the T_1 states possess a mainly $^3\pi\pi^*$ character in all cases. As is known comprehensively, T_x sublevels are the lowest in energy for $^3\pi\pi^*$ states [17]. Consequently, the order of the triplet sublevels was determined to be T_y , T_z and T_x from highest to lowest energy, respectively, in all molecules studied.

We can see from Table 1 that for cis-bpy and $[Zn(bpy)]^{2+}$ the

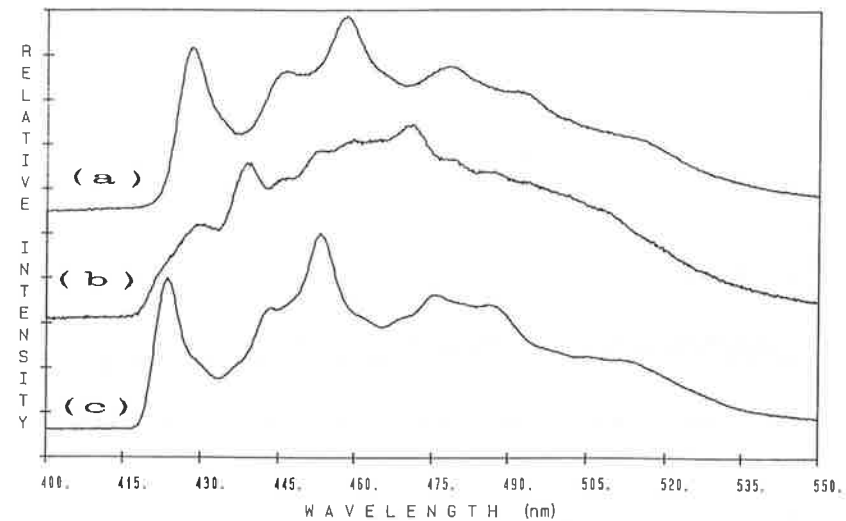


Fig. 2. Phosphorescence spectra of (a) trans-bpy in i-PrOH-H₂O (3:2, v/v), (b) cis-bpy in i-PrOH-H₂O (2:3, v/v) and (c) $[Zn(bpy)]^{2+}$ in i-PrOH-H₂O (2:3, v/v) at 4.2 K.

ZFS E parameter is less than one half that of trans-bpy. On the other hand, the ZFS D parameters of trans-bpy, cis-bpy and $[Zn(bpy)]^{2+}$ are nearly identical. It should be noted that the ZFS E parameter of bpy is determined mainly by the conformation and the effect of coordination to Zn^{2+} is small.

The total decay rate constants, k_i ($i = x, y, z$), of the spin sublevels of trans-bpy, cis-bpy and $[Zn(bpy)]^{2+}$ were determined from the analysis of the MIDP signals at 1.2 K with the method described by Schmidt, et al. [18]. The results are listed in Table 1. The assumption of negligible spin-lattice relaxation at 1.2 K was confirmed from the lack of temperature dependence of MIDP between 1.18 K and 1.43 K.

The microwave saturation recovery (MSR) method of Shain and Sharnoff [19] was used to obtain the relative radiative quantum yield of the T_i sublevel, $Q_i = k_i^r/k_i$, where k_i^r is the radiative rate constant of the T_i sublevel. The relative values of the steady-state populations of the sublevels, N_i^0 , were determined by Chan's and Nelson's method [20]. The relative values of the populating rates of the sublevels, P_i , were determined by the

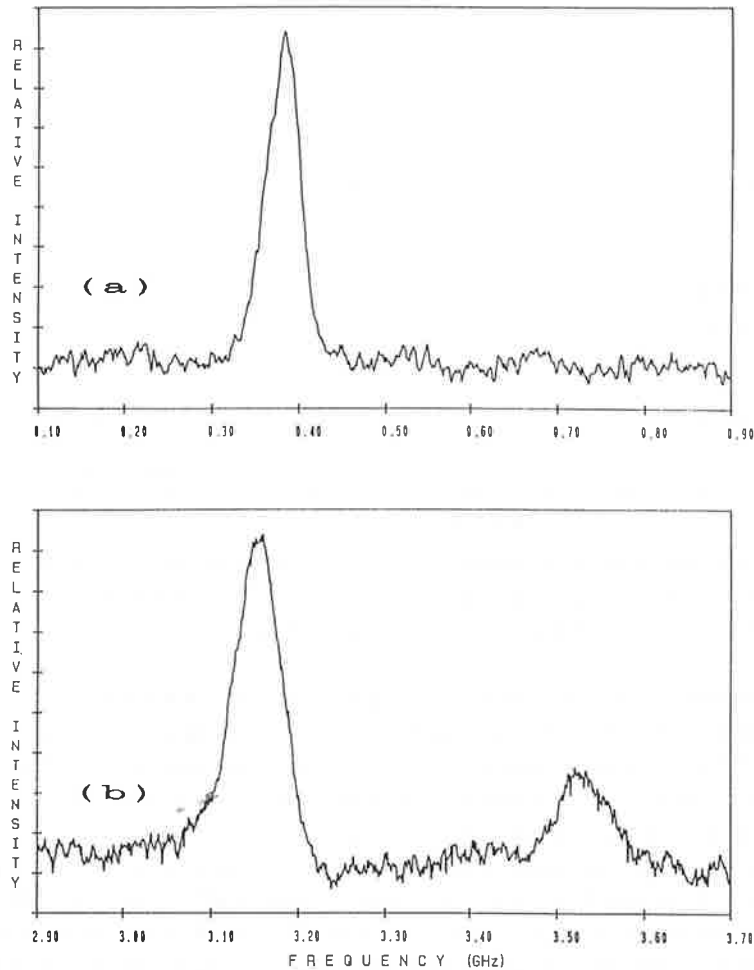


Fig. 3. Slow-passage ODMR transitions of $[Zn(bpy)]^{2+}$ in i-PrOH-H₂O (2:3, v/v) at 1.2 K. (a) T_y - T_z transition. The sweep rate was 18 MHz s⁻¹. The signal results from 2 scans. (b) T_x - T_z and T_x - T_y transitions. The sweep rate was 20 MHz s⁻¹. The signals result from 20 scans.

pulsed $S_1 \leftarrow G$ excitation method of El-Sayed and Olmsted [21].

The kinetic properties obtained are listed in Table 1. We can see from this table that the triplet sublevel kinetics are sensitive to both the conformational change and to metal complex forma-

Table 1

ZFS parameters (in GHz), k_i (in s⁻¹) and relative values of k_i^r , Q_i , P_i and N_i^0 observed at 1.2 K

Molecule ^a	$ D $ ^b	$ E $ ^c	k_x	k_y	k_z	k^d	k_x^r	k_y^r	k_z^r
trans-bpy	3.32	0.36	0.48	1.2	1.4	0.97	$k_y^r > k_z^r > k_x^r$		
cis-bpy	3.36	0.16	0.32	1.4	1.1	0.93	0.08	0.29	1
$[Zn(bpy)]^{2+}$	3.33	0.17	0.48	0.77	1.2	0.77	0.08	0.08	1
Q_x	Q_y	Q_z	P_x	P_y	P_z	N_x^0	N_y^0	N_z^0	
$Q_y > Q_x > Q_z$			$P_z > P_y > P_x$			$N_z^0 > N_x^0 > N_y^0$			
0.26	0.23	1	0.16	1	0.56	0.67	1	0.71	
0.2	0.1	1	0.48	1	0.65	0.78	1	0.40	

^a trans-bpy is in i-PrOH-H₂O (3:2, v/v). cis-bpy and $[Zn(bpy)]^{2+}$ are in i-PrOH-H₂O (2:3, v/v).

^b $D = (-3/2)X$.

^c $E = (1/2)(Z - Y)$.

^d Obtained from the phosphorescence decay at 4.2 K.

tion with Zn²⁺.

For cis-bpy, the most emissive sublevel is T_z , while it is T_y in trans-bpy. The out-of-plane T_x sublevels are the least emissive in both trans- and cis-bpy's, as is usual for planar ${}^3\pi\pi^*$ states of aromatic molecules. The sublevel which has the largest steady-state population is T_y in cis-bpy, while it is T_z in trans-bpy. T_z has almost the same steady-state population as T_x in cis-bpy. This observation is in accord with the fact that the slow-passage ODMR signal of the T_z - T_x transition was too weak to be observed for cis-bpy, although T_z is much more emissive than T_x . The k_i and relative k_i^r are inversely ordered in magnitude for the in-plane sublevels of both the trans- and cis-bpy's suggesting that the non-radiative contribution to k_z for trans-bpy and to k_y for cis-bpy is large. That intersystem crossing (ISC) from $T_1 \rightarrow G$ is efficient for these sublevels parallels the observation of preferential population of T_z from S_1 in trans-bpy and of T_y in cis-bpy.

The shortest-lived sublevel changes from T_y in cis-bpy to T_z

in $[\text{Zn}(\text{bpy})]^{2+}$. T_z is the most emissive in $[\text{Zn}(\text{bpy})]^{2+}$. The observed ordering of P_i of $[\text{Zn}(\text{bpy})]^{2+}$, $P_y > P_z > P_x$, is in good agreement with previous TREPR measurement in ethanol at 77 K [5]. The P_i ordering of $[\text{Zn}(\text{bpy})]^{2+}$ is the same as that of *cis*-bpy. T_y has the largest steady-state population in both *cis*-bpy and $[\text{Zn}(\text{bpy})]^{2+}$. However, the sublevel which has the least steady-state population is T_z in $[\text{Zn}(\text{bpy})]^{2+}$, while T_z has almost the same steady-state population as T_x in *cis*-bpy.

The $[\text{Zn}(\text{bpy})]^{2+}$ is believed to possess $^3\pi\pi^*$ type T_1 state because Zn^{2+} ion has a d^{10} closed shell configuration. The $d\pi^*$ states are expected to be located very high in energy due to the fully occupied 3d orbitals. In fact, the ZFS parameters, phosphorescence lifetime and the position of the 0-0 band of phosphorescence of the complex are almost the same as those of the metal-free *cis*-bpy in the same solvent and at the same temperature. This means that the T_1 state of $[\text{Zn}(\text{bpy})]^{2+}$ possesses almost pure $^3\pi\pi^*$ character for the local excitation within a ligand. The effect of coordination to Zn^{2+} on the T_1 state of bpy is believed to be small. However, the present work shows that Zn^{2+} plays an important role in determining the triplet sublevel kinetics of bpy.

Acknowledgment

We thank Professor Jiro Higuchi for several helpful discussions.

References

- [1] Y. Komada, S. Yamauchi and N. Hirota, *J. Phys. Chem.*, **90** (1986) 6425.
- [2] S. Yamauchi, Y. Komada and N. Hirota, *Chem. Phys. Lett.*, **129** (1986) 197.
- [3] A. P. Suisalu, A. L. Kamyshnyi, V. N. Zakharov, L. A. Aslanov and R. A. Avarmaa, *Chem. Phys. Lett.*, **134** (1987) 617.
- [4] M. Yagi, Y. Deguchi, Y. Shioya and J. Higuchi, *Chem. Phys. Lett.*, **144** (1988) 412.
- [5] M. Yagi, H. Shirai, J. Ohta and J. Higuchi, *Chem. Phys. Lett.*, **160** (1989) 13.
- [6] K. Nakamoto, *J. Phys. Chem.*, **64** (1960) 1420.
- [7] S. Castellano, H. Gunther and S. Ebersole, *J. Phys. Chem.*, **69**, (1965) 4166.
- [8] L. L. Merritt, Jr. and E. D. Schroeder, *Acta Crystallogr.*, **9** (1956) 801.
- [9] Y. Gondo and A. H. Maki, *J. Phys. Chem.*, **72** (1968) 3215.
- [10] K. Vinodgopal and W. R. Leenstra, *J. Phys. Chem.*, **89** (1985) 3824.
- [11] N. Okabe, T. Ikeyama and T. Azumi, *Chem. Phys. Lett.*, **165** (1990) 24.
- [12] M. Yagi, K. Makiguchi, A. Ohnuki, K. Suzuki, J. Higuchi and S. Nagase, *Bull. Chem. Soc. Jpn.*, **58** (1985) 252.
- [13] J. Higuchi, M. Yagi, T. Iwaki, M. Bunden, K. Tanigaki and T. Ito, *Bull. Chem. Soc. Jpn.*, **53** (1980) 890.
- [14] D. H. H. Tsao, J. R. Casas-Finet, A. H. Maki and J. W. Chase, *Biophys. J.*, **55** (1989) 927.
- [15] J. Kotlicka and Z. R. Grabowski, *J. Photochem.*, **11** (1979) 413.
- [16] J. Schmidt, W. S. Veeman and J. H. van der Waals, *Chem. Phys. Lett.*, **4** (1969) 341.
- [17] A. W. Hornig and J. S. Hyde, *Mol. Phys.*, **6** (1963) 33.
- [18] J. Schmidt, D. A. Anteunis and J. H. van der Waals, *Mol. Phys.*, **22** (1971) 1.
- [19] I. Y. Chan and B. N. Nelson, *J. Chem. Phys.*, **62** (1975) 4080.
- [20] A. L. Shain and M. Sharnoff, *J. Chem. Phys.*, **59** (1973) 2335.
- [21] M. A. El-Sayed and J. Olmsted III, *Chem. Phys. Lett.*, **11** (1971) 568.

Formation of Aminoxyl Radicals from 5,5-Dimethyl-1-pyrroline-N-oxide by Ferric Ion

Keisuke Makino, Akifumi Hagi, Hiroshi Ide, and Akira Murakami

Department of Polymer Science, Kyoto Institute of Technology, Kyoto 606
(Japan)

Masatoshi Nishi

Faculty of Pharmaceutical Sciences, Setsunan University, Hirakata, Osaka 573-01
(Japan)

Abstract

In order to assign unidentified ESR signals that are obtained with 5,5-dimethyl-1-pyrroline-N-oxide (DMPO) as a spin trap in samples containing metal ions, reactions of DMPO have been studied in the presence of ferric ion. It has been found that DMPO-OH (a spin adduct of hydroxyl radical) is produced by the nucleophilic addition of a water molecule to the double bond of DMPO as well as by the addition of hydroxyl radicals. This implies that the origin of a quartet due to DMPO-OH should be carefully attributed to since the adduct could be produced both by free radical and nucleophilic reactions. The products formed by the reaction between DMPO-OH and Fe(III) were separated by HPLC and their structures were analyzed spectrophotometrically. These results have revealed that 1-hydroxy-5,5-dimethyl-1-pyrrolid-2-one (HDMPN) and 2-hydroxy-5,5-dimethyl-1-pyrroline-N-oxide (HDMPO), which are tautomers with each other, are produced in the present system. HDMPN and HDMPO generate ESR visible aminoxyl radicals by oxidation reaction and/or addition of hydroxyl radicals. The background signals arising from these aminoxyl radicals prevent accurate assignment of the ESR spectra obtained in such systems.

1. Introduction

The method of spin trapping has been widely used to detect the formation of free radicals in biological systems in attempts to correlate the free radical formation to the initiation of various diseases [1,2]. In such investigations, 5,5-dimethyl-1-pyrroline-N-oxide (DMPO) has been used almost exclusively because it is so soluble in water that a small amount of short-lived free radicals will be trapped when its concentration is sufficiently high [3,4]. It is known, however, that ESR spectra obtained with DMPO are often difficult to assign because of the coexistence of unidentified signals.

In the present study, we have carried out detailed studies to elucidate the mechanism of generation of unidentified background ESR signals obtained when

DMPO is used as spin trap in biological systems. Since such unidentified ESR signals have been found to arise most frequently in Fenton systems, the role of ferric ion in the reaction of DMPO has been carefully assessed.

2. Experimental Section

DMPO with high purity was obtained from Mitsui-Toatsu Co. (Tokyo, Japan) and used without further purification [5]. Other reagents of reagent grade were purchased from Wako Pure Chemicals (Osaka, Japan). Water was purified sequentially by Milli R/Q and Milli QII (Millipore, MA, USA).

ESR spectra were measured with a JEOL Model PE-3X spectrometer (X-band, 100 kHz field modulation, JEOL, Tokyo, Japan). The markers used for the measurements of hyperfine splitting constants and g-values were Mn²⁺ and Cr³⁺, respectively. In the experiments performed at room temperature, an aqueous flat quartz cell (1.6 mm in thickness, 10.0 mm in width, and 180.0 mm in length) was used while a round quartz cell (5.0 mm i.d. and 262.5 mm long) was utilized for experiments performed at 77K.

HPLC separation was carried out under the conditions: column, Inertsil ODS (GL Science, Tokyo, Japan); eluent, (A) CH₃CN/H₂O (5%) and (B) CH₃CN/H₂O (20%); gradient, linear from A to B for 40 min; flow rate, 1 ml/min; detection, 210 nm.

All experiments were carried out in the dark to avoid photochemically induced reactions of DMPO [6].

3. Results and Discussion

ESR measurements of a sample containing DMPO and ferric ion performed at 77K showed a line at g=4.2 typical of a non-heme complex. This result indicates that a DMPO-Fe(III) complex is formed immediately after the sample preparation. In addition, an ESR signal attributed to DMPO-OH (a spin adduct of hydroxyl radicals) also appeared when the measurement was performed with a solution containing DMPO (100 mM) and Fe(III) (1mM) at room temperature. We have recently reported that this aminoxyl radical is produced by the nucleophilic addition of a water molecule to the DMPO-Fe(III) complex [7].

A reaction mixture composed of DMPO and ferric ion was separated by reversed-phase HPLC for product analysis (Fig.1). From NMR, MS and IR measurements of the main RPLC peak (Peak 1 in Fig.1), the structure of the main product was assigned to 1-hydroxy-5,5-dimethyl-1-pyrrolid-2-one (HDMPN) (data not shown). The detailed ¹H-NMR and MS fragmentation studies further indicate that 2-hydroxy-5,5-dimethyl-1-pyrroline-N-oxide (HDMPO) that is initially formed by the nucleophilic addition of a water

molecule to DMPO-Fe(III) isomerizes to HDMPN, a tautomer of HDMPO (Fig. 2).

The oxidative conversion of DMPO to HDMPN was accelerated by the addition of ferric ion to the sonicated aqueous DMPO solution (10 mM) containing both DMPO and DMPO-OH (ca. 50 μ M), suggesting that the precursor giving rise to HDMPO and HDMPN in the present systems is DMPO-OH (Fig. 3). Thus, we have concluded that unidentified background ESR signals often observed in biological systems are attributable to the aminoxy radical (HDMPO-OH and DMPOX) produced by the oxidation reaction of HDMPO and HDMPN by hydroxyl radicals (Fig. 3).

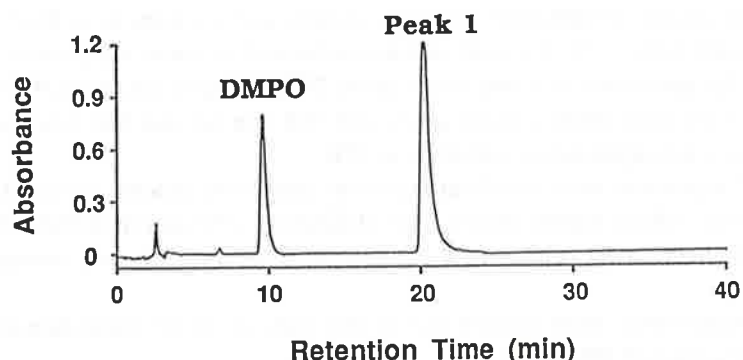


Fig. 1 HPLC separation of a system composed of DMPO and Fe(III).

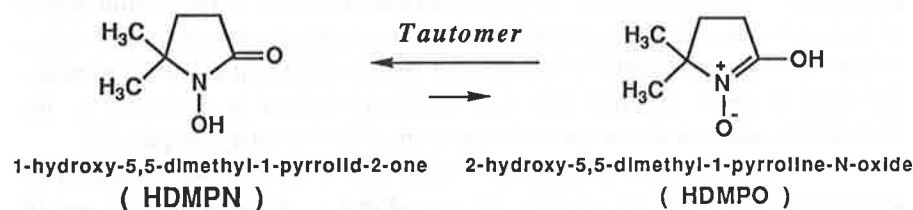


Fig. 2 Compounds produced from DMPO through DMPO-Fe(III).

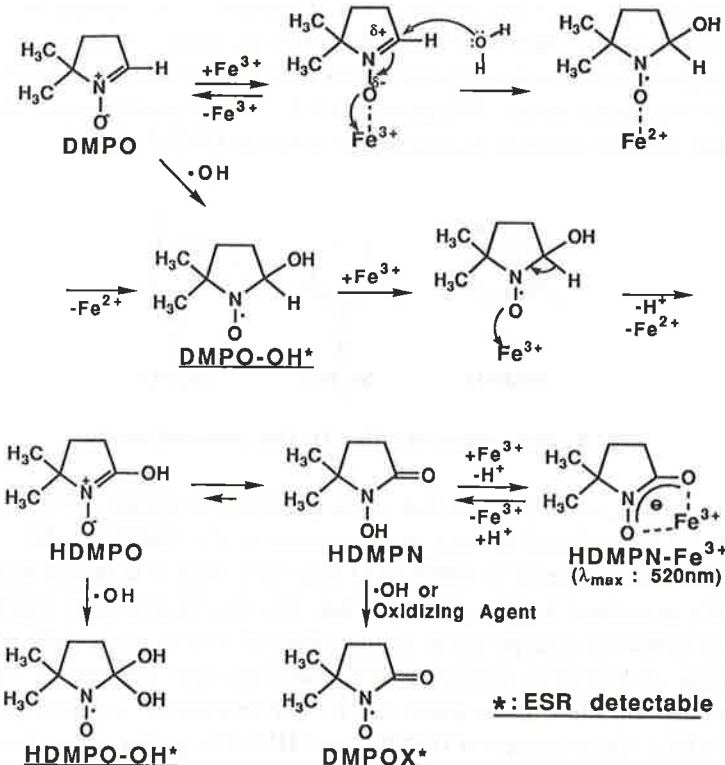


Fig. 3 Overall reactions of DMPO in the presence of Fe(III).

Based on the present results, the reaction mechanism of DMPO in the presence of Fe(III) is given as follows (see also Fig. 3). In the systems containing both DMPO and Fe(III), DMPO readily complexes Fe(III) to form DMPO-Fe(III), and subsequently DMPO-OH is produced by the nucleophilic addition of a water molecule to the complex. DMPO-OH undergoes further proton elimination to produce oxidation products such as HDMPO and HDMPN. These products give rise to background ESR signals by further reactions with hydroxyl radicals.

We have also investigated fundamental reactions of DMPO analogs including 2,5,5-trimethyl-1-pyrroline-N-oxide (M₃PO) and 3,3,5,5-tetramethyl-1-pyrroline-N-oxide (M₄PO) (Fig. 4). M₃PO was not subjected to the reactions

found for DMPO in the presence of Fe(III) because of substitution of CH₃ group for H at C2. The exact role of CH₃ at C2 to prevent such reactions is currently under investigation. M₄PO was degraded in the presence of Fe(III), but the rate of the degradation was much lower (1/10) than that of DMPO probably due to the steric hindrance by the CH₃ groups at C3. These results are on the whole consistent with the reaction mechanism proposed for DMPO (Fig. 3).

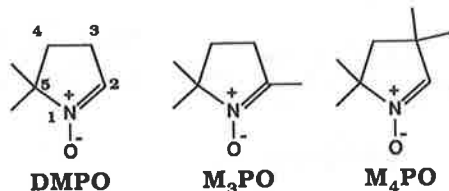


Fig. 4 Spin traps studied in the present study.

In summary, we will stress that in the presence of Fe(III), ESR detectable DMPO-OH is produced through the formation of the DMPO-Fe(III) complex, and ESR signals assigned to DMPO-OH may arise even if hydroxyl radicals are not really generated in the system. Thus, this misleading ESR signals could result in erroneous interpretation of the obtained results particularly when the generation of hydroxyl radicals is monitored by spin trapping in biological systems that are known to contain Fe(III). Furthermore, we have found that DMPO-OH is the precursor of HDMPO and HDMPN giving rise to background ESR signals in the presence of oxidative species. This also makes it difficult to analyze ESR signals obtained. Since a series of reactions shown in Fig. 3 are accelerated when H₂O₂ coexists in the systems (data not shown), assignment of each ESR signal obtained in biological systems should be carried out with great care. Such undesirable side reactions should be able to be prevented by using spin traps having CH₃ groups at C2 of pyrroline ring.

4. References

- [1] J. F. Mead in W. A. Pryor (ed.), *Free Radicals in Biology*, Academic Press, New York, 1980, Vol. I, p.51.
- [2] A. C. de Mello Filho and R. Meneghini, *Biochem. Biophys. Acta*, 847 (1985) 82.
- [3] E. G. Janzen in W. A. Pryor (ed.), *Methods in Enzymology*, Academic Press, New York, 1984, Vol. 105, p.188.

- [4] E. Finkelstein, G. M. Rosen and E. J. Rauckman, *Arch. Biochem. Biophys.*, 200 (1980) 1.
- [5] K. Makino, H. Imaishi, S. Morinishi, T. Hagiwara, T. Takeuchi and A. Murakami, *Free Rad. Res. Comms.*, 6 (1989) 19.
- [6] R. Bonnett, V. M. Clark and A. Todd, *J. Chem. Soc.*, (1959) 2102.
- [7] K. Makino, T. Hagiwara, A. Hagi, M. Nishi and A. Murakami, *Biochem. Biophys. Res. Commun.*, 172 (1990) 1073.

APPLICATIONS OF ESE SPECTROSCOPY IN THE STUDY OF ELECTRON SPIN POLARIZATION IN BACTERIAL PHOTOSYNTHESIS

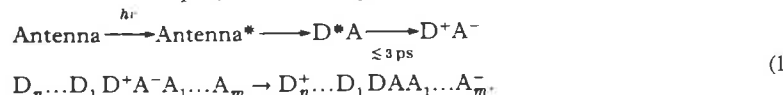
M.K. BOSCH, P. GAST AND A. J. HOFF

Department of Biophysics

Huygens Laboratory, University of Leiden
P.O. Box 9504, 2300 RA Leiden, The Netherlands

1. Photosynthetic Photochemistry

Photosynthesis is the conversion of the quantum energy of light by algae, higher plants and photosynthetic bacteria into the chemical energy of complex organic molecules and organized cellular structures. The light is absorbed by so-called antenna pigment-protein complexes, containing (bacterio)chlorophyll as their major pigment. The resulting electronic excited state is transferred among the antenna pigments by Förster resonant energy transfer until it is trapped by a specialized complex of (bacterio)chlorophyll, (B)Chl, molecules in a special protein, the reaction center (RC). In a few picoseconds, photochemistry on the excited specialized complex results in the donation of an electron to an electron acceptor, thus creating a pair of separated, charged radicals. Subsequent dark electron transport at either the donor or the acceptor side (or both) stabilizes the charges at the expense of free energy ("downhill" electron transport). Schematically:

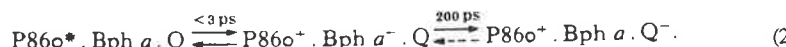


Here D stands for donor and A for acceptor molecules, and the asterisk denotes an excited state.

In this contribution we will limit ourselves to the photosystem of BChl *a* containing purple bacteria as this is simpler and better understood than the photosystems of plants (or other photosynthetic bacteria). Moreover, the salient Electron Spin Polarization (ESP) phenomena can all be found in the first few steps of photochemistry in the reaction center of these particular bacteria.

1.1. Bacterial photosynthetic reaction centers

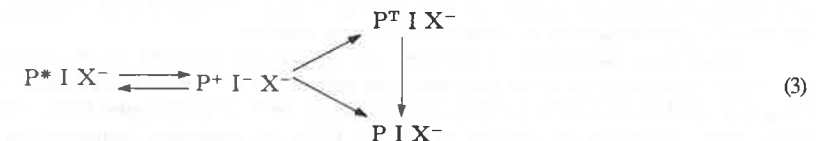
The primary photochemical reaction in the RC of BChl *a*-containing purple bacteria can be written as



Here P860 denotes the primary electron donor, a BChl *a* dimer having an absorption band

at 860 nm, BPh the first electron acceptor, a bacteriopheophytin *a* (BChl *a* without the central Mg atom) molecule, and Q the secondary electron acceptor, a ubiquinone. It is convenient to abbreviate these labels to P, I and X, respectively.

When the secondary acceptor is reduced, either photochemically or by adding a chemical reductant, the electron of the primary reaction cannot pass to the ubiquinone, and the primary radical pair decays by recombination, either to the singlet ground or excited state of P or to its triplet state, P^T:



In Eqn. 2 is indicated that the lifetime of the primary radical pair P^TI⁻ when X is not prereduced is about 200 ps. This time and the lifetime of the excited state P^TI depend very little on the temperature, so that it is possible to study the primary photochemistry at cryogenic temperatures, down to 1.5 K. In other words, the primary reaction of photosynthesis is a *solid state* reaction.

The complex machinery of the bacterial photosynthetic apparatus can be considerably simplified by isolating the RC protein from the photosynthetic membrane. The purified RC is fully capable of primary photochemistry. It has been crystallized and subjected to X-ray diffraction analysis, for which work J. Deisenhofer, R. Huber and H. Michel received in 1988 the Nobel prize for chemistry.¹ Their work, and subsequent similar work by the groups of Feher and Norris,^{2,3} has allowed to draw a detailed picture of the spatial configuration of the active components and of some other co-factors. A schematized version is shown in Fig. 1. It is seen that there are two chains of pigment co-factors, each followed by a quinone

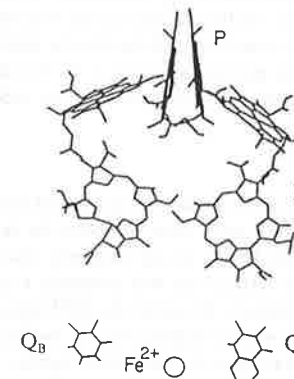


Fig. 1. Arrangement of the co-factors in the reaction center of *Rps. viridis*. Q_B is drawn symmetrically to Q_A, it is normally not seen by X-ray crystallography. Computed from coordinates obtained from Dr.J.Deisenhofer.

molecule, in a C_2 -symmetric arrangement. Surprisingly, only one chain, customarily labelled the A-chain, is photoactive, the second quinone molecule, Q_B , accepting the electron from Q_A^- . Q_B can be doubly reduced in two subsequent photoreactions, and when the RC is embedded in the photosynthetic membrane it leaves the RC to take part in further chemistry. In the isolated RC it is easily lost during the preparation procedure. The Q_A acceptor then cannot pass its electron further, and the charges on P^+ and Q_A^- recombine to the singlet state PIX in about 100 ms at room temperature and about 25 ms below 100 K. For RC having their full Q_B complement, electron transport from Q_A to Q_B is inhibited at lower temperatures and the P^+X^- pair decays by the same recombination reaction.

When Q_A is prereduced, or together with Q_B removed from the RC by extraction procedures, recombination of the photoproduced radical pair P^+I^- generates the triplet state P^+I with a yield of about 15% at 300 K and practically 100% at temperatures below 100 K. Under these conditions the lifetime of P^+I^- is 10-50 ns, depending somewhat on the temperature. The triplet state decays in a few μ s at 300 K, and in about 100 μ s below 100 K.

The many different redox states in which the RC can be prepared and the various regimes of radical pair lifetimes provide a rich playground for ESP enthusiasts. In the following Section a number of ESP observations for RC of the purple bacterium *Rhodobacter (Rb.) sphaeroides* strain R-26 will be discussed, some of which are unique and have as yet not been observed *in vitro*.

2. ESP of Bacterial Photosynthetic Reactants

Shortly after the first observation of ESP in plants,⁴ ESP was observed in bacterial RC.⁵ The latter observation showed conclusively that the Radical Pair Mechanism (RPM) and not the Triplet Mechanism (TM) was operative in generating ESP in (bacterial) photosynthesis. Further work showed that charge separation occurs from the singlet excited state, and that in all probability the exchange interaction J between P^+ and I^- is positive. Limiting values for both J and the z-component of the dipolar interaction between P^+ and X^- , D_{zz} , could be derived from extensive spectral simulation. In this Section a brief overview of ESP in the bacterial RC will be given, critically reviewing the information thus far gleaned.

2.1. ESP in active reaction centers

Unlike plants where ESP was observed without special treatment of the preparations, bacterial RC only showed ESP when they were subjected to detergent treatment.⁵ It was shown that this was due to the abolishment of the magnetic interaction between the (first) quinone acceptor and the high spin ferrous ion that normally is present in the RC (Fig. 1). In "native" RC this interaction enormously broadens the EPR signal of Q_A^- and makes it a fast relaxer. The latter property presumably is responsible for the destruction of ESP in native RC. In later work it was demonstrated that the same ESP signals are observed when the RC are depleted of the ferrous ion,⁶ but still functional with respect to primary photochemistry.⁷

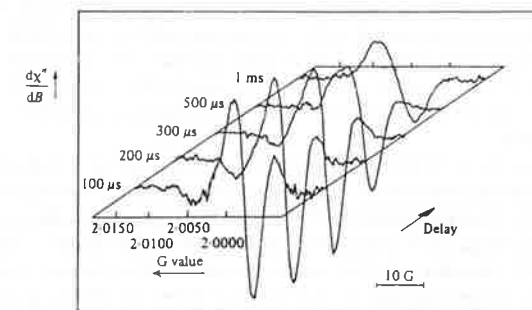


Fig. 2. Time-resolved flash EPR spectra of reaction centers of *Rb. sphaeroides* R-26 in which the quinone acceptor was magnetically decoupled from the iron. Delay times between the flash and the boxcar gate are indicated. From.⁸

The ESP signal depicted in Fig. 2 was recorded at 5 K with a cw X-band (9 GHz) EPR spectrometer having a time resolution of 20 μ s, employing boxcar integration of the initial part of the decay curve following a laser flash. The polarized spectrum is shown at several delay times after the flash. At early times, the signal is maximally polarized (as confirmed by direct detection measurements with < 1 μ s time resolution (A.J. Hoff and I.I. Proskuryakov, unpublished results). It decays within a few ms to the EPR signal in Boltzmann equilibrium, which consists of the overlapping EPR spectra of P^+ and Q_A^- .

2.1.1. Simulated ESP spectrum for active RC: the RPM approach

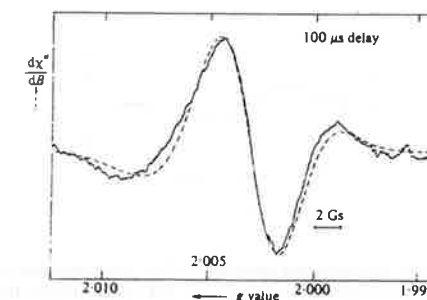


Fig. 3. Polarized spectrum of RC of *Rb. sphaeroides* at 5 K and a delay of 100 μ s (Fig. 2) compared with a simulation based on the RPM⁹ (broken line).

The maximally polarized experimental spectrum of Fig. 2 was simulated by Hore et al.⁹ using the RPM formalism for ESP in the solid state, in which for the first time the dipolar interaction was correctly introduced. The simulation was based on the assumption that multiplet and net polarization is generated in the primary radical pair P^+I^- , and that subsequently the electron is transferred to Q_A , conserving only the net polarization of I^- (the information on the hyperfine couplings is lost upon transfer). The anisotropy of the dipolar interactions between P^+ and I^- and I^- and X^- ($= Q_A$), and of the g -value of X^- was averaged over all angles. It is seen from Fig. 3 that the agreement between experimental and simulated spectrum is quite good.

It is instructive to compare the different contributions to the lineshapes of polarized P^+ and X^- (Fig. 4). The net effect for P^+ is emissive, corresponding with $\Delta g < 0$ and a singlet precursor to $J < 0$. The multiplet pattern of P^+ (dashed line) agrees with this sign. The dipolar contribution to the lineshape of P^+ averages to zero. For X^- the net effect is absorptive, since now $\Delta g > 0$, and the multiplet effect is absent because of the electron transfer step. The dipolar interaction no longer averages to zero because of the anisotropic g -value of X^- . It is seen to dominate the lineshape of the polarized X^- signal and to be responsible for the emissive low field lobe of the total ESP spectrum. Would one have naively interpreted this lobe as the emissive part of a multiplet pattern of X^- , then the purported E/A pattern would have led to $J > 0$, the opposite of the sign of J used for the simulation.

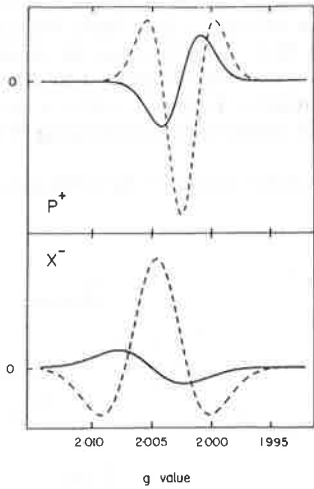


Fig. 4. The four contributions to the simulated spectrum of Fig. 3 corresponding to the net (solid line) and multiplet (broken line) ESP for P^+ and the net (solid line) and dipolar (broken line) components for X^- .⁹

Notwithstanding the success of the simulation a number of worrisome discrepancies remained. The linewidth of P^+ used for the simulation was almost half as small as that of the isolated P^+ *in vivo* (5.2 G vs. 9.7 G). The ratio $D_{P^+I^-}/J = 57$ derived from the best fit seemed very high compared with the value of $D_{P^+I^-}$ calculated from the crystal structure (~ 5.5 G^{8,10}) and the value of J estimated from a simulation of low-field Reaction Yield Detected Magnetic Resonance (RYDMAR) experiments, $|J| \approx 7$ G.^{11,12} In addition, the intensity of the polarized signal, about three times that of the EPR spectrum in Boltzmann equilibrium, together with a lifetime of the P^+I^- pair of 250 ps requires $J \approx -80$ G, a value that is clearly much too large and not compatible with the quoted value for the ratio $D_{P^+I^-}/J$. A last and serious discrepancy was the g -value of I^- needed for the simulation, 2.0007 compared to $g = 2.0035$ for the BPh^- radical *in vitro*.

2.1.2. Simulated ESP spectrum for active bacterial RC: the CRM approach

The above difficulties with the classical RPM for explaining the ESP signal of active bacterial RC prompted Hore et al.¹³ to take a radically different point of view. It was realized that an electron transfer time of 200 - 250 ps combined with a value of $|J_{pi}| < 10$ G is too short for generating appreciable polarization in the P^+I^- pair. In contrast, the magnetic interactions in the quasi-stable P^+X^- pair (lifetime ≈ 25 ms at 5 K) might be strong enough for generating the required magnitude of CRM polarization. Thus, a simulation was undertaken using the Correlated Radicals Mechanism (CRM)^{14,15} with sudden creation of the P^+X^- pair in the singlet state, taking into account the dipolar interaction between P^+ and X^- and the g -anisotropy of X^- . Averaging over all angles yielded the spectrum depicted in Fig. 5. It is seen that the correspondence between experimental and simulated spectrum is at least as good as for the earlier simulation based on the RPM. The parameter values, however, are now much more reasonable. The fit of Fig. 5 was obtained for $D_{P^+X^-} = -1.4$ G, $J_{P^+X^-} = 0$, literature values of the g -factor of P^+ and the g -tensor of X^- , and values for the angles defining the dipolar axis in the g -tensor coordinate frame of X^- that closely agreed with the values calculated from the crystal structure of RC of *Rhodopseudomonas (Rps.) viridis*,¹ which is homologous to that of *Rb. sphaeroides* R-26. The dipolar interaction agrees well with that found by De Groot et al.¹⁶ for the triplet state of P and X^- ; a small value of J is indicated by the large distance between P and X^- (about 3 nm). The calculated intensity of the ESP signal is about four times that of the corresponding equilibrium spectrum, in good agreement with the experimental ratio of about three.¹⁷ The linewidth of X^- was identical to the literature value; that of P^+ , however, was appreciably narrower (6.1 G vs. 9.4 G).

Comparing the results of the CRM simulation with that using the RPM approach, it appears that considerable progress is made in reconciling the values of the fit parameters to values derived from independent measurements. This lends credence to the validity of the CRM approach, but does not constitute proof. A point deserving further consideration is the lifetime of the P^+I^- pair, which was taken 200 ps as measured for native RC. For RC preparations that were depleted of the ferrous ion, however, it was reported¹⁸ that the lifetime of P^+I^- rose to 4.2 ns, long enough for substantial RPM polarization to develop. Since the lifetime of P^+I^- in the preparations used for recording the ESP spectra of Fig. 2 is not known, simulations were undertaken combining the RPM and CRM in a rigorous way, following the procedures outlined in Ref. 6. It was found that for reasonable values of D_{pi}

and J_{P_1} no significant effects on the X-band ESP spectrum occurred for lifetimes of P^+I^- up to 1 ns.¹⁶

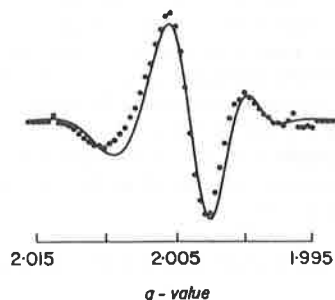


Fig. 5. Experimental ESP spectrum of Fig. 2 compared with a simulation based on the CRM.¹³

The question whether the ESP spectrum of RC of *Rb. sphaerooides* is due solely to the CRM or to an admixture of CRM and RPM could be answered if the lineshapes of the individual polarized radicals were known. In the following Section we will show that even at X-band such an unscrambling of complex overlapping ESP spectra can be achieved using a characteristic phenomenon of ESE spectroscopy, viz. that of *echo modulation*, or ESEEM.

2.1.3. MOdulation-Discriminated Echo Spectroscopy of Transient EPR (MODEST)

Measuring the echo intensity as a function of τ yields the echo decay curve. Often this curve is not smooth but shows deep modulations. These arise from interference of allowed and forbidden transitions that are simultaneous excited by the intense microwave pulse. Fourier transformation of the modulated curve yields the hyperfine and/or quadrupole interactions (see for an introduction Mims and Peisach,¹⁹ Dikanov and Astashkin,²⁰ and Schweiger.^{21,22} Thus, the modulations constitute a fingerprint of the radical studied. Considering the two radicals of a photoinduced radical pair, it is often possible to select a value of τ for which one radical shows a maximum echo amplitude, whereas that of the other radical is practically zero. If the EPR spectra of these two radicals overlap, recording the echo amplitude for that particular value of τ as a function of the magnetic field (so-called *field-swept ESE*) then yields almost exclusively the spectrum of the first radical, that of the second being suppressed. If for another value of τ the situation is reversed, then recording again the field-swept spectrum for the second τ -value yields the spectrum of the second radical. We will call this technique, which has proved to be particularly useful in unscrambling complex overlapping ESP spectra of polarized radicals, MOdulation-Discriminated Echo Spectroscopy of Transient EPR signals, or MODEST.

When using the MODEST technique, care must be taken to first record the ESEEM curves of the individual, unperturbed radicals for selecting appropriate values of τ . Furthermore it has to be ascertained that the photoproduced radicals do not exhibit strong interactions. In addition, one must be aware of the possibility that together with electron spin

polarization, the radicals may show nuclear spin polarization, which could affect the modulation pattern. Despite these caveats, MODEST is a powerful technique that allows measuring the ESP spectra of the individual radicals of a radical pair when the EPR spectra of these radicals overlap, as often happens in the solid state, even when employing high-frequency EPR.

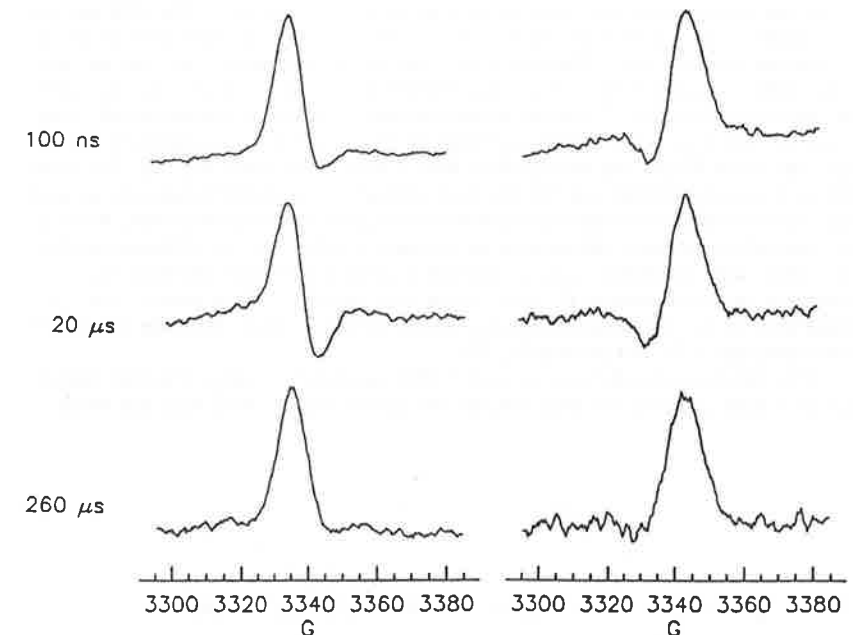


Fig. 6. MODEST spectra at 5 K of the radical pair P^*X^- . Lefthand column: $\tau = 325$ ns, righthand column: $\tau = 1055$ ns. Delay times as indicated.

Preliminary MODEST spectra of the radical pair P^*X^- are shown in Fig. 6. At $\tau = 325$ and 1055 ns the modulation amplitude of P^+ and X^- , respectively, is practically zero and the isolated polarized spectrum of X^- or P^+ (left- and righthand column, respectively) is recorded. It is seen that for short delay times after the laser flash the two spectra do not resemble the composite polarized spectrum of Fig. 2, indicating that good separation is indeed obtained. The spectrum of X^- conforms well to that expected from Fig. 4 (lower panel, the curves must be integrated). The polarized P^+ spectrum, however, deviates considerably from the expected curve; in fact the sum of the two spectra shows a net polarization not consistent with simple S - T_0 mixing. Note that the spectra are different from the simple CRM polarized spectra^{14,15} because of the presence of anisotropic dipolar and g -tensors. The extensive calculations necessary for the interpretation of the spectra are currently under way.

2.1.4. ESP of modified RC

Further progress in understanding the ESP spectrum of bacterial RC was made by recording the spectrum at higher microwave frequency (Q-band, 35 GHz), using RC preparations that were subjected to either perdeuteration, and/or to extraction of the native quinone and reconstitution with perdeuterated or protonated quinones.²³ The ESP spectra were recorded using 500 Hz light modulation, and thus represent an integration of all the time-resolved spectra of Fig. 2. This makes them unsuitable for simulation attempts, but they are nevertheless valuable for qualitative considerations as they show a much better resolution of the spectral features (Fig. 7) than the spectra previously obtained. Perdeuterated RC show the same X-band polarization pattern as previously observed (Fig. 2), viz. E/A/E/A, but the features are much sharper and the high-field lobe is more pronounced (Fig. 7a). The same pattern is observed at Q-band (Fig. 7b). RC reconstituted with perdeuterated quinone showed a polarized Q-band spectrum that was attributed to the perdeuterated quinone only, which is then completely in emission with peaks at the principal g-values (Fig. 7c). Perdeuterated RC reconstituted with protonated quinone showed a polarized Q-band spectrum that was attributed to the perdeuterated P⁺ only, which then shows a A/E/A pattern (Fig. 7d). Superposition of the two polarized spectra indeed yielded a spectrum similar to that of perdeuterated native RC displayed in Fig. 7b.

The interpretation with the conventional RPM supplemented with polarization transfer yields an X-band polarized spectrum with an A/E pattern (Fig. 4). At Q-band one would

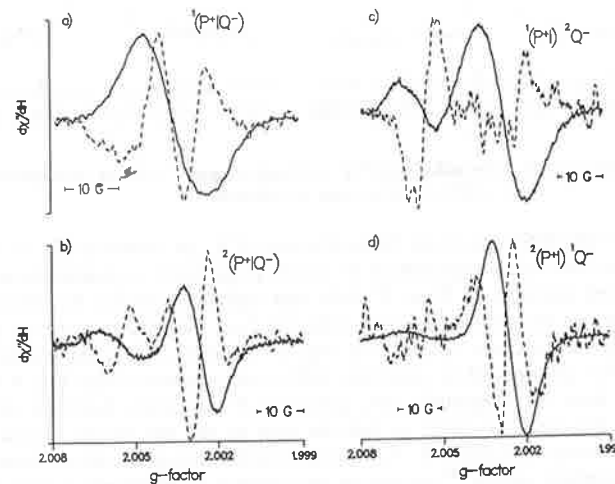


Fig. 7. Q-band EPR signal of RC of *Rb. sphaeroides* R-26 at 8 K (a) and 30 K (b,c,d) under continuous illumination (solid line) and 500 Hz light modulation (broken line).²³ Composition of the RC as indicated.

expect this pattern to change to predominantly net, emissive polarization (Fig. 4), since then the multiplet contribution is expected to be much smaller than the contribution due to the difference in Zeeman splitting. Experimentally one observes an A/E/A pattern at Q-band. Thus, it appears that polarization transfer alone cannot explain the ESP signals of active RC, in agreement with the rather satisfactory simulation of the X-band ESP spectrum by Hore et al.,¹⁵ which was based on the assumption that solely CRM polarization of the pair P⁺X⁻ contributes. As mentioned by Hore et al.,¹⁵ in reality iron-depleted RC may exhibit a lifetime of P⁺T⁻ that is long enough (> 1 ns) for significant polarization to build up. Simulations of ESP spectra of RC with known P⁺T⁻ lifetime are obviously needed to sort this out. Feezel et al.²³ have demonstrated that by carrying out such experiments on perdeuterated material at Q-band, a much higher resolution and therefore better discrimination of the simulations can be achieved.

2.2. ESP in blocked reaction centers

2.2.1. Experimental results

As discussed in Section 1.1. the secondary quinone acceptor can be prereduced, thereby blocking forward electron transport. The lifetime of the photoinduced P⁺T⁻ pair is then considerably enhanced compared to that in active RC (viz. 20-50 ns vs. 200-250 ps), allowing ample time for singlet-triplet mixing. The pair decays through recombination to either the singlet excited or ground state of P or to its triplet state, P^T. As a result of magnetic interactions between the reduced secondary acceptor X⁻ and the CRM polarized P⁺T⁻ pair, polarization is transferred to X⁻ with a lifetime corresponding to the spin-lattice relaxation time of X⁻. During this time the P⁺T⁻ pair may turn over several times, "pumping"

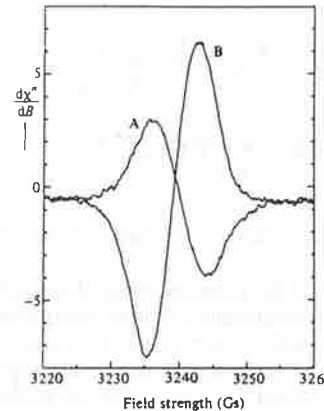


Fig. 8. Dark EPR spectrum of X⁻ of RC of *Rb. sphaeroides* at 5 K (trace A) and the spectrum under continuous illumination (trace B).²⁴

polarization into X^- . The result is striking²⁴ (Fig. 8): at 5 K under intense illumination the normal, absorptive cw EPR signal of X^- becomes completely emissive! Because of the "pumping" action one would expect that the emissivity depends on the intensity of the illumination. Moreover, it should inversely depend on the microwave power. Both predictions

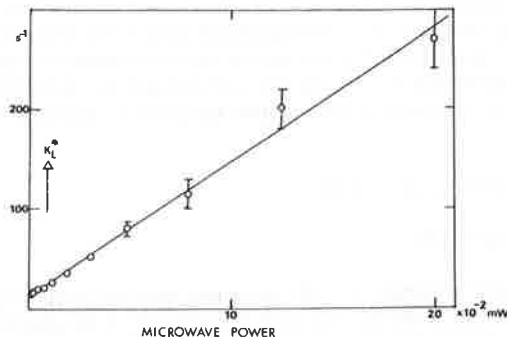


Fig. 9. Plot of the light flux at which the amplitude of the light-induced emissive signal of Fig. 14 is half-saturated as a function of the microwave power.²⁴

were verified. In Fig. 9 the microwave power is plotted against the half-saturation light intensity k_L^* , at which half the maximum emissivity is attained. Simple kinetic considerations based on the scheme of Fig. 10 predict a linear relationship²⁴, as observed.

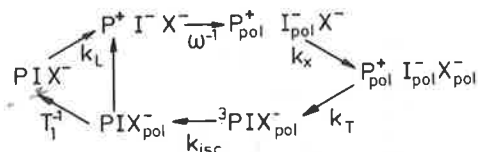


Fig. 10. Kinetic scheme of the "pumping" cycle for the generation of polarization in X^- .⁶

In spite of the success of the phenomenological description of the generation of emissive polarization of X^- , one observation remained unexplained. The emissive signal of Fig. 8 clearly shows a g-shift with respect to the dark signal, which depended on the microwave power. The g-shift is surprising as one would expect that an emissive, net-polarized signal (the transfer should be independent of nuclear spin) would faithfully reproduce the original lineshape. Possible explanations include the deformation of a true net-polarized signal of X^- by relaxation phenomena, emissive polarization of a radical other than X^- , and a polarization process more involved than simple transfer of polarization, which should then be non-uniform across the line of X^- . This phenomenon was therefore studied

in detail with ESE spectroscopy, which technique is free from the microwave power dependence and allows to record the T_1 and T_2 relaxation times across the X^- line.⁷ In addition, using the ESEEM option it is possible to unequivocally identify the polarized signal by recording its "fingerprint" echo modulation and comparing it to that of the dark signal.

The results of the ESE study are summarized in Fig. 11. In panel (a), the ESEEM traces of the emissive signal (inverted for clarity) and the dark signal are compared. It is seen that they are identical, positively identifying the emissive signal as due to X^- . In panel (b) the T_1 relaxation time, measured with a three-pulse sequence, is depicted as a function of magnetic field. The small dependence on field position within the line is symmetric and cannot explain the g-shift. This was confirmed comparing a medium-polarized signal (medium-intensity light flash) recorded directly after the flash with a signal produced with maximal polarization (saturating light flash) and recorded 1 s after the flash (Fig. 11c). The clearly non-uniformly polarized signal directly after the flash is identical with that recorded after the polarization has partly decayed, excluding that the non-uniform polarization is due to an anisotropic T_1 . In panel (d) the dark and emissive signals are compared for different echo-delay times $2t$. The g-shift is preserved over most of the echo decay period, excluding anisotropic T_2 as a possible source of the g-shift.

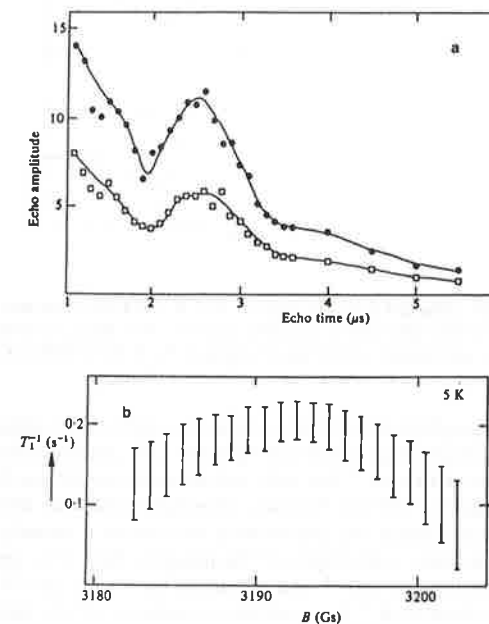


Fig. 11. (a) Echo-modulation envelope of the absorptive ESE signal of X^- at 5 K in the dark (open squares) and of the emissive signal under continuous illumination (filled circles, sign inverted).⁷ (b) Spin-lattice relaxation time of the emissive signal at 5 K as a function of magnetic field. Bars represent 90% error limits.⁷

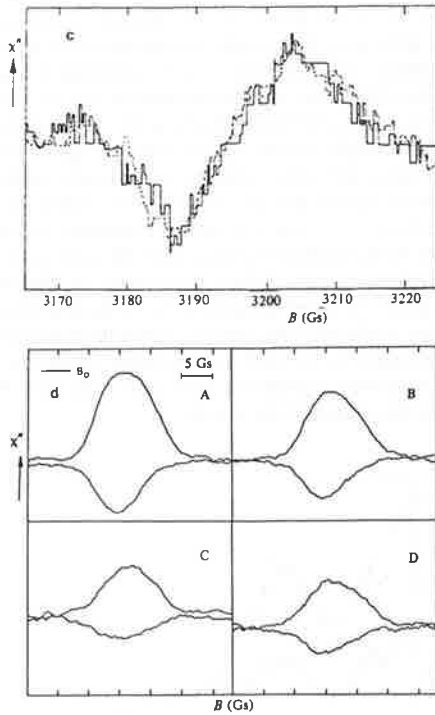


Fig. 11 cont'd. (c) Partially polarized ESE spectra of X^- at 5 K. Solid line: 1 ms after light flash of reduced intensity; broken line: 2 s after light flash of saturating intensity.⁷ Note that χ'' is monitored. (d) ESE spectra of the dark (upper traces) and emissive (lower traces) signals of X^- at 5 K for different echo delay times 2τ of 1.1 (A), 1.5 (B), 2 (C) and 4 (D) μ s.⁷

The remaining explanation, an inherent non-uniformity of the polarization mechanism, was investigated employing high-frequency (Q-band) EPR and perdeuterated material, thus allowing much greater resolution.²⁵ The dark and polarized spectra are displayed in Fig. 12. At the g_x and g_y positions, the line becomes emissively polarized, whereas at g_z there is almost no polarization. Clearly, the polarization mechanism is strongly dependent on the orientation of the X acceptor with respect to the magnetic field. This immediately suggests that the dipolar interaction between I^- and X^- and/or between P^+ and X^- plays a dominant role,⁹ and prompted Hore et al.²⁶ to undertake a simulation of the polarized signal at Q-band, to which work we will now turn.

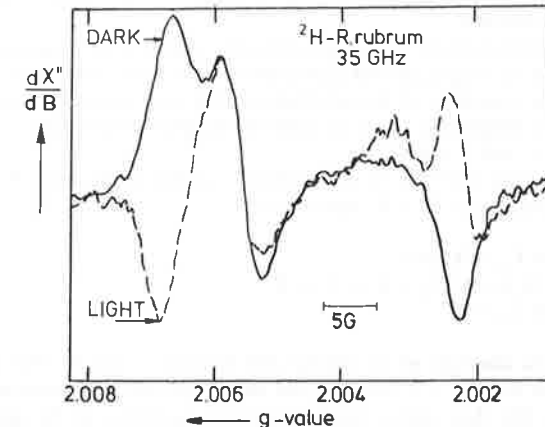


Fig. 12. Q-band spectrum of X^- in perdeuterated SDS-treated cells of *R. rubrum* at 80 K in the dark (solid line) and under continuous illumination of saturating intensity (broken line).²⁵

2.2.2. Calculation of polarization in the three-spin system $P^+I^-X^-$

In a first attempt to calculate the polarization of X^- in the $P^+I^-X^-$ three-spin system, Hoff and Hore²⁷ used the formalism of Stochastic Liouville Equation (SLE) with isotropic g -values, varying the values of the two exchange and the two dipolar couplings. (Those between P^+ and X^- were neglected.) It was found that for the parameters values searched, emissive polarization resulted only when $J_{Pi} > 0$. A more extended parameter search revealed that weak emissivity occurs for $J_{Pi} \approx -5$ G, $J_{IX} \approx -10$ G.²⁸ Clearly, just the sign of the polarized X-band spectrum of X^- is not a sufficiently discriminatory criterium.

To shed more light on the sign of J_{Pi} , Hore et al.²⁶ undertook a simulation of the well-resolved spectrum of Fig. 11, incorporating the anisotropic g -tensor of X^- . Since simulating the complete spectrum with variation of the large number of parameters, including the angles defining the position of the dipolar axes with respect to the g -tensor coordinate frame of X^- , over a considerable range would have been prohibitively demanding on computer time, it was decided to take as criteria for a successful fit the inequalities

$$\begin{aligned} 3\varphi_z &\geq \varphi_x \geq \varphi_z \geq 0.01 \\ \varphi_z &\geq 3\varphi_y \geq -\varphi_z \end{aligned} \quad (4)$$

i.e. somewhat more emission is found at g_x than at g_z , while that at g_y is much smaller. In addition the directions of the two dipolar axes were restricted to be parallel to one of the principal axes of the g -tensor of X^- (X , Y , and Z). From an extensive parameter search

during which more than 270.000 sets of polarizations were calculated, three general conclusions could be derived:

i. The X^- polarization is not sensitive to either the magnitude and direction of the P^+I^- dipolar coupling or to the magnitude and sign of the I^-X^- exchange interaction. Thus, both the magnitude *and* the anisotropy of the polarization must come from D_{IX} , whose absolute value indeed has to be larger than 5 G to generate the required polarization.

$$ii. k_T \geq 2 \cdot 10^8 \text{ s}^{-1} \text{ and } k_S \leq 8 \cdot 10^7 \text{ s}^{-1}.$$

iii. The magnitude and sign of the *exchange* interaction between P^+ and I^- are correlated with the direction of the I^-X^- dipolar axis:

$$\begin{aligned} J_{PI} &\leq -4 \text{ G and } \Gamma_{IX} = X \text{ or } Z \\ -4 \text{ G} &\leq J_{PI} \leq +4 \text{ G and } \Gamma_{IX} = X \text{ or } Y \text{ or } Z \\ J_{PI} &\geq +4 \text{ G and } \Gamma_{IX} = Y, \end{aligned} \quad (5)$$

where Γ_{IX} indicates the direction of the dipolar axis between I^- and X^- . For $|J_{PI}| \geq 4$ G, successful simulations with $\Gamma_{IX} = Y$ were 30-fold more numerous than those with the first condition of Eqn. 5. The three above conclusions were insensitive to the addition of an average hyperfine coupling, agreeing with the notion that at 35 GHz the differences in Zeeman interaction dominate.

From the crystal structure of *Rb. sphaeroides* R-26² and data on the *g*-tensors of model quinones,^{29,30} one finds that the direction of D_{IX} is roughly parallel to the Y axis. The modulus of J_{PI} as obtained from RYDMAR experiments and measurements of the effect of a magnetic field on the yield of P^+ falls within fairly narrow limits: $5 \text{ G} \leq |J_{PI}| \leq 8 \text{ G}$.^{12,31,32} It follows that only the last option of Eqn. 5 can explain the observed polarization pattern of Fig. 12 and that consequently J_{PI} is *positive*. The implications of this discovery for our understanding of primary electron transport in the RC will now be discussed.

3. Relevance of the Experimental Results for Electron Transport Theory

The mechanism of charge separation in bacterial RC is presently heavily debated. Two competing mechanisms have been proposed. Firstly, the so-called two-step mechanism, in which the accessory BChl, B_A , is reduced for a finite time before I is reduced.^{33,34,35} Secondly, the so-called superexchange mechanism in which B_A mediates electron transfer by coupling to both P and I, but is not reduced itself.^{36,37} Obviously, the relative importance of the two mechanisms depends on the position of the energy level of $P^+B_A^-$: if it lies well below that of P*, then the two-step mechanism is operative, if it lies well above P*, then the superexchange mechanism governs charge separation. Experimental evidence pro and contra the two proposed mechanisms is accumulating, but until now no consensus has been reached.^{38,39,40}

The energy difference between P* and $P^+B_A^-$, ΔG_1 , controls the energy of the singlet state of the radical pair, $[P^+I^-]$, but not the energy of its triplet state, $[P^+I^-]^T$. Therefore, knowledge of the magnitude and sign of the singlet-triplet splitting of P^+I^- , $2J_{PI}$, would in principle allow an assessment of magnitude and sign of ΔG_1 , hence of the importance of the superexchange vs. the sequential two-step model. Bixon et al.³⁷ calculated $2J_{PI}$ as the

difference in the energy shifts of the singlet and triplet state of P^+I^- , due to interactions with P* and P^+ :

$$2J_{PI} = \delta E_s(P^*) - \delta E_t(P^+) . \quad (6)$$

The two terms of Eqn. 6 are of comparable magnitude, have the same sign and practically cancel. Moreover, $\delta E_s(P^*)$ depends on the square of a reduction factor b that takes into account a possible relaxation of the nuclear configuration of P^+I^- following its formation from P*.³⁶ This means that the sign and magnitude of $2J_{PI}$ critically depends on *both* the position of the energy level of $P^+B_A^-$ relative to P* *and* the value of b .

Assuming that $P^+B_A^-$ lies 600 cm⁻¹ above P* and using $|2J_{PI}| = 10^{-3}$ cm⁻¹, Bixon et al.³⁷ found that $0.4 < b < 0.6$. The present work indicates that $2J$ is positive and has the value $2J = +14 \pm 1 \text{ G} (+1.3 \pm 0.1 \text{ cm}^{-1})$, which yields with the same value of ΔG_1 $0.33 < b < 0.36$.

The narrow range of possible values of b that results from the determination of the sign of J_{PI} suggests that either the assumed value of ΔG_1 is precisely correct, which would be surprising in view of the many approximations involved,³⁷ or that this energy difference needs adjustment so that the precise value of b is less critical.

Bixon et al.⁴¹ recently explored the consequences of varying ΔG_1 between -800 cm^{-1} ($P^+B_A^-$ below P*) and $+500 \text{ cm}^{-1}$ ($P^+B_A^-$ above P*). Four ranges were defined: (I) $\Delta G_1 \leq -400 \text{ cm}^{-1}$; sequential two-step mechanism at all temperatures, (II) $-400 \text{ cm}^{-1} \leq \Delta G_1 \leq 0$; superposition of sequential and superexchange mechanisms at all temperatures, (III) $0 \leq \Delta G_1 \leq +400 \text{ cm}^{-1}$; superposition of sequential and superexchange mechanisms at room temperature and superexchange mechanism at low temperature (100 K), (IV) $\Delta G_1 \geq +400 \text{ cm}^{-1}$; superexchange mechanism at all temperatures. Utilizing Eqn. 6 with somewhat different values of the reorganization energies than in their previous calculation³⁷ and taking $b = 1$, the authors found that over the range $\Delta G_1 = -600 \text{ cm}^{-1}$ to 0 the calculated value of $2J_{PI}$ was in accord with the experimental value of $|2J_{PI}|$. In other words, it was probable that the superexchange and sequential mechanism coexist at all temperatures, but a sequential mechanism at all temperatures could not be excluded.

The finding by Hore et al.²⁶ that J_{PI} is positive allows to narrow down the permissible values of ΔG_1 considerably. Taking the same parameter values as in Bixon et al.⁴¹ one finds for $J_{PI} > 0$, $\Delta G_1 \leq -100 \text{ cm}^{-1}$; for $2J_{PI} = +1.3 \cdot 10^{-3} \text{ cm}^{-1}$, $\Delta G_1 = -200 \text{ cm}^{-1}$. Thus, at all temperatures the sequential and superexchange mechanisms operate in parallel. Note that this agrees with the temperature independence of the absolute value of J_{PI} as found in¹¹.

As pointed out by Bixon et al.,⁴¹ the "peaceful coexistence" of the two routes for primary electron transport makes the primary process robust with regard to moderate variations of the energetic parameters. This, obviously, must have been of prime importance in the evolution of the various photosystems.

The above conclusion is valid for values of the reduction factor b , which lowers the contribution of $\delta E_s(P^*)$ to $2J_{PI}$, that are close to unity. If b is much smaller, then $\delta E_s(P^*)$ and consequently ΔG_1 are appreciably larger. For example, for $b = 0.5$, $\Delta G_1 = 20 - 30 \text{ cm}^{-1}$, favoring the superexchange mechanism at low temperatures. At physiological temperatures, however, and excepting values of b much smaller than 0.5, the parallelism of the two electron transport routes seems now well established.

4. Prospects

In this report we have endeavored to highlight the contribution that time-resolved EPR can make to the elucidation of the fundamental mechanisms of primary electron transport in bacterial photosynthesis. Much of what has been discussed is also applicable to the plant photosystems,⁴² be it in lesser detail. As mentioned, more work has to be done to firm up the conclusions. Conjunction of time-resolved EPR and optical spectroscopies is indispensable to allow extraction of meaningful values of the magnetic interactions between the various electron transport components. It is desirable to perform experiments on oriented samples in order to separate the contributions of the exchange and dipolar interactions. The work on the plant photosystems has to be extended, especially on the RC of Photosystem II, which although thought to be homologous to the bacterial RC, shows quite different behavior with respect to ESP phenomena. For all photosystems, work at higher frequencies with (per)deuterated material will considerably improve resolution and therefore narrow the limits of confidence for the parameters extracted from the simulation of ESP spectra. Finally, artificial systems modelling the photosynthetic transport chains should be screened for their potential to mimic the spin polarization behavior of the in vivo systems.⁴³

5. Acknowledgements

The simulations of ESP spectra discussed in this communication were all carried out in the group of Dr. P.J. Hore, whose important contributions to our understanding of electron spin polarization in the bacterial reaction center is gratefully acknowledged. The work done in Leiden was supported by the Netherlands Foundation for Chemical Research (SON), financed by the Netherlands Organization for Scientific Research (NWO).

6. References

1. J. Deisenhofer, O. Epp, K. Miki, R. Huber and H. Michel, *Nature* **318** (1985) 618-624.
2. J.P. Allen, G. Feher, T.O. Yeates, D.C. Rees, J. Deisenhofer, H. Michel and R. Huber, *Proc. Natl. Acad. Sci. USA* **83** (1986) 8589-8593.
3. C.H. Chang, D. Tiede, J. Tang, U. Smith, J. Norris and M. Schiffer, *FEBS Lett.* **205** (1986) 82-86.
4. R. Blankenship, A. McGuire and K. Sauer, *Proc. Natl. Acad. Sci. USA* **72** (1975) 4943-4947.
5. A.J. Hoff, P. Gast and J.C. Romijn, *FEBS Lett.* **73** (1977) 185-190.
6. P. Gast, R.A. Mushlin and A.J. Hoff, *J. Phys. Chem.* **86** (1982) 2886-2891.
7. R.J. Debus, G. Feher and M.Y. Okamura, *Biochemistry* **25** (1986) 2276-2287.
8. A.J. Hoff, *Quart. Rev. Biophys.* **17** (1984) 153-282.
9. P.J. Hore, E.T. Watson, J.B. Pedersen and A.J. Hoff, *Biochim. Biophys. Acta* **849** (1986) 70-76.
10. A. Ogrodnik, W. Lersch, M.E. Michel-Beyerle, J. Deisenhofer and H. Michel, in *Antennas and Reaction Centres of Photosynthetic Bacteria*, ed. M.E. Michel-Beyerle (Springer Verlag, Berlin, 1985) pp. 198-206.
11. K.W. Möhl, E.J. Lous and A.J. Hoff, *Chem. Phys. Lett.* **121** (1985) 22-27.
12. D.A. Hunter, A.J. Hoff and P.J. Hore, *Chem. Phys. Lett.* **134** (1987) 6-11.
13. P.J. Hore, D.A. Hunter, C.D. McKie and A.J. Hoff, *Chem. Phys. Lett.* **137** (1987) 495-500.
14. C.D. Buckley, D.A. Hunter, P.J. Hore, and K.A. McLauchlan, *Chem. Phys. Lett.* **135** (1987) 307-312.
15. G.L. Closs, M.D.E. Forbes and J.R. Norris, *J. Phys. Chem.* **91** (1987) 3592-3599.
16. A. de Groot, P. Gast and A.J. Hoff, *Biochim. Biophys. Acta* **808** (1985) 13-20.
17. P. Gast, *Doctoral Dissertation* (Leiden, 1982).
18. C. Kirmaier, D. Holten, R.J. Debus, G. Feher and M.Y. Okamura, *Proc. Natl. Acad. Sci. USA* **83** (1986) 6407-6411.
19. W.B. Mims and J. Peisach, in *Advanced EPR. Applications in Biology and Biochemistry*, ed. A.J. Hoff (Elsevier, Amsterdam, 1989) pp. 1-57.
20. S.A. Dikanov and A.V. Astashkin, in *Advanced EPR. Applications in Biology and Biochemistry*, ed. A.J. Hoff (Elsevier, Amsterdam, 1989) pp. 59-117.
21. A. Schweiger, in *Advanced EPR. Applications in Biology and Biochemistry*, ed. A.J. Hoff (Elsevier, Amsterdam, 1989) pp. 277-305.
22. A. Schweiger, *Angew. Chem. Int. Ed. Engl.* **30** (1991) 265-292.
23. L.L. Feezel, P. Gast, U.H. Smith and M.C. Thurnauer, *Biochim. Biophys. Acta* **974** (1989) 149-155.
24. P. Gast and A.J. Hoff, *Biochim. Biophys. Acta* **548** (1979) 520-535.
25. P. Gast, A. de Groot and A.J. Hoff, *Biochim. Biophys. Acta* **723** (1983) 52-58.
26. P.J. Hore, D.J. Riley, J.J. Semlyen and A.J. Hoff, *Biochim. Biophys. Acta* submitted.
27. A.J. Hoff and P.J. Hore, *Chem. Phys. Lett.* **108** (1984) 104-110.
28. P.J. Hore, in *Advanced EPR. Applications in Biology and Biochemistry*, ed. A.J. Hoff (Elsevier, Amsterdam, 1989) pp. 405-440.
29. B.J. Hales, *J. Amer. Chem. Soc.* **97** (1975) 5993-5997.
30. O. Burghaus, *Doctoral Dissertation* (Berlin, 1991).
31. J.R. Norris, C.P. Lin and D. Budil, *J. Chem. Soc. Faraday I* **83** (1987) 13-27.
32. W. Lersch, F. Lendzian, E. Lang, R. Feick, K. Möbius and M.E. Michel-Beyerle, *J. Magn. Res.* **82** (1989) 143-149.
33. R. Haberkorn, M.E. Michel-Beyerle and R.A. Marcus, *Proc. Natl. Acad. Sci. USA* **70** (1979) 4185-4188.
34. R.A. Marcus, *Chem. Phys. Lett.* **133** (1987) 471-477.
35. R.A. Marcus, *Chem. Phys. Lett.* **146** (1988) 13-22.
36. M.E. Michel-Beyerle, M. Bixon and J. Jortner, *Chem. Phys. Lett.* **151** (1988) 188-194.
37. M. Bixon, J. Jortner, M.E. Michel-Beyerle and A. Ogrodnik, *Biochim. Biophys. Acta* **977** (1989) 273-286.
38. J. Breton, J.-L. Martin, G.R. Fleming and J.-C. Lambry, *Biochemistry* **27** (1988) 8276-8284.
39. W. Holzapfel, U. Finkele, W. Kaiser, D. Oesterhelt, H. Scheer, H.U. Stilz and W. Zinth, *Chem. Phys. Lett.* **160** (1989) 1-7.
40. C. Kirmaier and D. Holten, *Proc. Natl. Acad. Sci. USA* **87** (1990) 3552-3556.
41. M. Bixon, J. Jortner and M.E. Michel-Beyerle, *Biochim. Biophys. Acta* **1056** (1991) 301-315.
42. D. Stehlík, C.H. Bock and M.C. Thurnauer, in *Advanced EPR. Applications in Biology and Biochemistry*, ed. A.J. Hoff (Elsevier, Amsterdam, 1989) pp. 371-403.
43. M.R. Wasielewski, G.L. Gaines, M.P. O'Neil, W.A. Svec and M.P. Niemczyk, *Mol. Cryst. Liq. Cryst.* **194** (1991) 201-207.

The Role of Spin Chemistry in the Primary Events of Photosynthesis

Gerd Kothe, Stefan Weber and Robert Bittl

Institut für Physikalische Chemie, Universität Stuttgart, D-7000 Stuttgart 80, Germany

James R. Norris^{**}, Seth S. Snyder, Jau Tang and Marion C. Thurnauer

Chemistry Division, Argonne National Laboratory, Argonne, Illinois, 60439

Andrea L. Morris, Richard R. Rustandi and Zhiyu Wang

^{**}Department of Chemistry, The University of Chicago, Chicago, Illinois, 60637

Abstract

The primary electron transfer process in many natural and artificial photosynthetic systems proceeds via a radical pair mechanism. We have developed theoretical treatments and have performed various transient experiments such as RYDMR (reaction yield detected magnetic resonance) [1] and FT-CIDEP (Fourier transform-chemically induced dynamic electron spin polarization) [2] to understand the role that spin chemistry may play in photosynthesis. In addition, understanding the mechanism and the dynamics for the unpaired electron spin system permits the characterization of the structure and function of natural and artificial photoreaction centers.

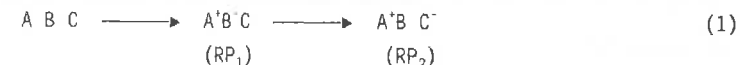
Previously, we presented a general description of electron spin polarization for interacting radical pairs and formulated a simple vector model as an aid to visualizing CIDEP [3]. In this current paper, we have extended our vector model to include the Redfield density matrix formalism in order to accommodate explicitly the processes of sequential electron transfer, relaxation and coherence. Even with the additional complications of relaxation and coherence, visualizing CIDEP with a vector diagram is straightforward. Such visualization is often helpful for planning and interpreting new experiments.

1. Introduction

The primary electron transfer process in many natural and artificial photosynthetic systems proceeds via a radical pair mechanism which can be studied by various direct or indirect magnetic resonance techniques. The role of spin chemistry can be understood by characterizing the mechanism and the dynamics for the unpaired electron spin system. With the advance of transient EPR techniques, one can probe the spin dynamics of the photo-induced charge separation processes at very early stages. By including relaxation effects explicitly we have extended our general description of electron spin polarization [3] for interacting radical pairs. Even though this treatment is considerably more complicated as a result of various explicit kinetic effects, a simple vector model description can be maintained as an aid for the visualization of CIDEP. In this version of our treatment, we have applied the Redfield density matrix formalism to accommodate processes such as sequential electron transfer, relaxation and coherence transfer.

2. Theory of the Time Evolution of Spin Correlated Radical Pairs

The sequential electron transfer reactions of photosynthesis produce two categories of radical pairs, RP₁ and RP₂, where



The time evolution of the density matrix of the system can be described as

$$d\rho/dt = \begin{pmatrix} C_{\rho_1} & 0 \\ 0 & C_{\rho_2} \end{pmatrix} + i \begin{pmatrix} [\rho_1, H_1] & 0 \\ 0 & [\rho_2, H_2] \end{pmatrix} \quad (2)$$

where H₁, ρ₁ correspond to the initial radical pair and H₂, ρ₂ correspond to the terminal radical pair.

A projection operator for RP₁ → RP₂ can be defined as

$$P = (1/2)(k_S|S><S| + k_T|T><T|) \quad (3)$$

where k_S, k_T are the decay rate constants for singlet and triplet, respectively. It follows that the time evolution of RP₁ and RP₂ is given by

$$d\rho_1/dt = i[\rho_1, H_1] - \{A, P\} \quad (4)$$

$$d\rho_2/dt = i[\rho_2, H_2] + \{A, P\} \quad (5)$$

where {ρ, P} is an anti-commutator. The simplest possible case to illustrate with a vector diagram involves the evolution from RP₁ to RP₂ in which interactions between spin degrees of freedom and the surrounding medium are not allowed. In this situation, the Hamiltonian of radical pair system is

$$H_i = E_{Si}|S\rangle\langle S| + E_{Ti}|T_0\rangle\langle T_0| + \Delta_i(|S\rangle\langle T_0| + |T_0\rangle\langle S|) \quad (6)$$

$$2J_i \equiv E_{Si} - E_{Ti} \quad i = 1, 2$$

Δ_i is the stationary transfer matrix element for the mixing of the singlet $|S\rangle$ and triplet $|T_0\rangle$ induced by electron spin-spin interactions. We define a density vector as

$$\vec{\rho}_i(t) = \rho_{ix}(t)\hat{x} + \rho_{iy}(t)\hat{y} + \rho_{iz}(t)\hat{z} \quad i = 1, 2 \quad (7)$$

with

$$\begin{aligned} \rho_i(t) &= \rho_{ss}(t) - \rho_{tt}(t) \\ \rho_i(t) &= 2\text{Re}[\rho_{ST}(t)] \\ \rho_i(t) &= 2\text{Im}[\rho_{ST}(t)] \end{aligned} \quad (8)$$

and the Hamiltonian vector as

$$\vec{\Omega}_i = (-J_i)\hat{z} + (-\Delta_i)\hat{x} \quad (9)$$

By further assuming that $k_S = k_T = k$ for the projection operator, the time development of RP_1 and RP_2 can be expressed as a simple vector diagram representation.

$$\frac{d\vec{\rho}_1}{dt} = \vec{\Omega}_1 \times \vec{\rho}_1 - k\vec{\rho}_1 \quad (10)$$

$$\frac{d\vec{\rho}_2}{dt} = \vec{\Omega}_2 \times \vec{\rho}_2 + k\vec{\rho}_1 \quad (11)$$

The geometrical picture of this type of chemical kinetics is shown in Figure 2.

When a constant microwave field ω_1 is applied to the radical pair system to turn on the coupling between $|T_{+1}\rangle$, $|T_{-1}\rangle$ and $|T_0\rangle$, the Hamiltonian of the system (in the following we only deal with one radical pair) in the $|\phi_c\rangle = |T_{+1}\rangle$, $|\phi_a\rangle$, $|\phi_b\rangle$ and $|\phi_d\rangle = |T_{-1}\rangle$ basis is

$$H = \begin{pmatrix} \Delta' & \omega_1 \cos \theta / 2^{1/2} & -\omega_1 \sin \theta / 2^{1/2} & 0 \\ \omega_1 \cos \theta / 2^{1/2} & (\Delta^2 + J^2)^{1/2} - J & 0 & \omega_1 \cos \theta / 2^{1/2} \\ -\omega_1 \sin \theta / 2^{1/2} & 0 & -(\Delta^2 + J^2)^{1/2} - J & -\omega_1 \sin \theta / 2^{1/2} \\ 0 & \omega_1 \cos \theta / 2^{1/2} & -\omega_1 \sin \theta / 2^{1/2} & -\Delta \end{pmatrix} \quad (12)$$

$$\text{where } \Delta' \equiv E_{|T_{+1}\rangle} - E_{|T_0\rangle} = E_{|T_0\rangle} - E_{|T_{-1}\rangle}$$

Here $|\phi_a\rangle$, $|\phi_b\rangle$ are the eigenstates of $|S\rangle$, $|T_0\rangle$, and the electron-electron dipolar term E_T is set to zero. Using a first order approximation of ω_1 for the density matrix, we have

$$H = H' + \omega_1 S_x \quad (13)$$

$$\sigma = \sigma^{(0)} + \omega_1 \sigma^{(1)} \quad (14)$$

where σ is the density matrix of spin system in $|\phi_a\rangle$, $|\phi_b\rangle$ representation. (ρ is the density matrix in $|S\rangle$, $|T_0\rangle$ representation.) Then the time evolution of the system is governed by the following Liouville equation

$$d\sigma^{(0)}/dt = i[\sigma^{(0)}, H'] \quad (15)$$

$$d\sigma^{(1)}/dt = i[\sigma^{(0)}, S_x] + i[\sigma^{(1)}, H'] \quad (16)$$

With the microwave field set parallel to the x axis in Eq. (13), the EPR absorption mode detects the observable $M_y \sim \langle S_y \rangle = \text{Tr}[\sigma(t)S_y] \approx \text{Tr}[\omega_1 \sigma^{(1)}(t)S_y]$. The expression of $\langle S_y \rangle$ shows that four EPR transitions result, two absorption lines and two emission lines as shown in Figure 3. With the radio-frequency set close to the $|\phi_c\rangle \leftrightarrow |\phi_a\rangle$ resonance, the time development of the line $I_{ac}(t)$ is

$$I_{ac}(t) \sim \cos^2 \theta [1 + \sigma_z(0)]/2 - \sin^2 \theta [\sigma_x(0) \cos \omega_{ab} t + \sigma_y(0) \sin \omega_{ab} t]/4 \quad (17)$$

where $\text{tg} 2\theta = \Delta/J$, and for convenience we take $\sigma_z(t) = \sigma_{aa}(t) - \sigma_{bb}(t)$, $\sigma_x(t) = \sigma_{ab}(t) + \sigma_{ba}(t)$, $\sigma_y(t) = (-i)[\sigma_{ab}(t) - \sigma_{ba}(t)]$. The first term in $I_{ac}(t)$ is a resonance term, and the second term is an oscillation term with frequency $\omega_{ab} \approx 2(\Delta + J^2)^{1/2}$.

Now we consider a more general case, in which there are interactions within the radical pair system and with the surrounding bath, induced by fluctuations of the energy splitting $2J$ and coupling matrix element Δ . The relevant Hamiltonian of the system in $|S\rangle$, $|T_0\rangle$ basis is

$$H = H_0 + H_B + \delta H \quad (18)$$

$$H_0 = E_S|S\rangle\langle S| + E_T|T_0\rangle\langle T_0| + \Delta(|S\rangle\langle T_0| + |T_0\rangle\langle S|) \quad (19)$$

$$\delta H = \delta J(|S\rangle\langle S| - |T_0\rangle\langle T_0|) + \delta \Delta(|S\rangle\langle T_0| + |T_0\rangle\langle S|) \quad (20)$$

where H_B is the Hamiltonian of the surrounding medium or heat bath and δH is the interaction operator between the heat bath and the spin subsystem. By applying the Redfield reduced density matrix equation to the H_0 eigenstates (to second order δH), we derive the density matrix elements in $|\phi_a\rangle$, $|\phi_b\rangle$ representation as:

$$\sigma_x(t) = \sigma_x(0) \cos(\omega t) \exp(-t/T_2) \quad (21)$$

$$\sigma_y(t) = \sigma_y(0) \sin(\omega t) \exp(-t/T_2)$$

$$\sigma_z(t) = \sigma_z^{eq} + [\sigma_z(0) - \sigma_z^{eq}] \exp(-t/T_1)$$

where $\omega = [\omega_{ab}^2 - (1/2T_1)^2]^{1/2} = (4\Delta^2 + 4J^2 - 1/4T_1)^{1/2}$. So the vector diagram

representation of ST_0 mixing in $|S\rangle$, $|T_0\rangle$ basis in the presence of heat bath is given by

$$\begin{aligned}\vec{\rho}(t) = & ((\vec{\rho}(0) \cdot \hat{\Omega} - |\vec{\rho}^{eq}|) \hat{\Omega}) \exp(-t/T_1) + |\vec{\rho}^{eq}| \hat{\Omega} \\ & + (\vec{\rho}(0) - (\vec{\rho}(0) \cdot \hat{\Omega}) \hat{\Omega}) \exp(-t/T_2) \cos \omega t \\ & + (\hat{\Omega} \times \vec{\rho}(0)) \exp(-t/T_2) \sin \omega t\end{aligned}\quad (22)$$

Figure 4 gives the geometrical picture of time evolution of density vector $\vec{\rho}(t)$.

By incorporating the relaxation mechanism, the EPR line intensity in general is:

$$I_{ac}(t) \sim \cos^2 \theta [1 + \sigma_z(t)]/2 - \sin^2 \theta [\sigma_x(t) + \sigma_y(t)]/4 \quad (23)$$

$$\begin{aligned}= & \cos^2 \theta [1 + \sigma_z^{eq}] + (\sigma_z(0) - \sigma_z^{eq}) \exp(-t/T_1)/2 \\ & - \sin^2 \theta [\sigma_x(0) \cos \omega t + \sigma_y(0) \sin \omega t] \exp(-t/T_2)/4\end{aligned}\quad (24)$$

The quantum beat frequency of EPR line now is ω . Equation (24) shows that the resonance EPR line decays to its equilibrium value induced by a T_1 process with the quantum beat oscillations damped by T_2 .

The CIDEP variables are defined as before[3].

$$M = (I_{ac} + I_{bd} - (I_{bc} + I_{ad}))/2 \quad (25)$$

The resonance signal of CIDEP can be expressed as

$$\begin{aligned}M^{(R)} = & [\cos 2\theta + \sigma_z(t)]/2 \\ = & [-\hat{\Omega} \cdot \hat{z} + \vec{\rho}(t) \cdot \hat{\Omega}]/2 \\ = & [\vec{\rho}(t) - \vec{\rho}(0)] \cdot \hat{\Omega}/2 \\ = & \Delta \vec{\rho}(t) \cdot \hat{\Omega}/2\end{aligned}\quad (26)$$

This is the result of the general $\Delta \vec{\rho}$ model provided in a previous paper. With the existence of the relaxation process, the CIDEP effect can occur in both initial and terminal radical pairs. The quantum beat part of the CIDEP variable in Eq. (25) is

$$\begin{aligned}(QB) = & -\sin 2\theta [\sigma_x(t) + \sigma_y(t)]/2 \\ = & [\hat{y} \cdot (\hat{z} \cdot \hat{\Omega})] [\hat{y} \cdot (\hat{\Omega} \times \vec{\rho}(t))] + \hat{y} \cdot \vec{\rho}(t) \\ = & -[\vec{\rho}(0) \cdot (\hat{y} \cdot \hat{\Omega})] [\vec{\rho}(t) \cdot (\hat{y} \cdot \hat{\Omega})]\end{aligned}\quad (27)$$

Obviously, the quantum beat term only depends on the initial and final position of the stable vector $\vec{\rho}$.

The theoretical treatment provided above omits the diffusive motion of radical pairs, because in the sequential electron transfer reactions of photosynthesis, diffusion is not operative in the early charge separation

events, while other mechanisms such as kinetic decay, coherence and relaxation can play a central role.

3. Discussion of Theory and Experimental Requirements for Observation of Coherence

We now define radical pair 1, RP_1 , as a system of radical pairs with a common isotropic electron spin-spin coupling and a common anisotropic dipolar electron spin-spin coupling. Likewise we now define radical pair 2, RP_2 , as a system of radical pairs with a common isotropic electron spin-spin coupling and a common anisotropic dipolar electron spin-spin coupling. At least one of the couplings of radical pair 1 is different from the corresponding coupling of radical pair 2. Each radical pair system, 1 or 2, can have a variety of hyperfine interactions and orientations. To calculate the entire system an ensemble average must be performed.

In a previous treatment of CRP and CIDEP we showed that CIDEP requires at least one intermediate radical pair. Our former vector diagram treatment neglected three aspects that we now include: 1) spin lattice relaxation and spin-spin relaxation, 2) broad band detection of the dynamics associated with the time evolution of the spin system, and 3) an explicit kinetic modeling of the radical pair evolution. Point 2 only means that this previous vector diagram was primarily intended for explaining the time averaged CIDEP and CRP spectra and not for explaining coherent oscillations that in special circumstances should be observable experimentally. The description of the time averaged spectrum remains unaltered in this more elaborate approach but where now we have explicitly treated these coherent oscillations both theoretically and experimentally.

However, one additional feature arises with this explicit treatment of relaxation. This new feature has implications potentially useful in the study of ESP of radical pairs. If spin lattice relaxation occurs between the two middle eigenfunctions of a single radical pair, for example, radical pair 1, then CIDEP occurs anyway. In other words, CIDEP occurs even though an intermediate radical pair has not been formed. This effect is readily understandable. Without relaxation the intermediate radical pair is necessary to the production of CIDEP to prevent the product of Δn (the population difference) times p_i (the transition probability) being equal in absolute magnitude for all transitions[3]. Including spin lattice relaxation between the two center levels of the radical pair changes this product, the calculated EPR intensity, by altering Δn but not p_i . We also note that spin lattice relaxation between a middle level and an upper or a lower level will not

result in CIDEP as we have defined it here.

If relaxation is slow, then the magnetic moment of the radical pair system is expected to exhibit oscillations which eventually dissipate with time. However, the experimental observations of these oscillations is difficult because of several reasons. The vector diagram approach of visualization can be helpful in choosing an appropriate sample. The best chance to observe oscillations is to have a system which has a minimum of Ω s which have phase coherence maximized from the beginning and whose coherence lasts for as long as possible. Moreover, high time resolution is required in the EPR spectrometer and the light excitation pulse should be very short, preferably sub nanosecond in length. The chemistry of formation for the radical pair must be correspondingly fast. To prevent these oscillations from averaging out the dipolar coupling should be negligible and this in turn demands a large distance between the members of the radical pair. The sample geometry should be consistent and homogeneous. The hyperfine broadening should be minimized. All these factors are realized using fully photosynthetic reaction centers found in photosystem I of blue-green algae.

4. Experimental Method

Time domain cw-EPR has been used to explore radical pair systems for the presence of the coherent oscillation of the magnetic moment induced by a short laser excitation pulse. The spectrometer will be described in more detail elsewhere. Transient x-band EPR data were obtained using a LeCroy 9450 transient recorder with a 350 MHz bandwidth. A PTI PL2300 nitrogen laser at 337.1 nm, 1.6 mJ/pulse energy, 600 ps (fwhm) and repetition rate of 0 to 20 Hz was employed to excite the sample. Note the short duration of the laser excitation pulse. Fully deuterated (99.7%) *synechococcus lividus* at room temperature was employed as the sample of choice.

5. Experimental Results

In Figure 5 we show the standard time-domain, field-swept EPR spectrum of *synechococcus lividus* (99.7 atom% ^2H). Three field points, A, B and C, are marked in Figure 5 where the EPR intensity is followed in time as shown in Figures 1, 6, and 7. These oscillations are similar to those calculated previously[4] and as predicted[5]. More detailed simulations are now in progress which will address various kinetic, spin relaxation and spin-spin interactions associated with the radical pairs formed in photo-induced charge separation of *synechococcus lividus*.

6. Conclusion

We have presented a detailed treatment of electron spin polarization for

interacting radical pairs using the Redfield density matrix formalism. Mechanisms such as kinetic decay and relaxation and their effects on the EPR signal were also described. A vector representation was presented for the evolution of the electron spin polarization and quantum beat oscillation as an aid for visualization of the time evolution of spin correlated radical pairs. Finally, the CIDEP quantum beat phenomenon predicted by Salikhov et al. [5] has been illustrated using the photochemistry of photosynthesis by careful considerations of the necessary experimental conditions.

Acknowledgement

This work was supported by the U.S. Department of Energy, Office of Basic Energy Sciences, Division of Chemical Sciences under contract W-31-109-Eng-38.

References

- [1] J. R. Norris, M. K. Bowman, D. E. Budil, J. Tang, C. A. Wright and G. L. Closs, Proc. Natl. Acad. Sci., 79 (1982) 5532.
- [2] K. Hasharoni, H. Levanon, J. Tang, M. K. Bowman, J. R. Norris, D. Gust, T. A. Moore and A. L. Moore, J. Am. Chem. Soc., 112 (1990) 6477.
- [3] J. R. Norris, A. L. Morris, M. C. Thurnauer and J. Tang, J. Chem. Phys., 92 (1990) 4239.
- [4] R. Bittl and G. Kothe, Chem. Phys. Lett., 177 (1991) 547.
- [5] K. M. Salikhov, C. H. Bock and D. Stehlík, Appl. Magn. Reson., 1 (1990) 195.

Figure legends

Figure 1. Time domain profiles observed using a 600 ps nitrogen laser (1.6mJ pulse energy) for excitation of a sample of fully deuterated (99.7%) whole cells of *synechococcus lividus* at room temperature. Field position C of Figure 5.

Figure 2. The vector diagram for RP₁ switching to RP₂. Only a single Ω for each RP is visualized. In reality each RP has a multitude of Ω s.

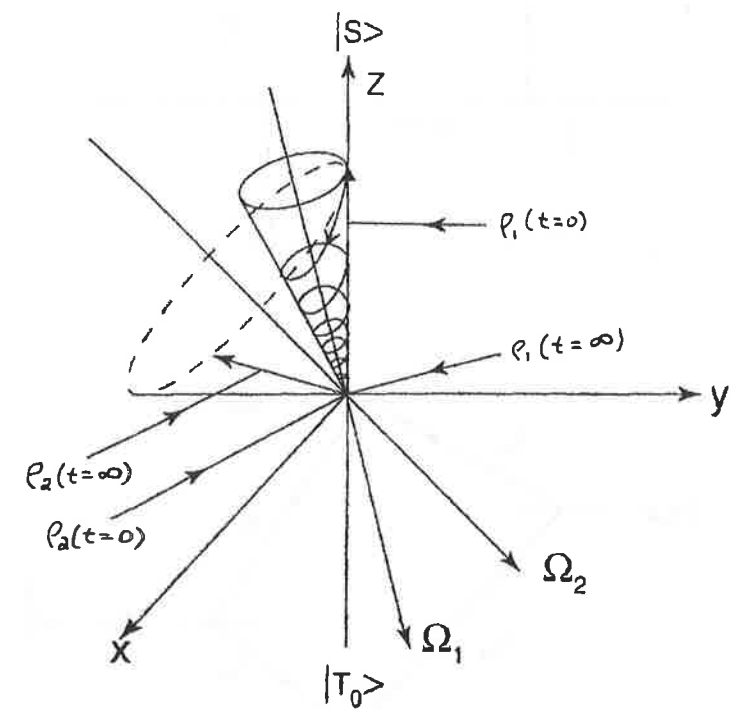
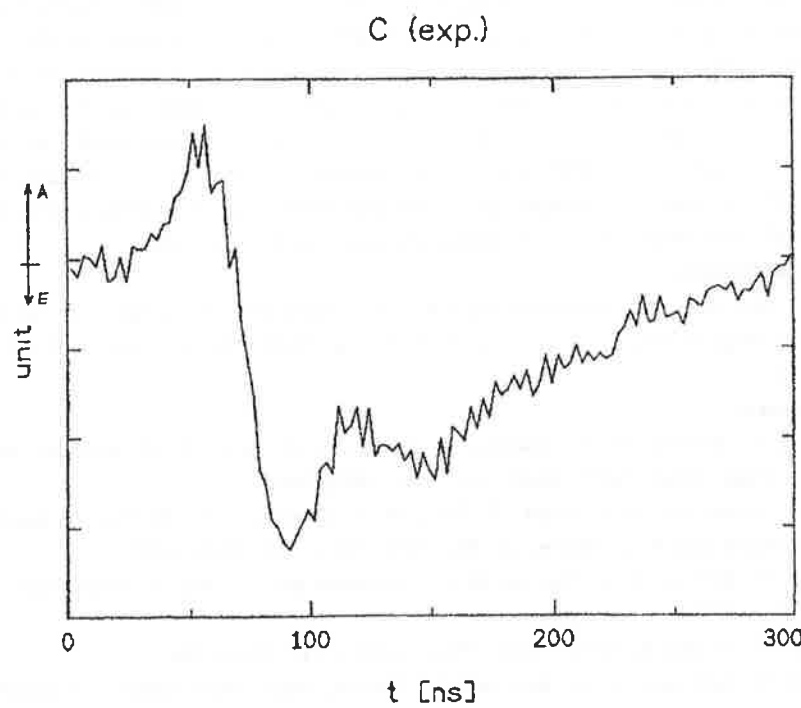
Figure 3. The EPR stick spectrum and associated energy level scheme for weakly interacting radical pairs characterized by a single Ω .

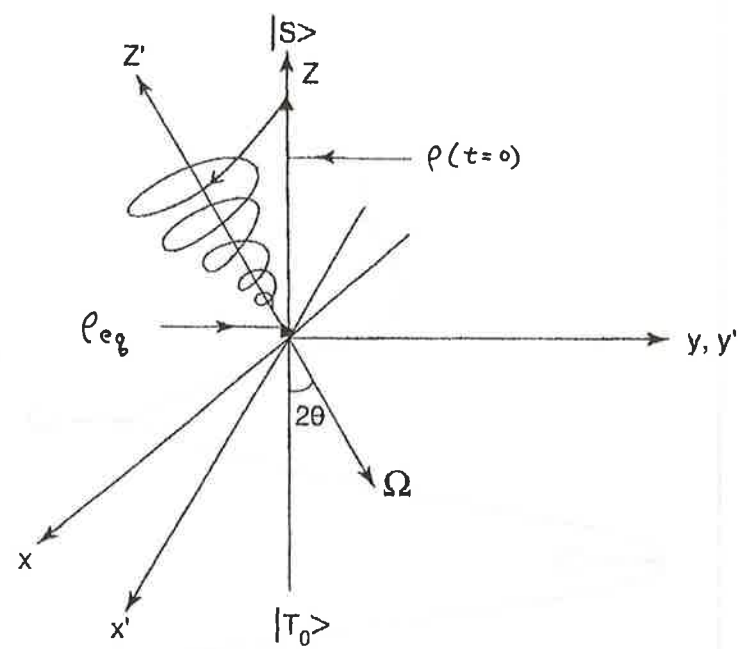
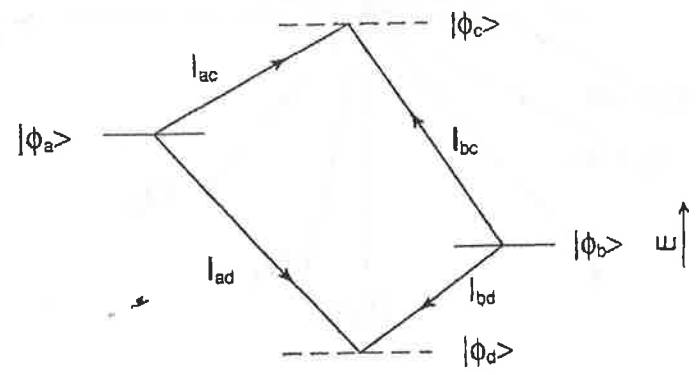
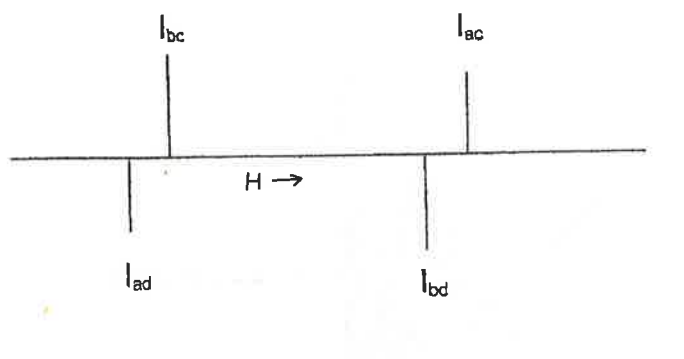
Figure 4. The general vector diagram for ST₀ mixing including relaxation effects. Again only a single Ω for the RP is visualized.

Figure 5. The x-band field swept EPR spectrum of *synechococcus lividus* at room temperature associated with Figures 1, 6 and 7.

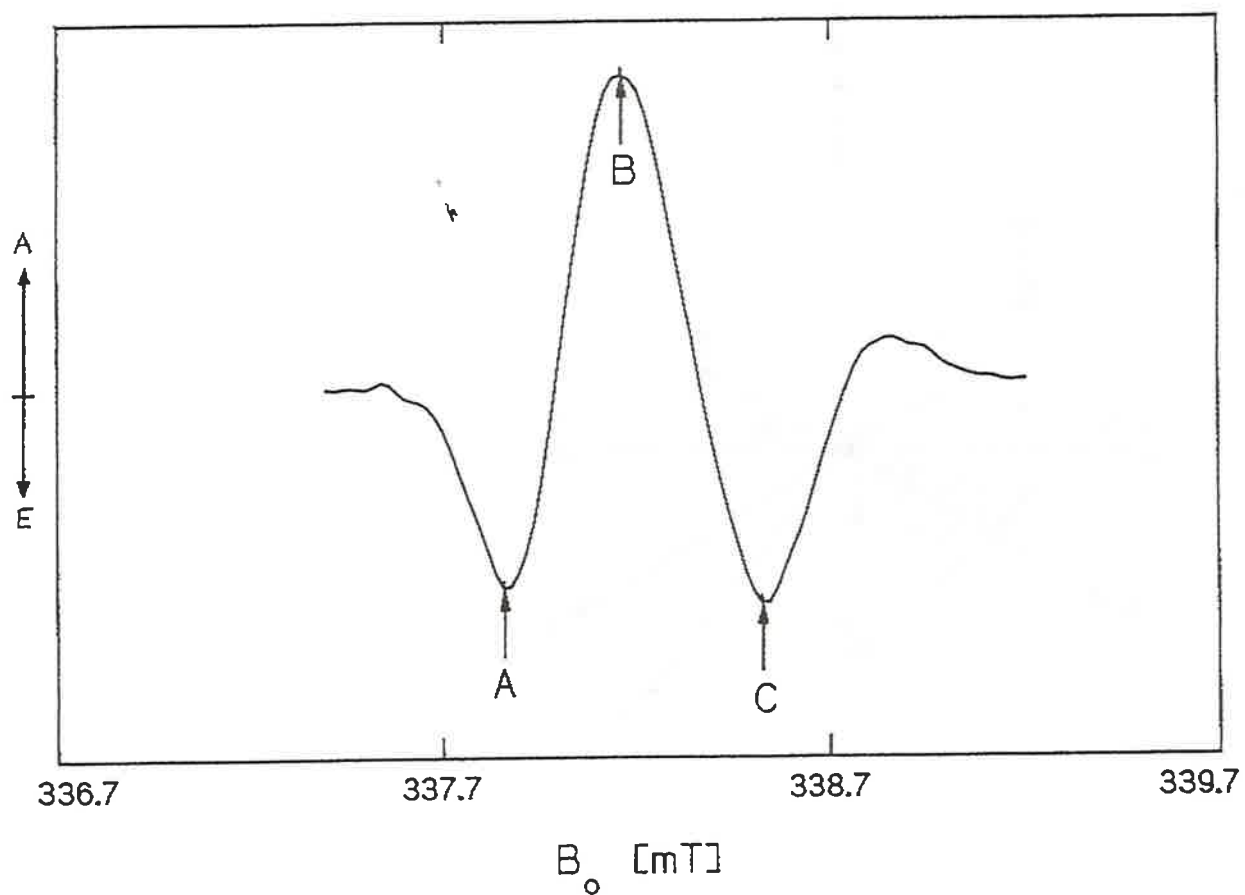
Figure 6. Same as Figure 1 except magnetic field point is at position B.

Figure 7. Same as Figure 1 except magnetic field point is at position A.



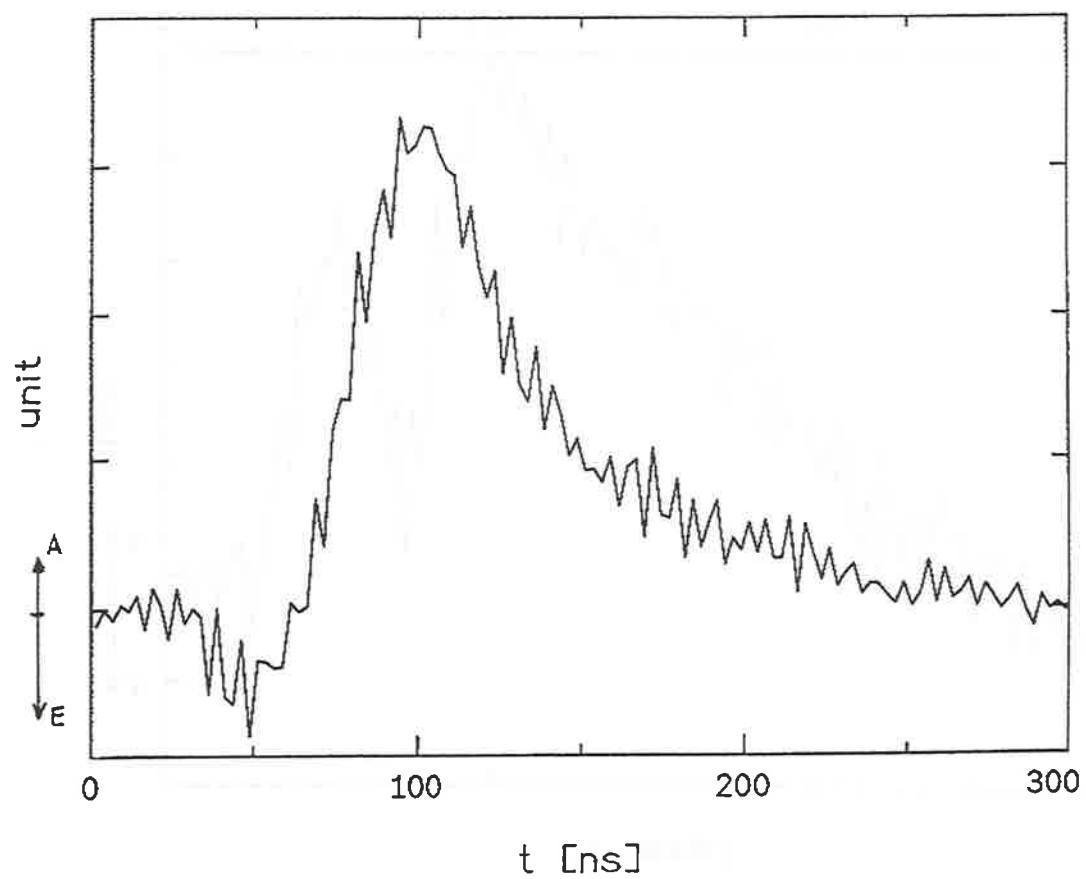


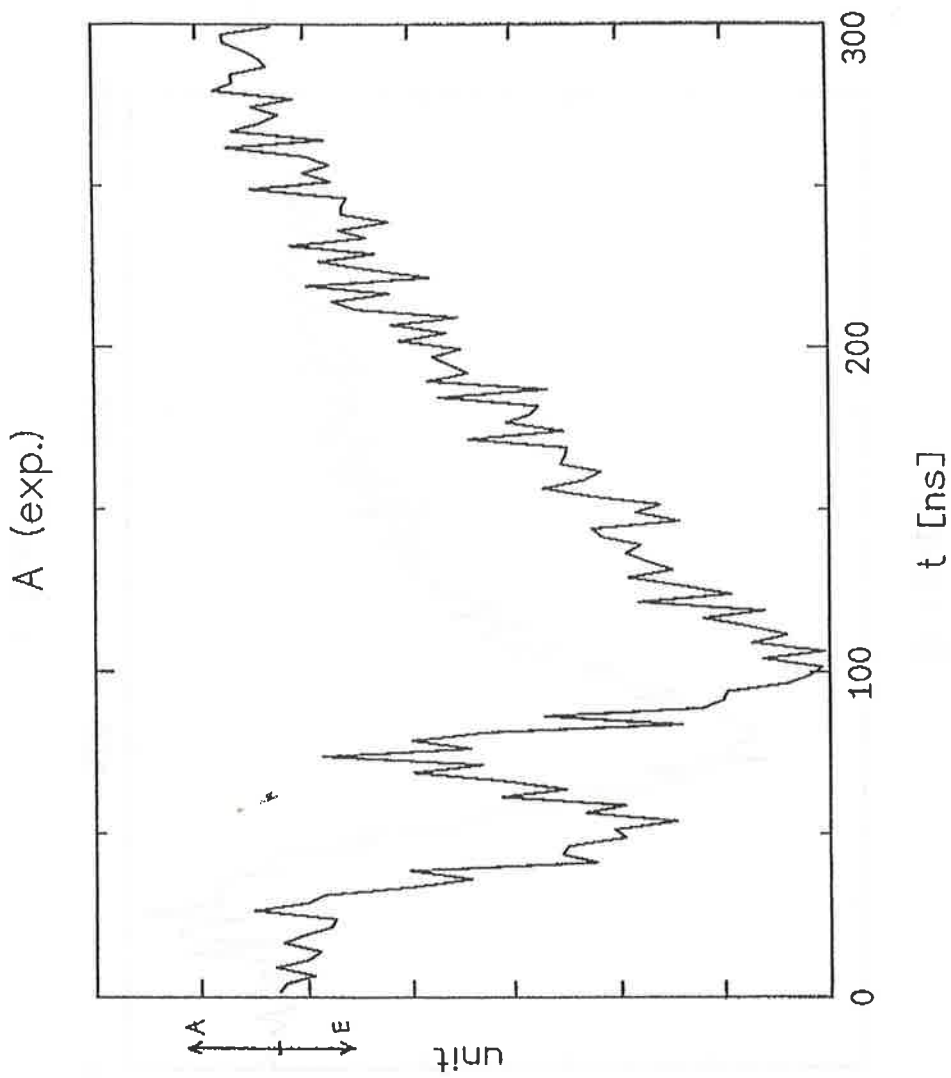
Synechococcus Lividus (99.7 atom% D) (exp.)



B_o [mT]

B (exp.)





ELECTRON SPIN POLARIZATION IN PHOTOSYNTHETIC BACTERIA. ANISOTROPIC CHEMICAL REACTIVITY

P. J. Hore, D. A. Hunter, D. J. Riley and J. J. Semlyen

Physical Chemistry Laboratory, Oxford University, United Kingdom

F. G. H. van Wijk and T. J. Schaafsma

Department of Molecular Physics, Wageningen Agricultural University, The Netherlands

P. Gast and A. J. Hoff

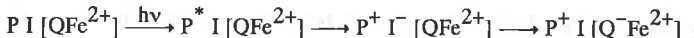
Department of Biophysics, University of Leiden, The Netherlands

Abstract

It is shown that electron spin polarization can be used to probe the anisotropy of singlet-triplet interconversion of radical pairs involved in photosynthetic charge separation. Anisotropic polarization may be observed with non-oriented reaction centres, provided an anisotropic interaction (e.g. zero-field splitting or g-tensor anisotropy) produces resolvable structure in the EPR spectrum of the reaction intermediates. Two examples, both for pre-reduced bacterial reaction centres, are discussed: (i) the triplet state of the primary donor (a bacteriochlorophyll dimer) and (ii) the reduced secondary acceptor (a semiquinone). Computer simulations are used to understand the observed behaviour and yield information on the magnetic and electronic interactions involved in electron transport.

1. Introduction.

The primary steps of bacterial photosynthesis take place in a pigment-protein complex known as the reaction centre, and may be summarized as follows:



The photo-excited electronic singlet state (P^*) of the primary donor (a bacteriochlorophyll dimer) undergoes rapid electron transfer (~ 3 ps) to the primary acceptor I (a bacteriopheophytin) which in turn transfers an electron (in about 200 ps) to the secondary acceptor, an iron-quinone complex $[QFe^{2+}]$.

In pre-reduced (i.e. $Q \rightarrow Q^-$) reaction centres, electron transfer to the iron-quinone complex is blocked, and different decay channels for the primary radical pair $[P^+I^-]$ become possible, Fig. 1. Formed from P^* in a spin-correlated singlet configuration, $^1[P^+I^-]$ can undergo charge recombination to give the primary donor in its ground (P) or excited singlet (P^*) state. At the same time, $^1[P^+I^-]$ is converted coherently by Zeeman, hyperfine, exchange and dipolar interactions into the triplet radical pair, $^3[P^+I^-]$, which may collapse with conservation of spin angular momentum, to give 3P , an excited triplet state of the primary donor, which in turn reverts slowly (~ 100 μ s) to P.

The presence of a third electron spin (on Q^-), affects the singlet-triplet interconversion of the primary radical pair, by facilitating both ST_{+1} and ST_{-1} mixing in addition to the usual ST_0 process. As shown in Fig. 2, the eight spin states of the three electron spin system (P^+ , I^- , Q^-) in a strong magnetic field, are grouped into four sets: $T_{+1}\alpha$, $\{T_{+1}\beta, T_0\alpha, S\alpha\}$, $\{S\beta, T_0\beta, T_{-1}\alpha\}$, $T_{-1}\beta$. In the high field approximation, singlet-triplet interconversion occurs within each of the two central sets of states. Briefly, $S\alpha$ and $T_0\alpha$ interconvert, as do $S\beta$ and $T_0\beta$, if P^+ and I^- have different EPR frequencies (e.g. due to coupling with Q^-) while $S\alpha$ and $T_{+1}\beta$ mix, as do $S\beta$ and $T_{-1}\alpha$, if either P^+ or I^- experiences a magnetic interaction with a third spin (e.g. the unpaired electron on Q^-) that can induce "flip-flop" transitions. These are, of course, just the interactions that give rise to CIDNP, CIDEPE and magnetic field effects on reaction yields, but with the interesting complication that there are now three unpaired electrons rather than the more usual two.

One consequence of the presence of Q^- is that the anisotropy of its magnetic interactions can lead to anisotropic electron spin polarization. This has been observed for both 3P and Q^-

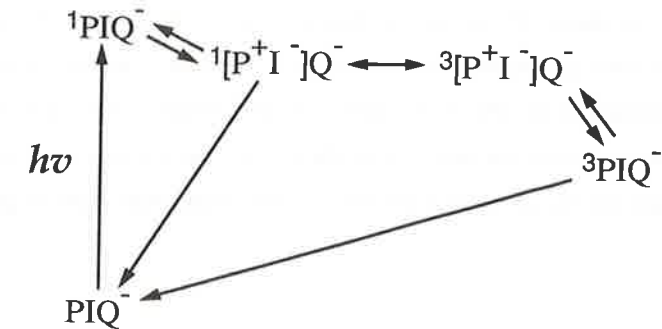


Fig. 1 Primary events in pre-reduced bacterial reaction centres.

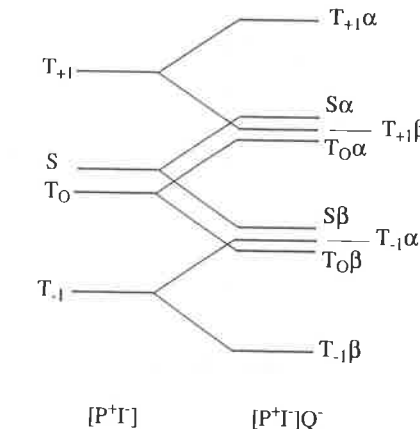


Fig. 2 Schematic energy level diagram for $[P^+I^-]$ (on the left) and $[P^+I^-]Q^-$ (on the right) in a strong magnetic field. The wavefunctions $S, T_0, T_{\pm 1}$ refer to $[P^+I^-]$; α, β refer to Q^- .

(see Refs 1 and 2 for reviews). In what follows, we discuss both sets of observations and outline how they may be understood and used to gain information on the magnetic and electronic interactions that affect photosynthetic electron transport. This work is already in print (3P [3]) or submitted for publication (Q^- [4]). Consequently, we shall describe rather briefly the computer simulations and devote more time than was possible in Refs 3 and 4 to developing simple models that give insight into the processes responsible for anisotropic polarization in photosynthetic systems.

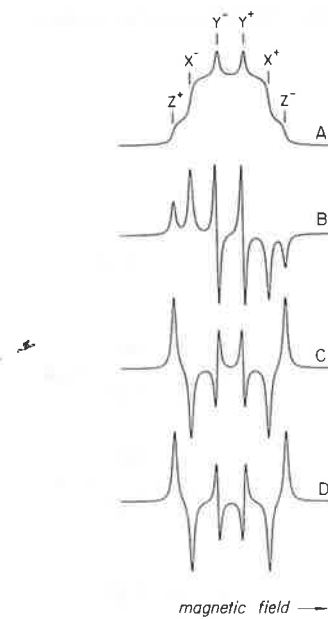


Fig. 3 Schematic EPR spectra of the donor triplet state, 3P , in *Rps. viridis*. (A) Unpolarized spectrum (χ''). (B) Unpolarized first derivative ($d\chi''/dB_0$) spectrum. (C) Low temperature polarized first derivative spectrum. (D) High temperature polarized first derivative spectrum. Reading from low field to high field, the polarizations in (C) and (D) are AEAAE spectrum and AEAEAE respectively, where A denotes absorption and E emission. [Taken from Ref. 3]

2. Spin polarization in 3P — experimental observations and computer simulations.

The appearance of the EPR spectrum of 3P is dominated by the anisotropic zero-field splitting due to the dipolar coupling of the two unpaired electrons, Fig. 3A, 3B. Under conditions of continuous illumination at low temperature (< 20 K), a spin-polarized EPR spectrum is observed [5,6], Fig. 3C, which may be designated AEAAE where A and E denote absorption and emission. This pattern of polarization is easily understood [6] within the framework of the ST_0 radical pair mechanism, which causes only the central triplet sub-level to be populated. Thus the $|+1\rangle \leftarrow |0\rangle$ transitions are absorptively polarized while the $|0\rangle \rightarrow |-1\rangle$ transitions are emissive. However, at temperatures above about 20 K, the spectrum for *Rhodopseudomonas viridis* changes to AEAEAE, Fig. 3D [7-10]. That is, the Y peaks are inverted, implying that the $|+1\rangle$ and $|-1\rangle$ states of 3P are more heavily populated than is $|0\rangle$ when the magnetic field is directed along the Y axis of the zero-field splitting tensor. This anisotropic inversion is only seen when the $[Q^-Fe^{2+}]$ complex is intact, and only in bacteria in which there exists a large exchange interaction between I^- and Q^- .

The key to understanding this behaviour lies in two additional experimental observations [11,12]: spin-lattice relaxation of the iron-semiquinone complex appears to accelerate substantially around 15 K; and the EPR frequency of $[Q^-Fe^{2+}]$ is strongly anisotropic due to zero-field splitting, Zeeman and exchange interactions.

Computer simulations of the yields of 3P in each of the three states $|+1\rangle$, $|0\rangle$ and $|-1\rangle$ were performed by integrating the Liouville equation of motion of the $P^+I^-[Q^-Fe^{2+}]$ system [3]. The anisotropy of the EPR frequency of $[Q^-Fe^{2+}]$, was modelled simply and approximately by treating the complex as a spin- $\frac{1}{2}$ entity (which we call X^-) with an anisotropic g-value, $g(X^-)$. All other anisotropic interactions are probably much smaller and so were ignored. The other two radicals, P^+ and I^- , were assumed to have equal, isotropic g-values: $g(P^+) = g(I^-) = g$. The reduced electron acceptors I^- and X^- were assumed to interact with an isotropic exchange interaction, $J(I^-X^-)$. Of the electron transfer steps in Fig. 1, only the primary charge separation

(assumed to be instantaneous) and the charge recombination of $[P^+I^-]$ to give 3P (rate constant k_T) were included, the other steps being rather slow at low temperatures. Spin-lattice relaxation of X^- (rate constant k_R) was introduced by means of a Redfield-type superoperator.

Some results of these simulations are summarized in Fig. 4, which shows the yields p_i ($i = +1, 0, -1$) of 3P in the three states $|+1\rangle$, $|0\rangle$ and $| -1\rangle$ as a function of $g(X^-)$ for four values of the relaxation rate, k_R . The value of $J(I^-X^-)$, -200 G, was chosen to match the experimental value for *Rps. viridis*. In this diagram the quantum yields for $g(X^-) \leq g$ are shown; symmetrical behaviour is found for $g(X^-) > g$, except that the T_{+1} and T_{-1} labels are interchanged.

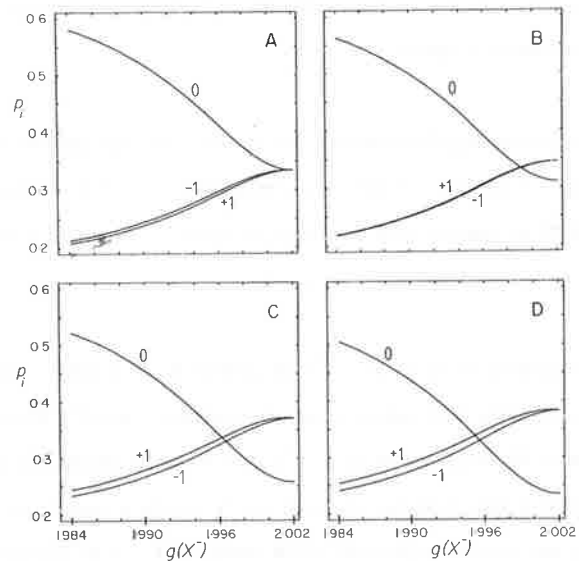


Fig. 4 Calculated yields of 3P in states $|+1\rangle$, $|0\rangle$ and $| -1\rangle$ as a function of $g(X^-)$. (A) $k_R = 0$; (B) $k_R = 10^8 \text{ s}^{-1}$; (C) $k_R = 10^9 \text{ s}^{-1}$; (D) $k_R = 10^{10} \text{ s}^{-1}$. Other parameters: $g(P^+) = g(I^-) = 2.002$; $k_T = 3 \times 10^8 \text{ s}^{-1}$; $J(I^-X^-) = -200 \text{ G}$. [Taken from Ref. 3]

In Fig. 4A, where $k_R = 0$, the yield of the central state $|0\rangle$ is always greater than (or, when $g(X^-) = g$, equal to) the yields of $|+1\rangle$ and $| -1\rangle$, as predicted by the radical pair mechanism. However as k_R increases (Fig. 4B, C and D) p_0 falls below p_{+1} and p_{-1} over a range of g -values close to 2.002, corresponding to polarization inversion in the EPR spectrum of 3P . When the calculation is repeated, with a much smaller value of $J(I^-X^-)$ (-2 G, roughly appropriate for *Rhodobacter sphaeroides*, for which no inversion is found experimentally), p_0 is larger than p_{+1} and p_{-1} for essentially all $g(X^-)$.

In short, our simulations suggest that inversion should occur when three conditions are satisfied: the g -value of X^- is close to those of P^+ and I^- ; the exchange interaction of I^- and X^- is large; and X^- undergoes rapid spin-lattice relaxation. To account for the observed AEAEAE pattern we require that $g(X^-) \approx 2.00$ when the magnetic field is directed along the Y axis of the zero-field splitting tensor of 3P , but rather different from 2.00 when the field is along X or Z.

3. Spin polarization in 3P — a physical picture.

To get an understanding of what is happening we consider the mixing of the following states of $P^+I^-X^-$ (which are combinations of S, T_0 and $T_{\pm 1}$ states of $[P^+I^-]$ and α and β states of X^-): $S\alpha$ with $T_{+1}\beta$, and $S\beta$ with $T_{-1}\alpha$ (which behave essentially identically to $S\alpha$ and $T_{+1}\beta$). The relevant matrix elements of the spin Hamiltonian H are:

$$\langle T_{+1}\beta | H | T_{+1}\beta \rangle - \langle S\alpha | H | S\alpha \rangle = \Delta_{ST} = [g - g(X^-)]\mu_B B_0$$

$$\langle S\alpha | H | T_{+1}\beta \rangle = \frac{1}{2}J(I^-X^-) .$$

When $|\Delta_{ST}|$ is large compared to $|\frac{1}{2}J(I^-X^-)|$, there will be little mixing of $S\alpha$ and $T_{+1}\beta$, and ST_0 mixing will dominate (i.e. no inversion). For values of $|\Delta_{ST}|$ comparable to $|\frac{1}{2}J(I^-X^-)|$, the states $S\alpha$ and $T_{+1}\beta$ are able to interconvert. Let us consider what happens when $\Delta_{ST} = 0$. In the absence of relaxation, $ST_{\pm 1}$ mixing is exactly balanced by ST_0 mixing such that all three

states of 3P are equally populated (see Fig. 4A). When the relaxation of X^- is fast enough, $S\alpha/T_{+1}\beta$ mixing evidently outweighs $S\alpha/T_0\alpha$ mixing and leads to inversion (Figs 4B, C and D).

To give some insight into how this comes about, we consider the somewhat simplified reaction scheme in Fig. 5. The coherent interconversions of singlet and triplet states of P^+I^- are treated as reversible first order processes, an approximation that is not so very far from what actually happens in radical pairs with many hyperfine couplings [13]. As indicated, the rate constants for singlet \rightarrow triplet and triplet \rightarrow singlet intersystem crossing are k_{ST} and k_{TS} respectively for ST_0 mixing, and $2k_{ST}$ and k_{TS} respectively for $ST_{\pm 1}$ mixing (the reason for the

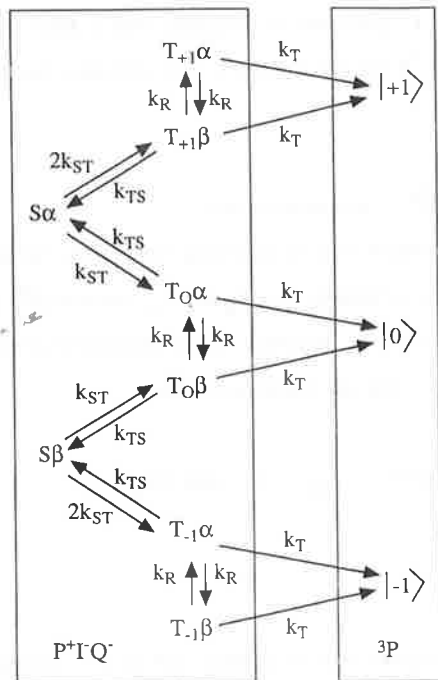


Fig. 5 The important steps involved in the process: ${}^1[P^+I^-]X^- \rightarrow {}^3[P^+I^-]X^- \rightarrow {}^3PI^-$. The wavefunctions $S, T_0, T_{\pm 1}$ refer to the radical pair $[P^+I^-]$, α, β refer to Q^- .

factor of two will emerge shortly). In addition, the spin-lattice relaxation of X^- and the charge recombination of ${}^3[P^+I^-]$ to give 3P are included with first order rate constants k_R and k_T . Using square brackets to indicate populations of states, we have $[S\alpha] = [S\beta] = \frac{1}{2}[S]$ and $[T_q\alpha] + [T_q\beta] = [T_q]$ ($q = +1, 0, -1$). Applying the steady state approximation to the reaction intermediates $T_q\alpha$ and $T_q\beta$ ($q = +1, 0, -1$) gives, in the limit $k_R = 0$:

$$[T_{+1}\alpha] = 0 \quad [T_{+1}\beta] = 2k_{ST}[S\alpha]/(k_{TS} + k_T)$$

$$[T_0\alpha] = k_{ST}[S\alpha]/(k_{TS} + k_T) \quad [T_0\beta] = k_{ST}[S\beta]/(k_{TS} + k_T)$$

$$[T_{-1}\alpha] = 2k_{ST}[S\beta]/(k_{TS} + k_T) \quad [T_{-1}\beta] = 0$$

and hence:

$$dp_{\pm 1}/dt = dp_0/dt = k_T k_{ST}[S]/(k_{TS} + k_T) .$$

Thus, all three triplet sub-levels are formed at the same rate as shown in Fig. 4A for $\Delta_{ST} = 0$. (The factors of 2 in the rate constants for $S\alpha \rightarrow T_{+1}\beta$ and $S\beta \rightarrow T_{-1}\alpha$ ensure that this is true.)

However, when $k_R \gg k_T$, rapid relaxation causes the previously empty states $T_{+1}\alpha$ and $T_{-1}\beta$ to be populated such that:

$$[T_{+1}\alpha] = [T_{+1}\beta] = 2k_{ST}[S\alpha]/(k_{TS} + k_T)$$

$$[T_{-1}\beta] = [T_{-1}\alpha] = 2k_{ST}[S\beta]/(k_{TS} + k_T) .$$

The populations of $T_0\alpha$ and $T_0\beta$, which are already equal, are not affected by relaxation of X^- . So:

$$\frac{dp_{\pm 1}}{dt} = 2dp_0/dt = 2k_T k_{ST} [So]/(k_{TS} + k_T) .$$

Thus, according to this simple scheme, the effect of fast relaxation of X^- is to increase the rate of formation of the $|\pm 1\rangle$ states of 3P by up to a factor of two, leading to an excess population of $|\pm 1\rangle$ relative to $|0\rangle$.

To conclude, rapid spin-lattice relaxation of the reduced iron-quinone complex can influence the population rates of the three sub-levels of 3P , in a way which depends on the anisotropy of the EPR frequency of $[Q^-Fe^{2+}]$ and hence gives rise to anisotropic spin polarization in 3P .

4. Spin polarization in Q^- — experimental observations and computer simulations.

The EPR spectrum of Q^- in reaction centres in which the iron-semiquinone coupling has been disrupted, is also anisotropically spin-polarized [14-18]. Fig. 6 shows 35 GHz EPR spectra of a frozen solution of perdeuterated cells of *Rhodospirillum rubrum* [18]. The dark spectrum (solid line) is the familiar powder pattern for a radical with an orthorhombic g-tensor. The dashed line is the spectrum of spin-polarized Q^- resulting from continuous illumination. For g -values near g_{zz} and g_{xx} the polarization is emissive (with somewhat smaller emission for $g \approx g_{yy}$), while for $g \approx g_{yy}$ very little polarization is seen.

The key to understanding this observation turns out to be the dipolar interaction between I^- and Q^- . Inspection of the X-ray coordinates for *Rps. viridis* shows that the I^-Q^- dipolar axis (roughly the vector connecting the centres of the two radicals) is nearly parallel to the Y axis of Q^- (the axis in the semiquinone plane, perpendicular to the oxygen-oxygen direction). Since the strength of the dipolar coupling is proportional to $3\cos^2\xi - 1$, where ξ is the angle between the dipolar axis and the magnetic field direction, it is plausible that the polarization at $g \approx g_{xx}$ and g_{zz} , for which $\xi \approx \pi/2$, should differ from that at $g \approx g_{yy}$ for which $\xi = 0$.

This idea has been investigated using computer simulations [4] similar to those described above. The results of these calculations may be summarized as follows. 1. Neither the P^+I^- dipolar coupling nor the I^-Q^- exchange interaction are significant in determining the observed pattern of spin polarization. 2. The I^-Q^- dipolar coupling is crucial: values of $D(I^-Q^-)$ between -5 and -40 G generally gave the desired polarization (a value of -9.5 G has been calculated from the crystallographic coordinates for *Rps. viridis* [19,20]). 3. k_T must be larger than about $2 \times 10^8 s^{-1}$ and k_S less than about $8 \times 10^7 s^{-1}$ [in agreement with Reaction Yield Detected Magnetic Resonance (RYDMR) experiments and static magnetic field effects (MARY)]. 4. With the I^-Q^- dipolar axis parallel to the Y axis of the semiquinone g-tensor, the P^+I^- exchange interaction $J(P^+I^-)$ must be greater than about +4 G (to be compared with $5 \text{ G} \leq |J(P^+I^-)| \leq 8 \text{ G}$ from RYDMR and MARY measurements).

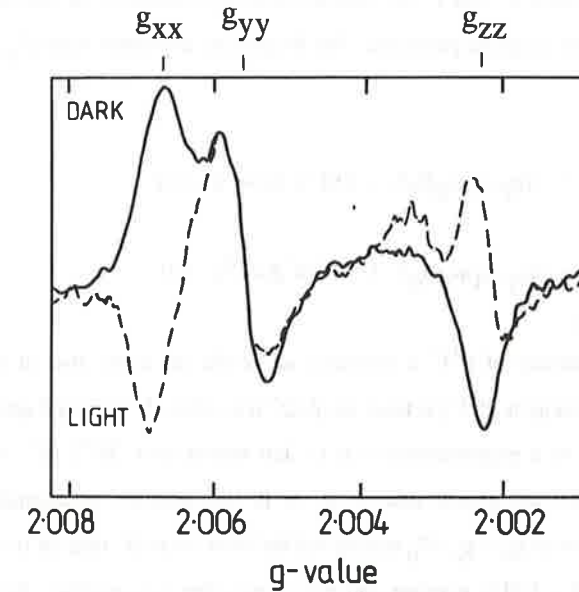


Fig. 6 Light (dashed line) and dark (solid line), first derivative, 35 GHz EPR spectra of Q^- in pre-reduced, perdeuterated cells of *Rhodospirillum rubrum* at 80 K. [Adapted from Ref. 18]

5. Spin polarization in Q^- — a physical picture.

A simple rationale for the anisotropy of the polarization (emission at both g_{xx} and g_{zz} , and very little polarization at g_{yy}) comes from a consideration of the ST_0 mixing of $[P^+I^-]$ induced by the I^-Q^- dipolar coupling. Assuming that the only significant interactions of P^+ and I^- are their isotropic Zeeman interactions and an axial dipolar coupling between I^- and Q^- , we have the following EPR frequencies:

$$\omega_P = g_P \mu_B B_0 / \hbar$$

$$\omega_I^\alpha = g_I \mu_B B_0 / \hbar + D(I^-Q^-)[\cos^2 \xi - 1/3]$$

$$\omega_I^\beta = g_I \mu_B B_0 / \hbar - D(I^-Q^-)[\cos^2 \xi - 1/3]$$

where ω_P and ω_I refer to P^+ and I^- , the superscripts (α and β) denote the spin states of Q^- , and $D(I^-Q^-)$ is the dipolar coupling parameter. The frequencies associated with ST_0 interconversion are therefore:

$$\omega_{PI}^\alpha = |\omega_P - \omega_I^\alpha| = |(g_P - g_I) \mu_B B_0 / \hbar - D(I^-Q^-)[\cos^2 \xi - 1/3]|$$

$$\omega_{PI}^\beta = |\omega_P - \omega_I^\beta| = |(g_P - g_I) \mu_B B_0 / \hbar + D(I^-Q^-)[\cos^2 \xi - 1/3]|$$

The major decay pathway of P^+I^- is formation of 3P via the triplet state of the radical pair. Therefore, if ST_0 mixing in $[P^+I^-]$ is faster for $\beta-Q^-$ (i.e. when Q^- is in its β spin state) than for $\alpha-Q^-$, there should be a preponderance of $\beta-Q^-$ left behind after ${}^3[P^+I^-]Q^- \rightarrow {}^3PIQ^-$ charge recombination. Since the ground state of Q^- is β , this situation corresponds to absorptive polarization. Now, since $g_P < g_I$, ST_0 mixing will be faster for $\beta-Q^-$ than for $\alpha-Q^-$ ($\omega_{PI}^\beta > \omega_{PI}^\alpha$) when $D(I^-Q^-)[\cos^2 \xi - 1/3]$ is negative, and vice-versa when it is positive. For a radical pair, $D(I^-Q^-)$ should be negative, so that we predict absorptive polarization for $\xi = 0$ (i.e. when the field is along the Y axis of Q^-) and emission for $\xi = \pi/2$ (i.e. when the field is parallel to either

the X or the Z axes). This is just what is observed (Fig. 6) except that the polarization at g_{yy} is essentially zero rather than absorptive. The discrepancy arises because this value of $g(Q^-)$ does not correspond to a unique orientation of the reaction centre, but to a range of orientations some of which have $\xi \approx 0$ (i.e. absorption) and some of which have $\xi \approx \pi/2$ (i.e. emission).

This line of reasoning is precisely that used to explain the origin and signs of CIDNP enhancements [21], with two differences: anisotropic interactions do not average out in the solid state and the Zeeman splitting of Q^- is comparable to that of P^+ and I^- (Fig. 2) so that $ST_{\pm 1}$ mixing cannot be ignored. It turns out that $ST_{\pm 1}$ mixing can account for the asymmetry of the observed polarization (i.e. more emission at g_{zz} than at g_{xx}) provided that $J(P^+I^-) \gtrsim 4$ G. Other measurements (RYDMR) give at best ambiguous evidence for the sign of this parameter [22,23].

To summarize: the anisotropically spin-polarized EPR spectrum of Q^- in pre-reduced reaction centres can be understood in a straightforward manner. Unlike many other types of measurement, electron spin polarization is sensitive to the *signs* of exchange interactions — the sign of $J(P^+I^-)$ determined here may prove useful in determining details of the primary charge separation and the role of the accessory chlorophyll situated between P and I. Finally, anisotropic polarization promises to be a method for determining the orientation of Q in reaction centres whose structures are unknown.

References

- [1] A. J. Hoff, *Q. Rev. Biophys.*, **17** (1984) 153.
- [2] P. J. Hore in A. J. Hoff (ed.), *Advanced EPR. Applications in Biology and Biochemistry*, Elsevier, Amsterdam, 1989, p. 405.
- [3] P. J. Hore, D. A. Hunter, F. G. H. van Wijk, T. J. Schaafsma and A. J. Hoff, *Biochim. Biophys. Acta*, **936** (1988) 249.
- [4] P. J. Hore, D. J. Riley, J. J. Semlyen, and A. J. Hoff, *Biochim. Biophys. Acta*, submitted.
- [5] P. L. Dutton, J. S. Leigh, and M. Siebert, *Biochim. Biophys. Res. Commun.*, **46** (1972) 406.

- [6] M. C. Thurnauer, J. J. Katz, and J. R. Norris, *Proc. Natl. Acad. Sci. USA*, **72** (1975) 3270.
- [7] F. G. H. van Wijk, P. Gast and T. J. Schaafsma, *Photobiochem. Photobiophys.* **11** (1986) 95.
- [8] F. G. H. van Wijk, P. Gast and T. J. Schaafsma, *FEBS Lett.* **206** (1986) 238.
- [9] F. G. H. van Wijk, C. B. Beijer, P. Gast and T. J. Schaafsma, *Photochem. Photobiol.* **46** (1987) 1015.
- [10] F. G. H. van Wijk, Thesis, Wageningen Agricultural University, 1987.
- [11] W. F. Butler, R. Calvo, D. R. Fredkin, R. A. Isaacson, M. Y. Okamura and G. Feher, *Biophys. J.* **45** (1984) 947.
- [12] G. C. Dismukes, H. A. Frank, R. Friesner and K. Sauer, *Biochim. Biophys. Acta*, **764** (1984) 253.
- [13] K. M. Salikhov, Yu. N. Molin, R. Z. Sagdeev and A. L. Buchachenko, *Spin Polarization and Magnetic Field Effects in Radical Reactions*, Elsevier, New York, p. 69, 1984.
- [14] P. Gast and A. J. Hoff, *Biochim. Biophys. Acta*, **548** (1979) 520.
- [15] A. J. Hoff and P. Gast, *J. Phys. Chem.* **83** (1979) 3355.
- [16] P. Gast, R. A. Mushlin, and A. J. Hoff, *J. Phys. Chem.* **86** (1982) 2886.
- [17] A. J. Hoff, P. Gast, R. A. Isaacson, and G. Feher, in *Photosynthesis III. Structure and Molecular Organization of the Photosynthetic Apparatus*, G. Akoyunoglou (ed.), p. 1023, Balaban International Science Services, Philadelphia, 1981.
- [18] P. Gast, A. de Groot, and A. J. Hoff, *Biochim. Biophys. Acta*, **723** (1983) 52.
- [19] A. Ogrodnik, W. Lersch, M. E. Michel-Beyerle, J. Deisenhofer and H. Michel in *Antennas and Reaction Centres of Photosynthetic Bacteria*, M. E. Michel-Beyerle (ed.), p. 198, Springer, Berlin, 1985.
- [20] D. Stehlik, C. H. Bock, and J. Petersen, *J. Phys. Chem.* **93** (1989) 1612.
- [21] R. Kaptein in *Chemically Induced Magnetic Polarization*, L. T. Muus, P. W. Atkins, K. A. McLauchlan and J. B. Pedersen (eds), Reidel, Dordrecht, 1977.
- [22] J. R. Norris, M. K. Bowman, D. E. Budil, J. Tang, C. A. Wraight, and G. L. Closs, *Proc. Natl. Acad. Sci. USA*, **79** (1982) 5532.
- [23] J. Tang and J. R. Norris, *Chem. Phys. Lett.* **94** (1983) 77.